TECTONO-MAGMATIC AND METALLOGENIC EVOLUTION OF THE LATE TRIASSIC TO MIDDLE JURASSIC HAZELTON GROUP IN NORTHWEST BRITISH COLUMBIA

by

Tony Barresi

Submitted in partial fulfilment of the requirements
for the degree of Doctor of Philosophy

at

Dalhousie University
Halifax, Nova Scotia
March 2015

Table of Contents

List of Tables

List of Figures

Abstract

The Hazelton Group (Stikine terrane) in NW British Columbia represents a regionally extensive, Late Triassic to Middle Jurassic successor arc. It records two economically important metallogenic episodes associated with the final stages of subduction- and rift-related magmatism in the Stikine terrane, and collision of Stikinia with inboard and outboard terranes and their accretion to Laurentia. This comprehensive study attempts to indicate the environments most likely to contain exploitable mineral resources.

Volcanic and sedimentary rocks of the lower Hazelton Group were deposited along two arc axes and in an intervening basin. Near Terrace, British Columbia, lower Hazelton Group (Telkwa Formation) volcanism initiated by 204.8±0.3 Ma and continued for >10 My, creating 16 km of stratigraphy. The volcanic rocks have bimodal silica concentrations and geochemical characteristics of subduction-related island-arc magmatism. Mafic to intermediate rocks comprise a mantle-derived differentiated suite; rhyolites formed from anatexis of arc crust caused by magmatic underplating.

Circa 174 Ma bimodal volcanic rocks of the upper Hazelton Group Iskut River Formation define a 300 by 50 km discontinuous belt in northwestern B.C. (the Eskay rift). They represent the final episode of Jurassic magmatism in the Stikine terrane, and are interpreted to have been deposited in sub-basins that opened during arc-scale transcurrent shearing during collision of Stikinia and surrounding terranes. Two geochemically distinct types of tholeiitic basalts are present; both resemble back-arc basin basalts formed by melting of asthenospheric and sub-arc mantle sources. Group 1 is isotopically more juvenile, and less enriched in non-conservative incompatible elements then group 2 basalts, which are affected by crustal contamination.

The formation of latest Triassic to Early Jurassic porphyry-Cu deposits in Stikinia is temporally linked to initiation of Hazelton Group magmatic-arc activity ca 205 Ma. The porphyry intrusions are interpreted to be derived from subduction-related, oxidized, metalliferous magmas that underplated Stikinia. Circa 174 Ma VMS deposits (e.g. Eskay Creek and Anyox) are linked to rifting during post-subduction, orogenic-scale, terrane collisions. The VMS deposits are found in the southern portion of the Eskay rift, in association with group 1 basalts, which are interpreted to have formed from rapidly ascending magma in an advanced rift setting.

List of Abbreviations Used

Locations

Abbr.	Description
AB	Alberta
AN	Anyox
AR	Ashman Ridge
BC	British Columbia
BR	Bait Range
DM	Diagonal Mountain
EC	Eskay Creek
KP	Klastine Plateau
MD	Mount Dillworth
NM	Netalzul Mountain
NR	Nilkitkwa Range
NWT	Northwest Territories
OE	Oweegee East
OR	Omineca Range
OW	Oweegee West
PBR	Pillow Basalt Ridge
QM	Quinlan Mountain
TB	Table Mountain
TC	Tenas Creek
TG	Treaty Glacier
TM	Todagain Mountain
TR	Toodoggon River
W1	Mount Will 1
W2	Mount Will 2
YT	Yukon

Minerals

Abbr.	Description
Al	albite
An	anorthite
CPX	clinopyroxene
En	enstatite
Fs	ferrosilite
OL	olivine
PLAG	plagioclase
Wo	wollastonite

Geological Timescale

Bath	Bathonian
Callov	Callovian
Hettang.	Hettangian
J	Jurassic
K	Cretaceous
JL	Joan Lake
Kimmerid.	Kimmeridgian
LT	Late Triassic
MJ	Middle Jurassic
TJB	Triassic-Jurassic boundary

Geochemical Classification and Terminology

Abbr.	Description
AFC	assimilation and fractional crystallization
BABB	backarc basin basalts
E-TMORB	enriched to transition MORB
EMORB	enriched MORB
F	magma mass/initial magma mass
FAPB	forearc platform basalt
G1	group 1 basalt
G2	group 2 basalt
HFSE	high field strength elements
HREE	heavy rare earth elements
IAT	island arc-tholeiites
ICP-MS	inductively coupled plasma mass spectrometry
LA-ICP-MS	laser-ablation inductively-coupled-plasma mass-spectrometry
LOTI	low Ti tholelite
LREE	light rare earth elements
Mg#	molar Mg/(Mg + Fe)
MORB	mid-ocean ridge basalts
NMORB	normal MORB
OFB	ocean floor basalt
OIB	ocean Island basalts
PER	Pearce element ratio
ppm	parts per million
REE	rare-earth-elements
T	initial
TDM	depleted mantle model age
TIMS	thermal ionization mass spectrometry
WDS-XRF	wavelength-dispersive—X-ray fluorescence

Stratigraphic Units

Abbr.	Description
BLG	Bowser Lake Group
IRF	Iskut River Formation
KC	Kitselas Complex
LHG	lower Hazelton Group
MHC	Mount Henderson Complex
MOC	Mount O'Brien Complex
Rv	Recent basalt flows
UHG	upper Hazelton Group

General Abbreviations

AURIF	Atlantic Universities Regional Isotopic Facility
BSE	backscatter electron
CA-TIMS	chemical-abrasion thermal-ionization-mass-spectrometry
ca	circa
DEM	digital elevation model
GSC	Geological Survey of Canada
KK	Kanganui Kaersutite
KSM	Kerr-Sulphurets-Mitchell
Ma	million years ago
My	million years
NAD83	North American datum 1983
NTS	National Topographic System Maps
T-P	Temperature and Pressure
UTM	Universal Transverse Mercator
VHMS	Volcanic-Hosted-Massive-Sulfide
VMS	volcanogenic massive sulfide
WDS	wavelength-dispersive spectrometers
XRF	X-ray fluorescence

Acknowledgements

I would like to thank my wife Keirsten Wells, son Elliot Barresi and parents John and Jolien Barresi for their patience and support. I also thank my long suffering friends, whom I have not seen in a very long time.

JoAnne Nelson of the British Columbia Geological Survey Branch (BCGS) conceived of this project, facilitated the fieldwork, and has been a wise and gracious mentor to me.

I am thankful to my supervisors, Jaroslav Dostal, and Rebecca Jamieson for their guidance, support, and cheerful dispositions. Dr. Dostal has carried on as an advisor long into his retirement, for which I am grateful. I also thank the other thesis committee members Nicholas Culshaw and Marcos Zentilli for their guidance and efforts towards bettering this work.

Many others contributed to this project, including Dani Alldrick of the BCGS, Robert Anderson and Vicki McNicoll of the Geological Survey of Canada, Steven Piercey of Memorial University, Harold Gibson of Laurentian University, Maurice Colpron of the Yukon Geological Survey, John Waldron and Jean-François Gagnon of University of Alberta, and Richard Friedman of the University of British Columbia.

I appreciate all my classmates and the staff and faculty at Dalhousie and Saint Mary's universities who have exemplified a positive academic environment.

I acknowledge and appreciate the financial support that I received from the Killam Foundation, the Natural Sciences and Engineering Research Council, Natural Resources Canada, The Geological Society of America, and the Society of Economic Geologists.

Chapter 1 - Introduction

1.0 Statement of Problem

The Stikine terrane (Stikinia) in northwestern British Columbia is one of the largest tectono-magmatic elements that comprise the Canadian Cordillera (Fig. 1-1). The terrane has been mapped mainly at 1:250,000 scale, and studied largely without the benefit of modern geochronological or geochemical methods. Recent detailed studies in the Stikine and other terranes have begun to refine our understanding of the Canadian Cordillera, and made possible regional syntheses that better describe the geological history of the individual terranes and the orogenic scale tectonics of arc-accretion and crustal growth (e.g. Marsden and Thorkelson, 1992; Mihalynuk et al. 1994; Taylor et al. 2008; Nelson et al. 2013; Staples et al. 2014).

This thesis is based on geological mapping, geochemistry, and geochronology from two targeted areas (Fig. 1-2) that were deficient in modern detailed studies yet are critical to deciphering the geological, tectonic and metallogenic history of Stikinia. The target areas include: 1) a 3,500 km^2 area near Terrace, BC, which contains an unusually thick sequence of lower Hazelton Group, arc-related, volcanic rock (Telkwa Formation) that spans the full duration of Hazelton arc construction and is coeval with a regional belt of porphyry Cu deposits; and 2) a 300 by 50 km belt of post-subduction, syn-accretion, rift-related upper Hazelton Group volcanic rocks (Iskut River Formation) that host volcanogenic massive sulfide deposits. The two areas record 30 My, beginning with construction of the Hazelton arc and formation of porphyry copper mineral deposits in the latest Triassic, and ending with accretion of the Stikine terrane to ancestral North America, opening of a short-lived rift, and formation of VMS deposits in the early Middle Jurassic.

These focused studies address problems related to the local geology, document critical locations/periods in the evolution of the Hazelton arc, and refine hypotheses that link

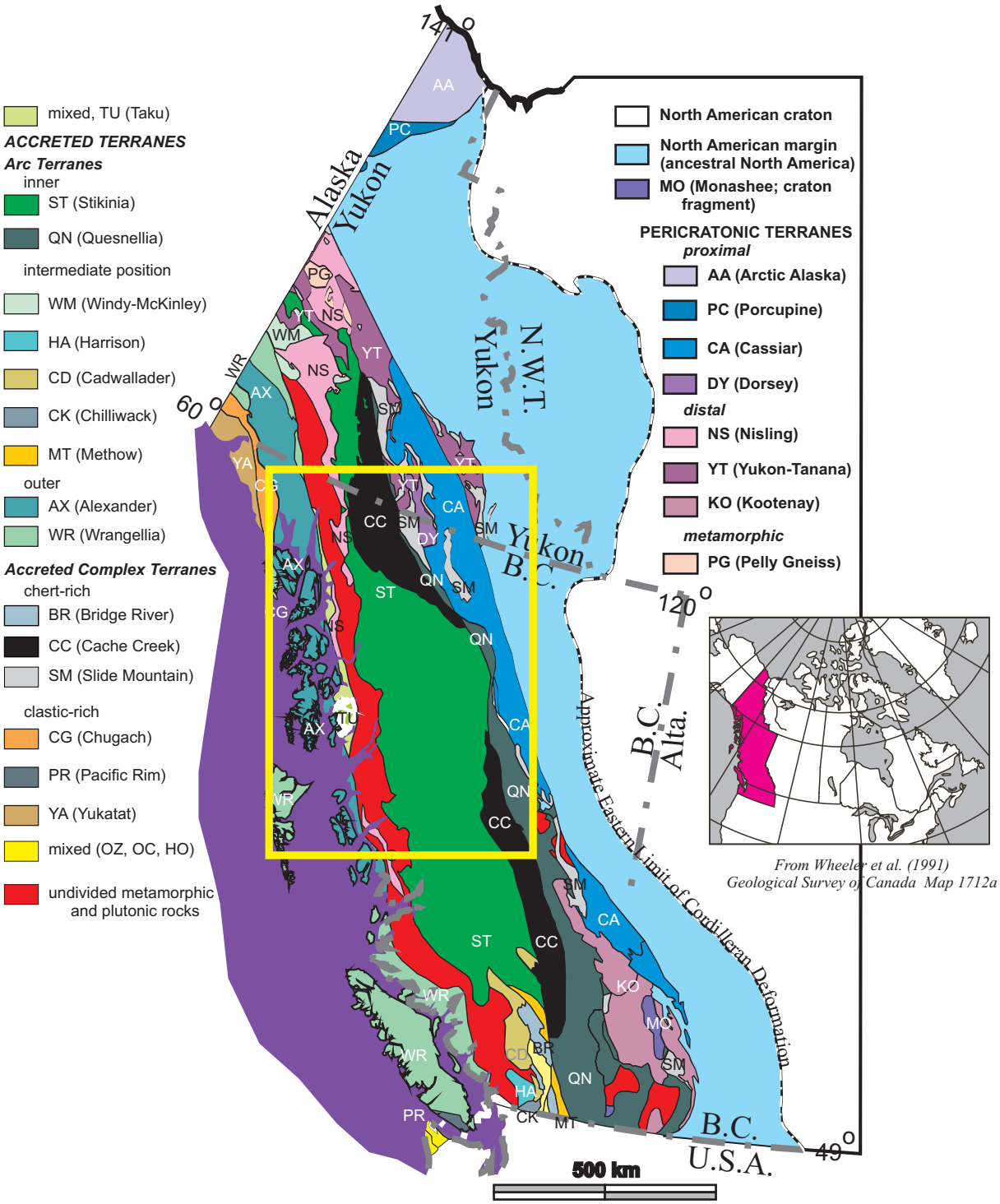

Fig. 1-1. Tectonic assemblage map (modified from Wheeler et al. 1991) showing the terranes that comprise the Canadian Cordillera. From west to east: 1) outer island-arc terranes with little or no continental influence (e.g. Alexander and Wrangellia terranes); 2) central island-arc (e.g. Stikinia) and oceanic (Cache Creek) terranes, some with minor continental affinity; 3) inner pericratonic terranes that have elements formed on or adjacent to the ancient North American continental margin; 4) inboard autochthonous continental margin and craton. Note the size of the Stikine terrane, sometimes described as a micro-continent. Inset shows location of Fig. 1-2.

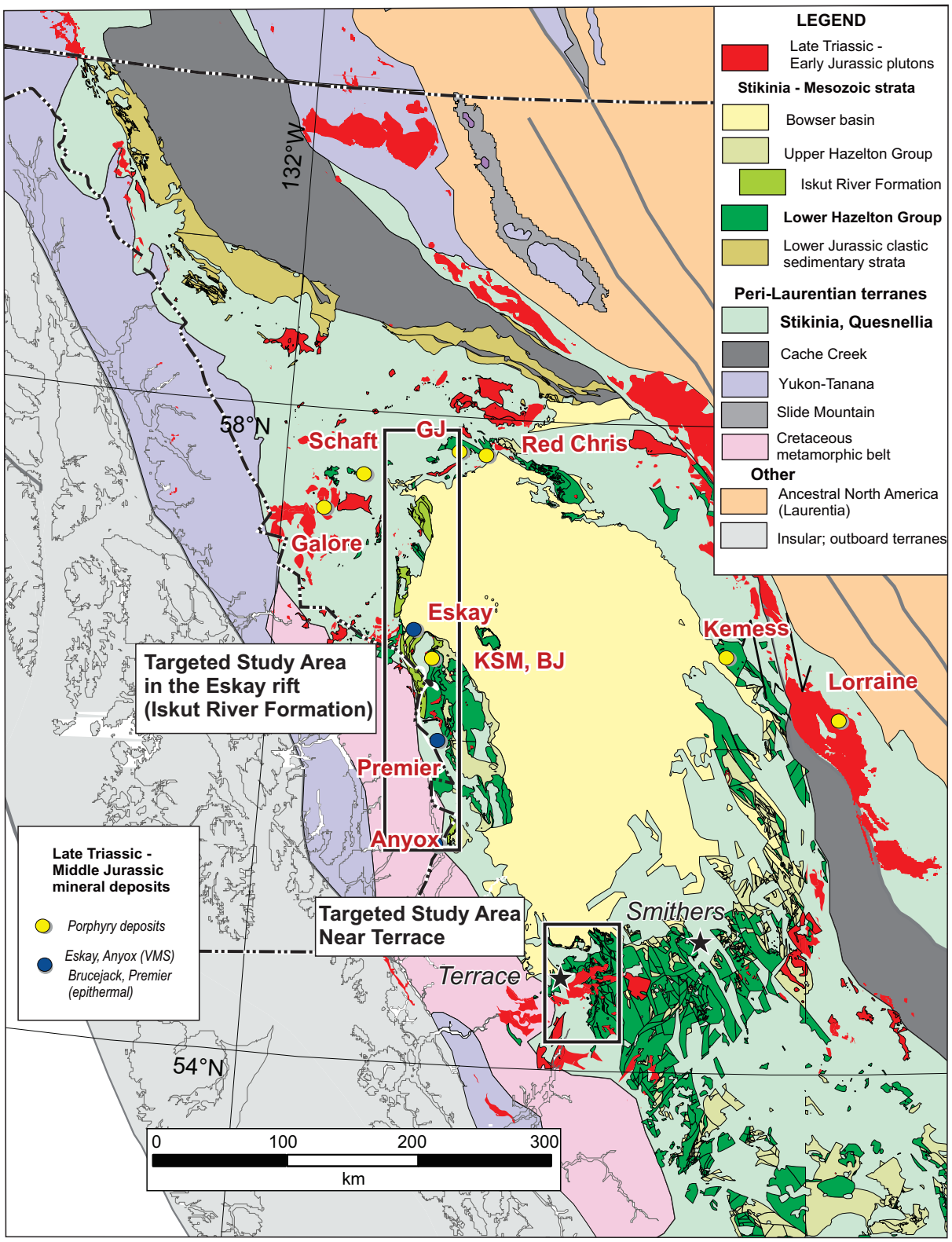

Fig. 1-2. Tectonic assemblage map of the northern Canadian Cordillera including Mesozoic geology of the Stikine terrane and location/context of significant mineral deposits. Insets for locations of areas targeted for mapping and geochemical and geochronological studies included in this thesis. Note that only areas where the Iskut River Formation outcrops were targeted within the Eskay rift area.

island-arc- and rift-related magmatism and subduction- and accretion-related tectonics to regional metallogeny.

1.1 State of Knowledge

1.1.1 Stikinia: Tectonic Framework and Stratigraphic Elements

The Canadian Cordillera is composed of ancestral North American rocks, Neoproterozoic and Paleozoic continental margin deposits, and terranes of various ages and origins that were accreted to the North American craton (Fig. 1-1 Coney et al. 1980). Terranes are fault-bounded fragments of the earth's crust with geological records that are distinct from those of other fault-bound crustal fragments (Monger and Berg 1984). Some terranes are recognized as having only oceanic and/or island arc stratigraphy with no pre-accretionary affinity to North America (Gabrielse and Yorath 1991). In contrast, pericratonic terranes have some elements that formed on or adjacent to the ancient North American continental margin (Fig. 1-1).

The Stikine island arc terrane defines the westernmost boundary of a geomorphic belt in the Cordillera composed of accreted island arc and pericratonic terranes structurally imbricated with oceanic rocks (intermontane belt). It is the largest island-arc terrane within the Cordillera and its extent can be followed, discontinuously, over a 2000 x 100-500 km area trending NW-SE along the general tectonic grain of the Cordillera (Fig. 1-1). Paleontological studies of Stikinian fossil assemblages (Stanley and McRoberts 1993) suggest that the terrane formed in a tropical environment at a southerly latitude in the eastern Pacific, before moving northward during the Jurassic. The Stikine terrane is inferred to have been deposited, at least in part, on pericratonic (Laurentian) basement of the Yukon-Tanana terrane (Jackson et al. 1991; Gehrels and Kapp 1998). It amalgamated with the more inboard Cache Creek subduction complex between 173.0 ±0.8 Ma and 172 Ma (Mihalynuk et al. 1992, 2004), and in turn the Alexander-Wrangellia block collided with the outboard side of Stikinia (van der Heyden 1992; Gehrels 2001). The composite terrane accreted to the western margin of Laurentia in the late Early to Late Jurassic, and was deformed along with the margin during Cretaceous (and older) orogenesis (Coney et

al. 1980; Monger et al. 1982; Wheeler et al. 1991; Mihalynuk et al. 1994; Nelson et al. 2013).

Rocks in the Stikine terrane record three episodes of island arc formation between the late Paleozoic and early Mesozoic (Table 1-1): 1) Devonian to Permian Stikine and Takhini assemblages and Asitka Group (Hart 1997; Logan et al. 2000; Gunning et al. 2006); 2) Middle to Late Triassic Stuhini and Takla groups (Souther 1977; Mortimer 1986; Dostal et al. 1999); and 3) Late Triassic to Middle Jurassic Hazelton Group (Tipper and Richards 1976; Monger et al. 1991; Marsden and Thorkelson, 1992; MacIntyre et al. 2001; MacIntyre 2006). Separated by unconformities, these three successions consist of isotopically juvenile, arc-related volcanic rocks (Samson et al. 1989) that either lie on, or interfinger with, carbonate and siliclastic rocks. Stikinia is overlain by middle to late Mesozoic rocks (Bowser Lake and Nechako groups) deposited in post-accretionary basins, and Tertiary to Recent volcanic rocks such as the Chilcotin Group (Miocene) and the Mt. Edziza Complex (Upper Miocene to Holocene).

Table 1-1 Important regional stratigraphic units in the study areas.

Age	Stratigraphic Element	Lithological and Structural Characteristics	Interpreted Tectonic Setting
Upper Miocene to Holocene	Mt. Edziza Complex	Alkaline basalt and rhyolite	Continental arc
Middle Jurassic to Cretaceous	Bowser Lake Group	Sedimentary rock, rich in clasts of black chert	Sedimentary overlap assemblage shed from near-by, obducted Cache Creek Terrane
Early to lower Middle Jurassic	Upper Hazelton Group; Iskut River Formation	Fault and unconformity bound conglomerates and bimodal tholeiitic volcanic rocks	Extension-related (rift) environment
Late Triassic to Early Jurassic	Lower Hazelton Group; Telkwa Formation	Mafic to felsic but dominantly andesitic calc-alkaline volcanic rocks and minor sedimentary rock.	Island arc
Late Triassic	Stuhini Group; Takla Group	Augite porphyritic, mainly mafic, alkalic or tholeiitic to calc-alkaline volcanic rocks	Island arc
Devonian to Permian	Stikine assemblage	Poly-deformed chert, carbonates, and intermediate volcanic rocks	Island arc

1.1.2 Geology of the Hazelton Group

The Hazelton Group is the youngest of the three arc/successor arc sequences that form Stikinia. Marsden and Thorkelson (1992) proposed that the Hazelton Group formed as a result of two concurrent and geometrically opposed subduction zones and related volcanic arcs on opposite sides of a Philippine-style micro-plate. The two belts of voluminous arc-related rocks are separated by a less volcanically active inter-arc basin. The lower Hazelton Group consists of mafic to felsic volcanic flows, tuffs, pyroclastic rocks, and volcanically derived epiclastic rocks (Tipper and Richards 1976; Greig and Gehrels 1995; Thorkelson et al. 1995; Gareau et al. 1997a, b; Duuring et al. 2009a,b). The volcanic rocks are interpreted to have been deposited in mainly subaerial environments and, along with sub-volcanic intrusions, to have built successive stratovolcanoes (Alldrick 1993). The upper Hazelton Group consists of Pliensbachian to late Callovian, regionally traceable, mainly sedimentary units, and a 300 km-long bimodal volcanic unit deposited in the "Eskay rift" (Evenchick and McNicoll 2002; Alldrick et al. 2005a,b). The Eskay rift represents post-subduction, extension/transtension-related volcanism during the amalgamation of the Stikinia, Cache Creek, and Quesnel terranes into an intermontane composite terrane and its subsequent accretion to North America. Although subduction-related magmatism was no longer active in northern Stiknia ca. 174 Ma, coeval, voluminous, calc-alkaline, Hazelton Group volcanics are represented in the Bella Coola and Whitesail Lakes area, approximately 450 km to the south, indicating a southward migration of the western Hazelton Group volcanic arc (Gordee 2005; Haggart et al 2006; Mahoney et al 2007)

1.1.3 Metallogenesis of the Hazelton Group

The Hazelton Group is host to a plethora of mineral deposits, including many that are economic (Macdonald et al. 1996a,b; Lang et al. 1995; Logan and Mihalynuk 2014). Particularly significant are porphyry copper deposits such as Red Chris, Kerr-Sulphurets-Mitchell (KSM), Snowfield, and GJ, volcanogenic massive sulfide deposits (VMS) such as Eskay Creek and Anyox, and epithermal deposits such as Brucejack, Premier, and Treaty Creek (Fig. 1-2). These deposits have been related to multiply reactive crustal-

scale faults and initiation of island-arc magmatism (Nelson and Kyba 2014), stalled subduction and the effects of slab windows (Logan and Mihalynuk, 2014), and late arc rifting (MacDonald et al. 1996a,b).

The Hazelton Group records two distinct and important metallogenic episodes. The first corresponds to subduction-related magmatism responsible for construction of the Hazelton arc ca 205 Ma to 195 Ma. During this time, emplacement of mineralizing porphyry intrusions formed porphyry copper deposits. Among these, the Red Chris deposit contains 936.2 million tonnes (proven and probable) grading 0.37% Cu and 0.385 grams per tonne (g/t) Au (Gillstrom et al. 2012), and the KSM deposits contain 2.2 billion tonnes (proven and probable) grading 0.21% Cu and 0.55 g/t Au (Huang et al. 2014). The porphyry copper deposits include calc-alkaline varieties, and unusual alkalic varieties that are very poorly represented outside British Columbia. The second metallogenic episode corresponds to ca 174 Ma rifting of the Stikine terrane, eruption of bimodal volcanic rocks (Iskut River Formation), and formation of volcanogenic massive sulfide deposits. These include Eskay Creek in the central Eskay rift and four deposits near Anyox in the southern Eskay rift, two of which were mined between 1914 and 1935. The Anyox deposits produced 21.73 million tonnes of ore with an average recovered grade of 1.68% Cu, 10.8 g/t Ag, and 0.2 g/t Au (Sherlock and Domvile 2008). The Eskay Creek deposit, which was mined between 1995 and 2007, is of particular importance because of its status as the world's highest-grade Au-rich VMS deposit (Mercier-Langevin et al. 2011). Eskay Creek contained 3.35 million tonnes of ore that graded 0.7% Cu, 2.9% Pb, 5.6% Zn, and an astonishing 45.97g/t Au and 2224 g/t Ag. For context, the world's second highest-grade Au-rich VMS deposit, Boliden in Skellefte Sweden, has an average Au grade of 15.50 g/t. The Eskay Creek deposit is divided into several zones of: 1) stratiform clastic-bedded sulfides and sulfosalts and/or barite hosted by marine mudstone; and 2) discordant quartz-sulfide veins in volcanic rocks that form the immediate footwall to the stratiform ore zones. The majority of the ore at Eskay Creek is contained in the 21B zone, a stratiform clastic sulfide and sulfosalt deposit. Sherlock et al. (1999) suggested, based on fluid inclusion data, that precious-metal precipitation at Eskay Creek was driven by boiling of hydrothermal fluid at a relatively low temperature (< 200°C) and shallow depth (< 1500 m). They concluded that low T-P

boiling, which is typically much more effective at precipitating Au and Ag than base metals, was the cause of high ratios of precious to base metals in the Eskay Creek deposit. The JADE hydrothermal field in the Okinawa trough is the only described modern analogue to the hydrothermal conditions represented at Eskay Creek (Sherlock et al. 1999).

1.2 Objectives and Motivation

Whereas the majority of detailed (e.g. 1:50,000 or smaller scale) geology maps and geochemical/geochronological studies in NW Stikinia that include the Hazelton Group are focused on the areas immediately surrounding mineral deposits, the objective of this study is to refine our understanding of the Hazelton Group by focusing on two targeted areas (Fig. 1-2) characterized by good exposure, and which together contain a continuous, unfragmented record of the Hazelton Group.

Previous 1:250,000 mapping of the Hazelton Group near Terrace (Duffel and Souther 1964; Woodsworth et al. 1985) showed that the area contains a complicated but unfragmented record of the Hazelton Group, from its initial deposition on basement rock through to foundering of the arc and deposition of overlying sedimentary units (upper Hazelton Group). The area (Fig. 1-2) was therefore targeted for a detailed mapping and geochemical/geochronological study, in order to characterize the lower Hazelton Group and understand its origin in the context of construction of the Hazelton Arc.

The following specific objectives apply to the Terrace map area:

1. Determine how the Telkwa Formation near Terrace differs from other areas (e.g. age, thickness, depositional environment, dominant composition, volcanic facies etc.) and link those variations to the overall geometry and/or geological history of the Hazelton arc.
2. Use modern geochemical and geochronological techniques, paired with detailed mapping, to determine the petrogenesis and evolution of the Hazelton magmatic arc.

3. Test the hypothesis that some or all of the roughly coeval porphyry Cu deposits in Stikinia are either co-magmatic with Hazelton arc volcanics, or were generated by related processes.
4. Test the hypothesis that the Kitselas volcanics (amphibolite facies) belong to the Hazelton Group and if so, determine their relationship to Telkwa Formation (zeolite facies) volcanic complexes or facies.
5. Determine the nature of the unconformity that separates the Stuhini and Hazelton groups near Terrace to see if it records erosion that is deep enough to explain the absence of Stuhini group volcanic rocks, which form thick accumulations to the north in the Stewart area.

In northern Stikinia, the upper Hazelton Group was traditionally considered to represent a predominantly sedimentary succession (e.g. Tipper and Richards 1976; Thomson et al. 1986; Marsden and Thorkelson 1992, Evenchick and Thorkelson 2005). However, in the Iskut River area refined geochronological and biostratigraphic work (e.g. Lewis et al. 1993; Macdonald et al. 1996a; Logan et al. 2000) provided constraints that showed the bimodal volcanic rocks of the Salmon River Formation[1] to be coeval with the more regionally extensive sedimentary successions in the upper Hazelton Group. The volcanic rocks were recognized by Anderson (1993) to extend along an approximately 300 km fault-bounded belt interpreted as a former rift (Eskay rift). In 1988, the high-grade 21 zone of the Eskay Creek VMS deposit was discovered in the central portion of the Eskay rift, initiating a staking rush and focusing academic and industry attention on the area. However, most studies of the upper Hazelton Group within the Eskay rift were concentrated in areas close to the Eskay Creek ore-body or other mineral occurrences, and the geochemical and field characteristics of coeval volcanic rocks that outcrop in the regions north and south of the mine received little attention. Geochemical studies were particularly restricted by the deposit-scale focus of previous work, because they could not incorporate regional variations, and the primary composition of the rocks were largely destroyed by hydrothermal alteration. Therefore, upper Hazelton Group volcanic rocks

[1] The term Salmon River Formation is superseded by the Iskut River Formation, which is introduced as part of the work in this thesis (Chapter 2).

exposed in the Eskay rift were targeted for this study (Fig. 1-2), in order to investigate the magmatic and tectonic processes that led to their formation.

The following specific objectives apply to the Eskay rift study area:

1. Map and define the strata that fill the Eskay rift in order to resolve the problems associated with conflicting and ambiguous nomenclature, and to better distinguish them from: a) the strata that fill the Hazelton trough, b) coeval regionally extensive sedimentary rock, and c) older island-arc volcanic rocks of the lower Hazelton Group.
2. Test the hypothesis that the Iskut River Formation was deposited in a single or multiple syn-depositional graben(s).
3. Characterize the Iskut River Formation rocks and stratigraphic or geographic variations in their lithology, volcanic facies, and/or chemistry.
4. Determine the petrogenesis of the volcanic rocks and their genetic, spatial, and temporal relationships to one another.
5. By using the outcome of the previous objectives, develop a conceptual model that accounts for the features of the upper Hazelton Group, and which can be used to test and possibly refine current theories that link the formation of VMS deposits to specific tectono-magmatic conditions or processes.

1.3 Methods

To fulfill the objectives, I have conducted fieldwork, petrographic, geochronological, and mineral and whole-rock geochemical analyses, as described below.

1.3.1 Fieldwork

The fieldwork component of this project lays the foundation for the remainder of the study by: a) describing the geology of the field areas including regional- to outcrop-scale lithological, structural and facies variations; and b) facilitating the collection of, and providing a geological context for, geochemical, petrographic, and geochronological samples. Fieldwork for this project was conducted during two three-month-long field-

seasons in the summers of 2004 and 2005, in cooperation with the British Columbia Geological Survey and collaborator JoAnne Nelson. The field areas were accessed mainly by helicopter, and mapping was conducted from 2-person bush-camps, at a maximum of 1:50 000 scale. This thesis incorporates the results of mapping conducted by a number of professional geologists and students who collaborated in the study.

Geochemical and geochronological sample collection was a vital aspect of the fieldwork. All samples were collected from surface exposures during mapping. Geochemical samples weighed a minimum of 1 kg. They were collected from the least altered examples of each volcanic rock type, from a range of stratigraphic levels in a number of separately defined volcanic complexes. Geochronology samples weighed a minimum of 10 kg and were collected from felsic volcanic flows or from conglomerates (for detrital studies). Sample locations were recorded using Universal Transverse Mercator (UTM) coordinates and the North America datum 1983 (NAD83), zone 9 projection. All sample locations were verified by ensuring agreement between UTM coordinates and observed topographic landmarks and features on 1:20,000 scale NTS maps.

1.3.2 Whole-Rock Geochemistry

Whole-rock geochemistry comprises an important data-set for this thesis; it is used to classify volcanic rock types, estimate physical and chemical magmatic conditions, and determine temporal and spatial variations in volcanic rock compositions. Thirty-seven samples from the upper Hazelton Group Iskut River Formation (IRF) were analyzed for major and trace element concentrations at the GSC's Analytical Chemistry Research and Development Laboratory in Ottawa. Preparation of rock samples for geochemical analysis was done at Dalhousie and Saint Mary's Universities where weathered surfaces were removed and samples were crushed in a hardened-steel shatter box. At the GSC four techniques were used for analysis: 1) fused bead X-ray fluorescence (XRF) to measure the major oxides; 2) infrared spectroscopy for measurement of H_2O and CO_2; 3) titration for FeO vs. Fe_2O_3, and 4) inductively coupled plasma mass spectrometry (ICP-MS) to measure the rare earth elements and selected trace elements e.g. Ni, Zr, Nb and Y. For ICP-MS analysis a Na_2O_2 sintering technique was used and rock powders were totally

dissolved using nitric, perchloric, and hydrofluoric acids. Precision of these techniques was maintained at better than 5% for 2σ error (at 10× detection limit) with accuracy determined by measurements made relative to in-house and international reference materials.

Twenty-six samples from the lower Hazelton Group Telkwa Formation were also analyzed for major and trace element concentrations. These analyses followed the same procedures as the IRF samples, but the XRF analyses were conducted at the Atlantic Geochemical Centre (Saint Mary's University), and ICP-MS analyses were conducted at the Earth Resources Research and Analysis Facility (Memorial University).

1.3.3 Isotope Geochemistry

Isotope geochemistry studies are essential to deciphering the relative contributions of specific mantle and crustal components in the generation of Hazelton Group volcanic rocks. Of the 63 geochemical samples collected from the study areas, 10 whole-rock samples were analyzed for Sm-Nd isotope composition and two for Rb-Sr isotope composition. Five samples from the IRF were analyzed at the GSC's Geochronology Laboratory in Ottawa and 5 samples from the Telkwa Formation were analyzed at the Atlantic Universities Regional Isotopic Facility (AURIF) at Memorial University. In both cases the isotopic compositions were measured by thermal ionization mass spectrometry (TIMS). Sm-Nd isotope ratios commonly remain unchanged during melting and recrystallization processes, and as a result they act as fingerprints of specific potential magma source reservoirs. By comparing the isotopic compositions of different Hazelton Group rock types, the relative influence of particular magma sources can be determined. The isotopic data have brought a greater level of resolution to questions concerning the tectono-magmatic system that generated Hazelton Group volcanic rock, such as variation in magma sources and the influence of crustal contamination in these magmas.

1.3.4 Geochronology

U/Pb zircon geochronology presented in this thesis places constraints on the timing, rate of deposition, and magma/sediment sources of the Telkwa Formation, and places geochemical samples into a temporally-constrained geological framework. Samples were collected for two types of U/Pb zircon dating: 1) four samples were collected from felsic volcanic flows in order to obtain igneous crystallization ages, and 2) two samples were collected from sedimentary rock to determine detrital zircon populations. Geochronological analyses were conducted by collaborator Richard Friedman at the Pacific Centre for Isotopic and Geochemical Research (University of British Columbia). Zircon crystals from the felsic volcanic flows were separated and isotopic concentrations were measured in multiple zircons by chemical-abrasion TIMS (CA-TIMS) analysis. Zircon crystals collected for the detrital studies were analysed by laser-ablation ICP-MS (LA-ICP-MS) analysis. Appendix C contains details of the analytical procedures.

1.3.5 Petrography and Mineral Chemistry

Petrography and in situ mineral chemistry investigations define textural and mineralogical features that help to elucidate the physical and chemical evolution of the magmas from which the rocks in this study formed. Analyses were conducted at Dalhousie University using a polarizing microscope and a JEOL 8200 electron microprobe. These studies were conducted using polished and normal thin sections prepared at Dalhousie University from representative samples that also underwent whole-rock geochemical analysis. Rock textures were used to establish primary vs. secondary phases, crystallization histories, and the processes that controlled crystallization. Mineral chemistry was used to help determine the chemical evolution of the magmas.

1.4 Thesis Organization

This thesis contains four sources of work: 1) published or in-revision peer-review articles; 2) published British Columbia government papers; 3) published British Columbia government open-file maps; and 4) unpublished work unique to this thesis. Copyright permissions for all previously published work are in Appendix D. Following the

introduction (Chapter 1), chapters 2, 3, 4, and 5 comprise individual or combined articles and government papers; Chapter 6 is a discussion that takes a broad view of the body of work. Appendices include open-file geological maps (Appendix E) and government papers (Appendix A) that are not included in the main chapters but are important supplements to chapters 3, 4, and 5. Chapter 2 describes, and in-part redefines, Hazelton Group stratigraphy; it provides the necessary background for the more focused work presented in the chapters that follow. Chapter 3 describes a focused study of the lower Hazelton Group near Terrace (Fig.1-2), and chapters 4 and 5 describe studies in the upper Hazelton Group within the Eskay rift (Fig. 1-2).

Chapter 2 - Stratigraphy of the upper Hazelton Group and the Jurassic evolution of the Stikine terrane, British Columbia

2.0 Preface

This chapter provides a current and broad stratigraphic context for the Hazelton Group relevant to the more focused studies found in chapters 3 and 4. The chapter is derived entirely from:

> Gagnon, J.-F., Barresi, T., Waldron, W.F., Nelson, J.L., Poulton, T.P., and Cordey, F. 2012. Stratigraphy of the upper Hazelton Group and the Jurassic evolution of the Stikine terrane, British Columbia. Canadian Journal of Earth Science **49**: 1027-1052.

The first author of this paper was a Ph.D. student at University of Alberta; the other authors included his supervisor J. Waldron, F. Cordey who conducted the research specific to radiolarians, and our collaborators in the BC Geological Survey and Geological Survey of Canada. I contributed substantially to the writing, figures, and ideas presented in the paper, in particular the sections regarding the newly defined Iskut River Formation, and the role of that formation in the Jurassic evolution of the Hazelton Group. I also contributed substantially to the development of the new stratigraphic framework and organized the concept that the Hazelton Group contains two distinct rifts. Detailed descriptions of sedimentary sections and fossil collections in the upper Hazelton Group that are not relevant to this thesis and that were contributed by the other authors have been omitted for purposes of this thesis.

Appendix D contains copyright agreement forms for all published manuscripts used in this thesis.

2.1 Abstract:

The Lower to Middle Jurassic Hazelton Group represents the final stage of magmatic arc activity in the intraoceanic Stikine terrane, which was followed by accretion within the Cordilleran terrane collage. The Hazelton Group is exposed in the following areas: (i) on the periphery of the Bowser basin, where arc and back-arc strata are overlain by mainly sedimentary strata of the upper Hazelton Group and then by the clastic basin fill of the Bowser Lake Group; and (ii) within a 300 km long rift system, the Eskay rift, west of the Bowser basin, where a predominantly bimodal volcanic succession contains significant mineral deposits. Examination of representative stratigraphic sections throughout the regional extent of the upper Hazelton Group has suggested significant revisions and clarification of its stratigraphy and include the following: (i) informal division of the Hazelton Group into upper and lower parts and recognition of a diachronous unconformity or unconformities at the boundary between them; (ii) establishment of a type section for the sandstone-dominated Smithers Formation; (iii) establishment of separate Quock and revised Spatsizi formations in the north and extension of the Quock Formation to include all lithostratigraphically equivalent units of blocky, thinly bedded siliceous mudstone and tuff around the periphery of the Bowser basin; and (iv) introduction of the Iskut River Formation for rift-related and volcanic facies in the Eskay rift area. Two independent rifting events occurred during deposition of the Hazelton Group: a Late Sinemurian to Early Pliensbachian phase in the northwest-trending Hazelton trough and a more restricted Aalenian to Bajocian extensional event in the Eskay rift.

2.2 Introduction

The Jurassic Period marked a key transition in the tectonics of the Canadian Cordillera. During this time, the western margin of North America was changing rapidly from a complex of island arcs, marginal basins, and offshore crustal fragments, analogous to tectonic elements in the modern southwest Pacific, to an accretionary orogen. The Stikine terrane, or Stikinia, is the largest arc terrane within the Canadian Cordillera (Fig. 2-1). Within Stikinia, the Lower to Middle Jurassic Hazelton Group is a widespread assemblage of volcanic and associated sedimentary strata that records the last volcanic

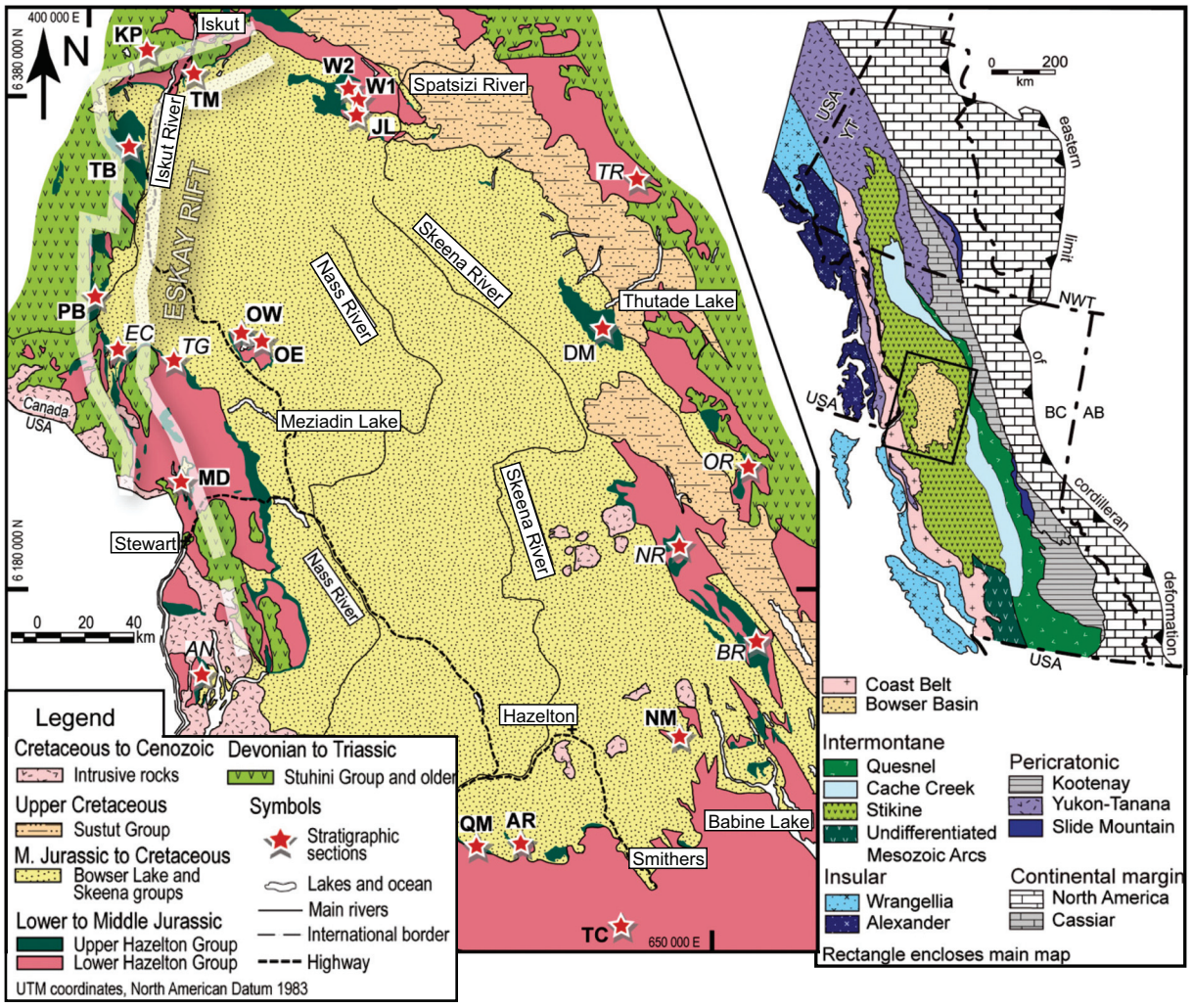

Fig. 2-1. Simplified geologic map showing the distribution of Hazelton Group rocks on the periphery of the Bowser Basin and the locations of stratigraphic sections. Inset shows locations in the Cordillera. BC: British Columbia; AB: Alberta; YT: Yukon; NWT: Northwest Territories. Section names (**bold**: sections described in this study; *italic*: sections compiled from cited literature): *AN*: Anyox; **AR**: Ashman Ridge; *BR*: Bait Range; *DM*: Diagonal Mountain; *EC*: Eskay Creek; **JL**: Joan Lake; **KP**: Klastine Plateau; **MD**: Mount Dillworth; **NM**: Netalzul Mountain; *NR*: Nilkitkwa Range; **OE**: Oweegee East; *OR*: Omineca Range; **OW**: Oweegee West; **PB**: Pillow Basalt Ridge; **QM**: Quinlan Mountain; **TB**: Table Mountain; **TC**: Tenas Creek; *TG*: Treaty Glacier; **TM**: Todagain Mountain; *TR*: Toodoggon River; **W1**: Mount Will 1; W2: Mount Will 2. Modified from Evenchick et al. (2009) and Alldrick et al (2006). Approximate outline of Eskay rift after Alldrick et al. (2004b). Coordinates are Universal Transverse Mercator (UTM) grid zone 9, North American datum 1983 (NAD83).

phase of the long-lived Stikine volcanic arc and also its demise. The Hazelton Group represents a time of critical change in the history of the Stikine terrane, as it evolved from an independent arc towards incorporation into the Cordilleran tectonic collage. Its lower part comprises voluminous, predominantly andesitic to dacitic arc-related volcanic accumulations with an intervening sedimentary basin, the Nilkitkwa trough (Marsden and Thorkelson 1992). Its upper part, the main focus of this paper, comprises generally thinner sedimentary strata and localized bimodal volcanic units, which record processes of arc extinction, rifting, and subsidence. The detailed regional analysis of the stratigraphic record of the upper part of the Hazelton Group, presented here, sheds light on a profound mid-Jurassic reconfiguration in the Cordilleran orogen.

The upper Hazelton Group is also of great economic interest in that it contains mid-Jurassic polymetallic massive sulfide deposits (Alldrick 1993; Barrett and Sherlock 1996; Macdonald et al. 1996a,b; Roth et al. 1999; Sherlock et al. 1999; Barresi and Dostal 2005) and potential petroleum source units (Evenchick et al. 2003, 2005; Ferri et al. 2004; Ferri and Boddy 2005; Osadetz et al. 2007).

2.3 Tectonic setting of the Hazelton Group

The Hazelton Group unconformably overlies arc-related strata of the Middle to Upper Triassic Stuhini and Takla groups (e.g., Tipper and Richards 1976; Monger and Church1977; Grove 1986; MacIntyre et al. 1989; Alldrick et al. 1989) and the Lower Devonian to Upper Permian Stikine assemblage (e.g., Monger 1977; Stevens and Rycerski 1989; Brown et al. 1991; McClelland 1992). All three successions contain volcanic arc rocks characterized by juvenile Sr and Nd isotopic signatures (Gabrielse et al. 1980; Armstrong 1988; Samson et al. 1989, 1991); together they represent a multistage arc terrane that developed in an intraoceanic setting isolated from the North American margin.

The Lower to Middle Jurassic Hazelton Group is an extensive assemblage of volcanic and sedimentary strata. The unusual width of the Hazelton volcanic field (450 km pre-deformation), combined with the lack of chemical variability in major and trace element profiles, led Marsden and Thorkelson (1992) to propose that volcanism was generated by

concurrent subduction of two opposing oceanic plates beneath the Stikine terrane. One involved east-facing subduction of the Cache Creek oceanic basin on the east side of the Stikine terrane; the other, west-facing subduction of oceanic lithosphere on the west side (directions in present-day coordinates). In this model, the Hazelton Group evolved on a Philippine-style microplate as a pair of coeval volcanic arcs separated by a northwest-trending interarc basin, the Hazelton trough.

The Hazelton Group is overlain by coarse clastic strata of the Middle to Upper Jurassic Bowser Lake Group, which were deposited in a large, deep, subsiding sedimentary basin that developed as Stikinia, and the terranes inboard, underwent a series of collisions that led to their accretion to the North American margin (e.g., Eisbacher 1985; Ricketts et al. 1992; Evenchick et al. 2007a, 2010; Gagnon et al. 2009). The Cache Creek ocean closed in the Middle Jurassic, and west-vergent shortening structures developed in rocks of the North American margin (Omineca belt), coeval with the southwest-vergent thrust faults that emplaced Cache Creek oceanic assemblages on top of the accreting Stikine arc terrane, or Stikinia (Fig. 2-1; Evenchick et al. 2007a). The western side of Stikinia was also affected by collision with outboard terranes (van der Heyden 1992), including the Alexander terrane (Gehrels 2001).

2.4 Hazelton Group stratigraphy: previous work

The upper parts of the Hazelton Group include a wide variety of sedimentary and volcanic rock types, discontinuously exposed around the periphery of the Bowser Basin (Fig. 2-1). These rocks have been described in detail by authors working in different areas, leading to significant advances in understanding but leaving overlaps and inconsistencies in stratigraphic nomenclature in the absence of a larger regional framework. This paper attempts to correlate and simplify mappable lithostratigraphic units at a regional scale by comparing multiple sections measured in the field and available in the literature. Existing nomenclature is reviewed first, to demonstrate the need for simplification and to highlight inconsistencies (Fig. 2-2). New paleontological data and measured sections are then presented. Where appropriate, ambiguous units are revised or recommended for abandonment and new formal stratigraphic names are

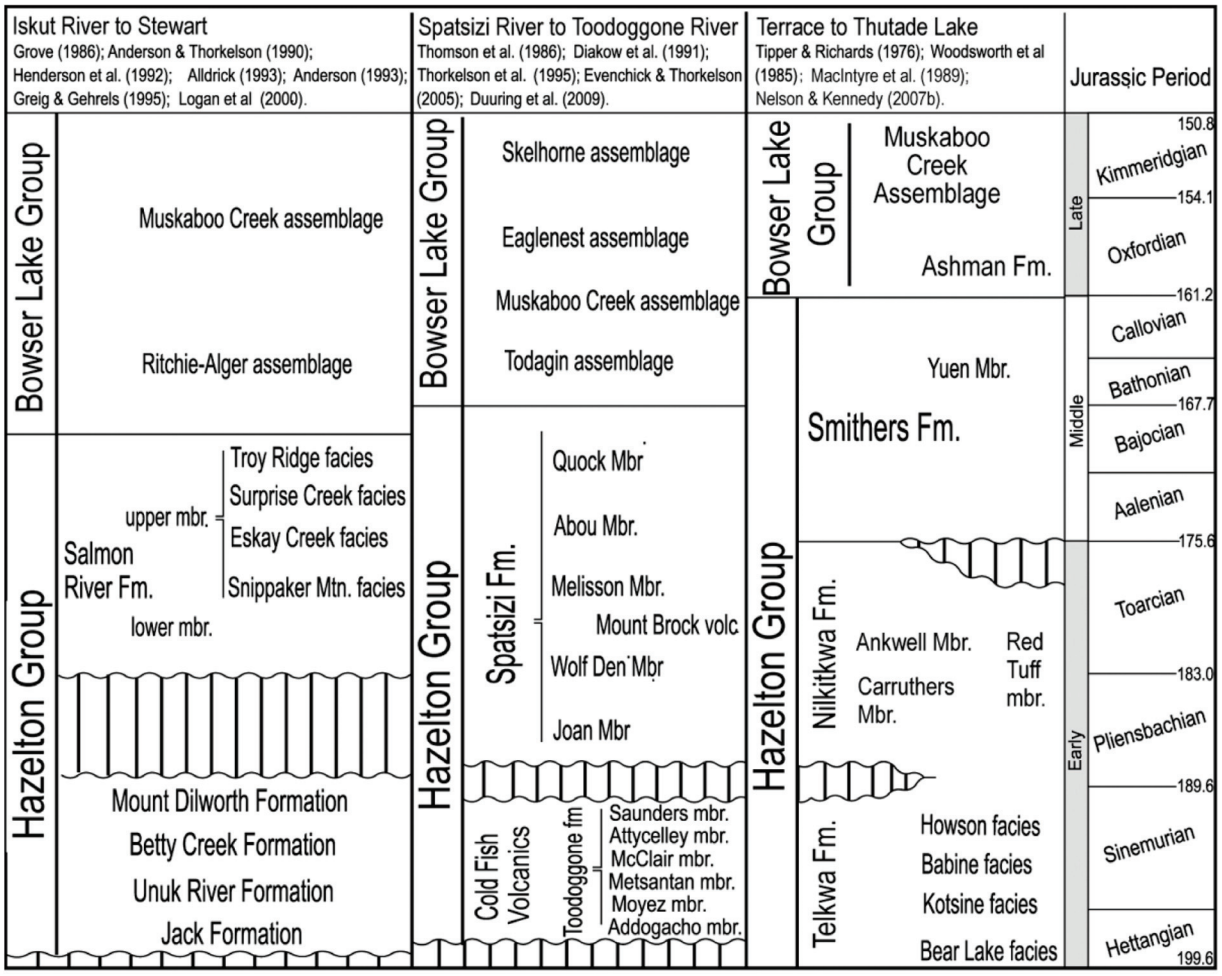

Fig. 2-2. Summary of previous stratigraphic nomenclature for the Hazelton Group in north-central British Columbia. Time scale modified from Ogg (2004). The new stratigraphic scheme proposed in this paper is shown in Fig. 2-7.

proposed, to highlight the main depositional themes and to facilitate understanding of this economically and tectonically important unit.

The term Hazelton Group was first introduced by Leach (1910) to describe a Jurassic assemblage of volcanic and sedimentary rocks exposed in north-central British Columbia. It replaced in part the broader term "Porphyrite Group" previously proposed by Dawson (1877). The Hazelton Group was subject to minor modifications later (e.g., Hanson 1925; Armstrong 1944; Duffell and Souther 1964) but remained imprecise owing to the lack of age control in the included units. Tipper and Richards (1976) completely revised the Jurassic stratigraphic nomenclature of north-central British Columbia and they established the first regional subdivision and interpretation of the Hazelton Group in the area between Terrace and McConnell Creek (Figs. 2-1, 2-2). They identified a thick, volcanic-dominated Early Jurassic lower unit, the mainly Sinemurian Telkwa Formation to the west and east. Between these exposures, Pliensbachian to Toarcian marine sediments and basalts of the Nilkitkwa Formation were deposited in the "Nilkitkwa trough". The uppermost unit, the Middle Jurassic Smithers Formation, is mainly clastic, with cherts and very fine tuffs in the Yuen Member (Fig. 2-2). The nomenclature of Tipper and Richards (1976) was subsequently extended to other areas around the margin of the Bowser Basin (Woodsworth et al. 1985; Diakow and Mihalynuk 1987; MacIntyre et al. 1989, 1997).

Northwest of McConnell Creek, in the Spatsizi River and Toodoggone River areas (Fig. 2-1), lower volcanic units of the Hazelton Group were assigned different formation names (Marsden and Thorkelson 1992; Thorkelson 1992; Thorkelson et al. 1995; Diakow et al. 1991) (Fig. 2-2). Above this volcanic succession, a distinct Pliensbachian to Bajocian mainly sedimentary succession, 700 m thick, was named the Spatsizi Group by Thomson et al. (1986). However, other authors (Marsden and Thorkelson 1992; Evenchick and Thorkelson 2005) pointed out that this contradicted Tipper and Richards' (1976) widely accepted definition of the Hazelton Group and made regional correlations more difficult, as other clastic-dominated successions at similar stratigraphic levels were included within the Hazelton Group. These arguments led Evenchick and Thorkelson (2005) to demote

the Spatsizi Group to the Spatsizi Formation and, consequently, its five formations to members.

In the Iskut River area (Fig. 2-1), the Hazelton Group has been divided into five formations, shown in Fig. 2-2 (e.g., Grove 1986; Alldrick et al. 1989; Anderson and Thorkelson 1990; Henderson et al. 1992; Anderson 1993; Greig and Gehrels 1995). A recently enlarged geochronological and biostratigraphic database in this area has provided improved age constraints on these units (e.g., Lewis et al. 1993; Macdonald et al. 1996a; Logan et al. 2000). A Pliensbachian to Toarcian hiatus apparently separates the four lower, predominantly volcanic units from the overlying Salmon River Formation (Anderson 1993; Greig and Gehrels 1995). The latter includes, in its upper member, a unit of thinly interbedded and laminated dark cherty mudstone and light-coloured ash tuff termed the Troy Ridge facies. These rocks became known informally but widely as "pyjama beds", a term coined by Howard Tipper in the late 1980s to describe their pinstriped appearance, and subsequently applied to similar facies throughout the upper Hazelton Group. We propose in the following text that this distinctive, mappable facies be recognized throughout the region as the Quock Formation, a name defined by Thomson et al. (1986).

In the Iskut River area, a zone of thicker mid-Jurassic volcanic and coarse to fine clastic rocks occupies a narrow, elongate N–S belt, characterized as the Eskay rift (e.g., Evenchick and McNicoll 2002, Alldrick et al. 2005a). These rocks are laterally equivalent to the upper parts of the Hazelton Group elsewhere, but they display distinct facies and occupy a unique tectonic setting; we propose the new Iskut River Formation to include these rocks.

In all these areas, the Hazelton Group is conformably overlain by an assemblage of mudstone, siltstone, sandstone, and chert-pebble conglomerate of the Bowser Lake Group (Fig. 2-2). In the Smithers area, Tipper and Richards (1976) originally assigned Upper Bajocian to Middle Oxfordian clastic rocks, including "pyjama beds", to the Ashman Formation, and therefore to the Bowser Lake Group, largely based on their age. However, Evenchick et al. (2007b, 2008a, 2008b, 2010) and Gagnon and Waldron (2008)

showed that the Ashman Formation comprises facies elsewhere divided between the Hazelton Group and the Bowser Lake Group. Consequently, the term Ashman Formation has been abandoned; beds previously assigned to the latter were reassigned to either the upper Hazelton Group or the Bowser Lake Group based on the presence or absence of tuffs, respectively (Evenchick et al. 2007b, 2008a, 2008b, 2010).

2.5 Stratigraphic sections[2]

New lithostratigraphic sections were measured at locations around the margin of the Bowser Basin and within the Eskay rift (Fig. 2-1). These sections, and others compiled from previous publications, are identified by two-letter codes in two profiles, running roughly S–N and W–E across the basin, shown, respectively, in Figs. 2-3 and 2-4.

2.5 Iskut River area

The Hazelton Group shows much greater lateral variation in the Iskut River area, beneath the NW extremity of the Bowser Basin, than in the areas to the east and south. Thick volcanic sections of Middle Jurassic age host significant mineral deposits, contemporaneous with condensed successions deposited elsewhere. The thick volcanic strata occupy a N–S belt, the Eskay rift (e.g., Alldrick et al. 2005a,b). The sections described here illustrate the contrast between the volcanic-dominated rift-fill assigned to the new Iskut River Formation and flanking successions assigned to the revised Spatsizi and Quock formations.

2.5.1 Table Mountain (TB)

Table Mountain (informal name) is a highland ~40 km SW of Iskut (Fig. 2-1). Section TB is compiled from our observations supplemented by reports and maps of Alldrick et al. (2004a,b, 2006) and Simpson et al. (2004). The lowest unit exposed along the western slope consists mainly of maroon and green plagioclase-phyric andesite flows and dacite

[2] The original paper, Gagnon et al (2012) has been edited here to include only sections that were worked on by the thesis author. The reader is directed to the original article to see these sections, which although not directly relevant to the subject of this thesis, are relevant on a broader scale, and to the overall theme of the paper.

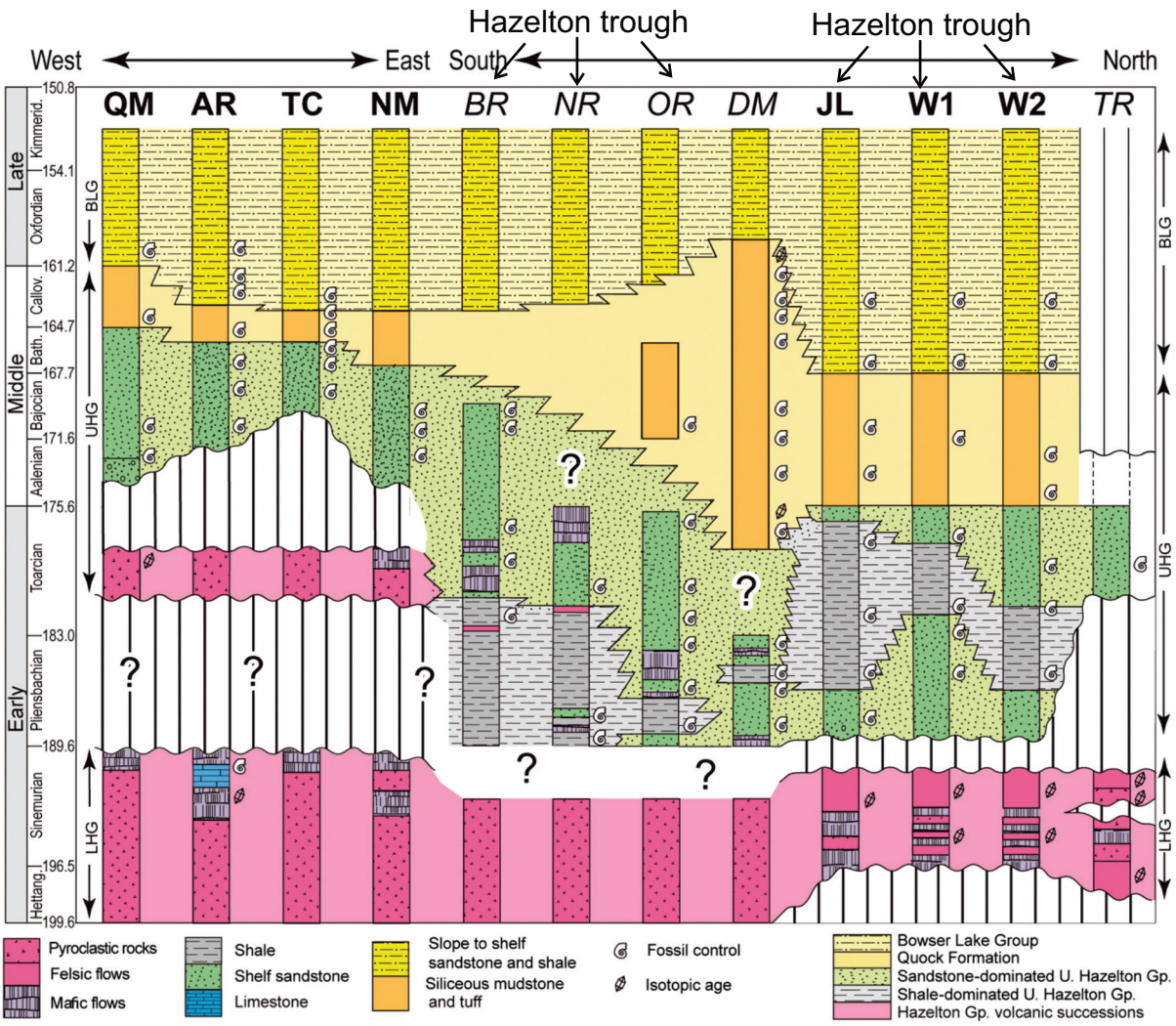

Fig. 2-3. Regional lithostratigraphic subdivisions of the Hazelton Group. Line of cross-section is oriented W-E across the southern Hazelton trough, then SE-NW along the eastern part of the trough. Section locations shown in Fig. 2-1 (**Bold**: sections described in this study; *italic*: section information compiled from Tipper and Richards 1976; Daikow et al. 1991; Jakobs 1993; Evenchick et al. 2007*b*; Duuring et al. 2009). Vertical axis shows time scale modified from Ogg (2004). BLG: Bowser Lake Group. UHG: upper Hazelton Group. LHG: lower Hazelton Group. Refer to Fig. 2-1 for abbreviations of section names. Full names of abbreviated Jurassic stages are shown in Fig. 2-2.

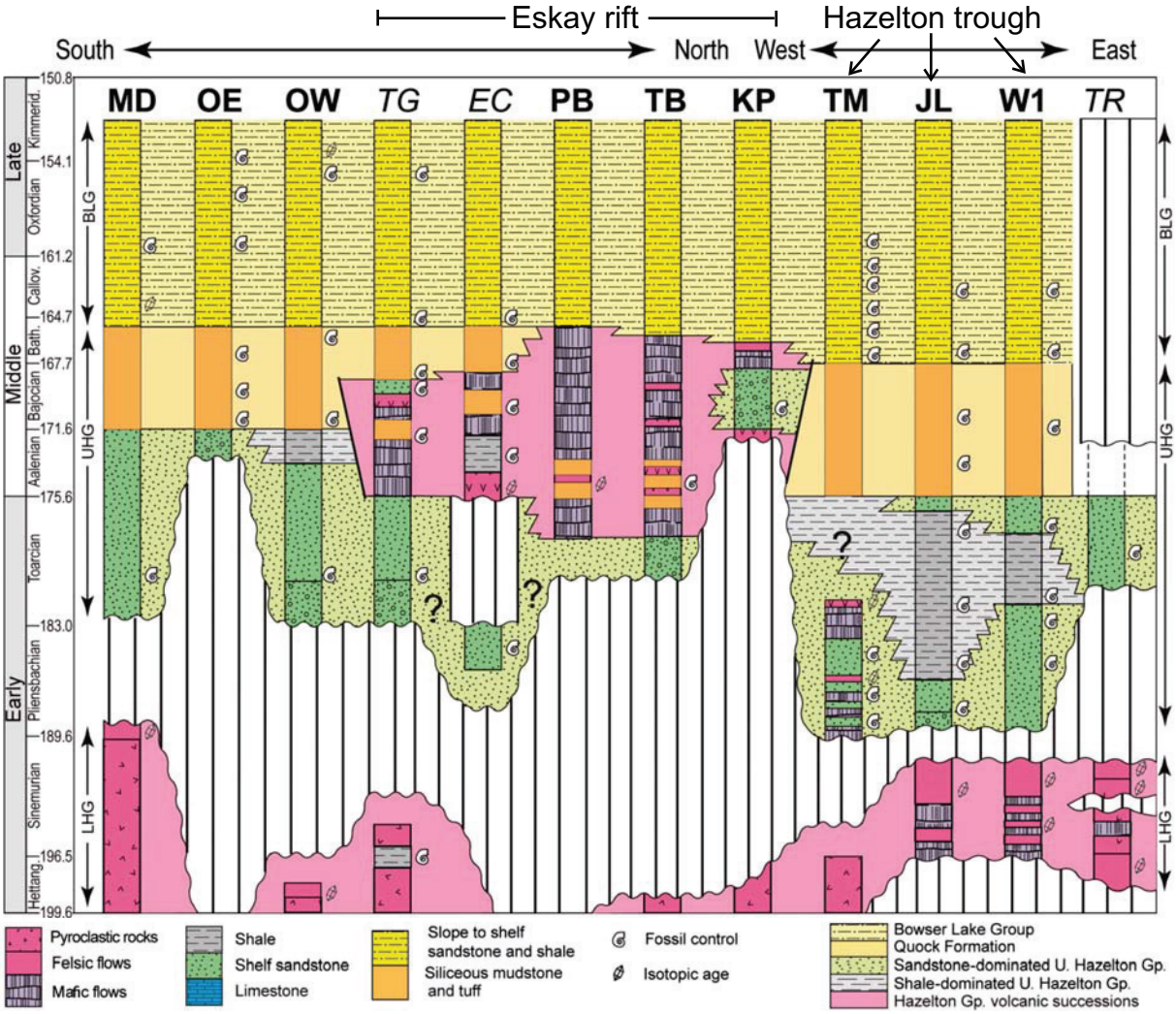

Fig. 2-4. Lithostratigraphic subdivisions of the Hazelton Group in the vicinity of the Iskut River area, S-N across the Eskay Rift, then W-E across northern Hazelton trough. In the Iskut River area, deposition of siliceous siltstone beds of the Quock Formation was contemporaneous with accumulation in the Eskay rift of thick bimodal volcanic rocks of the Iskut River Formation. Section locations shown in Fig. 2-1 (**bold**: sections described in this study; *italic*: section information compiled from Lewis et al. 1993; Roth 2002; Diakow et al. 1991; Duuring et al. 2009). For abbreviations of section names, refer to Fig 2-1. Vertical axis shows time scale modified from Ogg (2004). BLG: Bowser Lake Group. UHG: upper Hazelton Group. LHG: lower Hazelton Group. Full names of abbreviated Jurassic stages are shown in Fig. 2-2.

breccias (Fig. 2-5A), with sparse black mudstone and greyish-blue ash tuff. Minor diorite intrusions with pegmatitic pods cut the section. This unit is at least 720 m thick, but only the uppermost 100 m are shown in Fig. 2-5B. Despite the absence of age control, rock types identified in this unit suggest correlation with the lower Hazelton Group, but lower parts of the section could include Stuhini Group.

These intermediate volcanic rocks are unconformably overlain by volcanic and sedimentary rocks mapped as part of the informal "Willow Ridge Complex" by Alldrick et al. (2006); in this paper, these rocks are assigned to the new Iskut River Formation. The unconformity at the base of the Iskut River Formation dips steeply east and is onlapped by varied lithologies along strike, including polymictic conglomerate, basalt, and rhyolite (Fig. 2-5A). Its best exposed locality (Fig. 2-5A) is at UTM (Universal Transverse Mercator) zone 9 coordinates 415200 E, 6352500 N, NAD83 (North American datum 1983), where the unconformity is overlain by a heavily altered rhyolite unit ~70 m thick. Hematite and limonite give the regolithic groundmass a distinctive red to orange colour. In the few unaltered outcrops, the rhyolite consists of 1–7 mm pale white spherulites in a semi-translucent pale blue-green siliceous groundmass.

The rhyolite is overlain by 1770 m of dark to olive-green basalt (lower basalt unit of Alldrick et al. 2004b), typically aphanitic or feldspar-phyric, which forms eruptive units of pillowed flows and pillow breccias typically 5–20 m thick (Fig. 2-6A). Simpson et al. (2004) listed three basalt facies in this unit: aphyric, massive, and coherent pillow basalt; monomictic, blocky basalt breccia, and fluidal-clast breccia. Common devitrification variolites, 3–5 mm in diameter, appear on weathered surfaces as overlapping pale yellow spots (Fig. 2-6B). The uppermost 5 m are highly altered and contain up to 40% sulfides by volume; the hyaloclastite groundmass of the basalt breccia is partly to completely replaced by very fine-grained pyrite (Fig. 2-6C). This mineralization is bounded by the contact with the overlying mudstone at the base of the middle sedimentary unit of Alldrick et al. (2004b), where fluids responsible for the replacement mineralization were apparently capped (1940 m on Fig. 2-6B). Laminated beds of pyrite (up to 5 cm thick) immediately above the contact suggest that exhalative vents were still active during sedimentation. The 10 m unit of thinly bedded black mudstone and grey siltstone is

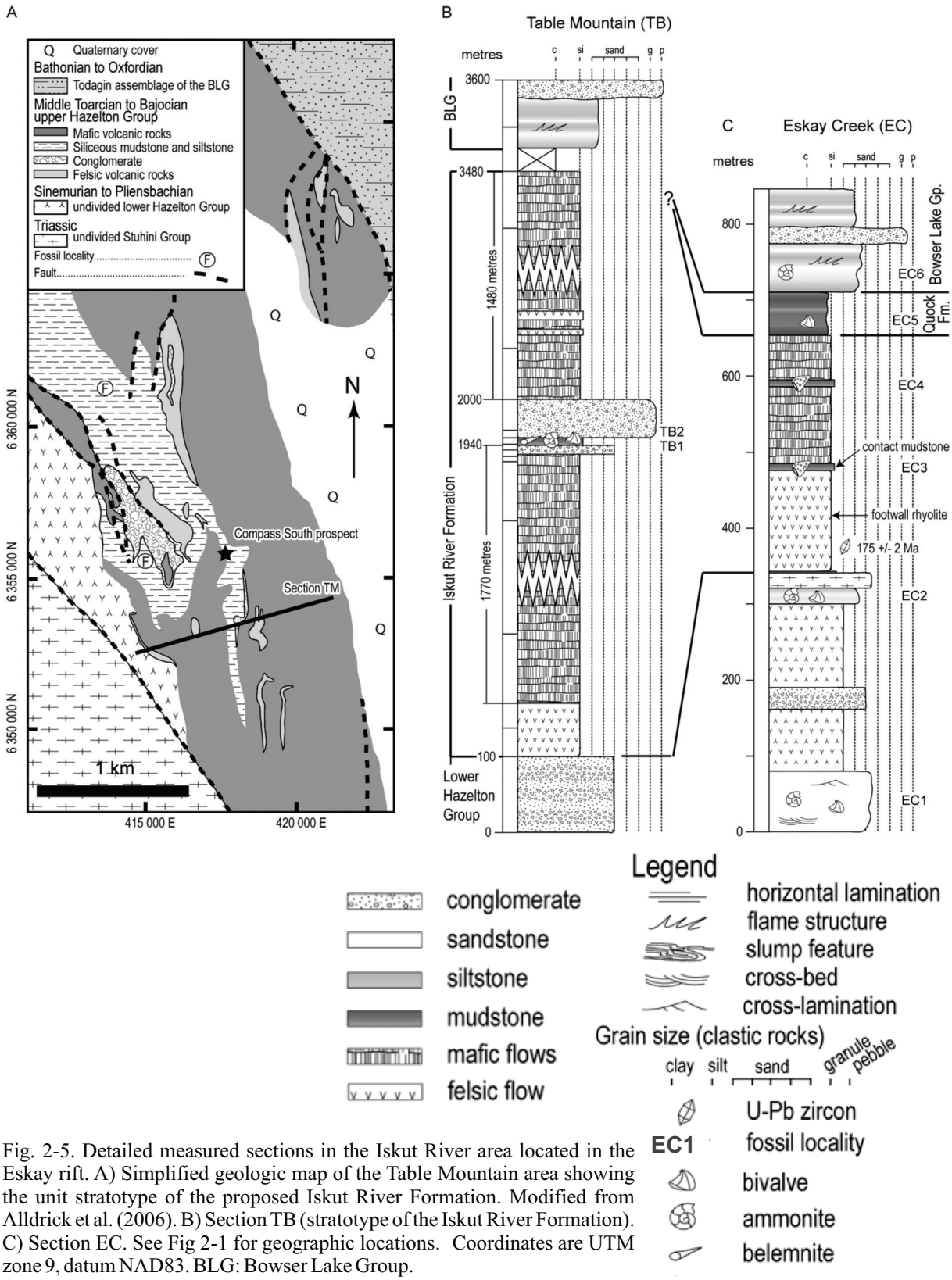

Fig. 2-5. Detailed measured sections in the Iskut River area located in the Eskay rift. A) Simplified geologic map of the Table Mountain area showing the unit stratotype of the proposed Iskut River Formation. Modified from Alldrick et al. (2006). B) Section TB (stratotype of the Iskut River Formation). C) Section EC. See Fig 2-1 for geographic locations. Coordinates are UTM zone 9, datum NAD83. BLG: Bowser Lake Group.

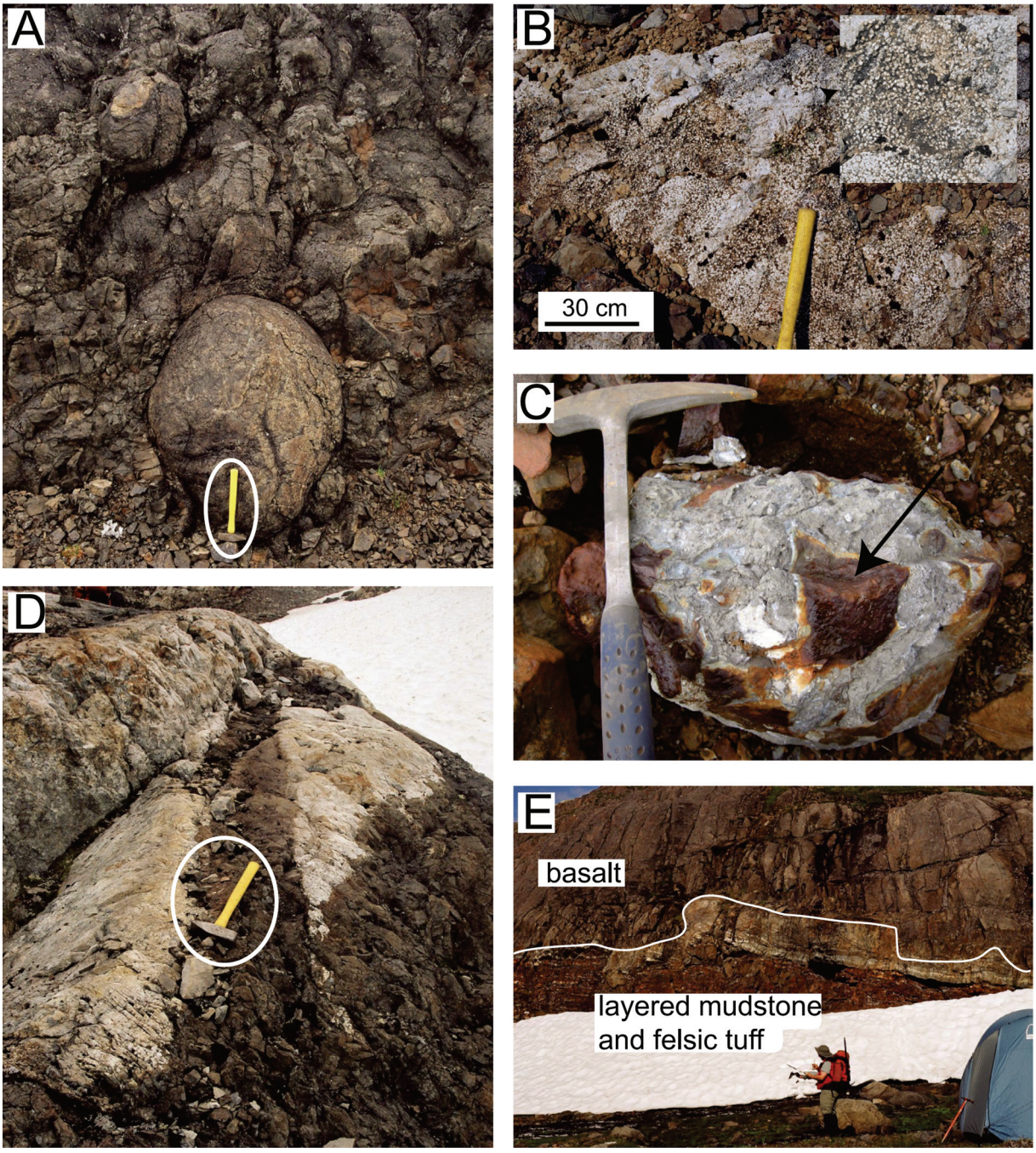

Fig. 2-6. Photographs of the Iskut River Formation showing distinctive lithological characteristics from units exposed at Pillow Basalt Ridge and Table Mountain (PB and TB on Fig. 2-1, respectively). A) Pillow basalts exposed on Pillow Basalt Ridge. Large (>1m diameter) pillows such as the one exposed near the base of the photograph are interpreted to indicate close proximity to eruptive centres. B) Basalt exposed at Table Mountain displaying variolitic texture. White-weathering variolites are characteristic devitrification features found on the glassy rims of basalt. C) Mineralized basalt breccia; dark rusty angular basalt fragments (arrow) are supported in a fine-grained sulphide matrix consisting mainly of pyrite. Photograph is from the Compass South prospect on Table Mountain. D) Bimodal volcanic rocks on Pillow Basalt Ridge. Light-coloured rhyolite flows were intruded by a sub-volcanic mafic dike swarm that fed eruptions responsible for the overlying pillow basalts. E) Rusty-weathering mudstone interbedded with felsic tuff, overlain by a basalt flow, on Pillow Basalt Ridge. The bedded rocks grade from mainly pyritic siliceous mudstones at the bottom to predominantly felsic tuff layers at the top. Incorporation of mudstone/tuff "rafts" into the overlying basalt during eruption resulted in an irregular contact.

overlain by 50 m of poorly sorted, matrix- to clast-supported, polymictic conglomerate with a matrix of coarse to very coarse sandstone. The sub-angular to sub-rounded clasts are basalt, mudstone, rhyolite, massive fine-grained pyrite, and limestone. This unit onlaps the basal unconformity directly in some places. Where it does, polymictic conglomerates grade into coarser fan-conglomerate with clasts that are identical to the underlying plagioclase-phyric andesites and dacites of the lower Hazelton Group. These relationships suggest that the Iskut River Formation was deposited unconformably against a surface with significant topographic relief, here interpreted to represent the floor and a bounding fault of the rift system.

Ammonoids and radiolarians from fine-grained sedimentary rocks that appear to be laterally equivalent to the middle sedimentary unit of Alldrick et al. (2004b) range from Late Toarcian to Middle Bajocian in age (Souther 1972; Evenchick et al. 2001). The sedimentary rocks are overlain by at least another 1480 m of basalt (upper basalt unit of Alldrick et al. 2004b) lithologically similar to the lower basalt unit, exposed on the east side of Table Mountain and on Willow Ridge (Fig. 2-5A). Its upper contact is not exposed and has been interpreted as a fault, based on discordance with turbiditic Bowser Lake Group strata to the east (Alldrick et al. 2004a,b). Regionally, however, this contact is conformable, as seen at section EC.

2.5.2 Eskay Creek (EC)

The geology of the Eskay Creek area (Fig. 2-1) is well known from detailed bedrock mapping, diamond drilling, and mining (e.g., Ettlinger 1992; Bartsch 1993; Nadaraju 1993; Roth 1993, 2002; Sherlock et al. 1994; Macdonald et al. 1996a). Section EC is compiled from these sources.

The Hazelton Group is exposed along the west limb and hinge of a NE-plunging anticline (Eskay anticline). These sedimentary and volcanic rocks, included previously in the Salmon River Formation (Anderson and Thorkelson 1990; Anderson 1993), are assigned here to the new Iskut River Formation. In contrast to the section TM (Fig. 2-5B), the lower contact is concordant but disconformable (340 m in Fig. 2-5C). Upper

Pliensbachian units comprising andesitic breccia, volcaniclastic, and dacitic volcanic rocks (lower Hazelton Group) are overlain by a thick felsic unit, the "footwall rhyolite", which varies in texture from massive to autobrecciated, and was interpreted by Bartsch (1993) to represent a series of flow-dome complexes. This rhyolite was dated at 175 ± 2 Ma, and a rhyolite in a similar stratigraphic position on the east limb of the Eskay anticline at 174 +2/-1 Ma (U–Pb zircon; both by Childe 1996). Overlying and interfingering in part with the rhyolite is a very fine-grained dark grey sedimentary unit known as the "contact mudstone". The contact is irregular along strike and is marked by rhyolite breccia, in which black mudstone fills the interstices of quench-fragmented rhyolite. This peperitic texture is interpreted to indicate that deposition of mudstone was contemporaneous with eruption/emplacement of the rhyolite. Clasts in the mudstone include altered rhyolite, barite, and fragmental sulfides and sulfosalts (Roth 2002). The former Eskay Creek mine exploited a stratiform volcanogenic massive-sulfide deposit at the base of the mudstone interval, producing 2.18 million tonnes of ore with an average grade of 46 g/tonne Au and 2267 g/tonne Ag (BC Geological Survey 2008). The mudstone yielded Aalenian to possibly Early Bajocian radiolaria (Nadaraju 1993). Massive basalt sills and pillowed basalt flows and breccia, with thin (<1 m thick) intervals of bedded argillite, chert, and felsic tuff, overlie the contact mudstone. Conformable above the basalt is a thicker succession of tuffaceous mudstone, here included in the Quock Formation, which yielded a collection of Early Bajocian bivalves (Roth 2002). Conformably overlying the Quock Formation are mudstone-siltstone turbidites and thickly bedded sandstone and conglomerate of the Bowser Lake Group (Richie-Alger assemblage) with Upper Bathonian to Lower Callovian ammonoids (Evenchick et al. 2001; Roth 2002).

2.6 New stratigraphic framework

The Hazelton Group rocks located outside the Eskay rift can be broadly divided into a lower volcanic-dominated suite and an upper sedimentary-dominated suite (Tipper and Richards 1976; Evenchick et al. 2009). Several authors (Ferri et al. 2004; Evenchick and Thorkelson 2005; Waldron et al. 2006; Gagnon et al. 2007; Evenchick et al. 2010) informally used the term "upper Hazelton Group clastic rocks" when referring to

sedimentary units of the Spatsizi, Salmon River, Smithers, or Nilkitkwa formations. Based on mapping relationships in the Oweegee Range, Todagin Mountain, and Joan Lake areas, in this study and previous work (e.g., Tipper and Richards 1976, Thomson et al. 1986, Marsden and Thorkelson 1992, Gagnon et al. 2007), the base of the upper Hazelton Group is marked by a widespread unconformity. Underneath this erosional surface, undivided intermediate volcanic lavas and associated volcaniclastic rocks and lahars were assigned to the lower Hazelton Group (Waldron et al. 2006; Gagnon et al. 2007). A new stratigraphic framework (Fig. 2-7) is here proposed based on this informal division of the group into the lower and upper Hazelton Group. In contrast, within the Eskay rift, the upper Hazelton Group comprises predominantly bimodal volcanic rocks, separated by an unconformity from older predominantly intermediate volcanic rocks of the lower Hazelton Group, the Triassic Stuhini Group, and the Paleozoic Stikine assemblage.

2.6.1 Lower Hazelton Group

The lower Hazelton Group comprises a wide range of lithologies dominated by maroon and green calc-alkaline andesitic to dacitic flows, associated volcanic breccias and tuffs, and sedimentary volcaniclastic rocks. It includes the Telkwa, Jack, Unuk River, Betty Creek, Mount Dilworth, and Toodoggone formations and the Griffith Creek and Cold Fish volcanics of previous authors (Figs. 2-2, 2-7). They rest unconformably above the Triassic volcanic rocks of the Stuhini Group (and equivalents) and, in some localities, Paleozoic rocks of the Stikine assemblage. The upper boundary of the lower Hazelton Group is typically defined by an erosional surface that separates it from the overlying upper Hazelton Group. The cluster of U–Pb ages at 190–200 Ma (Hettangian–Sinemurian) obtained from volcanic rocks of the Stuhini, Telkwa, and Toodoggone formations, and from the Cold Fish Volcanics, confirm that the main stage of lower Hazelton Group volcanism was contemporaneous across the Stikine terrane (Greig and Gehrels 1995; Thorkelson et al. 1995; Gareau et al. 1997a; Duuring et al. 2009a). Most volcanic rocks of the lower Hazelton Group are calc-alkaline to tholeiitic and have strong arc signatures (Tipper and Richards 1976; Anderson and Thorkelson 1990; Diakow et al.

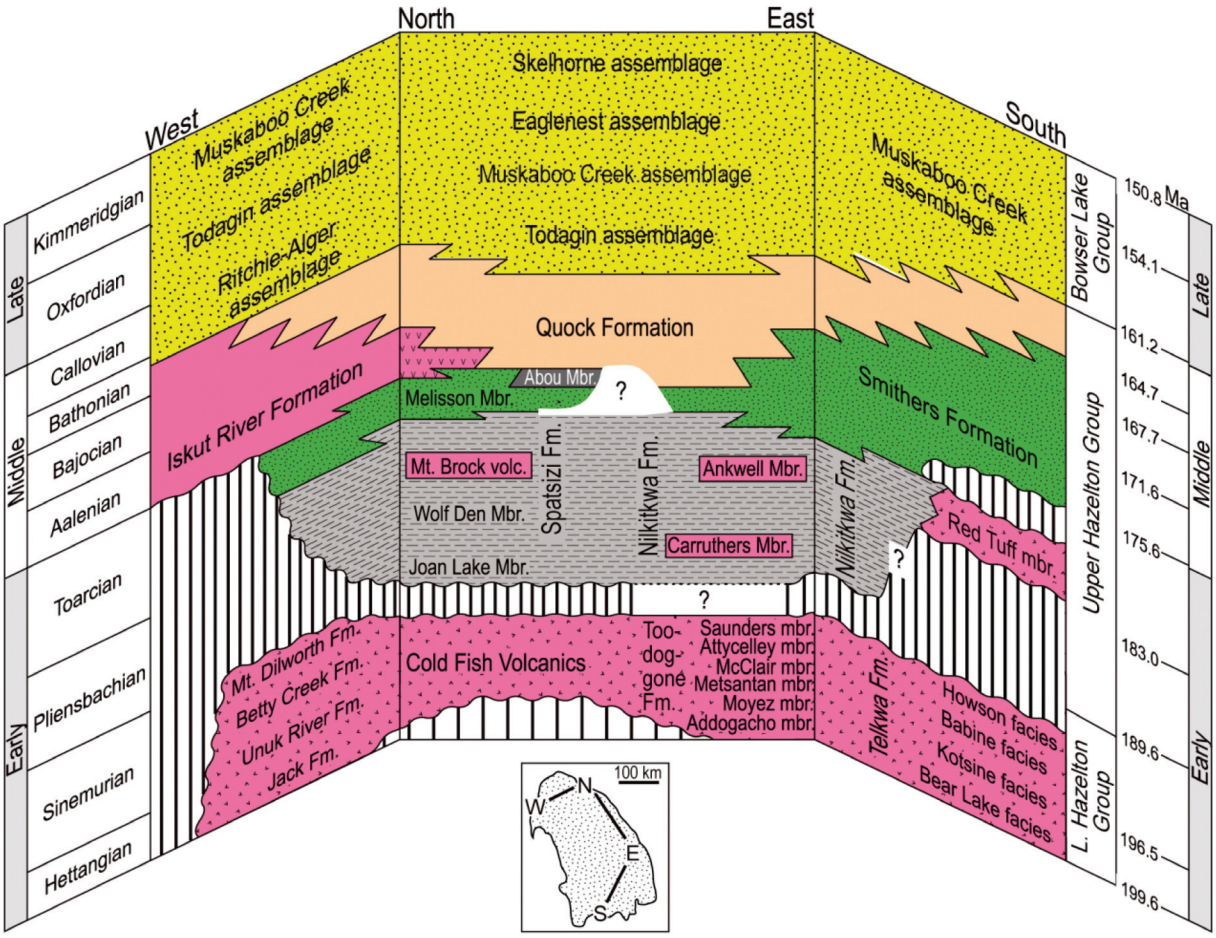

Fig. 2-7. Proposed stratigraphic nomenclature for the Hazelton Group exposed in the north-central Stikine terrane. Most significant changes include recognition of a diachronous unconformity at the base of the upper Hazelton Group, revision of the Spatsizi and Quock formations, and introduction of a new stratigraphic unit (Iskut River Formation) for the rift-related facies in the Iskut River area. Inset (bottom) shows the general position and orientations of the schematic sections (above); shaded area is geographic extent of Hazelton Group in north-central Stikine terrane. Time scale of Ogg (2004).

1991; Thorkelson et al. 1995; Logan et al. 2000). Most of these units were deposited in subaerial, oxidizing environments, and likely built stratovolcanoes on an evolving arc system (Alldrick et al. 1989). An exception is the Cold Fish Volcanics, which have a bimodal geochemical signature interpreted as a product of extensional volcanism in a back-arc setting (Thorkelson et al. 1995). Discontinuous siltstone beds bearing Hettangian to Upper Sinemurian ammonites highlight the marine setting of the emergent arc.

2.6.2 Upper Hazelton Group

Because of their greater lateral continuity and their relatively constant thickness, sedimentary units of the upper Hazelton Group are more traceable regionally than the volcanic units associated with the lower Hazelton Group. Three major stratified packages are recognized: the mainly sedimentary Smithers Formation and its equivalents, the overlying siliceous mudstones and thinly bedded tuffs of the Quock Formation, and the Eskay rift volcanic assemblage in the northwest, here named the Iskut River Formation.

2.6.2.1 Smithers Formation and equivalents

A recognizable lower package includes strata of the Smithers and Nilkitkwa formations, along with specific units previously assigned to the Spatsizi (Joan, Wolf Den, and Melisson members) and Salmon River (lower calcareous member) formations (Fig. 2-2). These units are here assigned to three formations: the Smithers and Nilkitkwa formations, and the revised Spatsizi Formation (Fig. 2-7). The unconformity at the base of these successions marks the boundary between the lower and upper Hazelton Group. In most parts of the basin, this unconformity is overlain by 1–5 m thick clast-supported conglomerate that fines upward into cross-bedded, coarse- to medium-grained sandstone, as seen at sections QM, JL, W1, W2, OW, and OA (Figs. 2-3, 2-4). One exception to the overall clastic nature of this package is the Toarcian Red Tuff Member of the Nilkitkwa Formation, which disconformably overlies lithologically similar red dacitic tuffs of the Sinemurian Telkwa Formation in sections AR and QM, and is in turn unconformably overlain by clastic units of the Smithers Formation.

For the most part, however, the three lower formations of the upper Hazelton Group, in part laterally equivalent, consist of interbedded tuffaceous siltstone and sandstone layers containing abundant marine fossils and trace fossils. These units are diachronous, ranging from Lower Pliensbachian – Upper Toarcian in the north to Lower Aalenian – Upper Bathonian in the south (Fig. 2-3). In the east, near the Nilkitkwa Range, there is a gradational lateral facies change northward from coarser clastics to finer-grained sedimentary rocks interbedded with mafic volcanics. This is attributed to deposition in a deeper water setting with continuing extensional volcanism, consistent with Tipper and Richards' (1976) definition of the "Nilkitkwa depression" as the main axis to the Hazelton trough. Deeper parts of the depression developed anoxic conditions and accumulated sediment rich in organic matter, preserved locally in the Nilkitkwa Formation and in the Wolf Den and Abou members of the revised Spatsizi Formation. In almost all the observed and compiled stratigraphic sections, units of the Smithers Formation and equivalents are overlain by thinly bedded siliceous mudstone and tuffaceous siltstone here assigned to the Quock Formation.

No type locality has been described for the Smithers Formation, and the reference sections measured by Tipper and Richards (1976) are incomplete. We propose section QM as the new stratotype (Fig. 2-3). Based on our observations, this section meets all the necessary criteria established by the North American Stratigraphic Code (North American Commission on Stratigraphic Nomenclature 2005) to serve as a type section (Table 2-1A).

In the eastern portion of the basin, the Nilkitkwa Formation type section described by Tipper and Richards (1976) is retained. Although individual units within the Nilkitkwa Formation are laterally continuous with some strata of the Smithers and revised Spatsizi formations, they are sufficiently different in lithology to merit separate formal designation. The stratotype proposed by Tipper and Richards (1976) contains interbedded basaltic flows, argillite, and sandstone, which are characteristic of this part of the basin.

The Nilkitkwa Formation is also retained in the southwestern part of the basin (Ashman Ridge – Quinlan Mountain). The Red Tuff Member is a thin but continuous blanket of fine-grained lithic tuff that in part is characterized by the presence of bombs. It represents an explosive eruption or eruptions in Middle Toarcian time that marked the last phase of arc volcanism in the area. It is significant that this postdated the end of lower Hazelton arc volcanism farther north by 10–20 million years.

A unit rich in thinly interbedded silicified tuffs and mudstones (revised Quock Formation) overlies the Smithers and Nilkitkwa formations in all measured sections (Fig. 2-3). This poses a problem in existing stratigraphic schemes, because where correlated with the northern part of the basin, this lithology has been included in the Spatsizi Formation as the Quock Member (Thomson et al. 1986; Evenchick and Thorkelson 2005). We propose removing the Quock unit from the Spatsizi Formation and revision of that formation to include only the lower three members (Joan, Wolf Den, and Melisson), justified under article 19 of the North American Commission on Stratigraphic Nomenclature (2005), as a minor change to make the unit more natural for common usage. The lowest three members of the Spatsizi Formation are lithostratigraphic lateral equivalents of the Nilkitkwa and lower Smithers formations (Fig. 2-3).

In the Iskut River area, the Salmon River Formation of previous authors now includes a Lower Toarcian member of bioclastic calcareous sandstone and siltstone, an Aalenian–Bajocian member mainly comprising thinly bedded tuffs and mudstones (Troy Ridge facies) equivalent to the Quock Formation, and bimodal volcanic flows (Eskay Creek facies). Furthermore, refinements and redefinitions of the Salmon River Formation in the last two decades (Anderson and Thorkelson 1990; Anderson 1993; Macdonald et al. 1996a) considerably changed the scope of the formation from the original description of Schofield and Hanson (1921), such that its type area, defined by Grove (1986), is no longer valid. In addition, its type section near Mount Dilworth actually includes sedimentary rocks of the Bowser Lake Group (Evenchick and McNicoll 2002; Gagnon and Waldron 2011; Waldron and Gagnon 2011) and lacks the pillow basalt which is a major component of the Salmon River Formation at Eskay Creek (Macdonald et al. 1996a; Logan et al. 2000; Alldrick et al. 2004b, 2005a,b; Barresi et al. 2005). To prevent

any further confusion, we recommend the abandonment of the Salmon River Formation following article 20 of the North American Commission on Stratigraphic Nomenclature (2005). As an alternative, we propose the following changes:

- inclusion of the Toarcian bioclastic calcareous lower member in the revised Spatsizi Formation;
- inclusion of the Troy Ridge facies in the Quock Formation;
- inclusion of the volcanic-dominated successions in a new unit, named here the Iskut River Formation (Chapter 2.6.2.3).

2.6.2.2 Quock Formation

In the course of this study a thinly interlayered grey to black siliceous siltstone and beige to pink ash tuff ("pyjama beds"), has been recognized at similar stratigraphic positions across the basin (Fig. 2-3), between the underlying Smithers Formation and equivalents, and the overlying Bowser Lake Group. In the north and west parts of the basin, these strata were assigned to the Troy Ridge facies of the former Salmon River Formation, and they are the only strata of that formation recognized outside the Iskut River area (Anderson and Thorkelson 1990; Greig 1991, 1992; Marsden and Thorkelson 1992; Anderson 1993; Evenchick and Porter 1993; Jakobs 1993; Ferri et al. 2004; Evenchick and Thorkelson 2005; Ferri and Boddy 2005; Waldron et al. 2006; Gagnon et al. 2007; Gagnon and Waldron 2008, Evenchick et al. 2010). Elsewhere, equivalent strata have been assigned to the Yuen and Bait members of the Smithers Formation (Tipper and Richards 1976) or the Quock Formation (Thomson et al. 1986). We follow Thomson et al. (1986) in considering the Quock to have formation rank, with its original type section at Joan Lake (JL) as the unit stratotype (Table 2-1B; see article 19e of North American Commission on Stratigraphic Nomenclature 2005). Outside the Eskay rift area (Fig. 2-3), the lowest occurrence of laminated siliceous and tuffaceous siltstone defines the base of the formation. Its top is at the contact with the overlying Bowser Lake Group, as redefined by Evenchick et al. (2010). However, in the Iskut River area, the characteristic siliceous mudstone and tuff lithologies interfinger laterally with thick sections of bimodal volcanic rock (Fig. 2-4). There, the mudstones interbedded with thick flows of volcanic rock are included in the proposed Iskut River Formation, and only the uppermost

package, dominated by laminated siliceous and tuffaceous siltstones, is included in the Quock Formation.

2.6.2.3 Iskut River Formation

With assignment of the calcareous bioclastic lower facies to the revised Spatsizi Formation, and the upper Troy Ridge facies to the Quock Formation, the remaining, dominantly volcanic facies of the current Salmon River Formation requires a lithostratigraphic name; we propose the new Iskut River Formation.

At many locations close to graben-bounding faults, the lower contact of the Iskut River Formation appears to be an angular unconformity where fan-conglomerates are juxtaposed on or against various units of the lower Hazelton Group, Stuhini Group, or Stikine assemblage. In a few locations, the lower part of the formation is exposed farther from the graben margin such that the conglomerates grade laterally into distal very fine-grained sedimentary rocks with intercalated tuff, and bimodal volcanics including rhyolite and voluminous tholeiitic basalt (Alldrick et al. 2005a; Barresi et al. 2005). At Eskay Creek, rhyolite of the Iskut River Formation disconformably overlies Upper Pliensbachian volcaniclastic rocks and felsic welded lapilli tuff of the lower Hazelton Group (Fig. 2-5C). The upper contact of the Iskut River Formation is typically conformable with either the Quock Formation or siliciclastic strata of the Bowser Lake Group. Since section TM is the thickest and includes the greatest variety of lithologies, we proposed it as the stratotype for the Iskut River Formation (Figs. 2-5A, 2-5B; Table 2-1C). The base of the formation is placed where feldspar-phyric andesite breccia of the lower Hazelton Group is overlain by rhyolite, which is heavily altered at this locality. Because the lower contact is along a contemporaneous faulted graben margin, section EC is designated as a reference section to define the disconformable lower contact farther into the basin.

Table 2 - 1. Definitions of new stratigraphic units.

A. Smithers Formation

1. Named by Tipper and Richards (1976) after the town of Smithers, British Columbia, located ~60 km east of the proposed typesection.
2. Lithological characteristics: bioturbated tuffaceous and calcareous siltstone and sandstone with abundant marine fossils.
3. Thickness at type section: 240 m.
4. Lower contact: unconformable above the oxidized tuffs of the Red Tuff Member of the Nilkitkwa Formation. Boundary defined at the base of a basal conglomerate fining upward into cross-bedded medium- to coarse-grained sandstone (UTM zone 9 555130 E 6077435 N).
5. Upper contact: conformable, defined by a fining-upward trend and gradational transition into units of the revised Quock Formation (see part B). The boundary is placed at the first occurrence of thinly interbedded siliceous siltstones and fine pale tuffaceous laminae (‘‘pyjama beds’’) (UTM 554870 E 6078650 N).
6. Age: extensive fossil collections indicate an age from Middle Aalenian to Upper Bathonian (see supplementary data[2]).

B. Quock Formation

1. Named by Thomson et al. (1986) for Mount Quock, ~1 km east of the type section. Equivalent to Quock member of Evenchick and Thorkelson (2005).
2. Lithological characteristics: thinly bedded, dark siliceous blocky mudstone and rusty-weathering tuff bands (‘‘pyjama beds’’). Thin section observations show abundant recrystalized radiolarian tests in the mudstone intervals as well as ferruginous clay. The tuff bands are characterized by angular volcanic fragments and feldspar grains, in addition to white micas and chlorite. Calcareous concretionary lenses and thin limestone beds are occasionally found throughout this unit. Discontinuous exposures of calcareous to siliceous dark shale outcropping in the lower portion of the section are included in the Quock Formation as the Abou Member.
3. Thickness at type section: 200 m.
4. Lower contact: as defined by Thomson et al. (1986); conformable and gradational contact above the uppermost bioturbated sandstone of the revised Spatsizi Formation (Melisson Member) (UTM 507560 E 6372125 N).
5. Upper contact: as defined by Thomson et al. (1986); conformable and gradational with the thinly bedded fissile siltstone and shale of the Bowser Lake Group (Todagin assemblage) (UTM 505685 E 6373530 N).
6. Age: Bajocian, possibly Upper Aalenian at type section; regionally, the base of the Formation may be as low as Late Toarcian, and the top may be as high as Lower Oxfordian (see supplementary data[2]).

C. Iskut River Formation

1. Named for Iskut River, the largest tributary of the Stikine River, British Columbia, which lies ~5 km east of the type section. The name of this river was previously informally applied to a Quaternary flow as Iskut River lava by Kerr (1948); also, MacIntyre et al. (1994) used the term ‘‘Iskut River stock’’ as an informal lithodemic term. Neither of these terms has found widespread use outside the original publications.
2. Lithological characteristics: thick volcanic piles of pillow basalt and pillow basalt breccia interbedded with intervals of rhyolite, conglomerate, and minor mudstone and dust tuff (‘‘pyjama beds’’) (Fig. 2-6).
3. Thickness at type section: at least 3480 m.
4. Lower contact: angular unconformity along the ancient graben margin at which various stratigraphic levels of the Iskut River Formation onlap against the lower Hazelton Group; at the best exposed part of the contact (UTM 415200 E 6352500 N), rhyolite of the Iskut River Formation rests above feldspar porphyritic andesite breccia of the lower Hazelton Group. The disconformable boundary at Eskay Creek (UTM 416800 E 6279000 N) is designated as a reference section to define the lower contact to the east, in the basin (Fig. 2-5C). At this location, rhyolite of the Iskut River Formation is in contact with Upper Pliensbachian volcaniclastic rocks and felsic welded lapilli tuff of the lower Hazelton Group.
5. Upper contact: not observed in outcrop but closely constrained with the overlying siliciclastic rocks of the Bowser Lake Group (UTM 420000 E 6370000 N). However, structural discordance suggests that the contact may be faulted. In the reference section at Eskay Creek (Fig. 2-5C) the Iskut River Formation is in conformable contact with thinly bedded siliceous mudstones and very thin tuff beds of the overlying Quock Formation.
6. Age: Upper Toarcian to Lower Bajocian fossils have been obtained from thin shale units here included in the Iskut River Formation (Souther 1972; Evenchick et al. 2001; see supplementary data[2]). However, undated lower and higher parts of the forma- tion could range as old as Early Toarcian and as young as Late Bajocian.

Note: Grid references are Universal Transverse Mercator coordinates in NAD83.

2.7 Discussion: Stratigraphic and tectonic evolution

Marsden and Thorkelson (1992) proposed that Early Jurassic arc volcanism in Stikinia was generated by concurrent subduction on opposite sides of the Stikine terrane. One involved a well-documented, east-facing subduction of the Cache Creek oceanic basin on the east side of the Stikine terrane; the other, a more speculative, west-facing subduction of oceanic lithosphere on the west side (directions in present-day coordinates). In the northern Hazelton trough (e.g., sections JL, W1, W2), the bimodal Upper Sinemurian to Lower Pliensbachian Cold Fish Volcanics accumulated in the back-arc area of a magmatic arc represented by calc-alkaline volcanic rocks of the Toodoggone Formation to the east (Diakow et al. 1991; Thorkelson et al. 1995). Farther north, English and Johnston (2005) interpreted the Whitehorse trough as an elongated sedimentary basin that originated in a fore-arc setting located between the arc magmatic rocks of Stikinia and the accretionary complex of the Cache Creek terrane.

The base of the upper Hazelton Group marks the transition from a volcanic arc to a post-arc tectonic environment in northern Stikinia. Stratigraphic cross-sections shown in Figs. 2-3 and 2-4 highlight the variable character and diachronous nature of the lower–upper Hazelton Group boundary, which ranges from Early Pliensbachian in the north to Early Aalenian in the south (Fig. 2-7). The end of Hazelton volcanism is much less diachronous in an E–W direction: the two separate arcs proposed by Marsden and Thorkelson (1992) both ceased activity during the Pliensbachian. The last vestige of arc-related volcanism is represented only in the far southwestern part of the study area by the Toarcian Red Tuff Member of the Nilkitkwa Formation. Southerly migration of the arc axis then continued with the renewal of magmatic activity in the Whitesail (Gordee 2005; Diakow 2006) and Bella Coola (Diakow et al. 2002) areas of southern Stikinia in Bajocian and Bathonian time.

The stratigraphic data presented in this paper show that the upper Hazelton Group includes both regionally extensive, mainly sedimentary units exposed around the margins of the Bowser Basin (Spatsizi, Smithers, and Quock formations), and the areally restricted and lithologically highly variable Iskut River Formation, which filled a narrow, well-defined rift at the western margin of the Bowser Basin.

Apart from the Iskut River Formation, most of the upper Hazelton Group represents a zone of regional, post-arc subsidence, controlled in part by the pre-existing paleogeography of the Hazelton trough and its elevated margins. The subsidence profile obtained by Gagnon et al. (2009) from the north-west portion of the Hazelton trough and overlying Bowser Basin indicates that extensional faulting and thermal contraction of the crust were responsible for high subsidence rates during the Pliensbachian. These results are consistent with the crustal subsidence model of Thorkelson et al. (1995), who proposed that accumulation of a thick volcanic pile in the lower Hazelton Group in the Spatsizi River area was accompanied by at least 2 km of synvolcanic subsidence. A protracted period of volcanism during the Late Sinemurian resulted in the abundant bimodal volcanic rock of the Cold Fish Volcanics (Marsden and Thorkelson 1992; Thorkelson 1992; Thorkelson et al. 1995) and the thick Telkwa Formation (Chapter 3, Tipper and Richards 1976). Subsequent thermal contraction of the lithosphere resulted in widespread subsidence of the Hazelton trough. Progressive reduction of volcanic activity after Sinemurian time (Fig. 2-8A) involved a few basaltic eruptions restricted to the Nilkitkwa depression (i.e., Mount Brock volcanics, Ankwell and Carruthers members). Exponentially decreasing thermal subsidence through the Middle Jurassic is suggested by the concave-up profile of the backstripped tectonic subsidence curve (Gagnon et al. 2009). This was followed by more rapid subsidence due to loading by clastic sediment derived from the Cache Creek terrane in the Late Jurassic.

The paleogeography established in Stikinia during development of the lower Hazelton Group, consisting of two arcs separated by a central trough, influenced subsequent crustal evolution. The lower–upper Hazelton Group contact appears conformable in the central part of the Hazelton trough (Fig. 2-3), where Lower Pliensbachian sedimentary rocks of the Nilkitkwa Formation directly overlie marine volcanic rocks of the Telkwa Formation (Tipper and Richards 1976). Elsewhere, outside the main trough axis, the base of the upper Hazelton Group is an unconformable surface but is somewhat diachronous (Figs. 2-3, 2-4). In the Spatsizi River area, Lower Pliensbachian shallow-marine sedimentary rocks of the Joan Member disconformably overlie the subaerial Cold Fish Volcanics, whereas a Toarcian hiatus has been reported in the Toodoggone, Iskut, Smithers, and Terrace areas (Diakow et al. 1991; Anderson 1993; Greig and Gehrels 1995; Waldron et

Fig. 2-8. Conceptual block diagrams showing the interpreted deposition environment of the upper Hazelton Group in the Early to Middle Jurrassic. Scale very approximate and vertically exaggerated. A) In the Pliensbachian (185 Ma), mafic volcanism and deep-water sedimentation dominated the central portion of the Hazelton trough, while coarser clastic rocks accumulated on the margins. B) In the Toarcian (180 Ma), progressive decrease in volcanic activity led to thermal subsidence of the Stikine terrane and relative sea-level rise. Siliceous mudstone and tuff of the Quock Formation began to accumulate in the central portion of the trough. C) In the Aalenian (173 Ma), mudstone and tuff (younger Quock Formation) were deposited throughout the basin while extension in the Iskut River area led to accumulation of rift-related facies of the Iskut River Formation.

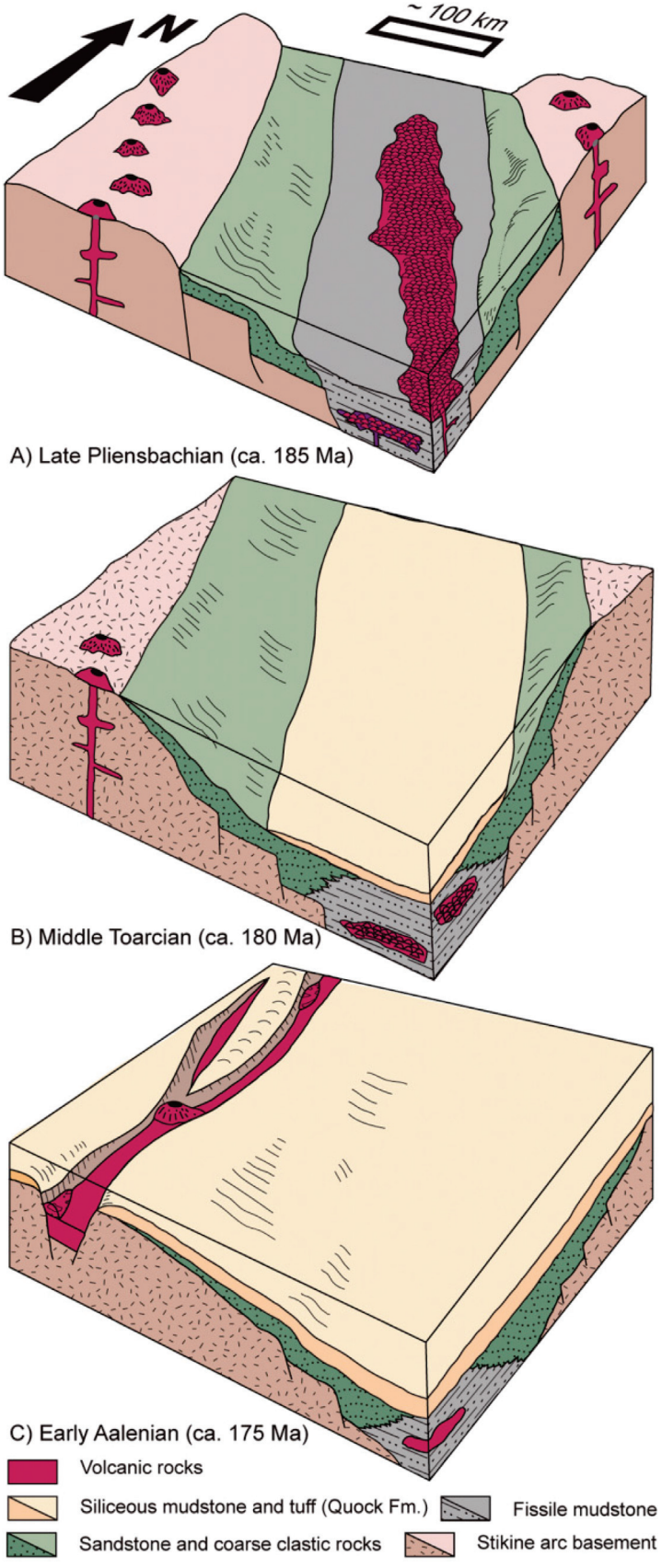

al. 2006; Gagnon et al. 2007; Nelson et al. 2007b). In this study, we recognize a 10–20 Ma hiatus at sections AR and QM separating the Sinemurian Telkwa Formation and the Toarcian Red Tuff Member of the Nilkitkwa Formation.

Stratigraphic cross-sections shown in Figs. 2-3 and 2-4 highlight the variability and diachronous nature of the lower–upper Hazelton Group boundary. Although development of a graben structure ensured continuous marine deposition within the Nilkitkwa depression, the rift margins of the Hazelton trough underwent periodic uplift and erosion (Tipper and Richards 1976).

Thermally subsiding volcanic remnants on the periphery of the graben were progressively submerged, to be overlain by transgressive shallow-water sedimentary rocks of the Smithers Formation and equivalents. This is a common feature in extensional settings such as back-arcs and continental rifts, where graben flanks become subaerially exposed in response to block tilting, which can lead to development of localized unconformities (cf. Baker et al. 1972; Kusznir and Egan 1990; Ebinger et al. 1991; Lin et al. 2003).

The diachronous nature of the lower–upper Hazelton Group transition reflects differential subsidence rates that affected the Hazelton arc during the Early to Middle Jurassic, linked to variations in the timing of the end of major volcanic activity. In depocentres characterized by intense volcanism and extensional faulting, onlap of the unconformity by shallow-marine sedimentary rocks occurred immediately after cessation of back-arc activity. This is attributed to greater post-rift subsidence rates in areas where the initial amount of lithospheric stretching was more significant (cf. McKenzie 1978; Steckler and Watts 1978). Where sedimentation around slower-subsiding areas began later, marine transgression reached its maximum extent around the Toarcian–Aalenian boundary (Fig. 2-8B), and a maximum flooding surface occurs close to the base of the Quock Formation.

The fine grain size and thinly bedded nature of the Quock Formation, combined with the high organic content in its mudstone components (total organic content values up to 6%, Ferri and Boddy 2005), suggest that it was deposited mainly from suspension in a deep-water, anoxic environment. These regionally extensive, condensed sections form a basin-wide stratigraphic marker near the top of the Hazelton Group (Fig. 2-3). The long time

interval demonstrated by fossil data from the Quock Formation at Diagonal Mountain (DM) indicates that tuff and siliceous mudstone accumulated there in a deep basin over a protracted period (Late Toarcian to Early Oxfordian) (Evenchick and Porter 1993; Jakobs 1993; Evenchick et al. 2001, 2010).

In the Iskut River area, extension-controlled volcanism prevailed in an elongate, narrow, north-trending rift basin during a short period, from Late Toarcian to Early Bajocian time (Fig. 2-4). Fault-controlled subsidence led to compartmentalization of at least 12 north-trending sub-basins within the 300 km long by 50 km wide volcanic belt of the Eskay rift (Alldrick et al. 2005a; Barresi et al. 2005; Fig. 2-8C). The irregular topography of the rift basement, characterized by depocentres and uplifted horst footwall blocks, hampers stratigraphic correlations within the Iskut River Formation. Volcanic and sedimentary units show great lateral and vertical variability because of the limited connectivity between sub-basins and the local nature of the volcanic processes. Nearly uninterrupted successions of pillow basalt up to 2 km thick (sections PB and TB) suggest rapid extrusion and basin filling, whereas other sub-basins (e.g., Eskay Creek and Treaty Glacier) have a higher proportion of fine-grained sedimentary rock and lack thick basaltic flows (Fig. 2-4). Intense volcanic activity above local feeder zones dominated the background accumulation of basinal tuffaceous mudstone successions in some places. Rare thin tuffaceous mudstone intervals between basaltic flows attest to lulls in volcanic activity and help link the Iskut River Formation with equivalent condensed successions (Quock Formation) elsewhere in the region. Such quiescent depositional environments were more prone to accumulation and preservation of exhalative sulfides (Alldrick et al. 2004b). Felsic volcanism is closely associated with mudstone intervals within the Eskay rift and is the most likely source of Aalenian-Bajocian tuffaceous intervals in the Quock Formation regionally.

Rift-related, bimodal volcanism in the Iskut area has been interpreted to have occurred in a back-arc setting (cf. Macdonald et al. 1996a). However, this resurgence of extension and volcanism occurred 10–15 million years after the significant decline of arc activity in all but the southern regions of the Hazelton trough. Even in the southern area of sections AR and QM, arc volcanism ended in the Toarcian, at about the same time as the inception

of the Eskay rift and the beginning of the volcanic activity represented by the Iskut River Formation. Geometrically the north-trending Eskay rift (Fig. 2-1) does not appear to be related to the remnant "Red Tuff" arc of the southern sections. The Eskay rift and the Iskut River Formation therefore probably represent an independent rifting episode. In addition, the short duration of this episode (~178–168 Ma) overlaps in time with final amalgamation of Stikinia and the Cache Creek subduction complex. This deformational event is well constrained by the age of the youngest blueschists in the Cache Creek terrane (173.0 ± 0.8 Ma; Mihalynuk et al. 2004) and by the age of the oldest post-kinematic intrusions that stitched the two domains together (ca. 172 Ma; Mihalynuk et al. 1992; Bath 2003). The Alexander terrane to the southwest also became accreted to Stikinia during this interval (van der Heyden 1992; Gehrels 2001). The Eskay rift and the Iskut River Formation may therefore reflect radical plate reorganization during terrane accretion that possibly led to transcurrent shearing across Stikinia (Nelson and Colpron 2007). This would explain their unique character in a region in which post-arc thermal subsidence and mild lithospheric thinning dominated. During the Miocene in Baja California and Sonora Mexico, a similar post-subduction transtensional rift developed. Circa 12.5 Ma the Baja Peninsula transferred to the Pacific plate, reconfiguring the North American-Pacific plate boundary. This resulted in a change in relative plate movement from convergent to oblique-divergence between 12.5 and 6 Ma (Lionsdale 2006, Till et al, 2009).

2.8 Conclusions

1. The Hazelton Group can be divided into two distinct intervals separated, in most places, by an unconformity:
    a. the lower Hazelton Group, which is dominated by arc-related volcanic rocks, and
    b. the upper Hazelton Group, which contains mainly fine-grained clastic rocks and geographically limited bimodal rift-related volcanic rocks.
2. An abrupt decline of volcanic activity, following back-arc rifting in the Sinemurian, led to widespread thermal subsidence of the lower Hazelton Group magmatic arc and Pliensbachian initiation of upper Hazelton Group sedimentation

in the Hazelton trough. Thick mudstone-dominated successions (Nilkitkwa Formation and most of the revised Spatsizi Formation) accumulated in the central portion of the trough, whereas topographically higher margins were loci of coarser-grained clastic sediments rich in volcanic detritus (Smithers Formation and parts of the revised Spatsizi Formation).

3. Progressive onlap of the unconformity by lowermost strata of the upper Hazelton Group was diachronous at the basin scale and reflects differential subsidence rates across the Stikine terrane.
4. Relative rise in sea level led to accumulation of siliceous mudstone and tuff of the Quock Formation in deep basinal conditions at the Toarcian – Aalenian boundary.
5. Laterally equivalent bimodal volcanic rocks and associated Ag-Au-Cu VMS deposits of the Iskut River Formation were deposited in sub-basins within a 200 by 50 km rift on the northwestern portion of the basin.
6. The northern Stikine terrane was affected by two independent rifting events during deposition of the Hazelton Group:
    a. a widespread Late Sinemurian to Early Pliensbachian extension phase in the northwest-trending Hazelton trough, and
    b. a much more focused and intense Aalenian to Bajocian extensional event in the north-trending Eskay rift, recorded in the Iskut River Formation.

Recognizing the distinctiveness of these independent units is important for tectonic models of the evolution of Stikinia and for predictive models in mineral and hydrocarbon exploration.

Chapter 3 - Evolution of the Hazelton Arc Near Terrace, British Columbia: Stratigraphic, Geochronological, and Geochemical constraints on a Late Triassic-Early Jurassic arc and Cu-Au porphyry belt

3.0 Preface

This chapter documents the geology of the lower Hazelton Group near Terrace, BC and discusses implications for regional metallogenesis. The chapter is derived entirely from:

> Barresi, T., Nelson, J.L., Dostal, J. and Friedman, R. in review 2015. Evolution of the Hazelton arc near Terrace British Columbia: Stratigraphic, geochronological, and geochemical constraints on a Late Triassic-Early Jurassic arc and Cu-Au porphyry belt. Canadian Journal of Earth Sciences.

The paper is based on 1) fieldwork that I conducted in conjunction with co-author JoAnne Nelson in 2005, and that J. Nelson conducted in 2006 and 2007; 2) geochemical analyses of rock samples that I collected or supervised the collection of; and 3) geochronology based on samples, collected by me or J. Nelson. Coauthor, R. Friedman conducted all of the laboratory work for the geochronology, created preliminary concordia diagrams and collaborated in interpreting ages. I wrote the article, drafted or touched-up all of the figures, processed the geochemistry samples, and in collaboration with co-authors conceived of the ideas presented in the paper.

The following government reports and open-file map reflect my original contribution to the fieldwork aspect of this project and describe the geology of the lower Hazelton Group near Terrace in greater detail. The reports and map are found in appendices A and E respectively.

> Nelson, J., Barresi, T., Knight, E. and Boudreau, N. 2006. Geology and Mineral Potential of the Usk Map Area (NTS 103I/09), Terrace, British Columbia. In

Geological Fieldwork 2005, British Columbia Ministry of Energy and Mines, British Columbia Geological Survey Paper 2006-1, p. 149-162.

Barresi, T., Nelson, J. 2006. Usk Map Area (NTS 103I/09), Near Terrace, British Columbia: Cross-Sections and Volcanic Facies Interpretation. In Geological Fieldwork 2005, British Columbia Ministry of Energy and Mines, British Columbia Geological Survey Paper 2006-1, p. 21-28.

Nelson, J.L., Barresi, T., Knight, E., Boudreau, N. 2006. Geology of the Usk Map Area (NTS 103I/9). British Columbia Ministry of Energy and Mines, British Columbia Geological Survey Open File 2006-03.

Appendix D contains copyright agreement forms for all published manuscripts used in this thesis.

3.1 Abstract

Understanding the development of island arcs that accreted to the North American craton is critical to deciphering the complex geological history of the Canadian Cordillera. In the case of the Hazelton arc (part of the Stikine terrane, or Stikinia) in northwestern British Columbia, understanding arc evolution also bears on the formation of spatially associated porphyry Cu-Au, epithermal, and volcanogenic massive sulfide deposits. The Hazelton Group is a regionally extensive, long-lived and exceptionally thick Upper Triassic to Middle Jurassic volcano-sedimentary succession considered to record a successor arc that was built upon the Paleozoic and Triassic Stikine and Stuhini arcs. In central Stikinia, near Terrace, British Columbia, the lower Hazelton Group (Telkwa Formation) comprises three volcanic-intrusive complexes (Mt. Henderson, Mt. O'Brien, and Kitselas) which, at their thickest, constitute almost 16 km of volcanic stratigraphy. Basal Telkwa Formation conglomerates and volcanic rocks were deposited unconformably on Triassic and Paleozoic arc-related basement. New U-Pb zircon ages indicate that volcanism initiated by ca. 204 Ma (latest Triassic). Detrital zircon populations from the basal conglomerate contain abundant 205-233 Ma zircons, derived

from regional unroofing of older Triassic intrusions. Eleven kilometres higher in the section, ca. 194 Ma rhyolites show that arc construction continued for >10 My. Strata of the Nilkitkwa Formation (upper Hazelton Group) with a U-Pb zircon age of 178.90 ± 0.28 Ma represent waning island arc volcanism. Telkwa Formation volcanic rocks have bimodal silica concentrations ranging from 48.1 - 62.8 and 72.3 - 79.0 wt.%, and display characteristics of subduction-related magmatism (i.e. calc-alkaline differentiation with low Nb and Ti and high Th concentrations). Mafic to intermediate rocks form a differentiated suite that ranges from high-Al basalt to medium-high K andesite. They were derived from hydrous melting of isotopically juvenile spinel lherzolite in the mantle wedge and from subsequent fractional crystallization. Compared to basalts and andesites (ε_{Nd} = +5 to +5.5), rhyolites have higher positive ε_{Nd} values (+5.9 - +6.0) and overlapping incompatible element concentrations, indicating that they are not part of the same differentiation suite. Rather, the rhyolites formed from anatexis of arc crust, probably caused by magmatic underplating of the crust. This study documents a temporal and spatial co-occurrence of Hazelton Group volcanic rocks with a belt of economic Cu-Au porphyry deposits (ca 205 – 195 Ma) throughout northwestern Stikinia. The coeval relationship is attributed to crustal underplating and inter-arc extension associated with slab rollback during renewed or reconfigured subduction beneath Stikinia, following the demise of the Stuhini arc in the Late Norian.

3.2 Introduction

The Late Triassic-Early Jurassic was a peak period for the formation of porphyry and related mineral deposits in the exceptionally well-endowed Stikine terrane (Stikinia) of the Canadian Cordillera (Fig. 3-1; Lang et al. 1995; Macdonald et al. 1996; Logan and Mihalynuk 2014). Past, present and potential future producers include porphyry copper-gold deposits such as Red Chris, Galore Creek, Schaft Creek, Kerr-Sulphurets-Mitchell (KSM), and GJ, and Au-Ag epithermal deposits such as Brucejack and Premier. The plate tectonic setting of these deposits has long been a topic of interest. However, insights into the tectonic setting of the porphyry and related deposits have been hampered

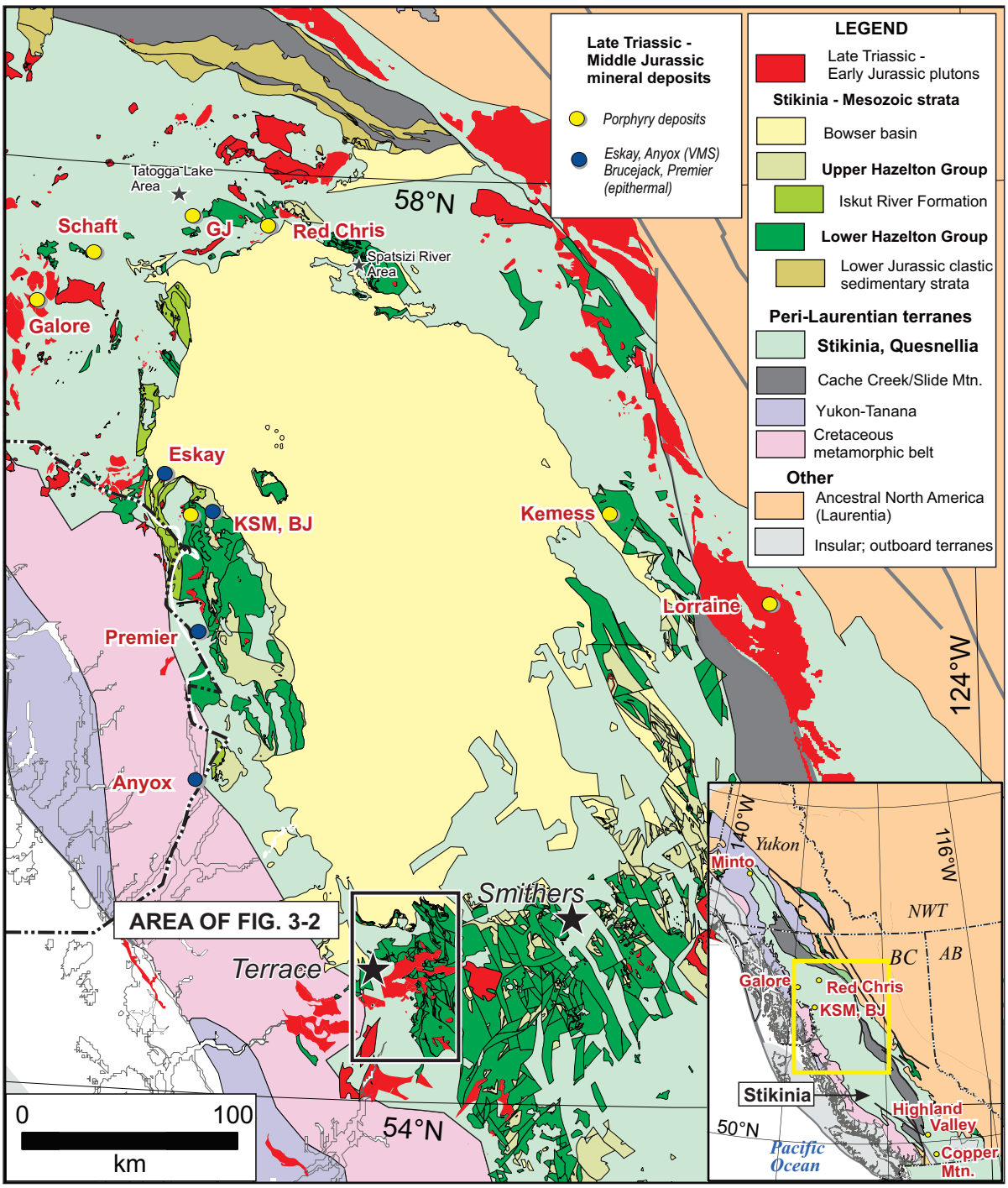

Fig. 3-1. Geology of northern Stikinia with a focus on Hazelton Group and related intrusions and location/context of major associated mineral deposits. Inset shows location of this area in the Canadian Cordillera. Area of Fig. 3-2 noted at bottom center.

by the inability to link specific intrusive events in the Triassic-Jurassic arc infrastructure with arc-building volcanic pulses, due to lack of supporting geochronological and geochemical data from extrusive rocks. The mineralizing intrusions fall into three age groups: 1) Late Triassic (ca. 222-210 Ma), including Schaft Creek (ca. 222 Ma, Scott et al. 2008) and Galore Creek (ca. 210 Ma, Mortensen et al. 1995; Logan and Mihalynuk 2014); 2) latest Triassic (205-201 Ma) including GJ (205 Ma, Friedman and Ash 1997), Red Chris (204 Ma, Friedman and Ash 1997), and Kemess South (ca. 201 Ma, Duuring et al. 2009); and 3) Early Jurassic, including KSM (197-190 Ma, Febbo et al. 2015). They are associated spatially and temporally with two early Mesozoic arc successions, the Stuhini and Hazelton groups. The Stuhini Group is a succession of Upper Triassic sub-alkaline to locally alkaline arc-related volcanic and sedimentary rocks (Logan et al. 2000; Simmons et al. 2007), which is recognized throughout northern Stikinia. The unconformably overlying and equally widespread Hazelton Group (Fig. 3-1) has been considered as exclusively Jurassic in age (Tipper and Richards 1976; Marsden and Thorkelsen 1992; MacDonald et al. 1996; Evenchick et al 2010; Gagnon et al. 2012; Logan and Mihalynuk 2014). In this geological context, the ca. 222-210 Ma porphyries were related to main-stage Stuhini magmatism and the ca. 197-190 Ma porphyries to main-stage Hazelton magmatism. The latest Triassic porphyries (205-201 Ma) formed during a poorly understood interval during and after the demise of the Stuhini arc but before the inception of the Hazelton Group at the Triassic-Jurassic boundary, now well constrained at 201.3 ± 0.2 Ma (Cohen et al. 2012). Their origin has been ascribed to a hiatus in arc activity (Lang et al., 1995), possibly triggered by collision of the intraoceanic Kutcho arc, with resulting slab break-off (Logan and Mihalynuk, 2014). The latest Triassic porphyry episode is of great economic significance; it has been estimated that over 90% of BC's copper endowment was acquired between 211 and 199 Ma (Logan and Mihalynuk, 2014). Precise data from potentially correlative supracrustal rocks would aid in constraining tectonic/metallogenetic models.

In this study we integrate geological/stratigraphic, geochronologic, major- and trace-element geochemical, and Nd isotopic data from a thick, well exposed but previously poorly studied section through the Hazelton Group near Terrace, British Columbia, in

central Stikinia (Fig. 3-1). We then use these data to document Mesozoic magmatic arc evolution and its relationship to mineralizing intrusions.

3.3 Geologic Setting

3.3.1 Stikinia

Outboard (westward) of the autochthonous and parautochthonous ancient Laurentian continental margin, the Canadian Cordillera consists of allochthonous terranes (Fig. 3-1), roughly classified as eastern peri-Laurentian terranes that comprise the Intermontane belt, and western exotic terranes that comprise the Insular belt. The terranes accreted to the western margin of Laurentia in the late Early to Late Jurassic, and were deformed along with the margin during Cretaceous (and older) orogenesis (Coney et al. 1980; Monger et al. 1982; Wheeler et al. 1991; Mihalynuk et al. 1994; Nelson et al. 2013). Stikinia is one of the Intermontane terranes, which also include the Yukon-Tanana, Quesnel, and Cache Creek terranes. Stikinia is over 500 km wide in northern British Columbia but tapers near the southern Canada-USA border and in Yukon. Rocks in the Stikine terrane record three episodes of island arc formation between the late Paleozoic and early Mesozoic: 1) Devonian to Permian Stikine and Takhini assemblages, and Asitka Group (Hart 1997; Logan et al. 2000; Gunning et al. 2006); 2) Middle to Late Triassic Stuhini and Takla groups (Souther 1977; Monger, 1977; Dostal et al. 1999); and 3) Hazelton Group, considered by previous authors as entirely of Jurassic age (Tipper and Richards 1976, Monger et al. 1991, Marsden and Thorkelson, 1992, MacIntyre et al. 2001, MacIntyre 2006, Gagnon et al. 2012). Separated by unconformities, these three successions consist of isotopically juvenile, arc-related volcanic rocks (Samson et al. 1989) that either lie on, or interfinger with, carbonate and siliclastic rocks. Near Terrace, the Paleozoic and Triassic successions comprise, respectively, the Zymoetz Group (Stikine assemblage, Nelson et al. 2006) and a thin section (≈ 50m) of sedimentary rocks assigned to the Stuhini Group. Locally the Zymoetz Group is divided into upper Paleozoic volcanogenic and marine sedimentary strata (Mt. Attree Formation, Nelson et al 2008a), overlain unconformably by Permian limestone (Ambition Formation, Gunning et al. 1994). The Stikine terrane is inferred to have been deposited, at least in part, on pericratonic

basement of the Yukon-Tanana terrane (Jackson et al. 1991; Gehrels and Kapp 1998). Stikinia amalgamated with the more inboard Cache Creek subduction complex between 173.0 ± 0.8 and 172 Ma (Mihalynuk et al. 1992, 2004), and in turn the Alexander terrane, part of the Insular belt, collided with the outboard side of Stikinia (van der Heyden 1992; Gehrels 2001). Stikinia is overlain by middle to late Mesozoic rocks (e.g. Bowser Lake and Skeena groups) deposited in post-accretionary basins, and Tertiary to Recent volcanic rocks such as the Nechako and Ootsa Lake groups (Eocene-Oligocene), Chilcotin Group (Miocene) and the Mt. Edziza complex (Pleistocene).

3.3.2 The Hazelton Group

The Hazelton Group is the youngest of three arc/successor arc sequences in Stikinia. Marsden and Thorkelson (1992) proposed that the Hazelton Group formed as a result of two concurrent and geometrically opposed subduction zones and related volcanic arcs on opposite sides of a Philippine-style micro-plate. The two belts of voluminous arc-related rocks are separated by a less volcanically active inter-arc basin. Stratigraphic nomenclature for the Hazelton Group was most recently formalized by Gagnon et al. (2012), who divided it into the lower Hazelton Group and upper Hazelton Group (Fig. 3-1). The lower Hazelton Group consists of mafic to felsic volcanic flows, tuffs, pyroclastic rocks, and volcanically derived epiclastic rocks (Greig and Gehrels 1995; Thorkelson et al. 1995; Gareau et al. 1997a, b; Duuring et al. 2009). The volcanic rocks are interpreted to have been deposited in mainly subaerial environments and, along with sub-volcanic intrusions, to have built successive stratovolcanoes (Alldrick 1993). The upper Hazelton Group was deposited diachronously, its base younging southward from Early Pliensbachian to Late Callovian (Gagnon et al. 2012). It consists of regionally traceable, mainly sedimentary units, and a 300 km-long bimodal volcanic unit deposited in the "Eskay Rift" (Evenchick and McNicoll 2002; Alldrick et al. 2005; Gagnon et al. 2012; Barresi et al. 2015). The upper Hazelton Group represents terminal arc-related and post-arc volcanism and related sedimentation during the amalgamation of Stikinia, Cache Creek, and Quesnellia into an intermontane composite terrane and its accretion to North America.

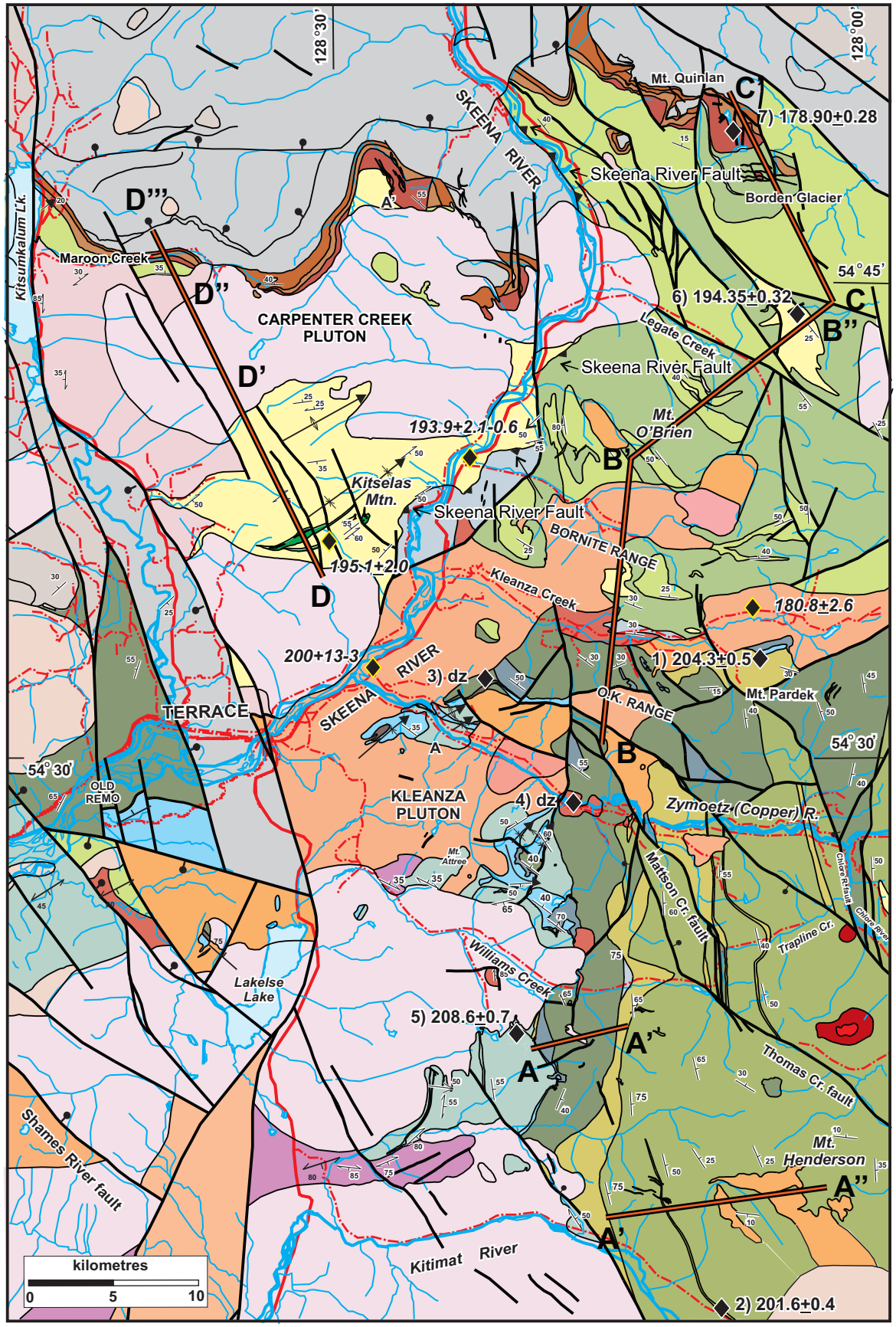
128°30'
128°00'
54°45'
54°30'
Mt. Quinlan
C
C'
7) 178.90±0.28
SKEENA RIVER
Skeena River Fault
Borden Glacier
Kitsumkalum Lk.
D'''
A'
Maroon Creek
D''
CARPENTER CREEK PLUTON
6) 194.35±0.32
B''
Legate Creek
Skeena River Fault
D'
193.9+2.1-0.6
Mt. O'Brien
B'
Kitselas Mtn.
Skeena River Fault
BORNITE RANGE
195.1±2.0
D
Kleanza Creek
180.8±2.6
200+13-3
RIVER
3) dz
1) 204.3±0.5
SKEENA
O/K. RANGE
Mt. Pardek
TERRACE
A
B
OLD REMO
KLEANZA PLUTON
4) dz
Zymoetz (Copper) R.
Mt. Attree
Mattson Cr. fault
Chlore R. fault
Chlore River
Trapline Cr.
Williams Creek
Lakelse Lake
5) 208.6±0.7
A'
A
Thomas Cr. fault
Shames River fault
Mt. Henderson
A''
A'
Kitimat River
2) 201.6±0.4
kilometres
0
5
10

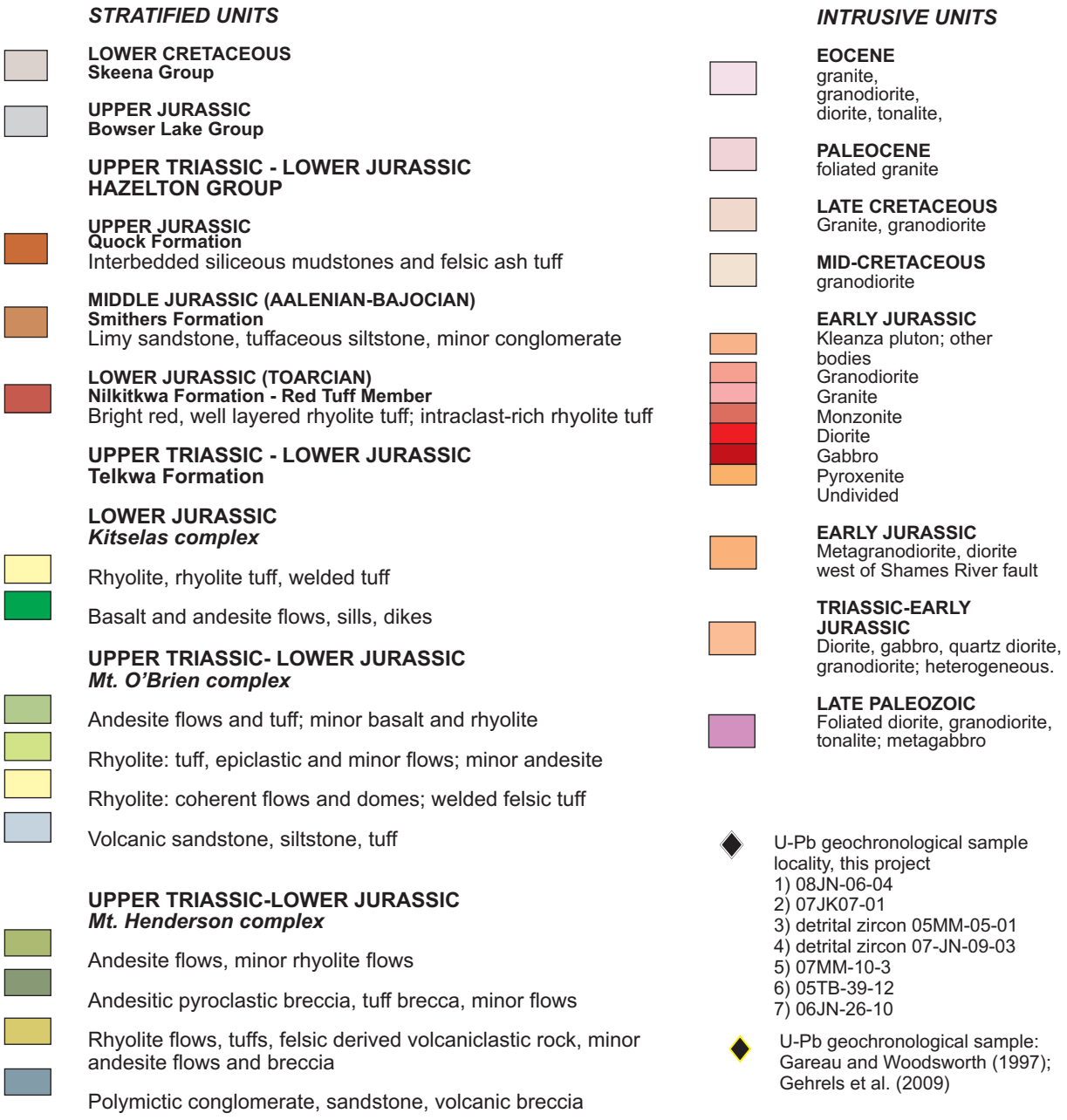

Fig. 3-2. Geology of the Terrace area. Note i) three volcanic complexes of the Telkwa Formation, Mount Henderson in the south, Mt. O'Brien in the north, and Kitselas to the northwest; (ii) the Telkwa Formation lies above narrow sections of Stuhini Group and Ambition Fm. in central map area, and above Mt. Attree Fm. in southern areas indicating a deepening of an unconformable contact southward; (iii) juxtaposition of Paleozoic (Mt. Attree Fm.) over Jurassic rocks across the Skeena River fault; and iv) the presence of the tri-part upper Hazelton marker units overlying Telkwa Formation on both sides of the Skeena River fault.

In west-central Stikinia, near Terrace (Fig. 3-2), the lower Hazelton Group is represented by the Telkwa Formation, defined in the Smithers area by Tipper and Richards (1976). The Telkwa Formation rests unconformably above the Stuhini Group (Triassic) and the Zymoetz Group (upper Paleozoic; Nelson et al. 2006, 2007, 2008a, b; Figs. 2, 3). Near Terrace, the Telkwa Formation comprises three volcanic centres referred to herein as the Mt. Henderson, Mt. O'Brien, and Kitselas volcanic-intrusive complexes (Fig. 3-2, 3-3, 3-4). The upper Hazelton Group is represented by the Red Tuff Member (Nilkitkwa Formation; Lower Jurassic), the Smithers Formation (Middle Jurassic) and the Quock Formation (Upper Jurassic; Gagnon et al 2012), and is overlain by sedimentary rocks of the Bowser Lake Group (Figs. 2, 3, 4).

3.4 Stratigraphic Elements of the Lower Hazelton Group

3.4.1 Basal Unconformity

The Telkwa Formation fills an erosional surface cut into Stuhini Group sedimentary rocks, and Permian limestone (Ambition Formation) and deformed volcanic rocks (Mt. Attree Formation) of the Zymoetz Group. The overall low-angle unconformity cuts gradually down-section from the north, where Telkwa Formation basal conglomerates lie on Stuhini Group, to the south where they typically lie on lower portions of Ambition Formation limestone (Fig. 3-5A), or on Mt. Attree Formation volcanic rocks (Fig. 3-2). Where the basal Telkwa Formation conglomerate lies on the Mt. Attree Formation, at least 200 metres of section has been removed by erosion. Greenschist-grade metavolcanic rocks of the Mt. Attree Formation are in part penetratively foliated and isoclinally folded. Both the Stuhini Group and underlying Ambition Formation lack a penetrative foliation, suggesting a pre-Permian deformational event. There is no evidence for folding of the Permian and Triassic units prior to deposition of the Telkwa Formation. Local sharp, small-scale relief on the unconformity surface contrasts with its overall low angle to underlying layering.

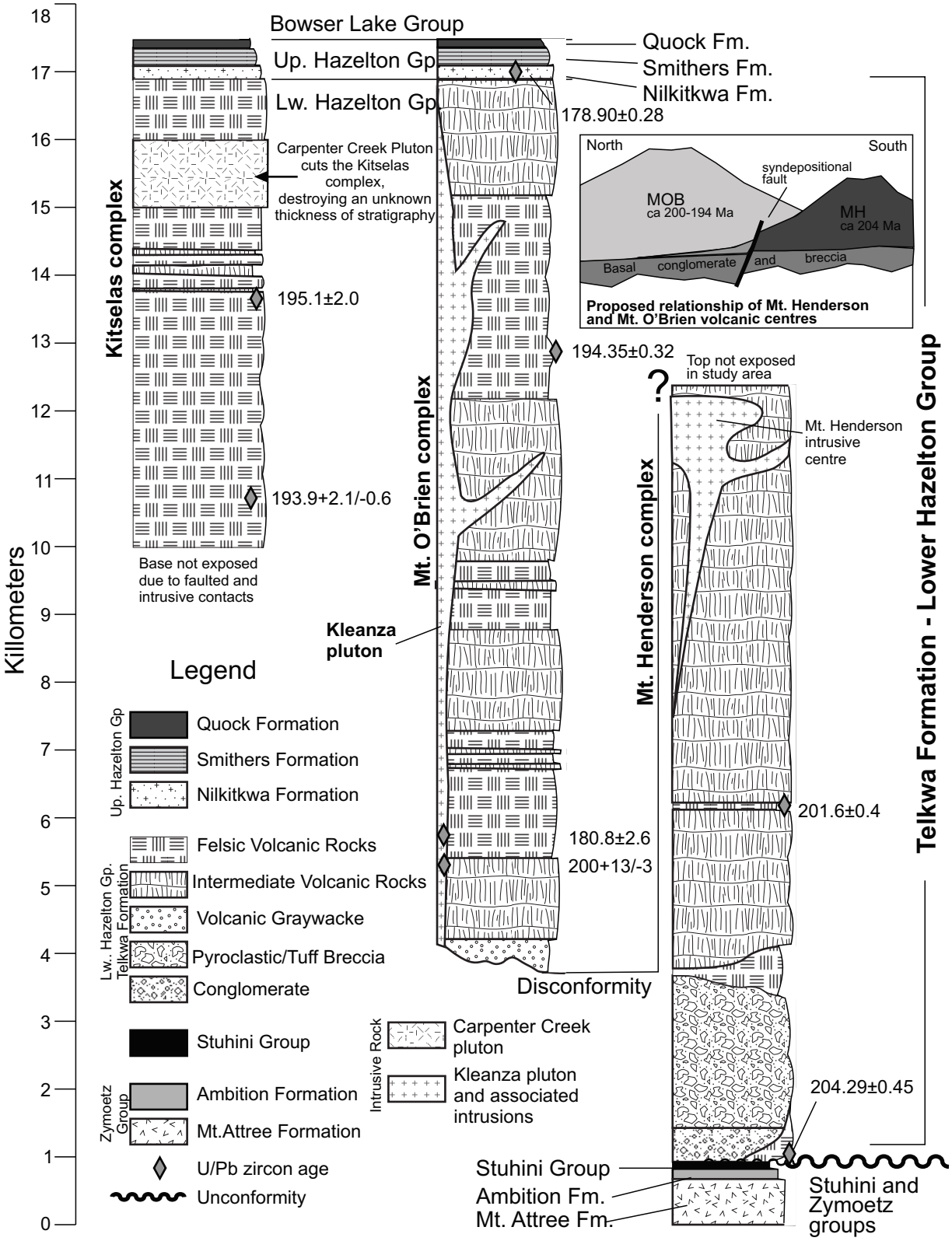

Fig. 3-3. Stratigraphic columns scaled to thickness. Note the basal unconformity beneath the Mt. Henderson complex and disconformity that separates the base of the Mt. O'Brien complex from the lower portion of the Mt. Henderson complex. Also note the significant differences in the abundances of felsic vs. intermediate volcanics between complexes. The columns show ≈16 km thickness of Hazelton Group stratigraphy.

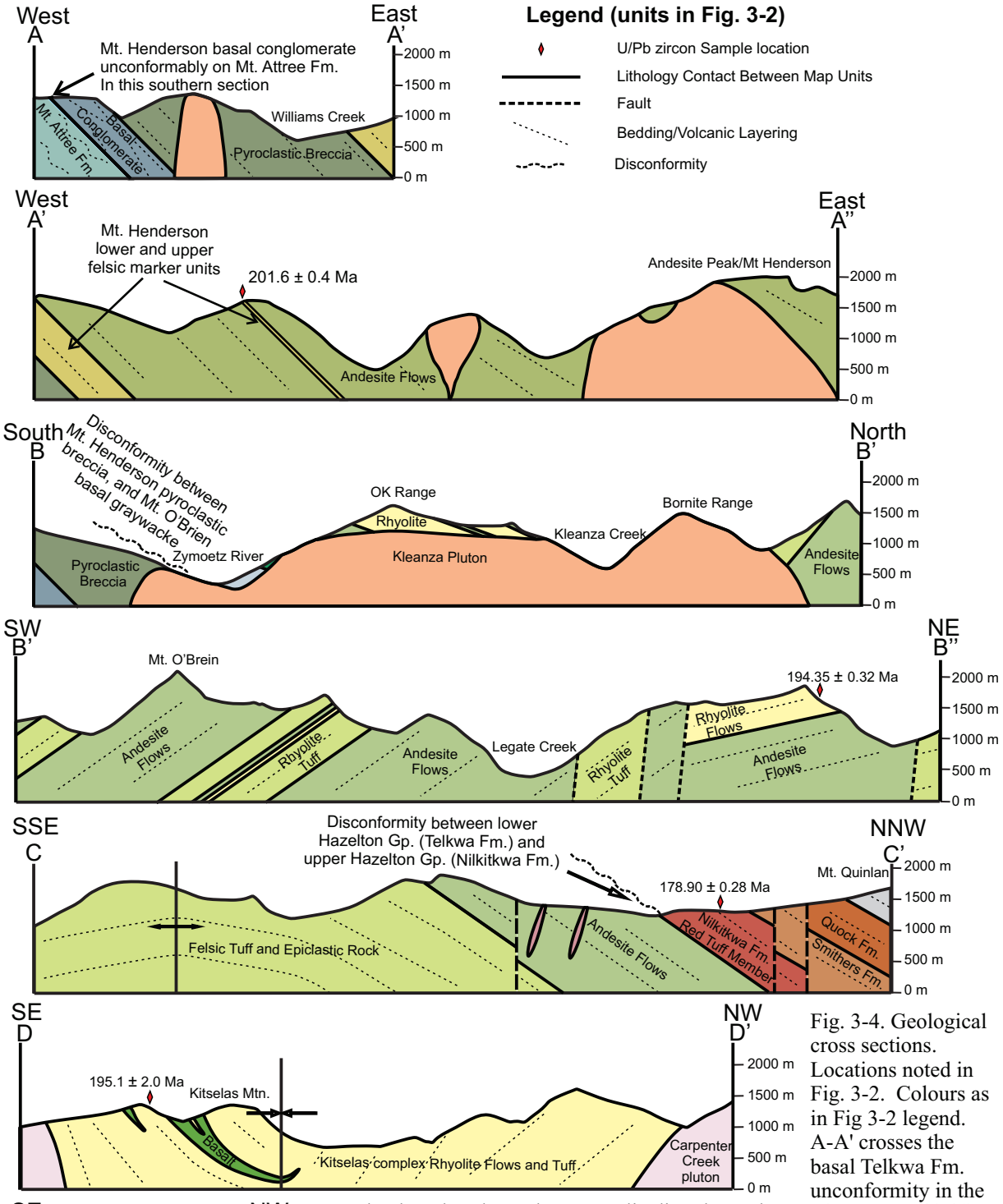

Fig. 3-4. Geological cross sections. Locations noted in Fig. 3-2. Colours as in Fig 3-2 legend. A-A' crosses the basal Telkwa Fm. unconformity in the south where basal conglomerates lie directly on the Mt. Attree Fm. A'-A" shows a thick accumulation of andesitic volcanics that form the Mt. Henderson complex. B-B' crosses the disconformity between the base of the Mt. O'Brien and Mt. Henderson complexes. It also shows the syn-volcanic Kleanza pluton, which cores the Mt. O'Brien complex. B'-B" and C'-C' and D=D'' show the very thick accumulation of intermediate and felsic volcanic rock that comprise the Mt. O'Brien and Kitselas complexes. D"-D'" shows that the Kitselas complex is overlain by the same upper Hazelton Group strata as the Mt. O'Brien complex (C-C").

3.4.2 Mt. Henderson Complex

Basal conglomerates

The base of the Mt. Henderson complex consists of polymictic conglomerate, up to 500 m thick, with less abundant sandstone and volcanic breccia interbeds (Figs. 3, 4A-A', B-B'). At its base, the conglomerate contains coarse subangular clasts derived from underlying Mt. Attree Formation volcanic rocks, Ambition Formation limestone, and Stuhini Group chert and argillite (Fig. 3-5B). It grades upward into a polymictic, matrix-supported conglomerate that includes volcanic intraclasts. Sandstone intervals and volcanic intraclasts increase upsection. The conglomerate locally pinches out, placing an overlying pyroclastic breccia unit directly on the basal unconformity. The highly variable thickness of the basal conglomerate and the presence of locally derived clasts indicates significant syn-depositional relief, possibly the result of penecontemporaneous block faulting superimposed on the gentle basal unconformity.

Basal felsic volcanic rocks

Several small felsic bodies outcrop near the base of the Mt Henderson complex, and at least one large felsic volcanic centre is exposed at Mt. Pardek between the Zymoetz River and Kleanza Creek (Fig. 3-2). At Mt Pardek, approximately 1100 metres of well-bedded felsic crystal tuffs and rhyolite unconformably overlie Permian limestone. Rhyolite at the base of Mt. Pardek extruded through the underlying limestone regolith or talus (Fig. 3-5C), leaving a transitional contact that grades from rhyolite-cemented limestone breccia to coherent rhyolite with entrained limestone xenoliths. Unlike the dark green and red plagioclase-porphyritic intermediate volcanic rocks that typify higher stratigraphic levels of the Telkwa Formation (Fig. 3-5D,E,F), these felsic rocks have a waxy, semi-translucent pale-green appearance and commonly contain abundant euhedral, vitreous quartz-eye phenocrysts. The basal felsic volcanic rocks erupted from a series of localized felsic centres which generated voluminous explosive material and minor rhyolite flows proximal to the centres. Few intact rhyolite centres are exposed at the base of the Telkwa Formation, but in places the basal conglomerate consists mainly of locally-derived felsic clasts.

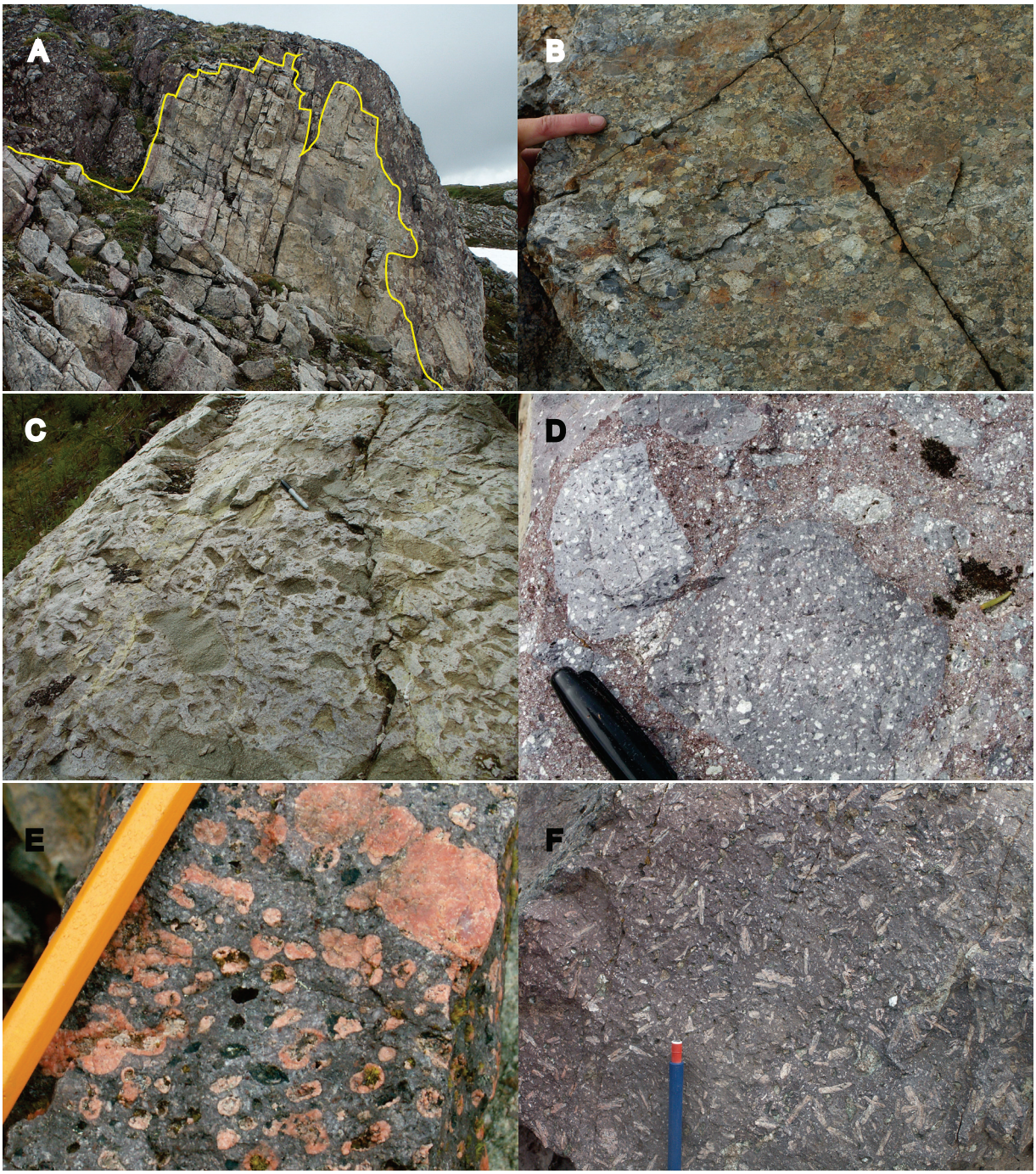

Fig. 3-5. Photographs of Telkwa Formation. A) Telkwa Formation basal conglomerate unconformably overlying Ambition Formation limestone. The unconformity surface is highly irregular and largely controlled by jointing in the limestone. The Telkwa Formation locally consists mainly of limestone clasts. B) Mt. Henderson complex, typical polymictic basal conglomerate with subangular to subrounded clasts of Stuhini Group shale (black), Ambition Formation limestone (light gray), and intraformational feldspar porphyry volcanic fragments. C) Rhyolite at the base of the Telkwa Formation, Mt. Henderson complex, which has intruded through, and incorporated clasts of Ambition Formation limestone. D) Typical pyroclastic breccia deposits, Mt. Henderson complex, with plagioclase phenocrysts in clasts and matrix. E) Mt. O'Brien complex, andesitic flows with vesicles and heulandite + chlorite + calcite amygdules. F) Mt. O'Brien complex, andesitic flows with abundant subhedral to euhedral, blocky to bladed feldspar phenocrysts.

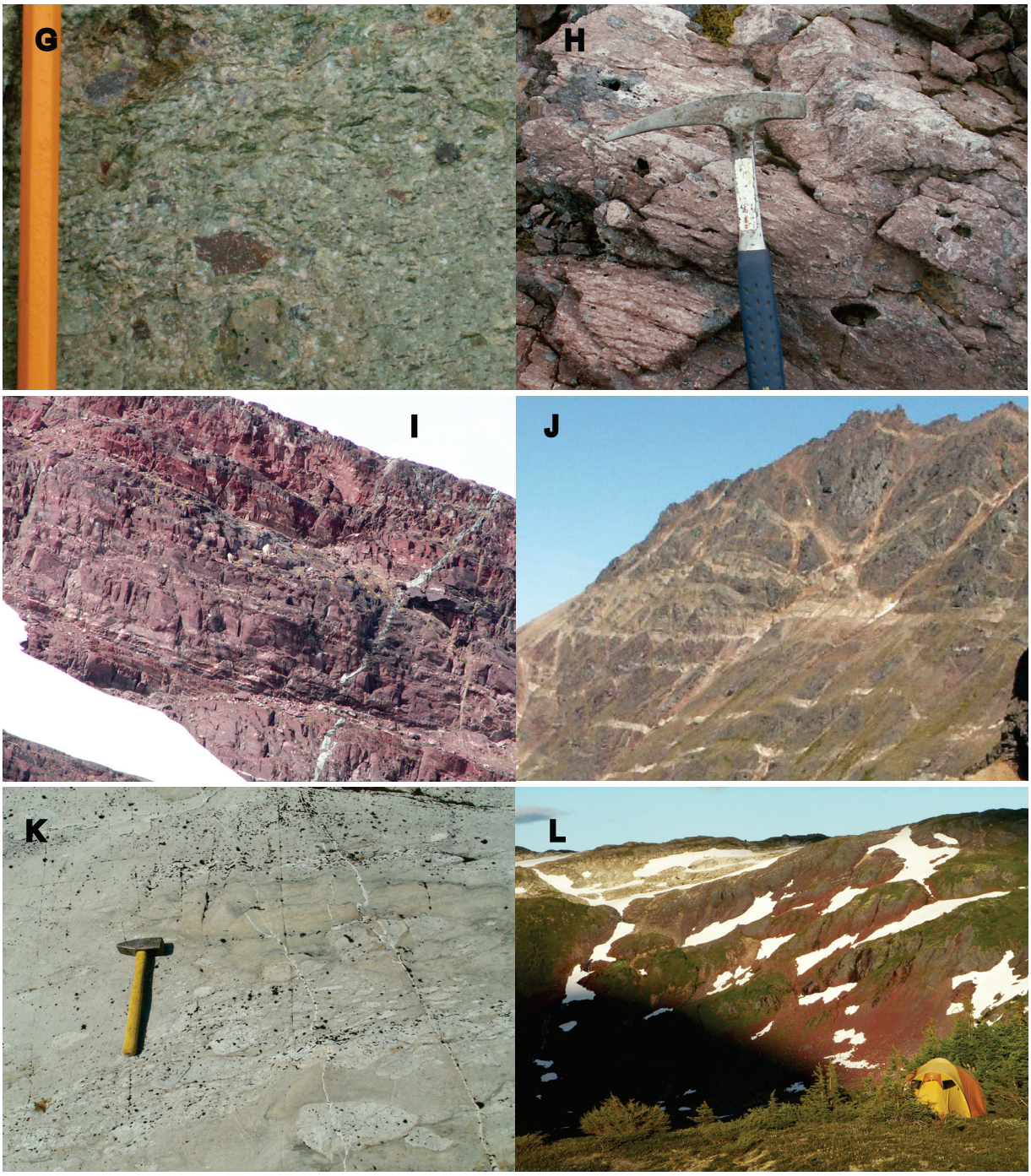

Fig. 3-5 cont'd. G) Mt. O'Brien complex ignimbrite with strongly welded green pumice fragments and more angular rhyolite clasts. H) Mt. O'Brien complex, lithophysae in rhyolite. I) Well-stratified Red Tuff member of the Nilkitkwa Formation. Approximate height of cliff-face: 100m. J) Mt. O'Brien complex, Kleanza pluton-related dikes cutting Telkwa Formation volcanic rocks, Mount O'Brien. K) Kitselas complex, thickly bedded felsic tuff with layers that contain abundant rhyolite lapilli. L) Gray sandstones of the Smithers Formation disconformably overlie red tuffs of the Nilkitkwa Formation.

Pyroclastic Unit

The basal conglomerate and felsic volcanic rocks interfinger with, and grade upward into, a 2000 to 2500 metre-thick unit of thickly bedded pyroclastic breccia with local thin intermediate volcanic flows, volcanically derived mudstone and sandstone, and rhyolitic lapilli and vitric-crystal tuffs (Fig. 3-4A-A', B-B'). Both groundmass and pyroclasts contain small (2-5 mm long), stubby, euhedral to subhedral plagioclase phenocrysts in a fine-grained holocrystalline groundmass (Fig. 3-5D); hornblende and clinopyroxene phenocrysts are rare. Overlying andesite and rhyolite flows also have abundant plagioclase phenocrysts, but these are up to 1 cm long and display distinct bladed or blocky habits. Although the pyroclastic breccia is compositionally homogeneous, textural variations include differences in the proportion and size of plagioclase phenocrysts, and the size, shape, and colour of pyroclasts.

Andesitic flow unit

The pyroclastic unit is overlain by nearly 9 km of plagioclase-porphyritic and amygdaloidal andesitic flows and local coarse, heterolithic andesitic breccias that were derived from erosion of proximal volcanic edifices. Amygdules and scattered large irregular cavities are filled with laumontite, quartz, epidote, chlorite, prehnite and pumpellyite (Mihalynuk 1987). The unit contains two laterally continuous felsic marker intervals. The lower is 100-800 m thick, and overlies the pyroclastic unit; the upper felsic marker unit lies about 2500 m upsection (Fig. 3-3, 3-4 A'-A''). Felsic lithologies include flow-banded rhyolite, welded tuff, bedded vitric-crystal tuff, and felsic breccia. Variations in thickness and extreme heterogeneity of lithologies within the felsic units indicate that a number of volcanic eruptive centres are represented.

Centred around the present day Mt Henderson massif (Fig. 3-2) is a transitional contact between intrusive stocks and dikes, and the roughly coeval andesitic volcanic rocks that they intruded. Structural orientations of volcanic layering, which are typically ENE facing, are roughly concentric around the massif, indicating that it is the core of an ancient stratovolcano.

3.4.3 Mt. O'Brien Complex

The Mt. O'Brien complex is cored by the Kleanza pluton (Figs. 3-2, 3-3, 4B-B'). The complex lies above the basal conglomerate, felsic centres, and pyroclastic breccia units that form the lower part of the Mt. Henderson complex. The lowermost unit consists of well-bedded maroon and green, volcanogenic graywacke, siltstone, and minor conglomerate and waterlain tuff. From a few metres up to 500 m thick, the unit drapes an irregular paleotopography, thickening in depressions and thinning over paleotopographic highs. It is interpreted to represent denudation and erosion during a period of volcanic quiescence following deposition of voluminous pyroclastic flows on the northern flank of the Mt. Henderson complex. Above the basal unit is a 5-12 km thick section of predominantly andesitic and rhyolitic flows centred near the Bornite range, 30 kilometres north of the inferred Mt. Henderson volcanic centre.

Andesitic and rhyolitic flow unit

The main constituents of the Mt. O'Brien complex are andesitic and rhyolitic flows, pyroclastic breccias, and thin basalt flows (Figs. 2, 4B-B', B'-B''). Near the Bornite Range, the unit is 12 km thick; near Legate Creek to the north it thins to about 5 km (Fig. 3-2). Andesites are characteristically plagioclase-glomeroporphyritic and amygdaloidal (Fig. 3-5E). Amygdules range from mm-scale ovals to cm-scale irregular cavities and are filled with laumontite, heulandite, calcite, quartz, epidote, chlorite, and/or pumpellyite. Plagioclase phenocrysts are typically tabular crystals, 5-10 mm long, with straight edges and subhedral terminations (Fig. 3-5F). Some flows contain clinopyroxene phenocrysts. Eruptive units define large (> 100 metres wide) lobes with steep to gently sloping margins.

The Mt. O'Brien complex contains several rhyolitic centres (Figs. 2, 3, 4B-B', B'-B''). Felsic intervals consist of coherent rhyolite as flows, flow breccias, domes, and cryptodomes and related pyroclastic rocks, with minor interbedded mafic and intermediate flows. Rhyolitic pyroclastic rocks include massive to thickly bedded pyroclastic breccia, highly siliceous well-bedded vitric tuff, and ignimbrite deposits with

siliceous lithic fragments and strongly welded pumice clasts (Fig. 3-5G). Interbedded coarse epiclastic sandstones indicate coeval reworking of rhyolite and pyroclastic deposits. Coherent rhyolite and rhyolite fragments in tuffs range from aphanitic to porphyritic, with 1-4 mm angular subhedral to anhedral K-feldspar and/or plagioclase phenocrysts. They are commonly flow-banded and spherulitic, and locally contain lithophysae (Fig. 3-5H). Felsic lapilli in tuffs commonly have strongly eutaxitic rims. Local reworked pyroclastic breccia clasts indicate multiple explosions from the same centre. The irregular geometry of felsic intervals (Fig. 3-2) is the result of an uneven depositional topography, probably on the slopes of a stratovolcano, where rhyolitic lava and pyroclastic flows first filled lows between 100 metre-scale lobes of andesite, and then deposited uniform pyroclastic drapes. The top of the andesitic and rhyolitic flow unit is overlain, with apparent conformity, by the distinct Red Tuff Member (Nilkitkwa Formation), which consists of well-bedded red tuff and resedimented volcanic deposits (Fig. 3-5I).

The Mt. O'Brien complex was intruded by the multi-phase Kleanza pluton (200 + 13/-3 Ma, Gareau et al. 1997a; 180.8 ± 2.6 Ma, Gehrels et al. 2009), and by younger Eocene granites of the Carpenter Creek pluton. The core of the Kleanza pluton, as exposed on the OK Range, is equigranular, medium-grained biotite granite and granodiorite. Border phases include stocks and dikes that cross-cut both the pluton and volcanic rocks (Fig. 3-5J), and near the peak of Mt. O'Brien, amygdaloidal andesitic flows grade transitionally into an andesite dike swarm of identical texture and composition. Breccias near the contact contain clasts derived from the pluton, and the pluton contains volcanic xenoliths. Based on these observations, we interpret the Kleanza pluton and Telkwa Formation to be co-magmatic.

Volcanic layering in the Mt. O'Brien complex generally dips to the east-northeast, but in the area around the Kleanza pluton the layering is variable and tends to wrap around the pluton. This pattern is interpreted to represent deposition of flows and coarse breccia units on the slopes of a former stratovolcano centred around the current location of the Kleanza pluton. By contrast, steeply-dipping, south-facing layers on the northern side of

the Kleanza pluton were probably tilted towards the intrusion during syn-intrusive block faulting, which would have also controlled the somewhat elongate distribution of the pluton (Fig. 3-2).

3.4.4 The Kitselas Complex

The Kitselas complex (195 ± 2.0 Ma, 193 +2.1/-0.6 Ma, Gareau et al. 1997a) is a 4.5 km thick succession of mainly felsic volcanic rocks (Fig. 4D-D', D''-D''') exposed along the Skeena River and west into the Kitselas Mountain area, and as remnants north of the Carpenter Creek pluton (Fig. 2). It lies in the footwall of a regional thrust fault (Skeena River fault), the trace of which follows the east side of the Skeena River valley (Figs. 2, 3). Nelson and Kennedy (2007) document 12 km of NE directed thrust-related displacement across the fault. However, Gareau et al. (1997b) interpreted the Skeena River fault as a detachment fault responsible for unroofing the Kitselas complex which was interpreted, based on its higher metamorphic grade (upper greenschist) relative to other Telkwa Formation rocks (zeolite to lower greenschist), to be an exhumed core complex. Therefore, we propose a two stage history of motion on the Skeena River fault: 1) early north-northeasterly directed thrust faulting, and 2) subsequent local detachment faulting east of Kitselas Mountain. The early NE directed thrust faulting, which was responsible for the imbrication of the Stikinian stratigraphic section (Fig. 2), is attributable to the regional mid-Cretaceous northeast-directed Skeena fold and thrust belt (Evenchick 2001). Subsequent normal motion on the fault, which was responsible for exhumation of the Kitselas complex from a deeper crustal level, is consistent with Eocene unroofing and detachment faulting in the Coast Mountains to the west (Rushmore et al. 2005).

The stratigraphically lowest exposed part of the Kitselas complex consists of coherent flow-banded white, gray and buff-coloured aphanitic rhyolite and locally-derived rhyolite agglomerate. Higher units in the complex are mostly thick-bedded volcaniclastic rock, including moderately to strongly welded lapilli and crystal tuff (Fig. 3-5K). Sparse beds of felsic agglomerate and ash flow tuff (Nelson et al. 2006) and a few thin basaltic and andesitic flows and associated dikes are also present (Fig. 3-2). The top of the Kitselas

complex, exposed in Maroon Creek, is separated from the main bulk of the complex by the Carpenter Creek pluton (Eocene; Gareau et al. 1997a, b). Here, the uppermost rocks are rhyolitic flows and tuff similar to those near the top of the Mt. O'Brien complex. One fault-bounded panel in Maroon Creek contains a thin unit of felsic tuff texturally similar to that in the main Kitselas complex to the south.

3.4.5 Upper Hazelton Group

Red Tuff Member, Nilkitkwa Formation

The Red Tuff Member of the Nilkitkwa Formation, formerly considered the "Red Tuff unit" of the Smithers Formation (Tipper and Richards 1976, Gagnon et al 2012), overlies the Mt. O'Brien and Kitselas complexes (Fig. 3-3, 3-4C-C', D''-D'''). It is a 200 m-thick succession of thin-bedded, fine-grained maroon felsic tuffs, with lesser interbedded thin amygdaloidal basaltic flows and, in places, very thin (approximately 10-30 cm) limestone layers. It has a paraconformable contact with underlying volcanic flows and felsic pyroclastic deposits and a disconformable and abrupt upper contact with brown bivalve-bearing sandstones and tuffs of the Smithers Formation (Fig. 3-5L; Gagnon et al. 2012). The Red Tuff Member represents the waning stage of volcanism in the Hazelton Group. A regionally extensive marker unit at the top of the member consists of brick red, strongly indurated vitric and crystal tuff with mm-scale angular anhedral, plagioclase crystals and large (up to 40 cm diameter) deformed sub-rounded clasts scavenged from underlying well-bedded tuffs and limestone. These unusual clasts show evidence of violent incorporation, as they commonly consist of large layered clasts, that have been plastically deformed and "metamorphosed" by the pyroclastic material that entrained them. Gagnon et al. (2012) interpreted the disconformity that separates the Nilkitkwa Formation from the overlying Middle Aalenian to Early Bajocian Smithers Formation to span 2 million years.

Smithers and Quock Formations

Near Terrace (Figs. 2, 3, 4C-C', D''-D'''), the Smithers Formation is a Middle Aalenian to Early Bajocian, 265 m-thick accumulation of siliciclastic sedimentary rocks (Gagnon et

al. 2012). The section consists of a 10 m-thick conglomerate that is overlain by interbedded limey sandstone and tuffaceous siltstone with abundant ammonoids and bivalves (Gagnon et al. 2012), and a unit of gray siltstone.

The Quock Formation is a regionally extensive unit of bedded siliceous mudstones and white to orange vitric tuff which are about 120 metres thick on Mt. Quinlan (Fig. 3-2; Gagnon et al. 2012). They are overlain by laminated partial Bouma sequences of sandstone and siltstone of the Bowser Lake Group.

3.5 Geochronology

3.5.1 Results

We present five new uranium-lead (U-Pb) chemical-abrasion thermal-ionization-mass-spectrometry (CA-TIMS) zircon ages from volcanic rocks of the Telkwa and Nilkitkwa formations, and two new (U-Pb) laser-ablation inductively-coupled-plasma mass-spectrometry (LA-ICP-MS) detrital zircon analyses from fragmental rocks at the base of the Telkwa Formation. Sample locations are displayed on Figs. 2 and 3, analytical results are presented in Table 3-1 and Appendix B.1, and analytical methods are described in Appendix C.

3.5.1.1 CA-TIMS U-Pb Zircon Results

Sample 08JN06-04 was collected from the Mt. Pardek rhyolitic centre at the base of the Mt. Henderson complex. Zircon recovery was low and nearly all very fine-grained. Two zircons, coarse enough to be analysed as single grains, give concordant and overlapping results that provide the basis for a weighted $^{206}Pb/^{238}U$ age of 204.29 ± 0.45 Ma (Fig. 3-6A; Table 3-1). This is considered a reasonable estimate for the crystallization age of the rock.

Table 3-1 TIMS U/Pb Zircon Geochronology Data Table

U-Th-Pb isotopic data

	Compositional Parameters								Radiogenic Isotope Ratios									Isotopic Ages					
	Wt.	U	Th	Pb	$^{206}Pb^*$	mol %	Pb^*	Pb_c	^{206}Pb	^{208}Pb	^{207}Pb		^{207}Pb		^{206}Pb		corr.	^{207}Pb		^{207}Pb		^{206}Pb	
Sample	mg	ppm	U	ppm	x10^{-13} mol	$^{206}Pb^*$	Pb_c	(pg)	^{204}Pb	^{206}Pb	^{206}Pb	% err	^{235}U	% err	^{238}U	% err	coef.	^{206}Pb	±	^{235}U	±	^{238}U	±
05TB39-12	**UTM Location:** Datum - NAD83, UTM Zone -9, Northing - 6065425, Easting -559420																						
A	0.006	392	0.360	12.4	2.9964	98.94%	27	2.63	1742	0.114	0.049853	0.506	0.210260	0.604	0.030589	0.254	0.563	188.14	11.78	193.77	1.06	194.23	0.48
B	0.004	358	0.326	11.2	1.8275	99.06%	31	1.42	1969	0.103	0.049789	0.771	0.210210	0.855	0.030621	0.224	0.486	185.16	17.96	193.73	1.51	194.43	0.43
C	0.005	118	0.473	6.2	0.9096	89.84%	3	8.45	182	0.151	0.051240	3.298	0.261310	3.499	0.036987	0.512	0.454	251.64	75.87	235.72	7.36	234.13	1.18
D	0.004	265	0.349	8.4	1.3352	98.35%	18	1.82	1124	0.111	0.049882	1.410	0.207672	1.515	0.030195	0.369	0.398	189.48	32.80	191.60	2.65	191.77	0.70
08JN06-04	**UTM Location:** Datum - NAD83, UTM Zone -9, Northing - 6045121, Easting - 5571040																						
B	0.001	165	0.434	7.6	0.2211	89.24%	2	2.18	172	0.138	0.050296	6.272	0.222345	6.548	0.032062	0.650	0.465	208.71	145.38	203.86	12.09	203.44	1.30
C	0.001	233	0.219	8.3	0.3129	95.95%	7	1.08	456	0.070	0.050445	2.227	0.224077	2.349	0.032216	0.241	0.545	215.56	51.56	205.30	4.37	204.41	0.48
07JK07-01	**UTM Location:** Datum - NAD83, UTM Zone -9, Northing - 6006266 , Easting - 555652																						
A	0.004	219	0.356	7.5	1.1010	97.58%	12	2.25	761	0.113	0.050084	0.563	0.219345	0.647	0.031764	0.177	0.577	198.88	13.08	201.36	1.18	201.58	0.35
B	0.004	150	0.410	5.2	0.7284	98.13%	15	1.14	986	0.130	0.049911	0.964	0.222207	1.053	0.032289	0.203	0.516	190.84	22.41	203.74	1.94	204.86	0.41
C	0.007	124	0.432	4.2	1.0795	99.02%	30	0.87	1895	0.137	0.050070	0.516	0.222475	0.653	0.032225	0.334	0.624	198.26	11.97	203.97	1.21	204.46	0.67
D	0.006	68	0.486	2.4	0.5185	97.70%	13	1.00	803	0.157	0.050743	3.247	0.215931	3.516	0.030863	0.787	0.440	229.15	75.00	198.52	6.34	195.95	1.52
E	0.007	120	0.464	3.9	1.0153	98.62%	21	1.17	1336	0.149	0.050555	1.332	0.210997	1.578	0.030270	0.736	0.541	220.60	30.82	194.39	2.79	192.24	1.39
07MM-10-3	**UTM Location:** Datum - NAD83, UTM Zone -9, Northing - 6023013, Easting - 543533																						
A	0.002	787	0.469	27.8	2.1887	99.21%	38	1.43	2351	0.149	0.050182	0.287	0.230664	0.442	0.033338	0.290	0.769	203.42	6.66	210.75	0.84	211.40	0.60
B	0.003	609	0.378	20.6	2.5879	99.39%	48	1.31	3030	0.121	0.050441	0.436	0.228543	0.640	0.032861	0.424	0.737	215.36	10.08	209.00	1.21	208.43	0.87
C	0.004	473	0.391	16.1	2.4659	99.25%	39	1.53	2460	0.124	0.050240	0.230	0.228187	0.683	0.032941	0.622	0.942	206.12	5.32	208.70	1.29	208.93	1.28
D	0.003	322	0.383	11.3	1.2523	98.66%	22	1.40	1376	0.122	0.050392	0.399	0.231421	0.487	0.033307	0.189	0.618	213.10	9.25	211.37	0.93	211.22	0.39
E	0.005	473	0.449	16.9	3.1325	98.40%	18	4.20	1151	0.143	0.050324	0.397	0.229668	0.552	0.033100	0.325	0.704	210.00	9.20	209.92	1.05	209.92	0.67
06JN20-8	**UTM Location:** Datum - NAD83, UTM Zone -9, Northing - 6076584, Easting - 556100																						
F	0.003	184	0.446	5.8	0.6478	97.49%	12	1.37	736	0.142	0.050	1.317	0.192	1.423	0.028	0.227	0.53	175.56	30.71	178.50	2.33	178.72	0.40
G	0.003	134	0.305	4.1	0.4719	97.45%	11	1.01	727	0.097	0.049	1.086	0.192	1.184	0.028	0.232	0.50	167.60	25.37	178.26	1.94	179.06	0.41
H	0.003	63	0.160	2.2	0.2613	96.51%	8	0.78	531	0.052	0.051	6.255	0.236	6.679	0.033	0.716	0.63	257.75	143.71	215.35	12.96	211.49	1.49
I	0.003	66	0.463	2.2	0.2334	96.41%	8	0.72	515	0.150	0.051	3.046	0.196	3.297	0.028	0.771	0.43	218.49	70.49	181.90	5.49	179.09	1.36

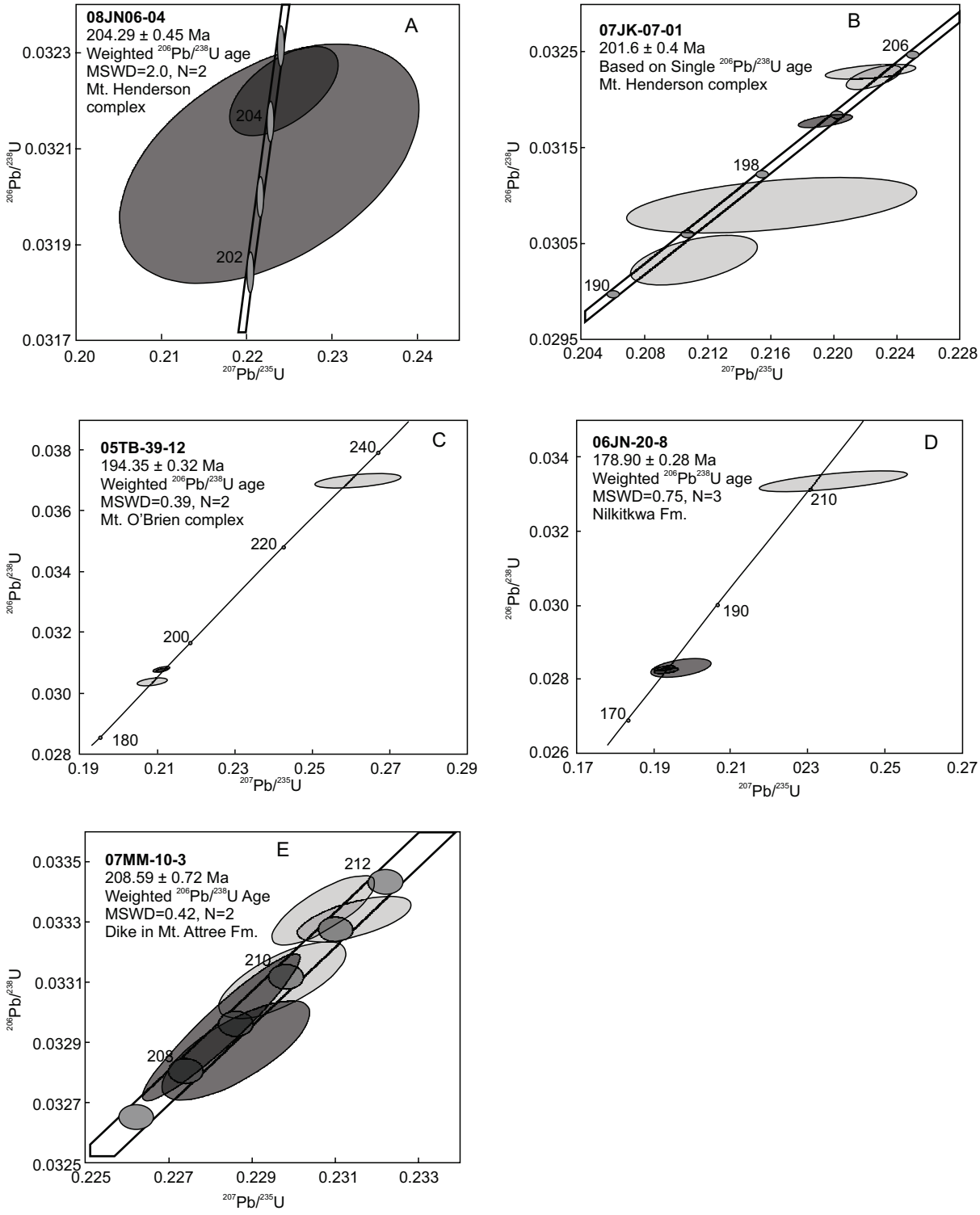

Fig. 3-6. Concordia diagrams for thermal-ionization-mass-spectrometry (TIMS) U/Pb zircon analyses. All ellipses represent 2 σ error. Dark coloured ellipses represent dates used to calculate the given ages. The data indicate a ca. 204 Ma. initiation of volcanic activity in the Telkwa Fm. (A), and continuation of volcanism until at least ca 194 Ma (C); waning volcanism represented in the Red Tuff Member of the Nilkitkwa Fm. occurred as late as ca 179 Ma (D). *S*ee text for details.

Sample 07JK07-01 was collected from a welded tuff with sparse mudstone xenoliths in the higher of two felsic intervals in the middle of the Mt. Henderson complex, approximately 6 km upsection from the rhyolitic center at the base of the complex. Five single and multi-grain analyses from this sample yield results that are concordant between about 205 and 192 Ma (Fig. 3-6B; Table 3-1). This range of ages is thought to reflect both the presence of xenocrystic grains for the older, and Pb loss for the younger, results. It is likely that the two younger and marginally concordant fine fractions retained grain sectors affected by Pb loss. The remaining three analyses lie squarely on concordia, two at ca. 205 Ma and one single grain analysis at ca. 202 Ma. Given the position of this tuff unit well above the ca. 204 Ma rhyolite centre at the base of the Mt. Henderson complex, the younger of these grains, with a $^{206}Pb/^{238}U$ date of 201.6 ± 0.4 Ma is considered as the best estimate for the age of the rock. The two older grains are interpreted as xenocrystic zircon in this tuffaceous rock, possibly derived from units in the lower portions of the Mt. Henderson complex.

Four single and multi-grain fractions were analysed from a rhyolite in the upper part of the Mt. O'Brien complex (Sample 05TB39-12). Concordant and overlapping results from two single grain analyses give a weighted $^{206}Pb/^{238}U$ age of 194.35 ± 0.32 Ma, considered as the best estimate for the crystallization age of this rock (Fig. 3-6C; Table 3-1). A multi-grain (n=4) finer fraction at ca. 192 Ma provides an absolute minimum age and an older multi-grain (n=3) analysis with results at ca. 235 Ma likely contains inherited or xenocrystic components.

Sample 06JN20-8 was collected from the brick-red marker tuff unit at the top of the Nilkitkwa Formation. Of four single zircon grains analysed three yield concordant and overlapping results that provide the basis for a weighted $^{206}Pb/^{238}U$ age of 178.90 ± 0.28 Ma (Fig.6D; Table 3-1). A fourth analysed grain with results that intersect concordia at ca. 211 Ma is interpreted to be xenocrystic or to contain an older inherited core.

Sample 07MM10-03 was collected from a quartz-feldspar porphyry dike that cuts the Paleozoic Mt. Attree Formation. Five analysed single zircon grains give concordant

results ranging from about 212 to 209 Ma. While we favour a weighted $^{206}Pb/^{238}U$ age of 208.59 ± 0.72 Ma, based on the younger two grains, we cannot rule out that these zircons may still retain sectors disturbed by minor Pb loss and that the older two grains at ca. 211 Ma could record the crystallization age of this rock. (Fig. 3-6E; Table 3-1).

3.5.1.2 Detrital Zircon LA-ICP-MS Results

Sample 07JN09-03 was collected from a sandstone bed within a volcanic-dominated conglomerate near the base of the Mt. Henderson complex basal conglomerate. The zircon yield from this sample was low with only 40 grains coarse enough for analysis; 35 of these are <10% discordant with $^{206}Pb/^{238}U$ date 2σ errors ranging from 0.9% to 10% (Appendix B.1). Thirty-five grains define a population with $^{206}Pb/^{238}U$ dates ranging from 211 ± 6 to 233 ± 5 Ma, with a peak at 221 Ma; a single grain has a $^{206}Pb/^{238}U$ date of 253 Ma (Fig. 3-7A).

Sample 07MM05-01 was collected from a volcanogenic sandstone, with a reworked felsic ash and lapilli component, near the top of the Mt. Henderson complex basal conglomerate. Of 60 zircons analysed, 50 were <10% discordant. The zircon ages are mainly distributed between 199.8 Ma and 228.6 Ma, with an asymmetric peak at 210 Ma, including a shoulder at 205 Ma; a single grain yielded an age of 289.6 Ma (Fig. 3-7B).

3.5.2 Discussion of Geochronology

A compilation of new and previously documented geochronological data in the Terrace area places constraints on: 1) age; 2) rate of deposition; and 3) magma/sediment sources, of the Telkwa Formation (Fig. 3-8). The rhyolite center at the base of the Mt. Henderson complex with a U-Pb zircon age of 204.29 ± 0.45 Ma, confirms that Telkwa Formation volcanism in the Terrace area initiated in the Late Triassic. Approximately 6 km of volcanic rocks accumulated at the Mt. Henderson complex before felsic volcanics of the "upper marker unit" erupted at ca. 201.6 Ma, approximately at the Triassic-Jurassic boundary. Late Triassic initiation of volcanism is also supported by the presence of two ca. 205 Ma zircon in the "upper marker unit" sample, interpreted to be xenocryts, which

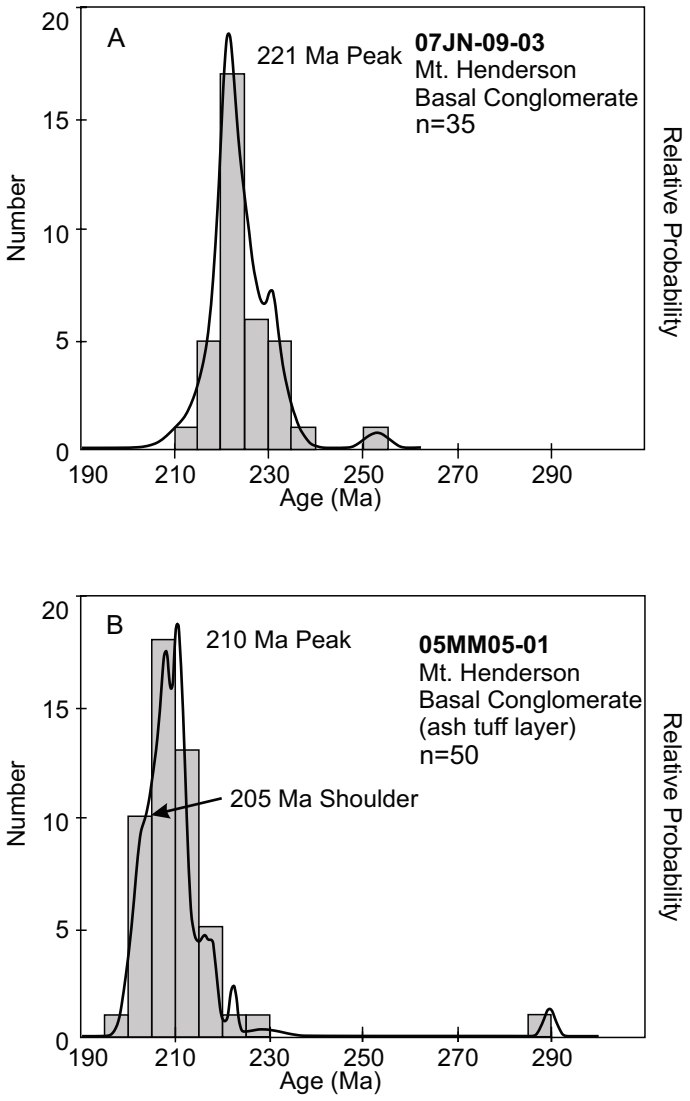

Fig. 3-7. Relative probability plots for detrital zircon samples collected from the base of the Telkwa Fm. Both samples contain mainly Late Triassic zircon and a single Permian zircon. The 205 Ma shoulder in sample 05MM05-01 probably represents intraformational Telkwa Fm. zircon and is therefore consistent with a ca. 205 Ma. iniation of volcanism in the Telkwa Fm. Older zircons were derived from unroofing of Late Triassic intrusions exposed beneath the basal unconformity.

indicate the importance of magmatism during that time. Crystallization ages from the Mt. O'Brien (194.35 ± 0.32 Ma) and Kitselas (193 + 2.1/-0.6 Ma, 195 ± 2 Ma, Gareau et al 1997a) complexes indicate that Telkwa Formation volcanism spanned the Triassic-Jurassic boundary (Figs. 6, 8).

Although most geochronological and biogeochronological data from the Hazelton Group is Jurassic (e.g. Tipper and Richards 1976; MacDonald et al., 1996), in a few instances previous workers have reported Triassic ages. For example, in the Tatogga Lake area (Fig. 3-1), Ash et al. (1997) and Friedman and Ash (1997) documented syn-volcanic porphyry intrusions as old as 205 Ma, with field relations indicating that they were coeval with a trachyandesite breccia unit assigned to the base of the Hazelton Group. However, the supporting geochronological data for these dates were not published. In the Spatsizi River area, Thorkelson et al. (1995) dated the Griffith Creek volcanics at the base of the Hazelton Group at ca. 206 Ma. Combined with the robust evidence for circa 204 Ma initiation of volcanism in the Telkwa Formation presented in this paper, it is now possible to infer that latest Triassic Hazelton arc initiation took place regionally between Terrace, Spatzizi and Tatogga Lake (Fig. 3-1).

Circa 204-194 Ma U-Pb ages of Telkwa volcanic rocks are consistent with the 200 +13/-3 Ma age (Gareau et al. 1997a) of a western phase of the Kleanza pluton. This age was obtained using multi-grain TIMS analyses of zircon and titanite fractions and is considered to be a less robust age than those obtained using CA-TIMS analyses. However, we consider 200 +13/-3 Ma to be a legitimate minimum age for the Kleanza pluton (where sampled along its western extent near the Skeena River) because it is the youngest possible interpretation of the data, and is based on three concordant fractions including a titanite fraction that yielded a 199.7±2.4 Ma $^{206}Pb/^{238}U$ date (Gareau et al. 1997a). The 204.29 ± 0.45 Ma age obtained from the base of the Mt. Henderson complex (this study), predates deposition of the volcanic rocks intruded by the Kleanza pluton, and therefore places a maximum age on the Kleanza pluton, bracketing the timing of initial emplacement between 204.29 + 0.45 Ma (this study) and ca. 200 Ma (Gareau et al. 1997a). Gehrels (2009) obtained an 180.8 ± 2.6 Ma age for an eastern lobe of the Kleanza

pluton based on spot analyses on single zircons using LA-ICP-MS techniques. This robust, but very different age, which is roughly coeval with the Nilkitkwa Formation, indicates that the Kleanza pluton was emplaced during two or more episodes that span most of the length of Hazelton Group volcanism.

Voluminous felsic volcanics in the upper portion of the Mt. O'Brien complex erupted ca. 194 Ma, based on a rhyolite with a U-Pb zircon age of 194.35 ± 0.32 Ma. Gareau et al. (1997a) obtained two ages for felsic volcanics from the Kitselas complex using multi-grain TIMS analyses of zircon fractions. They yielded: 1) a 195.1 ± 2.0 Ma age based on a lower discordant intercept from a 4-point regression (upper intercept at 1.3 Ga); and 2) a 193.9 +2.1/-0.6 Ma $^{206}Pb/^{238}U$ age from a single concordant zircon fraction. These nearly identical ages show that concurrent, voluminous felsic volcanism was active at both volcanic centers circa 194-195 Ma (Sinemurian). Both complexes are overlain by the ca. 179 Ma Nilkitkwa Formation.

The ≈15 million years that separate the 194 Ma felsic volcanism in the upper Mt. O'Brien and Kitselas complexes from the Nilkitkwa Formation are accounted for by continued sporadic and waning volcanism in the upper and undated portion of the Telkwa Formation and a hiatus that separates the formations.

Detrital zircon samples (07JN09-03 and 07MM05-01) contain zircons with dates that are consistent with derivation largely from Triassic igneous rocks below the sub-Hazelton unconformity. Both also contain single grains of Permian zircon, probably derived from the underlying Zymoetz Group, (ca 289 Ma; Gareau et al. 1997a). Sample 07MM05-01, which represents the top of the basal conglomerate unit, also contains ca 205 Ma intraformational zircon. Six zircons in sample 07MM05-01 yield $^{206}Pb/^{238}U$ dates that range between 199.8 ± 1.75 and 202.5 ± 0.98 Ma; they appear to be younger than the ca 204 Ma crystallization ages derived from allied rhyolitic rocks at Mt. Pardek. We therefore interpret the basal conglomerate to have been deposited episodically during a roughly 2 My time span and to have been contemporaneous with local volcanic centers such as at Mt. Pardek. We interpret the two youngest zircons in sample 07MM05-01

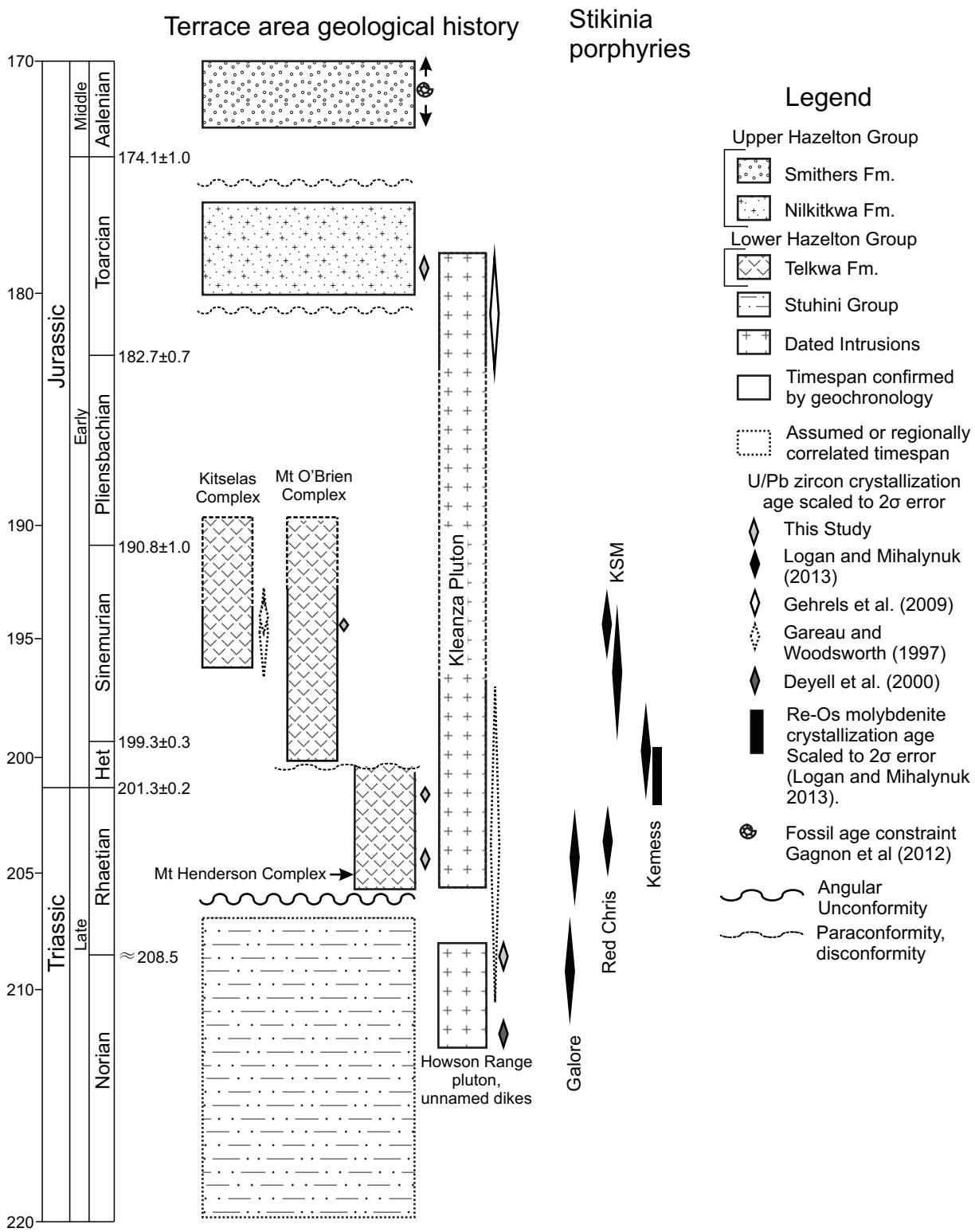

Fig. 3-8. Stratigraphic columns scaled to time (Cohen et al. 2013) with geochronological constraints from this study and other sources; including age data for selected porphyry copper + gold deposits of Stikinia. Note the similarity in age between mineralizing intrusions at Galore Creek and Red Chris, and the Mt. Henderson complex; and between concurrent felsic volcanism in the Kitselas and Mt. O'Brien complexes and intrusions at the Kerr-Sulphurets-Mitchell (KSM) deposits.

(199.8 ±3.5, and 200.3 ± 2.4 Ma) to represent ages close to the older limit allowed within the 2σ error (e.g. 203.1 and 202.7 Ma), so that they are compatible with the 201.6 ± 0.4 Ma age obtained from the upper marker unit, 6 km higher in the stratigraphy.

The abundance of pre-Hazelton (i.e. pre-205 Ma) Triassic zircons in the basal Telkwa Formation conglomerate is unexpected. The basal conglomerate appears to be primarily composed of local Zymoetz Group basement and Telkwa Formation intraclasts, which would yield Permian (or older), and contemporaneous (e.g. ca. 204-205 Ma) age zircon respectively. Except where the basal conglomerate directly overlies the Triassic Stuhini Group, clasts of fine-grained siltstone and shale derived from it are rare. Stuhini Group volcanics, which are abundant north of Terrace in the Stewart region, are not represented in the local geology near Terrace or Smithers and were not identified as clasts in the basal conglomerate. Therefore, we propose that the Triassic age zircons are mainly contained in the fine fraction (matrix) of the basal Telkwa Formation conglomerate and that they were derived from Late Triassic plutons exposed by tectonic uplift and denudation. The proposed source is supported by: 1) the presence of a regional unconformity which developed between deposition of the Stuhini and Hazelton groups, 2) local evidence of uplift and denudation between 210 and 204 Ma in the form of a dramatic shift from deep-water pelagic sedimentation to subaerial high-energy sedimentation and deep erosion; and 3) regional plutonic suites that yield similar ages (Fig. 3-8) (e.g. Schaft Creek porphyry, 216.6 ± 2 Ma, Logan et al. 2000; Williston Bay pluton, 216.6 ± 4 Ma, Mihalynuk et al. 1997; Topley Intrusive Suite, 219.5 +2/-3 Ma, MacIntyre et al. 2001); as well as a local Triassic dike (this study, 208.59 ± 0.72 Ma), and a pluton in the Howson Range 30 kilometres east of the study area dated at 212 ± 0.6 Ma (Deyell et al. 2000).

3.6 Geochemistry

3.6.1 Results

Twenty-five samples of Telkwa Formation volcanic rocks were collected from representative units in the Mt. O'Brien, Mt. Henderson, and Kitselas complexes. The

samples represent the most coherent flows or flow-like intervals with the least amount of alteration and/or weathering.

One sample was screened from the study because it was collected from a dike with unknown affinity. All obvious signs of alteration and weathering were trimmed from the samples with a diamond saw and the rocks were pulverized in a hardened steel shatterbox.

Major elements were determined using fused bead X-ray fluorescence at the Atlantic Geochemical Centre (Saint Mary's University). Analytical errors, as determined from replicate USGS standard rock analyses, are less than 2% (Dostal et al., 1994). Trace elements were analyzed by inductively coupled plasma mass-spectrometry (ICP-MS) at Memorial University of Newfoundland (St. John's, Newfoundland) using a Na_2O_2-sintering technique. The method and its is described by Longerich et al. (1990), and the precision is between 2 and 4% (Longerich et al. 1990). Five samples were analyzed for Nd isotopic ratios. The concentrations of Sm and Nd and Nd isotopic ratios were determined by isotope dilution mass spectrometry at the Atlantic Universities Regional Isotopic Facility (AURIF) at Memorial University. The precision of concentrations of Nd and Sm is ± 1%. The isotopic ratios were determined using a multicollector Finnigan MAT 262 V thermal ionization mass spectrometer operated in a static mode. Measured $^{143}Nd/^{144}Nd$ values were fractionation-corrected to a natural $^{146}Nd/^{144}Nd$ value of 0.721903, normalized to the JNdi-1 standard, with $^{143}Nd/^{144}Nd$ values accurate to 0.002% and the $^{147}Sm/^{144}Nd$ ratio accurate to 0.1%. Replicate analyses of JNdi-1 standard yielded $^{143}Nd/^{144}Nd = 0.512134 \pm 1$ (n= 91). Details of analytical techniques and precision and accuracy were described by Kerr et al. (1995). The ε_{Nd} values were calculated using $^{147}Sm/^{144}Nd = 0.1967$ and $^{143}Nd/^{144}Nd = 0.512638$ values for the present day chondrite uniform reservoir (CHUR) and ages of 194 and 204 Ma (Table 3-3). Second stage T_{DM} were calculated using a linear evolution for a mantle separated from CHUR at 4.55 Ga and having a present day ε_{Nd} value of +10.

3.6.1.1 Alteration

Telkwa Formation rocks were affected by sea-floor alteration in the subaqueous parts of the active volcanic environment, and subsequently by zeolite- to lower amphibolite facies metamorphism. Major and other mobile element ratios show systematic variations vs. SiO_2 and vs. immobile elements (e.g. Zr and Th). Alteration indices (e.g. Al_2O_3/Na_2O, $Al_2O_3/Na_2O+CaO+K_2O$) are very low (<8 for Al_2O_3/Na_2O) and relatively consistent, indicating that bulk-rock compositions are not significantly affected by alteration. However, alkali metals show some scatter and probably were subject to some degree of mobility during sea-floor alteration; therefore they are only used for petrogenetic interpretations where those interpretations are supported by data from other less mobile elements. High-field-strength (HFS) elements, transition elements, and the REE display strong correlations against Zr and are thus considered to represent primary magmatic compositions. These elements are immobile under most metamorphic conditions (Winchester and Floyd 1977) and display trends similar to those in modern volcanic rocks.

3.6.1.2 Major Element Chemistry and Rock Type Classification

The SiO_2 concentrations for Telkwa Formation volcanic rocks range from 48.1 to 79.0 wt.%, with a distinct gap between 62.8 and 72.3% (Table 3-2, Fig. 3-9). On Harker variation diagrams, FeO, MnO, TiO_2 and MgO show systematic decreases with increasing SiO_2, whereas K_2O shows a systematic increase (Fig. 3-9). Rock type classification based on SiO_2 vs. alkalis (Fig. 3-10A) shows that Telkwa Formation rock compositions are continuous from basalt/trachy basalt to andesite and form a gap between andesite and rhyolite. On the same diagram, $NaO+K_2O$ concentrations are transitional between alkaline and sub-alkaline. Trace element systematics, e.g. Zr/Ti and Nb/Y, are consistent with sub-alkaline compositions (Fig. 3-10B, C). Overall the samples span both typical calc-alkaline and high-K calc-alkaline island-arc compositions (Peccerillo and Taylor 1976; Fig. 3-10D). On an AFM diagram (Irvine and Baragar 1971; Fig. 3-10E) the samples show a clear calc-alkaline differentiation trend, and on a multi-element tholeiitic vs. calk-alkaline discrimination plot (Fig. 3-10F) samples follow the calc-alkaline trend.

Table 3-2. Geochemistry of Telkwa Formation Rocks

Sample	Detection	05NB-28-2	05NB-26-1	05NB-29-2	05NB-28-1	05NB-07-1	05NB-26-3	05NB-03-6	05NB-01-1
Easting	Limit	533533	534067	534106	533902	544867	534149	542012	544820
Northing		6053571	6053227	6053337	6053500	6063411	6052997	6056788	6047528
Complex		KC	KC	KC	KC	KC	KC	MHC	MHC
SiO_2 (%)	0.03	48.1	52.9	54.2	54.8	72.3	77.8	49.2	51.7
Al_2O_3 (%)	0.03	18.1	15.9	15.9	16.4	13.4	11.2	17.7	16.0
Fe_2O_{3Total} (%)	0.03	10.2	10.2	10.8	7.7	3.0	2.3	10.0	8.4
MnO (%)	0.005	0.28	0.20	0.39	0.12	0.04	0.02	0.16	0.14
MgO (%)	0.03	11.5	5.0	6.2	2.1	0.5	0.0	7.0	5.2
CaO (%)	0.03	1.1	6.3	1.4	3.9	1.2	0.2	6.5	6.3
Na_2O (%)	0.03	4.8	3.5	4.8	6.0	4.8	4.5	4.3	3.0
K_2O (%)	0.03	1.4	2.6	2.2	2.6	2.5	2.8	0.1	1.4
TiO_2 (%)	0.005	1.06	0.97	1.09	1.14	0.57	0.30	1.08	0.86
P_2O_5 (%)	0.005	0.23	0.20	0.22	0.38	0.13	0.06	0.27	0.29
LOI (%)		4.01	1.70	2.36	4.12	0.04	0.20	3.29	6.06
Total (%)		100.9	99.5	99.5	99.3	98.4	99.4	99.5	99.3
V (ppm)	5	376	311	316	196	15	13	247	5
Cr (ppm)	20	36	40	25	<20	<20	<20	191	91
Co (ppm)	1	56	41	53	26	7	6	54	35
Ni (ppm)	20	60	<20	<20	<20	<20	<20	76	42
Cu (ppm)	10	<10	<10	8	<10	17	26	13	<10
Zn (ppm)	30	521	92	423	163	32	34	101	101
Ga (ppm)	1	20	20	21	16	12	9	18	16
Rb (ppm)	1	38	47	35	52	77	66	9	39
Sr (ppm)	2	158	452	94	161	199	65	402	316
Y (ppm)	0.5	18.4	19.9	22.6	30.3	30.0	25.5	17.7	16.1
Zr (ppm)	1	76.1	82.9	96.9	161.4	181.1	116.2	78.1	95.6
Nb (ppm)	0.2	3.8	3.2	3.8	7.5	9.7	6.8	5.4	6.6
Ba (ppm)	3	805	1130	1728	1243	639	775	80	668
La (ppm)	0.05	8.8	7.9	9.4	10.2	20.6	8.8	9.9	12.0
Ce (ppm)	0.05	18.9	17.1	20.1	24.1	39.5	24.3	21.8	25.6
Pr (ppm)	0.01	2.67	2.39	2.77	3.63	5.14	3.67	3.09	3.47
Nd (ppm)	0.05	12.5	11.5	12.8	17.7	22.0	16.4	14.3	15.4
Sm (ppm)	0.01	3.16	2.94	3.31	4.57	4.99	3.75	3.35	3.31
Eu (ppm)	0.005	0.93	0.97	1.07	1.34	1.28	1.11	1.08	0.89
Gd (ppm)	0.01	3.64	3.56	3.96	5.34	5.16	4.21	3.59	3.36
Tb (ppm)	0.01	0.58	0.59	0.65	0.84	0.81	0.69	0.53	0.49
Dy (ppm)	0.01	3.68	3.90	4.27	5.51	5.17	4.55	3.31	3.02
Ho (ppm)	0.01	0.74	0.80	0.90	1.15	1.15	0.95	0.70	0.64
Er (ppm)	0.01	2.15	2.34	2.68	3.39	3.39	2.90	2.00	1.80
Tm (ppm)	0.005	0.32	0.35	0.40	0.50	0.51	0.45	0.29	0.27
Yb (ppm)	0.01	2.11	2.3	2.61	3.37	3.47	3.08	1.87	1.76
Lu (ppm)	0.002	0.31	0.34	0.39	0.51	0.50	0.45	0.27	0.25
Hf (ppm)	0.1	2.0	2.3	2.5	4.2	4.2	2.4	2.1	2.4
Ta (ppm)	0.01	0.13	0.09	0.09	0.24	0.51	0.36	0.15	0.21
Th (ppm)	0.05	0.9	1.2	1.5	3.0	4.2	3.0	1.0	1.4

Table 3-2. Geochemistry of Telkwa Formation Rocks - continued

Sample	Detection	05NB-15-5	05-TB-24-3	05-TB-23-4	05TB-25-3	05-TB-24-4	05-TB-37-3	05TB-31-1	05-TB-26-1
Easting	Limit	561974	557350	559085	557244	557522	558081	549597	555511
Northing		6043018	6042269	6042819	6044009	6041830	6065652	6049588	6051317
Complex		MHC	MHC	MHC	MHC	MHC	MOC	MOC	MOC
SiO_2 (%)	0.03	54.2	55.3	56.6	60.1	60.5	48.1	49.6	49.7
Al_2O_3 (%)	0.03	18.5	16.6	17.8	16.5	16.2	15.9	17.9	17.6
Fe_2O_{3Total} (%)	0.03	6.6	7.2	6.9	6.2	5.9	10.3	10.9	11.2
MnO (%)	0.005	0.20	0.13	0.13	0.12	0.08	0.30	0.19	0.21
MgO (%)	0.03	3.1	3.7	2.4	3.0	2.6	9.6	5.6	4.8
CaO (%)	0.03	6.5	9.2	7.4	6.5	1.5	3.5	9.0	7.2
Na_2O (%)	0.03	3.8	3.1	3.5	2.6	6.7	5.2	2.6	4.1
K_2O (%)	0.03	2.4	0.5	1.2	1.8	1.9	0.6	0.6	0.6
TiO_2 (%)	0.005	0.78	0.76	0.57	0.46	0.71	0.92	1.03	1.13
P_2O_5 (%)	0.005	0.32	0.22	0.27	0.13	0.21	0.21	0.22	0.25
LOI (%)		3.04	3.35	2.05	2.18	2.70	4.89	2.51	2.48
Total (%)		99.4	100.1	98.8	99.5	99.0	99.5	100.1	99.3
V (ppm)	5	150	228	167	148	163	276	305	364
Cr (ppm)	20	<20	50	<20	32	40	320	105	20
Co (ppm)	1	23	22	15	23	15	41	4	30
Ni (ppm)	20	<20	<20	<20	<20	<20	80	62	<20
Cu (ppm)	10	30	190	10	<10	30	<10	135	120
Zn (ppm)	30	123	70	90	86	100	220	105	130
Ga (ppm)	1	19	18	18	18	16	16	21	19
Rb (ppm)	1	45	7	17	40	27	16	15	11
Sr (ppm)	2	573	317	827	387	121	107	371	545
Y (ppm)	0.5	15.0	15.1	14.9	9.9	17.7	19.7	17.1	17.0
Zr (ppm)	1	109.2	88.0	79.0	77.0	129.0	56.0	48.8	50.0
Nb (ppm)	0.2	7.4	3.7	3.1	4.6	5.4	2.1	3.3	2.8
Ba (ppm)	3	1238	222	785	893	537	390	373	507
La (ppm)	0.05	14.9	11.0	12.5	8.1	18.4	7.1	7.2	8.7
Ce (ppm)	0.05	31.3	23.4	26.2	16.0	34.7	15.8	16.2	19.6
Pr (ppm)	0.01	4.11	2.72	3.03	2.06	4.30	2.06	2.33	2.49
Nd (ppm)	0.05	17.5	10.9	11.8	8.9	16.1	9.4	11.0	11.0
Sm (ppm)	0.01	3.58	2.62	2.81	1.86	3.84	2.56	2.80	3.01
Eu (ppm)	0.005	0.99	0.81	0.92	0.64	1.01	0.91	0.99	1.07
Gd (ppm)	0.01	3.23	2.49	2.51	1.90	3.37	2.97	3.17	2.97
Tb (ppm)	0.01	0.45	0.40	0.39	0.29	0.51	0.51	0.52	0.47
Dy (ppm)	0.01	2.74	2.41	2.36	1.83	2.93	3.14	3.28	2.84
Ho (ppm)	0.01	0.58	0.50	0.49	0.38	0.59	0.65	0.68	0.58
Er (ppm)	0.01	1.69	1.51	1.57	1.12	1.78	1.95	1.97	1.70
Tm (ppm)	0.005	0.24	0.23	0.24	0.17	0.26	0.29	0.29	0.25
Yb (ppm)	0.01	1.63	1.45	1.53	1.14	1.66	1.89	1.94	1.56
Lu (ppm)	0.002	0.24	0.22	0.23	0.17	0.25	0.29	0.29	0.24
Hf (ppm)	0.1	2.9	2.3	2.3	2.2	3.6	1.6	1.4	1.5
Ta (ppm)	0.01	0.23	0.25	0.18	0.17	0.38	0.12	0.09	0.17
Th (ppm)	0.05	3.4	2.5	1.6	1.3	4.1	0.7	0.9	1.1

Table 3-2. Geochemistry of Telkwa Formation Rocks - continued

Sample	Detection	05-TB-29-3	05-TB-34-3	05NB-23-4	05NB-23-2	05TB-39-9	05-TB-34-9	05-TB-38-12	05TB-33-1
Easting	Limit	556400	553601	548589	548011	558470	553206	559686	548697
Northing		6051240	6061099	6056878	6057018	6065163	6061785	6065099	6050376
Complex		MOC	MOC	MOC	MOC	MOC	MOC	MOC	MOC
SiO_2 (%)	0.03	52.20	52.32	62.78	74.43	76.20	77.65	78.71	78.97
Al_2O_3 (%)	0.03	17.64	16.76	14.83	12.64	12.76	11.56	9.83	11.98
Fe_2O_{3Total} (%)	0.03	7.84	8.99	6.01	4.79	1.58	1.94	1.80	1.49
MnO (%)	0.005	0.18	0.16	0.08	0.07	0.05	0.02	0.05	0.08
MgO (%)	0.03	3.4	4.5	0.6	0.1	0.2	0.1	0.1	0.5
CaO (%)	0.03	3.4	8.6	2.5	0.3	0.4	0.1	0.4	1.8
Na_2O (%)	0.03	6.7	3.2	3.1	5.0	4.6	1.9	1.4	2.8
K_2O (%)	0.03	1.82	1.59	4.87	2.36	2.54	7.26	6.92	2.89
TiO_2 (%)	0.005	0.67	0.95	0.89	0.53	0.21	0.08	0.17	0.12
P_2O_5 (%)	0.005	0.16	0.32	0.35	0.13	0.05	0.03	0.04	0.05
LOI (%)		4.53	1.97	3.82	0.71	0.87	0.37	0.64	0.48
Total (%)		98.5	99.4	99.9	101.1	99.4	100.9	100.0	101.2
V (ppm)	5	106	255	99	32	5	18	37	12
Cr (ppm)	20	30	70	<20	<20	<20	20	<20	<20
Co (ppm)	1	23	26	16	16	<1	<1	1	<1
Ni (ppm)	20	<20	<20	<20	<20	<20	<20	<20	<20
Cu (ppm)	10	10	20	<10	13	27	<10	<10	29
Zn (ppm)	30	270	110	247	50	32	<30	<30	41
Ga (ppm)	1	15	17	15	12	12	10	7	11
Rb (ppm)	1	38	30	92	53	79	125	109	84
Sr (ppm)	2	333	546	76	44	100	39	23	166
Y (ppm)	0.5	16.2	22.3	34.5	27.6	18.6	35.3	14.1	25.8
Zr (ppm)	1	54.0	89.0	157.9	111.6	158.3	130.0	192.0	78.3
Nb (ppm)	0.2	2.4	4.5	9.8	8.6	6.9	5.9	5.4	8.5
Ba (ppm)	3	1411	587	1417	705	978	2088	1342	1161
La (ppm)	0.05	8.7	12.9	21.9	17.8	13.9	19.2	5.1	21.382
Ce (ppm)	0.05	17.2	28.2	44.8	34.8	27.6	41.9	9.7	41.54
Pr (ppm)	0.01	2.16	3.37	5.83	4.59	3.50	4.97	1.34	5.12
Nd (ppm)	0.05	9.2	14.5	25.3	19.5	14.7	20.4	5.9	20.6
Sm (ppm)	0.01	2.43	3.61	5.74	4.41	3.07	4.79	1.57	4.23
Eu (ppm)	0.005	0.86	1.21	1.64	1.19	0.87	0.69	0.21	0.77
Gd (ppm)	0.01	2.52	3.70	6.41	5.03	3.04	4.80	1.76	4.25
Tb (ppm)	0.01	0.42	0.61	1.03	0.81	0.49	0.85	0.32	0.69
Dy (ppm)	0.01	2.53	3.63	6.64	5.32	3.16	5.57	2.14	4.48
Ho (ppm)	0.01	0.53	0.75	1.36	1.08	0.68	1.23	0.49	0.93
Er (ppm)	0.01	1.60	2.28	4.08	3.22	2.16	3.89	1.70	2.89
Tm (ppm)	0.005	0.24	0.34	0.61	0.48	0.35	0.61	0.29	0.45
Yb (ppm)	0.01	1.49	2.15	4.05	3.24	2.54	4.13	2.04	3.15
Lu (ppm)	0.002	0.23	0.33	0.59	0.47	0.39	0.64	0.34	0.47
Hf (ppm)	0.1	1.6	2.4	4.1	2.5	3.3	4.4	5.1	2.8
Ta (ppm)	0.01	0.17	0.26	0.36	0.43	0.36	0.49	0.42	0.44
Th (ppm)	0.05	1.1	1.3	5.3	4.7	3.2	6.9	3.8	5.3

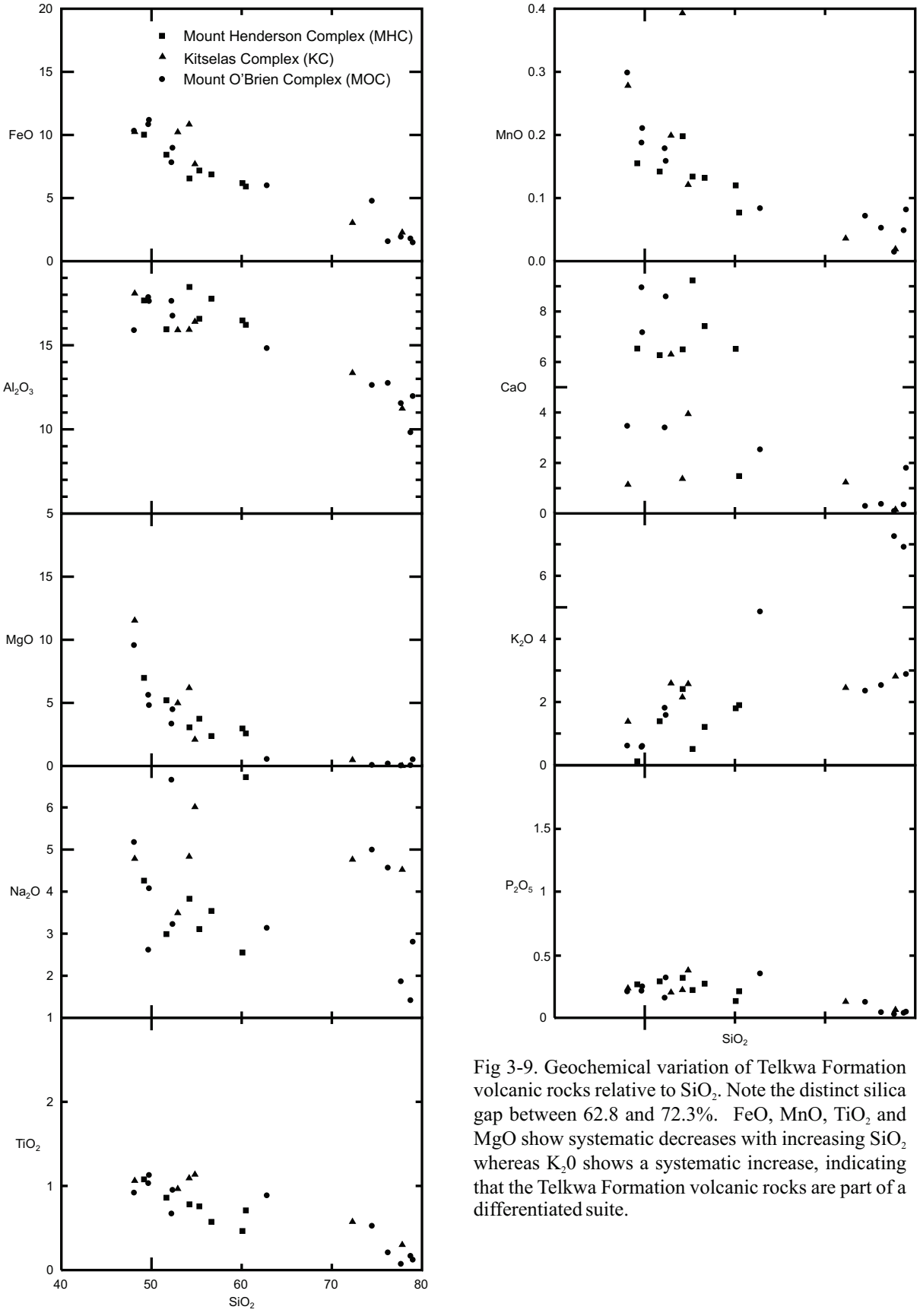

Fig 3-9. Geochemical variation of Telkwa Formation volcanic rocks relative to SiO_2. Note the distinct silica gap between 62.8 and 72.3%. FeO, MnO, TiO_2 and MgO show systematic decreases with increasing SiO_2 whereas K_20 shows a systematic increase, indicating that the Telkwa Formation volcanic rocks are part of a differentiated suite.

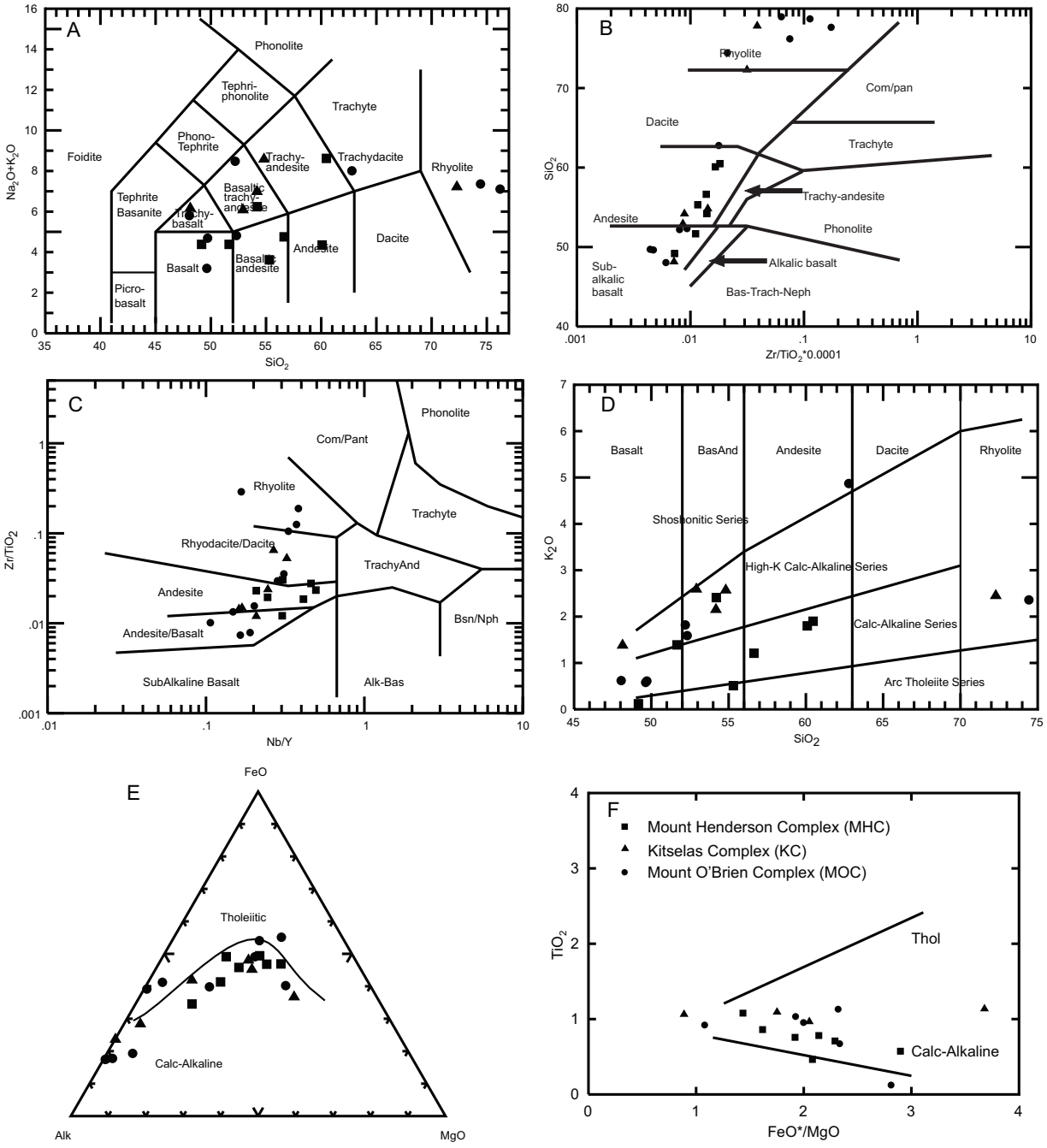

Fig. 3-10. Geochemical classification of Telkwa Formation volcanic rocks. A) LeBas et al. (1986); B) Winchester and Floyd (1976); C) Winchester and Floyd (1977); D) Peccerillo and Taylor (1976); E) Irvine and Baragar (1971); F) Miyashiro (1974). Immobile trace-element classification systems place the Telkwa Fm. rocks in the sub-alkaline field (B, C), and they follow typical calc-alkaline differentiation trends (E, F).

Basalt falls into the high-Al classification, with 17-21 wt.% Al_2O_3, which is typical of parental magmas for the calc-alkaline differentiation series. Andesites are medium- to high-K with 0.51-4.87 wt. % K_2O. Rhyolites have high SiO_2 (72.3 – 79.0 wt. %) and low concentrations of Al_2O_3 (9.83-13.35 wt.%) and TiO_2 (0.075 – 0.547 wt. %). Field observations of three main rock compositions typified by fine-grained dark basalt, lighter and variably coloured porphyritic andesite and highly siliceous rhyolite, are consistent with the silica gap defined by the geochemistry.

3.6.1.3 Trace Element and Rare Earth Element Chemistry

On chondrite-normalized REE plots (Fig. 3-11), Telkwa Formation basalt has a moderate negative LREE slope with an average $(La/Sm)_{chondrite}$ ratio of 1.83, lacks prominent Eu anomalies, and displays very slight negative HREE slopes with an average 1.47 $(Gd/Yb)_{chondrite}$ ratio. Plots of intermediate and felsic rocks show: 1) increasing absolute abundances of the LREE; 2) increase in LREE slopes (e.g., $(La/Sm)_{chondrite}$ ratios increase to 2.28 in intermediate and 2.49 in felsic samples); 3) a subtle negative Eu anomaly in intermediate rocks and a pronounced negative Eu anomaly in the most felsic samples; and 4) an increase in the absolute concentrations of HREE and decrease in $(Gd/Yb)_{chondrite}$ ratios for felsic but not intermediate samples (e.g., $(Gd/Yb)_{chondrite}$ ratios are 1.38 for intermediate samples and 1.07 for felsic samples).

On primitive mantle-normalized incompatible element spider diagrams (Fig. 3-12), basalts have lower normalized values of Th than La and pronounced negative Nb anomalies ($(Th/La)_{primitive\ mantle} = 0.72$; $(Th/Nb)_{primitive\ mantle} = 2.08$). They have a negative slope from La to Ti ($(La/Ti)_{primitive\ mantle} = 2.63$), and a very slight negative profile from Ti to Lu ($(Ti/Yb)_{primitive\ mantle} = 1.25$). Basalts display a minor negative Ti anomaly relative to Eu and Gd, and some samples from the Mt Henderson and Mt. O'Brien complexes have subtle positive Eu anomalies. Relative to basaltic profiles, intermediate and felsic profiles have increased absolute concentrations of all incompatible elements (normalized Yb is 3.96 ppm for mafic, 4.75 ppm for intermediate, and 5.33 ppm for felsic samples). Intermediate and felsic profiles have increasingly negative slopes between Th and La ($(Th/La)_{primitive\ mantle}$ = 1.61 and 2.29), Th and Sm ($(Th/Sm)_{primitive\ mantle}$ 3.64 and 5.82) and

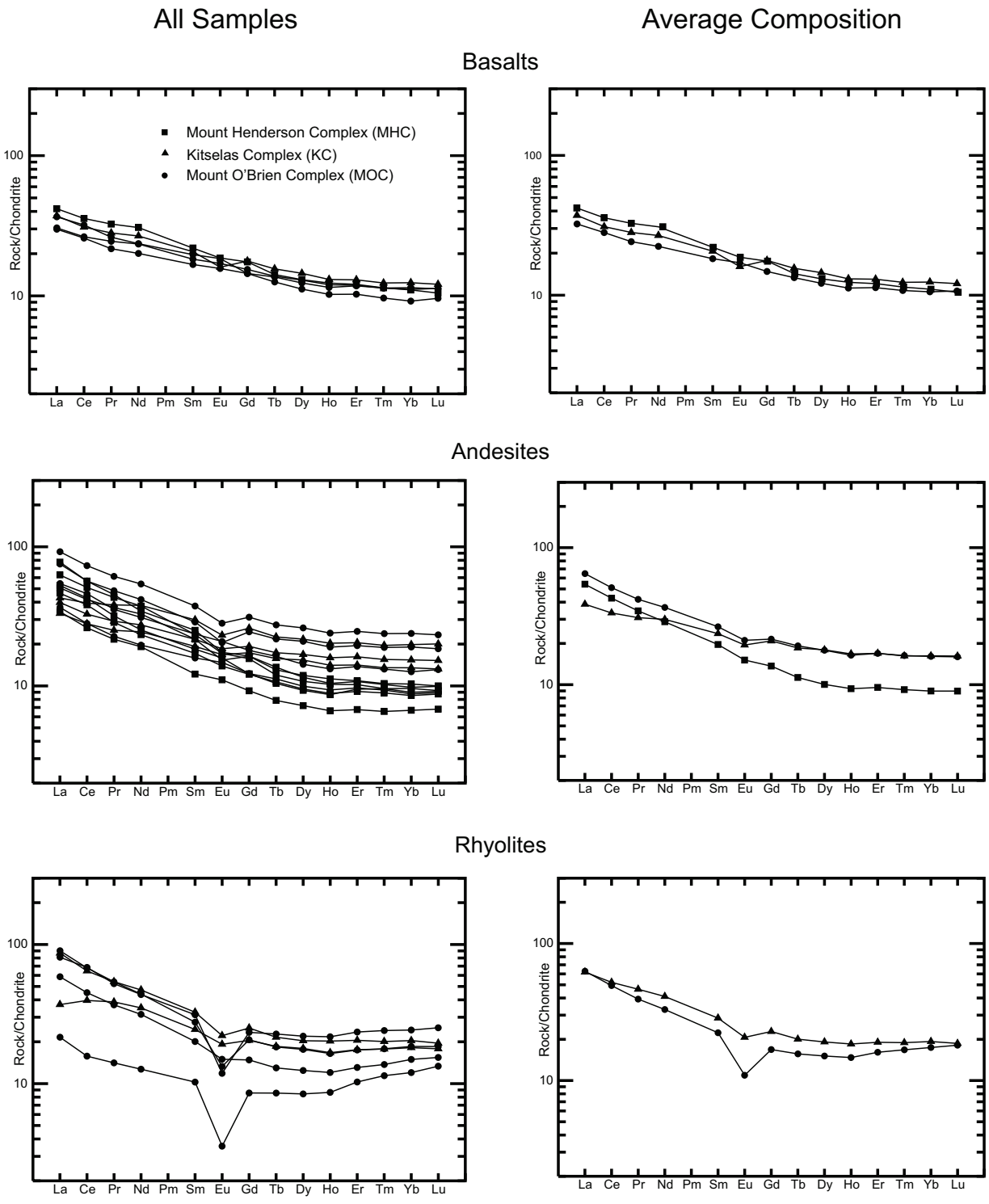

Fig. 3-11. Chondrite-normalized (Sun and McDonough 1989) rare-earth-element plots. Note that rocks from all three complexes have similar REE characteristics. Rhyolites and andesites have similar ranges of LREE and HREE concentrations and both have negative LREE slopes and nearly flat HREE slopes, while basalts have lower absolute concentrations of REE and a continual negative La/Lu slope. Some andesites and rhyolites display negative Eu anomalies indicating fractionation of feldspar.

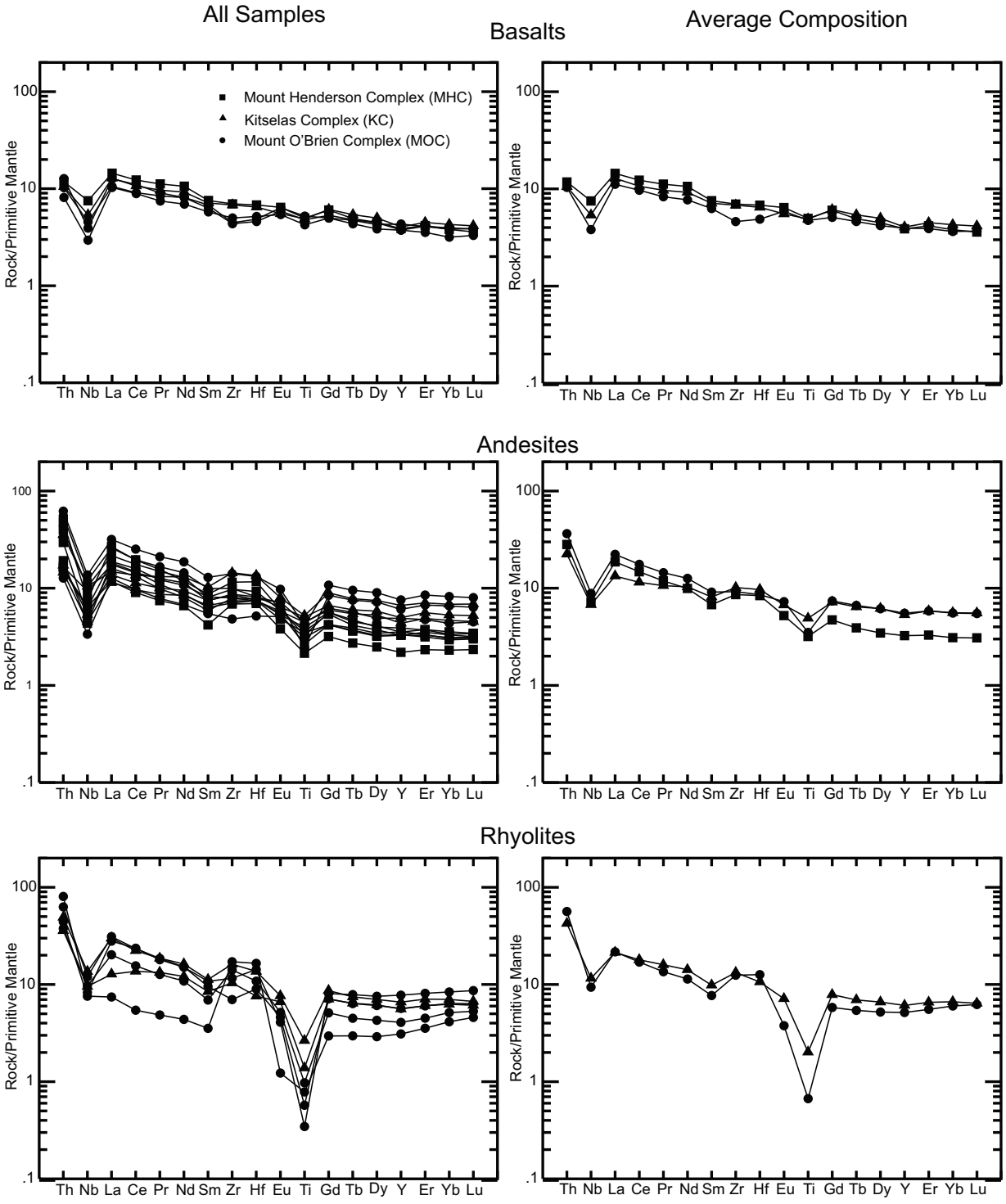

Fig. 3-12. Mantle-normalized (Sun and McDonough, 1989) incompatible element plots. Negative Nb and Ti anomalies are typical of arc-related magmas, where hydrous melting occurs in the mantle wedge above a subducting slab. Nb and Ti are typically thought to be immobile in these environments, while the other incompatible elements are incorporated into the melts, explaining the negative Nb and Ti anomaly.

strong negative Nb and Ti anomalies ($(Th/Nb)_{primitive\ mantle}$ = 3.78 and 4.84). Variably positive Zr and Hf anomalies are present in some of the samples; they have flat to weakly positive or weakly negative profiles with respect to the least incompatible elements.

3.6.1.4 Nd Isotope Geochemistry

Sm-Nd isotope ratios were determined for two basaltic, one andesitic, and two rhyolitic samples. The andesitic sample is from the Mt. Henderson complex, the other four samples are from the Mt. O'Brien complex. The age-corrected ε_{Nd} values range from +5.0 to +6.0 (Table 3-3). They fall well into the range of -0.5 to +7.7 established by Samson et al. (1989) for all types of Stikine terrane rocks, and are comparable to data reported by Dostal et al. (2005) from lower Hazelton Group volcanic rocks (Buck Creek complex – central British Columbia). They are less juvenile than rocks of the Triassic Takla Group (+6.09 to + 8.05; Dostal 1999). While the overall range of ε_{Nd} is quite limited, within it, the samples are distinctly distributed with regard to SiO_2; mafic samples have the lowest positive ε_{Nd} values, followed by the andesite sample, and the rhyolite samples have the highest positive ε_{Nd} values (Fig. 3-13), and therefore the most juvenile source(s). Although Precambrian xenocrystic zircon is indicated in geochronology samples from the Kitselas complex (Gareau et al. 1997a), high positive ε_{Nd} values and a positive correlation between ε_{Nd} and SiO_2 (Fig. 3-13) are inconsistent with significant contribution from older continental crust (or sedimentary derivatives) to Telkwa Formation melts. Instead, the atypical positive correlation between ε_{Nd} and SiO_2 must be explained by other petrogenetic processes.

Table 3-3. Sm-Nd Isotope Data – samples locations noted in Table 2-3

Sample	Age (Ga)	Nd (ppm)	Sm (ppm)	$^{147}Sm/^{144}Nd$	$^{143}Nd/^{144}Nd$	2σ	$\varepsilon^{143}Nd$
05TB29-3	0.194	10.01	2.746	0.1659	0.512853	5	5.0
05TB26-1	0.194	12.12	3.093	0.1544	0.512858	5	5.4
05TB34-9	0.194	20.94	4.906	0.1417	0.512867	5	5.9
05TB38-12	0.194	5.899	1.549	0.1588	0.512893	4	6.0
05TB23-4	0.204	12.99	2.800	0.1303	0.512830	6	5.5

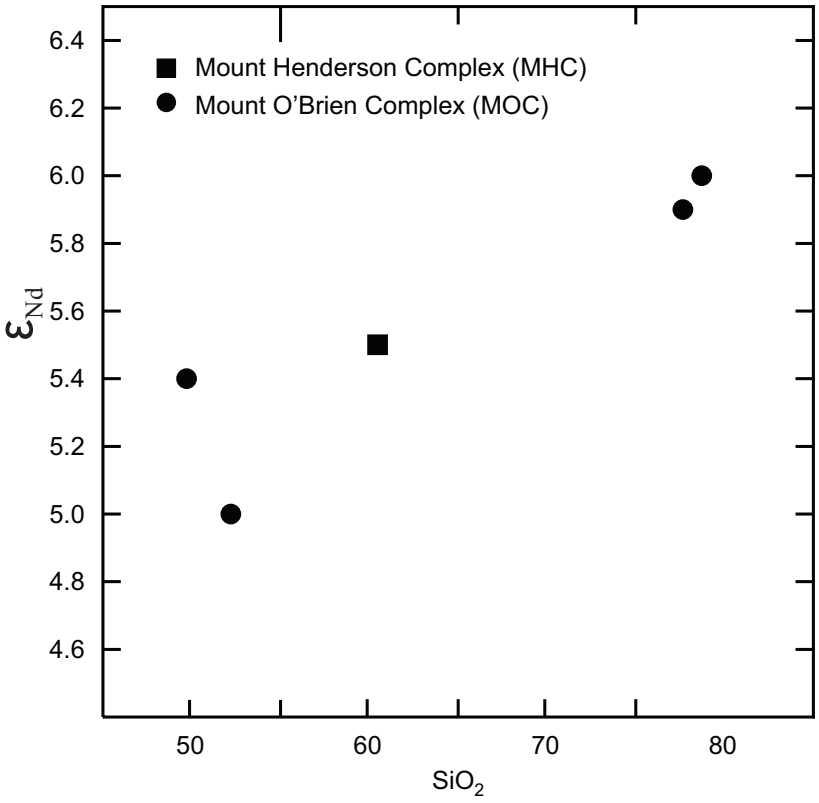

Fig. 3-13. ε_{Nd} values in Telkwa Formation volcanic rocks relative to SiO_2. Felsic rock have higher ε_{Nd} values than intermediate and mafic rocks suggesting that they are derived from a different source-rock and are not part of a differentiation trend.

3.6.2 Discussion of Geochemistry: Petrogenesis of the Telkwa volcanic suite

Telkwa Formation volcanic rocks have compositions consistent with a medium- to high-K, calc-alkaline, differentiated suite. Island arc volcanic suites commonly range from basalt to andesite, with high-Al basalts and elevated K_2O concentrations relative to other differentiated suites (e.g. Whalen 1985). Major and trace element variations are consistent with fractionation of titanomagnetite, olivine, and clinopyroxene in basalt, increased fractionation of plagioclase feldspar in intermediate rocks, and fractionation of apatite in the most felsic rocks. Based on the lack of correlation of Y with SiO_2, amphiboles were not a significant fractionating phase.

Telkwa Formation basalt displays negative sloping LREE and flat HREE profiles, indicating derivation by partial melting of spinel lherzolite. The basalts span a range of Th/Nb ratios (0.15-0.4), with limited variation in La/Sm ratio (Fig. 3-14). This indicates that geochemical variations within the basalts are largely a result of subduction-related enrichment rather than source enrichment or crustal contamination (Pearce 2008). The overall trace element profile of Telkwa Formation basalt (Fig. 3-12) is typical of island arc-related magmas, with characteristic negative Nb and Ti anomalies, and higher normalized concentrations of the most incompatible elements. This is reflected in standard tectonic discrimination diagrams (Fig. 3-15), which place the samples in island arc fields. Sm-Nd isotopic data for Telkwa Formation basalts suggest that they were derived from a juvenile source similar to other primitive rocks in Stikinia. The geochemical characteristics of the Telkwa Formation basalts are consistent with derivation by hydrous melting of spinel lherzolite in a mantle wedge during subduction.

Telkwa Formation intermediate rocks form a geochemical continuum with basalts: they follow the same differentiation trends relative to SiO_2 (Fig. 3-9), and have increased absolute concentrations and relative enrichment in the most incompatible trace elements (Fig. 3-11, 3-12). These characteristics, along with abundant feldspar and, more rarely, clinopyroxene phenocrysts, suggest derivation from basalts via fractional crystallization.

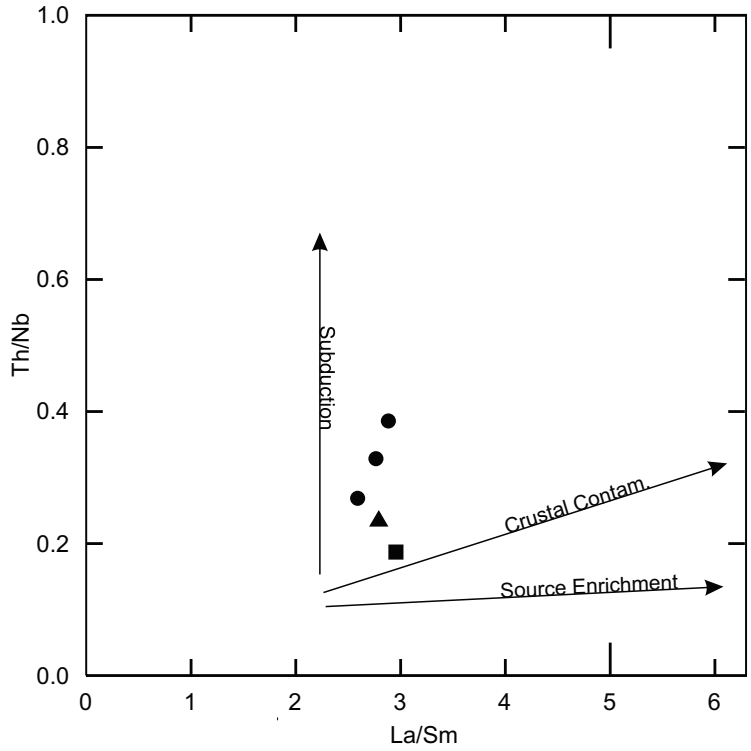

Fig. 3-14. Comparison of Telkwa Formation basalts to various differentiation vectors. An increase in Th/Nb without accompanying increase in La/Sm is typical of subduction-related enrichment, as opposed to enrichment via crustal contamination or increased partial melting.

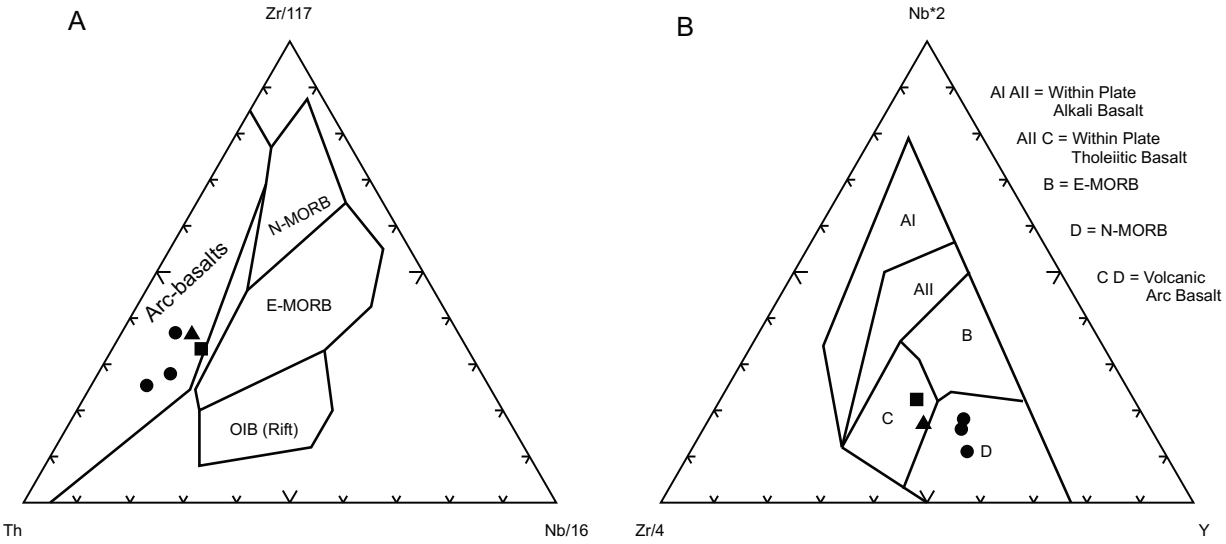

Fig. 3-15. Geochemical tectonic discrimination of Telkwa Formation basalts is consistent with a subduction-related origin. A) Wood (1980); B) Meschede (1986).

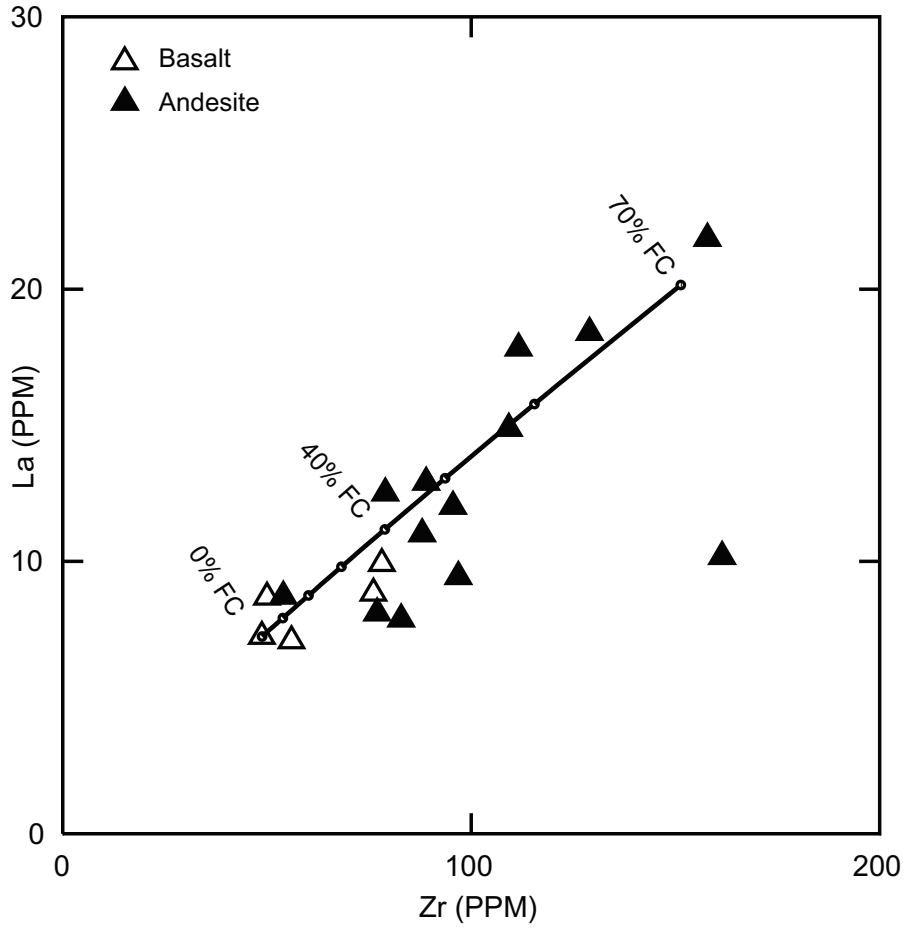

Fig. 3-16. Trace element modeling of fractional crystallization, using partition coefficients of McKenzie and O'Nions (1991) for andesites, assuming 95% plagioclase and 5% clinopyroxene fractionation. Fractional crystallization modeling predicts the trend defined by geochemical variations between Telkwa Formation basalts and andesites.

In addition, trace element modelling of removal of feldspar and clinopyroxene from the melt via fractional crystallization predicts the observed andesite compositions (Fig. 3-16).

Telkwa Formation rhyolite plots in volcanic arc fields on trace element tectonic discrimination diagrams (Fig. 3-17). Arc rhyolites are most abundant in continental arcs, where they are thought to be generated by crustal melting in and above the MASH zone (crustal melting, assimilation, storage and homogenization by underplated mafic magmas; Hildreth and Moorbath 1988) at the base of the thick crust. MASH zones and crustal underplating are not well developed in oceanic island arcs, and the volumetrically minimal felsic rocks found in present-day arcs are commonly considered to be a result of extreme differentiation of a basaltic parent magma (e.g. Ewart et al. 1973; Woodhead 1988; Pearce et al 1995). However, a number of recent studies have shown that some silicic rocks in modern island arcs were generated via partial melting of basaltic crust (e.g. Tonga-Kermadec arc, Smith et al. 2003a, b; Wright et al 2006; Lzi-Bonin arc, Tamura and Tatsumi 2002; Vanuatu arc, Monzier et al. 1994; South Sandwich arc, Leat et al. 2007). These authors suggest that the same processes that generate silicic rocks in continental arcs may apply to island arcs: 1) hydrous primary arc magmas pond at the base of the crust due to density differences; and 2) gabbro at the base of the crust is heated by the ponded basic magmas as they crystallize, generating partial (felsic) melts. These findings are supported by geochemistry, thermal modeling (e.g. Kawate and Arimar 1998; Jackson et al. 2005), and melting experiments which show that hydrous lower-crustal gabbro can generate 25-40% partial melts at 1050-1100°C (Rapp and Watson 1995).

Two lines of evidence suggest that the Telkwa Formation rhyolites were generated via partial melting of crustal rock, as opposed to fractionation of a basaltic parent: 1) the lack of dacites, which should be well represented in a differentiated suite, and 2) rhyolites have higher ε_{Nd} values (+5.9 and +6.0) than the basalts and andesites (+5.0 - +5.5), a difference that cannot be explained by differentiation because Sm-Nd isotopic ratios are unaffected by fractional crystallization (DePaolo 1981). Low Al_2O_3, Nb, and Ti concentrations and positive co-variation of Zr with Ti are also consistent with melts

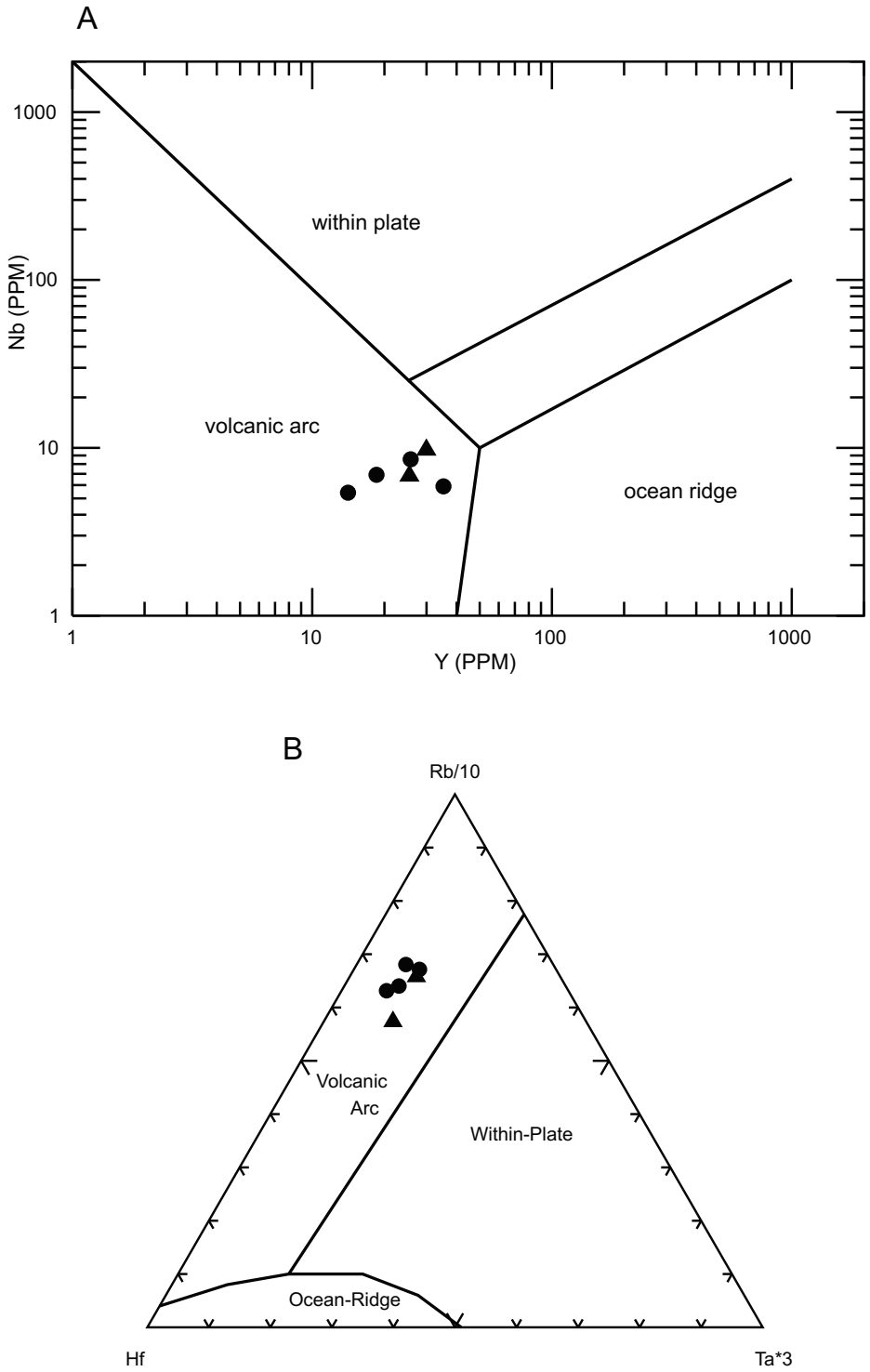

Fig 3-17. Geochemical tectonic discrimination of Telkwa Formation rhyolites. A) Pearce et al. (1984); B) Harris et al. (1986). The rhyolites, like the Telkwa Fm. basalts (Fig. 3-15), have a volcanic arc affinity.

produced by crustal fusion (Lentz 1996; Dostal 1989). Variable negative Eu anomalies indicate that the magmas experienced some fractionation of feldspar.

I propose that post-Stuhini-arc, renewed or reconfigured subduction beneath Stikinia resulted in crustal underplating and low-degree partial melting within the crust, generating felsic magmas that erupted from local rhyolitic centres at the base of the Mt. Henderson complex. Shortly after, fractionated mantle-derived magmas ascended, producing the voluminous andesitic pyroclastic rocks that also characterize the lower part of the Mt. Henderson complex. The relative scarcity of felsic rocks in the Mt. Henderson complex is consistent with its rapid construction, which required fast ascent of mantle-derived magmas, possibly reducing the volume of magma ponding at the base of the crust. In contrast, the Mt. O'Brien complex, which was built much more slowly (over at least 6 million years), encompassed multiple periods of quiescence during which underplating could have generated felsic magmas via crustal anatexis. Felsic volcanism during construction of the upper portion of the Mt. O'Brien complex, and which built most of the Kitselas complex (ca 194 Ma), may have resulted from prolonged underplating, similar to that which generated the 1980 eruption of felsic magma at Mt. St. Helens (Severs et al. 2013) in the Cascade Arc.

3.7 Evolution of the Hazelton Group near Terrace

Near Terrace, the Hazelton Group records a 25 My span of latest Triassic to Early Jurassic island-arc magmatism (Fig. 3-8, 3-18). In the lower Hazelton Group, the Telkwa Formation represents a successor arc built upon Paleozoic arc-related rocks of the Zymoetz Group, and deep-water sedimentary rocks of the Stuhini Group (Upper Triassic). A profound tectonic break during the Late Triassic involved cessation of deep-water sedimentation of thin, starved sequences of black chert and argillite, rapid uplift above wave-base, and regional erosion. The slightly younger (latest Triassic) rocks at the base of the Telkwa Formation were deposited on an irregular, and in places steep, topography which promoted high-energy deposition of locally derived coarse clasts and regionally derived finer matrix (Fig. 3-18A). The steep topography necessary for high-energy deposition is not consistent with the paleotopography locally observed on the

unconformity surface between the Telkwa Formation and older units. This surface is characterized by a gentle bevelling from the north to the south, where approximately 100 metres of material was removed; the surface was also incised by numerous channels which range from a few metres to 500 metres apparent width. We propose that Telkwa-age (ca. 204 Ma) syn-depositional faulting superimposed a rugged topography on the otherwise gentle unconformity surface, allowing for high-energy deposits of the basal Telkwa Formation conglomerate (Fig. 3-18A). Channels incised into the unconformity surface likely formed during this later high-energy erosional and depositional event.

By ca 204 Ma, small felsic volcanic centres were widely distributed (e.g., Mt. Pardek; Figs. 3-2, 3-3, 3-8). The felsic magmatism resulted from crustal anatexis driven by heat from subduction-related mantle melts that initially underplated Stikinia. Deposition of the basal conglomerate and formation of local volcanic centers spanned approximately 2 My and was followed by rapid ascent of hydrous mantle-derived melts that led to explosive and then effusive eruptions from a centre at Mt. Henderson. These eruptions deposited andesitic pyroclastic breccias that formed a regionally extensive, relatively homogeneous drape (Fig. 3-18B), overlain by voluminous andesitic lava flows. Detrital zircon age constraints from the base (ca 202.5 Ma), and a zircon crystallization age from the middle (201.8 Ma), of the Mt. Henderson complex indicate rapid accumulation of an ≈ 6 km thickness of predominantly andesitic volcanic rocks.

A second former stratovolcano is represented by the Mt. O'Brien complex, 8-30 km north of the Mt. Henderson complex (Fig. 3-2, 3-18C). The base of the volcano is built on pyroclastic fall deposits, interpreted to have originated from the Mt. Henderson complex, constraining the age of initial Mt. O'Brien complex volcanism to between ca 202.5 Ma (approximate age of top of basal conglomerate) and ca. 200 Ma (approximate age of older phase of the Kleanza Pluton). At the base of the complex, volcanogenic sandstone, siltstone, and minor conglomerate fill an erosional surface cut in the Mt. Henderson pyroclastic fall deposits, demarking a subtle unconformity that formed during an episode of volcanic quiescence. The Mt. O'Brien complex is centred on the Bornite Range and Mt. O'Brien, where it is intruded by the long-lived, co-magmatic and multi-phase

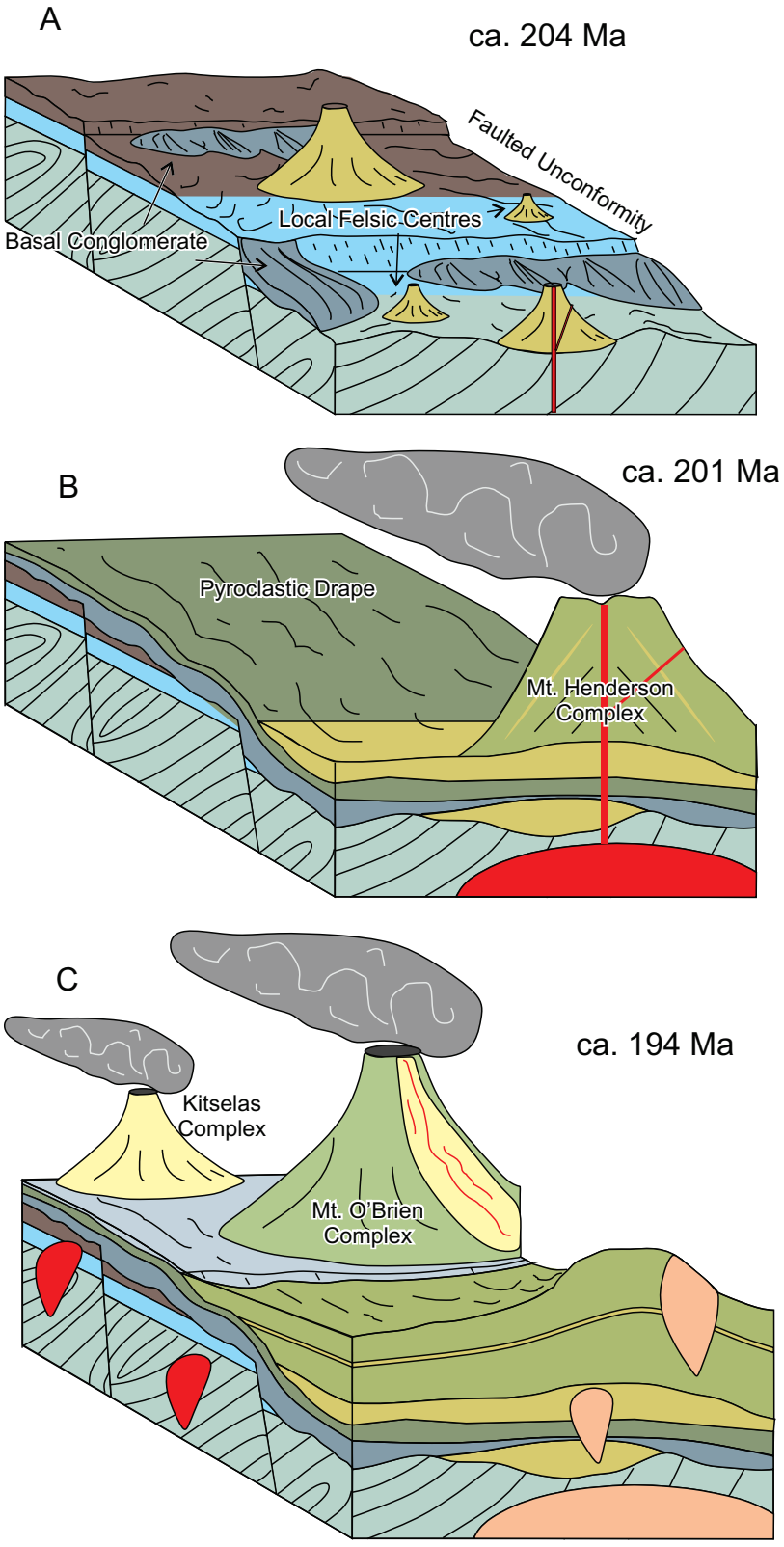

Fig. 3-18. Block diagrams showing evolution of the Hazelton Group near Terrace, BC; colours as in legend for Fig. 3-2. A) Deposition of basal Telkwa Formation conglomerate and development of local felsic centres on a faulted unconformity surface that gently cuts through Stuhini Group (brown), Ambition Fm. (blue) and into deformed Mt. Attree Fm. rocks. B) Regional drape of pyroclastic breccia (dark green) and the construction of the Mt. Henderson stratovolcano. C) Construction of the Mt. O'Brien and Kitselas complexes/stratovolcanoes.

Kleanza pluton. Most of the volcanic rocks, especially at the base of the complex, consist of coherent, mantle-derived, andesitic flows. Higher in the sequence, the proportion of felsic volcanic rocks increases. A voluminous pulse of felsic volcanism, which erupted ca. 194 Ma, is represented in the upper portion of the stratigraphy. Near the top of the Mt. O'Brien complex, tuffs become finer grained and are overlain by the Nilkitkwa Formation (178.90±0.28 Ma), which consists of red vitric and crystal tuff with minor basaltic flows and limestone intervals. The transition into the Nilkitkwa Formation represents a gradual decrease in volcanic activity over approximately 15 My. The majority of the Mt. O'Brien volcanic rocks have characteristics typical of sub-aerial environments (welding of clasts, red oxidized volcanic rocks, absence of pillow basalts, scarce sedimentary rocks, and very little lateral continuity). Limestone intervals in the Nilkitkwa Formation are evidence that the Telkwa arc was at least partly submerged by Toarcian time.

The Kitselas complex (195 ± 2 Ma, 193.9 +2.1/-0.6 Ma; Gareau et al. 1997a) is roughly coeval with felsic flows near the middle to upper parts of the Mt. O'Brien complex (194.35 ± 0.32 Ma). Although felsic magmatism was coeval in the two complexes, it was less voluminous at the mainly andesitic Mt. O'Brien complex (Fig. 3-18C). Early Jurassic felsic centres are sparse in Stikinia; at least 4.5 km thick, the Kitselas complex is one of the most significant, comparable only to those in Whitesail Lake area 100 km to the south-east of Terrace (Gordee 2005), and in the Toodoggone Formation of eastern Stikinia (Duuring et al., 2009). The thick felsic volcanic section at the Kitselas complex and coeval felsic intervals at the Mt. O'Brien complex imply partial melting of significant volumes of lower-crustal rocks, as indicated by geochemical data. The felsic volcanism was likely preceded by crustal underplating that generated the heat necessary for crustal melting.

3.8 Economic Implications: Northern Stikine Porphyry Cu-Au Belt

This study shows that two key suites of high-level intrusions that host porphyry copper deposits, latest Triassic (205-201 Ma) and Early Jurassic (197-190 Ma) were coeval and co-magmatic with Hazelton Group volcanism (Fig. 3-8). Ages of felsic volcanism in the

Mt. Henderson, Mt. O'Brien and Kitselas complexes corresponds to the timing of formation of porphyry copper deposits (Fig. 3-8). Basal felsic volcanism at ca 204 Ma in the Mt Henderson complex corresponds to Red Chris, GJ and a pulse of mineralization at Galore Creek, and ca 194 Ma felsic volcanism in the Mt. O'Brien and Kitselas complexes corresponds to the age of the Kerr-Sulphurets-Mitchell deposits (Fig. 3-8).

The temporal and geographic association of ca 205-195 Ma Hazelton Group arc-related volcanism and a belt of porphyry Cu-Au deposits of identical age suggests a genetic relationship. We propose that the timing of felsic volcanism in the Telkwa Formation is linked to mineralized porphyry intrusions through shared dependence on crustal underplating (Fig. 3-19): larger volumes of ponded magmas, and sufficient time to allow crystallization of those magmas, are required to produce the heat necessary to generate felsic crustal melts; likewise, crystallization of subduction-generated, oxidized magmas, ponded at the base of the crust, will produce the volatile-rich, metalliferous magmas that are parent magma to mineralizing porphyry intrusions (Richards 2003). The re-initiation or reconfiguration of subduction beneath Stikinia, which is marked by the initiation of Hazelton Group arc volcanism, may have led to conditions favourable for porphyry copper deposit formation including: 1) a new source of metals and a mechanism for mobilizing them during dehydration of the subducting slab; 2) development of structural conduits for emplacement of high-level intrusions via hinge-retreat induced inter-arc extension; and 3) deposition of thick sections of highly permeable conglomerates that may have enhanced hydrothermal circulation and focussed mineralizing fluids (e.g. Nelson and Kyba 2014).

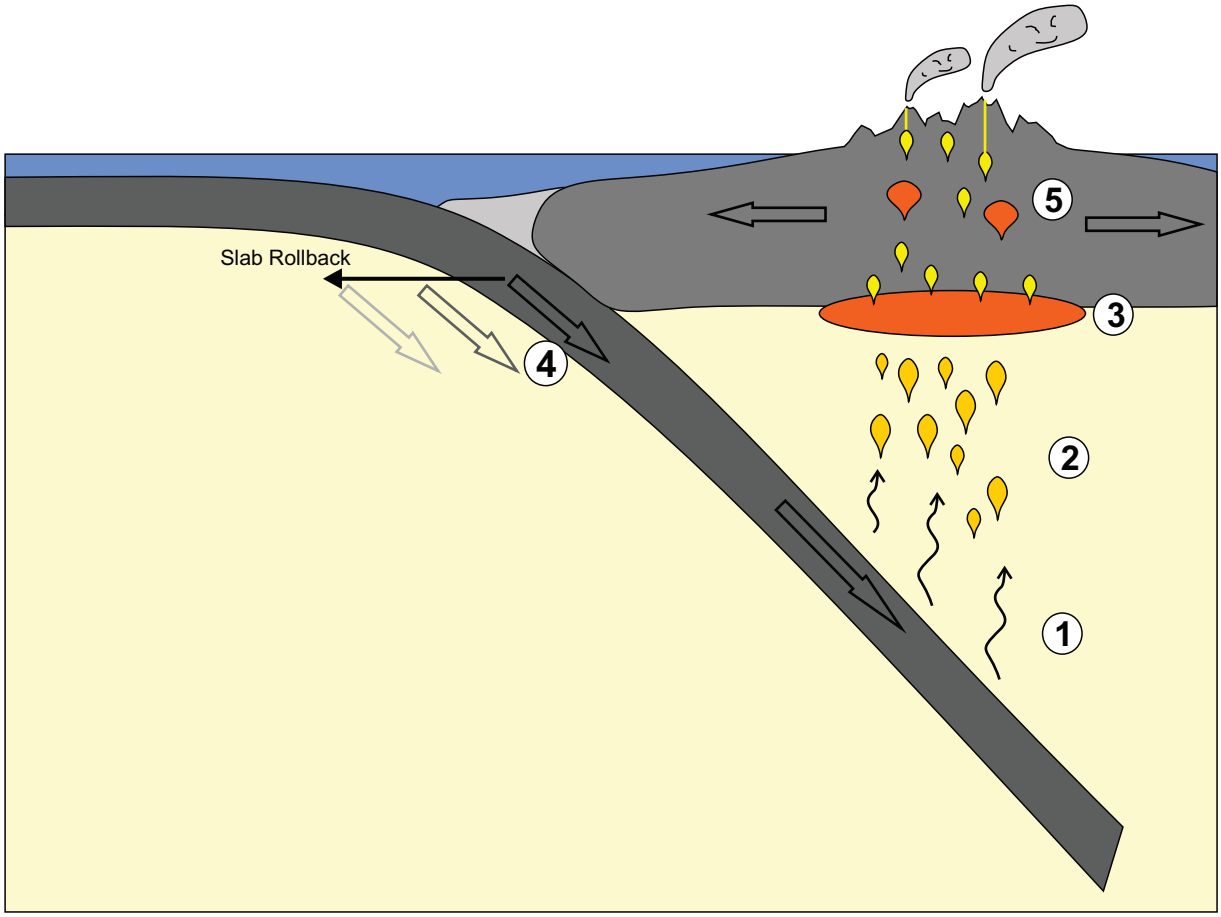

Fig. 3-19. Shared dependance on magmatic underplating explains the similarity in ages between pulses of felsic volcanism in the Telkwa Formation and Stikinian porphyry Cu deposits. Dehydration of a subducting slab beneath Stikinia led to upwelling of metalliferous fluids (1), which resulted in dehydration melting of the mantle and generation of highly oxidized, metalliferous magmas (2). The magmas ponded at the base of the crust due to density differences, creating a MASH zone (see text) (3). Crystallization of magma within the MASH zone resulted in further enrichment of the metals found in porphyry copper deposits. Heat from the ponded magma and latent heat of crystallization resulted in crustal anatexis and generation of felsic magma. An extensional tectonic regime related to slab-rollback (4) facilitated emplacement of the metalliferous magmas to high crustal levels (porphyry Cu deposits), as well as ascent and eruption of the crustally derived felsic melts (5).

3.9 Conclusions

The Hazelton Group in central Stikinia near Terrace records 25 My of subduction-related magmatism that extended from latest Triassic to late Early Jurassic. The Telkwa Formation (lower Hazelton Group) comprises up to 16 km of volcano-sedimentary rocks that define two former stratovolcanoes and a rhyolitic centre. The Telkwa Formation is separated from older Paleozoic and Triassic age rocks of the Zymoetz and Stuhini groups by a Late Triassic angular unconformity. Telkwa Formation volcanism began ca 204 Ma as a series of felsic centres and was followed by explosive eruptions of voluminous, volatile-rich, intermediate lavas. Subsequent volcanism at the Mt. Henderson, Mt. O'Brien and Kitselas volcanic-intrusive complexes comprised mafic to felsic, medium- to high-K, calc-alkaline, island-arc volcanic rocks, and coeval plutons, stocks, and dikes. Mafic and intermediate volcanics are interpreted to be the result of a relatively homogenous, mantle-derived differentiated suite generated from hydrous melting of isotopically juvenile spinel lherzolite in the mantle wedge. Felsic rocks are interpreted to have formed by crustal anatexis driven by heat from crustal underplating.

New U/Pb zircon ages presented in this study place initiation of Hazelton Group volcanism in the latest Triassic (ca 205-204 Ma). Initiation or reconfiguration of subduction at that time created structural and magmatic conditions that were favourable for the formation of mineral deposits and, in particular, for the emplacement of intrusions hosting ca 205-190 Ma porphyry Cu-Au deposits found throughout northern Stikinia.

Chapter 4 - The Upper Hazelton Group (Iskut River Formation): Tectonomagmatic and Stratigraphic Controls on Metallogenesis in the Eskay-Rift

4.0 Preface

Chapter 4 focuses on establishing geological context for geochemical data presented in Chapter 5 and integrates data from a number of different sources including my own collaborative work conducted with the Geological Survey Branch of the British Columbia Ministry of Energy and Mines and the Geological Survey of Canada.

This chapter contains original material as well as material published in the following three articles:

> Barresi, T., Nelson, J.L., Dostal, J. 2015. Geochemical constraints on magmatic and metallogenic processes: Iskut River Formation, volcanogenic massive sulfide-hosting basalts, NW British Columbia, Canada. Canadian Journal of Earth Sciences 52: 1-20.
>
> Barresi, T., Nelson, J.L., Alldrick, D.J., Dostal, J. 2005. Pillow Basalt Ridge Facies - detailed mapping of Eskay Creek equivalent stratigraphy. Geological Fieldwork 2004, Paper 2004-3: 41-52.
>
> Alldrick, D.J., Nelson, J.L., Barresi, T. 2005a. Geology and mineral occurrences of the upper Iskut River area: Tracking the Eskay Rift through northern British Columbia. Geological Fieldwork 2004, Paper 2004-2: 2-39.

Two relevant government open-file maps, which include mapping data acquired during the 2004 field season by the thesis author, are included in Appendix E:

> Alldrick, D.J., Nelson, J.L., Barresi, T. 2005b. Geology of the Volcano Creek - More Creek Area, British Columbia. British Columbia Ministry of Energy, Mines and Petroleum Resources, Open File Map 2005-5, scale 1:50 000.

Alldrick, D.J., Nelson, J.L., Barresi, T., Stewart, M.L. and Simpson, K.A. 2006a. Geology of upper Iskut River area, northwestern British Columbia. BC Ministry of Energy and Mines, Open File Map 2006-2, Scale 1:100 000.

Appendix D contains copyright agreement forms for all published manuscripts used in this thesis.

4.1 Geological Setting of the Eskay Rift

The Canadian Cordillera, outboard of the parautochthonous continental margin, is made up of allochthonous tectono-stratigraphic terranes (Fig. 4-1), mostly accreted to the western margin of Laurentia (ancestral North America) in Jurassic–Cretaceous time (e.g., Coney et al. 1980; Monger et al. 1982; Monger et al. 1991; Wheeler et al. 1991; Mihalynuk et al. 1994; Nelson et al. 2013). The inner peri-Laurentian terranes formed part of, or were proximal to, the western margin of Laurentia. Prominent among these, the Stikine terrane (Stikinia) stretches along the full length of British Columbia and extends into the Yukon (Fig. 4-1). It is over 500 km wide, tapering to <100 km in southern British Columbia and Yukon. The upper Paleozoic – Lower Mesozoic geological record of Stikinia consists of (*i*) Devonian to Permian, volcano-sedimentary, arc-related, and pericratonic rocks (Stikine assemblage, Asitka Group; Hart 1997; Logan et al. 2000; Colpron et al. 2006; Gunning et al. 2006; Roots et al. 2006), and (*ii*) Middle–Upper Triassic Takla and Stuhini groups unconformably overlain by the Lower–Middle Jurassic Hazelton Group (Tipper and Richards 1976; Monger et al. 1991; MacIntyre et al. 2001; MacIntyre 2006). Both Mesozoic sequences consist of arc-related, mafic-intermediate pyroclastic rocks, massive flows, and epiclastic rocks, and lie on, or laterally interfinger with, argillites, limestones, and minor volcanogenic epiclastic rocks. The Paleozoic Stikine assemblage, at least in part, is inferred to overlie the pericratonic Yukon–Tanana terrane (Jackson et al. 1991; Gehrels and Kapp 1998).

The Iskut River Formation (IRF) lies within a 300 km long and 50 km wide northtrending belt (Fig. 4-1) first described by Anderson (1993). It is informally referred to as the Eskay rift. Work by Alldrick et al. (2004a,b, 2005a,b, 2006), Simpson et al. (2004), and Barresi et al. (2005) further delineated the extent and significance of the Eskay rift north of Eskay

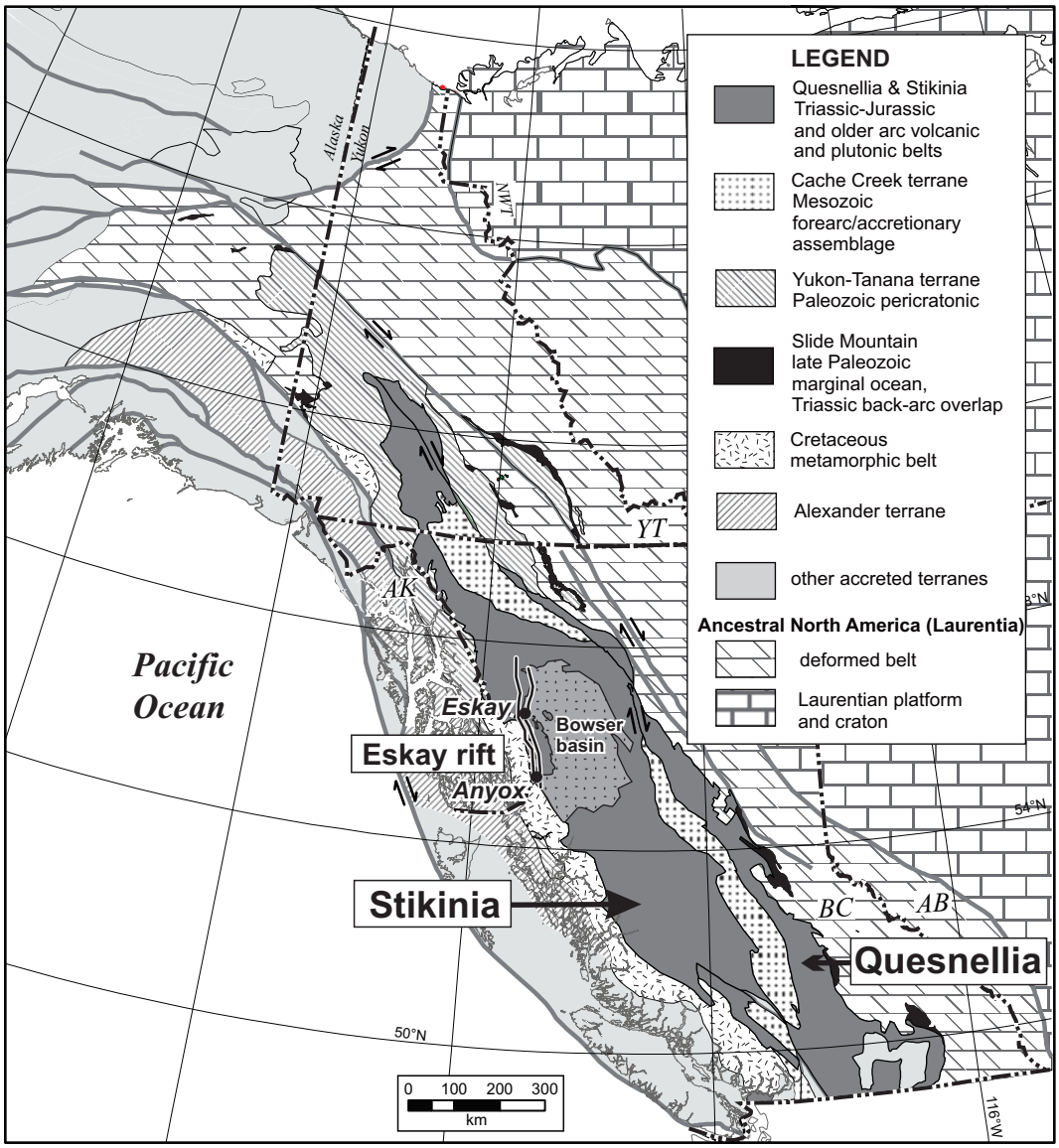

Fig. 4-1. Tectonic assemblage map showing the position of Stikinia in the Cordillera and the Eskay rift in Stikinia. Note the length and width of Stikinia, a terrane that represents a sub-continent that accreted to ancestral North America (Laurentia). The Bowser Basin (east of the Eskay rift and separating eastern and western portions of Stikinia) is a sedimentary tectonic overlap assemblage that formed following the accretion of Stikinia, Quesnellia and the intervening Cache Creek terrane to Laurentia. The Cache Creek terrane is a sliver of obducted oceanic and forearc crust that may have been entrapped between an originally contiguous composite Stikine and Quesnel terrane during oroclinal rotation (Mihalynuk et al. 1994).

Creek by defining nine individual rift sub-basins, each with similar rock types, ages (ca. 174–176 Ma; Childe 1996; Evenchick et al. 2004; Alldrick et al. 2005a), and graben-like characteristics. Together with sub-basins identified south of Eskay Creek (Evenchick et al 2004; Lewis 2013), the Eskay rift belt includes at least 12 sub-basins. The sub-basins are interpreted by Nelson et al. (2013) to be en-echelon transtensional grabens that formed as a result of oblique collision between Stikinia and adjacent inboard and outboard terranes.

Bimodal volcanic rocks within the Eskay rift have been assigned formal and informal stratigraphic names, including "upper Hazelton Group" (Ferri et al. 2004; Evenchick and Thorkelson 2005; Waldron et al. 2006; Gagnon et al. 2007; Evenchick et al. 2010), "Salmon River Formation" (Anderson and Thorkelson 1990; Anderson 1993; Lewis et al. 2001; Lewis 2013), and Mount Dilworth Formation (Alldrick et al. 1989; Alldrick and Britton 1992; Alldrick 1993). Gagnon et al. (2012) clarified and revised Hazelton Group stratigraphy to recognize the regional extent and diachronous age of the included formations. They formally defined the IRF to comprise the dominantly volcanic rock successions that fill the Eskay rift. The Quock Formation (Gagnon et al. 2012), a thin succession of sedimentary rock and felsic tuff that is stratigraphically equivalent to the IRF, but occurs outside the margins of the rift basins, shows a broader range in ages than the IRF, from Toarcian in the north to Callovian in the south.

The Iskut River and Quock formations represent the uppermost units of the Jurassic Hazelton Group (Gagnon et al. 2012). They are onlapped by turbiditic siltstones and shales of the Bowser Lake Group (Figs. 4-1, 4-2). The IRF comprises the most voluminous and volcanic-rich Middle Jurassic strata of the Stikine terrane. It was deposited during a brief period at the boundary between the Aalenian and Bajocian epochs ca. 174–176 Ma (Fig. 4-3; Childe 1996; Evenchick et al. 2004; Alldrick et al. 2005a) within syn-depositional extensional grabens. The IRF is composed of tholeiitic pillow basalts and basalt breccias (>90%) and conglomerates that were deposited near graben-bounding faults, which grade into distal turbidites with interlayered felsic tuff, sandstone, and chert, and intervals of alternating rhyolite, mudstone, and basalt (Fig. 4-3; Alldrick et al. 2005a,b; Barresi et al. 2005). Typically, the rift-filling IRF strata are in angular discordance with the underlying basement rock; however, in a few rift segments,

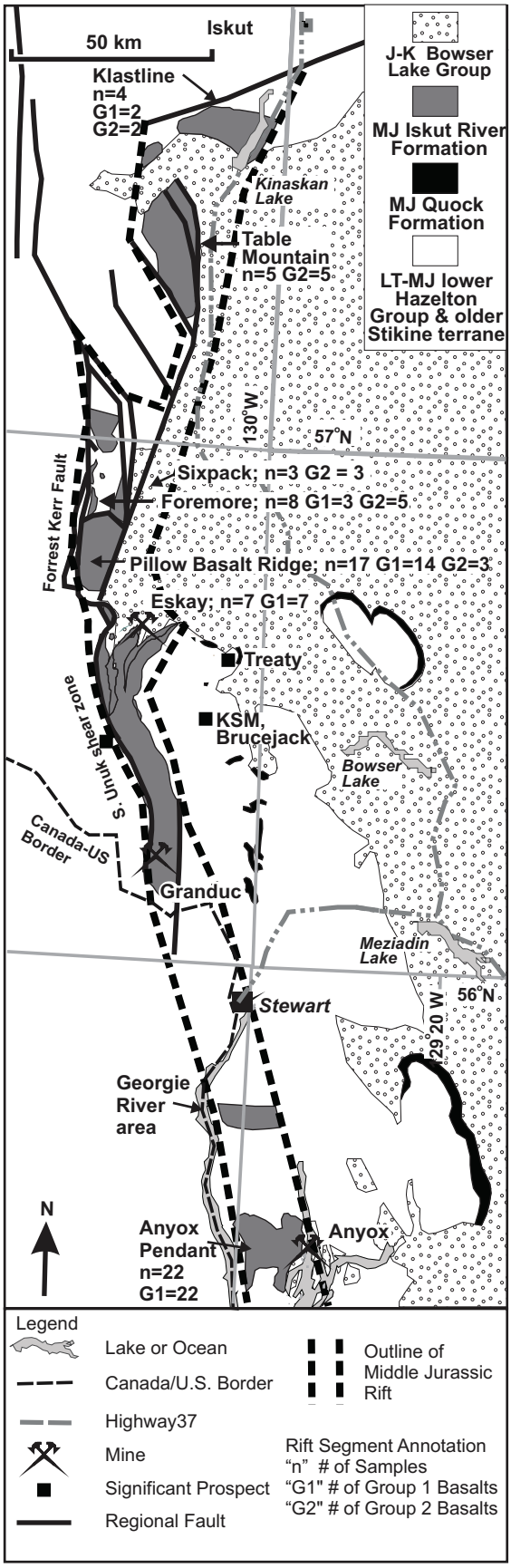

Fig. 4-2. Map showing the regional distribution and geological context of the IRF, including the location and names of rift segments. Note that the boundaries of the IRF are typically major regional faults, reflecting the structural control on their distribution. Numerical annotation beneath segment name is relevant to geochemical data presented in Chapter 5: n, number of geochemical samples (see section 5.7.0); G1 and G2, number of samples that are group 1 versus group 2 basalts. All geochemical data are newly presented in this thesis except those from Anyox (MacDonald et al 1996b; Smith 1993), Eskay Creek (Lewis 2001 and reference therein), and some Table Mountain samples (Barresi and Dostal 2005). Modified after Evenchick et al (2004). J, Jurassic; K, Cretaceous; KSM, Sulphurets-Mitchell; LT, Late Triassic; MJ, Middle Jurassic.

IRF strata are locally conformable with underlying Lower Hazelton Group rocks. A hiatus of some 10 million years separates the ca. 174 Ma IRF rocks from ca. 185 Ma and older strata of the Lower Hazelton Group (e.g., Betty Creek and Mount Dilworth formations).

The IRF represents the last stage of Mesozoic volcanism in northern Stikinia. It marks a distinct shift in the tectonomagmatic evolution of Stikinia from typical subduction-related island-arc volcanism of the Lower Hazelton Group, with calcalkaline, predominantly intermediate, volcanic rocks (Marsden and Thorkelson 1992), to a bimodal volcanic suite typical of back arc basins (Macdonald et al. 1996a).

4.2 Comparative Stratigraphy[3]

The rift segments compared in this study represent a range of geological settings within the Eskay rift, from roof pendants, to fault slivers, and fully preserved sections. Variations in the stratigraphy include: the overall thickness of the graben-bound packages, proximity to graben-bounding structures, and the sequence and thicknesses of individual sedimentary and bimodal volcanic units. While variations in the stratigraphy are expected within and between rift segments, marked and dramatic differences in the thickness and sequence of the stratigraphic sections in adjacent segments suggests that these sections are separate sub-basins with little interconnectivity, but which nevertheless experienced similar but volumetrically diverse, sedimentary and volcanic events.

The general geological setting and locations of the sub-basins are located on Fig. 4-2; Figs. 4-3 and 4-4 show more detailed geology and topography between Eskay Creek in the south and Moore Creek in the north. Comparative stratigraphic columns are illustrated on Fig. 4-5, and their locations are demarked on Fig. 4-2. The detailed geology of all areas north of Eskay Creek are included on the 1:50 000 and 1: 100 000 scale geological maps in appendices E.2, E.3.

[3] Refer to chapter 2.6 for descriptions of the Eskay Creek and Table Mountain sections, and to section 4.4 of this chapter 4.4 for detailed descriptions of the Pillow Basalt Ridge section.

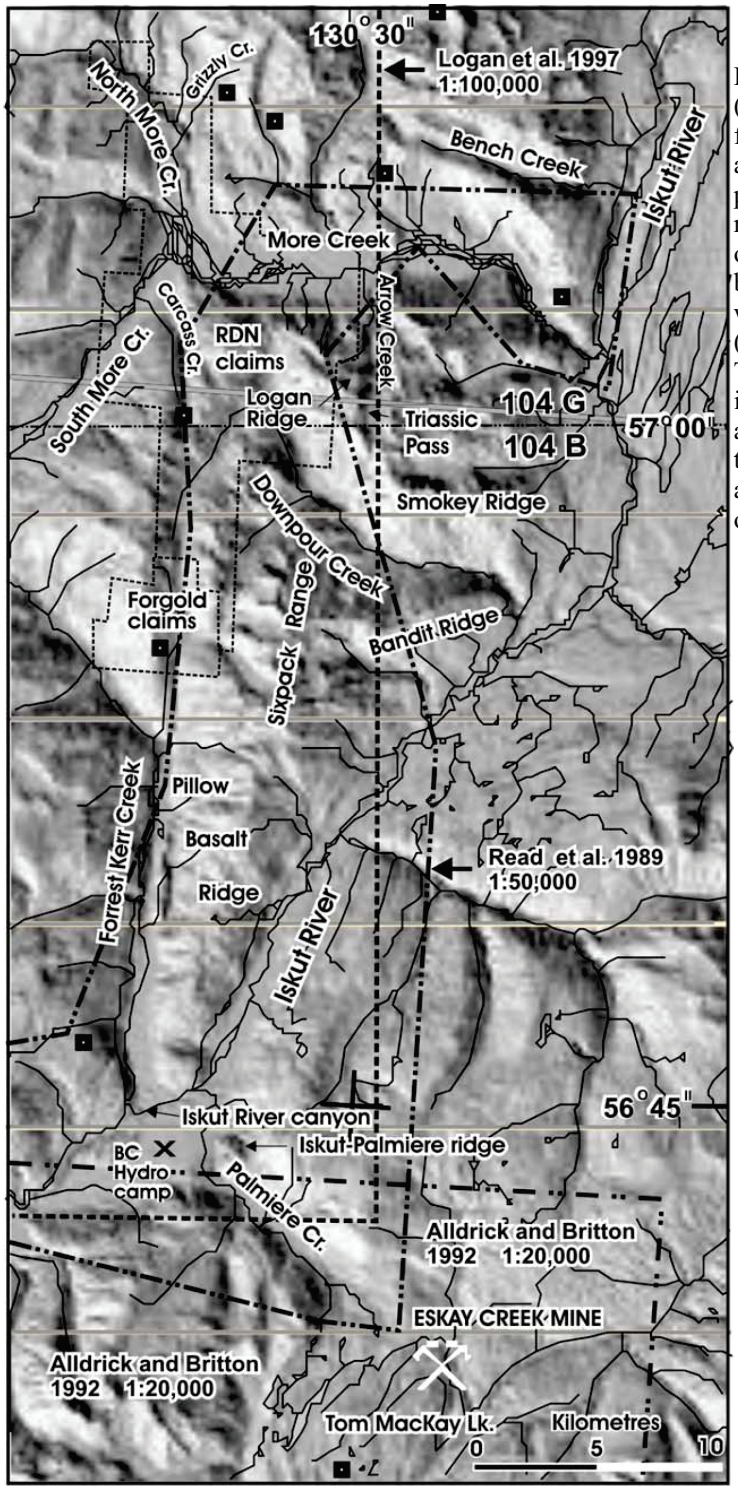

Fig. 4-3. Shaded digital elevation model (DEM) map showing major topographic features in the map area between Eskay Creek and More Creek and the boundaries of previous regional mapping projects. Note that recessive topographic linears bound sections of IRF. For example, Pillow Basalt Ridge is bordered on the west by Forest Kerr Creek, which juxtaposes IRF with Paleozoic rock (Fig. 4-4), and the Iskut river to the east. These topographic features, which are interpreted to be a result of faulting that was active during the deposition of the IRF, extend to the north through Triassic Pass and Carcass and North More creeks where they bound other sections of IRF.

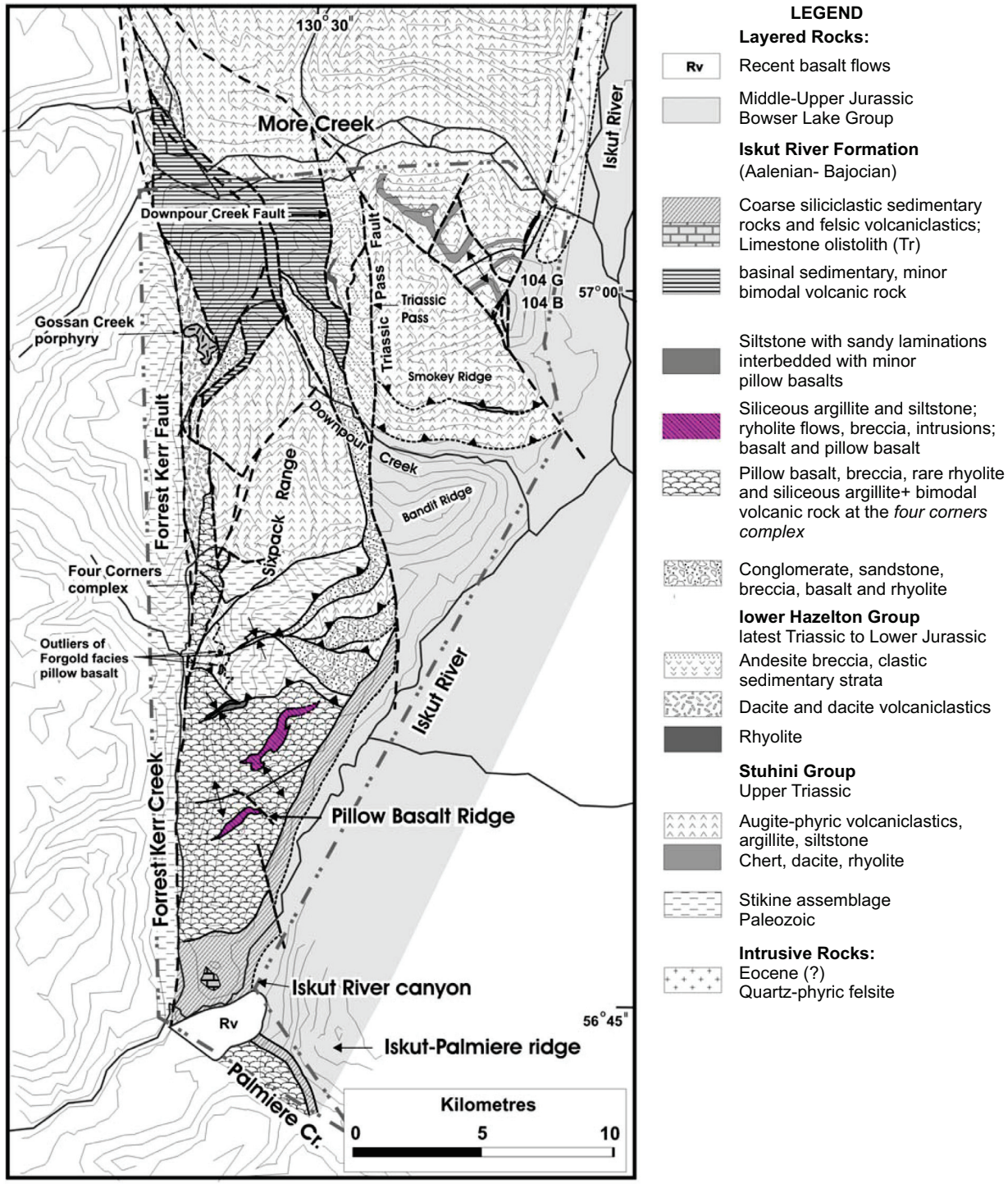

Fig. 4-4. Simplified geologic map of the More Creek - Palmiere Creek Area. The IRF is composed mainly of pillow basalts in the south, and has variable high- and low-energy deposits of sedimentary rock (along with bimodal volcanic rock) to the east and north surrounding a central (uplifted) core of older lower Hazelton and Stuhihi groups and Stikine assemblage rock. Note the IRF is largely bound by faults, but in places is in depositional contact with older rock units including the Paleozoic Stikina assemblage, indicating exhumation and deep erosion.

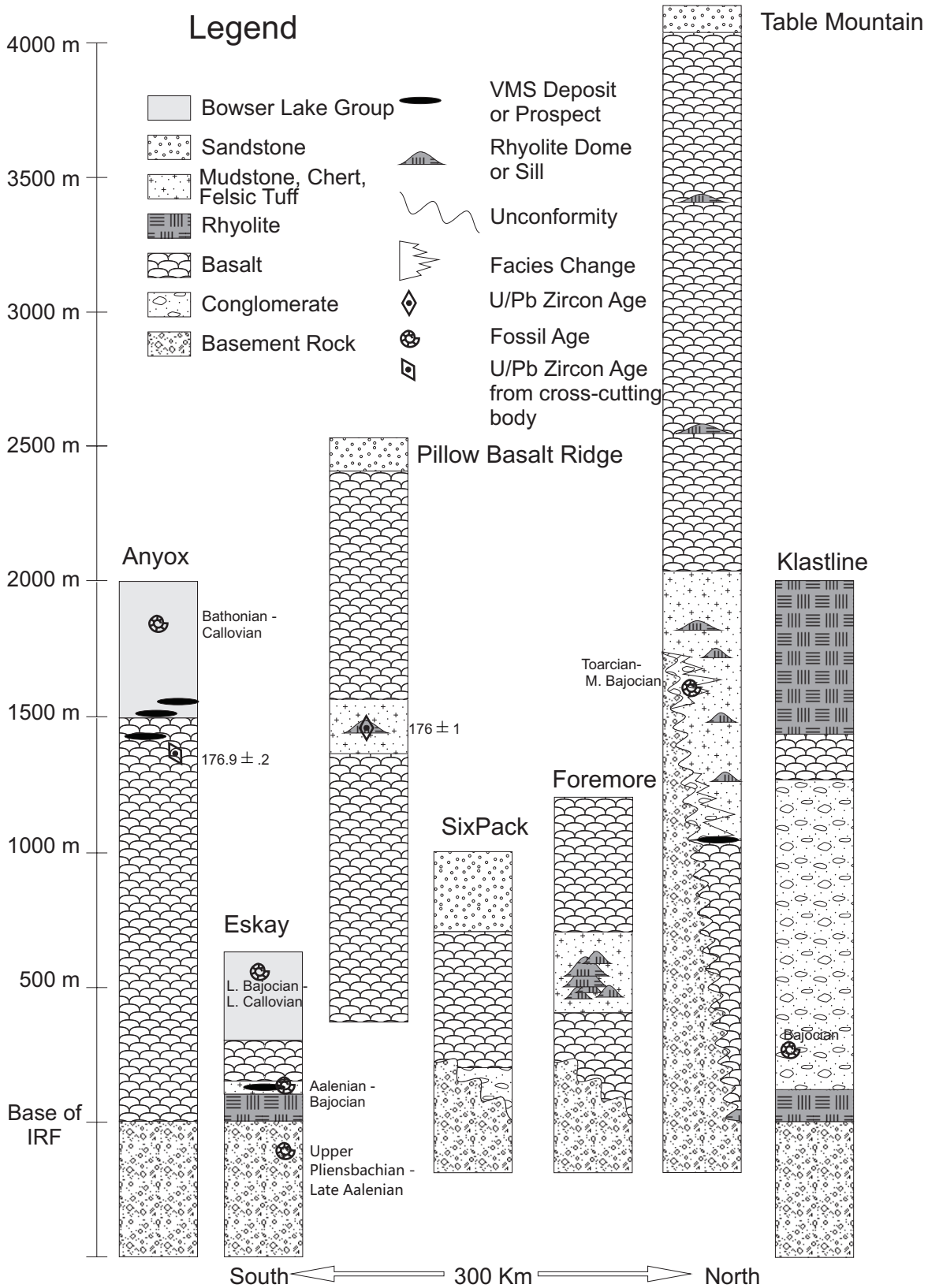

Fig. 4-5. Stratigraphic columns for seven sub-basins that are a primary focus of this thesis. Note that while the sub-basins contain similar rock types, the main lithologies occur in different sequences and thicknesses. This is interpreted to be a result of limited connectivity between sub-basins.

4.2.1 Anyox

The Anyox pendant (Figs. 4-2, 4-5) is the most southerly section of known IRF rock (Fig. 4-2). It is preserved as a structurally complex, metamorphosed roof pendant in a Tertiary granitoid body (Smith 1993, Evenchick and McNicoll 2002). At Anyox the IRF lies above, but in faulted contact with, Early Jurassic Hazelton Group metasedimentary and volcanic rocks. It consists of an approximately 1.5 km thick pile of pillow basalt and pillow basalt breccia. The basalt is conformably overlain by sand- and silt-stones turbidites correlated with the Bowser Lake Group. An extensive geochronological study in the Anyox area (Evenchick and McNicoll 2002) constrains the IRF basalts to the late Early – early Middle Jurassic, ca. 178 + 1/-1.5 Ma (Palfy et al. 2000). Pods of massive sulfides, which form the Hidden Creek and Bonanza VMS deposits, are near the top of the sequence where IRF basalts are interbedded with thin mudstone intervals.

4.2.2 Iskut River Unit

The Iskut River unit overlies the *PBR unit* in the lowlands along the west side of the Iskut River (Fig. 4-4), east and downslope of the crest of Pillow Basalt Ridge, and on the low hill south of Pillow Basalt Ridge and extending into the Iskut River Canyon near the old BC Hydro camp (Fig. 4-4). Correlative strata occur on the Iskut-Palmiere Ridge, where they were deposited between basalt assigned to the Eskay hangingwall unit, and basal strata of the Bowser Lake Group. Samples collected along the Iskut River canyon have yielded Middle Jurassic or possibly early Late Jurassic fossils (Collection F141; H.W. Tipper in Read et al., 1989), making it one of the youngest units in the Lower-Middle Jurassic Eskay Rift sequence.

Downhill and east of Pillow Basalt Ridge, the *Iskut River unit* consists of mixed siliciclastic and felsic volcanic strata, with a preponderance of coarse clastic material. The felsic rocks are mostly light green to pale grey volcaniclastics, rhyolite and dacite breccias, and fine crystal-ash tuffs. One outcrop ridge of massive rhyolite was located in the course of two traverses in the area; it is likely that more could be identified with further detailed work. The siliciclastic rocks comprise interbedded white arkosic sandstone, sedimentary breccia, quartz-feldspar granule conglomerate, and dark grey silty

argillite. In some areas, thinly interbedded sandstone and argillite resemble the Bowser Lake Group. They are distinguishable, however, based on the presence of felsic detritus and the absence of chert clasts in the sandstones, and on the presence of interbeds of felsic volcaniclastic material. In other exposures, bedding is uneven and soft-sediment deformation structures and sedimentary intraclasts are present. Large felsic volcaniclastic olistoliths and small white, pale green and bright sea-green felsic clasts within sedimentary breccias are notable features of this sequence. The felsic clasts show irregular, wispy outlines indicating incorporation in the matrix while still unconsolidated. Felsic detritus decreases in abundance northward. North of Pillow Basalt Ridge (north of the Kerr Bend fault), the sequence consists of a thick, cliff-forming unit of white arkosic sandstone overlain by dark grey slate that extends east as far as the Iskut River.

South of Pillow Basalt Ridge, the *Iskut River unit* is dominated by dacitic volcaniclastic material, with subordinate black argillite and other rock types. The felsic breccias are chaotic and unsorted. Clasts range in size from < 1cm up to olistoliths many metres across. All clasts are angular. Concentrations of coarser clasts show incipient fragmental (crackle breccia) to disaggregated (mosaic breccia) textures. Pulverised, fine-grained, sand-sized material forms both clasts in an aphanitic groundmass, and groundmass for larger clast populations. The source volcanic rock, as seen in clasts, is pale green, aphanitic to porphyritic dacite with small, sparse feldspar crystals. Massive dacite is rare. One outcrop of black, flow-banded rhyolite was noted. Its contact relationships are unknown, it could be either a local flow or a large block within the breccia.

Read et al. (1989) reported a single outcrop of limestone at the base of the felsic unit on the south slope of Pillow Basalt Ridge from which they extracted Early Permian conodonts (collection F129). This limestone is an olistostromal block surrounded by felsic breccia matrix. Other smaller limestone exposures occur within the felsic breccia. The nearest exposures of Early Permian limestone are 4 km west of Forrest Creek, and 10 km to the north within an uplifted block of Paleozoic rocks north of the Kerr Bend fault.

The hill immediately south of Pillow Basalt Ridge, and immediately northeast of the mouth of Forrest Kerr Creek, is underlain by basalt, andesite and dacite flows or tuffs and mixed sedimentary rocks intruded by small diorite and gabbro plugs. These strata are cut

by a recent volcanic chimney south of the summit, where a small circular lake fills the vent. Carbonates on this hill have given Triassic conodont ages (Collection F138, Read et al., 1989); they could be olistrostromes like the Paleozoic body described above.

North of Palmiere (Volcano) Creek, a thin unit of felsic volcaniclastic rocks and argillite crops out in the saddle between the main high ridge to the northeast and the small spur that overlooks the lower Iskut River Valley to the west. The lower part of this unit consists of chaotic, unsorted felsic breccia similar to the breccias of the Iskut River unit exposed at the south end of Pillow Basalt Ridge. The source rock is a pale grey-green to white, aphanitic to microporphyritic dacite or rhyolite. Clasts of medium-grained granodiorite are also present in the breccia. Most common are angular-clast breccias and crystal-ash tuffs, all without visible bedding. Rhyolite mosaic breccia with a black, siliceous matrix is present in places. The felsic breccias grade upwards into black, siliceous, pyritic argillite, which hosts the Iskut-Palmiere mineral occurrence (Alldrick at al 2005). The base of the argillite is interbedded with felsic breccia and stray felsic clasts are found supported within the argillite. All these rocks overlie basalt correlated with the Eskay Creek hangingwall unit and the PBR basalts, and these rocks are overlain in turn by sandstones and mudstones of the Bowser Lake Group.

The Iskut River unit overlies the pillow basalts and siliceous siltstones of Pillow Basalt Ridge facies with angular discordance, truncating units in the gently folded underlying sequence. A strong set of northeasterly topographic lineations on southeastern PBR, interpreted as flow-layering between separate eruptions of pillow basalt, is deflected northwards towards the base of the Iskut River unit. The Kerr Bend fault does not penetrate the base of the Iskut River unit. North of the fault, Iskut River unit arkose overlies rocks of the hangingwall strata of the Kerr Bend fault. The upper contact of the Iskut River unit with the Bowser Lake Group was not observed during this study.

The Iskut River unit exhibits a marked departure in volcanic and sedimentary regime from the underlying PBR facies. Effusive eruptions of basalt were succeeded by explosive felsic, mainly dacitic volcanism, while the pelagic, distal sedimentation associated with PBR was succeeded by coarse siliciclastic sedimentation in the *Iskut River unit*. Steep slopes are indicated by coarse grain sizes, synsedimentary deformation,

and olistoliths derived from both felsic breccias within the sequence, and from Paleozoic and Triassic limestones and possibly other strata from within the basement. Its unconformable relationships with the PBR rocks and with the Kerr Bend fault suggest that it postdated thrust displacement on the fault. Thus the Iskut River unit marks a profound change in basin geometry, with renewed exposure of rift margins, fault reactivation, and the development of new fault patterns.

4.2.3 Forgold area and the *four corners complex*

The Forgold area, which hosts the *four corners complex*, is a north-south elongated, fault-bounded segment of mainly volcanic rocks (Figs 4-2, 4-4, 4-5). The main Forest Kerr fault to the west, and a splay of the fault to the east, juxtapose rocks of the Forgold area with Paleozoic, Triassic and Lower Jurassic units. To the south, basalts of the Forgold area lie in unconformable contact on Paleozoic and Triassic strata, exposed in a waterfall as remnant patches of undeformed pillow basalt resting on highly deformed basement. At the northernmost extent of the Forgold area, pillow basalts lie in unconformable contact on Lower Jurassic strata to the west and in faulted contact with Triassic strata to the east.

Overall, volcanic and sedimentary rocks of the Forgold area are similar to those of Pillow Basalt Ridge. In contrast to Pillow Basalt Ridge, the Forgold area is dominated by a local felsic volcanic centre (the *four corners complex*), which is similar to, but larger than, the volcanic components in the *middle unit* on Pillow Basalt Ridge. With the exception of the four corners felsic volcanic complex, the Forgold area is composed of aphanitic, rarely vesicular, pillow basalt, pillow basalt breccia, and rare flow-banded basalt.

The *four corners complex* is a volcanic and intrusive centre constructed of extrusive rhyolite and hypabyssal equivalents and fine- to medium-grained basalt; it is onlapped by pillow basalts and fine-grained, siliceous sedimentary rock. The structural orientations of sedimentary and layered volcanic rocks on and around the dome are largely controlled by the paleotopography of the dome (Appendix E.2). The core of the dome is composed of feldspar-phyric rhyolite (Fig. 4-6A) that is crosscut by 1- to 3-m thick aphanitic and feldspar-phyric, flow-banded felsic dikes, and sets of medium-grained mafic dikes. Near the core of the dome, the contacts between felsic and mafic dikes, and between the dikes

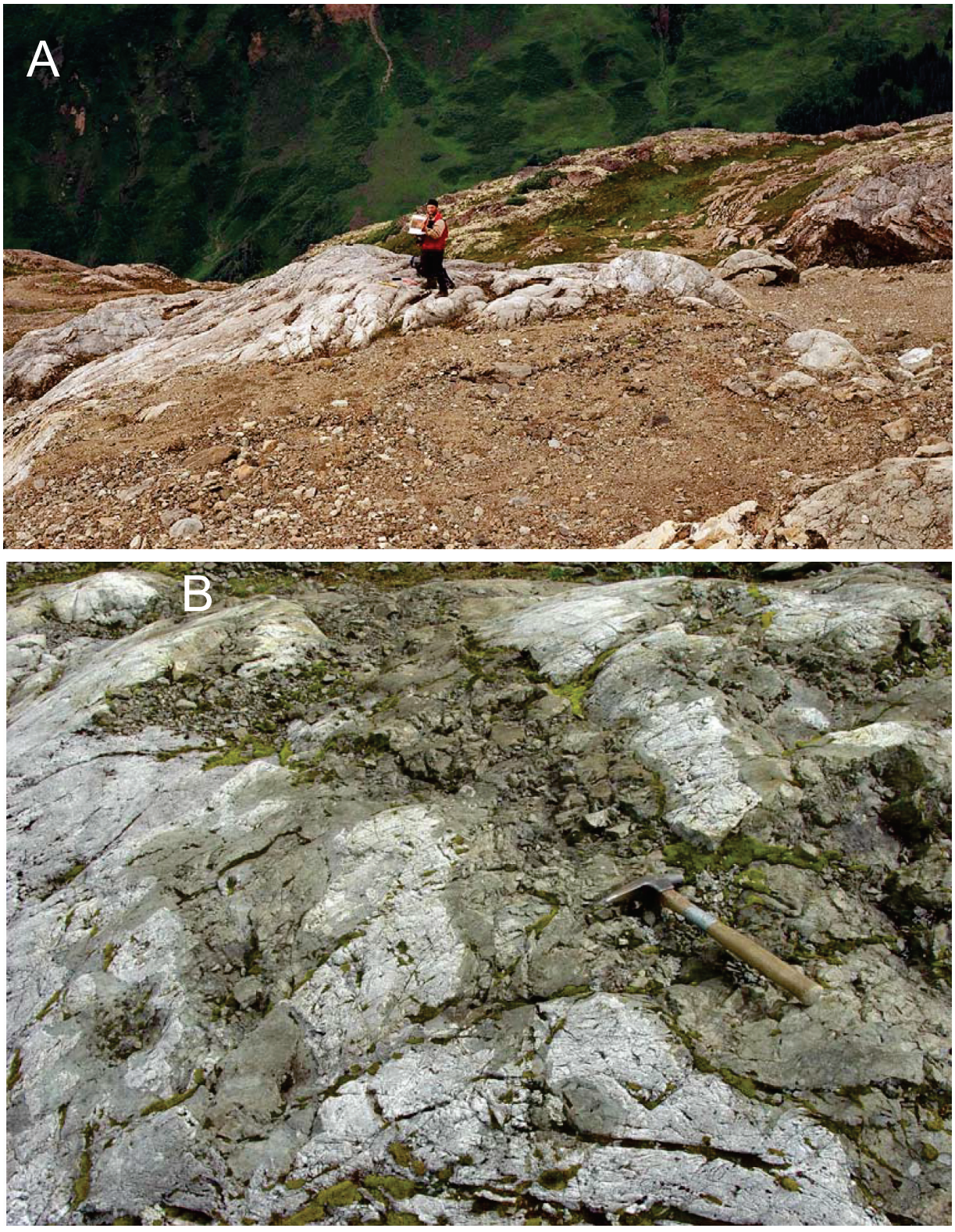

Fig. 4-6. A) Felsic intrusion in the centre of the four corners complex composed of massive aphanitic to K-feldspar and (or) quartz phyric felsite and flow-banded felsite dikes that are equivalent to rhyolite domes and flows higher up. B) Detail of irregular contacts between felsic and mafic dikes in the complex, indicating coeval emplacement.

and the surrounding dome, are amoeboid (Fig. 4-6B), indicating magma-mixing between coeval intrusions. The flanks of the dome are composed of 1- to 5-m thick, layered rhyolite flows with interbedded layers of siliceous sedimentary rocks, massive basalt flows and pillow basalt flows. Felsic dikes cut all the lithologies that comprise the dome. Above the felsic dome is a decreasing proportion of felsic dikes, coarse-grained massive basalt flows and fine-grained rhyolite flows, and an increasing proportion of pillow basalts. Basalt that erupted above the felsic dome was likely superheated, as suggested by deposits of irregular-shaped fluidal clasts in a matrix of blocky and curviplanar fragments (fire-fountain deposits). Fire-fountain deposits are characterized by Simpson and McPhie (2001), and were identified on Table Mountain by Simpson et al. (2004), and also on Pillow Basalt Ridge (Chapter 4.3.2 Fig. 4-11A) They are interpreted to be deposited proximal to (within 10 m) of a submarine volcanic fissure or vent.

The suite of rocks that comprise the *four corners complex* and immediately surrounding area is similar to that found in the *middle unit* of the Pillow Basalt Ridge area. Felsic rocks include aphanitic white- and cream-weathering, flow-banded rhyolite with semi-translucent medium-gray fresh surfaces; and white- to salmon-weathering feldspar-phyric rhyolite. These are accompanied by medium-grained basalt that has characteristic radiating feldspar microlites (first described near the Eskay Creek mine by Lewis *et al.* 2001) and, in places, a distinctive feldspar and/or pyroxene glomeroporphyritic texture. On the flanks of the dome, these rocks are extrusive, and take the form of breccias and flows. In one location, a breccia of toppled columnar-jointed basalt is preserved. Onlapping sedimentary rocks are rusty weathering, siliceous, pyritic, fine-grained, dark grey to black mudstones and/or chert. They are bedded on a 1 to 15 cm scale and have sharply eroded upper contacts. Some beds have spherical, white-weathering prehenite crystal aggregates up to 1 cm in diameter, similar to prenite found in the mudstones at the Eskay Creek mine and on Pillow Basalt Ridge (Ettlinger 2001).

The Forgold area is fault-bounded. Consequently its relationship to other rift segments is uncertain. It bears a strong resemblance to Pillow Basalt Ridge, and may represent a narrower northern extension of the rift basin that hosted Pillow Basalt Ridge stratigraphy. Alternatively it may be an independent rift fragment. The unconformable contact between

Foregold and underlying Upper Paleozoic, Upper Triassic and Lower Jurassic strata suggests that it was deposited on a block of these strata which had already undergone significant uplift and erosion.

4.2.4 Sixpack Range

Strata of the IRF crop out extensively on the eastern slopes of Sixpack Range (Figs. 4-2, 4-4). The basal units are well exposed immediately north of Kerr Bend fault. The basal talus breccia (Fig. 4-7A) is overlain by a thick (>500 m) interval of massive crystalline basalt flows cut by rare white rhyolite dikes, sills and flows. Towards the top of the thick mafic volcanic interval, the flows are progressively interlayered with overlying monolithic to heterolithic volcanic breccias, conglomerates and sandstones. These thick sequences of volcanic sandstones and granule to pebble conglomerates consist predominantly of felsic volcanic clasts. Locally, clast composition varies and can include up to 20% limestone, up to 25% hornblende-plagioclase porphyritic K-feldspar megacrystic granodiorite, or up to 10% black siltstone. Local concentrations of pyritic siltstone produce weakly gossanous weathered surfaces. Sandstones locally display graded bedding and good cross-bedding (Figs. 4-7B, 4-7C). Intercalated rock units are grey to black limestone, black siltstone, a single minor rhyolite flow, and minor sills and dikes of rhyolite and hornblende-plagioclase porphyritic potassium feldspar megacrystic granodiorite.

At its southern limit, the base of this stratigraphic unit is a thick talus breccia of predominantly carbonate clasts that rests unconformably above foliated Permian carbonate rocks. The talus breccia evolves in character up section from the Permian footwall rocks, changing from monolithic carbonate breccia, to heterolithic, volcanic-dominated breccia to coarse, well-bedded to cross-bedded sandstones and grits. These in turn are overlain by the thick succession of massive basalt flows.

Elsewhere the basal contact of the IRF strata is an unconformity, overlying Triassic or Permian footwall rocks (Fig. 4-7D). Where exposed, the upper contact for these strata is a thrust fault with Permian or Triassic rocks in the hangingwall.

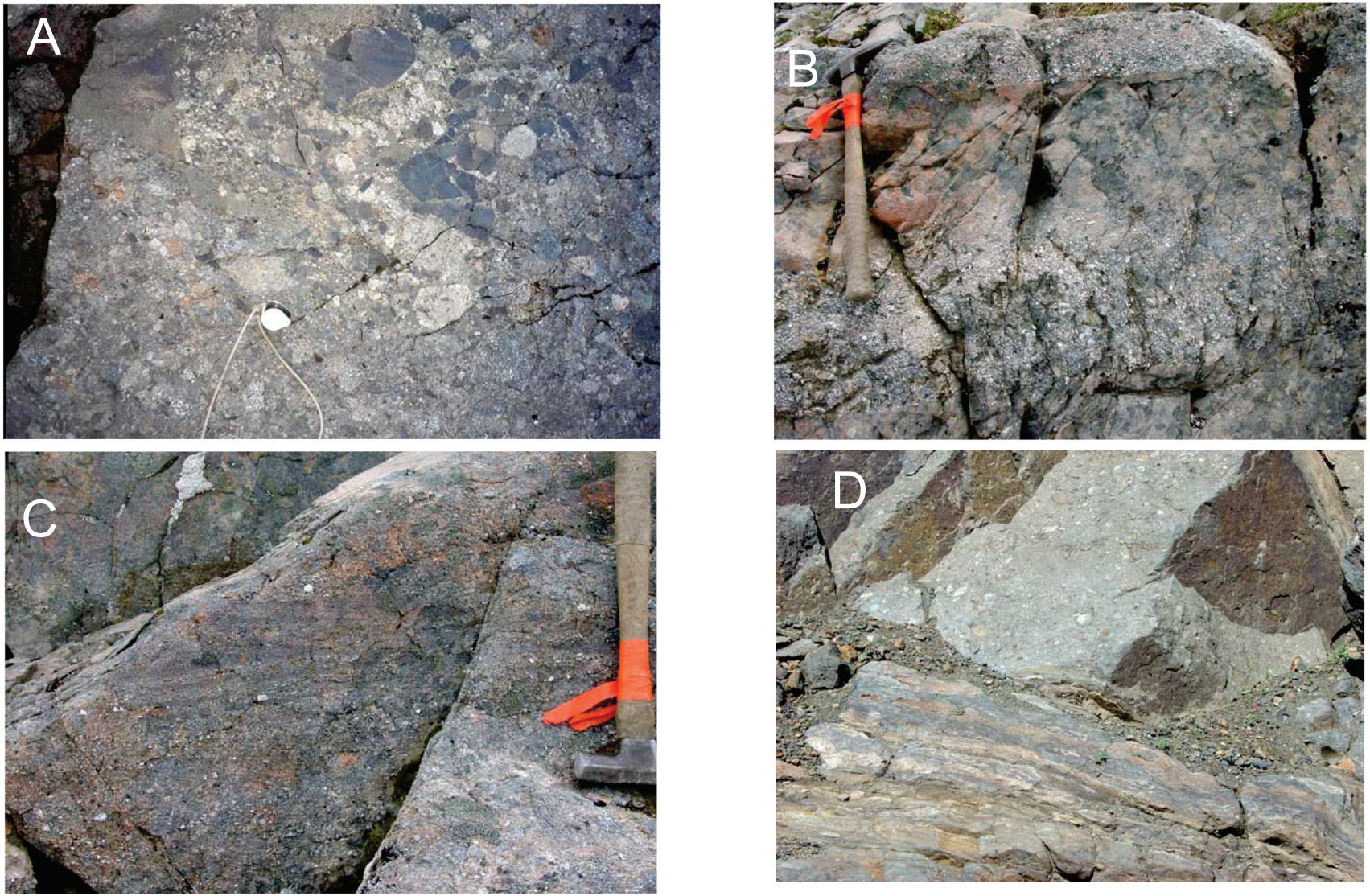

Fig. 4-7. Sixpack Rage exposures that show high-energy depositional environment at the base of the IRF. A) Polymictic talus breccia. B) Graded bedding in granule conglomerate. C) Crossbedding in pebble conglomerate. D) Basal unconformity (angular, but not apparent due to coarse-grained nature of basal conglomerate) showing polymictic conglomerate overlying well-foliated Paleozoic Stikine assemblage tuffs.

4.2.5 Downpour Creek

The Downpour Creek area is exposed north of Downpour Creek on both sides of the pass that separates Downpour Creek from Moore Creek (Figs 4-3, 4-4). To the west, these rocks are cut off by the Forrest Kerr fault. Their eastern limit is the north-striking Downpour Creek fault that juxtaposes them against Lower Jurassic strata (Fig. 4-8A).

These rocks were previously mapped by Read et al. (1989) and Logan et al. (2000). Remapping in 2004 has led to a modified structural interpretation and revised stratigraphic context. The Downpour Creek area is dominated by fine-grained clastic rocks, with less than 10% basalt, diabase, gabbro, and felsic volcanic and intrusive rocks. Clastic rocks are dark grey to black argillite with minor thin beds of orange-weathering ankeritic siltstone and sandstone, and rare granule to pebble conglomerate (Fig. 4-8B). Laminated siliceous siltstone beds become more common in the higher parts of the sequence, whereas coarser interbeds become rarer.

A variety of volcanic rock suites are exposed in the Downpour Creek area. Lenticular pillow basalt flows, black matrix rhyolite breccia, and cobble conglomerate are present within the thick sedimentary sequence. In addition, the ridgetops to the west and northwest of Downpour Creek are capped by volcanic and intrusive rock. The resistant igneous caprock mapped by Logan *et al.* (2000) includes Lower Jurassic and Middle Jurassic volcanic sequences as well as mafic intrusive bodies. The Lower Jurassic volcanic sequences, like those of the IRF, have pillow basalts and rhyolites, but also contain varied volcaniclastic rocks including volcanic conglomerates and ash and lapilli tuffs. Complicating the volcanic stratigraphy in this area are stocks of diabase and gabbro that have the same radiating microlites and glomeroporphyritic textures as the extrusive IRF basalt mapped at Pillow Basalt Ridge, the *four corners complex*, and the Sixpack Range.

The internal stratigraphy of the Downpour Creek area is not completely understood. Fossil collections are reported from this unit by Souther (1972), Read et al. (1989) and Logan et al. (2000). Along the ridgecrest west of the pass between Downpour and Moore creeks, Late Toarcian conodonts occur at two sites (Read et al., 1989); however, Logan et

Fig. 4-8. Downpour Creek exposures. A) View eastward to the fault contact of black, carbonaceous Downpour Creek area argillite and siltstone against Lower Jurassic rhyolite on Logan Ridge, east of the Downpour Creek fault. B) View northwest towards the pass between Downpour Creek and More Creek (distant background). Downpour Creek area argillites and thin ankeritic sandstone beds in foreground that overlie ankeritic lower Hazelton Group volcanics. Topographic linears (recessive zones) in background are splays of the main Downpour Creek multiply-reactivated normal (down to the west) and strike-slip fault.

al. (2000) reported Bathonian macrofossils from the same area. Further north, Logan *et al.* (2000) collected an Aalenian ammonite. Souther (1972) listed Middle Bajocian macrofossil collections east of the pass. Structures in the Downpour Creek area are complex, involving tight folds and multiple fault strands that significantly modify the single syncline inferred by Logan et al. (2000).

On the eastern side of Downpour Creek, fine-grained sedimentary beds of the Downpour Creek area overlie coarse polymictic conglomerates of the Sixpack Range in a gradational, interfingering contact. A similar relationship can be inferred several kilometres to the southwest near the headwaters of Downpour Creek, in spite of extensive fault slivering. There, conglomerates are accompanied by monolithologic, chaotic, volcanic-derived debris-flow breccias and minor basalt flows like those seen farther south in the Sixpack Range. East of Downpour Creek, the conglomerates are relatively thin and overlie plagioclase-phyric volcanic rocks correlated with the lower Hazelton Group (Fig. 4-8B). Based on these observations, the conglomerate in the Sixpack Range area is interpreted as a basal conglomerate to the finer-grained Downpour Creek area sedimentary succession, and as its more southerly, coarse-grained, more proximal equivalent.

4.2.6 Klastline Plateau

The Klastline Plateau section is 2000 meters thick and composed predominantly of a polymictic conglomerate containing clasts of older Triassic and Paleozoic country rocks, interclasts of basalt and rhyolite, and fragments of fossilized wood (Figs. 4-2, 4-5). The basal and top units are rhyolite, and basalt is a minor part of the stratigraphy. Interference ripples in sedimentary rock, fiamme in felsic tuffs, and massive (non-pillow) basalt flows indicate that this section was deposited in a shallow water to sub-aerial environment.

4.3 Case Study: Detailed Mapping of Eskay Creek–Equivalent Stratigraphy at Pillow Basalt Ridge

4.4.1 Background

Previous mapping of PBR identified its major bounding structures and the PBR anticline (Read et al., 1989; Logan et al., 1990). Read et al. (1989) depicted PBR as consisting entirely of pillow basalt. Logan et al. (1990; 1997) identified five narrow sedimentary intervals within the pillow basalt, which they depicted as discontinuous sedimentary lenses.

The rocks exposed on PBR are closely affiliated, both spatially and stratigraphically, with the hangingwall sequence of pillow basalts at the Eskay Creek mine. Mapping of the central and southern portion of PBR by Homestake Mining Company (Vaskovic and Huggins 1998) identified a zone approximately 300 m thick, which contains siliceous argillite beds up to 4 m thick, interbedded with pillow basalt. Homestake collared a diamond-drill hole (PBR01-01) in this zone, at what was then mapped as the crest of the PBR anticline (Fig. 4-9). The hole penetrated 1419 m of basalt with minor intervals of mudstone. In 2003, Roca Mines re-entered the hole, drilling to 1770 m without penetrating through the basalt or intersecting the Eskay-equivalent contact mudstones and rhyolites that were hypothesised to underlie PBR.

4.3.2 Stratigraphy

This study describes 1:20 000-scale mapping conducted on Pillow Basalt Ridge in 2004 that defined new stratigraphy and refined previously described structures (Fig. 4-9). Pillow Basalt Ridge is divided into four geological units: the *lower* and *upper pillow basalt* units are separated by a *middle unit*, and overlying the *upper pillow basalt unit* are distinctive sedimentary rocks of the *upper sedimentary unit*. The *middle unit* varies in thickness from 130 to 200 m and contains bimodal volcanics and horizons of siliceous argillites and tuffs (Fig. 4-10).

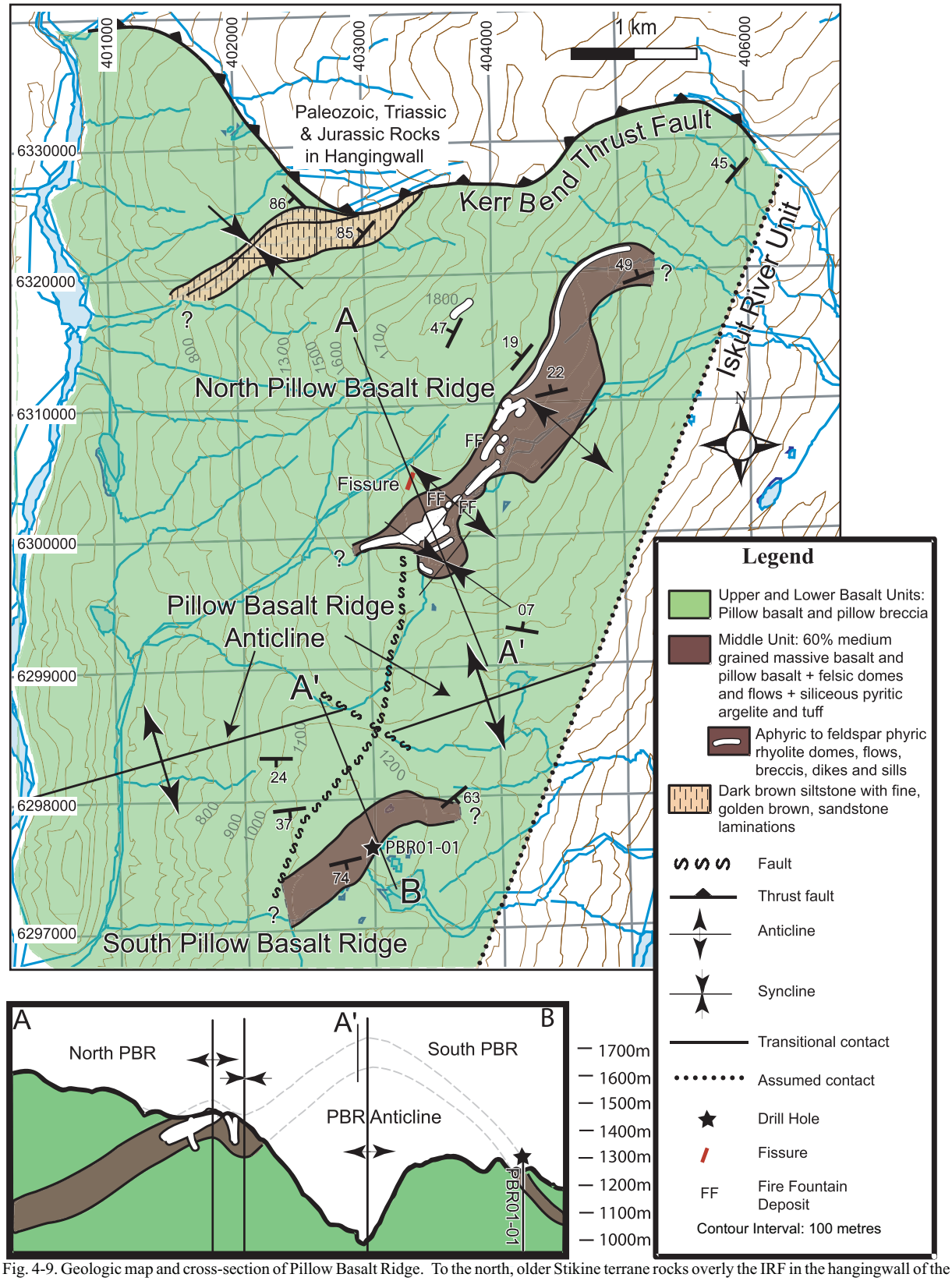

Fig. 4-9. Geologic map and cross-section of Pillow Basalt Ridge. To the north, older Stikine terrane rocks overly the IRF in the hangingwall of the Kerr Bend thrust fault. There, exposed in a syncline parallel to the main PBR anticline, sand- and siltstones interbedded with pillow basalts comprise the stratigraphic top of the IRF. To the south, and lower in the stratigraphy, *upper* and *lower* basalt units are separated by the *middle unit.* The cross-section demonstrates the relationship between the *middle unit*, and *upper* and *lower* pillow basalt units on north and south Pillow Basalt Ridge, which is largely controlled by the main PBR anticline.

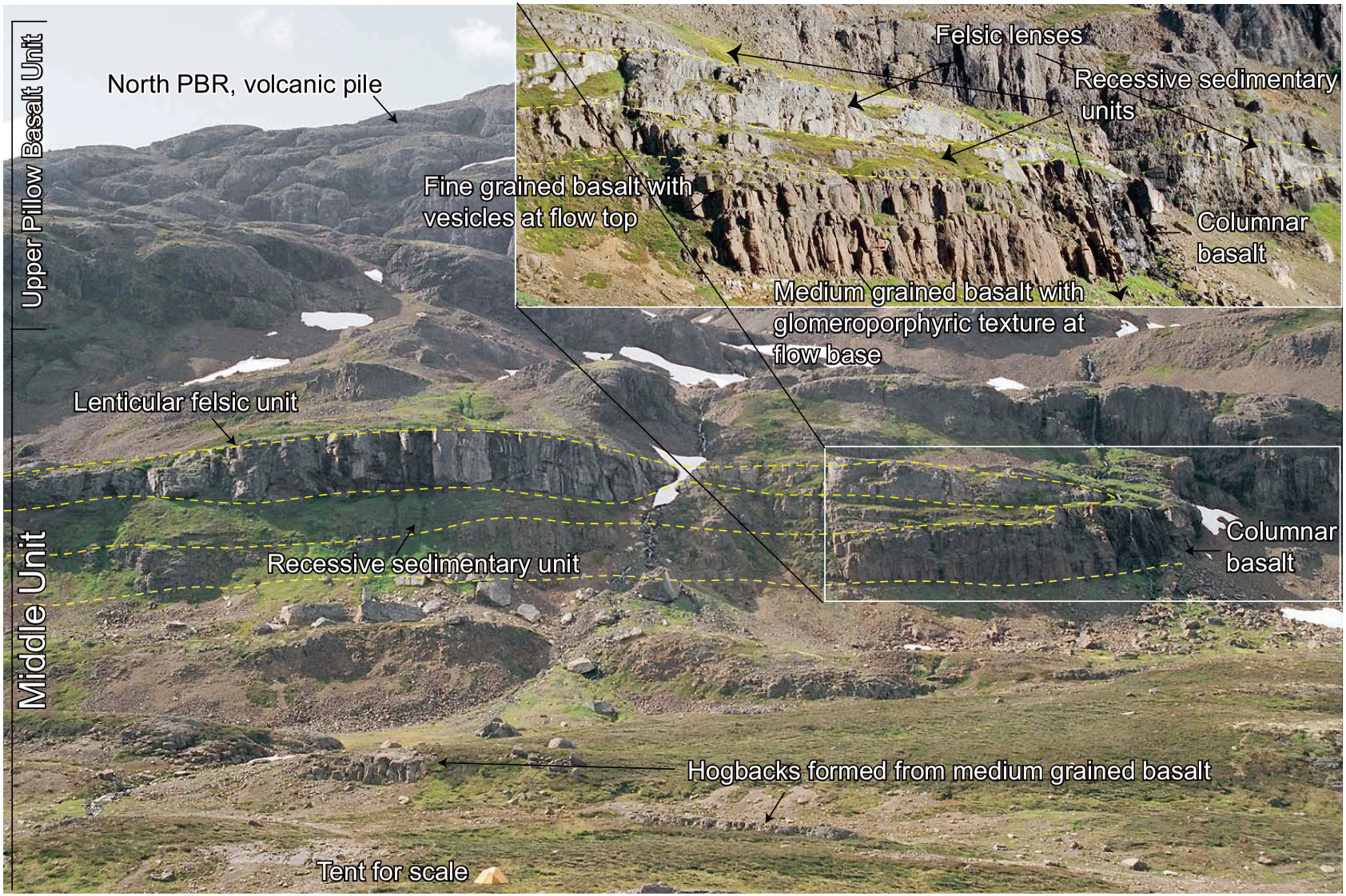

Fig. 4-10. Northern Pillow Basalt Ridge, facing west towards the *middle unit* (centre and bottom of photo) and *upper pillow basalt unit* (top of photo). The *middle unit* has characteristic steep sided, resistant, edifices associated with lenticular felsic flows and columnar basalt (see inset), that are interlayered with recessive sedimentary rock (see inset); in areas with low relief, resistant units form hogbacks. The *upper pillow basalt unit* comprises discontinuous lobe-shaped flows that onlap one

Lower and upper pillow basalt units

The *lower pillow basalt unit* is at least 1000 m thick and the *upper unit* is at least 850 m thick. Together they form a volcanic pile which accounts for over 90% of PBR. Both pillow basalt units are composed of two main variants: pillow basalts and pillow basalt breccias with transitional intervals of intact pillows in a breccia matrix. The volcanic pile is made up of many flows that interfinger and onlap one another. Individual flows are 5 to 30 m thick and are defined on a broad scale by different textures and weathering characteristics. There are a great variety of pillow forms, which range in size from 15 cm to 1.5 m in diameter (Figs. 4-11B, 4-11C). Pillow geometries range from spheres to flattened lobes; most pillows display tail and drape geometry.

The basalt is mainly aphanitic, with medium to dark green fresh surfaces and orange-brown weathered surfaces. Most pillow rims are thin and have textures similar to the pillow centres. However, in some layers, pillow rims are glassy and moderately thick (up to 4 cm). These basalts have a black vitreous appearance and the pillows are surrounded by a hyaloclastite matrix. Rarely PBR basalts have a porphyritic texture; plagioclase phenocrysts range up to 8 mm long. Variolites (spherical, white-weathering, devitrification features typically 1 to 3 mm in diameter) and chlorite-filled vesicles are present in approximately 25% of PBR basalts.

A number of fire-fountain deposits were identified in both the lower and upper basalt units (Figs. 4-2, 4-11A). These volcanic deposits, which indicate close proximity to loci of eruption, were also identified above the *four corners* complex (section 4.2.3) and by Simpson et al. (2004) in IRF rocks exposed on Table Mountain, 50 km to the north of PBR.

In the *upper pillow basalt unit*, a crack-and-fill feature was identified. A 20 m wide fissure cuts 65 m vertically through a massive pillow basalt layer. This gap is completely filled with a dense basalt breccia. On the fissure margins the basalt breccia drapes over intact pillows of the fissure wall. Although the *upper* and *lower basalt* units strongly resemble one another, the following features set them apart: 1) fire-fountain deposits, and the pillows with the largest diameters are concentrated in the *upper pillow basalt unit* immediately above the *middle unit*; 2) in northern PBR, the *upper pillow basalt unit* has

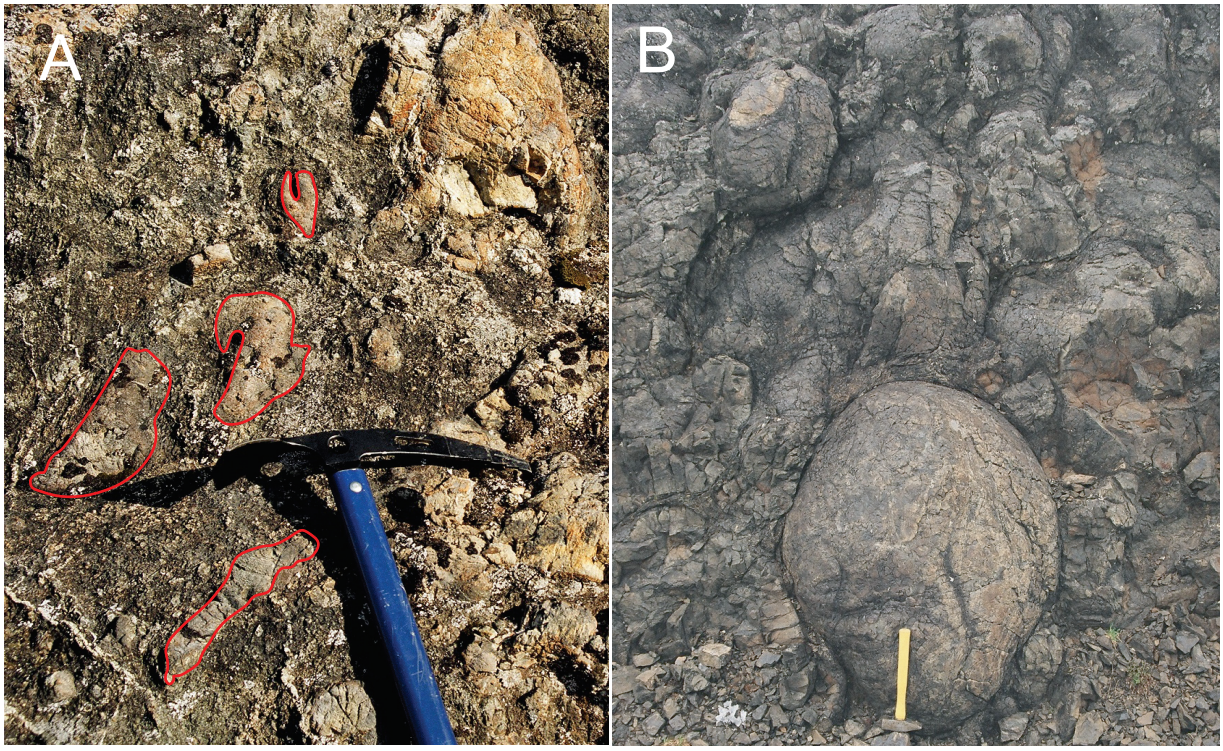

Fig. 4-11. Pillow Basalt Ridge lithologies and textures.
A) fluidal-shaped clasts (outlined in red) in a matrix of smaller, vitric, curviplanar and blocky clasts (fire-fountain deposit), indicating proximity to a submarine eruptive center.
B) Typical well-developed basalt pillows.
C) Pillow from the *upper basalt unit* directly above the *middle unit*, that range up to 1.5 m in diameter. Tail and drape geometry indicates a tops-up orientation.
D) Siliceous dark argillites and light felsic tuffs in the *middle unit*.

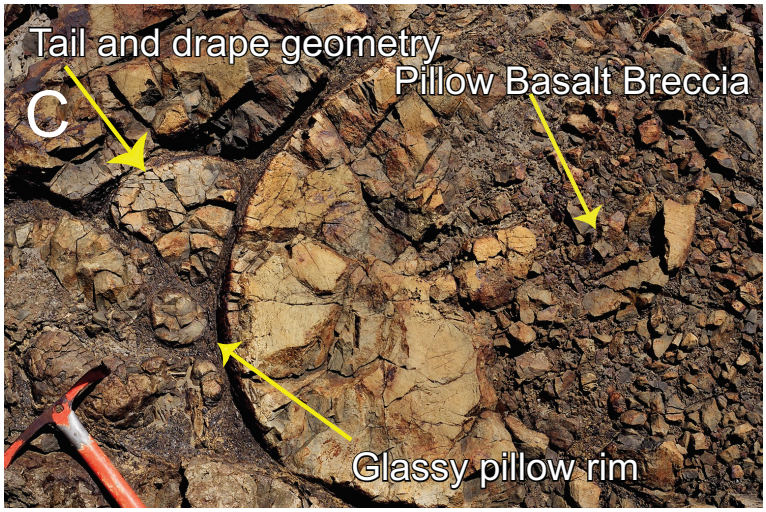

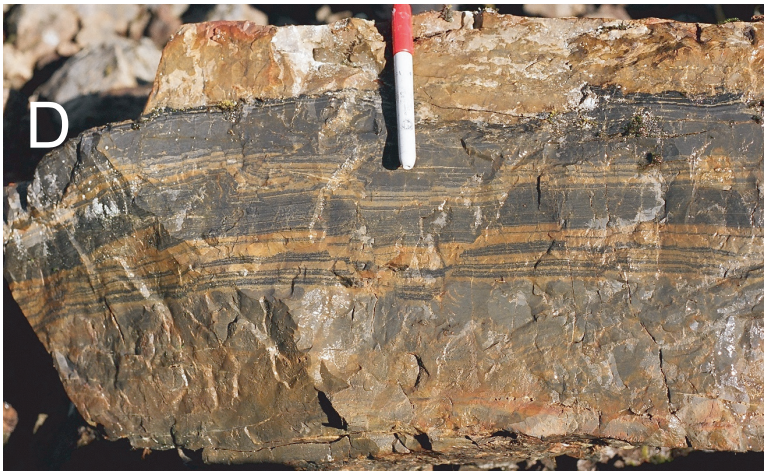

higher proportions of thick glassy rims and hyaloclastite matrix (Fig. 4-11B); 3) in the northwestern portion of PBR, just below the *upper sedimentary unit*, a breccia in the *upper pillow basalt unit* consists of angular basalt clasts supported within a blue-grey limestone matrix.

Middle unit - Bimodal Igneous and Sedimentary Rocks

The middle unit is exposed on both limbs of the PBR anticline (Fig. 4-9). Pillow basalts in the *middle unit* are interlayered with other lithologies that represent a distinct depositional and volcanic regime, different from that seen on the majority of PBR. The thickness of the *middle unit* varies and is partly controlled by the paleotopography defined by the top surface of the *lower pillow basalt unit*. The *middle unit* is a bimodal igneous and sedimentary interval predominately composed of mafic volcanic rocks interbedded with clastic sedimentary lithologies and felsic volcanic rocks. Overall, 60% of rock exposures in the zone are mafic, but in particular intervals, felsic and sedimentary rocks are the dominant rock types. On cliff exposures, medium-grained, massive basalt forms 5 to 25 m thick, orange-brown weathering, vertical faces, with metre-scale columnar joints (Fig. 4-10). Felsic units form 0.5 to 10 m thick, pale weathering, vertical, resistant cliff faces. Sedimentary intervals are typically 1 to 6 m thick, rusty weathering and recessive. A 30 m thick section that also contains the bimodal igneous and sedimentary rock suite occurs as a discontinuous band within the *upper pillow basalt unit* (Fig. 4-9).

Mafic Rock of the *middle unit*

Where the m*iddle unit* crops out on southern PBR, all mafic layers are pillow basalts. On northern PBR, the majority of mafic rock is medium-grained, non-pillowed basalt, which forms massive, columnar-jointed, outcrops. However, pillow basalt is also present. The presence of vesicles and absence of upper chilled margins, indicate that the medium-grained massive basalt layers are extrusive. They exhibit gradational stratification with the coarsest texture at the bottom of each flow and a vesicular, finer grained texture near the flow tops. The medium-grained basalt commonly contains radiating plagioclase microlites, and locally displays a distinctive glomeroporphyric texture with feldspars up to 2.5 mm long. Lewis et al. (2001) described a similar texture in the hangingwall basalts of the Eskay Creek mine.

Sedimentary Rock of the *middle unit*

Sedimentary layers are discontinuous and onlap both felsic and mafic flows. Their upper contacts with igneous flows are locally peperitic, and in one location several beds are entrained and folded within a felsic flow. Sedimentary rocks of the *middle unit* are medium-bedded (5 to 25 cm thick) and can be internally laminated or graded. Some beds have an undulating base, are normally graded, and have flat upper contacts, typical of beds deposited by density currents in a deep basin (Bouma 1962). The most common rock types are interbedded dark brown to black siliceous argillites and light-coloured felsic tuffs (Fig. 4-11D), known as "pyjama beds" (Anderson 1993). Light-coloured felsic tuff layers are generally more abundant near the tops of sedimentary intervals. Other sedimentary lithologies include light green intermediate to mafic tuff, dark blue-grey massive siltstone, and thin graphite-rich mudstone beds. Beds are typically siliceous; some are highly siliceous with a conchoidal fracture. Disseminated pyrite crystals, less than 1 mm in size, can constitute up to 10% of the rock volume. Rarely, 1 to 3 mm thick pyrite laminations are preserved. Approximately 20% of the black argillite beds have spherical, white-weathering prehnite rosettes up to 1 cm in diameter. These have also been identified in other IRF rocks, including the *contact mudstones* in the Eskay Creek mine area (Ettlinger, 2001) and in the mudstones of the *four corners complex* in the Forgold area.

Felsic Rock of the *middle unit*

Intrusive and extrusive felsic rocks are an important part of the *middle unit* on northern PBR. Intrusive bodies include dikes, sills and cryptodomes; extrusive bodies include flows, domes, and breccias. Felsic flows are typically autobrecciated, white to light grey, and locally display flowbanding. Some flows are peperitic, incorporating up to 30% sedimentary clasts and matrix. The felsic rock is aphanitic, locally spherulitic, has a semi-translucent dove-grey fresh surface, and is frequently pyritic. Most felsic rocks have small (less than 1 mm) K-feldspar phenocrysts, and rarely quartz and plagioclase microphenocrysts, in a groundmass of K-feldspar and quartz. Some quartz microphenocrysts are partly resorbed, and they form aggregates with K-feldspar. Flow

facies are highly variable and change abruptly between massive flows, autobrecciated flows, and breccias and conglomerates. Some felsic breccias are polymictic with sedimentary clasts and a variety of distinct felsic clasts. At least one flow has a thickness of 10 m or more over a strike length of 3 km; other felsic bodies form lenticular exposures that are less than 10 m across. Two small felsic volcanic centres were delineated within the *middle unit* on northern PBR. These show rapid thickening into roughly dome-shaped exposures (Fig. 4-9). The two felsic complexes are composed of massive, mainly unbrecciated, felsic rock which is intruded by both felsic and mafic dikes. The contacts between the felsic and mafic dikes, and between the dikes and the surrounding dome, are highly irregular and curviplanar, indicating intrusion into semi-solid bodies. The domes are surrounded by sedimentary rocks and networks of feeder dikes and sills underlie them. Large wedges of sedimentary rock up to 4 m thick were incorporated into the magma as giant xenoliths. Bedding attitudes in the sedimentary strata adjacent to the domes depart from the normal PBR structural grain, indicating that they may be controlled locally by the paleoslope of the domes, or deformed by the mafic and felsic dikes.

Upper Sedimentary Unit

The *upper sedimentary unit* overlies the *upper pillow basalt unit* at the northwestern edge of Pillow Basalt Ridge (Fig. 4-9). Here, a syncline in the immediate footwall of the Kerr Bend fault exposes the depositional contact between the two units. The *upper sedimentary unit* is composed of dark grey siltstone with golden brown sandstone laminations. The sedimentary strata interfinger with pillow basalts and in places form the matrix in pillow breccia. This intimate association with the volcanic rocks indicates that the sedimentary rocks are part of the Iskut River Formation, rather than Bowser Lake Group as suggested by Read et al. (1989).

4.3.3 Structure

Pillow Basalt Ridge is structurally bounded to the north by the Kerr Bend thrust fault, and to the west by the Forrest Kerr fault (Fig. 4-4, 4-9). As described by Alldrick et al. (2005a), these may be original basin-bounding faults. Although the present Kerr Bend fault places older strata over PBR, and was therefore active following PBR deposition, there is evidence that it was also a controlling structure for a horst of Paleozoic and Triassic rock that was uplifted during PBR deposition (see next section). Alldrick et al. (2005a) proposed that two stress regimes controlled the major structures on PBR. An early extensional regime was responsible for the northeasterly orientation of the felsic eruptive centres, dikes, fissures, and fire-fountain deposits preserved in Pillow Basalt Ridge. These extensional features are syn-rift. A later compressional stress regime was responsible for the folding which produced the PBR anticline, a broad regional fold that affects all of PBR. The PBR anticline trends 060°, and has been offset by an inferred east-southeast– trending fault that occupies the deep valley separating northern and southern PBR (Fig. 4-9). Minor folds trending north-northeast to northeast within the *middle unit* are probably related to this shortening. This small-scale buckling of the *middle unit* helped accommodate the space requirements of the fold in the thicker, more rigid, pillow basalt units. The later compressional regime was related to sinistral shear couple that straddled PBR (Alldrick et al., 2005a). Shearing on the eastern side of PBR was responsible for northward deflection of PBR bedding close to the Iskut River. This shearing also accommodated deposition of the overlying *Iskut River unit* in a narrow transtensional basin (Alldrick et al 2005a). In contrast to the high-energy deposits of the *Iskut River unit*, the syncline at the northwestern edge of PBR exposes conformable, fine-grained distal sedimentary rocks that were deposited in a relatively quiescent part of the basin.

4.3.4 Facies Interpretation

Pillow Basalt Ridge represents a major rift segment where more than 2 km of pillow basalt filled a subsiding subaqueous basin. The total thickness of the PBR facies remains

unknown, as does the type of rock that lies beneath it. Alldrick et al. (2005a) suggested that basal Middle Jurassic deposits of coarse clastic rocks interfingered with medium-grained basalt and felsic rock that are exposed in the hangingwall of the Kerr Bend fault, may also underlie the PBR facies. The *middle unit* records an interruption in the volcanic and depositional events that characterize the thick *upper* and *lower pillow basalt* units on PBR. Fine-grained felsic turbidites in this interval suggest that there was a significant period during which the extrusion of mafic lava was suppressed. If, rather than erupting, mafic magmas underplated the crust or formed intra-crustal magma chambers, they could have provided sufficient heat to cause crustal-level partial melting (Galley 1996, 2003; Hart et al. 2004) leading to the felsic volcanism also recorded by the *middle unit*. The same heat source may also have initiated a convective hydrothermal system, making this unique horizon especially prospective for VMS deposits.

The massive, medium-grained, characteristics of the *middle* unit mafic rocks are interpreted to represent lava ponds which resulted from slow effusion of low-volatile-content lavas in a deepwater environment (> 800m) with shallow or no slopes (Clague et al. 2000). The ponds formed in topographic lows that resulted from the irregular topography of the *middle unit* lower contact (Fig. 4-9) and/or other confining bodies including rhyolite domes, and small-scale fault-scarps. The felsic domes and cryptodomes of the PBR *middle unit* are too small to have produced the adjacent felsic flows and breccias. At least one felsic centre, now either buried or eroded, must have been significantly larger than those currently exposed on PBR.

Sparse paleo-direction indicators, including branching pillows, lava tubes, and the orientation of sedimentary layers entrained into lava flows, show southerly flow. This suggests that the main eruptive centre was located on northern PBR or even farther to the north. The relatively thin (150 m thick) interval of pillow basalt in the hangingwall of the Eskay Creek mine may represent the fringe of this volcanic accumulation. The differences between the *middle unit* exposures on northern and southern PBR are also consistent with north-south, proximal-to-distal progression. The *middle unit* on northern PBR is thicker than on southern PBR. It contains significant amounts of felsic and medium-grained mafic volcanics. The thinner *middle unit* on southern PBR contains only

pillow basalts with sedimentary intervals; it does not contain any of the rhyolite or massive basalts that characterize the northern exposures. Farther to the north, in the Forgold area (see section 4.3.5), a larger felsic centre, the *four corners complex*, is present. If the Forgold area was initially part of the same rift segment as PBR, it may represent further northward thickening of the *middle unit*. The suite of rock types that comprise the *middle unit* of PBR is not restricted to the *middle unit*. A narrow, discontinuous zone that repeats the *middle unit* lithologies is also present within the *upper pillow basalt unit*. Variations of the *middle unit* rock suite were also observed in the *four corners complex* in the Forgold area, and in the Sixpack Range (see section 4.3.6). This suggests that the events that led to the suppression of voluminous mafic volcanism, deposition of sediments, generation of felsic volcanism, and production of coarser grained massive basalt, were repeated several times throughout the history of the rift. Each of these intervals may represent favourable stratigraphy for the formation and preservation of VMS mineralization.

4.3.5 Summary of Pillow Basalt Ridge

Detailed mapping of Pillow Basalt Ridge has defined four map units: a *lower pillow basalt unit*; a *middle unit* which consists of bimodal volcanic rocks and intercalated clastic sedimentary strata; an *upper pillow basalt unit*; and the overlying siltstones of the *upper sedimentary unit*. The PBR volcanic facies is interpreted to have been deposited in an extensional submarine setting where basin subsidence kept pace with the accumulation of at least 2 kilometers of volcanic and sedimentary rocks. The *middle unit* represents a time interval when mafic volcanism waned. I speculate that heat from mafic magma chamber(s) or crustal underplating generated felsic magmas from partial melting of the crust, and could potentially have driven VMS mineralizing systems. Bimodal volcanism, fire-fountain deposits, and pyritic sedimentary and felsic horizons are all indications that the *middle unit* of PBR may have been a favourable host for VMS style mineralization. The presence of similar bimodal igneous and sedimentary rock suites similar to the PBR *middle unit*, located elsewhere on PBR and in other rift segments, indicates that otherwise

less prospective thick piles of pillow basalt sequences do contain strata that are favourable to VMS formation and preservation. Strata underlying PBR at depth may also represent an attractive exploration target. The new interpretation of the location and orientation of the PBR anticline presented here should facilitate future exploration of these blind strata.

4.4 Discussion– Stratigraphic and Structural Evolution of the Eskay Rift between Eskay Creek and More Creek

The units described above illustrate pronounced facies variations in time and space that characterize the late Early to early Middle Jurassic rift environment between the Eskay Creek mine and More Creek.

Pillow Basalt Ridge is a 2000 m thick basaltic sequence with a prominent interval in which rhyolites and rhythmically bedded, siliceous, pyritic siltstones are also important. The PBR basalt, which thins dramatically southwards towards the Eskay Creek mine, is overlain by coarse siliciclastic and felsic breccia deposits of the Iskut River unit, which indicates voluminous felsic volcanic eruption and rapid erosion. This unit records a higher energy depositional environment developed prior to the onset of Bowser Lake Group sedimentation. By contrast, in the syncline on northwestern Pillow Basalt Ridge, only siltstones and sandstones interfinger with the uppermost PBR basalts, indicating a more quiescent part of the basin.

The massif north of the Kerr Bend fault contains two distinct facies (Fig. 4-12). On its eastern side, facing the Iskut River, conglomerates, debris-flow breccias, rhyolites and basalts of the Sixpack Range unconformably overlie deformed Paleozoic and Triassic basement rocks. To the west, north of the Kerr Bend fault on the slopes facing west over Forrest Kerr Creek and its northern tributary, thin sediment-free pillow basalt outliers of the Forgold area unconformably overlie the same basement. These sub-Middle Jurassic unconformities on rocks as old as Paleozoic are unique within the Eskay rift system: everywhere else, the base of the sequence ranges from conformable on slightly older Jurassic strata to an unconformity on Upper Triassic or Lower Jurassic basement.

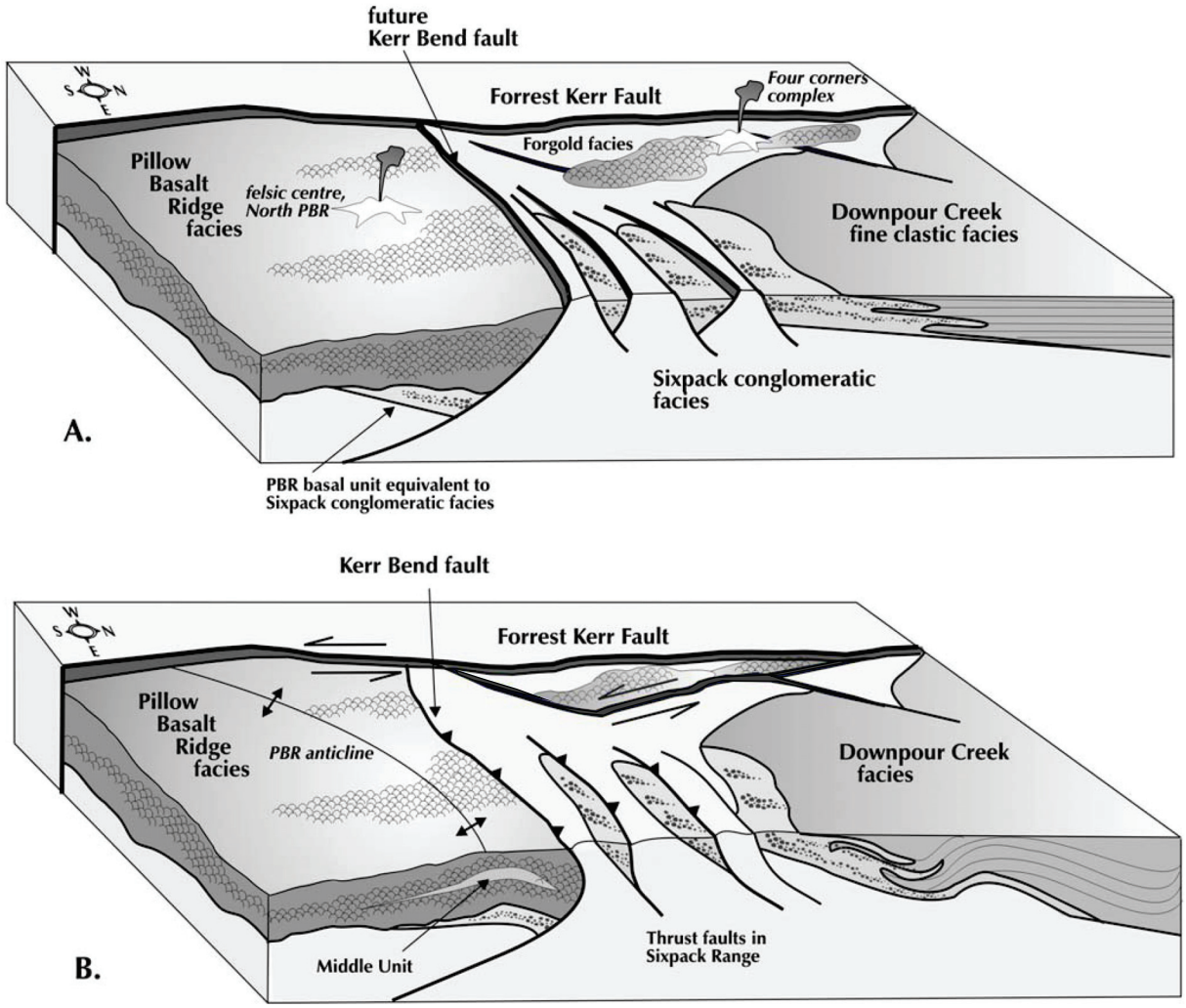

Fig. 4-12. Block diagram of the Eskay rift between Pillow Basalt Ridge and More Creek. Shows the relationship between different IRF facies: A) in their inferred syn-rift structural context, and B) later, when the basin-bounding faults were reactivated as a sinistral shear couple (fault in foreground/east-side, not shown in diagram) and the rift basin was transformed into a compressional transfer zone, causing basin inversion (e.g. folds: PBR anticline, and thrust faults: Kerr Bend fault).

The relationships between the two facies north of Kerr Bend fault to each other and to the Pillow Basalt Ridge area are not well understood. Clasts in the polymictic conglomerates are correlated with rocks exposed in the core of an uplifted block of Paleozoic and early Mesozoic rock exposed between Pillow Basalt Ridge and Downpour Creek, including quartz-plagioclase-K-feldspar porphyry intrusions that are known to occur both in the core of the uplift and to the northwest, along the northern tributary of Forrest Kerr Creek. It seems reasonable that these conglomerates were derived from the west. If so, the lack of a basal conglomerate below the pillow basalts on the west side of the Sixpack Range must be explained. A possible explanation is that this area was initially exposed sub-aerially and eroded, and later became a north-trending rift basin.

Both of these areas are juxtaposed abruptly with the thick, monotonous pillow basalt pile south of the Kerr Bend fault (Fig. 4-12). The base of PBR is not exposed. It is not known whether it has a basal conglomerate like the Sixpack Range to the northeast, or whether the pillow basalts lie directly on older basement as seen to the northwest.

Facies relationships northwards into the Downpour Creek area are clearer. The coarse, proximal Sixpack Range facies passes northward into basinal sediments and lesser bimodal igneous rocks of the Downpour Creek facies (Fig. 4-12). The northernmost basalts of the Forgold area unconformably overlie Lower Jurassic dacites in the headwaters of Downpour Creek, just southwest of the proximal to distal transition in the clastic strata. These basalts are over 200 m thick and have no associated sedimentary strata, like those along strike to the south in the western hangingwall strata above the Kerr Bend fault.

The following proposed geological history integrates the various volcano-sedimentary packages (Figs. 4-3, 4-12). The Sixpack Range proximal clastic facies is probably oldest, since it in part underlies the Late Toarcian and younger Downpour Creek basinal facies. It is inferred that these two clastic facies were deposited on the eastern and northern flanks of a horst within the Eskay rift system, now preserved as the Paleozoic-Triassic uplift in the core of the Sixpack Range. The horst could have been an elongate, north-tilted block with steepest scarps along its southeastern margin near the present Kerr Bend fault where the coarsest conglomerates and breccias occur. The adjacent graben to the immediate

south of this scarp is inferred to have filled first with clastic detritus from the north, and later became the site of eruption for the voluminous PBR pillow basalts. The absence of a basal conglomerate in the Forgold area and *four corners complex* suggests that these volcanic rocks were erupted later, as faulting and uplift waned and the exposed highlands were drowned.

The Kerr Bend fault separates two distinctive Middle Jurassic facies - a thick pile of basalts to the south versus a clastic-dominated package to the north (Fig. 4-12). Thrust faults that demarcate abrupt facies and thickness changes may be remobilized original growth faults (McClay et al. 1989). As shown in Figure 4-12, the locus of the present Kerr Bend fault is interpreted as a remobilized graben-bounding fault which separated the Sixpack Range horst from an adjacent graben to the south. The Kerr Bend fault corresponds roughly in position and orientation to the precursor normal fault. Read et al. (1989) inferred 2.5 km of post-Middle Jurassic displacement on the Forrest Kerr fault, based on offsets of the northeast- to east-northeast–trending faults and folds such as the PBR anticline. These features, which are only developed near the Forrest Kerr fault, can be related kinematically to sinistral transcurrent motion along it (Fig. 4-12).

The change in kinematics to sinistral transpression first steepened the original fault surface, and then overturned it to the south. Continued thrust motion on this fault would have obscured any basal clastic facies rocks on the southern (PBR) side, burying them in the footwall.

Since deposition of the *Iskut River unit* likely post-dates the last movement on the Kerr Bend fault, its Middle to early Late Jurassic fossil age constrains the onset of sinistral motion on the north-trending Forrest Kerr fault and related deformation of the PBR facies to immediately after the formation of the Eskay Creek orebodies. Rejuvenated high relief created by offsets on the Forrest Kerr and Kerr Bend faults could account for the high-energy sedimentary deposits and transport of olistoliths into the basin.

4.5 Conclusions

Middle Jurassic sedimentary and bimodal volcanic rocks of the Iskut River Formation define a 300 km by 50 km discontinuous belt in northwestern British Columbia. They

represent the final significant episode of Jurassic magmatism in the Stikine Terrane and are interpreted to have been deposited in an extensional tectonic environment.

There is a general correlation in stratigraphies, rock types, age, and compositions amongst the strata in the separate sub-basins which define the belt. For example the sections at Table Mountain and the Pillow Basalt Ridge, separated by 100 km, are characterized by basal and upper sequences of basaltic pillowed lava, 1000 m thick, separated by medial successions of sedimentary and bimodal volcanic rocks. The medial units closely resemble strata that host the Eskay Creek deposit and are potentially prospective for similar types of mineral deposits.

Important elements of the Iskut River Formation geological setting include: a) thick sequences of sedimentary and bimodal volcanic rock; b) the presence of original graben-bounding faults; c) unconformities associated with proximal, graben-filling conglomerates, including several that grade into distal facies argillite; and c) significant transcurrent displacements and kinematic indicators on some of the graben-bounding faults, which appear coeval with graben development. The traditional interpretation of these regional-scale tectonic and stratigraphic elements has been that the Iskut River Formation represents a west-facing, back-arc environment (Anderson 1989). This hypothesis is based largely on the proposed presence of three parallel time-equivalent facies: a central volcanic facies (thought to be a back-arc facies), a distal facies to the east composed of marine sediments, and a hypothetical intrusive "arc facies" to the west. However, the work presented in this chapter documents syn-rift structures that suggest a strong transcurrent tectonic regime during deposition. A transcurrent régime could have accommodated extension-related volcanic and sedimentary rocks by opening transtensional basins in an arc environment. The Iskut River Formation north of the Eskay Creek mine contains indications it was subjected to both compressional and extensional stress regimes, and one rift segment, PBR, records a syn-rift shift from an extensional to a compressional regime. This suggests that the IRF records both transtensional and transpressive tectonic regimes in an intra-arc environment affected by major transcurrent motion.

Chapter 5 - Petrology and Metallogenesis of the Iskut River Formation

5.0 Preface

Chapters 5 focuses on the petrology of the IRF basalts and their significance to regional metallogenesis and tectonics. The chapter is derived entirely from:

Barresi, T., Nelson, J.L., Dostal, J. 2015. Geochemical constraints on magmatic and metallogenic processes: Iskut River Formation, volcanogenic massive sulfide-hosting basalts, NW British Columbia, Canada. In press, Canadian Journal of Earth Science.

I am the first author of the article and co-authors are my thesis supervisor and our collaborator with the Geological Survey Branch of the British Columbia Ministry of Energy and Mines. I contributed significantly to the article by writing it, drafting or modifying all of the figures, collecting and processing all the samples and analysing the data, which led to the results and interpretations presented in the article.

Appendices A.3, E.2, E.3 contain maps and articles relevant to this chapter and chapter 4. An additional relevant geochemistry article is included as Appendix A.4:

Barresi, T., Dostal, J. 2005. Geochemistry and petrography of uppermost Hazelton Group volcanics: VHMS favourable stratigraphy in the Iskut River and Telegraph Creek map areas, northwest BC. Geological Fieldwork 2004, Paper 2004-2: 30-40.

Appendix D contains copyright agreement forms for all published manuscripts used in this thesis.

5.1 Abstract

Volcanic rocks of the Jurassic Iskut River Formation (IRF) in northwestern British Columbia (Canada) host several volcanogenic massive sulfide (VMS) deposits, including the exceptionally high-grade Eskay Creek Ag–Au–Cu–Pb–Zn deposit. The IRF comprises voluminous pillow basalt (>90%), minor rhyolite, and sedimentary rock of late Early to early Middle Jurassic age, filling a series of sub-basins along a 300 by 50 km north-trending belt. Two geochemically distinct types of tholeiitic basalts interfinger; both

resemble back-arc basin basalts formed from the melting of asthenospheric and sub-arc mantle sources. Group 2 basalts are more enriched in light rare-earth elements, Ba, K, Sr, Th, and U, and have lower positive ε_{Nd} values than group 1 basalts (+3.2 to +6.3 versus +6.9 to +8.4, respectively). The compositional differences between group 1 and group 2 basalts are interpreted to result from crustal contamination in group 2. Group 1 basalts are most common in the southern part of the IRF belt where they are closely associated with the Eskay Creek, Bonanza, and Hidden Creek (Anyox) VMS deposits. Group 2 basalts are most abundant in the northern half of the belt and are not associated with exploited mineral deposits. The lack of crustal contamination in group 1 basalts indicates that they formed from rapidly ascending magma in an advanced rift setting and were associated with high heat flow that drove hydrothermal circulation. Group 1 and group 2 basalts are reliably discriminated by Th/Ta <2.5 in the former and >2.5 in the latter. This geochemical criteria can therefore be used as an exploration tool to identify VMS permissive sub-basins and (or) stratigraphy in the IRF.

5.2 Introduction

Volcanogenic massive sulfide (VMS) deposits are important sources of copper, zinc, lead, gold, and silver (e.g., Franklin et al. 2005). They form at or near the sea floor as a result of the focused discharge of deeper circulating metal-rich hydrothermal fluids driven by magmatic heat (Barrie and Hannington 1999b). The compositional characteristics of the host volcanic rocks are predictors of regional VMS prospectivity (Lesher et al. 1986; Swinden 1996; Lentz 1998; Hart et al. 2004; Piercey 2010, 2011). However, based on the limited data available, there is still controversy about the setting of some large and (or) rich VMS districts (e.g., Iberian pyrite belt, Leistel et al. 1997; Abitibi belt, Gaboury and Pearson 2008). Among these are the Jurassic deposits of the Stikine terrane of the Canadian Cordillera in northwestern British Columbia. These deposits, some of which are associated with the bimodal volcanic rocks of the Jurassic Iskut River Formation (Table 5-1), include the Au-rich Eskay Creek deposit (Barrett and Sherlock 1996; Childe 1996; Macdonald et al. 1996a; Roth et al. 1999; Roth 2002) as well as the past-producing Hidden Creek and Bonanza Cu-rich VMS deposits at Anyox (Smith 1993; MacDonald et al. 1996b; Evenchick and McNicoll 2002). A number of other VMS prospects are hosted

by this formation or are proximal to it (Alldrick 1993; Evenchick and McNicoll 2002; Alldrick et al. 2004b, 2005a; Evenchick et al. 2004). While the geographic extent of the prospective IRF is broad, geochemical studies have been focused near the major deposits, including several studies of the rocks at or near the Eskay Creek mine (Barrett and Sherlock 1996; Childe 1996; Roth et al. 1999; Bartsch 2001; Lewis 2001; Roth 2002), the Anyox deposits (Smith 1993; MacDonald et al. 1996b), Georgie River (Evenchick et al. 2004), and Table Mountain (Barresi et al. 2005). Because of this, many samples discussed by previous studies are affected by strong alteration and much of the geochemical analysis was devoted to determining alteration-related geochemical vectors for exploration. A regional-scale geochemical study, focusing on determining the petrogenesis and variations in primary compositions of least-altered IRF rocks, has not been conducted.

Table 5-1. Mineral resources for VMS deposits in the IRF (Franklin et al. 2005 and references therein).

Deposit Name	Metric Tons Ore (millions)	Cu (%)	Pb (%)	Zn (%)	Au (g/t)	Ag (g/t)
Eskay Creek	3.35	0.7	2.9	5.6	45.97	2224
Hidden Creek	45.95	1.37	-	0.6	-	-
Bonanza	0.65	2.57	-	-	0.10	10

The objectives of this petrological study are to (i) describe the volcanological, petrographic, and geochemical characteristics of IRF basalts along a 300 km long belt (rift zone); (ii) elucidate petrogenetic and tectonic processes recorded in these rocks; (iii) interpret the processes responsible for this fertile metallogenic province; and (iv) evaluate how these factors can be used in future exploration by characterizing magmatic patterns along the length of the belt.

5.3 Physical volcanology

The sub-basins that host the IRF contain mainly basalt. Most sub-basins record nearly uninterrupted, 1 – 2 km thick, successions of pillow basalt and pillow basalt breccia (Figs. 4-4, 5-1, 5-2A). Individual flows are 5–30 m thick (Fig. 5-2A), and typically interfinger

and onlap one another. Pillows have geometries that range from spheres to flattened lobes, and tail and drape geometry is common (Fig. 5-2B). They range from 20 to 150 cm in diameter. Typically, the pillows have 1–5, or infrequently, up to 10 cm thick glassy rinds and aphanitic, equigranular phaneritic or rarely plagioclase- or glomero-porphyritic interiors. Collapsed pillows with 5–10 cm thick glassy tube rinds are locally abundant. The pillow basalts commonly contain 15%–20% vesicles or amygdules (chlorite or rarely calcite and (or) quartz), which are normally 2–4 mm in diameter but range up to 1 cm in some locations. Variolites on weathered surfaces form 4–10 mm diameter pale-weathering spheres, which can occupy up to 70% of the surface-area of the most glassy and fine-grained basalts. Locally, larger pillows are associated with deposits of fluidal coherent basalt clasts supported in a matrix of finely fragmented splintery basalt.

5.4 Petrography

The IRF basalts have variable grain size and crystallinity ranging from devitrified glass – holohyaline basalt to phaneritic holocrystaline basalt. Variations can be measured on the scale of pillows (from rim to center), eruptive units, and regionally, as basalts in the south are typically aphanitic and basalts in the north are typically phaneritic. Feldspar and (or) clinopyroxene phenocrysts are present in 20% of the flows, which are otherwise, and more typically, aphyric (Figs. 5-2C, 5-2E).

The finest-grained basalts have a brown, pseudo-isotropic groundmass with up to 10% radiating swallow-tailed plagioclase crystallites. Remnants of dendritic iron-oxide phases are locally present, and backscatter electron (BSE) microprobe images show feathery intergrowths of skeletal, quench-textured, clinopyroxene and plagioclase (Fig. 5-2C). The thickest flow units comprise phaneritic, aphyric basalts that typically have an equigranular texture with plagioclase and clinopyroxene grains up to 2 mm. They have subophitic textures, with 30%–40% clinopyroxene, 55%–70% plagioclase, and 5% iron oxides (discounting alteration products). They are commonly autobrecciated, with narrow, irregular interstices of altered volcanic glass or cryptocrystalline basalt.

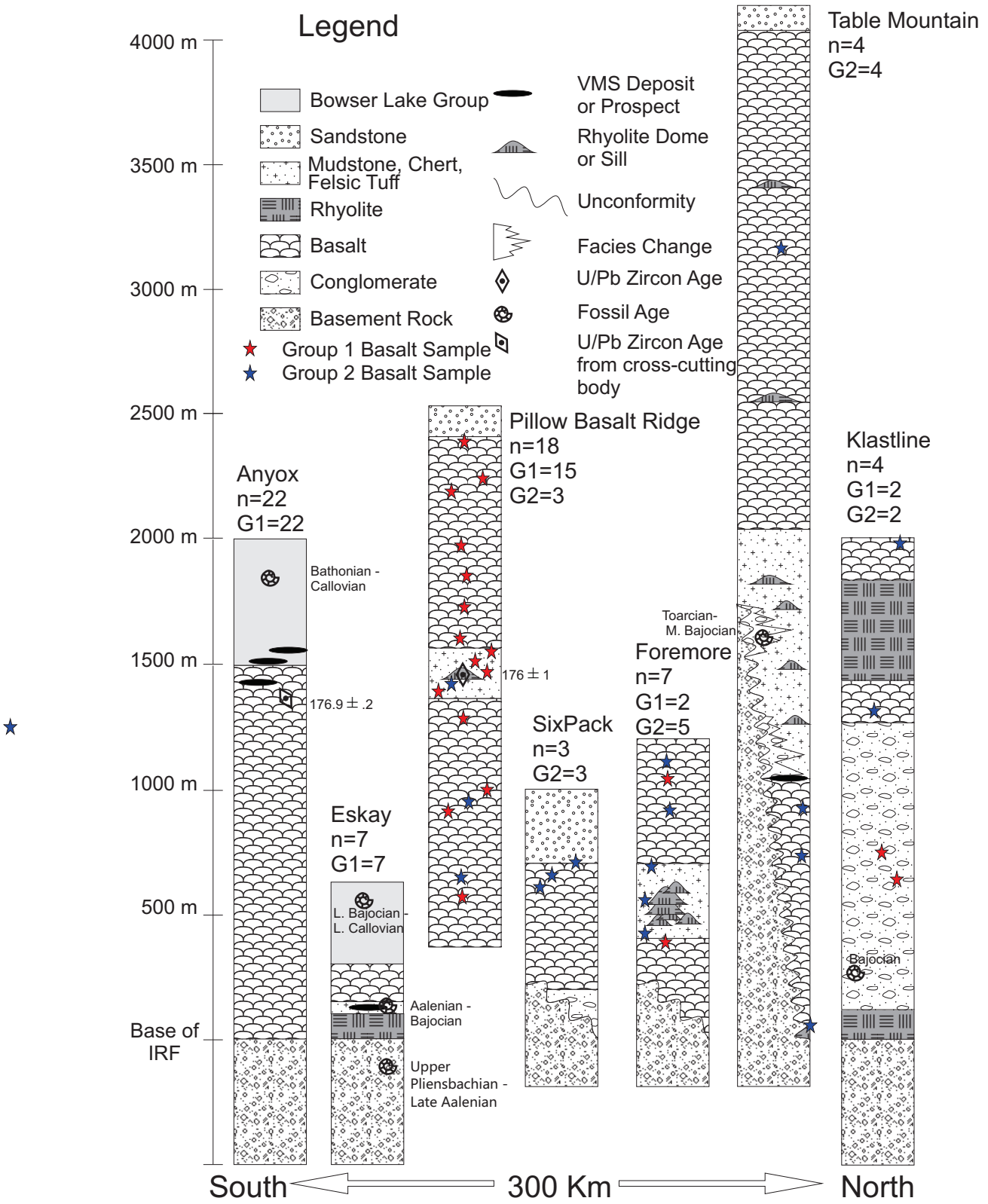

Fig. 5-1. Stratigraphic columns for seven sub-basins that are a primary focus of this thesis. Sample locations are depicted on the columns with stars (red = group 1; blue = group 2). Numerical notation at top of column indicates the number of samples (n) and how many are group 1 (G1) and group 2 (G2). Exact locations of samples from Eskay Creek and Anyox are not known but the samples are from within the pillow-basalt intervals.

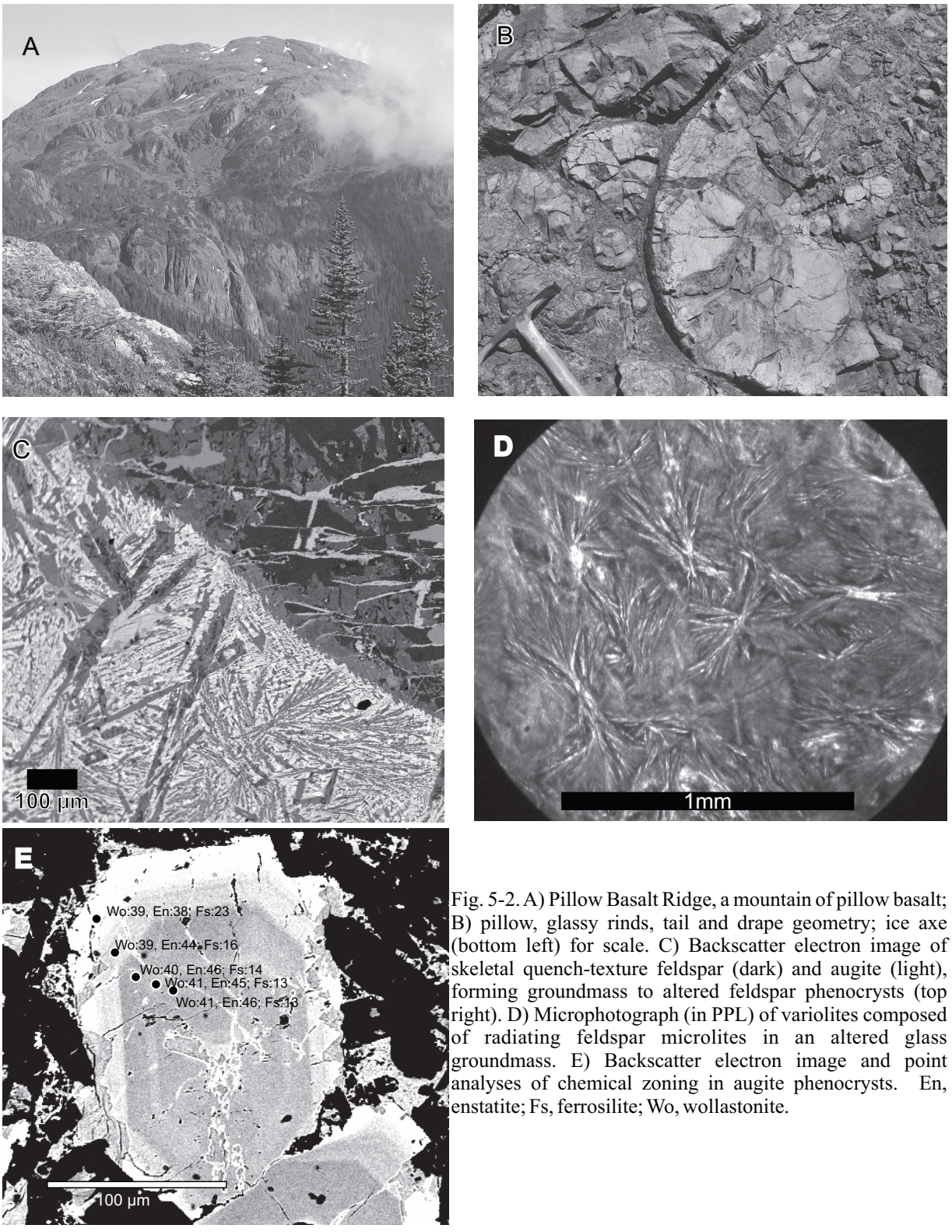

Fig. 5-2. A) Pillow Basalt Ridge, a mountain of pillow basalt; B) pillow, glassy rinds, tail and drape geometry; ice axe (bottom left) for scale. C) Backscatter electron image of skeletal quench-texture feldspar (dark) and augite (light), forming groundmass to altered feldspar phenocrysts (top right). D) Microphotograph (in PPL) of variolites composed of radiating feldspar microlites in an altered glass groundmass. E) Backscatter electron image and point analyses of chemical zoning in augite phenocrysts. En, enstatite; Fs, ferrosilite; Wo, wollastonite.

Within porphyritic flows, feldspars are the most common phenocryst phase, constituting up to 15% by volume of particular flows. The feldspar phenocrysts are lath-shaped, up to 5 mm long, and commonly have ragged fractured margins. Clinopyroxene phenocrysts are less abundant and smaller than plagioclase phenocrysts. They are euhedral to subhedral and show optical (colour) zoning from the core to the rim. In some basalts, clinopyroxene and plagioclase phenocrysts form glomerophenocrysts up to 1 cm in diameter. Variolites, a common macroscopic feature of the IRF basalts, comprise discrete spherical zones with radial plagioclase microlites hosted in a colour-zoned cryptocrystalline groundmass (Fig. 5-2D).

Electron microprobe analyses (Appendix B.2) show that clinopyroxene is augite (wollastonite $Wo_{37–46}$; enstatite $En_{26–49}$; ferrosilite $Fs_{9–30}$). Geochemical traverses across augite grains show that FeO increases from the cores to rims (Fig. 5-2E). Two ranges of plagioclase composition are present: primary labradorite to bytownite (anorthite, $An_{66–74}$) and secondary albite to oligoclase ($An_{4–13}$).

The volcanic rocks have been regionally metamorphosed to prehnite–pumpellyite faces as indicated by the presence of chlorite + epidote + prehnite in basaltic and sedimentary rocks (Alldrick et al. 2005a). Unzoned albite to oligoclase in some samples could have formed during low-grade metamorphism or sea-floor– hydrothermal alteration (Vallance 1974; Moody et al. 1985; Alt 1999).

5.5 Geochemistry

5.5.1 Analytical Techniques

Thirty-seven whole-rock samples of IRF mafic rocks were collected for major and trace-element analysis during regional mapping (Table 5-2; Appendix B.3). The samples represent the geographic, compositional, and stratigraphic range of IRF mafic rocks (Fig. 5-1). From these, six representative samples were selected for whole-rock Sm–Nd isotopic analysis, and two for Rb–Sr isotopic analysis (see Table 5-4 in section “Isotopic

Table 5-2. Examples of geochemical data for IRF basalts.

Location	Table Mtn.	6 Pack	Formore	Formore	Klastline	Klastline	PBR	PBR
Sample#	04TB24-7A	04JN6-6	04JN1-8A	04TB11-4	04JN8-10	04TB21-12	04TB10-2	04TB2-3
Group	2	2	2	1	1	2	1	1
UTM East	415314	405382	400954	402193	431990	426401	403181	401969
UTM North	6352203	6303669	6311052	6302414	6388080	6384867	6301058	6298303
SiO_2 (wt.%)	48.5	54.6	49.0	45.1	44.0	49.2	46.1	46.3
TiO_2	1.73	0.85	0.94	1.88	0.75	0.84	1.31	0.75
Al_2O_3	13.7	15.1	14.9	15.4	16.8	16	15.6	17.8
$Fe_2O_{3\_Total}$	16.5	8.7	11.5	13.1	9.7	9.9	11.3	9.5
MnO	0.23	0.16	0.29	0.18	0.17	0.17	0.20	0.17
MgO	4.37	5.27	3.19	6.39	9.39	7.71	9.03	5.66
CaO	6.62	6.93	7.23	11.14	11.66	6.56	8.80	12.13
Na_2O	4.3	5.5	4.5	2.7	1.6	3.6	2.4	2.7
K_2O	1.55	1.07	1.54	0.21	0.27	2.24	1.85	1.07
P_2O_5	0.46	0.18	0.34	0.21	0.08	0.18	0.13	0.08
LOI	2.1	2.3	6.5	3.8	6	3.8	4.2	3.3
TOTAL	100.5	100.6	100.5	100.0	100.0	100.2	100.3	100.1
Select Trace Elements (ppm)								
Co	47	30	33	45	47	41	50	39
Ni	0	18	27	71	212	80	128	55
V	499	194	252	340	179	233	80	234
Sc	37	30	20	42	35	34	36	35
Rb	31	18	24	3.8	6.2	35	43	25
Sr	339	184	449	257	273	448	288	87
Ga	19	19	17	20	12	12	17	15
Nb	6.3	6.9	2.9	4.6	1.2	3.1	3.0	1.3
Y	36	27	24	41	19	23	30	20
Zr	93	90	67	100	43	54	67	38
Ba	1340	344	556	130	345	699	1210	236
Cr	16	34	50	243	272	270	547	270
Cs	0.39	0.56	2.30	1.40	0.96	0.38	2.80	0.88
Hf	2.3	2.4	2.1	2.9	1.2	1.4	1.9	1.1
U	1.10	1.20	1.00	0.28	0.06	0.24	0.11	0.29
La	14.0	11.0	9.9	6.4	3.0	7.4	4.2	2.3
Ce	29	22	24	17	8	17	11	6
Pr	3.8	2.8	3.4	2.5	1.3	2.3	1.7	0.9
Nd	17.0	13.0	16.0	13.0	6.1	10.0	8.8	4.8
Sm	4.4	3.1	4.1	4.4	2.1	2.8	3.1	1.7
Eu	1.30	1.10	1.20	1.60	0.81	0.87	1.10	0.68
Gd	5.3	3.9	4.4	6.2	2.8	3.4	4.5	2.6
Tb	0.88	0.67	0.69	1.10	0.47	0.58	0.77	0.47
Dy	5.5	4.5	4.2	7.3	3.0	3.6	4.8	3.1
Ho	1.20	0.99	0.87	1.60	0.66	0.78	1.10	0.70
Er	3.3	2.7	2.3	4.3	1.9	2.2	3.0	2.0
Tm	0.52	0.44	0.36	0.68	0.29	0.35	0.45	0.31
Yb	3.6	2.9	2.3	4.3	1.9	2.3	3.0	2.0
Lu	0.56	0.44	0.34	0.67	0.31	0.37	0.46	0.33
Ta	0.35	0.38	0.19	0.80	0.08	0.18	0.18	0.10
Th	2.20	2.30	1.50	0.49	0.16	0.56	0.28	0.19

Note: Full table of whole-rock geochemical data is in Appendix B.3. Fe_2O_{3total}, total iron as Fe_2O_3; LOI, loss on ignition. Location coordinates in Universal Transvers Mercator (UTM) North American Datum 1983 (NAD83).

composition"). Visible effects of weathering and alteration were removed with a diamond saw during sample processing.

Major elements and trace elements analyses were performed at the Geological Survey of Canada's (GSC) analytical chemistry laboratory in Ottawa, Ontario. Major elements and Ba, Sr, Rb, Nb, and Zr were analyzed by wavelength dispersive – X-ray fluorescence (WDS–XRF). FeO was determined by titration, while H_2O total and CO_2 total were determined by infrared spectrometry (IRS). The rare-earth elements (REEs), and a suite of additional trace elements (Table 5-2; Appendix B.3) were determined by inductively coupled plasma – mass spectrometry (ICP–MS). Precision and accuracy of these techniques were maintained at better than 5% for 2σ error (σ, level of error) (at 10× detection limit) with measurements made relative to in-house and international reference materials. Analytical precision was monitored with blind duplicates (5% of all samples; duplicate analyses included in appendix B.3).

Nd and Sr isotopic ratios were determined by thermal ionization mass spectrometry (TIMS) at the GSC's Geochronology Laboratory in Ottawa, Ontario. Details of the analytical techniques used and their precision and accuracy were described by Thériault (1990).

Mineral compositions were determined using a JEOL Superprobe 8200, equipped with five wavelength-dispersive spectrometers (WDS), at Dalhousie University. The probe was operated with an accelerating voltage of 15 kV, 20 nA beam current, 1-2 μm beam diameter, and counting time of 20 s on each peak, and 10 s each on lower and upper backgrounds (double for the Fe peak and backgrounds). International reference standards were used to calibrate the probe and the standard Kanganui Kaersutite (KK) was analyzed periodically to monitor precision and accuracy. Unaltered groundmass and phenocrysts were chosen for analysis, and where possible core and rim compositions were measured.

5.5.2 Alteration effects

Only the visibly least-altered rocks were sampled for this project, and all visible effects of alteration were removed during sample processing. However, low-grade (prehnite–

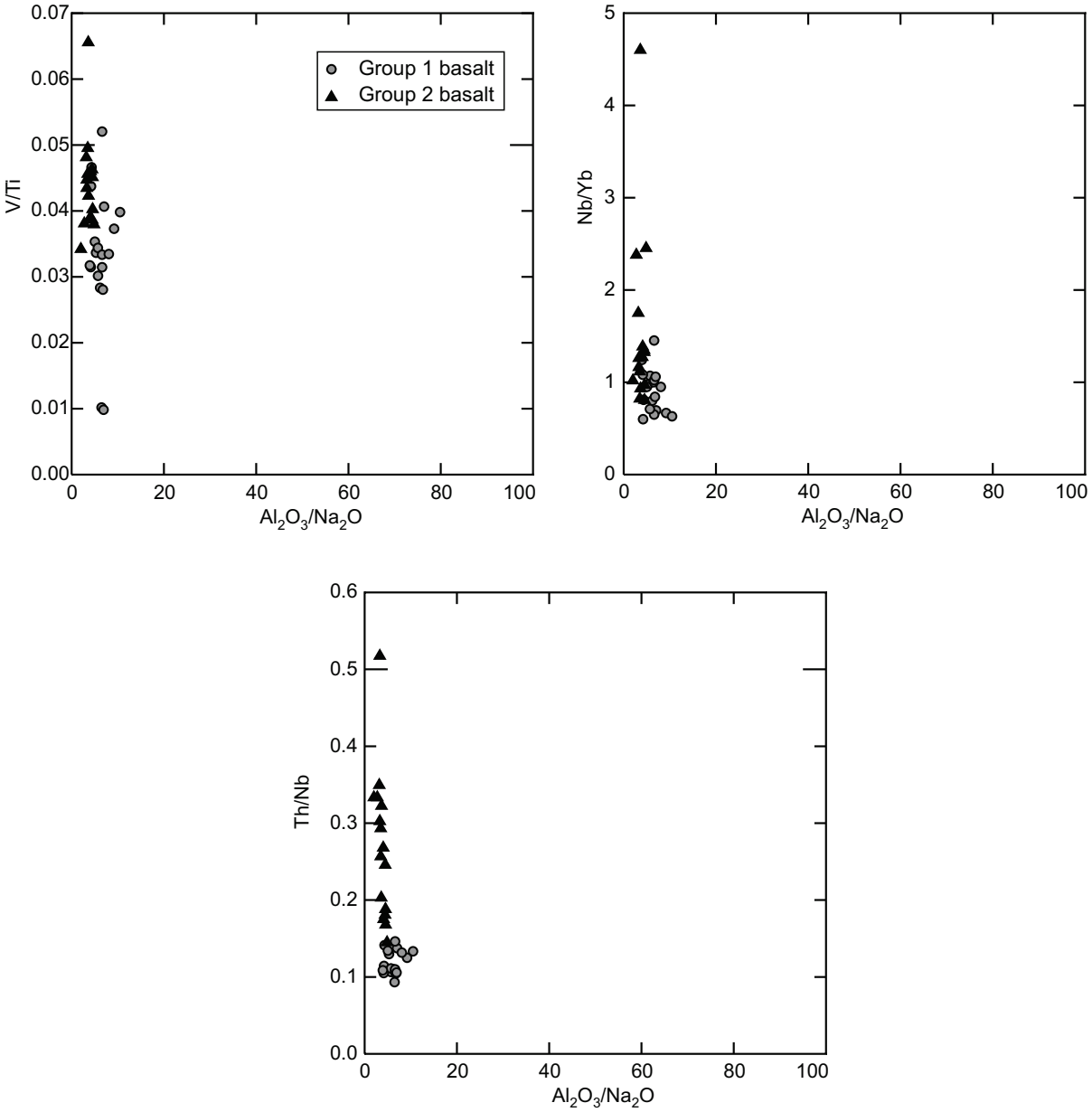

Fig. 5-3. Trace-element ratios plotted against Al_2O_3/Na_2O alteration index (Spitz and Darling 1978) indicate that the sampled IRF basalts are not strongly altered and that selected ratios do not vary with alteration.

pumpellyite facies) metamorphism, and weak (rare traces, noted below, mostly removed) sea-floor and hydrothermal alteration, have affected the IRF rocks. Petrographic evidence for hydrothermal alteration includes the rare presence of veins and partial replacement of primary minerals. Typical alteration indices (e.g., Al_2O_3/Na_2O, $Al_2O_3/Na_2O + CaO + K_2O$) are very low and relatively consistent, indicating that bulk-rock compositions were not significantly affected by alteration. Spitz and Darling (1978) found that Al_2O_3/Na_2O ratios in rocks affected by significant alkali mobility due to alteration of feldspar typically range from 10 to >100, whereas most samples in this study fall between 2 and 7 (Fig. 5-3). Furthermore, mobile–immobile element pairs (e.g., Na_2O/Th, MgO/Th) show well-defined trends, with few outliers (Fig. 5-3). It is likely that bulk-rock trends in CaO, Na_2O, and K_2O reflect petrogenetic processes. However, small-scale mobility via sea-floor and (or) hydrothermal alteration has affected these elements on a mineralogical scale, as evident from albitization of feldspar and calcite in amygdules. Therefore, these elements were not used to assess petrogenetic processes. The concentrations and ratios of high field strength elements (HFSE) and REE show well-defined linear correlations against Th (Fig. 5-4), indicating that these elements were immobile during alteration (Maclean 1990). This is consistent with numerous other studies of elemental behavior during alteration (e.g., Lesher et al. 1986; Maclean 1990; Polat et al. 2002), indicating that measured HFSE and REE concentrations represent their primary relative concentrations in IRF rocks and can therefore be used for petrogenetic interpretations.

5.5.3 Classification and Geochemical Variations

The IRF mafic rocks form two geochemical suites, here termed group 1 and group 2, with distinct major and trace-element characteristics. Thorium/tantalum ratios were used to classify the samples: group 1 samples have Th/Ta ratios below 2.5 and group 2 samples have ratios higher than 2.5.

All IRF mafic rocks have SiO_2 concentrations that range from 44–56 wt.%. The SiO_2 concentrations and Zr/TiO_2 versus Nb/Y ratios are consistent with sub-alkaline basalt to basaltic andesite compositions (Figs. 5-5A, 5-5B). Low Zr/Y and a negative correlation between Mg# and TiO_2 (Figs. 5-5C, 5-5D) indicate that the rocks are tholeiitic (Barrett

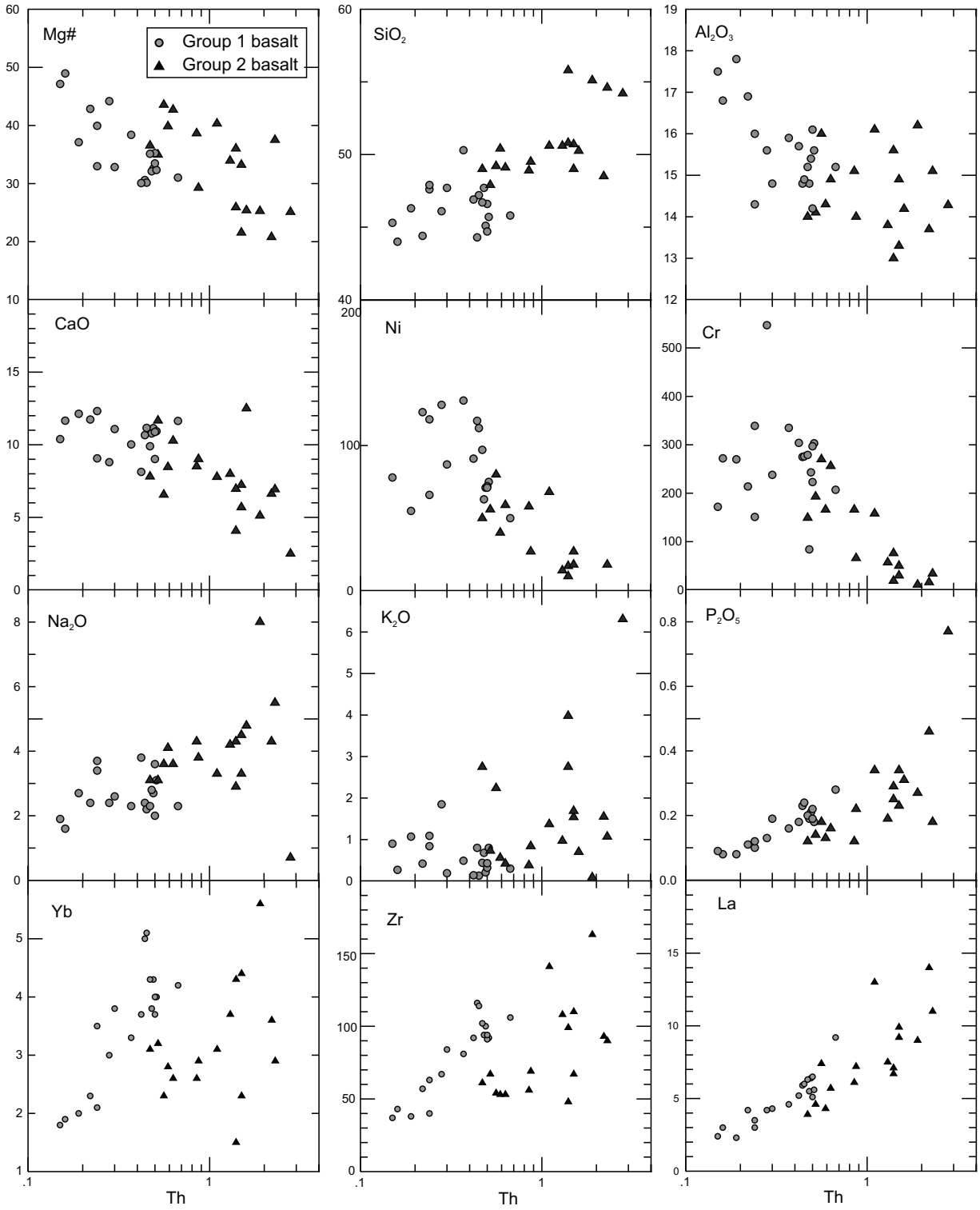

Fig. 5-4. Mobile versus immobile element (Th), and trace-element versus immobile element. In some cases, group 1 and group 2 basalts must be considered individually to identify trends. Where trends are well defined, they suggest that alteration has not had a significant effect on the mobile element concentrations.

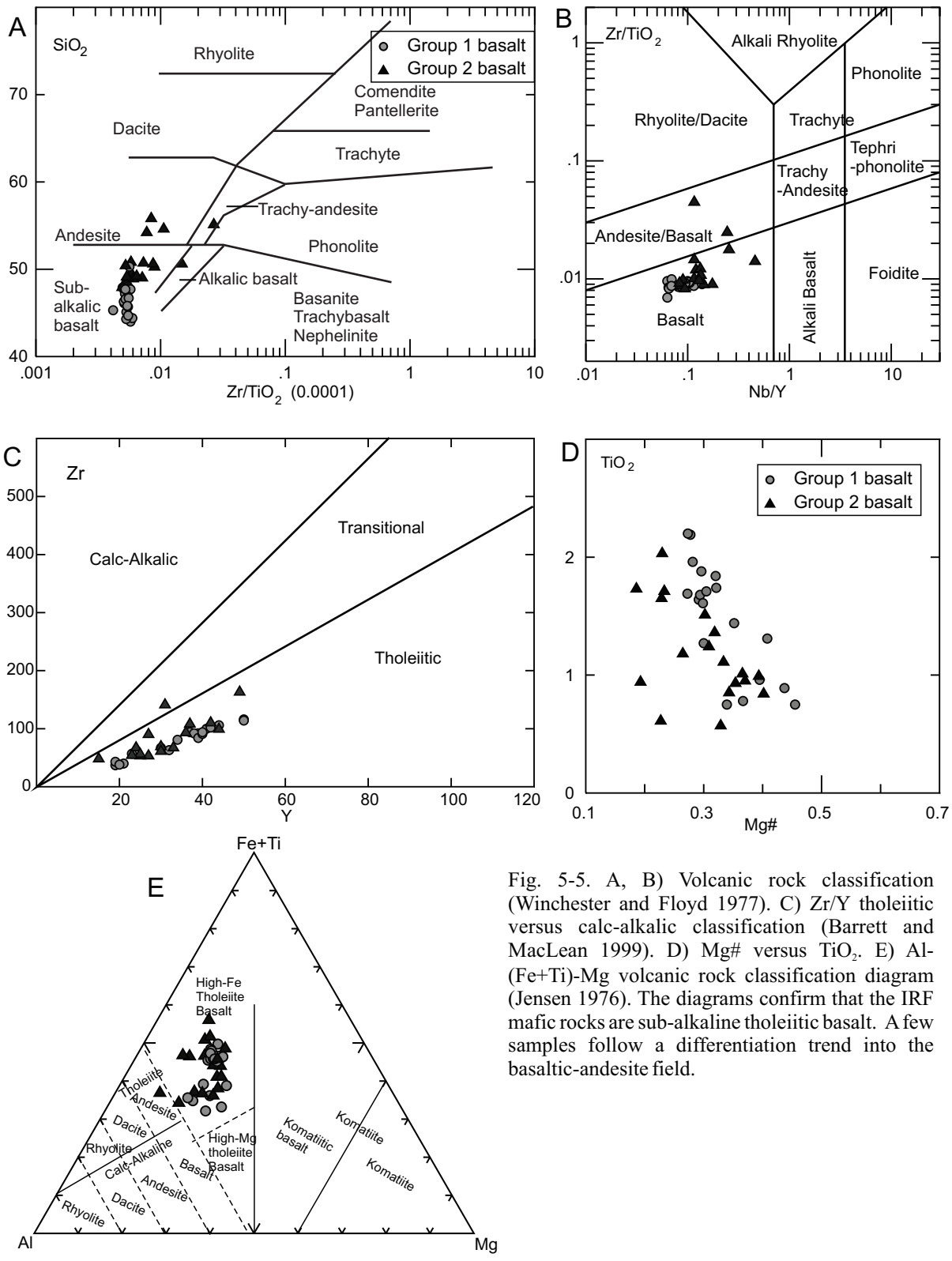

Fig. 5-5. A, B) Volcanic rock classification (Winchester and Floyd 1977). C) Zr/Y tholeiitic versus calc-alkalic classification (Barrett and MacLean 1999). D) Mg# versus TiO_2. E) Al-(Fe+Ti)-Mg volcanic rock classification diagram (Jensen 1976). The diagrams confirm that the IRF mafic rocks are sub-alkaline tholeiitic basalt. A few samples follow a differentiation trend into the basaltic-andesite field.

and MacLean 1999). This is consistent with the Al−(Fe + Ti)−Mg ternary plot (Jensen 1976), in which the IRF rocks plot as high-Fe tholeiitic basalts (Fig. 5-5E). The wide range in concentration of MgO (2.7 – 9.4 wt.%), Fe_2O_{3total} (total iron as Fe_2O_3; 7.6 – 16.5 wt.%), TiO_2 (0.57 – 2.2 wt.%), and Mg# (molar Mg/(Mg + Fe) indicates that the basalts are differentiated. Bivariate major oxides diagrams show increases in Na_2O and P_2O_5 and decreases in Al_2O_3, CaO, MgO, Ni, and Cr with increasing SiO_2 (Fig. 5-6). These variations, as well as Pearce element ratios (Fig. 5-7), support fractionation of typical major rock-forming phases, such as clinopyroxene, olivine, apatite, and plagioclase. Generally, the two groups of basalts form contiguous trends on bivariate diagrams, with the most differentiated group 1 basalts overlapping with the least differentiated group 2 basalts. Group 1 basalts have a lower average SiO_2, P_2O_5, and alkalis, and higher average Al_2O_3, MgO, Mg#, Ni, and Cr than group 2 basalts (Table 5- 3).

Based on trace-element systematics, the two basalt groups are best discriminated using La/Sm versus Th/Ta (or Th/Nb) ratios, reflecting an overall enrichment in highly incompatible elements and light REE (LREE) in group 2 basalts relative to group 1 (Fig. 5-8). Group 1 basalts have 10–30 times chondritic REE values; group 2 basalts have similar concentrations of the heavy REE (HREE) but higher LREE concentrations (15–65 times chondritic La; Fig. 5-9). Chondrite-normalized REE patterns (Sun and McDonough 1989) from group 1 basalts have a flat profile, whereas those from group 2 basalts have a downward slope from La to Sm; La_n/Sm_n (n, normalized) values for groups 1 and 2 basalts average 0.89 and 1.51, respectively. Slight negative Eu anomalies in some of the most differentiated basalts from both groups are consistent with minor plagioclase fractionation. Both groups have flat HREE patterns, which are consistent with derivation via partial melting of spinel peridotite (Dostal et al. 1976) at depths <85 km (i.e., above the garnet–spinel transition; Robinson and Wood 1998).

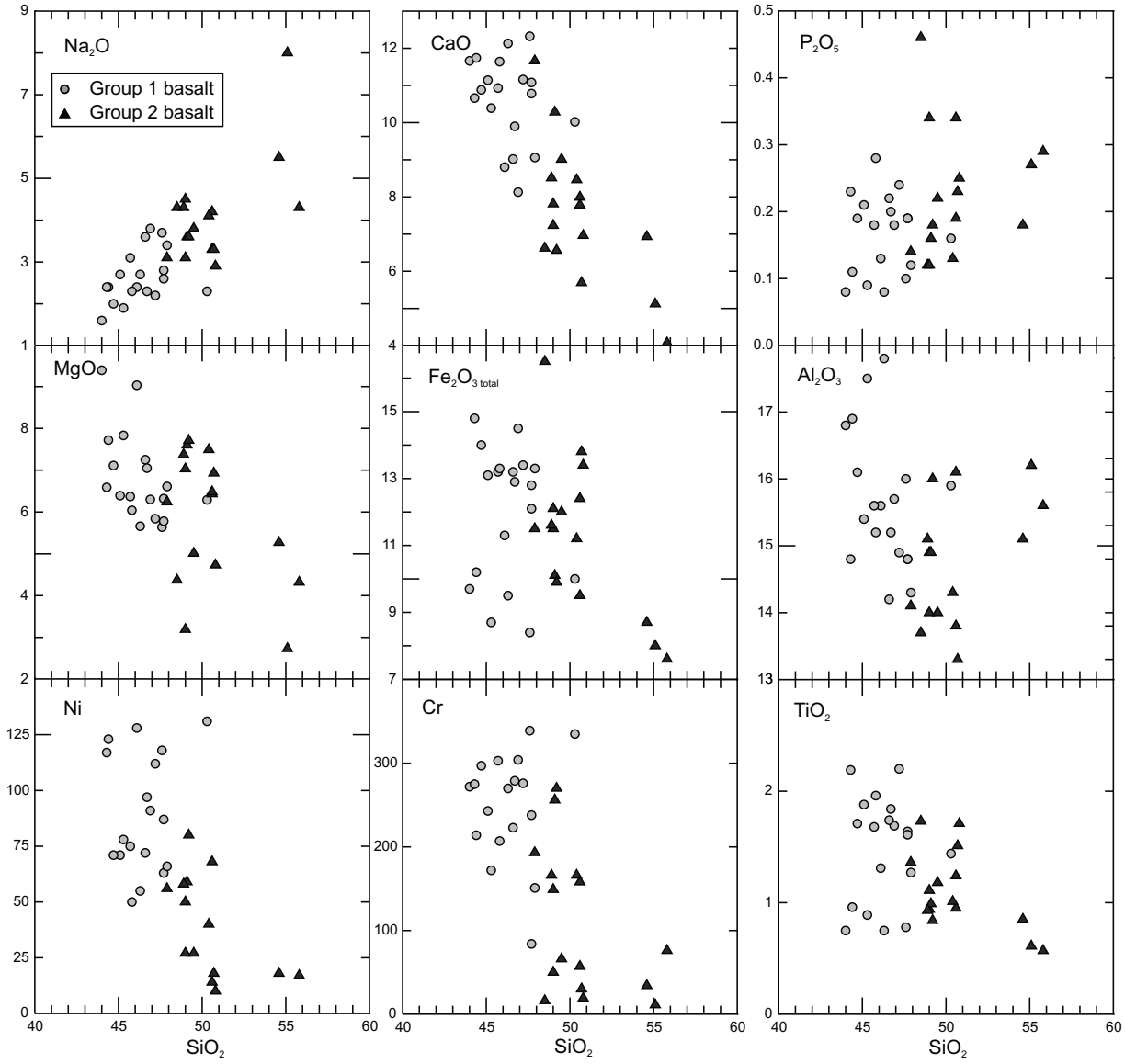

Fig. 5-6. Major elements, Ni and Cr plotted against SiO_2. Values of major elements in weight percent, Ni and Cr in parts per million. The range in values of SiO_2, MgO and Fe_2O_{3total} indicate that the basalts are differentiated. Increases in Na_2O and P_2O_5 and decreases in Al_2O_3, CaO, Mgo, Ni and Cr with increasing SiO_2 support fractional crystallization of clinopyroxene, olivine, apatite and plagioclase. Group 1 basalts have lower SiO_2, P_2O_5 and alkalis and higher Al_2O_3, MgO , Ni and Cr than group 2 basalts.

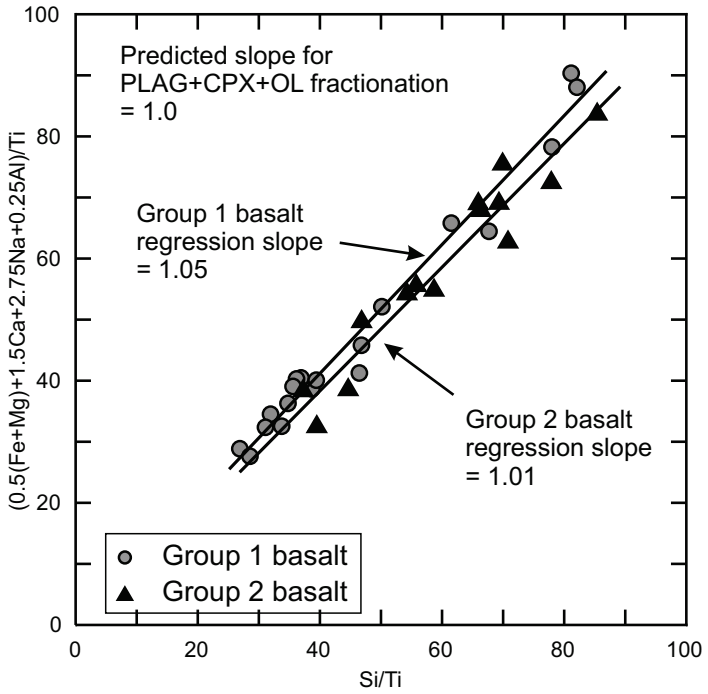

Fig. 5-7. Pearce element ratio (PER) diagram. Regression lines for groups 1 and 2 basalt samples have slopes consistent with the 1.00 predicted slope for plagioclase (PLAG), clinopyroxene (CPX), and olivine (OL) fractionation (Russell and Nicholls 1988; Stanley and Russell 1989). Note that PERs do not provide positive evidence of fractionating mineral phases, they only show that the chemistry is consistent with the hypothesis. PERs eliminate the closure problem in Harker style diagrams (Chayes 1964). Titanium was selected for the denominator because it is generally considered to be a conserved element during crystallization of mafic tholeiitic magmas; TiO_2 concentrations of IRF basalt CPX are low: average 0.81% n=39 (Appendix B.2).

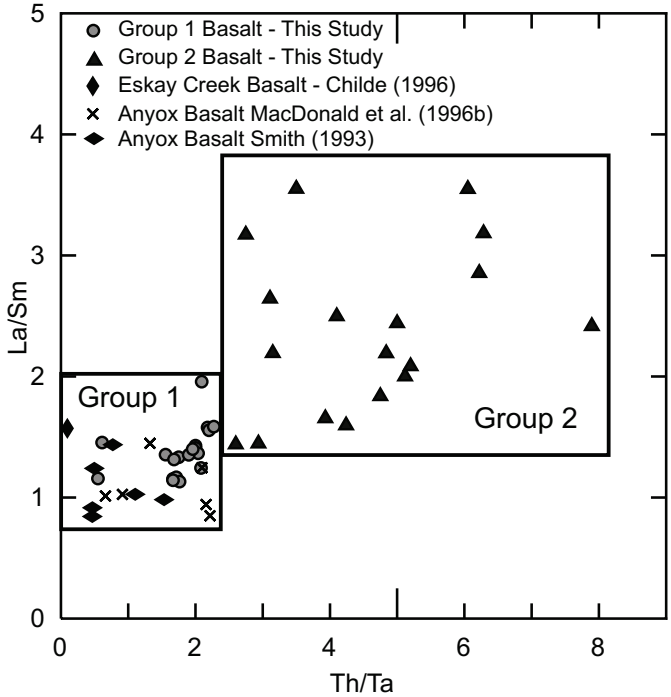

Fig. 5-8. Discrimination of group 1 and group 2 basalts. The boxes are defined by this study and outline the range of element ratios encompassed by group 1 and 2 basalts, effectively discriminating them. The selected ratios show the overall enrichment in highly incompatible elements and light REE in group 2 basalts relative to group 1. Eskay and Anyox samples all fall in the field of group 1 basalt.

Table 5-3. Average concentrations and ratios of selected elements for group 1 and group 2 basalts.

	Group 1			Group 2		
	Min	Max	Avg	Min	Max	Avg
SiO_2 (wt. %)	44.0	50.3	46.3	47.9	55.8	54.6
TiO_2 (wt. %)	0.75	2.20	1.49	0.57	1.73	0.85
Th (ppm)	0.15	0.67	0.37	0.47	2.3	2.30
Ni (ppm)	50	212	963	0	80	17
Cr (ppm)	84	547	265	11	270	34
Yb (ppm)	1.8	5.1	3.4	1.5	5.6	2.9
Al_2O_3/TiO_2	6.7	23.7	12.1	7.6	27.3	14.9
Mg#	27.25	45.50	33.07	18.59	40.17	30.78
Ti/V	19.21	101.55	36.10	15.25	29.25	23.19
Ti/Zr_{pm}	0.87	1.24	0.98	0.19	1.05	0.75
Nb/La_{pm}	0.37	0.74	0.62	0.28	0.94	0.56
Th/Nb_{pm}	0.82	1.28	1.02	0.23	0.82	0.50
Nb/Th_{pm}	0.78	1.23	1.00	1.21	4.34	2.24
La/Sm_c	0.73	1.26	0.89	0.93	2.29	1.51
Nb/Y	0.06	0.14	0.09	0.08	0.46	0.16
Nb/Yb	0.60	1.45	0.91	0.81	4.60	1.54
Zr/Y	1.90	2.54	2.27	1.96	4.55	2.66
Zr/Nb	17.38	35.83	26.14	6.96	28.60	19.58
Zr/Yb	18.00	25.24	22.71	18.93	45.48	26.16
Hf/Sm	0.52	0.69	0.61	0.50	0.82	0.63
Sm/Yb	0.85	1.17	1.03	0.87	1.78	1.11

On primitive mantle-normalized multi-element diagrams (Sun and McDonough 1989), group 1 basalts have a mainly flat profile with slight depletion of strongly incompatible elements, Th and Nb (Fig. 5-9). Group 2 basalts typically have higher concentrations of strongly incompatible elements and LREE, accompanied by higher Th/Nb ratios (Table 5-3). Their primitive mantle-normalized profiles show positive Th but negative Nb and Ti anomalies (Fig. 5-9). These trace-element characteristics, as well as high Ni and Cr concentrations, are geochemically intermediate between island-arc tholeiites (IAT) and mid-ocean ridge basalts (MORB), and more closely resemble back-arc basin basalts (BABB) (Fig. 5-10). Tectonic discrimination based on V, Ti, and Zr ratios (Shervais

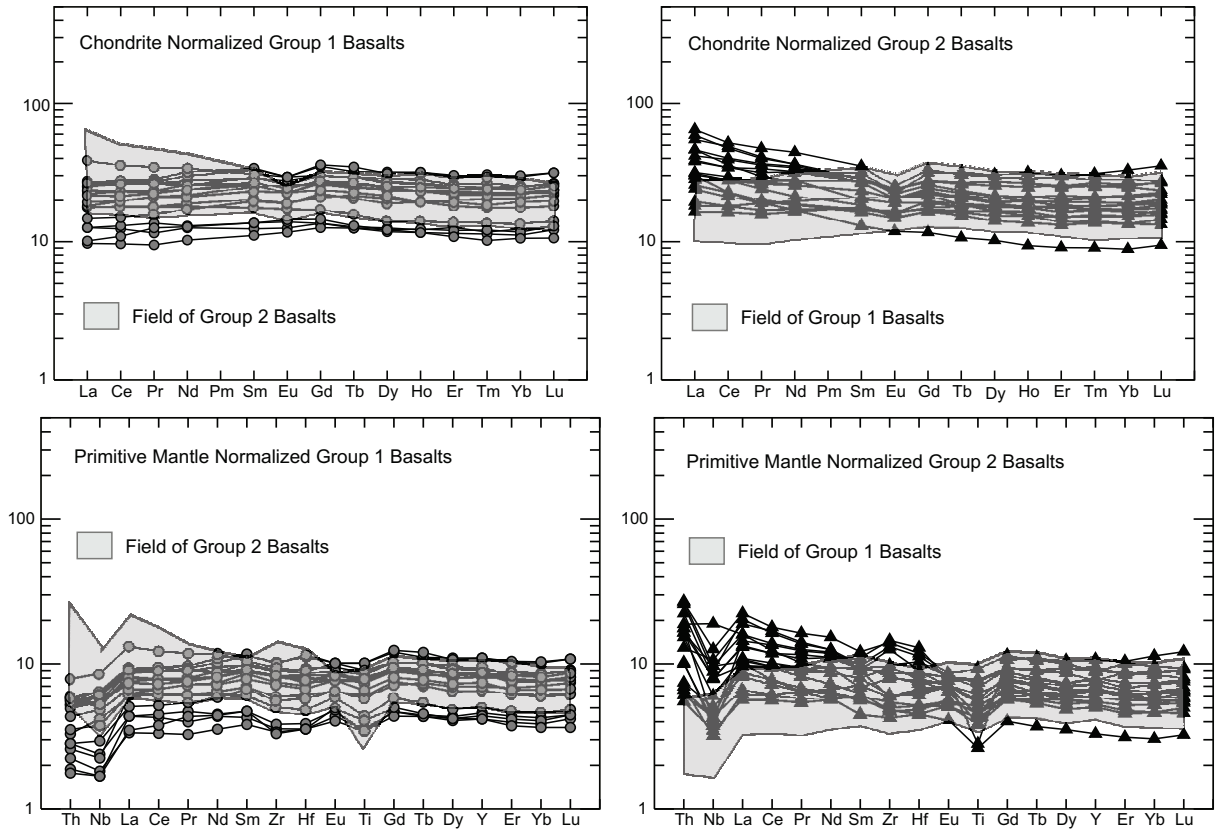

Fig. 5-9. Chondrite-normalized REE (top), and primitive mantle-normalized (bottom) multi-element diagrams comparing the characteristics of group 1 (left) and group 2 (right) basalts. Normalization data from Sun and McDonough (1989). The data for group 1 and 2 basalts have consistent profiles that are distinct from one another. Distinguishing features include lower Th and LREE concentrations in group 1 basalt and negative Nb and Ti anomalies in group 2 basalt, generally indicating a stronger subduction-related influence in group 2 basalt. Both groups of basalt have variable $Sm/Eu_{chondrite}$ ratios indicating that some samples from each group were affected by fractionation of feldspar.

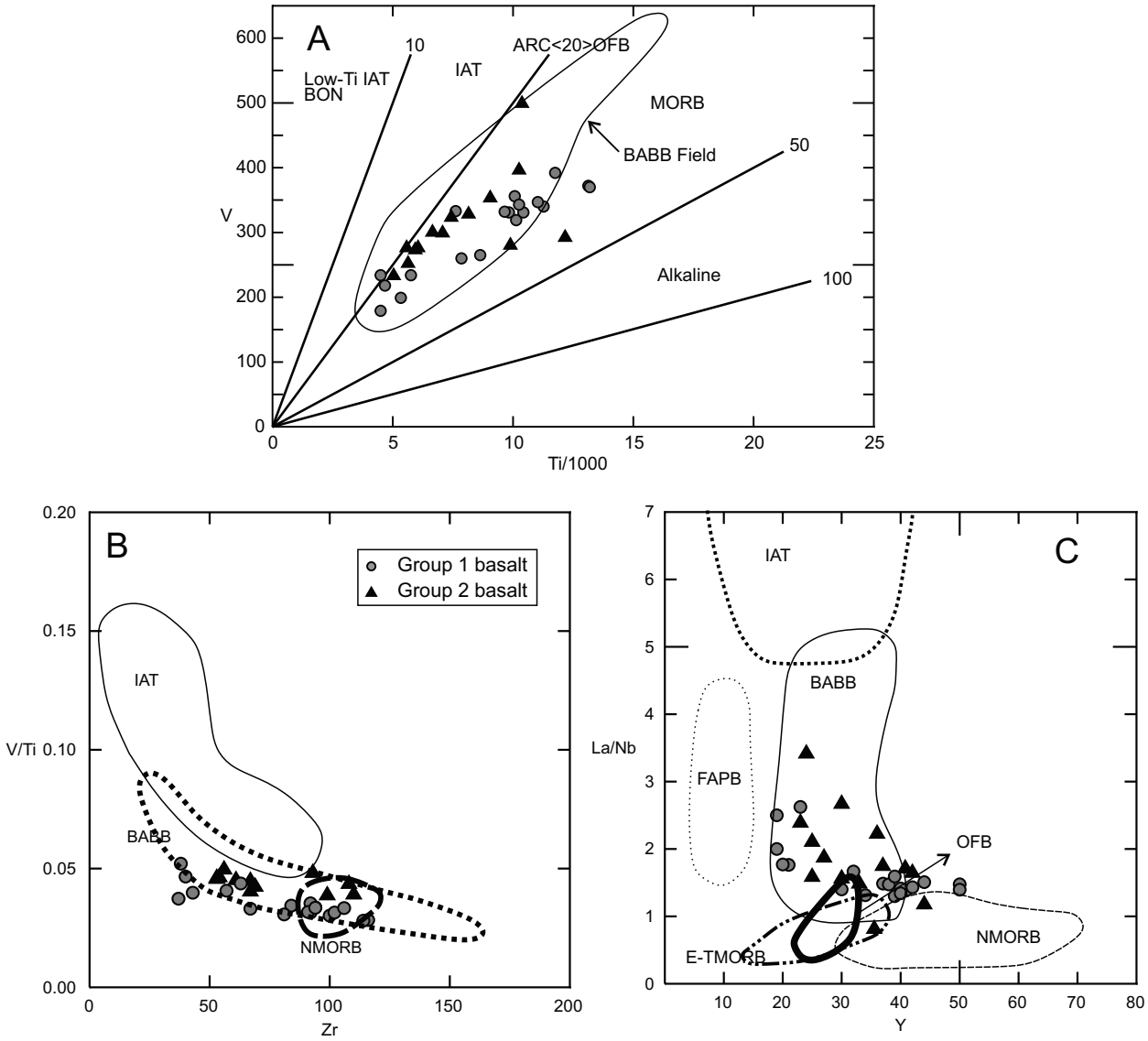

Fig. 5-10. Tectonic discrimination of the IRF basalts. Only samples that plot in the basalt fields of Figs 4-16A and 4-16B are plotted on these diagrams. A) V/Ti (Shervais 1982); B) V/Ti-Zr (Woodhead et al. 1993); C) La/Nb-Y (Woodhead et al. 1993. Teconic discrimination classifies both group 1 and 2 basalts as BABB; Group 1 basalts plot closer to MORB fields and group 2 basalts plot closer to IAT fields. Bon, bonnites; NMORB, normal MORB; E-TMORB, enriched to transition MORB; OFB, ocean-floor basalt; FAPB, forearc platform basalt.

1982; BABB field compiled by Metzger et al. 2002; Woodhead et al. 1993), indicate that the IRF basalts have BABB and (or) MORB affinities (Figs. 5-10A, 4-10B). However, using La/Nb versus Y ratios (Floyd et al. 1991), they can be classified as BABB (Fig. 5-10C). Although all of the IRF basalts have a BABB affinity, the geochemical characteristics of group 1 basalts are closer to MORB, whereas group 2 basalts have a stronger arc-related signature.

5.5.4 Isotopic Composition

The Nd isotope ratios were determined for one group 1 basalt, four group 2 basalts, and one andesite[4], collected from four separate sub-basins. The age-corrected ε_{Nd} values range from +3.2 to +6.9 (Table 5-4). Group 1 basalt has the highest positive value (+6.9) and two of the group 2 basalts and the andesite fall within the range +3.2 to +3.5. However, two samples of group 2 basalt have higher positive ε_{Nd} values, closer to those of group 1 (Figs. 5-11A, 5-11B). Previously published Nd isotopic data from the IRF include one basalt sample from the Eskay Creek mine (Childe 1996) that yielded ε_{Nd} +6.9 and six samples from the Anyox area (Smith 1993) that yielded ε_{Nd} values of +7.8 to +8.4. The major and trace-element characteristics of samples from Eskay and Anyox are similar to group 1 basalts (Fig. 5-22A). Overall, group 1 basalts have higher positive ε_{Nd}, whereas group 2 basalts typically fall into a lower range, from +3.2 to +6.3.

The ε_{Nd} Nd values of non-IRF rocks throughout the Stikine terrane range from –0.5 to +7.7 (Samson et al. 1989). With the exception of the most juvenile group 1 basalts, the ε_{Nd} values of IRF rocks are typical of other mafic volcanic and intrusive rocks from Stikinia. High positive ε_{Nd} values are inconsistent with a significant contribution from substantially older continental crust or sedimentary rocks derived from it (DePaolo 1981). However, the Nd isotopic data cannot exclude contamination by juvenile crust with a short crustal residence time, or limited contamination by older continental crust (Gonzales and Van Schmus 2007).

[4] Whole-rock data for MS03-23-05 are reproduced in Appendix B.3 and originally reported in Barresi and Dostal (2005). With the exception of being more differentiated, it has trace-element geochemical characteristics that are consistent with the group 2 basalts.

Table 5-4. Nd/Sm and Rb/Sr isotope concentrations and ratios.

Sample	Location	[Nd] ppm	[Sm] ppm	$^{147}Sm/^{144}Nd$	2σ	$^{143}Nd/^{144}Nd$	2σ	$\varepsilon^{143}Nd(174)$	2σ
04JN5-D	Six Pack	7.33	2.41	0.19847	0.00020	0.512962	0.000024	6.33	0.47
04TB24-2	Table Mtn.	11.10	3.34	0.18218	0.00019	0.512929	0.000022	6.05	0.43
MS03-23-05	Table Mtn.	22.34	5.67	0.15346	0.00018	0.512762	0.000021	3.43	0.41
04TB2-4	Pillow Basalt Rdg.	10.36	3.52	0.20563	0.00022	0.513002	0.000022	6.94	0.42
04TB21-12	Klastline	9.12	2.41	0.15958	0.00017	0.512759	0.000021	3.24	0.41
04TB16-6	Formore	8.00	2.40	0.18144	0.00019	0.512796	0.000032	3.46	0.63

Sample	Location	[Sr] ppm	[Rb] ppm	$^{87}Rb/^{86}Sr$	2σ	$^{87}Sr/^{86}Sr$	2σ	$^{87}Sr/^{86}Sr$ (174)	2σ
MS03-23-05	Table Mtn.	92.09	1.2	0.0368	0.0001	0.705316	0.000025	0.70522	0.00003
04TB2-4	Pillow Basalt Rdg.	162.94	9.7	0.1721	0.0012	0.704258	0.000026	0.70383	0.00004

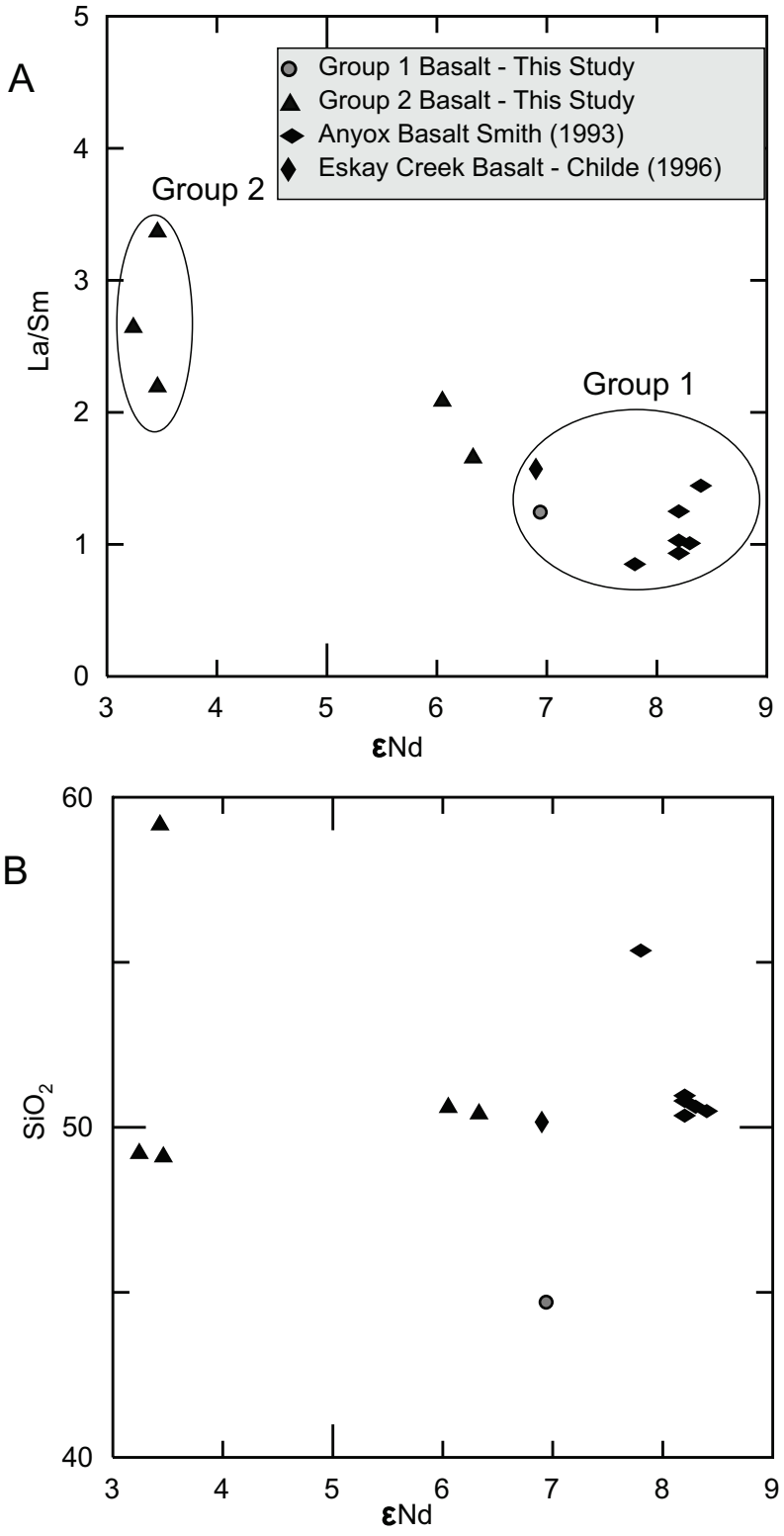

Fig. 5-11. ε_{Nd} data versus A) La/Sm, and B) SiO_2. The group 1 and 2 basalts have distinct ranges of ε_{Nd}, whereby group 1 basalt has higher positive ε_{Nd} values than group 2 basalt. ε_{Nd} values do not vary systematically with SiO_2 (an indices of differentiation or crustal contamination), or La/Sm (an index of subduction input) suggesting that isotopic heterogeneities within one or more of the magma sources influenced Nd isotopic ratios.

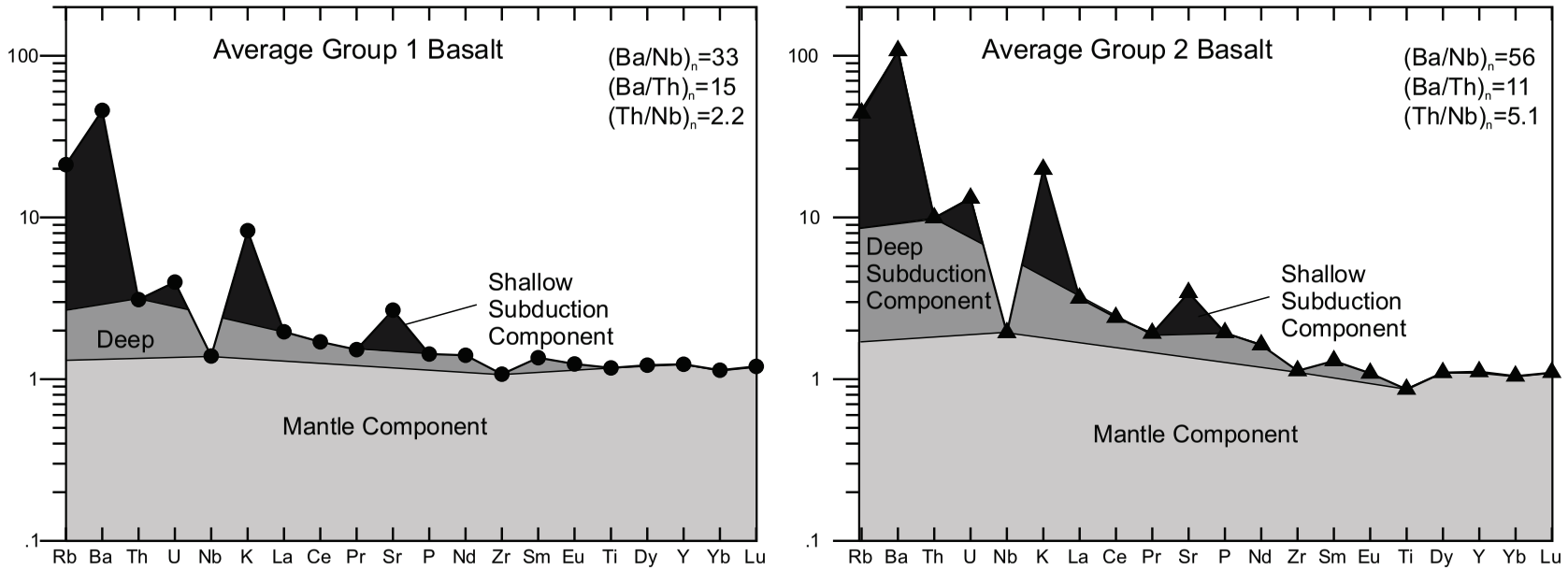

Fig. 5-12. NMORB-normalized average group 1 and group 2 multi-element profiles, highlighting mantle component and deep and shallow subduction components using the method of Pearce et al (2005). Group 1 and 2 basalts have similar mantle components but group 2 basalts have significantly higher total and deep subduction components than group 1 basalts. n, normalized.

5.5.5 Spatial distribution of group 1 and group 2 basalts

Group 1 basalts are more abundant in the south of the study area, whereas group 2 basalts are more abundant in the north (Figs. 4-2, 5-1). Eskay Creek and Anyox, the most southerly rift segments with geochemical data, consist entirely of group 1 basalts. Groups 1 and 2 basalts are intercalated in central rift segments (e.g., Pillow Basalt Ridge and Formore), and group 2 basalts are the only type sampled in the northern Sixpack and Table Mountain areas. The northernmost rift segment (Klastline) is an exception to this overall pattern in that it contains both group 1 and 2 basalts.

5.6 Discussion

5.6.1 Petrogenesis

A petrogenetic model for the IRF basalts must account for the simultaneous eruption of geochemically distinct group 1 and 2 basalts. The model should also account for within-group and between-group variations in major and trace elements, trace-element ratios, and Nd isotope data. Several processes that may have been responsible for the genesis of groups 1 and 2 basalts are considered in turn.

Variations as a result of fractional crystallization

The range of major-element compositions, Ni and Cr concentrations, Mg#, and Zr/Ti and Pearce element ratios (Tables 5-2, 5-3; Figs. 5-6, 5-7) are consistent with the fractional crystallization of olivine, clinopyroxene, and plagioclase. In group 1 basalts, molar proportions of Si decrease by 66% compared to Ti, which is conserved during fractionation of mafic tholeiitic rocks, indicating up to 33% fractionation (Fig. 5-7). Slightly lower Mg#, and Ni and Cr concentrations and elevated SiO_2 and Zr/Ti ratios in group 2 basalts indicate more advanced fractional crystallization relative to group 1 basalts (Figs. 5-5, 5-6). However, fractional crystallization cannot account for differences in the ratios of strongly incompatible trace elements such as La/Sm, Nb/La, Th/La, and Th/Nb, or differences in Nd isotopic ratios. Assimilation of crustal rock accompanying fractional crystallization (AFC process, e.g., DePaolo 1981; Kimura and Yoshida 2006) could affect incompatible trace-element ratios. However, before determining any possible effect of crustal contamination, the composition of the parent magma must be determined.

Mantle and subduction components in IRF basalts

The IRF basalts exhibit geochemical characteristics of BABB (Pearce and Stern 2006). Back-arc basin basalts are typical of extensional tectonic settings and can be distinguished from MORB based on the presence of a subduction-related geochemical signature that can vary considerably in magnitude and character. Pearce et al. (2005) argued that when normalized to NMORB (normal MORB), the composition of a subduction-influenced basalt can be broken down into three components: (*i*) the approximate mantle component (asthenosphere), defined by elements thought to be immobile during subduction (Nb, Ta, Zr, Hf, Ti, HREE); (*ii*) a deep subduction component that includes all elements that are mobile in melts or supercritical fluids released in deep subduction environments (Rb, Ba Th, U, Sr, K, P, LREE); and (*iii*) a shallow subduction component that includes elements, which in addition to being mobile in deep subduction environments, are also mobile in low-temperature (shallow) aqueous fluids (Rb, Ba, K, Sr, Ca, Na). According to this technique, NMORB-normalized ratios of Ba/Th, Th/Nb, and Ba/Nb represent shallow, deep, and total subduction components, respectively (Fig. 4-11). The IRF basalts are significantly enriched in all of the subduction–mobile elements. However, groups 1 and 2 basalts differ significantly in their NMORB-normalized profiles (Fig. 5-12). Average NMORB-normalized Th/Nb ratios, which represent the deep subduction component, are only slightly elevated in group 1 basalts (2.2× NMORB), but Th/Nb ratios of group 2 basalts have a larger range and on average much higher values (5.1× NMORB). Both groups have an additional shallow subduction signature, with high NMORB-normalized Ba/Nb ratios and positive Rb, Ba, Sr, and K anomalies relative to the trend defined by the deep subduction component (Fig. 4-12). The mantle component, defined by subduction–immobile elements, has a nearly flat, slightly enriched, NMORB-normalized trend (Fig. 4-12). Therefore, according to the technique of Pearce et al. (2005), the IRF basalts are interpreted to have been derived from a depleted mantle source that was slightly enriched relative to the source of NMORB. They have significant shallow and deep subduction components relative to NMORB, with group 2 basalts showing a greater subduction influence than group 1 basalts.

Source(s) of subduction components

Pearce and Stern (2006) described four mechanisms to explain the addition of a subduction component to BABB: (a) melting of sub-arc mantle that was enriched in mobile subduction components via metasomatism (Pearce et al. 2005); (b) contamination of ascending magma through assimilation of arc-derived crust (Pearce et al. 2005); (c) mixing of shallow subduction-related fluids with MORB (Elliott et al. 1997); and (d) mixing of subduction-generated magma with MORB (Davies and Stevenson 1992). In the case of the IRF basalts, which have both deep and shallow subduction components (Fig. 5-12; Pearce et al. 2005), it is unlikely that either the addition of subduction mobile components via subduction-related fluids (hypothesis c) or melts (hypothesis d) are exclusive enrichment processes because they only enrich the melt in shallow or deep components, respectively (Pearce and Stern 2006). In addition, hypotheses c and d would require that the IRF basalt formed during active subduction; however, there is no local or regional geological record of arc magmatism coeval with the IRF in northern Stikinia. Therefore, the subduction signature in IRF basalts is best attributed to either relict enrichment in the mantle source (hypothesis a), and (or) to contamination by arc-derived crust (hypothesis b). These hypotheses are considered viable because (*i*) both processes allow for enrichment in deep and shallow subduction components, and (*ii*) the long-lived pre-IRF arc magmatism recorded in the Stikine terrane can account for both crust and a sub-arc mantle enriched in subduction mobile components.

A plot of Th versus Nb, normalized to Yb to reduce the effects of partial melting and fractional crystallization, (e.g. Th/Yb versus Nb/Yb, Pearce and Pete 1995, Fig. 5-13) is useful to compare multiple enrichment processes, including enrichment via a mantle source (e.g., within-plate), subduction, and crustal contamination. The IRF basalts form two distinct trends, both parallel to the NMORB to ocean-island basalt (non-arc) mantle array (Pearce 2008). Both groups display elevated Th/Yb relative to the mantle array. Group 1 basalts have lower Th/Yb and Nb/Yb ratios than group 2, and their compositions plot just barely above the mantle array, whereas group 2 basalts form a trend farther above the mantle array (Fig. 5-13). Active subduction produces a vertical enrichment trend on this plot because during subduction Th is mobile and Nb is immobile (Rudnick

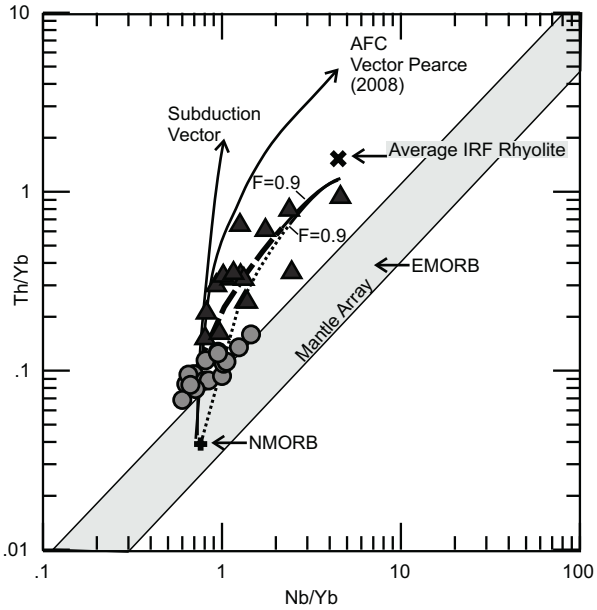

Fig. 5-13. IRF basalts on Th/Yb versus Nb/Yb plot (Pearce 2008) with fields for the mantle array (Pearce 2008), and modeled geochemical vectors for subduction and AFC; Solid lines from Pearce (2008); dashed line calculated using samples 05TB03-03 as the parent magma and average IRF rhyolite as the contaminant; dotted line calculated using NMORB as the parent magma and average IRF rhyolite as the contaminant. Partition coefficients calculated from McKenzie and O'Nions (1991); rate of assimilation to crystallization, $R = 0.5$. EMORB, enriched MORB; F, magma mass/initial magma mass.

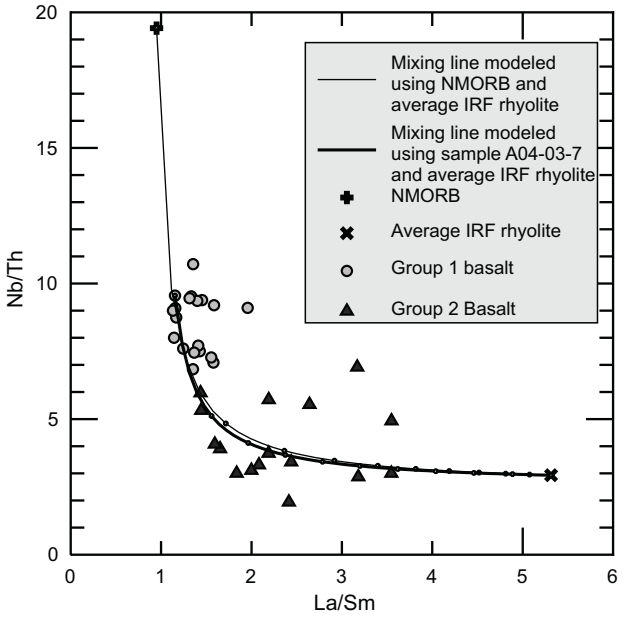

Fig. 5-14. Nb/Th versus La/Sm with calculated mixing lines between NMORB and average IRF rhyolite compositions. Both mixing lines pass through the field of group 1 basalts and define a best-fit-line through the group 2 basalts indicating that the geochemical characteristics of group 2 basalts may result from assimilation of arc-crust. The similarity of the two mixing lines indicates that group 1 and 2 basalts have the same or similar parent magmas.

1995; Plank 2005; Zack and John 2007). Enrichment as a result of assimilation–fractional crystallization (AFC) forms a trend intermediate between the mantle array and subduction enrichment (Pearce 2008). Both groups of basalts are enriched in subduction components relative to the mantle array, but the magnitude of enrichment is higher and more variable in group 2. Because the mantle array also reflects variable degrees of melting (Pearce 2008), some of the array-parallel enrichment may be a result of variable partial melting.

The AFC vector calculated by Pearce (2008) (Fig. 5-13) assumed contamination by Archean felsic rock (Rudnick and Fountain 1995); it does not adequately represent either between-group or within-group variations in IRF basalts. However, IRF rhyolites (Barrett and Sherlock 1996; Evenchick et al. 2004; Barresi and Dostal 2005) correspond to A-type granites of Pearce et al (1984) and Whalen et al. (1987) and fall in the A2 field of Eby (1992), indicating that they are crustal melts and therefore good approximations of a crustal contaminant. If AFC is modeled using the average composition of least-altered IRF rhyolites, (Appendix B.3) as the contaminant, the resulting vector approximates a best fit line through the field of group 2 basalts (Fig. 5-13). This suggests that crustal contamination (hypothesis b) probably contributed to enrichment of group 2 basalts, but not group 1 basalts. Based on Nb/Th versus La/Sm ratios (Fig. 5-14), which are also sensitive to crustal contamination, group 1 basalts show little variation, but fall on a mixing line between NMORB and the IRF rhyolite composition that also approximates a best fit line through the group 2 basalts. In both diagrams (Figs. 5-13, 5-14), the NMORB starting composition results in a trend that is almost identical to one calculated using the most primitive group 1 basalts. Group 1 and group 2 basalts could therefore have been formed from the same, or similar, mantle source(s), with the increased, and more variable, subduction components in group 2 basalts reflecting assimilation of a heterogeneous arc-related crust. The static subduction component found in group 1 basalts, and probably in the uncontaminated parent of group 2 basalts, is not explained by crustal contamination. Therefore, the source rock for both groups is interpreted to have contained a component of sub-arc mantle with a relict subduction signature (hypothesis a).

Petrogenesis based on trace elements

Based on incompatible element ratios and geochemical models, the IRF basalts formed from melting of composite asthenospheric and sub-arc mantle sources. The asthenospheric source was slightly enriched relative to NMORB (depleted mantle), and the sub-arc mantle source contained relict enrichment of deep and shallow subduction components (Pearce et al. 2005). Compositional variations in group 1 basalts result from variable degrees of partial melting and fractional crystallization. Group 2 basalts have a precursor composition similar to that of group 1 basalt, but they were affected by subsequent contamination by older arc crust that significantly altered their composition through the addition of subduction-mobile elements.

Petrogenesis based on variations in major elements

Group 1 basalts have lower SiO_2 and alkalis and higher TiO_2 and Mg# than group 2 basalts. While these variations can be accounted for by fractional crystallization alone, they are also consistent with AFC because the most fusible crust is enriched in SiO_2 and alkalis and depleted in TiO_2 and MgO relative to uncontaminated magma. The major-element characteristics are inconsistent with the competing hypothesis that the variation in subduction signatures between groups 1 and 2 results from melting of heterogeneous mantle sources. According to this hypothesis, there should be little variation in major-element concentrations between the two groups of basalt.

Petrogenesis based on variations in ε_{Nd}

Stikinia comprises isotopically juvenile rock with ε_{Nd} that ranges from –0.5 to +7.7 (Samson et al. 1989). The high positive ε_{Nd} values of group 1 basalts, as well as those from Eskay Creek and Anyox, are consistent with data from mafic rocks in Stikinia (ε_{Nd} +5.1 to +7.7; Samson et al. 1989). In group 2 basalts, ε_{Nd} values cluster between +3.2 and +3.6, with some lying closer to the high positive group 1 values. Group 2 ε_{Nd} values do not vary consistently with any indices of crustal contamination, subduction input, or differentiation. The lack of correlation between ε_{Nd} and any other elements or ratios suggests that isotopic heterogeneities within one or more of the magma source(s) influenced the Nd isotopic ratios. Possible sources are (*i*) asthenosphere, (*ii*) sub-arc mantle, and (*iii*) crust via contamination. The first two sources are common to groups 1

and 2 basalts, and would produce uniformly high positive ε_{Nd} values. Therefore, the isotopic heterogeneity of group 2 basalts can be explained by the assimilation of an older isotopically heterogeneous arc crust.

5.6.2 Tectonic and Metallogenic Significance

Volcanogenic massive sulfide (VMS) deposits are associated with specific magmatic suites and petrotectonic assemblages (e.g., Lesher et al. 1986; Swinden 1996; Lentz 1998; Hart et al. 2004; Piercey 2010, 2011). The IRF conforms to the "bimodal mafic" VMS lithotectonic assemblage of Franklin et al. (2005), comprising mainly mafic volcanic rocks, with up to 25% felsic volcanic or hypabyssal rock. The Noranda, Flin Flon, and Kidd Creek VMS camps are hosted in assemblages that also fall into this category. Bimodal mafic assemblages typically form in juvenile tectonic environments with little or no evidence of continental influence (e.g., back-arc and forearc basins; Piercey 2010, 2011). Basalts in these assemblages have MORB, BABB, or boninitic affinities. Boninites are interpreted to be derived from ultra-depleted mantle and therefore require higher melting temperatures than MORB (1200–1500 °C; Pearce et al. 1992; Falloon and Danyushevsky 2000). Bimodal mafic assemblages are typically associated with the initiation of subduction in forearcs or extension in back-arcs (Crawford et al. 1981; Bédard 1999). The generation of high-temperature basaltic magmas and their rapid ascent within these extensional tectonic environments is a critical controlling factor in driving higher temperature sub-sea-floor hydrothermal convective systems responsible for VMS formation (e.g., Cathles 1981; Sillitoe 1982; Barrie et al. 1999a; Syme et al 1999; Franklin et al. 2005; Hyndman et al. 2005; Currie and Hyndman 2006; Piercey 2010).

The composition of IRF basalts varies from the north, where basalts record crustal contamination (group 2), to the south where the basalts are uncontaminated (group 1). These compositional and geographic variations can be related to differences in structural permeability along the length of the rift, and ultimately to variations in heat-flow and the potential for generation of VMS deposits via the development of sub-seafloor hydrothermal convective systems (Fig. 5-15). Crustal contamination occurs through chemical and mechanical processes that are time-dependent (Huppert et al. 1985).

Fig. 5-15. Schematic cross sections (not to scale) of northern (*top*) and southern (*bottom*) rift segments depicting differences in structural permeability and resultant variations in magma ascent rates and potential for VMS deposit formation. In this model, high structural permeability in southern rift segments permitted rapid emplacement of high-temperature magmas that drove sub-seafloor convection systems ultimately responsible for VMS deposit formation. Lower structural permeability in northern rift segments resulted in a slower ascent of magma. These magmas cooled and were affected by crustal contamination during their protracted ascent and were not favorable heat sources for driving higher-temperature convection systems.

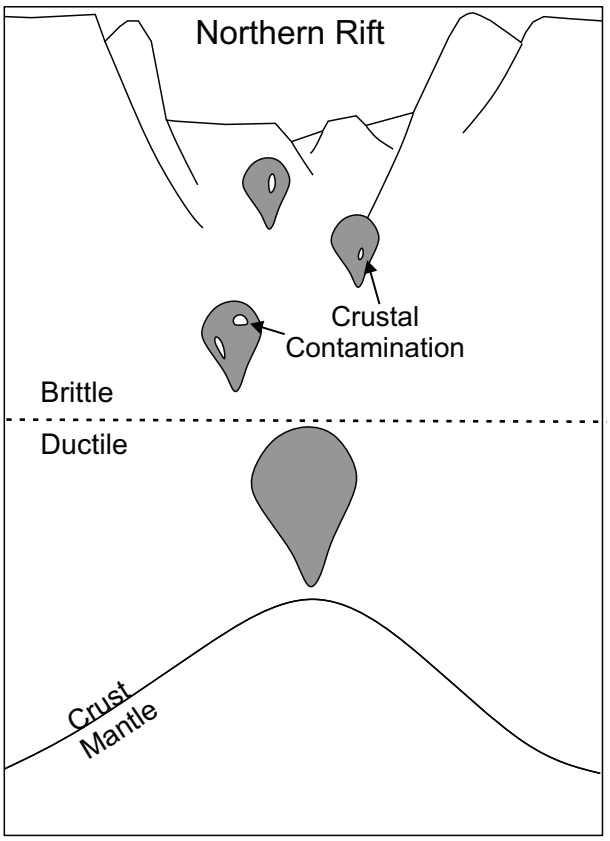

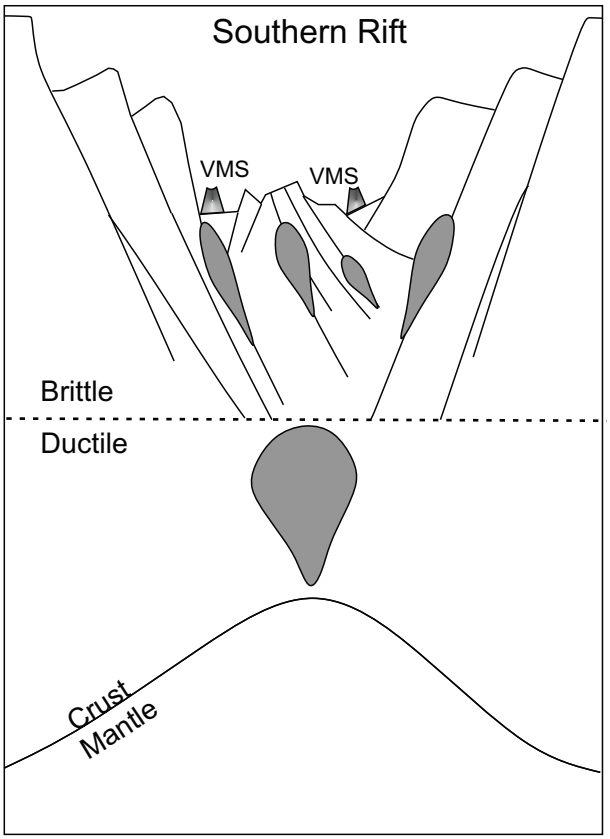

Rapidly ascending mantle-derived magmas have short crustal residency, and as a result, less opportunity for crustal rock to be assimilated by, and affect the bulk composition of, the ascending magma. The comparative lack of crustal contamination in magmas that formed group 1 versus group 2 basalts, is interpreted to be a result of the comparatively rapid ascent of group 1 magmas through the crust. Rapidly ascending magmas are most likely associated with more tectonically active portions of the rift, where higher proportions of deep penetrating and multiply reactivated faults would have been present (Syme et al 1999; Franklin et al. 2005; Hyndman et al. 2005; Currie and Hyndman 2006). The preferential distributions of group 1 and group 2 basalts, therefore, likely record variable intensities of tectonic activity, where the southern portion of the Eskay rift was more tectonically active than the northern portion.

The three best known and exploited VMS deposits hosted by the IRF are localized in southern sub-basins that contain only group 1 basalt. The high cross-stratal structural permeability in these sub-basins facilitated emplacement of high-temperature magmas into near-surface and surface environments, and likely contributed to the development of more localized, vertically penetrating, hydrothermal systems (Fig. 5-15). The resulting increased heat flow and potential for higher temperature hydrothermal circulation are important criteria for VMS deposit formation (Cathles 1981; Galley 1996; Franklin et al. 2005; Currie and Hyndman 2006; Piercey 2010). In contrast, sub-basins containing mainly group 2 basalts are interpreted to have had comparatively low structural permeability and less heat flow, which negatively affected the viability of sustained, high-temperature, hydrothermal convective systems. The presence of group 1 basalt is therefore a good geochemical indicator of prospective VMS stratigraphy in the IRF.

5.7 Conclusions

Although IRF basalts have identical field characteristics, and are intercalated within some sub-basins, two distinct types of tholeiitic basalts (groups 1 and 2) associated with minor felsic volcanism have been identified based on trace-element and isotopic characteristics. Both have compositional characteristics consistent with back-arc basin volcanism, and their geological setting shows that they formed in extensional basins. A comparison of non-subduction mobile element concentrations (e.g., Nb, Zr, Ti, and HREE) with those of

NMORB indicates that both groups of basalts are derived, in part, from an asthenospheric source similar to that of NMORB. Deep and shallow subduction components in both groups were probably added by melting of a sub-arc mantle that was enriched in subduction–mobile elements. In this case, subduction-related chemical signatures in the sub-arc mantle were introduced by metasomatism resulting from long-lived subduction beneath the Stikine terrane. Further variations in the composition of group 1 basalts are interpreted to reflect variable degrees of partial melting and fractional crystallization. Group 2 basalts had a similar source, and trace-element modeling indicates that contamination by an older arc-derived crust is the main process by which they became further enriched in subduction–mobile elements relative to group 1 basalts. Crustal contamination is also consistent with major-element contrasts between groups 1 and 2 basalts and with the lower positive and more variable ε_{Nd} values of group 2 basalts.

The distribution of the two basalt types is geographically constrained. Group 1 basalts are most abundant in the south and group 2 basalts in the north, and they are intercalated in centrally located sub-basins (Figs. 4-2, 5-1). The distinct lack of crustal contamination in group 1 basalts is consistent with well-developed rifting where deep penetrating structures facilitated rapid magma ascent through the crust (Fig. 5-15). In contrast, crustal contamination in group 2 basalts is a consequence of lower structural permeability and resulting slower magma ascent rate. The southern portion of the Eskay rift is interpreted to have represented a more advanced stage of rifting, associated with a higher density of deep penetrating structures, higher heat flow and increased potential for vigorous, higher temperature, hydrothermal circulation. This is consistent with the locations of all three exploited VMS deposits in the IRF, in the southern part of the rift, and their association with group 1 basalts. The identification of group 1 basalts is an important criteria for focusing exploration to the most VMS permissive sub-basins and (or) stratigraphy in the IRF.

This petrogenetic–metallogenic model is consistent with previous tectonic interpretations (e.g., Alldrick et al 2005a; Nelson et al. 2013), which suggested that the voluminous volcanics of the IRF were deposited in a series of en-echelon transtensional basins formed during protracted, oblique collision of Stikinia with more inboard peri-Laurentian terranes

and outboard terranes such as the Alexander–Wrangellia block. Together, the petrogenetic interpretations predict a productive metallogenic environment, whereby large volumes of rapidly ascending mafic magmas, derived from a depleted mantle source, were localized to drive hydrothermal circulation within specific sub-aqueous grabens or rift segments.

Chapter 6 - Discussion and Conclusions

6.1 Volcanogenic Massive Sulfide Exploration Criteria in the Eskay Rift and Beyond

6.1.0 Overview

Volcanogenic massive sulfides (VMS) comprise a class of mineral deposit that forms at, or near, the seafloor in an active submarine volcanic environment (Galley et al. 2007). They form as fluids that are highly enriched in metals, and driven by hydrothermal convection, precipitate metals during focused discharge at or near the sea-floor. The deposits comprise statabound lenticular bodies of massive sulfide (>80% sulfide) surrounding central vents or fumaroles (black smokers) that lie above discordant feeder zones. Historically they account for >20% of Canada's Cu, Pb, Zn, and Ag production and 3% of its Au production (Galley et al. 2007), signifying the importance of VMS deposits to Canadian mining and related industries.

A wide variety of exploration techniques are used to identity prospective VMS districts and deposits within those districts. The most universal criteria, on a district scale, are ones that link modern-day or ancient geological environments to extensional tectonics (e.g. Swinden et al. 1989; Swinden 1991, 1996; Bailes and Galley 1999; Syme et al. 1999, Wyman 1999; Wyman et al. 1999; 2004; Franklin et al. 2005; Galley et al. 2007 Piercey 2011). VMS deposits form from high-temperature, sub-seafloor, hydrothermal convection, and the intrinsic characteristics of extensional tectonic environments facilitate development of these mineralizing systems through: 1) high densities of deep-penetrating faults that allow efficient sub-seafloor convection, and 2) high heat flow as a result of crustal thinning, rapidly ascending hot magmas, and/or crustal underplating.

While extensional tectonic settings in modern environments are easily recognized on heat-flow maps, and by their other distinct characteristics (e.g. rift valleys), recognizing ancient extensional environments is more problematic. However, with the advent of modern geochemical techniques, the chemical compositions of rocks or suites of rocks can, along with other geological evidence (e.g. local and regional stratigraphy or

preserved syn-volcanic structures), support the interpretation that a particular set of ancient volcanic rocks formed in an extensional setting. As a result, the identification of particular geochemical suites of volcanic rocks has been widely accepted as a tool for VMS deposit exploration. Extensional tectonic settings span a wide array of specific environments, ranging from Archean environments for which there are no modern analogues, to ocean spreading centers and island and continental fore- inter- and back-arcs. As a result, there is no single geochemical, or other, criterion for identifying former extensional environments. One of the most reliable initial indicators of a relict extensional environment is bimodal volcanism. Bimodal volcanic rock suites typically encompass mafic and felsic end-member compositions (basalts or basaltic-andesite, and rhyolites or rhyodacites) and lack intermediate rock compositions (andesites and dacites). The genesis of end-member composition lavas in extensional tectonic regimes and their relationship to VMS deposits is discussed in the following sections.

An important recent advance in classifying VMS deposits is a new system that categorizes the deposits based on their lithostratigraphy and tectonic setting (e.g. Barrie and Hannington 1999a; Franklin et al. 2005; Piercey 2011). This system divides VMS deposits into five groups that can be roughly distinguished based on the interpreted tectonic setting and/or the relative abundances of mafic, felsic and sedimentary rock in the host stratigraphy (Table 6-1). Each of the five categories provides a model for the tectonic setting (e.g. juvenile or evolved crust, inter- back- or fore-arc, or oceanic) of the VMS deposit(s), and predicts particular petrochemical assemblages. Therefore, the specific stratigraphic and petrochemical criteria defined by the classification system can be useful for recognizing ancient extensional environments, and serve to focus exploration on particular areas that may have been especially productive environments for VMS deposit formation.

The work presented in Chapters 4 and 5 of this thesis defines three specific criteria (two geochemical and one stratigraphic) that are useful for VMS deposit exploration in the Iskut River Formation. It also describes the features of the IRF so that they can be recognized by explorationists on a property scale. The exploration criteria are intended to be specific to the IRF, however they also have implications for VMS deposit exploration

in general. Each criterion is discussed with regard to how it fits into, and could help inform, general theories that link geochemistry and/or stratigraphy to VMS-prospective environments. The criteria are:

1. In addition to basalt, which comprises more than 90% of the total stratigraphy of most sub-basins, the most prospective stratigraphic intervals in the IRF also contain mudstone, and locally rhyolite.
2. The IRF contains tholeiitic basalt with a BABB affinity. The most prospective sub-basins or stratigraphy have basalt with low Th/Ta ratios (< 2.5).
3. Rhyolite in the IRF corresponds to the FIII geochemical classification of Lesher et al. (1986). This is the category of felsic rock most closely linked to VMS deposits generally, and it can be used as a criterion to distinguish the IRF rhyolites from regionally extensive, but less prospective, FII-type felsic rocks of the lower Hazelton Group.

The final portion of this discussion deals with the relevance of shallow and deep sub-deposit intrusions in VMS deposit formation.

6.1.1 Stratigraphic considerations

Lithostratigraphic and tectonic classification

Documenting the basic stratigraphy of an area is a first, and essential, task in mineral exploration. Because VMS deposits are primarily found in extensional tectonic environments, identifying geological evidence of an ancient rift (e.g. grabens or calderas) is an exploration priority. The main stratigraphic units encountered in ancient rifted environments are: 1) pre-rift sedimentary or volcanic successions that are typically island or continental inter-, fore-, or back-arcs; 2) syn-rift bimodal volcanic and/or sedimentary rocks; and 3) post-rift, arc-related volcanic rock or basinal sedimentary rock (Gibson et al. 2007). These stratigraphic elements are accompanied by evidence of subsidence within the syn-rift stratigraphy (e.g. transition from shallow to deep marine sedimentary facies), and evidence of extension within an active volcanic environment (e.g. dike swarms, fracture-fill, syn-volcanic faults). Of these geological criteria, one of the most confounding for explorationists has been the wide array of within-rift strata that may be

present. Recent work by Barrie and Hannington (1999a) and Franklin et al. (2005) has refined the types of within-rift lithostratigraphy expected in particular tectonic environments. They defined five lithostratigraphic assemblages from different VMS-hosting extensional tectonic settings (Table 6-1). Using these categories to frame regional exploration can aid in identifying "rift-facies" stratigraphic sequences.

Table 6-1 VMS deposit classification. Additional row (bottom) lists regional characteristics of the IRF in the Eskay rift. MORB-mid-ocean-ridge-basalt; LOTI- low Ti tholeiite; BABB-backarc basin basalt; FII and FIII rhyolites as defined by Lesher et al. (1986) (Fig. 6-2). Modified after Franklin et al. 2005; Gibson et al 2007; Piercey 2007.

Type	Typical Lithofacies	Petrochemical Assemblage	Tectonic Setting(s)
Mafic	90% mafic flows, abundant mafic dills and dikes, <10% rhyolite	MORB; LOTI; Boninites	Mature intra-ocenaic backarcs
Pelitic-Mafic	composed of mafic sills and flows and abundant argillite, carbonaceous argillite, chert and trace to absent felsic volcanics	MORB; EMORB; Alkaline basalt	Sedimented mid-ocean ridges or backarcs
Bimodal-Mafic	composed mainly of mafic flows with <25% rhyolite and sedimentary rock	MORB; LOTI; BABB, Boninites. FIII rhyolites	Rifted oceanic arcs
Bimodal-Felsic	>50% felsic flows or volcaniclastic rock with subordinate mafic flows and terrigenous sedimentary rock	MORB, Alkaline basalt; FII or FIII rhyolite	Continental margin arcs and backarcs
Siliciclastic-Felsic	75% siliciclastic rocks with subordinate felsic flows and < 10% mafic flows/sills	MORB, Alkaline Basalt; FII or FII rhyolites	Mature epicontinental backarc
Eskay Rift	>90% mafic flows in most sub-basins. Minor rhyolite and sedimentary rock in discrete horizons.	BABB (two types); FIII rhyolite	Rifted ocean-island-arc

Iskut River Formation lithostratigraphy (Chapter 4) conforms to the "bimodal-mafic" category of Franklin et al. (2005). Geological evidence indicates that it was deposited in the corresponding inter-arc rift environment, lending credence to the classification

system. However, in a number of publications (Franklin et al. 2005; Gibson et al. 2007; Piercey, 2007, 2011), classification of the deposits hosted by the IRF is not consistent with the classification presented in this thesis. Franklin et al. (2005) included an extensive database of VMS deposits, their grade, tonnage, and classification according to the system they described. Their classification of the IRF deposits is problematic: It appears that the classification of the Eskay Creek deposit (bimodal-felsic) only took into account the stratigraphy local to the mine, which is an unusually thin stratigraphic section with a much higher proportion of felsic volcanic rocks than is usual in the IRF. In contrast, the bimodal-mafic classification of the deposits at Anyox was based on regional stratigraphy and disregarded the mine-sequence, which does not include felsic volcanic rock, a required lithostratigraphic component of the bimodal-mafic category.

The bimodal-mafic classification put forward in this thesis for both the Eskay Creek and Anyox deposits applies to, and takes into account, IRF stratigraphy exposed throughout the Eskay rift. However, there are conspicuous heterogeneities between sub-basins within the Eskay rift which, when not viewed in the context of a single tectonic environment, lend themselves to a variety of classifications: Eskay Creek and Georgie River (Evenchick and McNicoll 2002) as felsic-bimodal, Anyox as mafic, and Downpour Creek as pelitic-mafic. The most voluminous and geographically extensive lithostratigraphic assemblage in the IRF (bimodal-mafic) is also the one associated with the inferred tectonic environment of the Eskay rift. The IRF therefore stands as an example of "within-rift" lithostratigraphy that conforms to the lithostratigraphic assemblages predicted by Barrie and Hannington (1999a) and Franklin et al. (2005) based on its tectonic environment (rifted-arc). However, recognition and subsequent description of the entire belt of IRF rocks was necessary in order to classify the dominant lithostratigraphic assemblage accurately. If the specific assemblages that host the much more extensively studied deposits are taken out of regional context, they stand as counter-examples to the accuracy and usefulness of the classification system. This reinforces the importance of: 1) using the dominant regional lithostratigraphy when applying the classification system, and 2) within specific tectonic environments, allowing for significant lithostratigraphic variations on the scale of deposits or sub-basins. Many of the "rift-scale" exploration criteria will most likely need to be mapped and interpreted by

government or research geologists. Regardless of the sources of the information it can be applied to a "property-scale" project. In addition there are many "property-scale" geological observations and interpretations that lead to more effective VMS exploration (see below).

The importance of hiatuses

Once prospective "within-rift" stratigraphy is recognized, exploration may focus on identifying stratigraphic horizons that represent volcanic hiatuses (Gibson et al. 2007). Volcanic quiescence is critical for VMS deposit formation because it allows time for focused hydrothermal discharge zones to become established and precipitate economic quantities of metals, rather than being repeatedly buried by new volcanic deposits before significant metals can accumulate. Hiatuses may be marked by sedimentary rock, typically including exhalative units (Gibson et al 2007), or by changes in dominant volcanic lithofacies. The deposits at Eskay Creek and Anyox are hosted in sedimentary horizons that mark volcanic quiescence and that are otherwise very rare in IRF stratigraphy. Because the Eskay rift comprised many largely isolated sub-basins, the relative stratigraphic location of a deposit in one sub-basin is not necessarily predictive of prospective stratigraphy in the other sub-basins. For instance, the deposit at Eskay Creek is near the bottom of the IRF, whereas the Hidden Creek and Bonanza deposits at Anyox are near the top. The most important stratigraphic feature that connects the deposits is the evidence for a volcanic hiatus defined by the sedimentary rocks that host the deposits. Therefore, identifying strata that represent volcanic quiescence within specific sub-basins is more important than tracing particular deposit-bearing stratigraphic positions (e.g. the top or bottom of the "rift-fill" strata) between sub-basins.

Historical exploration drilling on Pillow Basalt Ridge (PBR) serves as an example that prospective stratigraphic positions in one sub-basin are not justification for exploration of that same position in other sub-basins. PBR and Eskay Creek sub-basins, which are less than 20 km apart, have conspicuously different stratigraphies, yet the stratigraphic position of the deposit at Eskay Creek was used as the model for exploration drilling on Pillow Basalt Ridge. The intention of the exploration program was to penetrate through the basalt, which at Eskay Creek is only about 150 m thick but at PBR comprises an

entire mountain, to intersect the contact-mudstone, which is host to the Eskay Creek deposit. The program resulted in a 1770 m diamond drillhole entirely in basalt (Vaskovic and Huggins 1998). Ironically, the drillhole on PRB was collared near the bottom of the PBR *middle unit*, which is described in this thesis and interpreted to represent a significant volcanic hiatus. The *middle unit* contains the most analogous strata on PBR to the contact-mudstone at Eskay Creek, yet it remains unexplored.

Based on evidence presented in this thesis I proposed that newly recognized strata on Pillow Basalt Ridge, at the Four Corners Complex, and on Table Mountain, may be prospective for VMS deposits, as these strata contain sedimentary rocks, as well as felsic volcanic rocks and coarse-grained basalts interpreted to have formed from lava ponding. This lithofacies, although different from those at Eskay Creek and Anyox, represents a hiatus during which sedimentary material accumulated, and small volumes of mafic lava ponded rather than forming pillows or breccia as would be expected in a more active volcanic environment. This, and other "quiescent" lithofacies described from the IRF can serve as examples to help identify similar prospective horizons in other VMS districts.

6.1.2 Mafic Rock Geochemistry

Although mafic rocks are associated with the vast majority of VMS deposits, historically there has been less work characterizing prospective *vs*. barren geochemical varieties of basalt, compared to work on felsic rocks (e.g. Lesher et al. 1986; Lentz 1998; Hart et al. 2004). This may be in part because of the ubiquity of mafic rocks, relative to felsic, and the association of VMS deposits with basalts that have a wide variety of chemical compositions. Swinden (1996) summarized a body of work on VMS prospective stratigraphy in the Dunnage Zone in Newfoundland. Based on what at the time were state-of-the-art geochemical techniques, they determined that VMS deposits within the belt are associated with a variety of basalt types, in a variety of tectonic settings, including primitive-, mature-, and continental-arcs. The chemical characteristics of the mafic rocks within this discrete, albeit large, zone include those of ocean-island basalts (OIB), boninites, low Ti tholeiites (LOTI), island arc-tholeiites (IAT), backarc basin basalts (BABB), MORB, and calc-alkaline basalt. Despite this variability, Swinden

(1996) argued that most VMS deposits in the Dunnage Zone are spatially associated with boninites or other refractory melts in areas that contain independent evidence of rifting. He also noted that the largest and richest deposits are associated with basalts that have arc geochemical signatures. Barrie et al. (1993) conducted a similar broad study on the highly productive Abitibi Subprovince. They found that >75% of all VMS deposits in the subprovince are associated with two volcanic rock suites that together account for 20% of the subprovince area. The prospective rock suites are both bimodal, one with tholeiitic rift-related basalts, and the other with both tholeiitic and calc-alkaline basalts to andesites that have rifted-arc tectonic affinities. These extension-related suites stand in stark contrast to the much more common suites of calc-alkaline and alkalic mafic to felsic (i.e. not bimodal) volcanic rocks with strong arc affinities that are barren of VMS deposits. Piercey (2011) linked particular petrochemical assemblages to the five groups of VMS deposits defined by Barrie and Hannington (1999a) and Franklin et al. (2005) (Table 6-1). He described boninites, LOTI, IAT, and MORB from the three most juvenile environments, and MORB and/or OIB from the two categories of evolved environments. Given a particular tectonic setting, these petrochemical assemblages aid in identifying "within-rift" stratigraphy. Piercey (2011) further refined exploration criteria by describing general stratigraphic variation or petrochemical evolution of the mafic rocks in each environment. However, his most important finding, consistent with the work of Swinden (1996), was that rocks crystallized from high-temperature magmas (e.g. boninites or LOTI) are closely associated with VMS deposits.

Mafic rocks of the IRF conform generally to petrochemical criteria for VMS prospective belts: 1) they are part of a bimodal suite; 2) they are tholeiites with a BABB affinity; and 3) they have arc-related geochemical characteristics. Based on the relative amounts of basalt, rhyolite and sedimentary rock, they generally conform to the bimodal-mafic classification of Franklin et al. (2005), which Piercey (2011) equated with suites of boninites, LOTI, IAT, MORB and BABB. The geochemistry of IRF basalts is not especially consistent with Piercey's associations because there are no IAT, LOTI or boninites. Piercey (2011) argued that basalts formed from these high-temperature magmas are genetically linked to VMS-hydrothermal systems because they "initiate, drive, and sustain hydrothermal circulation robust enough to generate metal-rich fluids

and form VMS mineralization". Although the IRF basalts are not boninites or LOTI, they are derived from high-temperature magmas similar to those that produce NMORB. Furthermore the IRF basalts are divided into two groups which, based on interpreted relative rates of ascent through the crust, represent higher- (group 1) and lower- (group 2) temperature magmas. In the Eskay rift, VMS deposits are directly correlated with the higher-temperature type of IRF basalt (Chapter 5). Although the IRF basalts do not strictly adhere to the petrochemical assemblages defined by Piercey (2011), they do adhere to the overall hypothesis that links VMS formation to higher-temperature magmas. Because the Eskay rift was both short-lived and very narrow, perhaps it could not facilitate the same high temperature melting that generated boninites in other more prolonged rifting environments. It is worth noting, from this example, that on a district scale, the nature of prospective high-temperature basalts may differ from those most commonly described, but within the context of the district, rocks derived from higher- vs. lower-temperature magmas are useful indices of prospectivity.

The Th/Ta geochemical signature which applies to IRF basalt prospectivity (Chapter 5) is an example of a district-scale criterion that can identify prospective volcanic stratigraphy. The ratio ostensibly identifies a subduction-related geochemical signature because is compares subduction-mobile (Th) to subduction immobile elements (Ta) (Rudnick 1995; Plank 2005; Zack and John 2007). However, Th/Ta ratios can be affected by multiple petrogenetic processes that need not include active subduction. The higher Th/Ta ratios relative to NMORB in IRF basalts do not a result from active subduction but were inherited from two distinct sources: i) melting of metasomatized sub-arc mantle, and ii) assimilation of island-arc crust (Chapter 5). In the IRF, VMS deposits are associated with basalts that have Th/Ta ratios <2.5, and basalts with higher Th/Ta ratios (>2.5) are considered to have lower prospectivity.

The same criterion, though with different limits, may be applied to other districts where VMS prospectivity may be affected by arc or subduction-related influences. DeWolfe et al. (2009) documented a subduction geochemical signature in the Hidden and Louis formations that comprise the hangingwall to the Flin Flon VMS deposits. In these formations rocks at the base of the stratigraphy, which are most likely genetically related

to the formation of the Flin Flon deposits, have the least amount of crustal contamination. In both cases (IRF and Flin Flon), increased ratios of subduction-related geochemical signatures, inherited via crustal contamination, reflect decreased prospectivity. However, in some districts higher Th/Ta ratios may reflect increased prospectivity. For example in the Dunnage Zone, Swinden (1996) noted that "by far the most, the largest, and the richest deposits occur in rocks with arc geochemical signatures". The same ratio may also be used to detect continental-arc influences where they are related to VMS prospectivity. For example, Au-rich VMS deposits on Wetar Island (Banda arc) are associated with the onset of continental subduction and associated contamination at ca. 4.7 Ma, as material derived from the Australian continent became a significant component of the down-going slab (Herrington et al. 2011).

6.1.3 Felsic Rock Geochemistry

Felsic rocks are associated with fewer VMS deposits than mafic rocks. For example, they are not essential components in two of the five categories of VMS deposits defined by Barrie and Hannington (1999a) and Franklin et al. (2005) (mafic and mafic-siliciclastic varieties), whereas mafic rocks are associated with all five (Table 6-1). However, because felsic rocks are much less common than mafic rocks generally in the geological record, their association with VMS deposits has long been a subject of interest. Lesher et al. (1986) wrote a pioneering paper that defined ore-bearing *vs*. barren VMS districts in the Superior Province based on the geochemistry of associated felsic metavolcanic rocks. They suggested, based on trace-element geochemical criteria (e.g. low Zr/Y and La/Lu ratios), that rhyolites associated with VMS deposits formed in high crustal-level magma

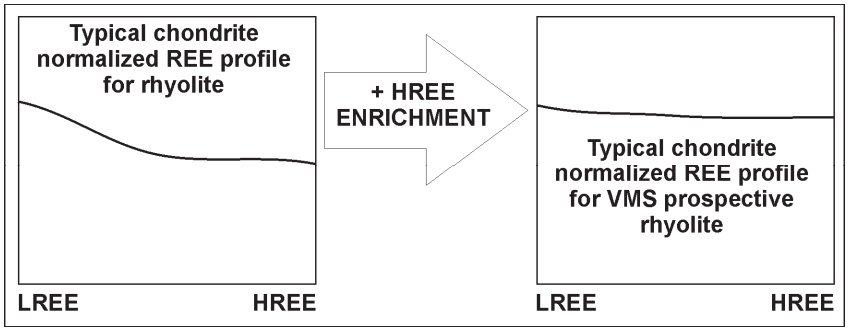

Fig. 6-1. The flat chondrite normalized REE profile in VMS prospective rhyolites (e.g. FIII rhyolites) is the result of HREE enrichment relative to typical LREE enriched felsic magmas (left). Hart et al. (2004) proposed that HREE enrichment is the result of high-level, low pressure, crustal melting where the magma equilibrates with garnet and amphibole free residua, allowing the HREE to be released into the melt. LREE= Light rare earth elements; HREE = heavy rare earth elements.

chambers that may also have been responsible for generating the hydrothermal systems that formed the deposits. In contrast, the generally much more common felsic rocks with geochemical characteristics indicating deep sources (e.g. high Zr/Y and La/Lu ratios) are not normally associated with VMS deposits. Hart et al. (2004) refined the work of Lesher et al. (1986) by expanding the scope of the study to include felsic rocks of Mesoarchean to Cenozoic age, and by re-examining the physical conditions that are necessary for the long-lived high heat flow that supports hydrothermal convective systems and generates hot felsic magmas. They found that high-pressure melting forms garnet residua with high HREE, but low-pressure melting generates garnet- and amphibole-free residua, releasing HREE into the melt (Fig. 6-1). They divided felsic rocks into four categories (including three categories originally defined by Lesher at al. 1986): FI rhyolites that equilibrate with garnet-bearing residua, FII with amphibole, and FIII and FIV with plagioclase and no garnet- or amphibole in the residua (Fig. 6-2). Based on the stability fields of the inferred residua, the depths at which the parent magmas were generated may be estimated: FI are derived from >30 km, FII from 30-10 km, and FIII and IV from <15 km. In addition, Hart et al. (2004) showed that, based on field relationships and thermodynamic constraints (Cathles et al. 1997), shallow felsic magma bodies are not the main heat source driving the hydrothermal convection necessary for VMS deposit formation, although they may contribute. Rather, the rhyolites are generated by partial melting high in the crust, from the same heat source(s) that drive the hydrothermal convection. Hart et al. (2004) proposed that the main heat sources for generating shallow felsic melts are mid-crustal-level mafic magma chambers. Although the rhyolites with the specified chemical characteristics do not generate VMS deposits, they are intimately associated with the most prospective environments, and since rhyolites with FIII and FIV characteristics are very rare compared to those with FI and FII characteristics, their identification is a useful tool in VMS deposit exploration.

Gaboury and Pearson (2008) provided an interesting counterpoint to the work of Lesher et al. (1986), Hart et al. (2004), and Piercey (2011). They showed that within the Abitibi belt, VMS deposits are associated with all types of rhyolites, and that rhyolite geochemistry may be more useful for targeting specific sub-types of VMS deposits than deposits generally. For instance, they found that FI rhyolites, which were considered

barren by Hart et al. (2004), host Au-rich VMS deposits including the world-class Laronde deposit. However, VMS deposits within the Noranda district of the Abitibi Belt are closely associated with FIII rhyolites, which are very rare elsewhere in the belt.

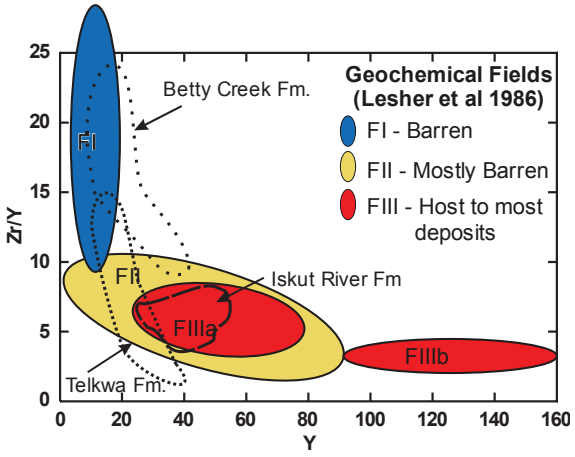

Fig. 6-2. FI, FII and FIII fields for prospective versus barren rhyolites as defined by Lesher et al. (1986). Dashed and dotted lines surround the fields of Betty Creek (Lewis et al 2001), Telkwa, and Iskut River formation rhyolites (excluding outliers). The IRF rhyolites fall within the field of prospective FIII rhyolites, whereas the Telkwa and Betty Creek formation rhyolites form a distinct trend that passes through FI and FII fields.

Although the geochemistry of rhyolite is not a focus of this thesis[5], where rhyolite compositions have been tested within the IRF (e.g.,Childe 1996; Evenchick et al. 2004; Barresi and Dostal 2005), they cluster within the FIII field of Lesher et al. (1986) (Fig. 6-2). Formation of the Eskay Creek VMS deposit was roughly coeval with the eruption of IRF rhyolites, which form the footwall to stratiform massive sulfide deposits, and host crosscutting feeder-zone type mineralization (Pumphouse and Pathfinder zones). Based on criteria defined by Lesher et al (1986), the FIII IRF rhyolites can be easily distinguished from FII to FI dacites of the Betty Creek Formation (Lewis et al. 2001), which are regionally extensive, and at Eskay Creek are located beneath a subtle disconformable contact at the base of the mine sequence (Roth et al. 1999). Data from Telkwa Formation rhyolites (Chapter 3) form a vertical trend on a Zr/Y versus Y diagram that overlaps with the field defined by the Betty Creek Formation dacites (Fig. 6-2). Together these units show that voluminous calc-alkaline felsic volcanism of the lower Hazelton Group differs significantly from the much rarer FIII rhyolite of the IRF, and therefore the geochemical signature of rhyolite in the Hazelton Group is a reliable guide for VMS exploration. However, while the identification of FIII rhyolite may be a positive indication of a prospective environments, and may aid in distinguishing segments of the Eskay rift from

[5] The IRF rhyolites are characterized in chapters 2 and 4, their average chemistry is in Appendix B.3, and appendix A.4 discusses the chemistry of rhyolite from Table Mountain and compares it to rhyolite at Eskay Creek.

lower Hazelton Group volcanics, it is not genetically related to the formation of the VMS deposits, and therefore its absence does not preclude VMS deposit formation. For example, the VMS deposits at Anyox, in the southern portion of the Eskay rift, have no associated rhyolites.

Unlike the Au-rich Laronde deposit in Abitibi Belt, which Gaboury and Pearson (2008) used to link FI rhyolites to a sub-set of Au-rich VMS deposits, the Eskay Creek deposit, arguably the best example of a Au-rich VMS deposit, is a positive example of the link between FIII rhyolites and VMS deposit formation/prospectivity. The rifted-arc tectonic environment that facilitated the eruption of IRF bimodal volcanics meets the criterion proposed by Hart et al. (2004) for 1) upper crustal melting to generate FIII rhyolite, and 2) high-temperature hydrothermal circulation, critical to VMS formation.

6.1.4 The Role of Sub-Deposit Intrusions

There has been long-standing debate and uncertainty regarding the role that shallow- (<3 km) and mid- (<15 km) crustal level intrusions play in the formation of VMS deposits. Many deposits are underlain by shallow mafic and/or felsic intrusions. The ubiquity of these intrusions has led to geophysical exploration methods (e.g. magnetic susceptibility) that identify buried intrusions in order to target prospective areas for VMS deposits (Galley 2007). Lesher et al. (1986) proposed that shallow sub-deposit felsic intrusions were the main source of heat in VMS hydrothermal systems. In contrast, Cathles (1978, 1983) showed that the heat from shallow felsic magma chambers would be insufficient to drive the high-temperature convection necessary for VMS formation, and Hart et al. (2004) proposed that mid- to shallow-level (< 15 km) mafic intrusions are the main heat source for both hydrothermal circulation and shallow melting that formed high-temperature silicic magmas. Many workers have suggested that in addition to driving hydrothermal convection near the sea-floor, mid-crustal and shallow intrusions are also responsible for adding metals to the hydrothermal system (e.g. Kamenesky et al. 2001; Yang and Scott, 2002, 2005; Beaudoin et al. 2007). In particular, magmatic contributions

may be important to Au-Ag rich VMS deposits, including Eskay Creek (Roth et al. 1999, Sherlock et al. 1999), as indicated by sulfur isotope and fluid inclusion studies; however, in the case of Eskay Creek the data are equivocal (Sherlock et al. 1999).

The Eskay Creek and Anyox deposits do not have shallow (1-3 km deep), sub-deposit, coeval intrusions. Therefore, in these cases at least, the formation of VMS deposits does not depend on heat from high-level magma chambers; rather, other heat sources must have sustained the hydrothermal convection system. Interestingly, it was once thought that the "Eskay porphyry" (MacDonald 2001), a K-feldspar-, plagioclase-, amphibole-, biotite- porphyritic monzonite that intruded the footwall of the Eskay Creek deposit approximately 500 m downsection, might have been the heat source for the hydrothermal convection responsible for the Eskay Creek deposit (e.g. Ettlinger 1991; Roth et al. 2001). However the ca 184 ± 2 Ma porphyry (MacDonald et al. 1992) is too old to be a heat source for the ca 174 Ma VMS deposit (Childe et al. 1994). In some cases, intrusions that are geographically associated with VMS deposits but have different ages, may have been preferentially emplaced along older crustal-scale faults than were later reactivated during the graben formation that controlled the locations of VMS mineralization (Nelson and Kyba 2014). The lack of associated shallow intrusions at Eskay Creek is consistent with the low-temperature hydrothermal system (<200°C, Sherlock et al. 1999) which was responsible for its formation and precious metal enrichment. The sustained heat necessary to drive this lower-temperature hydrothermal system may have been insufficient to generate enough crustal melting to produce sub-deposit magma chambers. However, the Anyox deposits, based on their higher base- to precious-metal ratios, were likely generated from a higher-temperature hydrothermal system.

Deeper, mid-crustal mafic intrusions, invoked by Hart et al. (2004) as heat sources, are difficult to verify because they may still be deeply buried and/or the stratigraphy may have been fragmented by post-emplacement tectonism. However, the interpreted petrogenesis of IRF group 1 and group 2 basalts (Chapter 5) may shed light on the importance of mid-level intrusions as heat sources for VMS-hydrothermal convection systems. The isotopically juvenile group 1 basalts, which host both the Eskay Creek and Anyox deposits, ascended rapidly from the mantle, while isotopically less juvenile group

2 basalts, which are barren, ascended over a protracted period during which they cooled and assimilated heterogonous crust. The protracted ascent of the group 2 basalts, and the heterogeneity of their isotopic signatures inherited through crustal contamination, indicate that at least some of the magmas stalled at mid-crustal levels, whereas the lack of crustal contamination in group 1 basalts indicates that they had little interaction with the crust, and did not mingle with magmas or other material at mid-crustal level. Based on this petrological interpretation, the main heat source beneath the Eskay rift is interpreted to have been deep-seated, probably ponded, magma at the base of the crust. The highest heat flow was associated with portions of the rift that had the greatest degree of crustal thinning and high densities of deep-penetrating faults which facilitated rapid emplacement of magmas. Where group 2 basalts are present, they indicate lower heat flow and represent cooler portions of the rift zone. This supports the interpretations of Galley (2003) and Piercey (2011) that the most important factor in VMS formation is a high-heat-flow "thermal corridor" or rift zone, and that associated shallow or mid-level intrusions may be proxies for high heat-flow but are not the cause of it.

3.1.5 Summary

1. The lithostratigraphy of the IRF conforms to the assemblage predicted by Barrie and Hannington (1999a) and Franklin et al. (2005) for a rifted island-arc environment. This lends credence to the classification system; however, the classification only works where based on the dominant regional lithostratigraphy. Where the specific assemblages that host the IRF VMS deposits are considered in isolation, they negate the accuracy and usefulness of the classification system. Therefore:
    1. it is important that the classification system be based on the dominant regional lithostratigraphy;
    2. within specific tectonic environments, allowances should be made for significant lithostratigraphic variations.
2. IRF VMS deposits formed within stratigraphic horizons that represent volcanic hiatuses. The horizons are not contiguous between sub-basins, and deposits

formed in markedly different positions in the stratigraphy. Therefore, VMS exploration should aim to:

    1. identify horizons that represent volcanic hiatuses,
    2. explore those horizons within the limits of the sub-basin;
    3. avoid targeting stratigraphic positions which, in other sub-basins, contain quiescence lithofacies, where there is no evidence supporting continuity of the lithofacies between sub-basins.

3. VMS deposits are associated with rocks derived from high-temperature magmas, but the specific high-temperature rock type can vary between districts. In many districts boninites or LOTI are the high-temperature rocks, but in the IRF all of the basalts are BABB and only a sub-set with low Th/Ta ratios (<2.5) are interpreted to have formed from higher-temperature magmas.
4. The Th/Ta geochemical criterion for prospective IRF basalts (Th/Ta <2.5) is an example of a district-scale criterion that can be developed to identify prospective volcanic stratigraphy. Although it cannot be applied directly to other districts, a similar criterion using the same elements could be developed in other districts where prospectivity is affected by subduction-related influence(s).
5. FIII rhyolite in the IRF indicates prospective stratigraphy. However, the deposits at Anyox do not have associated rhyolite, indicating that felsic rocks are not genetically related to VMS deposit formation although they may be a by-products of the same processes.
6. The deposits at Eskay Creek and Anyox, which both lack coeval sub-deposit intrusions, demonstrate that shallow magma chambers are not necessary to drive the hydrothermal convection that forms VMS systems.
7. Based on the recognition that VMS deposits in the IRF are closely associated with magmas that ascended rapidly, had little interaction with the crust, and did not mingle with magmas at mid-crustal level, I propose that the main heat source that drove hydrothermal convection was deep-seated, probably ponded, magma at the base of the crust.

6.2 Towards a Better Understanding of Hazelton Arc Evolution

6.2.1 Overview

The Hazelton Group consists of island-arc, volcano-sedimentary stratigraphy that is interpreted to have occupied an ~500 by 800 km area, forming a partly emergent microcontinent (Marsden and Thorkelson 1992) built on crystalline basement comprising Devonian-Triassic island-arc and pericratonic rocks (Logan et al 2000; Colpron et al. 2006; Gunning et al. 2006). Regional tectonic-stratigraphic syntheses of the Hazelton Group (Tipper and Richards 1976; Marsden and Thorkelson 1992; Gagnon et al. 2012) showed that it consists of two parallel belts of partly emergent volcanic arcs, separated by a NW-trending central trough (the Hazelton trough; Fig. 6-3; Tipper and Richards 1976; Marsden and Thorkelson 1992). In their current positions they form three roughly parallel NW-trending belts, but the central trough is poorly exposed because it is overlain by the sedimentary successions that fill the Bowser and Sustut basins. Marsden and Thorkeson (1992) proposed that the arc-basin-arc geometry of the Hazelton Group resulted from concurrent and opposite-facing subduction zones along eastern and western pate-margins, analogous to the tectonic setting of the modern-day Philippine microcontinent. By this model volcanic axes formed above each downgoing slab and were separated by a subsiding basin or incipient back-arc. The Hazelton Group spans approximately 40 My, at least half of which encompassed major plate reconfigurations as the Stikine terrane and inboard and outboard terranes collided and ultimately became accreted to the western margin of Laurentia.

6.2.2 Initiation of Hazelton Arc Volcanism – Implications of Timing

The Triassic-Jurassic boundary (TJB) has historically been considered a geologically significant division in the geological history of Stikinia because it separated volcano-sedimentary successions of the Triassic Stuhini Group and Jurassic Hazelton Group (e.g. Tipper and Richards 1976; Marsden and Thorkelson 1992; Ash et al. 1997). However, recent advances in radiometric dating methods, particularly those that determine isotopic U/Pb and Ar/Ar ages, have significantly refined relevant portions of the geological

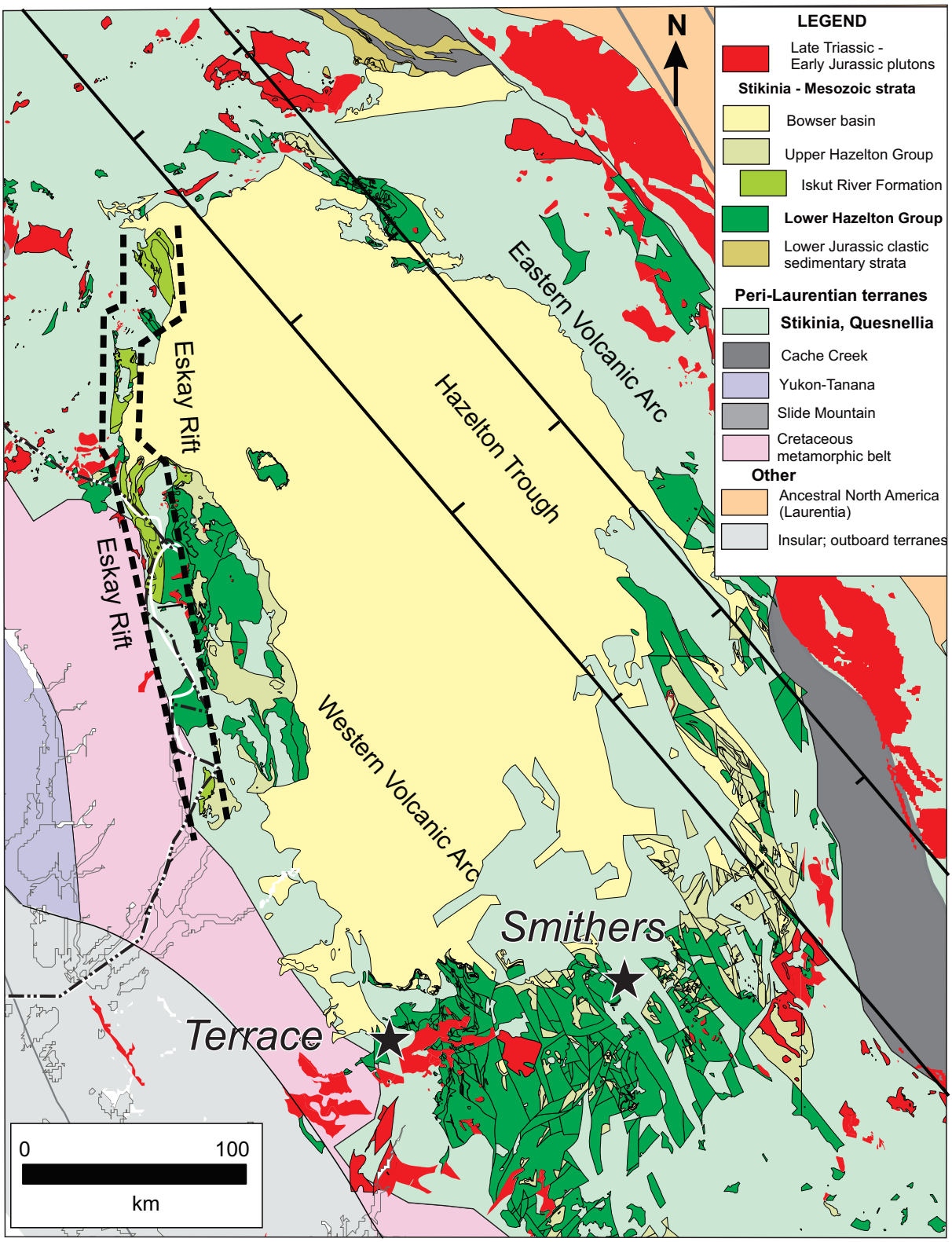

Fig. 6-3. Geological map of northwest BC highlighting upper and lower Hazelton Group divisions and the location of the Iskut River Formation. The proposed arc-basin-arc geometry (Tipper and Richards 1976) and a schematic outline of the Eskay Rift are illustrated. Note the differences in size and orientation of the two Hazelton Group rifts. The Hazelton trough is largely covered by sedimentary successions in the overlying Bowser Basin (yellow).

timescale. Prior to 1999, a number of timescales had been applied to the Canadian Cordillera (summarised by Harland et al. 1990). According to these timescales the TJB ranged between 210 and 203 Ma, and the most commonly used timescale (Harlan et al. 1990) placed the boundary at 208±7.5 Ma. Pálfy et al. (1999) were the first to base the Jurassic timescale entirely on modern (i.e. 1990 or later) U/Pb and Ar/Ar ages. They dated the TJB at 201±1 Ma based on data from three locations where the biostratigraphic TJB was directly dated with U/Pb zircon methods: i) 201.3 ±1.0 and 200.9±1.0 Ma from the Orange Mountain Basalt in the Newark Basin (Dunning and Hodych 1990); ii) 201.3±1.0 from the base of the North Mountain Basalt in the Fundy Graben (Hodych and Dunning 1992); and iii) 199.6±0.3 Ma from a tuff layer in the Queen Charlotte Islands (Pálfy et al. 1999). In a series of articles, Pálfy and coauthors redefined the TJB to 199.6 ±.3 Ma (Pálfy et al. 2000), redacted the refinement in favor of the 201±1 Ma age (Mundil and Pálfy 2005), and then based on new samples dated using CA-TIMS methods, restated the TJB to be 201.7 ±0.6 Ma (Friedman et al. 2008). The final age is consistent with a reported CA-TIMS U/Pb zircon age from Peru that dates the TJB at 201.58 ±0.28 Ma (Schaltegger et al. 2007). Therefore, publications such as maps, reports and peer-review articles that include stratigraphic classification of geological units, variably define those units as Triassic or Jurassic depending on the date of publication.

Although the updated timescales were adopted by workers in the Cordillera, little attention has been paid to how they bear on older, often pioneering or seminal, work in the Cordillera. One of the more notable effects of this oversight is that despite a roughly 7 My change in the TJB, the same boundary is still considered to separate the Stuhini and Hazelton Groups (e.g. Gagnon et al. 2012; Evenchick et al 2010; Logan and Mihalynuk 2014). Chapter 3 of this thesis represents the first time that volcano-sedimentary rocks of the Hazelton Group have been dated and referred to as Triassic. Previous studies that documented similar U/Pb ages (e.g. Thorkelson et al. 1995, Ash et al. 1997) near the base of the Hazelton Group considered these strata to be Early Jurassic. The U/Pb chronology presented in Chapter 3 documents a Late Triassic igneous crystallization age, and two supporting detrital zircon ages, from basal Hazelton Group conglomerates. Together these ages serve to formalize the Hazelton Group as a unit that spans the TJB. In addition, work by Thorkelson et al. (1995) and Ash et al. (1997) is re-evaluated in terms

of the current absolute age of the TJB, and shown to document Triassic age Hazelton Group strata in other regions of Stikinia.

Biostratigraphy is a widely used tool that helps to define and differentiate units of various relative ages. In NW Stikinia, bioclastic units that contain Norian or Rhaetian (Late Triassic stage) fauna were invariably classified as Stuhini Group, and only Jurassic fossil assemblages were considered Hazelton Group. Our reassessment of the timing of initial Hazelton Group deposition demonstrates that strata recognized as Rhaetian, or even as old as Late Norian[6], may be Hazelton Group. Based on this recognition and new detailed lithostratigraphic work, Kyba and Nelson (2015), reassigned a Late Norian conglomerate-bearing siliclastic unit in the Bronson Creek area of Stikinia, from the Stuhini Group to the Hazelton Group. Reassessment of Late Norian or Rhaetian rock units in Stikinia could result in a substantial shift in the geological framework that defines the demise of the Stuhini arc and initiation of the Hazelton arc. One possible outcome could be recognition that the Stuhini-Hazelton Group separation is not marked by a single continuous volcanic hiatus that included uplift and erosion as previously thought. It may be that localized uplift and erosion accompanied or preceded magmatism in particular regions, creating a serious of discontinuous or diachronous and locally nested unconformities (e.g. Thorkelson et al. 1995; Kyba and Nelson 2015) that separate regions that experienced magmatic pulses at different times. In addition, re-evaluation of Late Triassic strata may have implications for the genesis of coeval and possibly co-magmatic porphyry copper deposits in northern Stikinia, some of which are intimately associated with Late Norian strata (e.g. Galore Creek; Logan and Mihalynuk 2014).

The work described in Chapter 3 helps to explain why there are so few other U/Pb ages from the Hazelton Group that correspond to the Late Triassic on the modern timescale. The Telkwa Formation near Terrace is divided into three separate volcanic complexes. Only one of the three complexes is Triassic, and it contains by far the least felsic rock. The rapid volcanic facies changes in the lower Hazelton Group, noted by Tipper and Richards (1976) and almost all subsequent workers, represent at least in part different

[6] New work defining the Norian Rhaetian boundary (Wotzlaw et al. 2014) places it at 205.50±0.35 Ma

volcanic centers that may be of different ages. Detailed work, such as that presented in this thesis, is necessary in order to recognize ancient volcanic complexes, and thereby distinguish volcanic entities with potentially distinct eruptive histories. However, similar detailed work with accompanying geochronology is very limited in the Hazelton Group. Most previous ages obtained from lower Hazelton Group volcanics range from 200 to 190 Ma (Breitsprecher and Mortensen 2004, and references therein). These ages demonstrate a voluminous magmatic episode, however, they also likely reflect sampling bias towards felsic rocks. Felsic rocks are targeted for dating because they yield more zircon than other volcanic rock types, and they also form regional ash and other marker units as a result of explosive volcanism. Future identification of particular volcanic centers will help to eliminate sampling bias and will likely result in identification of adjacent centers with very different eruption histories.

6.2.3 Telkwa Formation volcanism near Terrace – Identification of the volcanic axis

The Telkwa Formation near Terrace was not discussed by Tipper and Richards (1976), and was given only cursory attention by Marsden and Thorkelson (1992). However, according to the arc-basin-arc model, it represents a position in the western volcanic belt that is farthest away from the Hazelton trough (Fig. 6-3), and presumably closest to the trench, and therefore worth studying in order to better understand facies changes across the width of the volcanic belt. Tipper and Richards (1976) described the Howson facies of the Telkwa Formation near Smithers as a subaerial volcanic facies with "calc-alkaline basalt to rhyolite flows, breccia, tuff; intravolcanic sediments; minor marl". This facies correlates well with the mainly subaerial volcanic rocks exposed in the Terrace area. However, Tipper and Richards (1976) documented a maximum thickness of 2500 m for the Howson facies, whereas in the Terrace area individual complexes are up to 13 km thick and composite sections are up to 16 km thick. These exceptionally thick sections must represent the main volcanic axis of the western Hazelton volcanic arc and are also consistent with other island arcs, which range between 10 and 70 km thick (Plank and Langmuir 1988). Island arcs in the Caribbean, which are significantly smaller than the Hazelton arc, typically include 5-10 km thick volcano-sedimentary sections (Larue et al. 1991), and the Philippine arc has estimated median crustal thicknesses between 30 and 40

km, and up to 65 km, beneath volcanic centers (Dimalanta and Yumul 2003). Given the thickness of the volcanic strata near Terrace, it is not surprising that they were mainly deposited in a subaerial environment. The first definitive evidence for submarine conditions is in the upper Hazelton Group red tuff member of the Nilkitkwa Formation, which lies disconformably above maroon andesites and dacites of the Telkwa Formation. Gagnon et al (2012) interpreted the contact between the Nilkitkwa and Telkwa formations on Mount Quinlan (in the Terrace area) as a disconformity that encompasses 10 My or longer. The eventual transgression that allowed submarine deposition of the Nilkitkwa Formation was probably related to volcanic loading along the axis of the arc which led to depression of the lithosphere, extensional faulting, and basin development, and subsequent thermal subsidence following the main stage of volcanic activity. While there is little structural evidence for syn-volcanic extension in the Terrace area, Richards (2003) noted that inter-arc extension is integral to the development of most arcs, but is not always easily identified in the geological record because positive feedback between magmatism and faulting results in structures being obscured by intrusive bodies. In the Terrace map areas the Kelanza and Carpenter Creek plutons may obscure extensional faults and the Skeena River thrust fault could be a reactivated extensional structure. However, large extensional structures which could account for significant inter-arc subsidence are probably present to the east beyond the boundaries of the study area described in Chapter 3. One candidate structure is approximately 45 km east of Terrace, where the Zymoetz River shifts abruptly from its E-W trend to a N-S trend, along the western margin of the Howson Range. A west-side-down normal fault in this N-S river valley could help account for the difference in thicknesses between the Telkwa Formation in the Howson Range and near Terrace. It is worth noting that 100 km to the south-east of Terrace, in the Whitesail Lake area, a comparable thickness (≈ 10 km) of significantly younger (ca. 176 Ma) Telkwa Formation rocks are present, and are associated with extensional faults (Gordee 2005; Mahoney et al. 2006). These volcanic rocks represent the southward migration of the Hazelton volcanic arc, and are limited to locations south of the Skeena Arch.

6.2.4 The Two Hazelton Group Rifts

The Hazelton Group includes two rifts: the Eskay rift and the Hazelton trough (Fig. 6-3). The Hazelton trough was first identified by Tipper and Richards (1976), whereas the Eskay rift was not discussed in literature until 1990 (Anderson and Thorkelson 1990), a year after the famous "Hole 109" struck gold at Eskay Creek. The two rifts differ in character and tectonic affinity (Table 6-2), yet in the mineral exploration community they

Table 6-2 Comparison of the two Hazelton Group rifts.

	Eskay Rift	**Hazelton Trough**
Age (Ma)	176-172	205-180
Width	>10 km	>50 km
Sedimentary Environment	Deep marine	Deep marine to locally subaerial
Stratigraphic thickness	Highly variable, up to > 2000m	Thin on margins, up to 4300m in the Nilkitkwa depression.
Dominant lithology	Basalt	Shale, sandstone
Other lithologies	Rhyolite, chert, mudstone, tuff	Basalt, rhyolite
Interpreted Tectonic Setting	Sub-basins opened during accretion-related transtensional tectonics.	Incipient back-arc basin
Nature of Extension	Graben formation. Rapid but short-lived.	Modest extension. Crustal thinning via block-faulting.

are not well understood or differentiated. The revised Hazelton Group stratigraphic nomenclature (Chapter 2) should help in distinguishing the two rifts. The Hazelton trough hosted modest extension over a long period in an incipient back-arc basin environment, whereas the Eskay rift represents short-lived but rapid extension related to arc-scale transcurrent shearing and the opening of transtensional basins.

To date, no VMS deposits have been discovered in the Hazelton trough. The Kotsine facies of the Telkwa Formation NE of Smithers was deposited in the Nilkitkwa depression, which represented a deep-water axis of the Hazelton trough (Tipper and

Richards 1976). This facies, which includes >1500 m of bimodal volcanic and sedimentary rocks deposited in a sub-aqueous environment, may have been a favorable environment for VMS deposit formation. Along the NE margin of the Hazelton trough, roughly coeval bimodal volcanic rocks (Cold Fish volcanics; Thorkelson 1992) are also interpreted to represent rift-related bimodal volcanism (Marsden and Thorkelson 1992). This indicates that there may be a buried belt of VMS-prospective, lower Hazelton Group, rift-related volcanics beneath sedimentary successions of the upper Hazelton and Bowser Lake groups.

The Eskay rift represents an important tectonic, magmatic, and metallogenic episode in the history of Stikinia. Ideas about the Eskay rift have evolved since Anderson and Thorkelson (1990) first introduced the "Eskay facies" of the Salmon River Formation, which they recognized as a belt of distinct submarine volcanic rocks within the Hazelton Group. Early interpretations of the Eskay rift suggested that it was related to inter- or back-arc extension (e.g. Marsden and Thorkelson 1992; Roth et al. 1999; Childe 1996; Barrett and Sherlock 1996; Sherlock 1999). The new interpretation presented in this thesis describes it as a short-lived, independent volcanic and tectonic event that post-dated arc-related Hazelton Group volcanism. This interpretation is based on three main observations: 1) volcanism in the Eskay rift post-dated arc magmatism and contrasted significantly with the coeval post-arc thermal subsidence recorded in the regionally extensive sedimentary units of the upper Hazelton Group; 2) the Eskay rift is not parallel to the volcanic axis of the Hazelton Group (Fig. 6-3), or to the general tectonic grain of Stikinia; 3) the timing of volcanism in the Eskay rift, ca 176 - 172 Ma, corresponds to the amalgamation of Stikinia and the Cache Creek terrane between 173.0 ±0.8 and ca 172 Ma. (Mihalynuk et al. 1992, 2004).

Nelson et al. (2013) suggested that the Eskay rift opened as a result of transcurrent shearing during "radical plate reorganization" associated with terrane amalgamation and collision with Laurentia. This hypothesis is supported by the structural interpretation presented in Chapter 4, which proposed that the opening of sub-basins north of Eskay Creek resulted from transtension between a pair of bounding sinistral faults. While the details of the complex series of tectonic events involved in the terrane collisions and

accretion are not well known, there are geological analogues for similar types of rifts. 1) During the Miocene a transtensional rift developed in Baja California and Sonora Mexico as a result of the capture of the previously-subducting Monterey plate by the Pacific plate, which was colliding with the North American plate at an oblique angle (Lonsdale 2006; Tiff et al. 2009). 2) During the Early Devonian, the rift that hosted VMS deposits of the Iberian Pyrite belt formed by transcurrent faulting related to oblique collision of the South Portuguese and the Ossa Morena Zones (Carvalho et al. 1999; Barrie et al. 2002). The improved understanding of the Eskay rift is largely based on geochronology, which demonstrates that the Eskay rift postdated arc magmatism and was contemporaneous with terrane collisions. Without these geochronological constraints, the Eskay rift would best fit an inter-arc rift model based on its location within the western volcanic axis of the Hazelton group and its bimodal-mafic lithostratigraphy. Instead it represents an unusual rift environment, maybe still classifiable as inter-arc, but not caused by typical inter-arc tectonics.

Prior to the current description and interpretation of the Eskay rift and Iskut River Formation, some of the IRF sub-basins had been studied and attributed to different tectono-magmatic origins. In particular, the Anyox sub-basin had been studied, largely due to the presence of the VMS deposits that it hosts (Sharp 1980; Smith 1993). The section at Anyox is exposed as a roof pendant in the Coast Plutonic Complex, so unlike sections in some of the other sub-basins, the geological context at Anyox is not well constrained. Smith (1993) proposed that the Jurassic section at Anyox represents a marginal basin that formed between the Stikine and Alexander terranes and that it was obducted during their collision. While this hypothesis is consistent with the geochemical data presented by Smith (1993), the data are also consistent with a hypothesis that includes Anyox as a southern extension of the Eskay rift, an idea first proposed by Evenchick and McNicoll (2002). The inclusion of Anyox in the Eskay rift model was originally based on the similarity in ages of Eskay Creek and Anyox (ca 174 Ma) and on their linear distribution, along with other sections of coeval marginal-basin type stratigraphy within Stikinia (Fig 4-2). The work in this thesis shows that the trace-element and isotopic geochemical data presented by Smith (1993) are consistent with IRF group 1 basalts (Figs. 5-8, 5-11), which are common throughout the central and southern Eskay

rift. Although the hypothesis that the Jurassic section at Anyox represents a marginal basin formed outboard of Stikinia cannot be ruled out, based on the geographical, geochronological and geochemical affinity of the rocks at Anyox to those in other Eskay rift sub-basins, the simplest and most preferable explanation is that it represents a southern extension of the Eskay rift.

6.3 Conclusions

1. A regional examination of the Hazelton Group resulted in significant revisions and clarification to its stratigraphy including:
    - Informal division of the Hazelton Group into upper and lower parts and recognition of a diachronous unconformity or unconformities at the boundary between them.
    - Redefinition of the Quock Formation to include all lithostratigraphically equivalent units of blocky, thinly bedded, siliceous mudstone and tuff around the periphery of the Bowser Basin.
    - Introduction of the Iskut River Formation for rift-related and volcanic facies in the Eskay rift area.
2. Near Terrace, British Columbia, the lower Hazelton Group Telkwa Formation comprises three Late Triassic to Early Jurassic volcanic-intrusive complexes (Mt. Henderson, Mt. O'Brien, and Kitselas) which, at their thickest, constitute almost 16 km of volcanic stratigraphy.
    - Detrital zircon populations from the basal conglomerate contain abundant 205-233 Ma zircons, derived from regional unroofing of older Triassic intrusions.
    - Volcanic rocks are calk-alkaline, isotopically juvenile, predominantly andesitic and silica-bimodal (no dacites).
    - Compared to basalts and andesites ($\varepsilon Nd = +5$ to $+5.5$), rhyolites have high positive εNd values ($+5.9$ - $+6.0$) and overlapping incompatible element concentrations, indicating that they are not part of the same differentiation suite.

3. Lower Hazelton Group volcanic rocks correlate in time and space with a belt of economic Cu-Au porphyry deposits (ca. 205 – 195 Ma) throughout the northwestern Stikine terrane. The coeval relationship is attributed to favourable structural (extensional) and magmatic conditions (underplating) associated with slab rollback during subduction beneath Stikinia.
4. Two independent rifting events occurred during deposition of the Hazelton Group: a Late Sinemurian to Early Pliensbachian phase in the northwest-trending Hazelton trough. and a more restricted Aalenian to Bajocian extensional event in the Eskay rift. The former resulted from extension in an incipient back-arc environment; the latter opened as a series of transtensional sub-basins during collision of the Stikine terrane with other inboard and outboard terranes and accretion to Laurentia.
5. The newly defined Iskut River Formation comprises the most voluminous and volcanic-rich Middle Jurassic strata of the Stikine terrane.
    - It was deposited during a brief period at the boundary between the Aalenian and Bajocian epochs, ca 176–172 Ma, within syn-depositional grabens that comprise the 300 by 50 km north-trending Eskay rift.
    - The lithostratigraphy of the IRF varies considerably between sub-basins, but it is typically composed of tholeiitic pillow basalts and basalt breccias (>90%) and conglomerates deposited near graben-bounding faults, which grade into distal turbidites with interlayered felsic tuff, sandstone, and chert, and intervals of alternating rhyolite, mudstone, and basalt. The rift-filling IRF strata are in angular discordance with the underlying basement rock.
    - The IRF represents the last stage of Mesozoic volcanism in northern Stikinia. It marks a distinct shift in the tectonomagmatic evolution of Stikinia from typical subduction-related island-arc volcanism of the Lower Hazelton Group, dominated by calc-alkaline, predominantly intermediate, volcanic rocks, to a strictly basalt - rhyolite bimodal volcanic suite typical of marginal basins undergoing extension.

- Two geochemically distinct types of tholeiitic basalts interfinger; both resemble back-arc basin basalts formed from the melting of asthenospheric and sub-arc mantle sources. Group 2 basalts are more enriched in light rare-earth elements, Ba, K, Sr, Th, and U, and have lower positive εNd values than group 1 basalts (+3.2 to +6.3 versus +6.9 to +8.4, respectively).
- Group 1 and group 2 basalts are reliably discriminated by Th/Ta <2.5 in the former and >2.5 in the latter. This geochemical criterion can therefore be used as an exploration tool to identify VMS prospective sub-basins and (or) stratigraphy in the IRF.
- The dominance of Group 1 basalts and VMS deposits in southern rift segments indicate that it represents a portion of the rift with deeper-penetrating faults and higher heat flow (i.e. more advanced rifting).

6. This work defines distinct porphyry-Cu(Ag) and VMS metallogenic episodes in the Stikine terrane and should lead to improved exploration models by refining the timing of each episode and linking them to specific tectono-magmatic processes. Specific stratigraphic, structural, and geochemical criteria presented in this thesis apply to exploration within the Hazelton Group specifically, and may serve as a guide for developing similar criteria in other metallogenic provinces.

References

Alldrick, D.J. 1993. Geology and metallogeny of the Stewart mining camp, northwestern B.C.. British Columbia Ministry of Energy, Mines and Petroleum Resources, British Columbia Geological Survey Bulletin 85, 105 p.

Alldrick, D.J. and Britton, J.M. 1992. Unuk River Area Geology (104B/7E, 8 & 9W, 10E). British Columbia Ministry of Energy, Mines and Petroleum Resources, British Columbia Geological Survey Open File 1992-22; scale: 1:20,000.

Alldrick, D.J., Britton, J.M., Webster, I.C.L., and Russell, C.W.P. 1989. Geology and mineral deposits of the Unuk area. British Columbia Ministry of Energy, Mines and Petroleum Resources, Open File 1989-10.

Alldrick, D.J., Stewart, M.L., Nelson, J.L. and Simpson, K.A. 2004a. Geology of the More Creek - Kinaskan Lake area, northwestern British Columbia. British Columbia Ministry of Energy, Mines and Petroleum Resources, Open File Map 2004-2, scale 1:50 000.

Alldrick, D.J., Stewart, M.L., Nelson, J.L. and Simpson, K.A. 2004b. Tracking the Eskay Rift through northern British Columbia - geology and Mineral occurrences of the Upper Iskut River area. *In* Geological Fieldwork 2003. British Columbia Ministry of Energy and Mines, Paper 2004-1, pp.1-18.

Alldrick, D.J., Nelson, J.L., and Barresi, T. 2005a. Geology and mineral occurrences of the upper Iskut River area: Tracking the Eskay Rift through northern British Columbia. *In* Geological Fieldwork 2004, British Columbia Ministry of Energy and Mines, British Columbia Geological Survey Paper 2005-2: 2-39.

Alldrick, D.J., Nelson, J.L. and Barresi, T. 2005b. Geology of the Volcano Creek - More Creek Area, British Columbia. British Columbia Ministry of Energy, Mines and Petroleum Resources, Open File Map 2005-5, scale 1:50 000.

Alldrick, D.J., Nelson, J.L., Barresi, T., Stewart, M.L. and Simpson, K.A. 2006. Geology of upper Iskut River area, northwestern British Columbia. BC Ministry of Energy and Mines, Open File Map 2006-2, Scale 1:100 000.

Alt, J.C. 1999. Hydrothermal alteration and mineralization of oceanic crust: mineralogy, geochemistry, and processes. *In* Barrie, C.T., Hannington, M.D. (*Eds*.). Volcanic-associated Massive Sulfide Deposits: Processes and Examples in Modern and Ancient Settings. Reviews in Economic Geology, **8**:133–155.

Anderson, R.G. 1993. A Mesozoic stratigraphic and plutonic framework for northwestern Stikinia (Iskut River area), northwestern British Columbia, Canada. *In* Mesozoic Paleogeography of the Western United States--II. *Edited by* G. Dunne and K. McDougall. Society of Economic Paleontologists and Mineralogists, Pacific Section, 71, pp. 477-494.

Anderson, R.G., and Thorkelson, D.J. 1990. Mesozoic stratigraphy and setting for some mineral deposits in Iskut River map area, northwestern British Columbia. *In* Current research. Geological Survey of Canada, Paper 90-1E, pp. 131-139.

Armstrong, J.E. 1944. Smithers, British Columbia. Geological Survey of Canada, Paper 44-23.

Armstrong, R.L. 1988. Mesozoic and early Cenozoic magmatic evolution of the Canadian Cordillera. Geological Society of America Bulletin, Special paper **218**: 55-91.

Ash, C.H., MacDonald, R.J.W., and Friedman, R.M. 1997. Stratigraphy of the Tatogga Lake area, northwestern British Columbia (104H/12 & 13, 104G/9 & 16). *In* Geological Fieldwork 1996, British Columbia Ministry of Energy and Mines, British Columbia Geological Survey Paper 1997-1: 238-290.

Bailes, A.H, and Galley, A.G. 1999. Evolution of the paleoproterozoic snow lake arc assemblage and geodynamic setting for associated volcanic-hosted massive sulphide deposits, Flin Flon Belt,

Manitoba. Canadian Journal of Earth Sciences, **36**: 1789–1805.

Baker, B.H., Mohr, P.A., and Williams, L.A.G. 1972. Geology of the Eastern Rift System of Africa. Geological Society of America Bulletin, Special Paper **136**: 1-67.

Barresi, T., and Dostal, J. 2005. Geochemistry and Petrography of Upper Hazelton Group volcanics: VHMS-Favourable Stratigraphy in the Iskut River and Telegraph Creek Map Areas, Northwestern British Columbia. *In* Geological Fieldwork 2004. British Columbia Ministry of Energy, Mines and Petroleum Resources, Paper 2005-1, pp. 39-47.

Barresi, T., and Nelson, J. 2006. Usk Map Area (NTS 103I/09), Near Terrace, British Columbia: Cross-Sections and Volcanic Facies Interpretation. *In* Geological Fieldwork 2005, British Columbia Ministry of Energy and Mines, British Columbia Geological Survey Paper 2006-1, p. 21-28.

Barresi, T., Nelson, J.L., Alldrick, D.J., and Dostal, J. 2005. Pillow Basalt Ridge Facies: Detailed mapping of Eskay Creek-Equivalent Stratigraphy in Northwestern British Columbia. *In* Geological Fieldwork 2004. British Columbia Ministry of Energy, Mines and Petroleum Resources, Paper 2005-1, pp. 31-38.

Barresi, T., Nelson, J.L., and Dostal, J. 2015. Geochemical constraints on magmatic and metallogenic processes: Iskut River Formation, volcanogenic massive sulfide-hosting basalts, NW British Columbia, Canada. Canadian Journal of Earth Sciences, **52**: 1-20.

Barresi, T., Nelson, J.L., Dostal, J. and Friedman, R. *in revision*. Evolution of the Hazelton arc, British Columbia: Stratigraphic, geochronological and geochemical constraints on a Late Triassic - Early Jurassic arc and Cu-Au porphyry belt. Canadian Journal of Earth Sciences.

Barrett, T.J. and MacLean, W.H. 1999. Volcanic sequences, lithogeochemistry, and hydrothermal alteration in some bimodal volcanic-associated massive sulfide systems; in Volcanic-associated Massive Sulfide Deposits; Processes and Examples in Modern and Ancient Setting. *Edited by* C.T. Barrie and M.D. Hannington, Reviews in Economic Geology, **8**: 101 – 131.

Barrett, T.J. and Sherlock, R.L. 1996. Geology, lithogeochemistry and volcanic setting of the Eskay Creek Au-Ag-Cu-Zn deposit, northwestern British Columbia. Exploration and Mining Geology**, 5**: 339-368.

Barrie, C. T., and Hannington, M. D. 1999a. Classification of volcanic-associated massive sulfide deposits based on host-rock composition. in Volcanic-associated massive sulphide deposits: Processes and examples in modern and ancient settings. *Edited by* C.T. Barrie and M.D. Hannington, Reviews in Economic Geology, **8**: 357-373.

Barrie, C. T., and Hannington, M. D., *editors* 1999b. Volcanic-Associated Massive Sulfide Deposits: Processes and Examples in Modern and Ancient Settings. Reviews in Economic Geology Volume **8**: 1-408.

Barrie, C.T., Ludden, J.N., and Green, T.H. 1993. Geochemistry of volcanic rocks associated with Cu–Zn and Ni–Cu deposits in the Abitibi Subprovince. Economic Geology, **88**: 1341–1358.

Barrie, C.T., Cathles, L.M., and Erendi, A. 1999. Finite element heat and fluid flow computer simulations of a deep ultramafic sill model for the giant Kidd Creek volcanic-associated massive sulfide deposit, Abitibi Subprovince, Canada. Economic Geology Monograph **10**: 529–540.

Barrie, C.T., Amelin, Y., and Pascual, E. 2002. U-Pb Geochronology of VMS mineralization in the Iberian Pyrite Belt. Mineralium Deposita, **37**: 687-703.

Bartsch, R.D. 1993. A rhyolite flow dome in the upper Hazelton Group, Eskay Creek area (104B/9, 10), British Columbia. *In* Geological Fieldwork 1992. Ministry of Energy, Mines and Petroleum Resources, Report Paper 1993-1, pp. 331-334.

Bartsch, R.D. 2001. Lithology, petrology and geochemistry of the Prout Plateau. *In* Metallogenesis of the Iskut River Area, Northwestern British Columbia. *Edited by* P.D. Lewis, A. Toma R.M. Tosdal. Mineral Deposit Research Unit, Special Publication Number 1, Chapter 3, pp. 31-46.

Bath, A. 2003. Middle Jurassic granitic plutons within the Cache Creek terrane and their aureoles: implications for terrane emplacement and deformation. *In* Geological Fieldwork 2002. Ministry of Energy, Mines and Petroleum Resources, Paper 2003-1, pp. 51–55.

BC Geological Survey. 2008. MINFILE Record Summary 104B 008. Available from http://minfile.gov.bc.ca/Summary.aspx?minfilno=104B++008 [accessed 19 February 2012].

Beaudoin, Y., Scott, S.D., Gorton, M.P., Zajacz, Z., and Halter, W. 2007. Pb and other ore metals in modern seafloor tectonic environments: evidence from melt inclusions. Marine Geology **242**: 271–289.

Bédard, J. H. 1999. Petrogenesis of boninites from the Betts Cove ophiolite, Newfoundland, Canada; identification of subducted source components. Journal of Petrology, **40**: 1853-1889.

Bouma, A.H. 1962. Sedimentology of some flysch deposits. Elsevier, Amsterdam, 168 p.

Breitsprecher, K., and Mortensen, J.K. 2004. BCAge 2004A-1-a database of isotopic age determinations for rock units from British Columbia. British Columbia Ministry of Energy and Mines, Open File 3 (2004).

Brown, D.A., Gunning, M.H., Orchard, M.J., and Bamber, W.E. 1991. Stratigraphic evolution of the Paleozoic Stikine assemblage in the Stikine and Iskut rivers area, northwestern British Columbia. Canadian Journal of Earth Sciences, **28**: 958-972.

Carvalho D, Barriga FJAS, and Munha J. 1999. Bimodal-siliciclastic systems – the case of the Iberian Pyrite Belt. *In*: Barrie CT, Hannington MD (*eds*) Volcanic-associated massive sulfide deposits: processes and examples in modern and ancient settings. Reviews in Economic Geology, **8**:375–408.

Cathles, L.M. 1978. Hydrodynamic constraints on the formation of Kuroko deposits: Mining Geology, **28**: 257-266.

Cathles L.M. 1981. Fluid flow and genesis of hydrothermal ore deposits. Economic Geology 75th Anniversary Volume (1905–1980).

Cathles, L.M. 1983. An analysis of the hydrothermal system responsible for massive sulfide deposition in the Hokuroko basin of Japan. Economic Geology Monograph **5**: 439–487.

Cathles, L.M., Erendi, A.H.J., and Barrie, T. 1997. How long can a hydrothermal system be sustained by a single intrusive event? Economic Geology, **92**: 766–771.

Chayes, Y. 1964. Variance-covariance relations in Harker diagrams of volcanic rocks. Journal of Pertrology, **5**: 219-237.

Childe, F.C. 1996. U-Pb Geochronology and Nb and Pb Isotopic Characteristics of the Au-Ag-Rich Eskay Creek Volcanogenic Massive Sulphide Deposit, British Columbia. Economic Geology, **91**, pp. 1209-1224.

Clague, D.A., Moore, J.G., and Reynolds, J.R. 2000. Formation of submarine flat-topped volcanic cones in Hawai'i. Bulletin of Volcanology, **62**: 214-233.

Cohen, K.M., Finney, S.C., Gibbard, P.L. and Fan, J.-X. 2013. The ICS International Chronostratigraphic Chart. Episodes, 36: 199-204.

Colpron, M., Nelson, J. L., and Murphy, D. C. 2006. A tectonostratigraphic framework for the pericratonic terranes of the Northern Canadian Cordillera. Special Paper - Geological Association of Canada, **45**: 1-23.

Coney, P.J., Jones, D.L., and Monger, J.W.H. 1980. Cordilleran suspect terranes. Nature, **288**: 329–333.

Crawford, A. J., Beccaluva, L., and Serri, G. 1981. Tectono-magmatic evolution of the west Philippine-Mariana region and the origin of boninites. Earth and Planetary Science Letters, **54**: 346-356.

Currie, C.A., and Hyndman, R.D. 2006. The thermal structure of subduction zone back arcs. Journal of Geophysical Research **111**: 0-B08404.

Davies, J. H., and Stevenson, D. J. 1992. Physical model of source region of subduction zone volcanics. Journal of Geophysical Research, **97**: 2037-2070.

Dawson, G.M. 1877. Report on explorations in British Columbia. Geological Survey of Canada.

DePaolo, D.J. 1981. Trace element and isotopic effects of combined wallrock assimilation and fractional crystallization. Earth and Planetary science Letters, **53**: 189-202.

Deyell, C.L., Thompson, J.F.H., Friedman, R.M. and Groat, L.A. 2000. Age and origin of advanced argillic alteration zones and related exotic limonite deposits in the Limonite Creek area, central British Columbia. Canadian Journal of Earth Sciences. **37**:1093-1107.

DeWolfe, Y.M., Gibson, H.L., and Piercey, S.J. 2009. Petrogenesis of the 1.9 Ga mafic hanging wall sequence to the Flin Flon, Callinan, and Triple 7 massive sulphide deposits, Flin Flon, Manitoba, Canada. Canadian Journal of Earth Sciences, **46**: 509-527.

Diakow, L. 2006. Geology between the Finlay River and Chukachida Lake, central Toodoggone River map area, north-central British Columbia (parts of NTS 94E/2, 6, 7, 10 and 11). British Columbia Ministry of Energy, Mines and Petroleum Resources, Open File Map 2006-1.

Diakow, L., and Mihalynuk, M.G. 1987. Geology of Whitesail Reach and Troitsa Lake map areas (93E/10W, 11E). *In* Geological Fieldwork 1986. British Columbia Ministry of Energy, Mines and Petroleum Resources, Paper 1987-1, pp. 171-180.

Diakow, L.J., Panteleyev, A., and Schroeter, T.G. 1991. Jurassic Epithermal Deposits in the Toodoggone River Area, Northern British Columbia: Examples of Well-Preserved, Volcanic-Hosted, Precious Metal Mineralization. Economic Geology, **86**: 529-554.

Diakow, L.J., Mahoney, J.B., Gleeson, T.G., Hrudey,M.G., Struik, L.C., and Johnson, A.D. 2002. Middle Jurassic stratigraphy hosting volcanogenic massive sulphide mineralization in eastern Bella Coola map area, southwest British Columbia; *In* Geological Fieldwork 2001. British Columbia Ministry of Energy, Mines and Petroleum Resources, Paper 2002-1, p. 119–134.

Dimalanta, C.B., and Yumul, G.P. 2003. Magmatic and Amagmatic Contributions to Crustal Growth of an Island-Arc System: The Philippine Example. International Geology Review, **45**: 922-935.

Dostal, J. 1989. Geochemistry of Ordovician volcanic rocks of the Tetagouche Group of southwestern New Brunswick. Atlantic Geology, **25**: 199-209.

Dostal, J., Dupuy, C., and Coulon, C. 1976. Rare-earth elements in high-alumina basaltic rocks from Sardinia. Chemical Geology, **18**: 251-262.

Dostal, J., Gale, V. and Church, B. N. 1999. Upper Triassic Takla Group volcanic rocks, Stikine terrane, north-central British Columbia: Geochemistry, petrogenesis, and tectonic implications. Canadian Journal of Earth Sciences **36**: 1483-1494.

Dostal, J., Owen, J. V., Church, B. N. and Hamilton, T. S. 2005. Episodic volcanism in the Buck Creek Complex (central British Columbia, Canada); a history of magmatism and mantle evolution from the Jurassic to the Early Tertiary. International Geology Review, **47**: 551-572.

Duffell, S., and Souther, J.G. 1964. Geology of Terrace Map-Area, British Columbia. Geological Survey of Canada, Memoir 329.

Dunning, G.R., and Hodych, J.P. 1990. U/Pb zircon and baddeleyite ages for the Palisades and Gettysburg sills of the northeastern United States: Implications for the age of the Triassic/Jurassic boundary. Geology, **18**: 795-798.

Duuring, P., Rowins, S.M., McKinley, B.S.M., Dickinson, J.M., Diakow, L.J., Kim, Y.-S., and Creaser, R.A. 2009. Examining potential genetic links between Jurassic porphyry Cu-Au+/-Mo and epithermal Au+/-Ag mineralization in the Toodoggone district of North-Central British Columbia, Canada. Mineralium Deposita, **44**: 463-496.

Duuring, P., Rowins, S.M., McKinley, B.S.M., Dickinson, J.M., Diakow, L.J., Kim, Y.S., and Creaser, R.A. 2009. Magmatic and structural controls on porphyry-style Cu-Au-Mo mineralization at Kemess South, Toodoggone district of British Columbia, Canada. Mineralium Deposita, **44**: 435-462.

Ebinger, C.J., Karner, G.D., and Weissel, J.K. 1991. Mechanical strength of extended continental lithosphere. Constraints from the Western Rift System. Tectonics, **10**: 1239-1256.

Eby, G. N. 1992. Chemical subdivision of the A-type granitoids; petrogenetic and tectonic implications. Geology **20**: 641-644.

Eisbacher, G.H. 1971. A subdivision of the Upper Cretaceous-Lower Tertiary Sustut Group, Toodoggone Map-Area, British Columbia. Geological Survey of Canada, Paper 70-68, 16p.

Eisbacher, G.H. 1985. Pericollisional strike-slip faults and synorogenic basins, Canadian Cordillera. In Strike-slip deformation, basin formation, and sedimentation. *Edited by* K.T. Biddle and N. Christie-Blick. Society of Economic Paleontologists and Mineralogists Special Publication, **37**, pp. 265-282.

Elliott, T., Plank, T., Zindler, A., White, W., and Bourdon, B. 1997. Element transport from slab to volcanic front at the mariana arc. Journal of Geophysical Research, **102**: 14-19.

English, J.M., and Johnston, S.T. 2005. Collisional orogenesis in the northern Canadian Cordillera: Implications for Cordilleran crustal structure, ophiolite emplacement, continental growth, and the terrane hypothesis. Earth and Planetary Science Letters, **232**: 333–344.

Ettlinger, A.D. 1991. A marriage of geologic processes: an epithermal massive sulphide origin for Eskay Creek? Abstract, Northwest Miner's Association Meeting, Spokane, Washington.

Ettlinger, A.D. 1992. Hydrothermal alteration and brecciation underlying the Eskay Creek polymetallic massive sulphide deposit (104B/9W), British Columbia. *In* Geological Fieldwork 1991. Ministry of Energy.

Ettlinger, A.D. 2001. Eskay Creek 21 Zone; in Lewis, P.D., Toma, A. and Tosdal, R.M. (*eds*.), Metallogenesis of the Iskut River Area, Northwestern British Columbia. Mineral deposit research unit, Special publication number 1.

Evenchick, C.A. 2001. Northeast-trending folds in the western Skeena fold belt, northern Canadian Cordillera: a record of Early Cretaceous sinistral plate convergence. Journal of Structural Geology, **23**: 1123-1140.

Evenchick, C.A. and McNicoll, V.J. 2002. Stratigraphy, structure, and geochronology of the Anyox Pendant, Northwest British Columbia, and implications for mineral exploration; Canadian Journal of Earth Sciences, **39**: 1313-1332.

Evenchick, C.A., and Porter, J.S. 1993. Geology of west McConnell Creek map area, British Columbia. *In* Current Research. Geological Survey of Canada, Paper 93-1A, pp. 47-55.

Evenchick, C.A., and Thorkelson, D.J. 2005. Geology of the Spatsizi River map area, north-central British Columbia. Geological Survey of Canada, Bulletin 577.

Evenchick, C.A., Mustard, P.S., Greig, C.J., Porter, J.S., and McNeill, P.D. 2000. Geology, Bowser Lake (NTS 104A), British Columbia. Geological Survey of Canada Open File, 3918.

Evenchick, C.A., Poulton, T.P., Tipper, H.W., and Braidek, I. 2001. Fossils and facies of the northern two-thirds of the Bowser Basin, British Columbia. Geological Survey of Canada, Open File 3956.

Evenchick, C.A., Ferri, F., Mustard, P.S., McMechan, M.E., Osadetz, K.G., Stasiuk, L.D., Wilson, N.S.F., Enkin, R.J., Hadlari, T., and McNicoll, V.J. 2003. Recent results and activities of the Integrated Petroleum Resource Potential and Geoscience Studies of the Bowser and Sustut Basins project, British Columbia. *In* Current Research. Geological Survey of Canada, Paper 2003-A13.

Evenchick, C.A., McNicoll, V.J. and Snyder, L.D. 2004. Stratigraphy, geochronology and geochemistry of the Georgie River area, northwest British Columbia, and implications for mineral exploration. Canadian Journal of Earth Sciences, **41**: 199-216.

Evenchick, C.A., Ferri, F., Mustard, P.S., McMechan, M.E., Ritcey, D., McNicoll, V.J., Osadetz, K.G., O'Sullivan, P.B., Stasiuk, L.D., Wilson, N.S.F., Poulton, T.P., Lowe, C., Enkin, R.J., Waldron, J.W.F., Snyder, D.B., Turner, R.J.W., Nowlan, G., and Boddy, M. 2005. Highlights of recent research in the Bowser and Sustut Basins Project, British Columbia. *In* Current research. Geological Survey of Canada, Paper 2005-A1.

Evenchick, C.A., McMechan, M.E., McNicoll, V.J., and Carr, S.D. 2007a. A synthesis of the Jurassic-Cretaceous tectonic evolution of the central and southeastern Canadian Cordillera: exploring links across the orogen. In Whence the mountains? *Edited by* J.W. Sears, T.A. Harms, and C.A. Evenchick. Geological Society of America, Special Publication, **433**. pp. 117-145.

Evenchick, C.A., Mustard, P.S., McMechan, M.E., Ferri, F., Porter, S., Hadlari, T., and Jakobs, G.K. 2007b. Geology, McConnell Creek, British Columbia. Geological Survey of Canada, Open File 5571, 1:125,000 scale.

Evenchick, C.A., Mustard, P.S., McMechan, M.E., Ritcey, D.H., and Smith, G.T. 2008a. Geology, northeast Terrace and northwest Smithers, British Columbia. Geological Survey of Canada, Open File 5895.

Evenchick, C.A., McMechan, M.E., Mustard, P.S., Ritcey, D., Smith, G.T., Ferri, F., and Waldron, J.W.F. 2008b. Geology, Hazelton, British Columbia. Geological Survey of Canada, Open File 5704.

Evenchick, C.A., Mustard, P.S., McMechan, M.E., Greig, C.J., Ferri, F., Ritcey, D., Smith, G., Hadlari, T., and Waldron, J.W.F. 2009. Geology, Compilation Geology of Bowser and Sustut Basins Draped on Shaded Relief Map, North-central British Columbia. Geological Survey of Canada, Open File 5794.

Evenchick, C.A., Poulton, T.P., and McNicoll, V.J. 2010. Nature and significance of the diachronous contact between the Hazelton and Bowser Lake groups (Jurassic), north-central British Columbia. Bulletin of Canadian Petroleum Geology, **58**: 235–267.

Eward, A., Bryan, W.G., and Gill, J.B. 1973. Mineralogy and geochemistry of the younger volcanic islands of Tonga, S. W. Pacific. Journal of Petrology **14**: 429–65.

Falloon, T. J., and Danyushevsky, L. V. 2000. Melting of refractory mantle at 1.5, 2 and 2.5 GPa under anhydrous and H (sub 2) O-undersaturated conditions; implications for the petrogenesis of high-ca boninites and the influence of subduction components on mantle melting. Journal of Petrology, **41**: 257-283.

Ferri, F., and Boddy, M. 2005. Geochemistry of Early to Middle Jurassic Organic-rich Shales, Intermontane Basins, British Columbia. *In* Summary of Activities 2005. British Columbia Ministry of Energy, Mines and Petroleum Resources, pp. 132-151.

Ferri, F., Osadetz, K., and Evenchick, C. 2004. Petroleum source rock potential of Lower to Middle Jurassic clastic, Intermountain basins, British Columbia. *In* Geological Fieldwork, 2003, BC Ministry of Energy and Mines Open File 2004-01 p. 163-166.

Floyd, P.A., Kelling, G., Gökçen, S.L., and Gökçen, N. 1991. Geochemistry and tectonic environment of basaltic rocks from the Misis ophiolitic mélange, south Turkey. Chemical Geology **89**: 263-80.

Franklin, J. M., Gibson, H. L., Jonasson, I. R., and Galley, A. G. 2005. Volcanogenic massive sulfide deposits. In Economic Geology; one hundredth anniversary volume, 1905-2005. *Edited by* J.W. Hedenquist, J.F.H. Thompson, R.J. Goldfarb, J.P. Richards, Society of Economic Geologists, Littleton, CO.

Friedman, R.M., and Ash, C.H. 1997. U-Pb ages of intrusions related to porphyry Cu-Au mineralization in the Tatogga Lake area, northwestern British Columbia (104H/12NW, 104G/9NE). *In* Geological Fieldwork 1996, British Columbia Ministry of Energy, Mines and Petroleum Resources, Paper 1997-1, 291–298.p.

Friedman, R., Mundil, R., and Pálfy, J. 2008. Revised zircon U-Pb ages for the Triassic-Jurassic boundary and the earliest Jurassic employing the chemical abrasion pretreatment (CA-TIMS) technique. Geochimica Et Cosmochemica Acta, **72**: 1.

Gaboury, D., and Pearson, V. 2008. Rhyolite Geochemical Signatures and Association with Volcanogenic Massice Sulfide Deposits: Examples from the Abitibi Belt, Canada. Economic Geology, **103**:1531-1562.

Gabrielse, H., Wanless, R.K., Amrstrong, R.L., and Erdman, L.R. 1980. Isotopic dating of Early Jurassic volcanism and plutonism in north-central British Columbia. *In* Current research. Geological Survey of Canada, Paper 80-1A, pp. 27-32.

Gagnon, J.-F., and Waldron, J.W.F. 2008. Ashman Ridge Section Revisited: New Insights for the Evolution of the Bowser Basin, Northwestern British Columbia (NTS 93L/13). *In* Summary of Activities 2007. Geoscience British Columbia, Report 2008-1, pp. 121-128.

Gagnon, J.-F., and Waldron, J.W.F. 2011. Sedimentation styles and depositional processes in a Middle to Late Jurassic slope environment, Bowser Basin, Northwestern British Columbia, Canada. Marine and Petroleum Geology, **28**: 698–715.

Gagnon, J-F., Loogman, W., Waldron, J.W.F., Cordey, F., and Evenchick, C.A. 2007. Stratigraphic Record of Initiation of Sedimentation in the Bowser Basin (NTS 104A, H), Northwestern British Columbia. Geological Fieldwork 2006. British Columbia Ministry of Energy, Mines and Petroleum Resources, Paper 2007-1, pp 275-283.

Gagnon, J.-F., Evenchick, C.A., Waldron, J.W.F., Cordey, F., and Poulton, T.P. 2009. Jurassic subsidence history of the Hazelton Trough-Bowser Basin in the area of Todagin Mountain, north-central British Columbia, Canada. Bulletin of Canadian Petroleum Geology, **57**: 1-19.

Gagnon, J.-F., Barresi, T., Waldron, W.F., Nelson, J.L., Poulton, T.P., and Cordey, F. 2012. Stratigraphy of the upper Hazelton Group and the Jurassic evolution of the Stikine terrane, British Columbia. Canadian Journal of Earth Science **49**: 1027-1052.

Galley A.G. 1996. Geochemical characteristics of subvolcanic intrusions associated with Precambrian massive sulphide deposits. *In* Trace Element Geochemistry of Volcanic Rocks: Applications for Massive Sulfide Exploration. *Edited by* D.A. Wyman; Geological Association of Canada, Short Course Notes, **12**: 239-278.

Galley, A.G. 2003. Composite synvolcanic intrusions associated with Precambrian VMS-related hydrothermal systems. Mineralium Deposita, **38**:443–473.

Galley, A.G., Hannington, M., and Jonasson, I. 2007. Volcanogenic massive sulphide deposits. Mineral deposits division. Geological Association of Canada Special Publication **5**: 141–161.

Gareau, S.A., Friedman, R.M., Woodsworth, G.J. and Childe, F. 1997a. U-Pb ages from the northeastern quadrant of Terrace map area, west-central British Columbia. *In* Current Research, Geological Survey of Canada, Paper 1997-A/B, p. 31-40.

Gareau, S.A., Woodsworth, G.J. and Rickli, M. 1997b. Regional geology of the north eastern quadrant of Terrace map area, west-central British Columbia. Geological Survey of Canada, Current Research 1997-A/B, pages 47–55.

Gehrels, G.E. 2001. Geology of the Chatham Sound region, southeast Alaska and coastal British Columbia. Canadian Journal of Earth Sciences, **38**: 1579–1599.

Gehrels, G. E. and Kapp, P. A. 1998. Detrital zircon geochronology and regional correlation of metasedimentary rocks in the Coast Mountains, southeastern Alaska. Canadian Journal of Earth Sciences, **35**: 269-279.

Gehrels, G. , Rusmore, M. , Woodsworth, G. , Crawford, M. , Andronicos, C. , Hollister, L. , Patchett, J. , Ducea, M. , Butler, R. , Klepeis, K. , Davidson, C. , Friedman, R. , Haggart, J. , Mahoney, B. , Crawford, W., Pearson D. and Girardi, J. 2009. U-Th-Pb geochronology of the Coast Mountains batholith in north-coastal British Columbia: Constraints on age and tectonic evolution. Geological Society of America Bulletin, **121**: 1341-1361.

Gibson, H.L., Allen, R.L., Riverin, G., and Lane, T.E. 2007. The VMS Model: Advances and Application to Exploration Targeting. Ore Deposits and Exploration Technology. Proceedings of Exploration, **7**: 713-730.

Gillstrom, G., Anand, R., and Robertson, S. 2012. 2012 Technical Report on the Red Chris Copper-Cold Project. Technical Report for Imperial Metals Corp. Available at www.sedar.com [accessed January 2014].

Gonzales, D.A., and Van Schmus, W.R. 2007. Proterozoic history and crustal evolution in southwestern Colorado: Insight from U.Pb and Sm/Nd data. Precambrian Research, **154**:31-70.

Gordee, S.M. 2005. Volcanostratigraphy, age, and geologic setting of the Lower-Middle Jurassic upper Hazelton Group, west-central British Columbia. Unpublished MSc. Thesis, University of British Columbia, Vancouver, BC, 161 pp.

Greig, C.J. 1991. Stratigraphic and structural relations along the west-central margin of the Bowser Basin, Oweegee and Kinskuch areas, northwestern British Columbia. *In* Current research. Geological Survey of Canada, Paper 91-1A, pp. 197-205.

Greig, C.J. 1992. Fieldwork in the Oweegee and Snowslide ranges and Kinskuch Lake area, northwestern British Columbia. *In* Current Research. Geological Survey of Canada, Paper 92-1A, pp. 145-155.

Greig, C.J., and Gehrels, G.E. 1995. U-Pb zircon geochronology of Lower Jurassic and Paleozoic Stikinian strata and Tertiary intrusions, northwestern British Columbia. Canadian Journal of Earth Sciences, **32**: 1155-1171.

Grove, E.W. 1986. Geology and mineral deposits of the the Unuk River - Salmon River - Anyox area. British Columbia Ministry of Energy, Mines and Petroleum Resources, Bulletin 63.

Gunning, M.H., Hodder, R.W.H. and Nelson, J.L. 2006. Contrasting volcanic styles within the Paleozoic Stikine assemblage, western Stikine terrane, northwestern British Columbia. *In* Paleozoic Evolution and Metallogeny of Pericratonic Terranes at the Ancient Pacific Margin of North America, Canadian and Alaskan Cordillera. *Edited by* M. Colpron and J.L. Nelson, Geological Association of Canada, Special Paper 45, p. 201-227.

Haggart, J.W., Diakow, L.J., Mahoney, J.B., Struik, L.C., Woodsworth, G.D., Gordee, S., M., and Rushmore, M. 2006. Geology, Bella Coola area (93D/01, /07, /08, /10, /15 and parts of D/02, D/03, /06, /09, /11, /14, /16, and 92M/15 and /16), British Columbia. Geological Survey of Canada, Open Fiel 5385 and B.C. Ministry of Energy, Mines and Petroleum Resources, Geoscience Map 2006-7, scale 1:100 000.

Hanson, G. 1925. Driftwood Creek map-area, Babine Mountains, British Columbia. *In* Summary Report 1924, Geological Survey of Canada, Part A, pp. 19-37.

Harland, W.B., Armstrong, R.L., Cox, A.V., Craig, L.E., Smith, A.G., and Smith, D.G. 1990. A Geologic time scale 1989. Cambridge University Press, Cambridge, p. 1-263.

Harris, N. B. W., Pearce, J. A., and Tindle, A. G. 1986. Geochemical characteristics of collision-zone magmatism. Geological Society Special Publications, **19**: 67-81.

Hart, C. J. R. 1997. A Transect Across Northern Stikinia: Geology of the Northern Whitehorse Map Area, Southern Yukon Territory (105D/13-16). Northern Affairs Program (Canada) Bulletin Yukon Region Exploration and Geological Services Division, v. 8.

Hart, T. R., Gibson, H. L., and Lesher, C. M. 2004. Trace element geochemistry and petrogenesis of felsic volcanic rocks associated with volcanogenic massive Cu-Zn-Pb sulfide deposits. Economic Geology and the Bulletin of the Society of Economic Geologists, **99**: 1003-1013.

Henderson, J.R., Kirkham, R.V., Henderson, M.N., Payne, J.G., Wright, T.O., and Wright, R.L. 1992. Stratigraphy and Structure of the Sulphurets Area, British Columbia. *In* Current research. Geological Survey of Canada, Paper 92-1A, pp. 323-332.

Herrington, R.J., Scotney, P.M., Roberts, S., Boyce, A.J., and Harrison, D. 2011. Temporal association of arc-continent collision, progressive magma contamination in arc colcanism and formation of gold-rich massive sulphide deposits on Wetar Island (Banda Arc). Gondwana Research, **19**: 583-593.

Hildreth, W.E., and Moorbath S. 1988. Crustal contributions to arc magmatism in the Andes of Central Chile. Contributions to Mineralogy and Petrology, **98**: 455-499.

Hodych, J.P., and Dunning, G.R. 1992. Did the Manicouagan impact trigger end-of-Triassic mass extinction? Geology, **20**: 51-54.

Huang, J.J., Hafex, S.A., Lechner, M.J., Parkinson, J.G., Gray, J.H., Brazier, N., Newcomen, W., Jones, K., Ghaffari, H., Parolin, R.W., Kreiz, D.K., Wachmann, T., Pelletier, P., and Hammett, R. 2014. Amended (2014) 2012 KSM (Kerr-Sulphurets-Mitchell) Prefeasibility Study. Technical Report for Seabridge Gold Corp. Available at www.sedar.com. [accessed Jan. 2014].

Huppert, H.E., Stephen, R., and Sparks, J. 1985. Cooling and contamination of mafic and ultramafic magmas during ascent through continental crust. Earth and Planetary Science Letters, **74**:371-385.

Hyndman, R.D., Currie, C.A., and Mazzotti, S.P 2005. Subduction zone backarcs, mobile belts, and orogenic heat. GSA Today **15**: 4–10.

Irvine, T. N. and Baragar, W. R. A. 1971. A guide to the chemical classification of the common volcanic rocks. Canadian Journal of Earth Sciences, **8**: 523-548.

Jackson, J. L., Gehrels, G. E., Patchett, P. J. and Mihalynuk, M. G. 1991. Stratigraphic and isotopic link between the northern Stikine Terrane and an ancient continental margin assemblage, Canadian Cordillera. Geology **19**: 1177-1180.

Jackson, M.D., Gallagher, K., Petford, N., and Cheadle, M.J. 2005. Towards a coupled physical and chemical model for tonalite–trondhjemite–granodiorite magma formation. Lithos **7**: 43–60.

Jakobs, G.K. 1993. Jurassic stratigraphy of the Diagonal Mountain area, McConnell Creek map area, north-central British Columbia. *In* Current research. Geological Survey of Canada, Paper 93-1A, pp. 43-46.

Jensen, L. S. 1976. A New Cation Plot for Classifying Subalkalic Volcanic Rocks. Ontario Geological Survey Miscellaneous Paper 66.

Kamenetsky, V.S., Binns, R.A., Gemmell, J.B., Crawford, A.J., Mernagh, T.P., Maas, R., and Steele, D. 2001. Parental basaltic melts and fluids in eastern Manus backarc basin; implications for hydrothermal mineralisation. Earth Planet Science Letters **184**:685–702.

Kawate, S., and Arimar, M. 1998. Petrogenesis of the Tanzawa plutonic complex, central Japan: exposed felsic middle crust of the Izu-Bonin-Mariana arc. Island Arc **7**: 342–58.

Kerr, F.A. 1948. Lower Stikine and western Iskut River Areas, British Columbia. Geological Survey of Canada, Memoir 246.

Kerr, A., Jenner, G.A. and Fryer. B.J 1995. Sm-Nd isotopic geochemistry of Precambrian to Paleozoic granitoid suites and the deep-crustal structure of the southeast margin of the Newfoundland Appalachians. Canadian Journal of Earth Science. **32**: 224-245.

Kimura, J., and Yoshida, T. 2006. Contributions of slab fluid, mantle wedge and crust to the origin of quaternary lavas in the NE Japan Arc. Journal of Petrology, **47**: 2185-2232.

Kusznir, N.J., and Egan, S.S. 1990. Simple-shear and pure-shear models of extensional sedimentary basin formation: Application to the Jeanne d'Arc Basin, Grand Banks of Newfoundland. In Extensional Tectonics of the North Atlantic Margins. *Edited by* A.J. Tankard and H.R. Balkwill. AAPG Memoir 46, pp. 305-322.

Kyba, J., and Nelson, J. 2015. Stratigraphic and tectonic framework of the Khyber-Sericite-Pins mineralized trend, lower Iskut River, northwest British Columbia. *In* Geological Fieldwork 2014, British Columbia Ministry of Energy and Mines, British Columbia Geological Survey Paper 2015-1, p. 41-58.

Lang, J. R., Lueck, B., Mortensen, J. K., Russell, J. K., Stanley, C. R. and Thompson, J. F. 1995. Triassic-Jurassic silica-undersaturated and silica-saturated alkalic intrusions in the Cordillera of British Columbia: Implications for arc magmatism. Geology, **23**: 451-454.

Larue, D.K., Smith, A.L., and Schellenkens, J.H. 1991. Ocean Island arc stratigraphy in the Caribbean region: don't take it for granite. Sedimentary Geology, **74**:289-308.

Leach, W.W. 1910. The Skeena River District. In Summary report 1910. Geological Survey of Canada, Sessional Paper 26, pp. 61-68.

Leat, P.T., Larter, R.D., and Millar, I.L. 2007. Silicic magmas of Protector Shoal, South Sandwich arc: indicators of generation of primitive continental crust in an island arc. Geological Magazine, **144**: 179-190.

LeBas, M.J., LeMaitre, R.W., Streckeisen, A., and Zanettin, B. 1986. A chemical classification of volcanic rocks based on the total alkali-silica diagram. Journal of Petrology, **27**: 745-750.

Leistel, J. M., Marcoux, E., Thieblemont, D., Quesada, C., Sanchez, A., Almodovar, G. R., and Sanchez, R. 1997. The volcanic-hosted massive sulphide deposits of the Iberian Pyrite Belt review and preface to the thematic issue. Review and preface to the thematic issue. Mineralium Deposita, **33**: 2-30.

Lentz, D. R. 1996. Trace-element systematics of felsic volcanic rocks associated with massive-sulphide deposits in the Bathurst mining camp; petrogenetic, tectonic and chemostratigraphic implications for VMS exploration. Short Course Notes - Geological Association of Canada, **12**: 359-402.

Lentz, D.R. 1998. Petrogenetic evolution of felsic volcanic sequences associated with Phanerozoic volcanic-hosted massive sulfide systems: The role of extensional geodynamics. Ore Geology Reviews, **12**: 289-327.

Lesher, C. M., Goodwin, A. M., Campbell, I. H., and Gorton, M. P. 1986. Trace-element geochemistry of ore-associated and barren, felsic metavolcanic rocks in the Superior Province, Canada. Canadian Journal of Earth Sciences, **23**: 222-237.

Lewis, P.D. (compiler) 2001. Whole rock geochemistry. *In* Metallogenesis of the Iskut River Area, Northwestern British Columbia. *Edited by* P.D. Lewis, A. Toma, and R.M Tosdal, Mineral Deposit Research Unit, Special Publication Number 1, Chapter 7.

Lewis, P.D. 2013. Iskut River Area Geology, Northwest British Columbia (104B/08, 09, 10 & part of 104B/01, 07, 11). Geoscience British Columbia Report 2013-05; 3 1:50,000-scale maps, legend and notes; .shp files.

Lewis, P.D., Thompson, J.F.H., Nadaraju, G., Anderson, R.G., and Johannson, G.G. 1993. Lower and Middle Jurassic stratigraphy in the Treaty glacier area and geological setting of the Treaty glacier alteration system, northwestern British Columbia. *In* Current research. Geological Survey of Canada, Paper 93-1A, pp. 75-86.

Lewis, P.D, Macdonald, A.J., and Bartsch, R.D. 2001. Hazelton group / Bowser Lake group Stratigraphy in the Iskut River Area - Progress and Problems. *In* Metallogenesis of the Iskut River Area, Northwestern British Columbia. *Edited by* P.D. Lewis, A. Toma, and R.M Tosdal, Mineral Deposit Research Unit, Special Publication Number 1, Chapter 2, p. 9-30.

Lin, A.T., Watts, A.B., and Hesselbo, S.P. 2003. Cenozoic stratigraphy and subsidence history of the South China Sea Margin in the Taiwan region. Basin Research, **15**: 453-478.

Logan. J.M., Koyanagi, V.M. and Drobe, J.R. 1990. Geology and Mineral Occurrences of the Forrest Kerr – Iskut River Area (104B/15). British Columbia Ministry of Energy Mines and Petroleum Resources, Open File Map 1990-2, scale 1:50,000.

Logan, J.M., Drobe, J.R., Koyanagi, V.M. and Elsby, D.C. 1997. Geology of the Forest Kerr - Mess Creek Area, Northwestern British Columbia (104B/10,15 & 104G/2 & 7W). British Columbia Ministry of Employment and Investment, Open File Map 1997-3, scale 1:100 000.

Logan, J.M., Drobe, J.R. and McClelland, W.C. 2000. Geology of the Forest Kerr - Mess Creek Area, Northwestern British Columbia (104B/10,15 & 104G/2 & 7W). British Columbia Ministry of Energy and Mines, and Petroleum Bulletin 104, 164p.

Logan, J.M. and Mihalynuk, M.G. 2014. Tectonic controls on Early Mesozoic paired alkaline porphyry deposit belts (Cu-Au + Ag-Pt-Pd-Mo) within the Canadian Cordillera. Economic Geology, **109**: 827-858.

Lonsdale, P. 2006. The opening of the Gulf of California Trough Within the North American Cordillera. Abstracts with Programs – Geological Society of America Specialty Meeting Backbone of the Americas, Mendoza, Argentina, pp. 82.

MacDonald, J. 2001. Eskay Porphyry. *In* Metallogenesis of the Iskut River Area, Northwestern British Columbia. *Edited by* P.D. Lewis, A. Toma, and R.M Tosdal, Mineral Deposit Research Unit, Special Publication Number 1, Chapter 13, p. 134-148.

MacDonald, A.J., van der Heyden, P., Lefebure, D.V., and Alldrick, D.J. 1992. Geochronometry of the Iskut River area – an update (104A and B). *In* Geological Fieldwork, British Columbia Ministry of Energy, Mines and Petroleum Resources Paper 1992-1, p. 495-501.

MacDonald, A.J., Lewis, P.D., Thompson, J.F.H., Nadaraju, G., Bartsch, R.D., Bridge, D.J., Rhys, D.A. Roth, T., Kaip, A., Godwin, C.I., and Sinclair, A.J. 1996a. Metallogeny of an Early to Middle Jurassic arc, Iskut River area, northwestern British Columbia. Economic Geology **91**: 1098-1114.

MacDonald, R.W.J., Barrett, T.J., and Sherlock, R.L. 1996b. Geology and lithogeochemistry of the Hidden Creek deposit, Anyox, west-central British Columbia. Exploration and Mining Geology, **5**: 311-314.

MacIntyre, D. 2006. Geology and mineral deposits of the Skeena Arch, west-central British Columbia; a geoscience BC digital data compilation project. *In* Geological Fieldwork 2006, British Columbia Ministry of Energy and Mines, British Columbia Geological Survey Paper 2007-1 p. 333-340.

MacIntyre, D.G., Desjardins, P., and Tercier, P. 1989. Jurassic stratigraphic relationships in the Babine and Telkwa Ranges (93L/10, 11, 14, 15). *In* Geological Fieldwork 2008. British Columbia Ministry of Energy, Mines and Petroleum Resources, Paper 1989-1, pp. 195-208.

MacIntyre, D., Ash, C., and Britton, J. 1994. Nass-Skeena (93/E, L, M; 94/D; 103/G, H, I, J, P; 104/A, B). British Columbia Department of Energy and Mines Open File, 1994-14.

MacIntyre, D.G., Webster, I.C.L., and Villeneuve, M. 1997. Babine Porphyry Belt Project: Bedrock Geology of the Old Fort Mountain Area (93M/1), British Columbia. *In* Geological Fieldwork 1996. British Columbia Ministry of Energy, Mines and Petroleum Resources, Paper 1997-1, pp. 47-68.

MacIntyre, D. G., Villeneuve, M. E., and Schiarizza, P. 2001. Timing and tectonic setting of Stikine Terrane magmatism, Babine-Takla Lakes area, central British Columbia. Canadian Journal of Earth Sciences, **38**: 579-601.

MacLean, W. H. 1990. Mass change calculations in altered rock series. Mineralium Deposita, **25**: 44-49.

Mahoney, J.B., Haggart, J.W., Hooper, R.L., Snyder, L.D., Woodsworth, G.J., and Friedman, R.M. 2007. New Geological Mapping and Implications for Mineralization Potential in the Southern and Western Whitesail Lake Map Area (NTS 093E), Southwestern British Columbia. *In* Geological Fieldwork 2006. British Columbia Ministry of Energy, Mines and Petroleum Resources, Paper 2007—1, pp 341-354.

Malpas, J. 1979. Two contrasting trondhjemite associations from transported ophiolites in Western Newfoundland. *In*: Barker, F. (*Ed*.), Trondhjemites, Dacites, and Related Rocks. Elsevier, Amsterdam, p. 465–487.

Marsden, H., and Thorkelson, D.J. 1992. Geology of the Hazelton volcanic belt in British Columbia: Implications for the Early the Middle Jurassic evolution of Stikinia. Tectonics, **11**: 1266-1287.

McClay, K.R., Insley, M.W. and Anderson, R. 1989. Inversion of the Kechika Trough, northeastern British Columbia; *in* M.A. Cooper and G.D. Williams, *eds*., Inversion Tectonics, Geological Society of London, Special Publication **44**: 235-257.

McClelland, W.C. 1992. Permian and older rocks of the southwestern Iskut River map area, northwestern British Colombia, Geological Society of America Bulletin, Special Paper **343**: 159-182.

McKenzie, D., and O'Nions, R.K. 1991. Partial melt distributions from inversion of rare earth element concentrations. Journal of Petrology, **32**: 1021-1091.

McKenzie, D. 1978. Some remarks on the development of sedimentary basins. Earth and Planetary Science Letters, **40**: 25-32.

Mercier-Langevin, P., Hannington, M.D., Dube, B., and Becu, V. 2011. The gold content of volcanogenic massive sulfide deposits. Mineralium Deposita, **46**: 509-539.

Meschede, M. 1986. A method of discriminating between different types of mid-ocean ridge basalts and continental tholeiites with the Nb-Zr-Y diagram. Chemical Geology, **56**: 207-218.

Metzger, E.P., Miller, R.B., and Harper, G.D. 2002. Geochemistry and tectonic setting of the ophiolite Ingalls complex, north Cascades, Washington: implications for correlations of Jurassic Cordilleran ophiolites. The Journal of Geology, **110**: 543-560.

Mihalynuk, M.G. 1987. Metamorphic, structural and stratigraphic evolution of the Telkwa Formation, Zymoetz River area (NTS 103I/08 and 93 L/05), near Terrace, British Columbia. M.Sc. thesis, Department of Earth Sciences, University of Calgary, Calgary, Alberta, 128 pages.

Mihalynuk, M. G., Smith, M. T., Gabites, J. E., Runkle, D., and Lefebure, D. 1992. Age of emplacement and basement character of the Cache Creek Terrane as constrained by new isotopic and geochemical data. Canadian Journal of Earth Sciences, **29**: 2463-2477.

Mihalynuk, M.G., Nelson, J., and Diakow, L.J. 1994. Cache Creek terrane entrapment: Oroclinal paradox within the Canadian Cordillera. Tectonics, **13**: 575–595.

Mihalynuk, M. G., Gabites, J. E., Orchard, M. J., and Tozer, E. T. 1997. Age of the Willison Bay pluton and overlying sediments; implications for the Carnian stage boundary. *In* Geological Fieldwork 1996, British Columbia Ministry of Energy and Mines, British Columbia Geological Survey Paper 2007-1, p., 171-179.

Mihalynuk, M. G., Erdmer, P., Ghent, E. D., Cordey, F., Archibald, D. A., Friedman, R. M. and Johannson, G. G. 2004. Coherent French Range blueschist: Subduction to exhumation in <2.5 m.y.? Bulletin of the Geological Society of America, **116**: 910-922.

Miyashiro, A. 1974. Volcanic rock series in island arcs and active continental margins. American Journal of Science, **274**:321-355.

Monger, J.W.H. 1977. Upper Paleozoic rocks of the western Canadian Cordillera and their bearing on Cordilleran evolution. Canadian Journal of Earth Sciences, **14**: 1832-1859.

Monger, J.W.H., and Church, B. 1977. Revised stratigraphy of the Takla Group, north-central British Columbia. Canadian Journal of Earth Sciences, **14**: 318-326.

Monger, J.W.H., Price, R.A., and Tempelman-Kluit, D.J. 1982. Tectonic accretion and the origin of two metamorphic and plutonic welts in the Canadian Cordillera. Geology, **10**: 70–75.

Monger, J.W.H., Wheeler, J.O., Tipper, H.W., Gabrielse, H., Harms, T., and Struik, L.C. 1991. Upper Devonian to Middle Jurassic Assemblages. *In* Geology of the Cordilleran Orogen in Canada. *Edited by* H. Gabrielse and C.J. Yorath. Geological survey of Canada, Geology of Canada, no. 4 Part B. Cordilleran Terranes, Chap. 8, pp. 281-327.

Monzier, M., Robin, C., and Eissen, J.-P. 1994. Kuwae (≈1425 A.D.): the forgotten caldera. Journal of Volcanology and Geothermal Research **59**: 207–18.

Moody, J.B., Jenkins, J.E., and Meyer, D. 1985. An experimental investigation of the albitization of plagioclase. Canadian Mineralogist, **23**:583-596.

Mortensen, J.K., Ghosh, D.K., and Ferri, F. 1995. U-Pb geochronology of intrusive rocks associated with copper-gold porphyry deposits in the Canadian Cordillera. Canadian Institute of Mining, Metallurgy and Petroleum Special Volume, **46**: 142–158.

Mortimer, N. 1986. Late Triassic, arc-related, potassic igneous rocks in the North American Cordillera. Geology, **14**: 1035-1038.

Mundil, R., and Pálfy, J. 2005. Triassic-Jurassic time scale and mass extinction; current status and new constraints. Geochimica Et Cosmochimica Acta, **69**: 310pp.

Nadaraju, G. 1993. Triassic-Jurassic Biochronology of the eastern Iskut River map area, northwestern British Columbia. M.Sc. thesis, Department of Earth and Ocean Sciences, The University of British Columbia, Vancouver, B.C.

Nelson, J.L., and Colpron, M. 2007. Tectonics and metallogeny of the Canadian and Alaskan Cordillera, 1.8 Ga to present. In Mineral Deposits of Canada: A Synthesis of Major Deposit Types, District Metallogeny, the Evolution of Geological Provinces, and Exploration Methods *Edited by* W.D. Goodfellow. Mineral Deposit Division, Geological Association of Canada, Special Publication, 5, pp. 755–791.

Nelson. J.L., and Kennedy, R. 2007a. Geology of the Doreen south half (103I/16S) and Terrace east half (103I/10E) map areas, near Terrace, British Columbia; BC Ministry of Energy, Mines and Petroleum Resources Open-File 2007-4, 1:50,000.

Nelson, J., and Kennedy, R. 2007b. Terrace Regional Mapping Project Year 2: New Geological Insights and Exploration Targets (NTS 103I/16S, 10W), West-Central British Columbia. *In* Geological Fieldwork 2006, British Columbia Ministry of Energy and Mines, British Columbia Geological Survey Paper 2007-1, p. 149-162.

Nelson, J., and Kyba, J. 2014. Structural and stratigraphic control of porphyry and related mineralization in the Treaty Glacier – KSM – Brucejack – Stewart trend of western Stikinia. *In* Geological Fieldwork 2013, British Columbia Ministry of Energy and Mines, British Columbia Geological Survey Paper 2014-1, p. 111-140.

Nelson, J., Barresi, T., Knight, E., and Boudreau, N. 2006a. Geology and Mineral Potential of the Usk Map Area (NTS 103I/09), Terrace, British Columbia. *In* Geological Fieldwork 2005, British Columbia Ministry of Energy and Mines, British Columbia Geological Survey Paper 2006-1, p. 149-162.

Nelson, J.L., Barresi, T., Knight, E., and Boudreau, N. 2006b. Geology of the Usk Map Area (NTS 103I/9). British Columbia Ministry of Energy and Mines, British Columbia Geological Survey Open File 2006-03.

Nelson, J.L., Kennedy, R., Angen, J., and Newman, S. 2007. Geology of Terrace area. British Columbia Ministry of Energy, Mines and Petroleum Resources, Open File 2007-04.

Nelson, J.L., McKeown, M., Cui, Y., Desjardins P. and Nakanishi, T. 2008a. Terrace Preliminary Geodata Release (Central West BC). B.C. Ministry of Energy, Mines and Petroleum Resources, Geofile 2008-11.

Nelson, J., Kyba, J., McKeown, M. and Angen, J. 2008b. Terrace Regional Mapping Project, Year 3: Contributions to Stratigraphic, Structural and Exploration Concepts, Zymoetz River to Kitimat River, East-Central British Columbia (BTS 103I/09). *In* Geological Fieldwork 2007, British Columbia Ministry of Energy and Mines, British Columbia Geological Survey Paper 2008-1, p. 159-174.

Nelson, J.L., Colpron, M. and Israel, S. 2013. The Cordillera of British Columbia, Yukon and Alaska: Tectonics and Metallogeny. *In* Tectonics, Metallogeny and Discovery: The North American Cordillera and Similar Accretionary Settings. *Edited by* M. Colpron, T. Bissig, B.G. Rusk, and J. Thompson, Society of Economic Geologists Special Publication **17**: 53-110.

North American Commission on Stratigraphic Nomenclature. 2005. North American Stratigraphic Code. AAPG Bulletin **89**: 1547-1591.

Ogg, J.G. 2004. The Jurassic Period. In A Geologic Time Scale 2004. *Edited by* F.M. Gradstein, J.G. Ogg, and A.G. Smith. Cambridge University Press. pp. 307–343.

Osadetz, K.G., Jiang, C., Evenchick, C.A., Ferri, F., Stasiuk, L.D., Wilson, N.S.F., and Hayes, M. 2007. Compositions and significance of crude oil stains in Bowser and Sustut basins (Intermontane Belt) British Columbia. Bulletin of Canadian Petroleum Geology, **55**: 285-305.

Pálfy, J., Smith, P.L., Mortensen, J.K., and Friedman, R.M. 1999. Integrated ammonite Biochronology and U-Pb geochronometry from a basal Jurassic section in Alaska. Geological Society of America Bulletin, **111**: 1537-1549.

Palfy, J., Mortensen, J. K., Smith, P. L., Friedman, R. M., McNicoll, V. and Villeneuve, M. 2000. New U-Pb zircon ages integrated with ammonite biochronology from the Jurassic of the Canadian Cordillera. Canadian Journal of Earth Sciences, **37**: 549-567.

Pearce, J.A. 2008. Geochemical fingerprinting of oceanic basalts with applications to ophiolite classification and the search for Archean oceanic crust. Lithos, **100**: 14–48.

Pearce, J.A., and Peate, D.W. 1995. Tectonic implications of the composition of volcanic arc magmas. Annual Reviews in Earth and Planet Science, **23** :251–285.

Pearce, J.A., and Stern, R.J. 2006. Origin of back-arc basin magmas; trace element and isotope perspectives. *In* Back-Arc Spreading Systems Geological, Biological, Chemical and Physical Interactions. *Edited by* D.M. Christie, C.R. Fisher, S-M Lee, S. Givens, Geophysical Monograph, **166**: 63-86.

Pearce, J. A., Harris, N. B. W. and Tindle, A. G. 1984. Trace element discrimination diagrams for the tectonic interpretation of granitic rocks. Journal of Petrology, **25**: 956-983.

Pearce, J. A., Thirlwall, M. F., Ingram, G., Murton, B. J., Arculus, R. J., and van der Laan, S.R. 1992. Isotopic evidence for the origin of boninites and related rocks drilled in the Izu-Bonin (ogasawara) forearc, leg 125. Proceedings of the Ocean Drilling Program, Scientific Results, **125**: 237-261.

Pearce, J.A., Baker, P.E., Harvey, P.K., and Luff, I.W. 1995. Geochemical evidence for subduction fluxes, mantle melting and fractional crystallization beneath the South Sandwich arc. Journal of Petrology **36**: 1073–1109.

Pearce, J. A., Stern, R. J., Bloomer, S. H., and Fryer, P. 2005. Geochemical mapping of the Mariana Arc-Basin system; implications for the nature and distribution of subduction components. Geochemistry, Geophysics, Geosystems - G3, **6**: 1-27.

Peccerillo, A., and Taylor, S. R. 1976. Geochemistry of Eocene calc-alkaline volcanic rocks from the Kastamonu area, northern Turkey. Contributions to Mineralogy and Petrology, **58**: 63-81.

Piercey, S.J. 2007. An overview of the use of petrochemistry in the regional exploration for volcanogenic massive sulfide (VMS) deposits. *In*: Milkereit B (*ed*.) Proceedings of exploration 07: Fifth Decennial International Conference on Mineral Exploration. Toronto, ON. pp 223–246.

Piercey, S.J. 2010. An overview of petrochemistry in the regional exploration for volcanogenic massive sulfide (VMS) deposits. Geochemistry: Exploration, Environment, and Analysis, **10**: p.119-136.

Piercey, S. J. 2011. The setting, style, and role of magmatism in the formation of volcanogenic massive sulfide deposits. Mineralium Deposita, **46**: 449-471.

Piercey, S.J., Murphy, D.C., Mortensen, J.K, and Paradis, S. 2001a. Boninitic magmatism in a continental margin setting, Yukon-Tanana Terrane, southeastern Yukon, Canada. Geology **29**:731–734.

Piercey, S,J,, Paradis, S., Murphy, D.C., and Mortensen, J.K. 2001b. Geochemistry and paleotectonic setting of felsic volcanic rocks in the Finlayson Lake volcanic-hosted massive sulfide (VHMS) district, Yukon, Canada. Economic Geology **96**:1877–1905.

Piercey, S.J, Murphy, D.C., Mortensen, J.K., and Creaser, R.A. 2004. Mid-Paleozoic initiation of the northern cordilleran marginal back-arc basin: geological, geochemical and neodymium isotopic evidence from the oldest mafic magmatic rocks in Yukon-Tanana terrane, Finlayson Lake district, southeast Yukon, Canada. Geological Society of America Bulletin **116**:1087–1106.

Plank, T. 2005. Constraints from Thorium/Lanthanum on sediment recycling at subduction zones and the evolution of the continents. Journal of Petrology, **46**: 921-944.

Plank, T., and Langmuir, C. 1988. An evaluation of the global variations in the major element chemistry of arc basalts. Earth and Planetary Science Letters, **90**: 349-370.

Polat, A., Hofmann, A. W., and Rosing, M. T. 2002. Boninite-like volcanic rocks in the 3.7-3.8 g.a. Isua Greenstone Belt, West Greenland; geochemical evidence for intra-oceanic subduction zone processes in the early earth. Chemical Geology, **184**: 231-254.

Read, P.B., Brown, R.L., Psutka, J.F., Moore, J.M., Journeay, M., Lane, L.S. and Orchard, M.J. 1989. Geology of More and Forest Kerr Creeks (parts of 104B/10,15,16 and 104G/1, 2), Northwestern British Columbia. Geological Survey of Canada, Open File 2094.

Richards, J.P. 2003. Tectono-Magmatic Precursors for Prophyry Cu-(Mo-Au) Deposit Formation. Economic Geology, **98**: 1515-1533.

Ricketts, B.D., Evenchick, C.A., Anderson, R.G., and Murphy, D.C. 1992. Bowser Basin, northern British Columbia: constraints on the timing of initial subsidence and Stikinia-North America terrane interactions. Geology, **120**: 1119-1122.

Robinson, J. A., and Wood, B. J. 1998. The depth of the spinel to garnet transition at the peridotite solidus. Earth and Planetary Science Letters, **164**: 277-284.

Roots, C. F., Nelson, J. L., Simard, R., and Harms, T. A. 2006. Continental fragments, Mid-Paleozoic arcs and overlapping Late Paleozoic arc and Triassic sedimentation in the Yukon-Tanana Terrane of northern British Columbia and southern Yukon. Special Paper - Geological Association of Canada, **45**: 153-177.

Roth, T. 1993. Surface geology of the 21A zone, Eslay Creek, British Columbia (104B/9W), British Columbia. *In* Geological Fieldwork 1992. British Columbia Ministry of Energy, Mines and Petroleum Resources, Report Paper 1993-1, pp. 325-330.

Roth, T. 2002. Physical and chemical constraints on mineralization in the Eskay Creek deposit, northwestern British Columbia: evidence from petrography, mineral chemistry, and sulfur isotopes, University of British Columbia, Ph.D. Thesis, 401p.

Roth, T., Thompson, J.F.H. and Barrett, T.J. 1999. The precious metal-rich Eskay Creek deposit, northwestern British Columbia. *in* Volcanic-associated massive sulphide deposits: Processes and examples in modern and ancient settings. *Edited by* C.T. Barrie and M.D. Hannington, Reviews in Economic Geology, **8**: 357-373.

Rudnick, R. L. 1995. Making continental crust. Nature, **378**: 571-578.

Rudnick, R. L., and Fountain, D. M. 1995. Nature and composition of the continental crust; a lower crustal perspective. Reviews of Geophysics, **33**: 267-309.

Rushmore, M.E., Woodsworth, G.J., and Gehrels, G.E. 2005. Two-stage exhumation of midcrustal arc rocks, Coast Mountains, British Columbia. Tectonics, **24**: 1-25.

Russell, J.K., and Nicholls, J. 1988. Analysis of petrologic hypothesis with Pearce element ratios. Contributions to Mineralogy and Petrology, **99**: 25-35.

Samson, S. D., McClelland, W. C., Patchett, P. J., Gehrels, G. E., and Anderson, R. G. 1989. Evidence from neodymium isotopes for mantle contributions to Phanerozoic crustal genesis in the Canadian Cordillera. Nature, **337**: 705-709.

Samson, S.D., Patchett, P.J., McClelland, W.C., and Gehrels, G.E. 1991. Nd isotopic characterization of metamorphic rocks in the Coast Mountains, Alaska and Canadian Cordillera: ancient crust bounded by juvenile terranes. Tectonics, **10**: 770-780.

Schaltegger, U., Schoene, B., Bartolini, A., Guex, J., and Ovtcharova, M. 2007. Precise ages for the Triassic/Jurassic boundary and Hettangian recovery from northern Peru. Goldschmidt conference abstract A884, Cologne, Germany.

Schofield, S.J., and Hanson, G. 1921. Salmon River District, British Columbia. *In* Summary Report 1920. Geological Survey of Canada, Part A, pp. 6-12.

Scott, J.E., Richards, J.P., Heaman, L.M., Creaser, R.A., and Salazar, G.S. 2008. The Schaft Creek Porphyry Cu-Mo-(Au) deposit, northwestern British Columbia. Exploration and Mining Geology, **17**: 163–196.

Severs, M.J., Gryger, K.J., Makin, S.A., Bodnar, R.K. and Bradford, W.B. 2013. Investigation of long-term geochemical variations and magmatic processes at Mount St. Helens. Geofluids **13**: 440-452.

Sharp, R.J. 1980. The geology, geochemistry and sulpur isotopes of the Anyox massive sulphide deposits. M.Sc. thesis, University of Alberta, Edmonton.

Sherlock, R., and Domvile, J. 2008. Great Mining Camps of Canada 2. The history and geology of the Anyox copper camp, British Columbia. **34**: 113-134.

Sherlock, R.L., Barrett, T.J., Roth, T., Childe, F.C., Thomson, J.F.H., Kuran, D., Marsden, H., and Allen, R. 1994. Geological investigations of the 21B deposit, Eskay Creek, northwestern British Columbia (104B/9W). *In* Geological Fieldwork 1993. British Columbia Ministry of Energy, Mines and Petroleum Resources, Report Paper 1994-1, pp. 357-364.

Sherlock, R.L., Roth, T., Spooner, E.T.C., and Bray, C.J. 1999. Origin of the Eskay Creek Pecious Metal-Rich Volcanogenic Massive Sulphide Deposit: Fluid Inclusion and Stable Isotope Evidence. Economic Geology, **94**: 803-824.

Shervais, J. W. 1982. Ti–V plots and the petrogenesis of modern and ophiolitic lavas. Earth and Planetary Science Letters **59**: 101–118.

Sillitoe, R.H. 1982. Extensional habitats of rhyolite-hosted massive sulfide deposits. Geology, **10**: 403–407.

Simmons, A.T., Tosdal, R.M., Awmack, H.J., Wooden, J.L., and Friedman, R.M. 2007. Early Triassic Stuhini Group Magmatism (NTS 104K/10W), Northwestern British Columbia: New U-Pb Grochronological Results. *In* Geological Fieldwork 2006, British Columbia Ministry of Energy and Mines, British Columbia Geological Survey Paper 2007-1, p. 211-224.

Simpson, K.A. and McPhie, J. 2001. Fluidal-clast breccia generated by submarine fire fountaining, Trooper Creek Formation, Queensland, Australia. Journal of Volcanology and Geothermal Research. **109**: 339-355.

Simpson, K. A., Nelson, J. L., and Hicock, S. R. 2004. Preliminary interpretations of mid-jurassic volcanic and sedimentary facies in the east telegraph creek map area. Current Research - Geological Survey of Canada, 2004-A1: 1-8.

Smith, A. D. 1993. Geochemistry and tectonic setting of volcanics from the Anyox mining camp, British Columbia. Canadian Journal of Earth Sciences, **30**: 48-59.

Smith, I.E.M., Steward, R.B., and Price, R.C. 2003a. The petrology of a large intra-oceanic silicic eruption: the Sandy Bay Tephra, Kermadec arc, southwest Pacific. Journal of Volcanology and Geothermal Research, **124**: 173–94.

Smith, I.E.M., Worthington, T.J., Stewart, R.B., Price, R.C., and Gamble, J.A. 2003b. Felsic volcanism in the Kermadec arc, southwest Pacific: crustal recycling in an oceanic setting. In Intra-oceanic Subduction Systems in Tectonic and Magmatic Processes (*eds* R. D. Larter and P. T. Leat). Geological Society of London Special Publication **219**: 99-118.

Souther, J.G. 1972. Telegraph Creek map-area, British Columbia (104G). Geological Survey of Canada, Paper 71-44.

Souther, J.G. 1977. Volcanism and Tectonic Environments in the Canadian Cordillera – a Second Look, Volcanics Regimes of Canada. Geological Association of Canada Special Paper Number 16, p. 1-24.

Spitz, G., and Darling, R. 1978. Major and minor element lithogeochemical anomalies surrounding the Louvem copper deposit, Val D'or, Quebec. Canadian Journal of Earth Sciences, **15**: 1161-1169.

Stanley, George D., and McRoberts, C. A. 1993. A coral reef in the Telkwa range, British Columbia; the earliest jurassic example. Canadian Journal of Earth Sciences, **30**: 819-831.

Staples, R.D., Murphy, D.C., Gibson, H.D., Colpron, M., Berman, R.G., and Ryan, J.J. 2014. Middle Jurassic to earliest Cretaceous mid-crustal tectono-metamorphism in the northern Canadian Cordillera; recording foreland-directed migration of an orogenic front. Geological Society of American Bulletin, **126**: 1511-1530.

Steckler, M.S., and Watts, A.B. 1978. Subsidence of the Atlantic-type continental margin off New York. Earth and Planetary Science Letters, **41**: 1-13.

Stevens, C.H., and Rycerski, B. 1989. Early Permian colonial rugose corals from the Stikine River area, British Columbia, Canada. Journal of Paleontology, **63**: 158-181.

Sun, S.S., and McDonough, W.F. 1989. Chemical and isotopic systematic of oceanic basalts; implications for mantle composition and processes. *In* Magmatism in the Ocean Basins. *Edited by* A.D. Saunders, and M.J. Norry, Geological Society [London] Special Publication **42**: 313-345.

Swinden, H.S. 1991. Paleotectonic settings of volcanogenic massive sulphide deposits in the Dunnage Zone, Newfoundland Appalachians. Canadian Institute of Mining Bulletin **84**:59–89.

Swinden, H.S. 1996. The application of volcanic geochemistry in the metallogeny of volcanic-hosted sulfide deposits in central Newfoundland. *In* Trace Element Geochemistry of Volcanic Rocks: Applications for Massive Sulfide Exploration. *Edited by* D.A. Wyman; Geological Association of Canada, Short Course Notes, **12**: 329-358.

Swinden, H.S., Jenner, G.A., Kean, B.F., and Evans, D.T.W. 1989. Volcanic rock geochemistry as a guide for massive sulphide exploration in central Newfoundland Current Research. Newfoundland Department of Mines. pp 201–219.

Syme, E.C., Lucas, S.B., Bailes, A.H., and Stern R.A. 1999. Contrasting arc and MORB-like assemblages in the Paleoproterozoic Flin Flon Belt, Manitoba, and the role of intra-arc extension in localizing volcanic hosted massive sulphide deposits. Canadian Journal of Earth Science, **36**: 1767-1788.

Tamura, Y., and Tatsumi, Y. 2002. Remelting of an andesitic crust as a possible origin for rhyolitic magma in oceanic arcs: an example from the Izu-Bonin arc. Journal of Petrology **43**, 1029–47.

Taylor, C. D., Premo, W. R., Meier, A. L., Taggart, J E, Piercey, S. J., Peter, J. M., and Mortensen, J. K. 2008. The metallogeny of Late Triassic rifting of the Alexander terrane in southeastern Alaska and northwestern British Bolumbia. Economic Geology and the Bulletin of the Society of Economic Geologists, **103**: 89-115.

Thériault, R. J. 1990. Methods for Rb-Sr and Sm-Nd isotopic analyses at the geochronology laboratory, Geological Survey of Canada. Geological Survey of Canada Paper 89-02, pp. 3-6.

Thomson, R.C., Smith, P.L., and Tipper, H.W. 1986. Lower to Middle Jurassic (Pliensbachian to Bajocian) stratigraphy of the northern Spatsizi area, north-central British Columbia. Canadian Journal of Earth Sciences, **23**: 1963-1973.

Thorkelson, D.J. 1992. Volcanic and Tectonic Evolution of the Hazelton Group in the Spatsizi River (104H) map-area, North-Central British Columbia. Ph.D. thesis, Department of Earth Sciences, Carleton University, Ottawa, Ont.

Thorkelson, D.J., Mortensen, J.K., Marsden, H., and Taylor, D.C. 1995. Age and tectonic setting of Early Jurassic episodic volcanism along the northeastern margin of the Hazelton Trough, northern British Columbia. *In* Jurassic magmatism and tectonics of the North American Cordillera. *Edited by* D.M. Miller and C.J. Busby. Geological Society of America Special Paper **299**: 83–94.

Till C.B., Gans P.B., Spera F.J., MacMillan I., and Blair K.D. 2009. Perils of petrotectonic modeling: A view from southern Sonora, Mexico. Journal of Volcanology and Geothermal Research, **186**: 160–168.

Tipper, H.W. and Richards, T.A. 1976. Jurassic stratigraphy and history of north-central British Columbia. Geological Survey of Canada, Bulletin **270**, 73 p.

Vallance, T.G. 1974. Spilitic degradation of a tholeiitic basalt. Journal of Petrology, **15**: 8-52.

Van der Heyden, P. 1992. A Middle Jurassic to Early Tertiary Andean-Sierran arc model for the Coast Belt of British Columbia. Tectonics, **11**: 82-97.

Vaskovic, M.S. and Huggins, C. 1998. Assessment Report on Rock and Stream Geochemical Sampling on the PBR Property. BC Ministry of Energy and Mines, Assessment Report No. 25,777, 20p.

Waldron, J.W.F., and Gagnon, J.-F. 2011. Recognizing soft-sediment structures in deformed rocks of orogens. Journal of Structural Geology, **33**: 271–279.

Waldron, J.W.F., Gagnon, J.-F., Loogman, W., and Evenchick, C.A. 2006. Initiation and deformation of the Jurassic-Cretaceous Bowser Basin: implications for hydrocarbon exploration. *In* Geological Fieldwork 2005. British Columbia Ministry of Energy, Mines and Petroleum Resources, Paper 2006-1, pp. 349-360.

Whalen, J. B. 1985. Geochemistry of an island-arc plutonic suite; the Uasilau-Yau Yau intrusive complex, New Britain, P.N.G. Journal of Petrology, **26**: 603-632.

Whalen, J. B., Currie, K. L., and Chappell, B. W. 1987. A-type granites; geochemical characteristics, discrimination and petrogenesis. Contributions to Mineralogy and Petrology, **95**: 407-419.

Wheeler, J.O., Brookfield, A.J., Gabrielse, H., Monger, J.W.H., Tipper, H.W., and Woodsworth, G.J. 1991. Terrane map of the Canadian Cordillera. Geological Survey of Canada, Map 1713A, scale 1:2,000,000.

Winchester, J. A. and Floyd, P. A. 1976. Geochemical Magma Type Discrimination: Application to altered and metamorphosed basic igneous rock. Earth and Planetary Letters, **28**: 459-469.

Winchester, J. A. and Floyd, P. A. 1977. Geochemical discrimination of different magma series and their differentiation products using immobile elements. Chemical Geology **20**: 325–343.

Wood, D. A. 1980. The application of a Th-Hf-Ta diagram to problems of tectonomagmatic classification and to establishing the nature of crustal contamination of basaltic lavas of the British Tertiary volcanic province. Earth and Planetary Science Letters, **50**: 11-30.

Woodhead, J.D. 1988. The origin of geochemical variations in Mariana lavas: a general model for petrogenesis in intraoceanic island arcs? Journal of Petrology **29**: 805–30.

Woodhead, J., Eggins, S., and Gamble, J. 1993. High field strength and transition element systematics in island arc and back-arc basin basalts; evidence for multi-phase melt extraction and a depleted mantle wedge. Earth and Planetary Science Letters, **114**: 491-504.

Woodsworth, G.J., Hill, M.L., and Van der Heyden, P. 1985. Preliminary geologic map of Terrace (NTS 103I East Half) map area, British Columbia. Geological Survey of Canada, Open File 1136.

Wotzlaw, J-F., Guex, J., Bartolini, A., Gallet, Y., Krystyn, L., McRoberts, C.A., Taylor, D., Schoene, B., and Schaltegger, U. 2014. Towards accurate numerical calibration of the Late Triassic: High-precision U-Pb geochronology constraints on the duration of the Rhaetian. Geology, **42**: 571-574.

Wright, I.C., Worthington, T.J., and Gamble, J.A. 2006. New multibeam and geochemistry of the 30◦–35◦ S sector, and overview, of southern Kermadec arc volcanism. Journal of Volcanology and Geothermal Research **149:** 263–96.

Wyman, D.A. 1999. A 2.7 Ga depleted tholeiite suite: evidence of plume-arc interaction in the Abitibi greenstone belt, Canada. Precambrian Research **97**: 27–42.

Wyman, D.A., Bleeker, W., and Kerrich, R. 1999. A 2.7 Ga komatiite, low Ti tholeiite, arc tholeiite transition, and inferred proto-arc geodynamic setting of the Kidd Creek deposit; evidence from precise trace element data. Economic Geology Monograph, **10**: 511–528.

Yang, K., and Scott, S.D. 2002. Magmatic degassing of volatiles and ore metals into a hydrothermal system on the modern sea floor of the eastern Manus back-arc basin, western Pacific. Economic Geology, **97**: 1079–1100.

Yang, K., and Scott, S.D. 2005. Vigorous exsolution of volatiles in the magma chamber beneath a hydrothermal system on the modern sea floor of the eastern Manus back-arc basin, western Pacific; evidence from melt inclusions. Economic Geology, **100**: 1085–1096.

Zack, T., and John, T. 2007. An evaluation of reactive fluid flow and trace element mobility in subducting slabs. Chemical Geology, **239**: 199-216.

Appendix A: Supplemental Articles

A.1: Nelson, J., Barresi, T., Knight, E., and Boudreau, N. 2006a. Geology and Mineral Potential of the Usk Map Area (NTS 103I/09), Terrace, British Columbia. In Geological Fieldwork 2005, British Columbia Ministry of Energy and Mines, British Columbia Geological Survey Paper 2006-1, p. 149-162.

Geology and Mineral Potential of the Usk Map Area (NTS 103I/09), Terrace, British Columbia

JoAnne Nelson, Tony Barresi[1], Ellie Knight[2] and Nicole Boudreau[3]

KEYWORDS: Telkwa Formation, Terrace, Skeena River, Hazelton Group, Kitselas, Stikinia, vein deposits, copper deposits

INTRODUCTION

The Usk map area spans the valley of the Skeena River and its tributaries, over a 530 km^2 area north and east of the town of Terrace, British Columbia (Fig. 1, 2). It includes the lower parts of the Zymoetz (= Copper) River and Kleanza Creek, which flow southwest from their remote headwaters in the Howson Range between Terrace and Telkwa. Chimdemash, St. Croix and Legate creeks drain the Mount O'Brien massif east of the Skeena River. Tributaries west of the river are Carpenter, Sand, Hardscrabble, Shannon, and Lowrie creeks. The topographic names suggest episodes in a long history of settlement. Zymoetz is an ancient name describing the spread of translucent pale blue colour where its waters join the turbid, brown Skeena River. Hardscrabble refers to early placer mining work; Ste.-Croix and Legate were prospectors. Mount O'Brien was named for a young Terrace man killed in World War II.

Within the Usk map area, there are sites and communities that date from roughly 5000 BP to the present day (Berthiaume, 1999). The sites at Kitselas canyon range from ancient encampments to the prosperous village of Gitlaxdzawk, which dominated the Skeena's rocky western bank in historic times. Based on trade and taxation of river traffic, it flourished up to about 1860–1880, when disease and depopulation wiped the settlement out. In the late 1800s, steamboat traffic turned the Skeena River into a major corridor to the interior and a new town, also named Kitselas, was built south of the canyon. The construction of the railroad from 1910 to 1914 refocused communities: the new Kitselas was abandoned and small settlements grew up beside the railroad. Usk was one of these. It is now accessed by a reaction ferry from the highway that was built east of the river in the early 1940s. Terrace itself arose as the railroad and highway developed, and grew with the logging industry. Its northeastern suburb of Thornhill extends into the Usk map area (Fig. 2). A new community, Gitaus, sited on a gravel bench east of the Skeena, has been developed by the Kitselas First Nation over the last 15 years.

[1]*Department of Earth Science, Dalhousie University, Halifax, NS*

[2]*Department of Earth Science, Simon Fraser University, Vancouver, BC*

[3]*Department of Geology, St. Mary's University, Halifax, NS*

This publication is also available, free of charge, as colour digital files in Adobe Acrobat PDF format from the BC Ministry of Energy, Mines and Petroleum Resources internet website at http://www.em.gov.bc.ca/Mining/Geolsurv/Publications/catalog/catfldwk.htm

EXPLORATION HISTORY

The role of mineral exploration in the local economy has waxed and waned through time. The Tshimshian word Kleanza means 'gold', an indication of early placer activity. The opening of the Skeena as a major river route, and the construction of the railway, brought prospectors into the country. Discoveries followed. More than 10 prospects, mainly gold-quartz veins and copper-silver massive sulphide mineralization, eventually saw at least limited production between 1890 and 1942. On a voters list from Kitselas in 1909, 25% of the male population stated their profession as 'miner' (Bennett, 1997, p. 172). In the early 1900s, up to a hundred prospecting parties might be out in a given summer (W. McRae, pers. comm., 2005). Horse trails were built to access workings through tens of miles of arduous mountain valleys and over steep ridges. One such trail joined the headwaters of Chimdemash and Ste.-Croix creeks via 67 switchbacks.

The coming of the Depression and World War II put an end to most of the mining activity. Forest wealth fueled the next economic resurgence. Small mills had been built near the railroad beginning in 1910. During World War I, Sitka spruce from the Skeena River valley was in high demand for airplane construction. Mill development intensified with the opening of the highway during World War II. The Skeena Mill (originally Skeena Forest products) was built in 1960. Between 1950 and 1990, extensive networks of logging roads were constructed into all of the valleys in the area. They offer excellent access to remote locations; however, most of them are presently deactivated and becoming increasingly difficult as routes of travel.

Terrace has a small but active prospecting community. However, compared to well-known mining camps such as Smithers and the Iskut-Stikine region, the area has seen a modest level of modern mineral exploration. In the Usk area, for instance, there are 80 listed mineral occurrences (MINFILE, 2005), but only 25 assessment reports were filed during the period 1980–2004. Most of the work has been done on behalf of individuals and small companies.

In the last three years, there has been a minor resurgence in local mineral exploration. Between 2003 and 2005, Eagle Plains Resources Ltd. has been exploring the bulk tonnage Au and Cu-Mo potential of its large Kalum property north of Terrace (Mihalynuk and Friedman, 2005). The Dardanelle Au-quartz vein mine (MINFILE 103I107) and the Treasure Mountain Cu property (MINFILE 103I090), both of them located immediately south of the Usk map area, were explored and drilled in the summer of 2005. Exploration work continues on a system

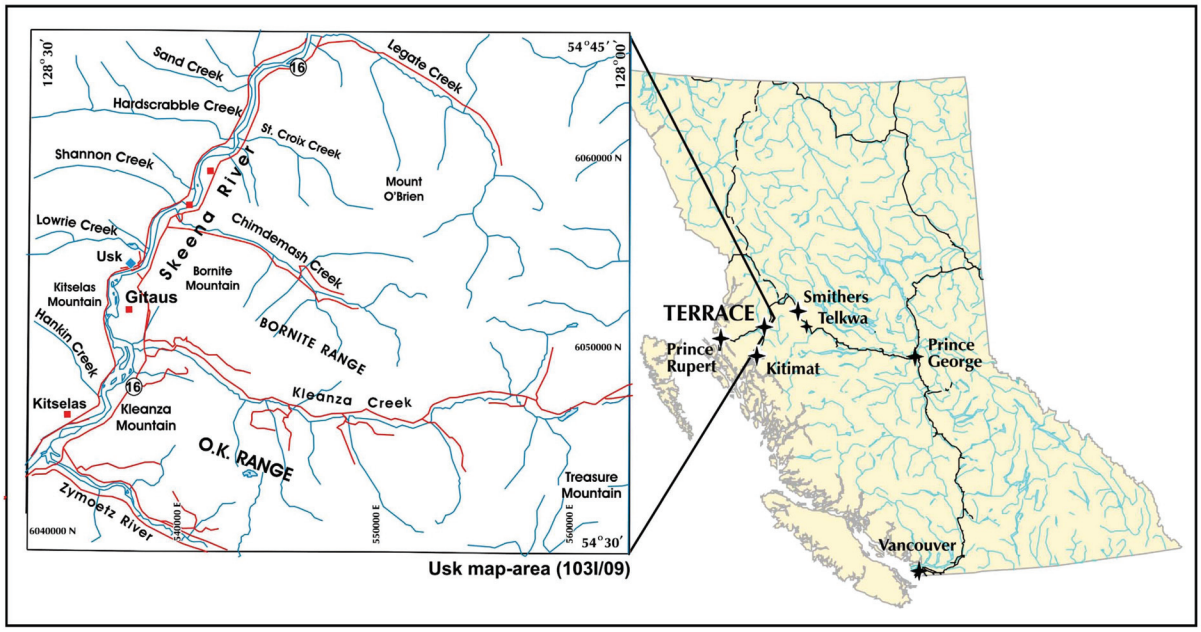

Figure 1. Location and physiography of Terrace, BC, and the Usk map area.

of veins and replacement-style occurrences, the Zona May (MINFILE 103I060) and M&K (MINFILE 103I065) in the upper Legate Creek drainage and Silver Basin in the upper Chimdemash drainage (MINFILE 103I065), by Argonaut Resources (Salat, 2005).

THIS PROJECT

Coastal and northwestern BC are relatively poorly covered by 1:50 000-scale regional geological mapping. At present, roughly 18% of the province has been mapped at 1:50 000 scale. Within NTS 103I, the large-scale sheet that includes Terrace, no 1:50 000-scale mapping is available, except for focused thesis work (Mihalynuk, 1987; Heah, 1991). The Terrace regional mapping project was initiated in 2005, in recognition of this knowledge gap and its potential effect on exploration interest in the area. Results for the Usk map area (NTS 103I/09) will be released as an open file map (Nelson *et al.*, 2006).

In connection with the present study, part of a Ph.D. thesis by Tony Barresi of Dalhousie University will address the volcanic stratigraphy and geochemistry of the Telkwa Formation (Barresi and Nelson, 2006), while an Honours B.Sc. thesis by Nicole Boudreau of St. Mary's University will examine the relationship between the Kitselas volcanic unit and the Hazelton Group.

This project was a cooperative effort between the BC Geological Survey Branch and the Resource Management Department of the Kitselas First Nation (KFN). In the summer of 2005, one BCGS geologist, three geology students and three KFN resource technicians surveyed the Usk map area, using trucks, bicycles and helicopter-supported fly camps. A total of 560 km^2 was mapped, including 160 linear kilometres of roads.

REGIONAL GEOLOGY

Terrace lies within the western extent of Stikinia, one of the intermontane terranes, a large crustal block dominated by the products of episodic Paleozoic through mid-

Figure 2. Looking north along the Skeena River from Thornhill, BC, with Kitselas Mountain on the western skyline and Bornite Mountain and Mount O'Brien on the east.

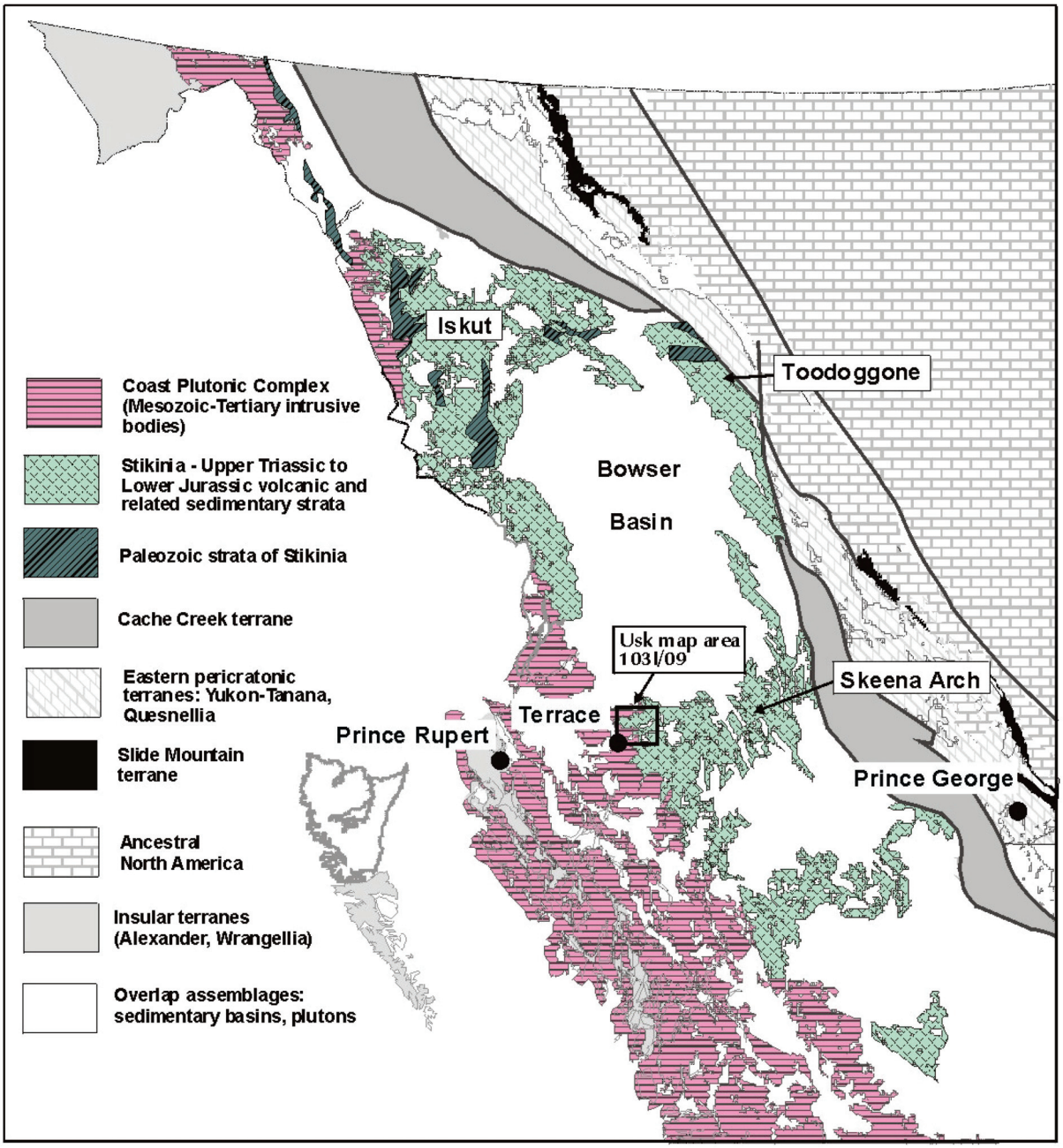

Figure 3. Tectonic setting of Terrace, BC in western Stikinia, on the eastern border of the Coast Plutonic Complex.

Jurassic island-arc magmatic activity (Fig. 3; Monger *et al.*, 1991).

Terrace also lies on the eastern fringe of the Coast Plutonic Complex, a linear belt dominated by granitoid and metamorphic rocks that occupies most of coastal BC. The Coast Plutonic Complex is the deeply eroded and tectonically denuded roots of the mid-Jurassic to Eocene successor arc, which developed along the new western margin of North America following accretion of the intermontane and insular terranes to the continent (van der Heyden, 1992).

Previous 1:250 000-scale mapping (Duffell and Souther, 1964; Woodsworth *et al.*, 1985) shows the general geological features of the Terrace area, which are refined by mapping of the present project (Fig. 4; see Nelson *et al.* [2006] for greater detail).

The oldest recognized stratigraphic unit is a section of upper Paleozoic volcanogenic rocks and limestone, corre-

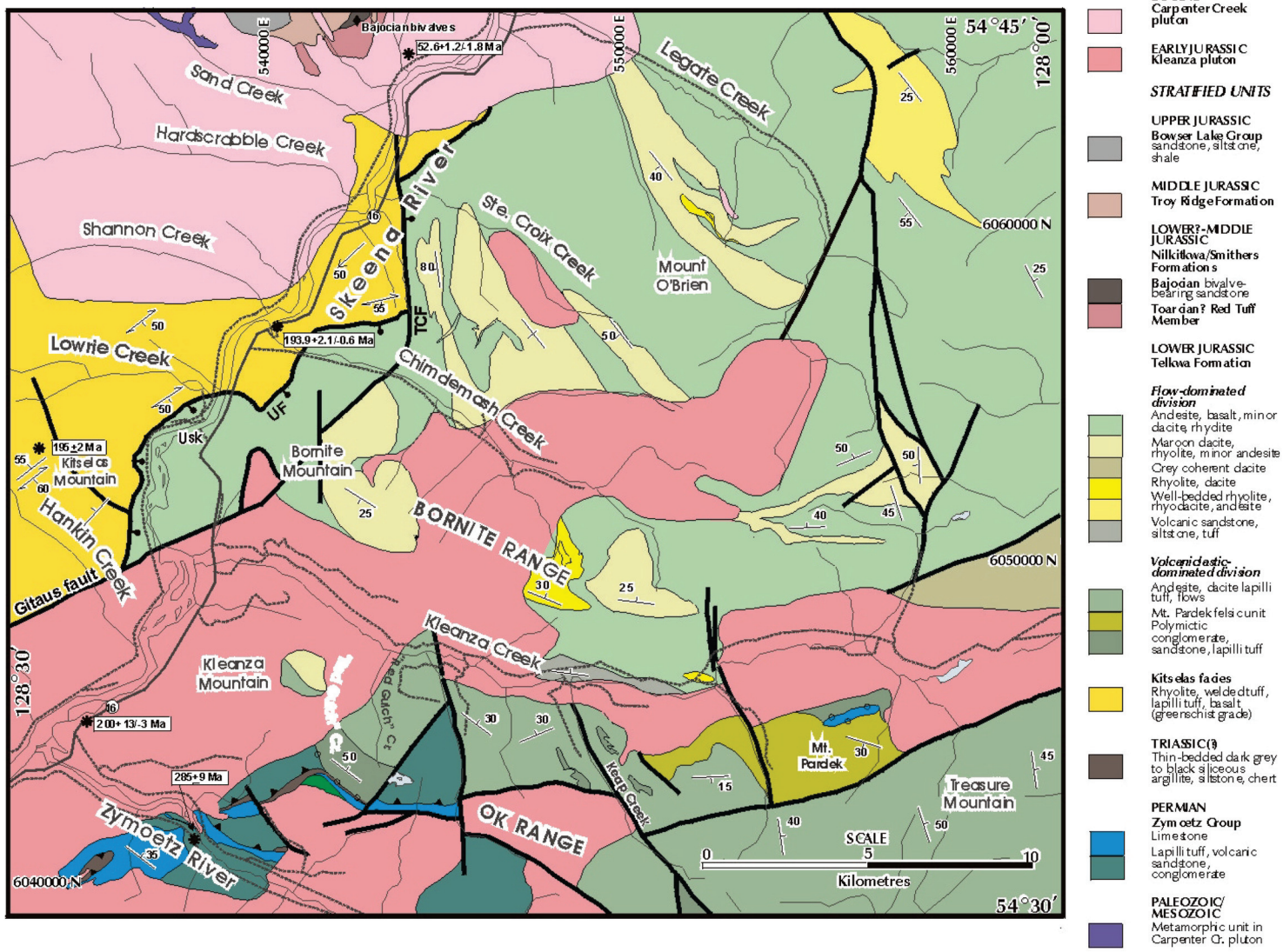

Figure 4. Geology of the Usk map area (NTS 103I/09), near Terrace, BC.

lative with younger strata in the Stikine 'assemblage' in the Iskut-Stikine area (Brown *et al.*, 1996; Logan *et al.*, 2000). It is overlain by Triassic sedimentary strata, which are in turn overlain by the primarily intermediate to felsic volcanogenic rocks that belong to a lower portion of the Hazelton Group, equivalent to the Telkwa Formation in the Smithers area (Tipper and Richards, 1976). North of the Usk map area, Telkwa strata are overlain by the Nilkitkwa, Smithers and Ashman formations and the Bowser Lake Group (Woodsworth *et al.*, 1985, and G. Woodsworth, unpublished mapping, 2006). Small exposures of these rocks occur within the Usk map area near Sand Creek.

Voluminous plutonic rocks occupy much of the drainages of the Zymoetz River and Kleanza Creek. Woodsworth *et al.* (1985) assigned them a Jurassic and/or Cretaceous age. Presently, published and unpublished zircon ages suggest that they are entirely Early Jurassic (*ca.* 200 Ma; Gareau *et al.*, 1997a; G. Woodsworth, pers. comm., 2005). The main body, termed the Kleanza pluton by Gareau *et al.* (1997b), is probably comagmatic with the Telkwa Formation. These rocks contrast with plutons in drainages to the west of the Skeena River, which are Eocene and belong to the Coast Plutonic Complex (Gareau *et al.*, 1997a, b).

A distinctive, mainly felsic volcanic unit underlies the Skeena valley between Gitaus and St. Croix Creek, and extends into the mountains west of the river. It has been named the Kitselas volcanic rocks, from a type locality on Kitselas Mountain (Gareau *et al.*, 1997b). Locally strong foliation and development of greenschist-facies mineral assemblages in this unit led to early interpretations of a Paleozoic age (Duffell and Souther, 1964). Gareau *et al.* (1997a) reported U-Pb zircon ages of *ca.* 194 and 195 Ma from this unit, coeval with the Telkwa Formation regionally (Marsden and Thorkelsen, 1992), and coeval with or slightly younger than the age of the Kleanza pluton locally. G. Woodsworth (unpublished data, 2006; pers. comm; see also Gareau *et al.*, 1997b) proposed that the comparatively high metamorphic grade and structural relationships of the Kitselas volcanic unit to the Telkwa Formation are suggestive of a detachment fault relationship. In this model, the Kitselas volcanic unit would lie in the footwall of an easterly-dipping detachment fault, with the zeolite-grade Telkwa Formation in its hangingwall.

A large, relatively undeformed bulbous pluton of Eocene age (53 Ma; Gareau *et al.*, 1997a) intrudes both the Kitselas volcanic unit and the Telkwa Formation in the northwestern part of the map sheet. Thus, motion on a fault between them must have ceased before this time. On the other hand, a 56 Ma pluton contains fabrics analogous to those in the Kitselas volcanic unit; Gareau *et al.* (1997a, b) considered it to be involved in the detachment-related deformation. Given these constraints, detachment faulting must have taken place in mid-Eocene time, coeval with other recognized crustal shear zones such as the Shames River shear zone west of Terrace (Heah, 1991).

LOCAL GEOLOGY

Detailed mapping of the Usk map area in 2005 (Fig. 4) focused on aspects of the regional geology that remain problematic, particularly those relating to mineral exploration models. The following questions formed the framework for investigation:

- What are the structural and stratigraphic relationships of the Triassic and Jurassic rocks to the underlying Paleozoic section? On one hand, the basal Telkwa Formation has been interpreted locally as Triassic to Jurassic in age (Gareau *et al.*, 1997b); regionally, on the other hand, it is restricted to the Early Jurassic (Tipper and Richards, 1976; Marsden and Thorkelsen, 1992).
- What was the nature and paleogeography of Telkwa volcanism? Prior to this study, the Telkwa Formation remained undivided in the Terrace area, except for one east-west transect south of the Usk map area (Mihalynuk, 1987).
- What are the nature and morphology of the Early Jurassic Kleanza pluton, and what is its relationship to the Telkwa Formation, which it intrudes?
- What are the volcanology and geochemistry the Kitselas volcanic unit, and what was its primary relationship to the Telkwa Formation?
- What is the nature of the structural boundary between the Kitselas volcanic unit and the Telkwa Formation?

Stratified Units

ZYMOETZ GROUP (NEW NAME)

A section of Permian volcanogenic and marine sedimentary strata, including thick limestone, outcrops within and south of the lower Zymoetz River valley (see Duffell and Souther, 1964; Woodsworth *et al.*, 1985). The authors propose that this isolated exposure, located 250 km south of the upper Paleozoic belt of northern Stikinia, be (informally) named the Zymoetz group.

Within the Usk map area, the Zymoetz group outcrops on Copper and Thornhill Mountains, and on the southern slopes of the OK Range (Fig. 4). It is divided into two units, limestone (uPls) and a mixed volcanogenic unit (Pvs) that includes pyroclastic and volcanic-derived sedimentary strata. The volcanogenic unit is highly variable; it includes coarse to fine lapilli and crystal-ash tuffs, well-bedded volcanic sandstone and polymictic volcanic conglomerate. Lapilli tuff ranges from mono to polymictic, and fragments range in size from dominantly sand to dominantly boulders. Clasts are mainly andesitic in composition, with subordinate quartz-phyric dacite and scattered limestone fragments. Plagioclase phenocrysts are ubiquitous; clinopyroxene is common in the andesite. Along the Zymoetz River, unstratified, dark green crystal-ash tuff predominates.

Conglomerate includes clasts derived from the lapilli tuff, as well as limestone and red to white, highly siliceous rocks that may be either rhyolite or chert, neither of which was observed *in situ*. They grade both into lapilli tuff and into volcanic sandstone. Green volcanic sandstone is well bedded and better sorted than the tuff. It interfingers with the limestone. Limy matrix is common, and aids in distinguishing it from Telkwa volcaniclastic units. Macrofossils occur on bedding planes in black shale, and isolated within volcanic sandstone beds.

Limestone in the Zymoetz group shows a strong variability in character. On top of Copper Mountain, outcrops are of pure, white to light grey crystalline marble with local

thin colour banding. This unit appears to be nonfossiliferous. On the northern slopes of Copper Mountain and along the road north of the Zymoetz River, thick-bedded grey limestone is interbedded with green volcanic sandstone that grades into crystal-lithic tuff. In both cases, the volcanogenic unit depositionally overlies the limestone. This limestone contains a wealth of macrofossils, including rugose corals, bryozoans and crinoids. Limestone in an isolated exposure southwest of Kleanza Lake is interbedded with laminated, siliceous green tuff and felsic conglomerate. Overall, the intimate relationships of limestone and volcanogenic strata are suggestive of a series of limy banks and small redeposited reefs that developed on an active arc edifice.

The Zymoetz group is dated both by macrofossils and by U-Pb zircon methods. Duffell and Souther (1964) reported extensive coral and brachiopod collections of Permian age, and Gareau *et al.* (1997a) obtained an Early Permian U-Pb age of *ca.* 285 Ma from lapilli tuff on the O.K. Range. These rocks correlate with Permian units in the Iskut-Stikine area (Brown *et al.*, 1996; Logan *et al.*, 2000). The limestone is age equivalent to the Ambition Formation of Gunning *et al.* (1994). One difference is that Zymoetz group limestone interfingers extensively with volcanic-derived clastic deposits, whereas the Ambition Formation contains almost no volcanic material and is interpreted to postdate arc volcanism.

TRIASSIC (?) SEDIMENTARY STRATA

Near the crest of the western O.K. Range, a distinctive unit intervenes between the highest exposure of Permian limestone and the Telkwa basal conglomerate. It consists of less than a hundred metres of thin-bedded, black and grey-laminated radiolarian chert. Bedding in it is roughly conformable with its external contacts, which are covered. This unit is considered to be of Triassic age (Duffell and Souther, 1964; G. Woodsworth, unpublished map, 2006). It resembles Middle Triassic chert in the Iskut-Stikine area (Logan *et al.*, 2000), as well as the Triassic Teh Formation on the BC-Yukon border (Roots *et al.*, in press). Radiolarians collected in this project will be evaluated paleontologically.

A band of thin-bedded black chert occurs in logging cut exposures farther downslope in the Zymoetz River valley, between two panels of Zymoetz group strata (Fig. 4). Bedding attitudes in it are highly variable and generally not parallel to its external contacts. The western contact is interpreted as a thrust fault that repeats Permian and Triassic strata. Similarly, coal black argillite and chert between Copper and Thornhill mountains, which lies structurally below white Permian marble, is interpreted as another Triassic unit in the footwall of a thrust fault.

TELKWA FORMATION (LOWER JURASSIC)

Overview

The Telkwa Formation of the Hazelton Group is the most widespread stratigraphic unit in the Usk map area (Fig. 4). It consists wholly of volcanic and volcanic-derived strata: mostly andesite and dacite but with some basalt and local rhyolitic centres. Stratigraphic relationships in it are complex, due to the irregularity of topography in volcanic environments, abrupt changes in volcanic facies, synvolcanic faulting and the localization of felsic accumulations.

At its base in the western O.K. Range, a polymictic conglomerate unconformably overlies thrust-imbricated Triassic and Paleozoic strata (Fig. 4). The conglomerate interfingers upward with a thick unit of andesitic and lesser dacitic volcaniclastic deposits and minor flows. This unit is divided into the informally named O.K. Range – Treasure Mountain and Kleanza Creek sections by an east-striking fault. The Kleanza Creek section underlies part of the southern slope of the Kleanza Creek valley, overlying (and interfingering with?) a local accumulation of felsic volcaniclastic rocks on Mount Pardek. Andesitic volcaniclastic and sedimentary strata north of Kleanza Creek are overlain by an extensive, flow-dominated unit, the Mount O'Brien section, which comprises andesite, dacite, rhyolite and basalt in decreasing order of abundance. Andesite constitutes about 70% of the unit, dacite 25% and rhyolite 5%. Three distinct rhyolitic centres have been identified in this section.

Conglomerate

Polymictic conglomerate is most abundant at the base of the Telkwa Formation, although lenses of it also occur

Figure 5. a) Polymictic conglomerate near the base of the Telkwa Formation in the western OK Range, containing pink and green siliceous volcanic rocks, chert, limestone, plagioclase and pyroxene-phyric andesite and dacite. b) Detail of pink, crinoidal limestone clast in conglomerate.

stratigraphically higher, interbedded with andesitic lapilli tuff and volcanic sedimentary intervals. It contains both intraformational (andesite, dacite and rhyolite) and extraformational (limestone, black chert, andesite, dacite and rhyolite) clasts (Fig. 5a).

Because both the Zymoetz group and Telkwa Formation are the remnants of mainly intermediate to felsic island arc edifices, distinction between clasts sourced from them must rely on subtle differences of composition and texture. For instance, clinopyroxene and quartz phenocrysts are much more abundant in the Permian volcaniclastic units, whereas well-formed, lath-shaped plagioclase predominates in the basal Telkwa.

Local clast composition of the conglomerate varies considerably. In some areas, limestone clasts are abundant; in others they constitute less than 1% of the population. Fossiliferous clasts contain corals, brachiopods and bryozoans, clearly reflecting their Permian source (Fig. 5b). Near the black Triassic chert band, the base of the conglomerate contains concentrations of black chert clasts.

The basal conglomerate is very coarse and thick bedded. Conglomerate higher in the section is finer grained, and interbedded with sandstone, siltstone and Telkwa lapilli tuff. Rare clasts of limestone in lapilli tuff on the west slope of Treasure Mountain, far upsection from the basal conglomerate, hint at continued (fault-related?) exposure of pre-Jurassic rocks during eruption and deposition of the Telkwa Formation.

O.K. Range – Treasure Mountain Section

From the middle of the O.K. Range east to Treasure Mountain and beyond, a section dominated by maroon and green andesitic volcaniclastic strata dips homoclinally to the east. In addition to andesite lapilli tuff, it comprises about 15% andesite flows, 5% thin intervals of fine-grained volcanic-derived sedimentary beds and 5% dacite lapilli and crystal-ash tuffs. Its basal contact with the conglomerate unit is an interpreted fault; however, rocks in this section are identical to those in the Kleanza Creek section, which demonstrably overlie and interfinger with the conglomerate. The two sections are separated by an east-striking, north-side-down normal fault (Fig. 4).

Andesitic lapilli tuff in the O.K. Range – Treasure Mountain section is thick bedded, ranging from coarse to fine clast dominated, and monomictic to polymictic. Overall, the clasts are mostly plagioclase phyric, with minor local hornblende and clinopyroxene (Fig. 6a).

Textural variations from unit to unit involve percentage and size of phenocrysts, which are typically lath shaped, euhedral and 2–5 mm long. Some tuff units contain crowded porphyritic and fine grained, holocrystalline clasts that tend to be strongly epidotized (Fig. 6b). The authors interpret these as hypabyssal clasts altered in place, prior to incorporation in an explosive eruptive unit. Similar alteration patches were observed in the Kleanza pluton in the Bornite Range.

Andesite flows are coherent, tabular to lensoid units 20–200 m thick, that in places grade through brecciated into lapilli tuff. Volcanic textures are identical to those in the tuff. These flows are only locally amygdaloidal, in contrast to flows in the Mount O'Brien section.

Thin units of bedded volcanic sandstone, siltstone and mudstone represent quiescent intervals. Subaqueous deposition is indicated by graded bedding and mudstone rip-up clasts.

Dacitic units are maroon, brick red, light grey, lavender and pink. They comprise lapilli and crystal-ash tuffs and minor coherent dacite. Clasts and coherent portions are very siliceous and aphanitic to glassy, and may contain sparse, very small (<1 mm) feldspar phenocrysts. West of Treasure Mountain, three thin dacitic units occur in association with thin-bedded volcanic sedimentary strata. One of them exhibits a polymictic base, involving andesite clasts from underlying units, and a monomictic top. Degree of welding increases upward within the unit.

Kleanza Creek Section and Mount Pardek

This section extends along the southern slopes of the Kleanza Creek valley, from Kleanza Mountain to Mount Pardek; its sedimentary upper part is exposed near the main logging road north of Kleanza Creek (Fig. 4). In the west, its base consists primarily of andesitic lapilli tuff that transitionally overlies and interfingers with polymictic conglomerate. To the east, the basal unit is the felsic tuff sequence exposed on Mount Pardek, which overlies Permian

Figure 6. a) Coarse-grained Telkwa Formation lapilli tuff from near Treasure Mountain, showing plagioclase-hornblende-phyric clasts with well-formed phenocrysts. b) Epidote-altered clasts in lapilli tuff.

limestone and conglomerate. This, in turn, is overlain by andesitic lapilli tuff and derived sedimentary layers. The authors interpret the Mount Pardek sequence as the products of a nearby felsic centre.

The Mount Pardek sequence consists of thin, quartz-feldspar-phyric flows, water-laid tuff units and resedimented volcaniclastic deposits (Fig. 7).

Although dominantly felsic, it also contains andesitic volcaniclastic layers. Felsic units are typically light pastel green. Unlike other felsic units in the Telkwa Formation, they contain up to 60% clear, euhedral quartz crystals. Evidence of subaqueous deposition includes grading and crude sorting in well-bedded units. They are probably of turbiditic origin. Overall, the sequence is up to 1200 m thick. The dominantly felsic unit grades upward into andesitic lapilli tuff, sandstone and siltstone that are identical to those of the O.K. Range – Treasure Mountain section.

Figure 7. Thick-bedded felsic lapilli tuff, Mount Pardek, looking north across Kleanza Creek to the main logging road.

West of Kipulta Creek, a lower felsic sequence consists of thin-bedded, colour-banded rhyolite tuff and waxy, translucent rhyolite. Lapilli tuff ranges from monomictic to polymictic, with green to pink rhyolite and also quartz-vein clasts. This sequence, like that on Mount Pardek, is overlain by volcaniclastic beds of intermediate composition, including lapilli tuff and maroon, well-bedded sandstone and siltstone.

Between Keap Creek and 'Red Gulch' Creek, andesite lapilli tuff with thin intervals of volcanic sandstone and siltstone overlies and interfingers with the basal Telkwa conglomerate. Polymictic conglomerate with limestone clasts occurs high in the section, particularly on the slopes west of Keap Creek. The conglomerate thickens southward, consistent with a topographic high south of the main Telkwa accumulation.

The northeast-facing sedimentary sequence north of Kleanza Creek is separated from the coarser lapilli tuff by an apophysis of the Kleanza pluton, although it is identical in lithology and bedding attitude to the volcanic-derived sedimentary intervals farther south. It is overlain by andesite flows and coarse lapilli tuff of the Mount O'Brien section along a transitional contact.

Mount O'Brien Section

This widespread unit extends from Kleanza Creek through the eastern and northern boundaries of the map area, including Bornite Mountain, Mount O'Brien and the ridges northeast of Legate Creek (Fig. 8a).

It is dominated by andesite and dacite flow/lapilli tuff eruptive units that alternate on scales of tens to hundreds of metres. The larger dacite bodies are shown on Figure 4. Rhyolite is also present in three separate centres, and aphyric basalt accompanies the andesite in places. In the western part of the section, beds are very thick and alternation between andesite/basalt, dacite and rhyolite occurs over hundreds of metres. East of Legate Creek and in the Treasure Creek area, the section is well bedded, individual flow units are thinner, and alternation between andesite and lesser dacite occurs at a scale too small to depict in regional mapping. These rocks are grouped with the andesite.

Andesite in this section is texturally (and compositionally?) different from that in the volcaniclastic-dominated sections to the south. Plagioclase is tabular rather than lath-shaped, and less euhedral. Synneusis (clumping of individual crystals due to weak attraction on flat faces) gives them a raggedly terminated appearance. Average plagioclase size varies from unit to unit, ranging from a few millimetres to, locally over a centimetre in length. Subsidiary clinopyroxene occurs in some of the flows. Mount O'Brien andesite flows tend to be amygdaloidal, from abundant tiny pinpricks to irregular, zeolite±quartz±epidote±chlorite±pumpellyite-filled cavities many centimetres across (Fig. 8b).

Dacite units are composite, consisting of coherent flows and flow breccias, lapilli tuff, welded to nonwelded tuff with lithic and pumice fragments, and less common crystal tuff (Fig. 8c). Texturally, they resemble the much less extensive dacite south of Kleanza Creek. Colours range from maroon to brick red to pastel shades of lavender, pink, cream and orange. All of these rocks are markedly more siliceous than the andesite. They are aphyric to finely porphyritic, with a small percentage of tiny, submillimetre plagioclase phenocrysts.

Three significant accumulations of rhyolitic volcanic rock occur within the Mount O'Brien section: they are located in the middle of the Bornite Range southwest of the headwaters of Chimdemash Creek, north of Mount O'Brien, on the northernmost ridge and cirques between St. Croix and Legate Creeks; and in the northeastern portion of the map area northwest of the headwaters of Legate Creek. These units are typically closely associated with minor amounts of dacite, basalt and andesite, but have been mapped at 1:50 000 scale wholly as rhyolite. Pyroclastic rocks within these units include nonwelded to strongly welded lapilli tuff with lithic and pumice fragments; coherent rhyolite (Fig. 8b,c) occurring as thin flows, minor domes and cryptodomes that commonly grade into flow breccia; beds of resedimented felsic debris ranging from conglomerate to sandstone; and local thin-bedded, aphani-

tic, highly siliceous units, which may represent felsic ash tuff or exhalitive chert.

Individual beds range in thickness from less than 1 m to more than 30 m and are normally laterally continuous with little change in volcanic or sedimentary facies. Coherent rhyolite and rhyolite fragments in volcaniclastic deposits are typically highly siliceous, flow banded, aphanitic, semitranslucent and white, pink, orange, lavender or brick red in colour. In these three locations, the high concentration of rhyolitic rocks, especially coherent rhyolite, leads to the interpretation that each location is proximal to a localized centre of felsic volcanism. These units lack the light green pastel colour, abundance of quartz phenocrysts and turbiditic sedimentary structures that characterize the Mount Pardek felsic unit located to the south.

Regional Variations in the Telkwa Formation

A dramatic regional change in the stratigraphy occurs between the O.K. Range – Treasure Mountain and Kleanza Creek sections located in the southern portion of the map area and the Mount O'Brien section in the north. The Mount O'Brien section is dominated by volcanic flows of intermediate composition, and local felsic accumulations that are proximal to eruptive centres; the O.K. Range – Treasure Mountain and Kleanza Creek sections are dominated by volcaniclastic deposits. It is clear that the southern sections represent a more distal volcanic facies than the coherent flows of the northern section (Barresi and Nelson, 2006). The authors propose that the southern sections are a thick accumulation of volcaniclastic material originating from volcanic centres in the Mount O'Brien section. This material was deposited in a subsiding basin south of Kleanza Creek. East-trending faults in the southern sections, particularly the fault separating the O.K. Range – Treasure Mountain section from the Kleanza Creek section, may be original basin-bounding faults. The differences in volcanic facies between the southern and northern sections are not due to a juxtaposition of different positions in a continuous stratigraphic sequence; rather, they represent a geographic change in facies (Barresi and Nelson, 2006).

Kitselas Facies (Lower Jurassic)

The Kitselas facies of the Telkwa Formation is well exposed in a homoclinal, northwest-facing sequence on Kitselas Mountain and the ridge between Shannon and Lowrie creeks. It also outcrops east of the Skeena River between Usk and the ridge north of St. Croix Creek. On Kitselas Mountain, cleavage development is spaced and original textures are very well preserved. The section is predominantly felsic, with >95% dacite or rhyolite along with a minor mafic component of basalt, andesite(?) and diabase. The base of the exposed section, which outcrops on the east side of the Skeena River and at the base of Kitselas Mountain, is primarily coherent rhyolite. The majority of the rocks higher in the section, which form Kitselas Mountain, are thick-bedded volcaniclastic units (Fig. 10a).

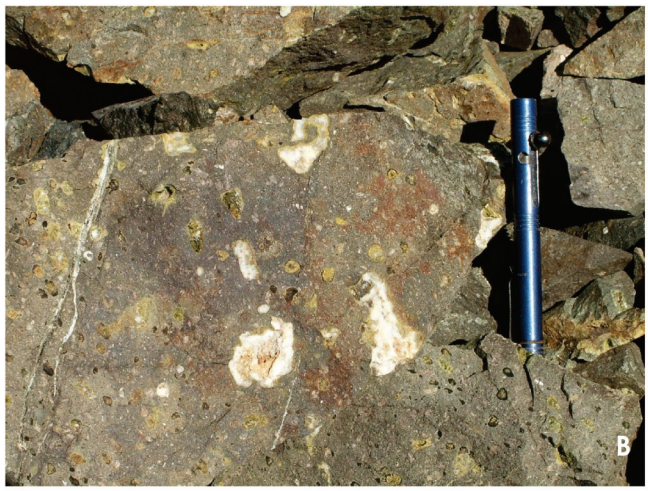

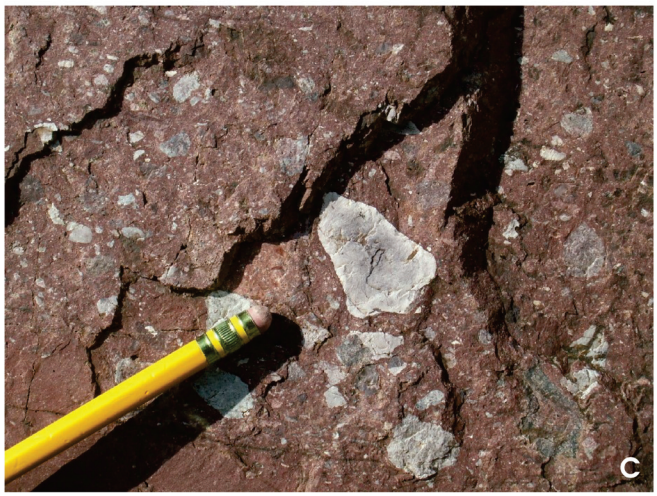

Figure 8. a) South face of Mount O'Brien, showing very thick, maroon andesite flows cut by a gently dipping diorite dike swarm related to the Kleanza pluton. b) Andesite with large, irregular amygdules from the Mount O'Brien section. c) Bright red dacite lapilli tuff with pale siliceous clasts.

The coherent rhyolite is typically medium grey to light purple and aphanitic with rare feldspar microphenocrysts. Flows, which are transitional into flow breccia, have similar characteristics to the larger coherent bodies but are colour and flow banded on a millimetre to centimetre scale. The volcaniclastic portion of the section includes rhyolitic to dacitic lapilli tuffs, welded tuff (Fig. 10b) and rare beds of crystal and/or ash tuffs and resedimented volcanic rocks. Lapilli and welded lapilli tuffs are monolithic, with dominantly sand to pebble-size lapilli. The dominant lapilli compositions are homogeneous aphanitic white, medium purple or grey rhyolite and pumice; minor plagioclase-phyric lapilli and scoriaceous bombs are locally present. Welded tuff exhibits both normal and normal-reverse grading, and the typical aspect ratio of pumice clasts is 1:5. One thin bed of resedimented volcanic rock grades upward from a laminated mudstone base to a conglomerate. Sedimentary structures within this section include flame structures, load casts and crossbeds, which together are suggestive of a subaqueous depositional environment.

Figure 9. Flow-banded rhyolite on the Bornite Range.

Basalt on Kitselas Mountain occurs as three continuous but thin (60–220 m) units. The thickest of these units caps the summit of Kitselas Mountain, and the other two outcrop on its western ridge. They are various shades of blue-grey and are defined by aphanitic, hackly and vesicular to scoriaceous textures. Several zones within the basalt on the Kitselas summit have been thoroughly epidotized, leaving them a brilliant pistachio green colour. These zones are texturally distinguishable from the unaltered basalt, as they have smaller and rarer amygdules and are holocrystalline as opposed to aphanitic. These zones are interpreted to represent proximity to eruptive fissures or centres where hydrothermal alteration would be concentrated. Other mafic rocks within the Kiteselas volcanic unit include minor diabase dikes on the southeast slope of Kitselas Mountain and thin concordant flows or sills exposed on the slopes east of the Skeena River.

Comparison of Kitselas Facies and Felsic Centres Elsewhere in the Telkwa Formation

The Kitselas facies is coeval with the Telkwa Formation (Gareau *et al.*, 1997a); however, its stratigraphic relationship to the Telkwa, locally or regionally, is uncertain. A brief comparison of the physical features of the Kitselas felsic rocks to felsic centres located within the Telkwa Formation in the Usk map sheet is presented here; a more detailed examination, including petrographic and geochemical comparisons is the subject of a B.Sc. thesis currently in progress by Nicole Boudreau.

The Kitselas volcanic rocks are dominantly rhyolitic in composition and consist of a thick section of coherent rhyolite at the base of the exposed section, overlain by an equally thick section of volcaniclastic rocks exposed on Kitselas Mountain. There is no analogue within the Usk map sheet for the thick coherent rhyolite body at the base of the section. However, the exposures of Telkwa felsic centres may be on the flanks of larger, unexposed rhyolite bodies, as is suggested by the thick accumulations of volcaniclastic material in these locations. The upper volcaniclastic section of the Kitselas volcanic rocks is very similar to Telkwa felsic rocks. Both are characterized by similar facies, textures and rock types, and are bedded on a similar scale. The most obvious differences between these rocks are that the Telkwa felsic rocks occur in a wide variety of colours and often have multiple rock types within individual tuff beds, whereas the Kitselas rocks are uniformly white to grey (or rarely purple) and are normally (apparently) monolithic.

Nevertheless, because the Kitselas rocks exhibit higher degrees of metamorphism and alteration, these features found in the Telkwa felsic rocks may simply be obscured in the Kitselas. Although there is no exact analogue for the Kitselas volcanic rocks within the Telkwa in the Usk map area, the physical features of the Kitselas volcanic rocks are consistent with those of the Telkwa.

NILKITKWA AND SMITHERS FORMATIONS

Along logging roads north of Sand Creek, inliers within the Carpenter Lake pluton consist of three units: bright maroon, thin-bedded felsic tuff and basalt; thin-bedded, siliceous and tuffaceous siltstone; and brown sandstone with large bivalve fossils. These units resemble, respectively, the 'Red Tuff' member of the Nilkitkwa Formation (Tipper and Richards, 1976); the so-called 'pyjama beds', correlative with the mid-Jurassic (Toarcian and Bajocian) Troy Ridge and Yuen formations (Tipper and Richards, 1976; Anderson, 1989); and the Smithers Formation (Tipper and Richards, 1976) and Toarcian to Bajocian sandstone intervals within the Eskay belt (Alldrick *et al.*, 2005).

The maroon felsic tuff-basalt unit is distinguished from Telkwa volcanic facies because of the uniformly thin-bedded, fine-grained character of the tuff, interbedded with thin, aphyric, amygdaloidal basalt flows. Accretionary lapilli were noted at one outcrop. The siliceous siltstone unit displays the dark and light colour banding typical of the 'pyjama beds', a lithotype also recognized within the Eskay belt (Alldrick *et al.*, 2005). The brown sandstone, with its lack of obvious chert detritus and abundance of large bivalves, more closely resembles mid-Jurassic clastic

units than it does the Bowser Lake Group. A collection of the bivalves was submitted to T. Poulton of the Geological Survey of Canada for identification. His report (Table 1) indicates a probable early Bajocian age, equivalent to the older part of the Smithers Formation.

In the area north of Sand Creek, G. Woodsworth *et al.* (unpublished mapping, 2006) showed Bowser Lake Group strata overlying the Nilkitkwa and Smithers units described above. These exposures were not visited in 2005.

METAMORPHIC UNIT IN SAND CREEK HEADWATERS

An enclave of metamorphic rocks lies within the Carpenter Lake pluton in the northeastern corner of the map area. They consist of brown, black and grey, variably pyritic hornfels with local limy pods. Microscopically, they contain grains of plagioclase, quartz and minor K-feldspar, along with metamorphic biotite, actinolite and diopside. Their protolith was probably thin-bedded tuffaceous wacke and dirty pelite. A strong, pre-contact metamorphic foliation is present. In character, the unit resembles impure clastic rocks of the Smithers Formation or Paleozoic volcaniclastic rocks of the Zymoetz group, but the exposure was too small to provide definitive information.

Intrusive Units

KLEANZA PLUTON (EARLY JURASSIC)

The Kleanza pluton is a large, sprawling, heterogeneous body with apophyses along the Zymoetz River, Kleanza Creek and southeast of Mount O'Brien (Fig. 4). It has been dated as Early Jurassic (*ca.* 200 Ma U-Pb date on zircon; Gareau *et al.*, 1997a). As is typical of intermontane plutons of this age (*cf.* Woodsworth *et al.*, 1991), it varies texturally from fine grained to porphyritic to coarse grained equigranular, and compositionally from gabbro to granite. Its marginal phases tend to be more mafic than those in its interior, and more variable. On Copper Mountain, for instance, microdiorite (a fine-grained, salt and pepper rock composed of 60% plagioclase and 40% pyroxene) alternates on a 10 m scale with porphyritic intrusive andesite, gabbro and very coarse grained hornblende pegmatite bodies. Microdiorite is common within the southwestern part of the pluton. Because of its fine-grained nature, it can be difficult to distinguish from similarly textured extrusive units. Key diagnostic features are the absence of phenocrysts, amygdules and fragmental textures.

South of Mount O'Brien, fine-grained border phases of the Kleanza pluton include pink plagioclase-phyric monzonite and green andesite that is texturally identical to nearby flows, except for its lack of amygdules and unstratified character. This part of the pluton is possibly a feeder to Telkwa extrusive units.

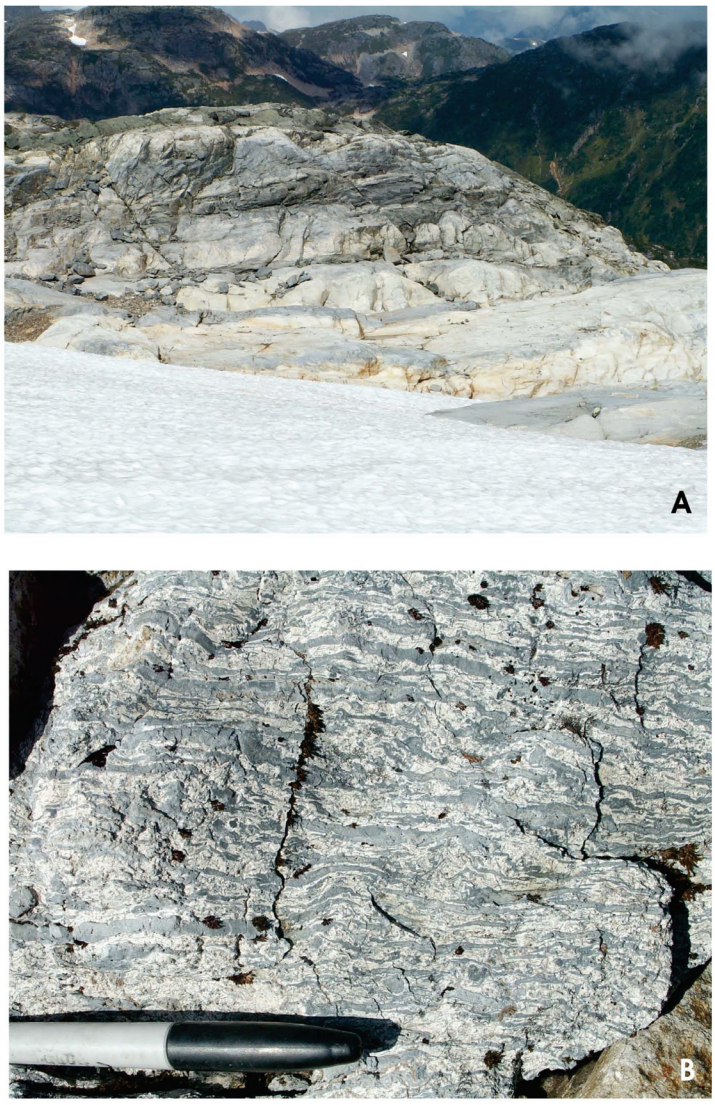

Figure 10. a) Part of the extensive, thick-bedded rhyolite to dacite volcaniclastic unit of the Kitselas member; looking west from near Kitselas Mountain. b) Welded tuff, Kitselas member.

Much of the interior of the Kleanza pluton consists of coarse-grained, equigranular hornblende-biotite granodiorite, with lesser diorite and granite.

The Kleanza pluton intrudes strata of the Zymoetz group, as well as the Telkwa Formation. Contacts both parallel and crosscut the stratigraphy. In the valley of Kleanza Creek, the pluton occurs at low elevations, flanked by Telkwa Formation on adjacent high ridges (Fig. 4; see also Barresi and Nelson, 2006). This configuration suggests a roof contact. Contacts in the Chimdemash Creek valley are steeper and more crosscutting. Overall, the pluton seems to have formed as a branching and possibly stacked set of laccolithic arms that delaminated and domed the stratigraphic section. It was probably emplaced at shallow depths. Contact metamorphism around its margins is only well developed in the Zymoetz group on Copper Mountain, where diopside-garnet assemblages occur in limestone. Farther

TABLE 1. REPORT ON MACROFOSSILS FROM SANDSTONE NEAR SAND CREEK.

Report No. J6-2005-TPP

Report on one collection of Jurassic bivalves collected by JoAnne Nelson, BC Geological Survey, in Terrace area, BC (NTS 103I/09), 2005

GSC Locality C-500768: Field no. 05NB5-6; UTM Zone 9V, 543161E, 6067163N

Identifications:

Plagiostoma sp. cf. *hazeltonense* McLearn
Ctenostreon(?) sp.
Lopha(?) sp.
other bivalves, indeterminate
belemnites, indeterminate
terebratulid brachiopod, indeterminate

Age: Early Bajocian probably

The fossils are very poorly preserved fragments and imprints. This fauna is represented best in British Columbia at Hudson Bay Mountain near Smithers and in central Whitesail Lake map area. It occurs in Early Bajocian beds of the Smithers Formation, together with the ammonite *Sonninia.* Other Middle Toarcian through Bathonian ages for these fossils are remotely possible, but very unlikely in the Terrace area.

T.P. Poulton
October 4, 2005

north, zeolite-facies assemblages persist to within metres of its margins.

CARPENTER LAKE PLUTON (EOCENE)

The Carpenter Lake pluton underlies a large area in the drainages of Carpenter, Sand and Hardscrabble creeks, as well as the lower reaches of Legate Creek. It has been dated as Eocene by a 53 Ma U-Pb date on zircon (Gareau *et al.*, 1997a), which is consistent with other plutons belonging to the Coast Plutonic Complex. It comprises large areas of homogeneous granodiorite, tonalite and granite, as well as areas of abundant dikes of variable compositions and textures. Among these, pink orthoclase-phyric granite, medium-grained granodiorite and diorite, and green andesite are most common. Pink pegmatite and aplite occur in parts of it, notably in the headwaters of Sand Creek.

STRUCTURE

The most important structure in the area is the Usk fault (UF), which abruptly separates footwall felsic rocks of the Kitselas volcanic unit from hangingwall Telkwa Formation andesite intruded by the Kleanza pluton (Fig. 4). It is an undulating surface that dips variably to the southeast, offset by the steep, east-side-down Gitaus and Tumbling Creek faults. The UF corresponds to an abrupt change in bedding attitudes. In its footwall, well-bedded Kitselas units strike uniformly southwest and dip and face northwest, away from the fault. In its hangingwall, Telkwa units strike southeast and dip moderately to steeply southwest, toward the fault. The UF is located within a metamorphic transition zone between greenschist and zeolite facies. Greenschist-facies assemblages are developed both within mafic rocks of the Kitselas volcanic unit and within the lower part of the Telkwa Formation, up to 300 m above the UF. Spaced, southeasterly-dipping zones of strong penetrative cleavage occur throughout the Kitselas volcanic unit. Strongly foliated zones are particularly well developed near its structural top (*e.g.*, in highway outcrops north of Chimdemash Creek). The broader shear zone persists hundreds of metres above the UF, expressed as strongly cleaved intervals and chloritic brittle shears within the Telkwa Formation and the Kleanza pluton.

Overall, the UF appears to be a discrete detachment fault corresponding to an abrupt lithological break, located within a broader zone of shearing and strong fabric development, the Usk shear zone. Attenuation occurred across the entire zone, with displacement focused on the UF. The original relationship of the Kitselas volcanic unit to the Paleozoic to Jurassic rocks in the hangingwall of the UF is still not known.

MINERALIZATION

The Usk map area contains about 80 documented mineral occurrences of several deposit types (Fig. 11; see also Kindle [1937a, b] for detailed descriptions of historic showings). Copper mineralization is common and widespread, and includes quartz vein, quartz-poor sulphide vein (bornite-chalcocite-epidote-specular hematite), shear-hosted, disseminated and replacement styles, in addition to the nearly ubiquitous malachite stains of uncertain origin. Silver is commonly associated with Cu minerals, particularly in veins and shears. Gold favours quartz veins, and occurs either with pyrite alone, as at Columario (MINFILE 103I077), or in polymetallic veins with chalcopyrite, bornite, sphalerite, galena, tetrahedrite and other sulphosalts. Molybdenite occurs within and near the Carpenter Lake pluton.

The origin and associations of the Cu and Au-bearing epigenetic mineralization are unclear, because the evidence is circumstantial. Four possibilities exist, listed in order of implied age of mineralization:

1) Copper-rich shear zone – hosted and replacement occurrences in the Telkwa Formation, notably on the north-south Treasure Mountain trend (Fig. 11) could be related to early fluid migration associated with Hazelton-age volcanic activity.
2) Hydrothermal systems associated with the Kleanza pluton could give rise to a broad spectrum of epigenetic occurrences, such as veins, shear-hosted, disseminated and replacement massive sulphide minerals.
3) The Early Tertiary Usk shear zone and Usk detachment fault could be implicated in the formation of local epigenetic mineralization.
4) Veins could relate to hydrothermal effects of the Eocene Carpenter Lake pluton.

The spatial distribution of Au and Cu-rich occurrences on Figure 11 points most strongly at the Kleanza pluton as a key factor in their formation. Most of the Au-rich veins concentrate in a band that corresponds to the northeast-trending northern lobe of the pluton, which extends from the mouth of the Zymoetz River to the headwaters of Legate Creek. This includes the cluster of veins on Kleanza Mountain, and the Silver Basin (MINFILE 103I067) to Zona May – Frisco area (MINFILE 103I063, 061).

The Kleanza pluton is a heterogeneous multiphase body. Outcrop patterns outline a curviplanar shallow top to both lobes. It was probably intruded as a sprawling, laccolith-shaped body to high crustal levels in zeolite-facies country rocks. The upper levels of the pluton and its volcanic cupola are extensively exposed in the area, constituting a highly favourable environment for mineralization. Major ankeritic alteration occurs in the Silver Basin area,

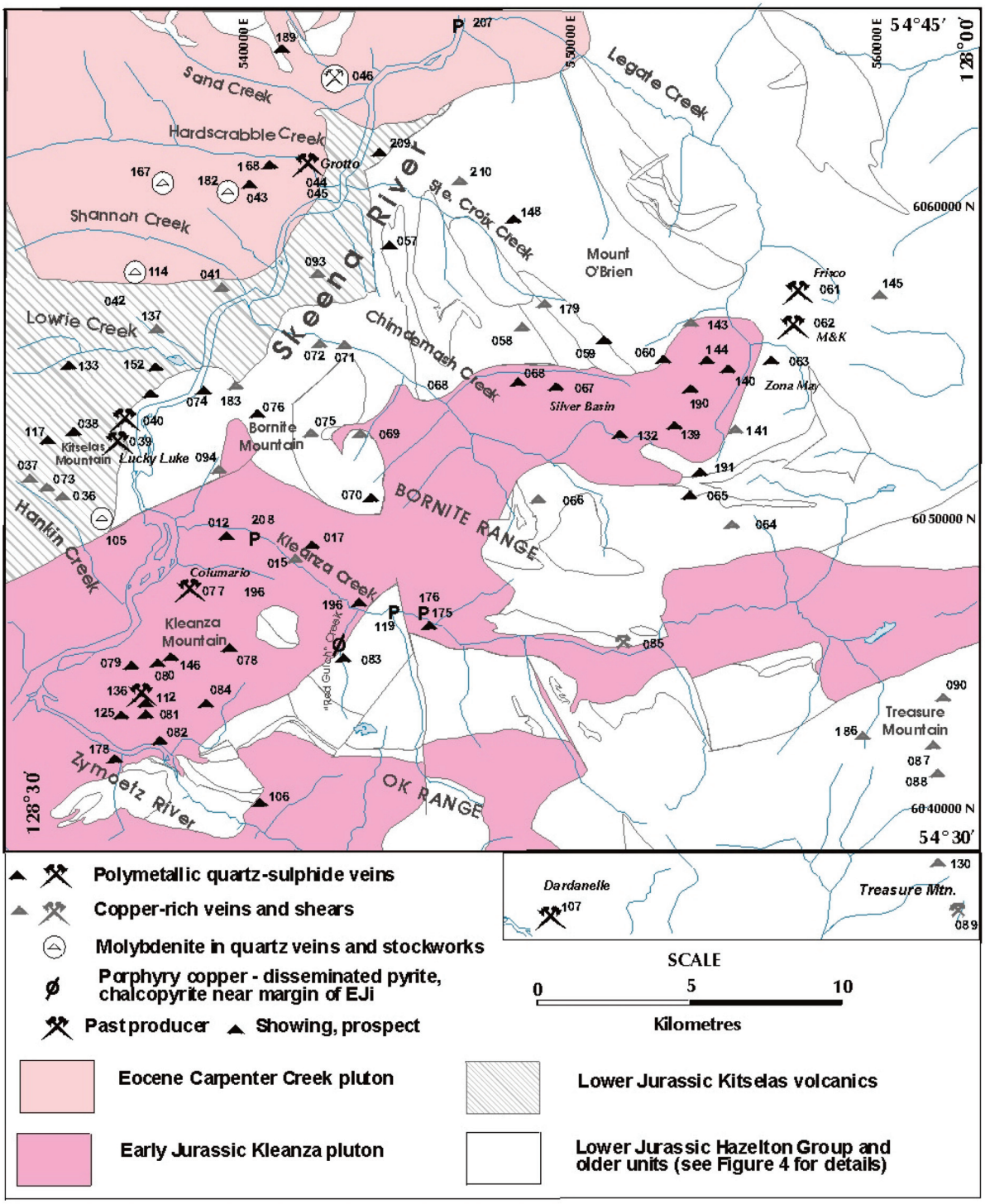

Figure 11. Mineral prospects in the Usk map area.

associated with an unusual porphyritic monzonite phase of the pluton. In 'Red Gulch' Creek and on the lower, western and southern slopes of Bornite Mountain, common occurrences of disseminated chalcopyrite and pyrite near the margins of the pluton may indicate a potential for porphyry-style mineralization.

The only cluster not clearly associated with the Kleanza pluton is that on Kitselas Mountain, including the Lucky Luke (MINFILE 103I039) and Gold Star veins (MINFILE 103I038; Carter, 1970). These crosscut S_1 fabrics in the Kitselas member, which are related to the Usk shear zone; therefore, they are probably of Eocene age and may relate to the detachment faulting event.

HIGHLIGHTS OF 2005 ROCK GEOCHEMICAL SAMPLING PROGRAM

As part of the regional mapping program, more than 70 samples were taken from mineralized zones and areas for geochemical and assay analysis (Table 2). Some correspond exactly or approximately to existing locations in the MINFILE database. Table 3 shows revised locations for selected mineral occurrences, based on the authors' work and that of Raymond Cook of Argonaut Resources.

Sampling carried out by the authors confirmed significant metal values from several known showings. Grab samples from the Columario (JN4-3; MINFILE 103I077) and Lucky Luke (JN2-5; MINFILE 103I039) returned 36.6 and 0.35 g/t Au, respectively. Many samples in the upper Chimdemash Creek area contain significant metal values, notably a vein float sample, TB-26-03, taken west of the Silver Basin (MINFILE 103I065) that contains 0.18 g/t Au. Showings on Treasure Mountain (EK 24 through 26 series; MINFILE 103I090, 086) returned high values of Cu and, in some cases, elevated Ag. The Alvija occurrence (MINFILE 103I089), located immediately north of the Kleanza Creek road, is a broad zone of fracturing and Cu mineralization. A representative sample contained 5.59% Cu and 99 g/t Ag. Quartz veins at the Shan occurrence (TB41-3, 4; MINFILE 103I167) contained up to 0.989% Mo.

Table 2 also shows many anomalies from samples not located near previously documented mineral occurrences. Although most are from thin veins and shear zones, some represent interesting new mineral potential for the area. They include the following:

- The highest Au value obtained from a new showing was 3670 ppb (3.6 g/t) from sample JN13-7, located on the ridge south of Mount O'Brien. It was obtained by digging through talus to a malachite-stained shear zone in rubble-crop. The width and length of this zone are unknown, because it is largely covered.
- Samples EK8-1 and 1a are from an outcrop on the north side of the Hardscabble Creek logging road, where several quartz veins with small, visible sulphide grains occur in a silicified zone associated with aplite dikes. The samples contain elevated values of W, Cu, Pb, Zn, Ag, Bi, Cd and Te (Table 2). The dike and vein system strike roughly east, subparallel to the road; they shortly disappear under cover in both directions. This locality is approximately 1 km west of the Grotto vein in the canyon of Hardscrabble Creek (MINFILE 103I044, 45).
- Samples from within and near the Silver Basin area tend to contain elevated base metal and silver values. These include JN7-3, JN8-2, TB26-3, TB26-6, TB26-13, TN27-5, TB27-8 and TB27-12. Combined with the widespread ankeritic alteration in the area, they indicate a significant metalliferous system.
- Samples of disseminated pyrite and chalcopyrite from near the borders of the Kleanza pluton include EK13-5, EK13-8, EK13-11, EK15-3, and TB4-2.They contain anomalous but sub-ore-grade Cu values, 419–3083 ppm, and negligible Au and Ag.
- Samples EK9-3 and 9-5, from the logging road south of Sand Creek, were of altered, quartz-veined granite of the Carpenter Lake pluton, with minor visible molybdenite. They returned anomalous Mo values of 38 and 164 ppm.

MINERAL POTENTIAL AND MODELS

Mineralization in the Usk area is controlled by the Early Jurassic Kleanza pluton, particularly its northern lobe; the Eocene Carpenter Lake pluton; possibly the Usk shear zone; and, in the case of the Cu(-Ag) occurrences on Treasure Mountain, fluid flow of unknown origin along a north-striking shear zone. The Kleanza system is generally expressed as polymetallic quartz veins and vein swarms with sporadic high values in Au and/or Ag. Replacement-style mineralization is reported in a tuff near its northeastern margin, at the Zona May occurrence (MINFILE 103I061; Salat, 2005; R. Cook, pers. comm., 2005). The widespread Silver Basin veins and alteration zones at the head of Chimdemash Creek provide a target of interest.

The Carpenter Lake pluton contains zones of molybdenite concentration, such as the Shan occurrence and the Sand Creek area.

Although, in general, the Treasure Mountain system is clearly shear related and shear controlled, there is an important zone south of the map area (MINFILE 103I090) from which stratabound zones have been reported (A. Burton, pers. comm., 2005). There, a 12.19 m surface chip sample assayed approximately 3.40% Cu and 18.6 g/t Ag (Sutherland Brown, 1965). Unclassified reserves are 28 120 tonnes grading 1.7% Cu (Sadlier-Brown, 1973). This zone offers the possibility of bulk-tonnage potential.

Exposures of Troy Ridge Formation equivalents in the northwestern corner of the map area hint at the potential for Eskay-equivalent stratigraphy along strike farther to the north.

SUMMARY AND CONCLUSIONS

Geological mapping by the BC Geological Survey in the area northeast of Terrace in 2005 has clarified stratigraphic, intrusive and structural relationships of upper Paleozoic, Triassic and Jurassic rock packages, including subdivision of the Jurassic Hazelton Group and Telkwa Formation.

It is suggested here that the Permian volcanogenic strata and limestone be informally named the Zymoetz group, as the nearest equivalent exposures (the Asitka Group and units in the Stikine 'assemblage') are 250 km distant.

The authors have recognized an unusual, volcanic-free Triassic section of black chert and basinal sedimentary strata. It, along with the underlying Permian rocks, was thrust imbricated prior to deposition of the basal conglomerate of the Lower Jurassic Telkwa Formation.

TABLE 2. GEOCHEMICAL AND ASSAY RESULTS FROM 2005 SAMPLING IN THE USK MAP AREA

					Element	Mo	W	Cu	Pb	Zn	Au	Ag	Bi	Cd	Te	As	Sb	Hg
					Units (note that assays in % and g/t are in bold)	ppm (%)	ppm	ppm (%)	ppm (%)	ppm (%)	ppb	ppb (g/tonne)	ppm	ppm	ppm	ppm (%)	ppm (%)	ppb %
					Method	ARMS	ARMS	ARMS	ARMS	ARMS	ARMS	ARMS	ARMS	ARMS	ARMS	ARMS	ARMS	ARMS
					Detection Limit	0.01	0.2	0.01	0.01	0.1	0.1	2	0.02	0.01	0.02	0.1	0.02	5
Station ID	**Easting**	**Northing**	**Sample Description**	**MINFILE name**	**MINFILE number**													
05EK03-2	536652	6041105	skarn? + chalcopyrite			0.36	-0.1	37.73	2	36.6	0.4	57	0.14	0.13	0.12	1.8	0.13	5
05EK04-1	549076	6046868	quartz vein + pyrite in microdiorite			0.96	2.3	18.92	2.18	28.4	2.2	149	1.06	0.11	0.37	0.7	0.12	5
05EK04-2	549227	6046833	quartz vein + pyrite in microdiorite			8.02	78.8	1518.63	2.5	31	17.8	1486	14.53	0.11	6.52	4.1	0.12	23
05EK08-01	540488	6062600	20 cm quartz vein in silicified aplite with pyrite, chalcopyrite, chalcocite, bornite, galena			4.17	>100	128.53	1042.78	370.5	17.4	30234	146.02	16.62	3.57	2	0.11	65
05-EK-08-01a	540488	6062600	20 cm quartz vein in silicified aplite with pyrite, chalcopyrite, chalcocite, bornite, galena			10.83	5.6	261.67	**0.41**	3137.3	41.3	**253**	646.65	159.04	19.87	2.6	21.93	204
05EK08-02	540593	6062598	quartz vein in silicified aplite with pyrite, chalcopyrite, chalcocite, bornite, galena			0.91	0.5	42.79	4.19	99	-0.2	75	0.71	0.67	0.04	1.1	0.21	13
05EK08-03	540646	6062609	quartz vein in silicified aplite with pyrite, chalcopyrite, chalcocite, bornite, galena			0.62	0.3	4.27	5.55	20.1	-0.2	69	0.39	0.06	-0.02	1.4	0.09	15
05EK08-10	543091	6062965	5 cm quartz vein with chalcopyrite wisps			61.78	0.1	2984.3	1.29	97.1	11.1	16081	1.83	1.81	0.39	-0.1	0.08	-5
05EK09-03	542074	6063990	quartz stockwork with molybdenite	Pitman	46	37.78	0.5	7.97	4.45	10.1	-0.2	227	4.39	0.06	0.33	0.6	0.12	-5
05EK09-05	541443	6064116	quartz stockwork with molybdenite	near Pitman	46	163.76	0.1	30.24	2.4	30.8	-0.2	83	1.56	-0.01	0.04	2.9	0.16	-5
05EK10-06	540517	6042837	pyritic zone at Kleanza pluton contact			1.12	-0.1	447.03	2.27	22.6	0.9	179	0.45	0.07	0.24	0.8	0.16	-5
05EK10-06rep	540517	6042837	pyritic zone at Kleanza pluton contact			0.97	-0.1	419.89	2.18	18.7	1.1	176	0.37	0.06	0.22	0.7	0.16	-5
05EK11-03	538339	6059735	altered Eocene granite with pyrite, azurite			1.92	-0.1	26.8	6.44	39.4	-0.2	264	0.76	0.06	0.13	0.5	0.06	-5
05EK13-05	543271	6046592	microdiorite with chalcopyrite, pyrite			43.58	0.3	481.64	4.21	44.6	5.9	336	0.12	-0.01	0.13	0.6	0.36	-5
05EK13-08	542834	6046628	microdiorite with chalcopyrite, pyrite			1.36	0.4	515.11	2.97	75.1	1.6	334	0.22	0.15	0.14	0.7	0.21	-5
05EK13-10	542936	6046450	microdiorite with chalcopyrite, pyrite			0.88	0.4	57.44	1.36	49.2	1	64	0.07	0.01	0.05	0.4	0.08	-5
05EK13-11	543211	6046552	andesite with chalcopyrite, pyrite			0.5	-0.1	699.52	631.29	55.9	17.4	2108	0.09	0.08	0.14	1.1	8.01	8
05EK15-03	540094	6053186	bornite with epidote alteration, quartz veining; in microdiorite			0.37	0.2	3038.05	3.32	90.2	55.2	3326	0.84	0.14	0.15	1.1	0.13	-5
05EK21-05	555527	6040284	thin quartz vein with malachite, azurite			1.45	0.2	**3.32**	7.25	38.7	6.6	**19**	0.03	2.82	0.02	1.2	0.04	74
05EK24-01	564027	6041719	Cu-stained shear zone	Treasure Mtn.	90	0.2	0.1	1409.7	10.68	130.5	0.8	1193	0.04	0.18	-0.02	2.2	0.27	6
05EK24-06	563187	6040694	Cu-stained shear zone - over 2 m wide	Treasure Mtn.	90	0.26	0.3	**5.091**	1.67	108.2	210.7	**34**	0.02	0.06	0.04	2.1	0.07	-5
05EK-24-06b	563187	6040694	second chip sample Cu-stained shear zone, 2 m	Treasure Mtn.		6.78	0.2	**1.853**	11.84	109.7	1092.2	**15**	1.36	0.39	0.06	1.6	0.85	7
05EK25-08	563061	6042263	malachite-stained andesite	Montana	88	1.17	-0.1	2597.7	40.73	79.7	13.3	1869	0.1	0.35	0.14	10.7	5.66	12
05EK26-01	563858	6042482	chalcocite+malachite in 30 cm+ shear	Treasure Mtn. - Wells showing	90	0.15	-0.1	**9.156**	3.95	101.2	339.7	**228**	0.12	0.21	0.1	0.9	0.1	65
05EK26-05	564139	6042351	bornite, chalcocite, chalcopyrite in shear	Treasure Mtn.	90	0.17	-0.1	**2.427**	1.31	76.8	136.2	**77**	0.09	0.67	0.03	1	0.13	28
05-EK-31-05	561796	6058684	1 m thick shear breccia with quartz veining			13.25	3.8	**3.2**	**0.44**	1640	364.3	10586	2.85	43.29	1.57	7.8	9.65	993
05-EK-31-05rep	561796	6058684	1 m thick shear breccia with quartz veining			13	2.9	**3.287**	**0.5**	1677.3	185.5	7714	2.78	46.16	1.4	6.9	2.93	1133
05EK35-12	561907	6062498	altered tuff with abundant malachite			0.32	-0.1	3750.53	31.78	140	13	25136	0.35	1.14	-0.02	78.7	116.86	162
05EK37-01	559887	6061626	rusty, malachite-azurite stained volcanic			0.35	-0.1	**1.341**	7.24	22.9	12.3	**270**	1.58	0.17	0.02	11.8	1.38	33
05EK41-02	562679	6043387	quartz stockwork with chalcopyrite, bornite, malachite, azurite			0.18	-0.1	2430.78	8.91	47.1	15.5	1270	0.07	0.14	-0.02	0.8	0.3	-5
05EK41-07	562848	6043929	minor chalcopyrite in shear	Copper King?	163	0.26	-0.1	118.3	0.7	14.9	6.6	447	0.02	0.06	-0.02	0.4	0.04	-5
05EK41-08	562893	6043778	20 cm shear with epidote, bornite, chalcocite, malachite, azurite	Copper King?	163	0.23	0.1	**6.116**	3.35	139	27.4	**88**	0.05	0.66	0.07	0.7	0.09	15
05JN02-5	536153	6052601	quartz vein with bornite, chalcocite, pyrite	Lucky Luke	39	17.52	1.4	**2.734**	3.68	34.2	3509.7	**70**	30.48	1.23	9	-0.1	0.09	8
05JN04-3	539757	6048084	quartz vein with coarse pyrite	Columario	77	1.23	0.1	**0.018**	7.09	28.1	38629.3	**137**	10.52	0.36	63.61	1.2	0.06	58
05JN05-3	560134	6043074	10 cm quartz vein with chalcocite, galena			0.47	-0.1	2094.4	2.23	22.7	34	1566	0.16	0.06	0.11	0.6	0.06	-5
05JN07-3	553460	6050340	20 cm quartz vein with epidote, hematite, chalcocite			0.25	<.1	**1.087**	**2.55**	**2**	113.5	**399**	0.1	778.5	0.7	**0.13**	**0.595**	**0.046**
05JN08-2	553704	6053780	quartz vein with pyrite, galena, trace chalcopyrite in altered monzonite porphyry			1.74	0.7	**0.06**	**0.53**	**1.41**	21.2	**10**	0.44	160.7	<.02	42.1	5.32	2965
05JN12-8	549820	6047287	40 cm rustry flat quartz vein			0.67	31.1	32.14	28.31	120.8	185.4	3646	23.23	0.61	11.15	8.8	0.07	18
05JN13-1	552164	6057440	frothy chalcedonic quartz vein 20 cm, irregular			0.88	0.5	41.62	5.81	113.5	1.4	475	0.95	1.78	0.05	0.8	0.09	39

TABLE 2 (CONTINUED)

						Element	Mo	W	Cu	Pb	Zn	Au	Ag	Bi	Cd	Te	As	Sb	Hg
						Units (note that assays in % and g/t are in bold)	ppm (%)	ppm	ppm (%)	ppm (%)	ppm (%)	ppb	ppb (g/tonne)	ppm	ppm	ppm	ppm (%)	ppm (%)	ppb %
						Method	ARMS	ARMS	ARMS	ARMS	ARMS	ARMS	ARMS	ARMS	ARMS	ARMS	ARMS	ARMS	ARMS
						Detection Limit	0.01	0.2	0.01	0.01	0.1	0.1	2	0.02	0.01	0.02	0.1	0.02	5
Station ID	**Easting**	**Northing**	**Sample Description**	**MINFILE name**	**MINFILE number**														
05JN13-7	551927	6056970	20 cm shear with chalcopyrite, pyrite	new showing		16.54	0.7	**5.314**	1413.18	929.7	3670	**17**	5	27.33	0.61	48.9	0.7	348
05NB04-3	536748	6044151	quartz vein with pyrite, molybdenite	New Harlequin	112	**0.214**	0.2	113	3.23	3.7	22.4	1118	0.75	0.55	0.45	0.1	0.03	30
05NB04-4	536890	6043614	coxcomb quartz vein with pyrite	Excelsior	181	9.14	3.4	733.1	9.2	81.8	959.7	13033	20.77	1.17	22.17	1	0.08	5
05NB06-4	546363	6063795	2 m fracture zone with chalcopyrite, malachite, chalcocite			0.66	0.4	2069.61	2.38	65.3	13.6	5110	2.59	0.91	0.27	0.2	0.07	-5
05-NB-07-06	545200	6062700	30 cm quartz vein with bornite			19.71	0.4	4165.32	1.88	27.5	246.9	11951	6.03	0.44	3.19	-0.1	0.28	-5
05NB10-6	540604	6045701	quartz vein in topographic linear, cryptocrystalline; stockwork			1.84	<.1	46.73	67.26	57.1	2.8	1314	0.04	1.37	0.02	3.7	8.77	1229
05NB10-8	540888	6045772	quartz stockwork			652.97	<.1	19.59	14.72	33.3	36.4	598	0.05	0.14	<.02	186	5.12	279
05NB24-3	534216	6065296	30 cm fine grained quartz vein + stockwork; in Eocene granite			0.78	-0.1	63.05	2.23	16	2.5	87	0.11	0.03	-0.02	0.2	0.03	-5
05TB03-7	552920	6046509	fractures with malachite, bornite: 20 m+wide zone	Alvija/ Lucky Jane?	85	3.23	0.1	**5.59**	36.42	184.6	14.7	**99**	0.23	1.68	0.57	1.4	0.2	660
05TB04-2	544488	6045917	disseminated pyrite in quartz veins; silicification	Kino	83	70.47	0.3	625.87	11.13	46.8	12.2	1276	0.17	0.4	0.12	1.6	1.27	7
05TB06-7	540244	6054066	flat quartz vein with pyrite, chalcopyrite, galena, sphalerite	Four Aces	76	0.3	-0.1	645.76	1433.4	6000.3	60.2	19066	9.29	195	7.79	0.1	0.04	11
05-TB-9-09	539333	6054456	quartz vein 2-3 m, with bornite, chalcocite	Emma	74	2.39	1.2	6271.25	3438.08	9155.5	43.6	61000	98.73	179.26	7.04	-0.1	1.36	16
05TB11-3	545285	6066873	1-2% visible pyrite in granodiorite			0.94	-0.1	928.45	8.92	108.8	1.2	11162	0.05	2.95	-0.02	23.4	117.19	210
05TB11-6	545706	6066895	thin quartz vein with pyrite, sphalerite, chalcopyrite			0.68	-0.1	890.26	10.14	120.5	0.7	10983	0.06	3.11	0.03	23	126.99	214
05TB13-3	541784	6050970	quartz vein with epidote alteration, chalcopyrite, bornite			1.19	0.1	9342.85	7.27	20	30.5	1754	0.21	1.84	0.74	0.6	0.56	-5
05TB13-5	541822	6050978	shear zone			0.36	-0.1	9309.3	1.61	40.9	11.3	3387	0.11	0.88	0.51	0.5	0.3	-5
05TB17-3	546337	6045678	5 m ankeritic shear zone with malachite, chalcocite			0.23	-0.1	1801.47	6.19	209.5	3.6	2820	0.07	0.07	0.02	0.8	0.78	-5
05TB22-6	557700	6044323	massive pyrite at dike margin			21.5	0.2	2222.15	8.05	21.8	9.4	840	4.22	0.03	5.22	59.8	2.15	66
05TB24-7	557660	6042014	40 cm zone of epidote veinlets with malachite, azurite, pyrite, chalcocite			0.44	0.1	**1.993**	1.7	42.5	2	8213	0.02	0.35	0.25	1.3	0.06	-5
05-TB-26-03	555087	6051416	polymetallic vein float, upper Chiimdemash Creek			4.69	17.6	**0.685**	4682.46	1326.6	1842.4	**1469**	0.5	149.35	0.02	125.3	**0.351**	2304
05TB26-6	555437	6051701	quartz veins with malachite, azurite, galena	Silver Basin	65	1.73	0.2	1362.83	8335.49	4974.6	102.4	96002	0.42	168.42	0.03	89.2	333.29	1213
05TB26-8	555673	6051584	chalcopyrite with epidote in amygdules	Silver Basin	65	0.3	<.1	66.15	12.91	196.6	1.6	603	0.03	3.9	0.02	1.4	0.73	26
05-TB-26-08	555673	6051584	barite-quartz vein 10 cm	Silver Basin	65	0.3	<.1	66.15	12.91	196.6	1.6	603	0.03	3.9	0.02	1.4	0.73	26
05-TB-26-13	555646	6051345	Main Trench vein 20 cm, with bornite, chalcopyrite, tetrahedrite	Silver Basin	65	9.04	0.5	**1.62**	79.43	1199.6	250.2	**1481**	0.28	279.63	0.03	180.7	9999	4472
05TB27-12	556713	6050629	rusty felsic dike			1.47	<.1	25.29	14.54	36.2	2.5	447	0.05	0.22	2.45	37.3	1.24	48
05TB27-5	554232	6051210	chalcocite, hematite and epidote in basalt			52.36	<.1	**1.412**	5	62.9	49	**55**	0.5	0.93	0.81	0.8	6.56	106
05TB27-8	553918	6050487	4 m patch of highly Cu-stained andesite			0.51	0.2	5418.61	12.73	65.8	0.8	4863	0.03	0.35	0.03	2.7	2.4	150
05TB39-10	559067	6065383	chalcopyrite-bornite in quartz vein breccia and epidote veins; sample is 2 - 1/2 m2 surfaces			0.7	-0.1	**4.28**	30.56	129.2	256.1	**161**	12.37	1.29	0.15	1.3	0.43	5
05TB39-10rep	559067	6065383	chalcopyrite-bornite in quartz vein breccia and epidote veins; sample is 2 - 1/2 m2 surfaces			8.27	-0.1	**4.507**	30.87	130.8	227.3	**166**	12.83	1.35	0.1	0.9	0.36	7
05TB41-3	536026	6058215	20 cm thick quartz vein with molybdenite in area of veining and disseminated pyrite-molybdenite			1328.84	0.2	115	1.24	2.9	-0.2	275	0.15	-0.01	0.04	0.1	0.04	-5
05TB41-4	536205	6058404	40 cm quartz vein with abundant pyrite, molybdenite	Shan	167	**0.989**	0.9	**0.035**	5.94	6.1	8	1380	4.88	0.26	0.53	0.4	0.11	6
05-TB-45-02	551591	6043380	one of several small sulfide (skarn?) zones in limestone olistolith within andesite tuff, each less than 30 cm wide			5.79	0.3	**1.123**	**1.28**	**10.94**	26.5	**2232**	0.43	1765.02	0.06	387.7	**0.686**	7393

TABLE 3. REVISIONS OF MINERAL DEPOSIT LOCATIONS FROM FIELD OBSERVATIONS, USK MAP AREA

MINFILE name	MINFILE number	Station	New easting	New northing	Description
Gold Star B zone	38	05JN11-2	534294	6053101	trench with quartz veins, chalcocite, bornite, chalcopyrite
Gold Star A zone	38	05JN11-3	534555	6052629	trench with quartz veins, chalcocite, bornite, chalcopyrite
Lucky Luke	39	05JN02-5	536153	6052601	quartz vein with bornite, chalcocite, pyrite
Pitman	46	05EK09-03	542074	6063990	quartz stockwork with molybdenite
Pitman	46	05EK09-05	541443	6064116	quartz stockwork with molybdenite
United St. Croix	59	05JN07-9	551722	6049346	complex quartz vein up to 1 m, with chalcopyrite, pyrite, chalcocite, malachite, azurite
Silver Basin main trench	65	05TB26-13	555646	6051345	quartz vein 20 cm with chalcocite, bornite; in WSW-striking shear zone
Emma	74	05TB09-9	539333	6054456	malachite-stained quartz veins in fault
Four Aces	76	05TB06-7	540244	6054066	flat quartz vein with pyrite, chalcopyrite, galena, sphalerite
Columario	77	05JN04-3	539757	6048084	quartz vein with coarse pyrite
Zymoetz	82	05NB04-5	536999	6043038	70 cm quartz vein with pyrite, galena, magnetite, sphalerite, chalcopyrite; in old adit
Kino	83	05TB04-2	544488	6045917	disseminated pyrite in quartz veins; silicification
Kino	83	05EK13-05	543271	6046592	microdiorite with chalcopyrite, pyrite
Kino	83	05EK13-08	542834	6046628	microdiorite with chalcopyrite, pyrite
Kino	83	05EK13-10	542936	6046450	microdiorite with chalcopyrite, pyrite
Kino	83	05EK13-11	543211	6046552	andesite with chalcopyrite, pyrite
Alvija	85	05TB03-7	552920	6046509	fractures with malachite, bornite; wide zone
Wells	87	05EK26-01	563858	6042482	chalcocite+malachite in 30 cm+ shear
Montana	88	05EK25-08	563061	6042263	malachite-stained andesite
Treasure Mtn. north	90	05EK24-06	563187	6040694	Cu-stained shear zone; over 2 m wide
New Harlequin	112	05NB04-3	536748	6044151	quartz vein with pyrite
Shan	167	05TB41-4	536205	6058404	40 cm quartz vein with abundant pyrite, molybdenite
Copper King	163	05EK41-08	562893	6043778	20 cm shear with epidote, bornite, chalcocite, malachite, azurite
Excelsior	181	05NB04-4	536890	6043614	coxcomb quartz vein with pyrite
Peerless	186	05JN06-3	560746	6044270	massive chalcocite vein in ankerite-altered andesite; 10 cm thick; flat dip
GPS locations of mineral occurrences established by Raymond Cook (pers. comm., 2005):					
Silver Basin headwall zone	65b		556552	6051171	disseminated tetrahedrite, bornite in amygdules
Pass	new		559633	6056738	gossan (breccia zone) 40 m wide, continuous 200 m in pass; assays pending
Frisco	61		558656	6058339	Cu, Ag in veins, stringers, disseminations in 12 m wide zone (MINFILE)
M&K main adit	62		558609	6057003	Quartz veins with Au, Ag values (0.38 g/t Au, 119 g/t Ag in grab sample; Salat, 2005) in sheared, brecciated zone
M&K (stratabound zone)	62b		558577	6056985	bedding-parallel mineralized zone, up to 1.2 m wide, in tuff; chalcopyrite, chalcocite, galena, bornite, minor tetrahedrite, pyrite, specularite
Zona May vein	60a		554523	6055208	0.2 3 m wide quartz vein over 700 (possibly 1800) m; strikes ESE; grab samples assayed 0.03 24 g/t Au, 0.3 3364 g/t Ag (Salat, 2005)
Zona May west wall breccia	60b		554296	6055299	see above
Zona May vein (glacier zone)	60c		554631	6055172	see above
Zona May east	60d		554674	6055172	see above
Dynasty	new		555343	6055033	extension of Zona May vein to east(?); east-striking quartz vein with Cu, Ag

The Telkwa Formation is regionally divisible into two distinct successions: a clastic-dominated section south of Kleanza Creek, and a flow-dominated succession north of Kleanza Creek. Although the flow-dominated section locally overlies the clastic section, the authors consider them to be volcanic facies variants as well: the flows were sourced locally within the map area and represent a major complex of andesite, dacite and rhyolite centres.

The Kitselas facies of the Telkwa Formation comprises mainly felsic volcaniclastic and coherent rocks, with minor basalt; it lies in the footwall of the Usk fault.

The top of the Hazelton Group comprises an equivalent of the 'Red Tuff' member of the Nilkitkwa Formation, sandstone fossil-dated as Bajocian, and banded siliceous strata equivalent to the Troy Ridge Formation. These are overlain by the Bowser Lake Group.

The 200 Ma Kleanza pluton is a sprawling laccolithic body with two major lobes. It is probably comagmatic with the Telkwa Formation, and may core the volcanic centre that generated flows in the Mount O'Brien section.

Mineralization in the area relates to the Kleanza pluton and the Eocene Carpenter Lake pluton, as well as possibly to the structures associated with the Usk shear zone and, in the case of Cu-Ag-rich shears and replacements, regional hydrothermal circulation in the Telkwa Formation.

ACKNOWLEDGMENTS

Glenn Woodsworth was generous with his knowledge of Terrace area geology, and it was our pleasure to confirm many of his observations and ideas in the field. Bill McRae, Jim Mulvey, George Chinn, Alex Burton and Ray Cook provided detailed information on mineral prospects in the area. We are deeply indebted to Bill and Helene McRae for every kind of help and support. This project was conducted in partnership with the Resource Management Department of the Kitselas First Nation. We thank Daniel Parker, Chad Gerow and Richard Seymour for able assistance in the field. Larry Diakow provided an insightful review of the text.

REFERENCES

Alldrick, D.J., Nelson, J.L. and Barresi, T. (2005): Geology and mineral occurrences of the upper Iskut River area: tracking the Eskay rift through northern British Columbia; *in* Geological Fieldwork 2004, *BC Ministry of Energy, Mines and Petroleum Resources*, Paper 2005-1, pages 1–30.

Anderson, R.G. (1989): A stratigraphic, plutonic and structural framework for the Iskut map area, northwestern British Columbia; *in* Current Research, Part E, *Geological Survey of Canada*, Paper 89-1E, pages 145–154.

Barresi, T. and Nelson, J.L. (2006): The Usk map area near Terrace, BC: Cross-sections and volcanic facies interpretation; *in* Geological Fieldwork 2005, *BC Ministry of Energy,*

Mines and Petroleum Resources, Paper 2006-1 and *Geoscience BC*, Report 2006-1.

Bennett, N., Compiler (1997): Pioneer Legacy: Chronicles of the Lower Skeena River; *R.E.M. Lee Hospital Foundation*, Terrace, BC, 240 pages.

Berthiaume, R. (1999): The Gitselasu: The People of Kitselas Canyon; *First Nations Education Centre*, Terrace, BC, 154 pages.

Brown, D.A., Gunning, M.H. and Greig, C.J. (1996): The Stikine Project: geology of western Telegraph Creek map area, northwestern British Columbia; *BC Ministry of Energy, Mines and Petroleum Resources*, Bulletin 95, 176 pages.

Carter, N.C. (1970): Gold Star; *in* Geology, Exploration and Mining in British Columbia 1970, *BC Ministry of Energy, Mines and Petroleum Resources*, pages 195–197.

Duffell, S. and Souther, J.G. (1964): Geology of Terrace map area, British Columbia; *Geological Survey of Canada*, Memoir 329, 117 pages.

Gareau, S.A., Friedman, R.M., Woodsworth, G.J. and Childe, F. (1997a): U-Pb ages from the northeastern quadrant of Terrace map area, west-central British Columbia; *Geological Survey of Canada*, Current Research 1997-A/B, pages 31–40.

Gareau, S.A., Woodsworth, G.J. and Rickli, M. (1997b): Regional geology of the northeastern quadrant of Terrace map area, west-central British Columbia; *Geological Survey of Canada*, Current Research 1997-A/B, pages 47–55.

Gunning, M.H., Bamber, E.W., Brown, D.A., Rui, L., Mamet, B.L. and Orchard, M.J. (1994): The Permian Ambition Formation of northwestern Stikinia, British Columbia; *in* Pangea: Global Environments and Resources, Embry, A.F., Beauchamp, B. and Glass, D.J., Editors, *Canadian Society of Petroleum Geologists*, Memoir 17, pages 589–619.

Heah, T.S.T. (1991): Mesozoic ductile shear and Paleogene extension along the eastern margin of the Central Gneiss Complex, Coast Belt, Shames River area, near Terrace, British Columbia; M.Sc. thesis, *University of British Columbia*, Vancouver, BC, 155 pages.

Kindle, E.D. (1937a): Mineral resources of Terrace area, Coast district, British Columbia; *Geological Survey of Canada*, Memoir 205.

Kindle, E.D. (1937a): Mineral resources, Usk to Cedarvale, Terrace area, Coast district, British Columbia; *Geological Survey of Canada*, Memoir 212.

Logan, J.M., Drobe, J.R. and McClelland, W.C. (2000): Geology of the Forrest Kerr – Mess Creek area, northwestern British Columbia; *BC Ministry of Energy, Mines and Petroleum Resources*, Bulletin 104, 164 pages.

Marsden, H. and Thorkelsen, D.J. (1992): Geology of the Hazelton volcanic belt in British Columbia: implications for the Early to Middle Jurassic evolution of Stikinia; Tectonics, Volume 11, pages 1266–1287.

Mihalynuk, M.G. (1987): Metamorphic, structural and stratigraphic evolution of the Telkwa Formation, Zymoetz River area (NTS 103I/08 and 93L/05), near Terrace, British Columbia; M.Sc. thesis, *University of Calgary*, Calgary, Alberta, 128 pages.

Mihalynuk, M.G. and Friedman, R.M. (2005): Gold and base metal mineralization near Kitsumkalum Lake, north of Terrace, west-central British Columbia; *in* Geological Fieldwork 2004, *BC Ministry of Energy, Mines and Petroleum Resources*, Paper 2005-1, pages 67–82.

MINFILE (2005): MINFILE BC mineral deposits database; *BC Ministry of Energy, Mines and Petroleum Resources*, URL <http://www.em.gov.bc.ca/mining/Geolsurv/Minfile/> [Nov 2005].

Monger, J.W.H., Wheeler, J.O., Tipper, H.W., Gabrielse, H., Harms, T., Struik, L.C., Campbell, R.B., Dodds, C.J., Gehrels, G.E. and O'Brien, J.A. (1991): Cordilleran terranes; Part B of Chapter 8 *in* Geology of the Cordilleran Orogen in Canada, Gabrielse, H. and Yorath, C.J., Editors, *Geological Survey of Canada*, Geology of Canada, No 4, p. 281–328 (also The Geology of North America, *Geological Society of America*, Boulder, Colorado, Volume G-2).

Nelson, J.L., Barresi, T., Knight, E. and Boudreau, N. (2006): Geology of the Usk map area, Terrace, British Columbia (103I/09); B.C. Ministry of Energy, Mines and Petroleum Resources, Open File 2006-3, 1:50,000 scale.

Roots, C.F., Nelson, J.L., Simard, R.-L., Mihalynuk, M., Harms, T.A., Friedman, R. and Heaman, L. (in press): Continental fragments, Paleozoic arcs and overlapping Triassic sediments in the pericratonic belt, northern British Columbia and southern Yukon; *in* Paleozoic Evolution and Metallogeny of Pericratonic Terranes at the Ancient Pacific Margin of North America, Canadian and Alaskan Cordillera, Colpron, M., Nelson J.L. and Thompson, R.I., Editors, *Geological Association of Canada*, Special Paper 45, in press.

Sadlier-Brown, T. (1973): Statement of material facts — Treasure Mountain; press release, prepared for *Spectroair Explorations Ltd*, June 16, 1973.

Salat, H.P. (2005): Report on the geological reconnaissance and evaluation of the Zona May – Silver Basin property, BC; submitted by Argonaut Resources Inc., *BC Ministry of Energy, Mines and Petroleum Resources*, AR 27786, 90 pages.

Sutherland Brown, A. (1965): Northwest Copper – Treasure Mountain; *BC Ministry of Energy, Mines and Petroleum Resources*, Minister of Mines Annual Report 1965, pages 71-72.

Tipper, H.W. and Richards, T.A. (1976): Jurassic stratigraphy and history of north-central British Columbia; *Geological Survey of Canada*, Bulletin 270, 73 pages.

van der Heyden, P. (1992): A Middle Jurassic to early Tertiary Andean-Sierran subduction model for the Coast Belt of BC; *Tectonics*, Volume 11, pages 82–97.

Woodsworth, G.J., Anderson, R.G. and Armstrong, R.L. (1991): Plutonic regimes; Chapter 15 *in* Geology of the Cordilleran Orogen in Canada, Gabrielse, H. and Yorath, C.J., Editors, *Geological Survey of Canada*, Geology of Canada, No 4, pages 491–531 (also *Geological Society of America*, The Geology of North America, Volume G-2).

Woodsworth, G.J., Hill, M.L. and van der Heyden, P. (1985): Preliminary geology map of Terrace (NTS 103I, east half) map area, BC; *Geological Survey of Canada*, Open File 1136, 1 map at 1:125 000 scale.

A.2: Barresi, T., and Nelson, J. 2006. Usk Map Area (NTS 103I/09), Near Terrace, British Columbia: Cross-Sections and Volcanic Facies Interpretation. In Geological Fieldwork 2005, British Columbia Ministry of Energy and Mines, British Columbia Geological Survey Paper 2006-1, p. 21-28.

Usk Map Area (NTS 103I/09), Near Terrace, British Columbia: Cross-Sections and Volcanic Facies Interpretation

By T. Barresi[1] and J.L. Nelson

KEYWORDS: Terrace, Stikine Terrane, Usk, Telkwa Formation, Zymoetz group, volcanic facies, facies analysis, cross-section

INTRODUCTION

In the summer of 2005, one geologist and three geology students working for the British Columbia Geological Survey, along with three Kitselas First Nation resource technicians, surveyed the Usk map area, near Terrace, BC (Fig. 1). A major objective of the project was to identify subdivisions within the Telkwa Formation, a unit that had previously been undivided in the Terrace area. This article presents four cross-sections of the map area (Fig. 2); it is a companion article to Nelson *et al.* (2006), where a full examination of the physical features and exploration potential of the Usk map area is presented. This paper highlights the details of the newly distinguished units within the Telkwa, as well as their stratigraphic, (paleo)geographic and structural relationships to one another and to local intrusive and older Triassic and Paleozoic units. Special emphasis is placed on variations in volcanic facies that occur between and within the divisions of the Telkwa Formation. Twenty samples have been collected along these transects for whole-rock major, trace and isotope geochemical analyses. These will be incorporated into a Ph.D. thesis currently in progress by the senior author at Dalhousie University.

GEOLOGICAL SETTING

The Usk map area falls within the western portion of the Stikine Terrane, or Stikinia. Stikinia is the largest of the intermontane terranes and is composed of Paleozoic to Middle Jurassic, island-arc-related volcanic, plutonic and sedimentary rocks (Anderson, 1993). The map area also falls along the eastern boundary of the Coast Plutonic Complex, a linear belt of subduction-related plutonic rocks emplaced after the accretion of the intermontane terranes to the North American continent (van der Heyden, 1992).

The cross-sections in this paper depict three main stratigraphic units and two plutonic units. The oldest stratigraphic unit, the Zymoetz group, is correlative with Paleozoic rocks of the Stikine 'assemblage' in the Iskut-Stikine area (Nelson *et al.*, 2006; see also Logan *et al.*, 2000; Brown *et al.*, 1991). These units are overlain, in places, by thin, well-bedded sedimentary rocks, which are thought to be Triassic in age and are correlative with the Stuhini Group. The youngest, and by far the most voluminous, stratigraphic unit represented in these cross-sections is correlative with the Telkwa Formation, the oldest formation of the Hazelton Group (Richards and Tipper, 1976); it is composed mainly of intermediate coherent volcanic and volcaniclastic rocks. A large, multiphase, anastomosing pluton, informally named the Kleanza pluton (Gareau *et al.*, 1997a, b), is represented in these cross-sections. A second plutonic suite, belonging to the Eocene Coast Plutonic Complex, is only represented in cross-section D–D′–D″, as it outcrops mainly in the northwestern corner of the Usk map area (Carpenter Lake pluton, Fig. 2).

CROSS-SECTIONS

Detailed descriptions of the geological units that are shown in these cross-sections are presented in Nelson *et al.* (2006) and will not be repeated here; rather, this paper will focus on observations, made along the transects of the cross-sections, that may be important to the interpretation of the environment of emplacement/deposition.

Section A–A′

The A–A′ transect (Fig. 3), which crosses from Copper Mountain on the south side of the Zymoetz River to the O.K. Range on the north side of the river, highlights the features of the Paleozoic Zymoetz group, Triassic strata, and their internal structure and relationship to overlying and intrusive Jurassic units.

Apophyses of the Jurassic Kleanza pluton outcrop on Copper Mountain and in the O.K. Range. The margins of this intrusive body represent both original intrusive contacts and faulted contacts. The Kleanza pluton forms a laccolith in the northwestern and central parts of the Usk map area. The laccolith is present at a shallow depth, as depicted on the northeastern portion of this cross-section. Its geometry, in this portion of the map, is inferred from 1) its regional outcrop characteristics (for instance, plutonic rocks commonly outcrop in low lying drainages); and 2) high concentrations of dikes, up to 50% of all outcrop, with rock types similar to those of the pluton.

The Paleozoic Zymoetz group is composed of two units, a fossiliferous limestone and a volcanic unit that is composed of interbedded intermediate lapilli tuff and volcanic conglomerate and sandstone. These units are considered by Nelson *et al.* (2006) to be a subaqueous-arc edifice with limestone reefs and limy banks that were periodically inundated by volcaniclastic debris. Limestone of the Zymoetz group is coeval with the Permian Ambition For-

[1]*Department of Earth Sciences, Dalhousie University, Halifax, NS (john.barresi@dal.ca)*

This publication is also available, free of charge, as colour digital files in Adobe Acrobat PDF format from the BC Ministry of Energy, Mines and Petroleum Resources internet website at http://www.em.gov.bc.ca/Mining/Geolsurv/Publications/catalog/catfldwk.htm

posed to the heterogeneous border phases that are normally observed. The centre of the pluton is more evolved than the border phases: it is a relatively homogeneous, coarse grained, equigranular, biotite granite with up to 60% quartz. Border phases, such as those exposed in the Kleanza Creek valley, on this cross-section are typically more mafic and are composed of hornblende±biotite granodiorite and diorite, rare granite, green microdiorite and aplite. These border phases of the Kleanza suite show extreme local variability and mutual crosscutting relationships.

Juxtaposed across the Kleanza Creek valley are distinct units of the Telkwa Formation, which Nelson *et al.* (2006) refer to as the O.K. Range – Treasure Mountain facies and Kleanza Creek facies in the south, and the Mount O'Brien facies in the north. Both are composed mainly of andesitic volcanic rocks, but the O.K. Range and Kleanza Creek facies are mainly volcaniclastic rocks, whereas those to the north are mainly coherent volcanic flow units. The differences between these units are not the result of a stratigraphic relationship; rather, they represent a paleogeographic difference in volcanic environments and depositional settings. The northern Mt. O'Brien facies is proximal to eruptive fissures and centres, and is therefore composed mainly of coherent volcanic flows. In the southern Kleanza and O.K. Range facies, there is very little coherent volcanic material; instead, they are composed mainly of primary and resedimented volcaniclastic material, particularly andesitic lapilli tuff. These are more distal facies and represent a subsiding basin. The basin accommodated large amounts of volcanic debris that erupted directly into it or washed into it from the volcanic edifice.

There are no exposures of Triassic or Paleozoic rocks, or the basal Telkwa conglomerate, beneath the andesite of the Mt. O'Brien facies. On the northern slopes of Kleanza Creek, a sequence of finely bedded green and maroon volcanic sandstone grades transitionally upward into coherent flows.

Two locally occurring bodies of dacite and rhyolite are depicted on the northeastern portion of the cross-section. Both coherent and volcaniclastic facies of these felsic rocks form irregular and discontinuous bodies within the coherent Mt. O'Brien facies andesite unit. Felsic intervals are rare in the O.K. Range and Kleanza facies, due to the distance of these rocks from the local felsic eruptive centres located to the north in the Mt. O'Brien facies. The characteristics of the Mt. O'Brien facies felsic units and their relationships with the andesitic units are discussed in further detail in the following two sections.

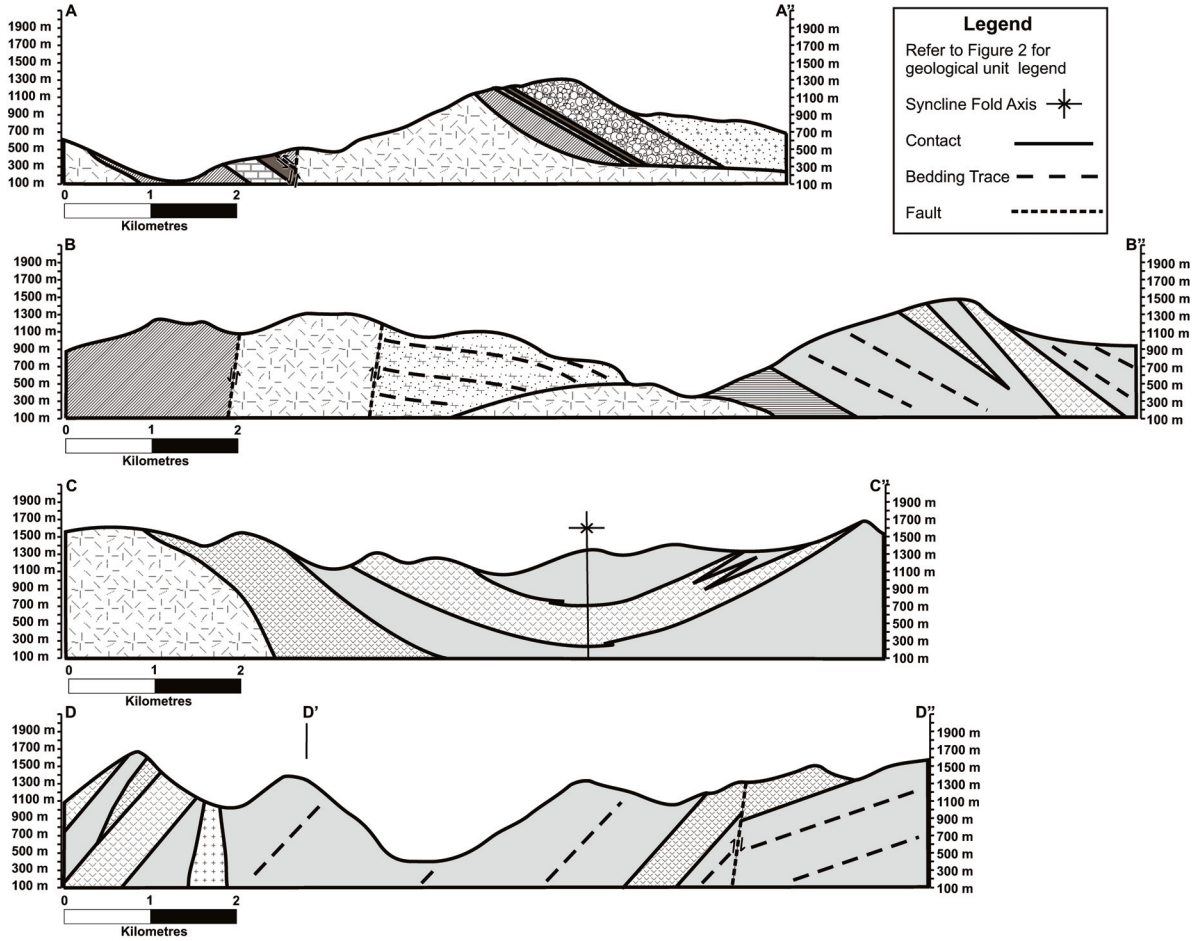

Figure 3. Cross-sections of the Usk map area. Rock unit patterns as on Figure 2.

Section C–C′

The C–C′ transect (Fig. 3), which spans a length of the Bornite Range between the headwaters of Chimdemash Creek to the north and Kleanza Creek to the south, depicts the physical distribution of dacitic and rhyolitic units within the Mt. O'Brien facies.

On the western portion of this cross-section, there is a contact between a body of the Kleanza pluton and a rhyolite volcanic unit. Closer to the centre of the intrusive body, the rock is relatively homogeneous, but, along its margin, it is composed almost entirely of dikes with variable composition, ranging from mafic to felsic. Of particular interest is the presence of highly epidotized, fine-grained, holocrystalline 'clasts'; these clasts are also found in abundance in certain tuff layers in the overlying rhyolitic units (Fig. 4). The close resemblance of many of the border phase felsic dikes to the rocks within the rhyolite unit, and the presence of holocrystalline epidotized clasts in both the pluton and the tuff layers, suggests that the contact between the pluton and the rhyolite may be transitional in the sense that the pluton was a feeder to the overlying eruptive volcanic unit.

The rhyolite unit is composed of laterally continuous layers of coherent, flow-banded white rhyolite, lapilli tuff and thin-bedded aphanitic siliceous sedimentary layers (Fig. 5). The fine-grained, well-bedded, siliceous sedimentary units may be intervals of felsic ash tuff or exhalitive chert. Lapilli tuff in this felsic unit is mono to polylithic, and some beds contain mafic as well as felsic lapilli. At least one 20 m thick bed is composed of resedimented lapilli tuff, which has scour-and-fill structures at its base and a coarsening-upward grading. Welding (*i.e.*, the flattening of pumice clasts due to compaction of hot volcanic material) is conspicuously absent in any of these beds. The continuity of beds in this unit, especially of the coherent rhyolite bodies, is unusual for these highly viscous volcanic rocks. It suggests that the section crosses very close to the volcanic centre but at a distance where beds can be deposited without being disrupted by further volcanic activity, probably on the moderately distal flanks of the eruptive edifice. The lateral continuity of beds, absence of welding, and presence of fine-grained, well-bedded sequences are all suggestive of a subaqueous depositional environment.

The dacitic unit in this cross-section is exposed on two limbs of what is interpreted to be a broad syncline. The syncline is inferred from the opposing dips of the rocks on each limb; however, within the dacitic unit, igneous layering orientations are highly variable. This can be explained by the viscous nature of the lava, the irregular topography of the underlying andesitic unit, and the general high-energy and chaotic nature of volcanic centres. The dacitic unit interfingers extensively with the surrounding andesite and typically fills paleotopographic depressions between large lobes of andesite that are typically hundreds of metres wide. In some places, thin veneers of fine-grained dacitic rock also cover paleotopographic highs. The dacitic unit is highly variable in its textures and individual facies are rarely laterally continuous. They are typically brick red or lavender in colour and variably feldspar phyric and vesicular. Coherent bodies are sometimes flow banded, spherulitic and rarely contain lithophysae (large vugs that form from the devitrification of volcanic glass). Volcaniclastic rocks include large breccia piles, lapilli tuff, and fine-bedded ash and crystal-ash tuffs. In at least two locations, lapilli tuff contains clasts of lapilli tuff (Fig. 6), an indication of multiple generations of explosive volcanism from the same centre. Other volcanic rocks are highly welded, with up to 1:10 aspect ratios on flattened pumice clasts. The overall geometry of deposition of the dacitic unit is consistent with subaerial pyroclastic flows (Wright *et al.*, 1980). The ubiquity of welded rocks in this unit also supports a subaerial depositional setting.

The andesite unit, which interfingers extensively with the dacitic unit, is composed mainly of green or maroon, vesicular, coherent flow units and minor amounts of lapilli tuff. The coherent units are fine grained to aphanitic and commonly have euhedral, lath-shaped plagioclase phenocrysts. The vesicles and amygdules, which range in size from 0.2 to 10 cm, occupy a large proportion of the coherent bodies, up to 60% by volume, and are filled with zeolite-facies metamorphic minerals, including chabazite, chlorite and natrolite (Fig. 7). These bodies form an irregular paleotopography composed of large flow units, as well as smaller flow lobes; no pillow forms were observed. The absence of pillow forms and the large vesicle size in these units is suggestive of a subaerial deposition. In addition, there is a virtual absence of interbedded sedimentary mate-

Figure 4. Holocrystalline epidotized clasts in the Kleanza pluton (left) and felsic lapilli tuff of the Telkwa Formation (right), Usk map area, near Terrace, BC.

Figure 5. Well-bedded rhyolitic ash and crystal ash tuff overlain by a 20 m thick bed of resedimented felsic lapilli tuff, Usk map area, near Terrace, BC.

rial, such as would be found in most proximal subaqueous depositional environments.

Section D–D′–D″

The D–D′–D″ transect (Fig. 3) crosses a cirque on the northern flank of Mt. O'Brien (D–D′) and then crosses Legate Creek, near its headwaters, to the northernmost mountain range in the Usk map area (D′–D″). This section crosses a small plug of probable Eocene age, and also two Telkwa rhyolitic units. It also crosses a major fault, which separates shallow-dipping strata in the north (Fig. 8) from more steeply dipping strata in the south. In addition, this section shows that regional trends in the orientation of beds are variable throughout the map area, as these beds dip to the southwest, whereas those in the other sections dip predominately to the northeast.

In the southwestern portion of this cross-section, a series of mainly coherent dacitic and rhyolitic units interfinger with andesite. These felsic units are similar to those described in cross-section C–C′. The andesite at this location also has similar characteristics to that on section C–C′; here, however, pipe vesicles may be present at the contacts between flows. Pipe vesicles commonly occur in subaerial environments where a flow passes over a moist surface, releasing vapours into the overlying lava (Wilmoth and Walker, 1993). The predominance of andesite shown in the lower slopes of the Legate Creek drainage is inferred, as this area is heavily forested and unexposed due to a thick Quaternary overburden.

The rhyolite unit in the northeastern portion of the cross-section is distinct from those elsewhere in the Usk map area. It is composed of a wide variety of coherent and volcaniclastic, 1–40 m thick beds of lapilli, ash and crystal-ash tuffs, and coherent rhyolite flows and domes that are transitional into flow breccias. This unit is also composed of approximately 30% dacite and 20% andesite beds. In one location, white flow-banded rhyolite was extruded through

Figure 6. Lapilli tuff with a 'clast' of a previously formed lapilli tuff, Usk map area, near Terrace, BC.

Figure 7. Amygdaloidal andesite, the vesicles partly filled with pink chabazite, Usk map area, near Terrace, BC.

Figure 8. Shallow-dipping, well-bedded layers in the northernmost rhyolitic unit (cross-section D'–D''), Usk map area, near Terrace, BC.

what was a nonlithified, red dacitic, crystal-ash tuff, creating an interval of peperitic white rhyolite in a red dacitic groundmass (Fig. 9). The andesite unit in this portion of the cross-section is composed of volcaniclastic and coherent flow rocks that are also bedded on a 1–40 m scale. Both the felsic and mafic rocks in this portion of the map area have been affected by high-angle, synvolcanic faults, which show between 1 and 10 m of vertical displacement. Rare welding of pumice clasts in rhyolitic beds suggests a subaerial depositional environment; however, limestone is found in the interstices of some andesite breccia, which suggests subaqueous deposition. In addition, rhythmic layering and normal grading of some tuff beds are also suggestive of subaqueous deposition by density currents. The volcanic rocks in this portion of the map area may have been deposited on a partly emergent, partly submerged volcanic edifice.

GEOLOGICAL HISTORY AND PALEOGEOGRAPHY OF THE STUDY AREA

The oldest rocks represented in the Usk map area belong to the Paleozoic Zymoetz group, which consists of limestone and volcanic rocks that were deposited on the limy shelf of an arc edifice. It was overlain by well-bedded Triassic chert and argillite in an oxygen-starved marine environment. These units were thrust imbricated prior to deposition of the Jurassic Telkwa Formation. During the Jurassic, they are interpreted to have formed an upstanding topographic high, which was present in the southwestern portion of the map area. These rocks were eroded and, along with a Telkwa volcanic influence, formed a basal Telkwa conglomerate, also exposed mainly in the southern portion of the map area. Overlying the basal conglomerate is a thick unit of mainly andesitic primary and resedimented lapilli tufts. These are interpreted to have been deposited in a mainly subaqueous, subsiding basin. Coeval, coherent volcanic rocks, which are voluminous to the north of Kleanza Creek, are the proximal and effusive equivalents of volcaniclastic rock deposited in the south. The northern section comprises andesite, dacite and rhyolite eruptive units, which interfinger extensively. Evidence of both subaerial and subaqueous deposition are present, often in close geographic or stratigraphic proximity to one another, suggesting that these rocks were deposited on a partly emergent arc edifice. Units of all ages have been intruded by the Jurassic Kleanza pluton and smaller bodies of Eocene age that relate to the eastern margin of the Coast Plutonic Complex. The relationship between the Kleanza pluton and the overlying Telkwa volcanic rocks is, in part, transitional, and similarities between the border phases of the pluton and Telkwa volcanic units suggest that these plutons were direct sources of volcanic magmas.

ACKNOWLEDGMENTS

We wish to thank Ellie Knight and Nicole Boudreau for their fine contributions to the Usk map; and Dan Parker, Richard Seymour and Chad Gerow of the Kitselas First Nations for their assistance in the field. The first author thanks Andrew McRae for his help in constructing the cross-sec-

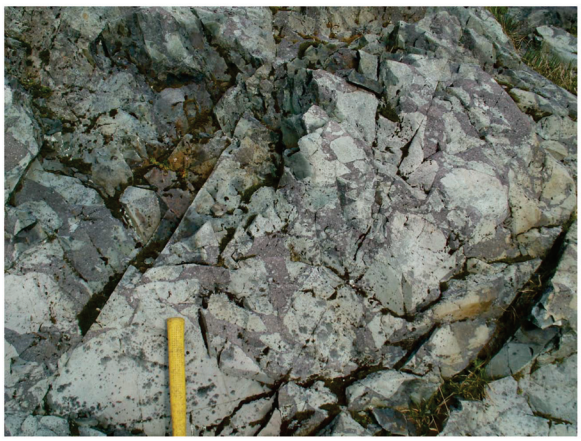

Figure 9. Peperitic, flow-banded white rhyolite in a red dacitic tuff groundmass, Usk map area, near Terrace, BC.

tions, and Jarda Dostal for his ever-present support and guidance.

REFERENCES

Anderson, R.G. (1993): A Mesozoic stratigraphic and plutonic framework for northwestern Stikinia, northwestern British Columbia, Canada; *in* Mesozoic Paleogeography of the Western United States – II; Dunne, G. and McDougall, K., Editors, Society of Economic Paleontologists and Mineralogists, Pacific Section, Volume 71, pages 477–494.

Brown, D.A., Logan, J.M., Gunning, M.H., Orchard, M.J. and Bamber, W.E. (1991): Stratigraphic evolution of the Paleozoic Stikine assemblage in the Stikine and Iskut rivers area, northwestern British Columbia; *Canadian Journal of Earth Sciences*, Volume 28, no 6, pages 958–972.

Gareau, S.A., Friedman, R.M., Woodsworth, G.J. and Childe, F. (1997a): U-Pb ages from the northeastern quadrant of Terrace map area, west-central British Columbia; *in* Current Research 1997-A/B, *Geological Survey of Canada*, pages 31–40.

Gareau, S.A., Woodsworth, G.J. and Rickli, M. (1997b): Regional geology of the northeastern quadrant of Terrace map area, west-central British Columbia; *in* Current Research 1997-A/B, *Geological Survey of Canada*, pages 47–55.

Gunning, M.H., Bamber, E.W., Brown, D.A., Rui, L., Mamet, B.L. and Orchard, M.J. (1994): The Permian Ambition Formation of northwestern Stikinia, British Columbia; *in* Pangea: Global Environments and Resources, Embry, A.F., Beauchamp, B. and Glass, D.J., Editors, *Canadian Society of Petroleum Geologists*, Memoir 17, pages 589–619.

Logan, J.M., Drobe, J.R. and McClelland, W.C. (2000): Geology of the Forrest Kerr – Mess Creek area, northwestern British Columbia; *BC Ministry of Energy, Mines and Petroleum Resources*, Bulletin 104, 164 pages.

Nelson, J.L., Barresi, T., Knight, E. and Boudreau, N. (2006): Geology and mineral potential of the Usk map area (NTS 103I/09), near Terrace, British Columbia; Geological Fieldwork 2005, *BC Ministry of Energy, Mines and Petroleum Resources*, Paper 2006-1 and *Geoscience BC*, Report 2006-1.

Richards, T.A. and Tipper, H.W. (1976): Jurassic stratigraphy and history of north-central British Columbia; *Geological Survey of Canada*, Bulletin 270, 73 pages.

van der Heyden, P. (1992): A Middle Jurassic to early Tertiary Andean-Sierran arc model for the Coast Belt of British Columbia; *Tectonics*, Volume 11, pages 82–97.

Wilmoth, RA and Walker, G.P.L. (1993): P-type and S-type pahoehoe: a study of vesicle distribution patterns in Hawaiian lava flows; *Journal of Volcanology and Geothermal Research*, Volume 55, pages 129–142.

Wright, J.V., Smith, A.L., and Self, S. (1980): A working terminology of pyroclastic deposits; *Journal of Volcanology and Geothermal Research*, Volume 8, pages 315–336.

A.3: Alldrick, D.J., Nelson, J.L., and Barresi, T. 2005a. Geology and mineral occurrences of the upper Iskut River area: Tracking the Eskay Rift through northern British Columbia. In Geological Fieldwork 2004, British Columbia Ministry of Energy and Mines, British Columbia Geological Survey Paper 2005-2: 2-39.

Geology and Mineral Occurrences of the Upper Iskut River Area: Tracking the Eskay Rift through Northern British Columbia (Telegraph Creek NTS 104G/1, 2; Iskut River NTS 104B/9, 10, 15, 16)

By D.J. Alldrick[1], J.L. Nelson[1] and T Barresi[2]

KEYWORDS: bedrock mapping, Eskay Creek, Eskay Rift, Hazelton Group, Stuhini Group, mineral deposits, VMS, Targeted Geoscience Initiative-II (TGI-II)

INTRODUCTION

The Eskay Creek gold-silver mine, located in northwest British Columbia, is the highest-grade precious-metal volcanogenic massive sulphide deposit in the world. The mining industry continues to spend more than $2 million each year on exploration for similar deposits in the area. The geologic setting at the minesite is well studied, but large tracts in north-central British Columbia require more detailed surveys to determine if favourable sites exist for formation and preservation of additional deposits. In 2003, the British Columbia Geological Survey and the Geological Survey of Canada launched a two-year mapping program to delineate the ore horizon through the region north of the mine, and to assess potential for additional Eskay Creek type deposits. This horizon lies within Lower to Middle Jurassic, arc-related, rift sequence rocks along the northwest perimeter of the Bowser Basin, a large (48,000 km^2) Middle Jurassic to Early Cretaceous sedimentary basin (Fig. 1).

The field portion of the project has now covered 1,300 km^2, extending 125 km north from the Eskay Creek mine to the Red Chris deposit (Fig. 2). The paved Stewart-Cassiar Highway (Highway 37) runs northward along the eastern edge of the map area. In 2003, the first field season, an eight-person team mapped 70 km along the rift sequence between Kinaskan Lake and More Creek (Fig. 2). In 2004, three geologists mapped 40 km along the rift sequence between More Creek and Palmiere (Volcano) Creek. Ongoing work will include compilation from published sources and completion of two final 1:50,000-scale maps and one 1:100,000-scale map, scheduled for release in 2005.

[1] *British Columbia Ministry of Energy and Mines, Email:* Dani.Alldrick@gems6.gov.bc.ca

[2] *Department of Earth Science, Dalhousie University*

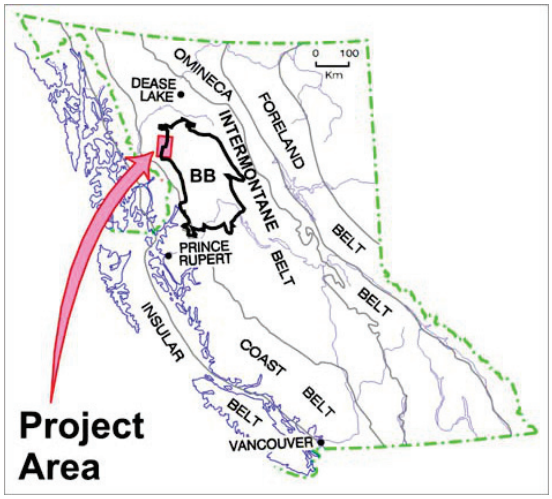

Figure 1. Project location map showing Bowser Basin (BB). Modified from Logan (2000).

The project area straddles the eastern edge of the Coast Mountains and the broad valley of the upper Iskut River. This area lies within the Tahltan First Nation traditional area and they participated directly in this project. Topography varies from rounded glacial valleys along the upper Iskut River, to the extensive Spatsizi Plateau, to high serrated ridges and peaks that are being actively glaciated. Elevations range from 250 m above sea level at the confluence of Iskut River and Forrest Kerr Creek, up to 2,662 m at the summit of Hankin Peak in the west-central region of the field area. Mount Edziza can be seen rising to 2780 m near the northern boundary of the study area. Vegetation comprises boreal spruce-pine-fir forest at low elevations. Timberline is at 1400 m elevation with subalpine fir and meadow areas above.

Regional-scale geology maps and reports for this area include Operation Stikine (1957), Souther (1972), Read *et al.* (1989), Evenchick (1991), Logan *et al.* (1990, 1992, 1993, 1997, 2000), Gunning (1996), Ash *et al.* (1995, 1996, 1997a, 1997b) and Evenchick *et al.* (2002) (Fig. 2). Detailed geological maps are available

in theses by Schmitt (1977) and Kaip (1997) and in many company assessment reports cited in ARIS and MINFILE. The most recent and most comprehensive study of the Eskay Creek orebodies is the PhD thesis by Tina Roth (2002) which offers an extensive bibliography of all previous reports on the deposit, including many progress reports and final reports that were part of the Iskut Metallogeny Project of the Mineral Deposits Research Unit at the University of British Columbia (Macdonald *et al.*, 1996).

Anderson (1993) interpreted the present study area as the northern extension of a large fault-bounded belt or rift. Sections of this rift have been mapped at 1:50,000 scale by Read (1991), Logan *et al.* (1990, 1992, 1993) and Ash *et al.* (1997b). The current project will complete 1:50,000-scale coverage between these earlier mapping projects, with more detailed mapping of the strata of the upper Hazelton Group, and detailed stratigraphic investigations within the Eskay Rift (e.g. Simpson and Nelson, 2004; Barresi *et al.*, this volume). The federal and provincial governments have jointly funded this study as part of the "Bowser Basin Energy and Mineral Resource Potential Targeted Geoscience Initiative".

REGIONAL GEOLOGIC SETTING

The project area lies on the western edge of the Intermontane Tectonic Belt, within Stikine terrane, and is bounded to the east by the Bowser sedimentary basin (Fig. 1). It straddles the tectonic elements of the Bowser structural basin and the Stikine Arch to the northwest.

Souther (1972) and Logan *et al.* (2000) describe the geological history of the area as a series of five mid-Paleozoic to mid-Mesozoic volcanic arcs developed in sediment-poor and sediment-rich marine settings. Lulls in volcanism at the Triassic-Jurassic boundary and in the uppermost Lower Jurassic were marked by tectonic uplift, deformation and erosion, termed the Inklinian and Nassian orogenies respectively (Souther, 1972).

Strata range in age from Devonian to Holocene (Fig. 3). The major stratigraphic units exposed within the project area are the Paleozoic Stikine Assemblage, Triassic Stuhini Group, Lower to Middle Jurassic Hazelton Group, Jurassic-Cretaceous Bowser Lake Group and Pleistocene Mount Edziza Complex. The Stikine Assemblage was defined by a Geological Survey of Canada team (Operation Stikine, 1957) and has most recently been described by Logan *et al.* (2000). It consists of Early Devonian to mid-Permian volcanic and sedimentary strata, characterized by thick carbonate members. The Upper Triassic Stuhini Group typically consists of pyroxene porphyritic basalt flows and breccias with intercalated clastic sedimentary rocks and minor carbonate units. The Early to Middle Jurassic Hazelton Group is an island arc succession composed of a lower package of intermediate volcanic rocks and derived clastic sedimentary units; a middle interval of thin, but widely distributed felsic volcanic rocks; and an upper unit of fine clastic sedimentary rocks with local bimodal volcanic rocks dominated by basalt.

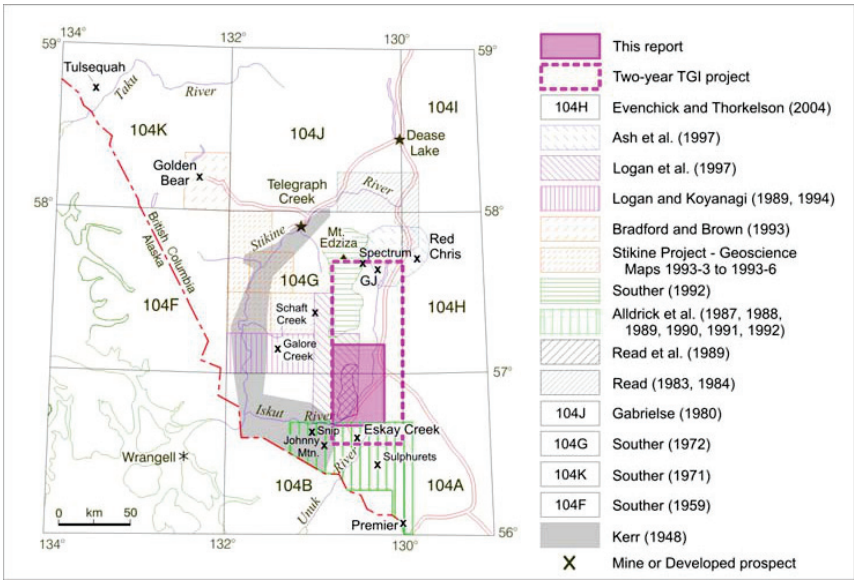

Figure 2. Current project outline and previous geologic mapping. Modified from Logan (2000).

Carbonate units are rare or absent in Hazelton Group strata. The Middle Jurassic to Early Cretaceous Bowser Lake Group is a thick, clastic marine sedimentary succession. Miocene to Recent volcanic strata from the Mount Edziza volcanic complex blanket the northwest part of the project area.

Regional-scale unconformities within the study area include a Late Permian - Early Triassic unconformity, a Late Triassic - Early Jurassic angular unconformity and nonconformity, and a late Early Jurassic angular unconformity.

Logan *et al.* (2000) describe five plutonic episodes in the area (Middle to Late Triassic Stikine; Late Triassic to Early Jurassic Copper Mountain; Early Jurassic Texas Creek; Middle Jurassic Three Sisters; Eocene Hyder). The four youngest plutonic suites generated important mineral deposits.

To the south, mid-Cretaceous regional metamorphism reached a maximum grade of lower greenschist facies (Alldrick, 1993). In the current field area, chlorite is rare to absent and prehnite is present, thus the regional metamorphic grade is interpreted as sub-greenschist, mid-prehnite-pumpellyite facies (Alldrick *et al.*, 2004).

GEOLOGY OF THE MAP AREA

Mapping in the 2004 field season covered Paleozoic to Middle Jurassic strata at the southern end of the two-year project area (Fig. 2). Several topographic features in this year's map area have been informally named to simplify description of locations (Fig. 4). Simplified geology of the 2004 map area is presented in Figure 5. Age control is provided by fossil collections from Souther (1972), Read *et al.* (1989), Logan *et al.* (2002) and Evenchick *et al.* (2001), and by isotopic age dates tabulated in the new BCAge database (Breitsprecher and Mortensen, 2004).

Stratified Rocks

STIKINE ASSEMBLAGE (MIDDLE TO UPPER PALEOZOIC)

Volcanic and carbonate upper Paleozoic strata of the Stikine Assemblage were mapped in this year's survey. A large tract of complexly faulted Permian, Triassic and Jurassic strata crops out immediately north of Pillow Basalt Ridge, underlying a well glaciated spine called Sixpack Range (Fig. 4 and 5). The strata are emplaced along a series of south verging thrust faults that stack Paleozoic to Jurassic stratigraphic successions into three repetitions (Fig. 5).

Stikine Assemblage rock types exposed in this area include green chloritic tuff, lapilli tuff, massive andesitic to dacitic feldspar-porphyritic flows, massive and flow-banded dacite and rhyolite, pillow basalt, tuffaceous and siliceous siltstone, ribbon chert and several thin, highly recrystallized white carbonate beds. These rocks are all interpreted to be Permian age.

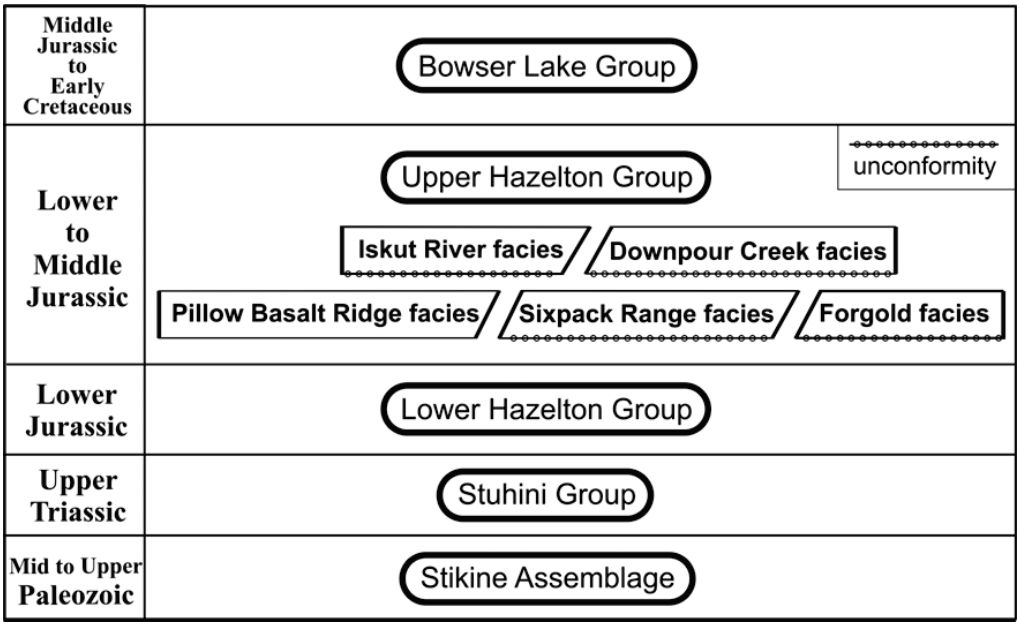

Figure 3. Schematic regional stratigraphy of the 2004 map area.

Permian strata are strongly foliated everywhere and multiple generations of foliation are apparent in most outcrops. Thin-bedded units may also show crenulations. Bedding is parallel or sub-parallel to the foliation. Some weathered outcrop surfaces in the carbonate rocks reveal sparse crinoid ossicles that are not visible on fresh surfaces of the recrystallized limestone.

Basal contacts are thrust faults. Upper contacts are commonly erosional unconformities. In one location close to Forrest Kerr Creek, pillow lavas of Early to Middle Jurassic age (?) lie unconformably upon strongly foliated Paleozoic strata.

STUHINI GROUP (UPPER TRIASSIC)

In the map area, the Stuhini Group consists of mafic to felsic (dacitic) volcanic flows; thin-bedded, interbedded black and olive green waterlain tuffs; derived clastic sediments including orange-weathering carbonate cemented sandstones; siliceous black siltstones; black and white limestone beds; and weakly pyritic black rhyolite and white rhyolite units.

Pyroxene-bearing basalts are common and typically fine-grained to weakly augite +/- feldspar porphyritic. Thick (20-30 m) massive andesitic to dacitic flow units are finely feldspar porphyritic and show faint columnar jointing in cliff-face exposures.

Extensive orange-weathering, well-sorted sandstone forms a thick stratigraphic interval that includes intercalated black siliceous siltstone, massive black and white limestone units and regionally extensive, flow-layered chert that varies from black to pale grey to white, and carries dust-size disseminated pyrite. Individual horizons within the buff- to orange-weathering sandstone host fossil wood debris.

The pyritic rhyolite units have been explored in three separate locations (Bench, Sinter and Southmore prospects) where structurally disrupted, crackled rhyolite beds are highly gossanous. Upper Triassic copper-bearing mafic volcanics exposed between 1800 to 2000 m elevation near the crest of Sixpack Range have not yet been explored (*see* Malachite Peak prospect).

On the southeast side of the Sixpack Range, these strata are cut by two small diorite and gabbro plugs and by a more extensive sill of hornblende and plagioclase porphyritic, potassium feldspar megacrystic granodiorite similar to the intrusions of the Texas Creek Suite exposed elsewhere in this region.

HAZELTON GROUP (LOWER TO MIDDLE JURASSIC)

Lower Jurassic

Strata of the Lower Hazelton Group form two belts in the northern part of the map area (Fig. 5). Northeast of Downpour Creek, a dominantly volcanic sequence includes andesite and rhyolite flows, hematitic epiclastic siltstones, sandstones and coarse, heterolithic epiclastic conglomerates, and black siltstones. The calcareous sandstone units are favourable hosts for fossil wood debris and fossil-rich bioclastic horizons that contain ammonites and bivalves. A collection from one of these intervals contains Sinemurian ammonites (Logan *et al.*, 2000, p. 45).

A second, north-trending belt of feldspar-phyric extrusive dacites and related plagioclase (± Kspar) phyric granodiorite to monzonite intrusions lies along the eastern side of the Forrest Kerr fault from the headwaters of Downpour Creek to north of More Creek. As described below, numerous showings and alteration zones on the RDN claims are related to this unit, including the Marcasite Gossan and the spectacular Gossan Creek Porphyry gossan. Three U-Pb ages of 193.0±1.3 Ma, 193.6±0.3 Ma and 193.6±1.0 Ma on both intrusive and extrusive bodies establish the age of these rocks as Late Sinemurian (Mortensen *et al.*, this volume). It is thus coeval with, but different in character from, the sequence east of Downpour Creek, giving an insight into the degree of local variability of volcanic facies in the lower Hazelton Group.

Lower to Middle Jurassic

Rocks of probable late Early Jurassic (Toarcian) to Middle Jurassic (Aalenian to Bathonian) age occur in several distinct outcrop areas located between Forrest Kerr Creek to the west, More Creek to the north, and the Iskut River to the east (Fig. 5). The different outcrop areas are described here as five different facies packages (Fig. 3 and 5) because of the pronounced variations in stratigraphy and thicknesses between them.

These units are considered to be broadly coeval (Fig. 3), although precise age controls are lacking in most areas. The Downpour Creek facies has been dated as Toarcian through Bathonian, based on macrofossils, conodonts and radiolaria (Read *et al.*, 1989; Logan *et al.*, 2000). The thick pile of pillow basalts that dominates the Pillow Basalt Ridge (PBR) facies has been correlated with the Middle Jurassic hangingwall basalt unit at the Eskay Creek mine. Similar, although much thinner, basalts crop out sporadically northwards from western PBR into the Forgold area. The Sixpack Range facies lies unconformably on Paleozoic and Triassic basement, and interfingers with and underlies the Downpour Creek facies. The Iskut River unit contains fossils dated as Middle to possibly early Late Jurassic (Collection F141, Read *et al.*, 1989). The Iskut River unit continues south and east across the Iskut River, to Iskut-Palmiere Ridge, where it overlies a basalt unit that is correlated with the hangingwall basalt at the Eskay Creek mine.

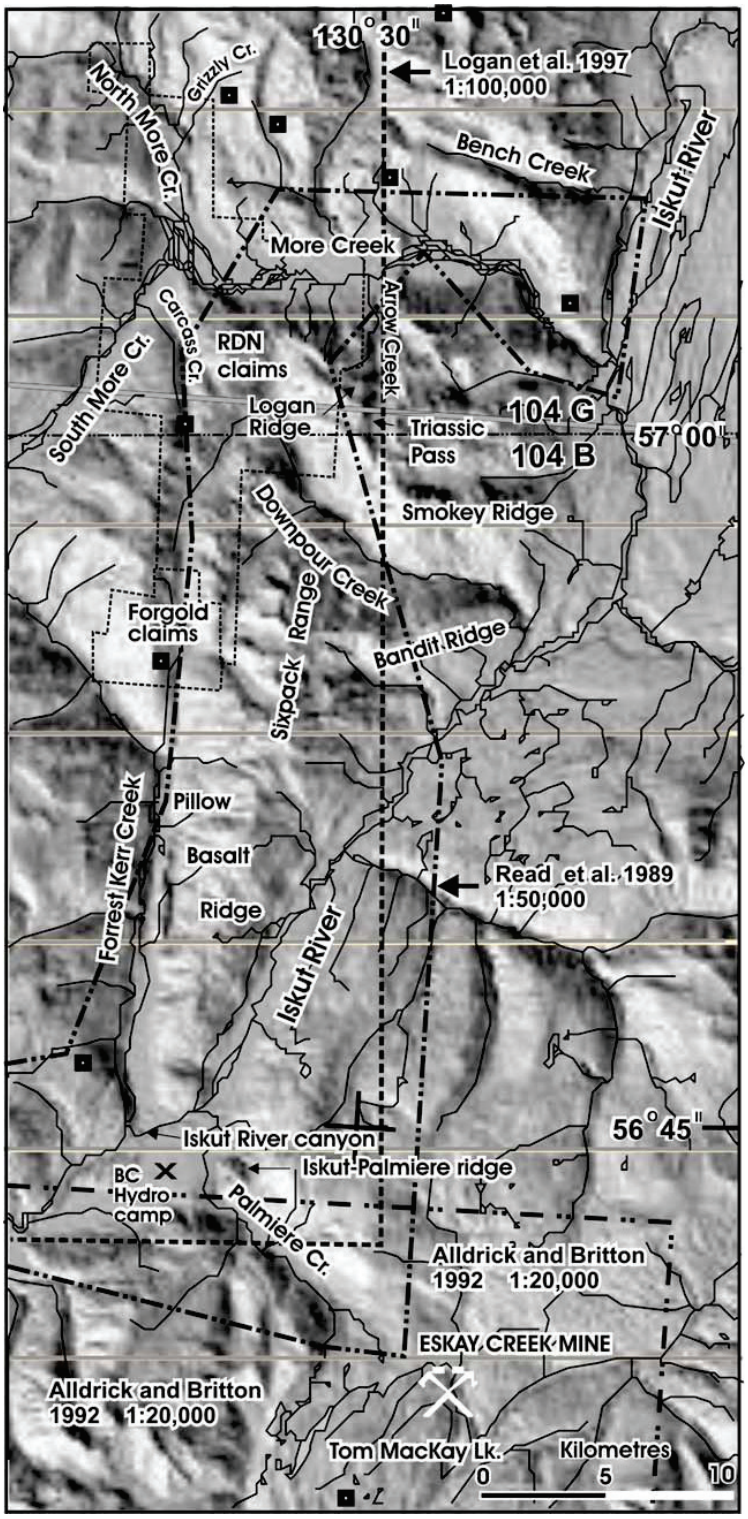

Figure 4. Shaded DEM map showing major topographic features in the 2004 map area and boundaries of previous regional mapping projects.

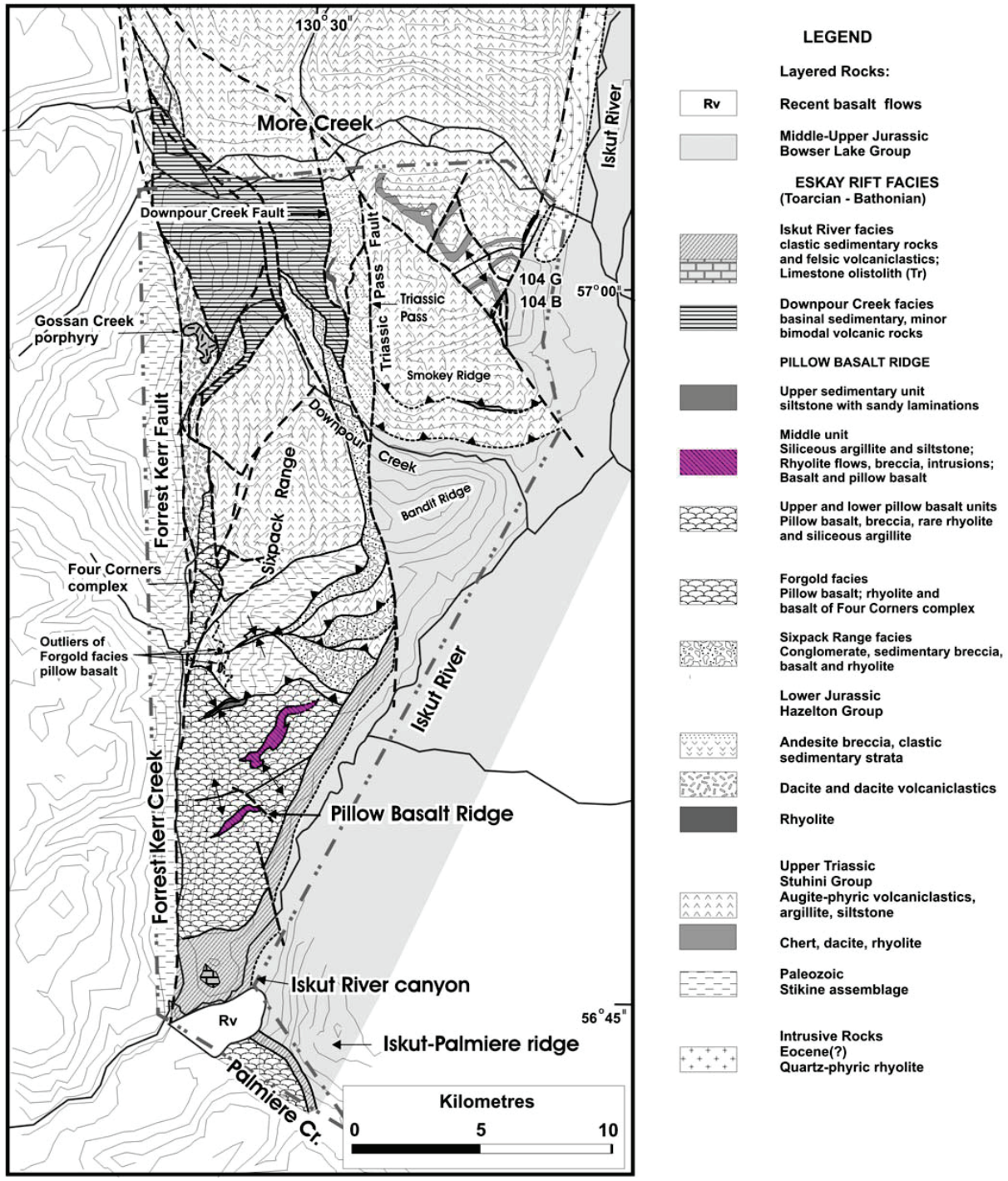

Figure 5. Simplified geologic map of the More Creek - Palmiere Creek area.

Pillow Basalt Ridge (PBR facies)

Pillow Basalt Ridge is 12 km long and 6 km wide. It is the main ridge between the Iskut River and lower Forest Kerr Creek. With the exception of overlying Iskut River unit rocks exposed at lower elevations to the east and south, the entire ridge is composed of PBR facies rocks. To the west, the Forest Kerr fault juxtaposes the PBR facies against Paleozoic rocks. To the north, the Kerr Bend fault thrusts Paleozoic, Triassic and Jurassic strata over PBR.

Features of the PBR facies are summarized here; they are fully described in Barresi *et al.* (this volume). Pillow Basalt Ridge is composed of over 2000 m of mostly pillow basalt and pillow basalt breccia. A "Middle Unit" of variable thickness within the pillow basalt sequence is composed of more than 50% mafic rock (fine- to medium-grained massive basalt and pillow basalt), rhyolite flows, domes, and breccias, and fine-grained siliceous pyritic argillite and tuff. Some individual rhyolite and sedimentary horizons within this bimodal igneous-sedimentary Middle Unit can be traced for at least 3 km along strike.

The voluminous volcanic rock and large regional extent of the Pillow Basalt Ridge facies suggests deposition within a major Middle Jurassic rift segment, similar to that of Table Mountain, located to the north (Alldrick *et al.*, 2004; Simpson and Nelson, 2004). The discovery of the bimodal igneous/sedimentary Middle Unit within the PBR facies indicates that significant intervals with potential to form and preserve Eskay Creek-style mineralization may be present within extensive, less prospective pillow basalt sequences throughout the length of the Eskay rift.

The PBR facies is overlain by two separate units: the Iskut River facies, described in the following section; and a homogeneous, siltstone-dominated unit that occupies the core of a small northeast-trending syncline next to the Kerr Bend fault (Barresi *et al.*, this volume). In the syncline, a transitional contact is observed. Pillow basalts interfinger with sand-laminated siltstone and limy siltstone fills inter-pillow interstices. The sedimentary rock types within this unit, and the nature of its contact with the PBR basalts, are in strong contrast to the Iskut River unit.

Iskut River unit

The Iskut River unit overlies the PBR facies in the lowlands along the west side of the Iskut River (Fig. 5), east and downslope of the crest of Pillow Basalt Ridge, and on the low hill south of Pillow Basalt Ridge and extending into the Iskut River Canyon near the old BC Hydro camp (Fig. 4). Correlative strata occur on the Iskut-Palmiere Ridge, where they lie depositionally between basalt assigned to the Eskay hangingwall unit, and basal strata of the Bowser Lake Group. A fossil age for this unit, from samples collected along the Iskut River canyon, is Middle Jurassic or possibly early Late Jurassic (Collection F141; H.W. Tipper in Read *et al.*, 1989), making it one of the younger units in the Lower-Middle Jurassic Eskay Rift sequence.

Downhill and east of Pillow Basalt Ridge, the Iskut River unit consists of mixed siliciclastic and felsic volcanic strata, with a preponderance of coarse clastic material. The felsic rocks are mostly light green to pale grey volcaniclastics, rhyolite and dacite breccias, and fine crystal-dust tuffs. One outcrop ridge of massive rhyolite was located in the course of two traverses in the area; it is likely that more could be identified with further detailed work. The siliciclastics comprise interbedded white arkosic sandstone, sedimentary breccia, quartz-feldspar granule conglomerate and dark grey silty argillite. In some areas, thinly interbedded sandstone and argillite resemble the Bowser Lake Group. They are distinguishable, however, based on the presence of felsic detritus and the absence of chert clasts in the sandstones, and on the presence of interbeds of felsic volcaniclastic material. In other exposures, bedding is uneven and soft-sediment deformation features and sedimentary intraclasts are present. A notable feature of this sequence is the common occurrence of large felsic volcaniclastic olistoliths as well as small white, pale green and bright sea-green felsic clasts within sedimentary breccias. They show irregular, wispy outlines indicative of incorporation in the matrix while still unconsolidated. Felsic detritus decreases in abundance northward. North of Pillow Basalt Ridge (north of the Kerr Bend fault), the sequence consists of a thick, cliff-forming unit of white arkosic sandstone overlain by dark grey slate that extends east as far as the Iskut River.

South of Pillow Basalt Ridge, the Iskut River unit is dominated by dacitic volcaniclastic material, with subordinate black argillite and other rock types. The felsic breccias are chaotic and unsorted. Clasts range in size up to olistoliths many metres across. All clasts are angular. Concentrations of coarser clasts show incipient fragmental (crackle breccia) to disaggregated (mosaic breccia) textures. Pulverised, fine-grained, sand-sized material occurs as both the clast component with an aphanitic groundmass, and as the groundmass component to larger clast populations. The source volcanic rock, as seen in clasts, is pale green, aphanitic to porphyritic dacite with small, sparse feldspar crystals. Massive dacite is rare. One outcrop of black, flow-banded rhyolite was noted. Its contact relationships are unknown, it could be either a local flow or a large block within the breccia.

Read *et al.* (1989) show a single outcrop of limestone at the base of the felsic unit on the south slope of Pillow Basalt Ridge from which they extracted Early Permian conodonts (collection F129). This limestone is an olistostromal block surrounded by felsic breccia matrix. Other smaller limestone exposures occur within the felsic breccia. The nearest present exposures of Early Permian limestone are 4 km west of Forrest Kerr

Creek, and 10 km to the north within the uplifted block of Paleozoic rocks north of the Kerr Bend fault.

The hill immediately south of Pillow Basalt Ridge, and immediately northeast of the mouth of Forrest Kerr Creek is underlain by basalt, andesite and dacite flows or tuffs and mixed sedimentary rocks, and is intruded by small diorite and gabbro plugs. This strata is cut by a recent volcanic chimney south of the hill's summit area, where a small circular lake fills the vent. Carbonates on this hill have given Triassic conodont ages (Collection F138, Read *et al.*, 1989); they could be olistrostromes like the Paleozoic body described above.

North of Palmiere (Volcano) Creek, a thin unit of felsic volcaniclastics and argillite crops out in the saddle between the main high ridge to the northeast and the small spur that overlooks the lower Iskut River Valley to the west. The lower part of this unit consists of chaotic, unsorted felsic breccia similar to the breccias of the Iskut River unit exposed at the south end of Pillow Basalt Ridge. The source rock is a pale grey-green to white, aphanitic to microporphyritic dacite or rhyolite. Clasts of medium-grained granodiorite are also present in the breccia. Most common are angular-clast breccias and crystal-dust tuffs, all without visible bedding. Rhyolite mosaic breccia with a black, siliceous matrix is present in places. The felsic breccias are overlain transitionally by black, siliceous, pyritic argillite which hosts the Iskut-Palmiere mineral occurrence. Beds of felsic breccia and individual felsic clasts occur within the basal part of the argillite. All these rocks overlie basalt, which is correlated with the Eskay hangingwall unit and the PBR basalts, and these rocks are overlain in turn by sandstones and mudstones of the Bowser Lake Group.

The Iskut River unit overlies the pillow basalts and siliceous siltstones of Pillow Basalt Ridge facies with angular discordance, truncating units in the gently folded underlying sequence. A strong set of northeasterly topographic linears on southeastern PBR, interpreted as flow-layering between separate eruptions of pillow basalt, is deflected northwards towards the base of the Iskut River unit. The Kerr Bend fault does not penetrate the base of the Iskut River unit. North of the fault, Iskut River unit arkose overlies rocks of the hangingwall strata of the Kerr Bend fault. The upper contact of the Iskut River unit with the Bowser Lake Group was not observed during this study.

The Iskut River unit exhibits a marked departure in volcanic and sedimentary regime from the underlying PBR facies. Quiet basalt effusion was succeeded by explosive felsic, mainly dacitic volcanism, while the pelagic, distal sedimentation associated with PBR was succeeded by coarse siliciclastic sedimentation in the Iskut River unit. Steep slopes are indicated by coarse grain sizes, synsedimentary deformation, and olistoliths sourced from both felsic breccias within the sequence, and from Paleozoic and Triassic limestones and possibly other strata from within the basement. Its unconformable relationships with the PBR rocks and with the Kerr Bend fault suggest that it postdated thrust displacement on the fault. Thus the Iskut River unit marks a profound change in basin geometry, with renewed uplift of rift margins, fault reactivation and the development of new fault patterns.

Forgold facies and the Four Corners complex

The Forgold facies, which hosts the Four Corners volcanic complex, is located east of Forest Kerr Creek, and south of the headwaters of Downpour Creek. It is a north-south elongated, fault-bounded segment of mainly volcanic rock, inferred to be Middle Jurassic rift-related strata (pending U/Pb dates). The main Forest Kerr fault to the west, and a splay of the Forest Kerr fault to the east, juxtapose the Forgold facies units with Paleozoic, Triassic and Lower Jurassic units. To the south, basalts of the Forgold facies lie in unconformable contact on Paleozoic and Triassic strata, exposed in a waterfall as remnant patches of undeformed pillow basalt resting on highly deformed basement. At the northernmost extent of the Forgold facies, on the eastern side of Downpour Creek's headwaters, pillow basalts lie in unconformable contact on Lower Jurassic strata to the west and in faulted contact with Triassic strata to the east.

Overall, the volcanic and sedimentary rocks of the Forgold facies are similar to those of Pillow Basalt Ridge. In contrast to Pillow Basalt Ridge, the Forgold facies is dominated by a local felsic volcanic centre (the Four Corners complex) which is similar to, but larger than, the volcanic complexes found in the Middle Unit of the Pillow Basalt Ridge facies. With the exception of the Four Corners felsic volcanic complex, the Forgold facies is composed of aphanitic, rarely vesicular, pillow basalt, pillow basalt breccia, and rare flow-banded basalt.

The Four Corners complex is a volcanic centre composed of intrusive and extrusive felsites and fine- to medium-grained basalt, with onlapping pillow basalts and fine, siliceous sedimentary rock. The structural orientations of sedimentary and layered volcanic rocks on and around the dome are largely controlled by the paleotopography of the dome. The core of the dome is composed of feldspar-phyric felsic rock (Fig. 6a) that is crosscut by 1 to 3 m thick aphanitic and feldspar phyric, flow-banded rhyolite dikes, and sets of medium-grained diabase (basalt) dikes. Near the core of the dome, the contacts between felsic and mafic dikes, and between the dikes and the surrounding dome, are amoeboid (Fig. 6b), indicating that they are magma-mixing textures developed between coeval intrusions. The flanks of the dome are composed of 1 to 5 m thick, layered rhyolite flows with interbedded layers of siliceous sedimentary rocks, massive basalt flows and pillow basalt flows. All are crosscut by rhyolite dikes. Overlying the felsic dome are a decreasing proportion of coarse-grained, massive basalt and fine-grained rhyolite flows, and an increasing proportion of pillow basalt flows. Felsic

A)

B)

Figure 6. A) Rhyolite intrusion in the centre of the Four Corners complex. B) Detail of irregular contacts between felsic and mafic dikes in the complex, indicating coeval emplacement.

dikes are less common. Basalt that erupted above the felsic dome was likely superheated, as suggested by the presence of fire fountain deposits.

The suite of rocks that comprise the Four Corners complex and immediate surrounding area is similar to that found in the Middle Unit of the Pillow Basalt Ridge facies. Felsic rocks include aphanitic white and cream weathering, flow-banded rhyolite with semi-translucent fresh surfaces; and white to salmon weathering feldspar-phyric rhyolite. These are accompanied by medium-grained basalt that has characteristic radiating feldspar microlites (first described near the Eskay Creek mine by Lewis *et al.* [2001]) and, in places, a distinctive glomeroporphyritic texture of feldspar and/or pyroxene. On the flanks of the dome, these rocks are extrusive, and take the form of breccias and flows. In one location, a breccia of toppled columnar-jointed basalt is preserved. Onlapping sedimentary rocks are rusty weathering, siliceous, pyritic, fine-grained, dark grey to black mudstones and/or tuff and/or chert. They are bedded on a 1 to 15 cm scale and have sharply eroded upper contacts. Some beds have spherical, white weathering crystals up to 1 cm in diameter, similar to prehnite found in the mudstones at Eskay Creek mine and on Pillow Basalt Ridge (Ettlinger, 2001; Barresi *et al.*, this volume).

The Forgold facies is fault bounded. Consequently its relationship to other rift fragments is uncertain. The facies bears a strong resemblance to that of Pillow Basalt Ridge, and may represent a narrower northern extension of the rift basin that accommodated the Pillow Basalt Ridge facies. Alternatively it may be an independent rift fragment. The unconformable contact between this facies and underlying Upper Paleozoic, Upper Triassic and Lower Jurassic strata suggests that it was deposited on a block of these strata which had already undergone significant uplift and erosion.

Sixpack Range facies

Strata of the Upper Hazelton Group crop out extensively on the eastern slopes of Sixpack Range, extending from the Kerr Bend fault in the south to Downpour Creek in the north.

The basal units are well exposed immediately north of Kerr Bend fault. The basal talus breccia (Fig. 7a) is overlain by a thick (>500 m) interval of massive crystalline basalt flows cut by rare white rhyolite dikes, sills and flows. Towards the top of this thick mafic volcanic interval, these rocks are progressively interlayered with overlying monolithic to heterolithic volcanic breccias, conglomerates and sandstones. These thick sequences of volcanic sandstones and granule to pebble conglomerates consist predominantly of felsic volcanic clasts. Locally, clast composition varies and can include up to 20% limestone clasts, up to 25% hornblende-plagioclase porphyritic potassium feldspar megacrystic granodiorite clasts, or up to 10% black siltstone clasts. Local concentrations of scattered clasts of pyritic siltstone produce weakly gossanous weathered surfaces. Sandstones locally display graded bedding and good cross-bedding (Fig. 7b and 7c). Intercalated rock units are grey to black limestone, black siltstone, a single minor rhyolite flow, and minor sills and dikes of rhyolite and hornblende-plagioclase porphyritic potassium feldspar megacrystic granodiorite.

At its southern limit, the base of this stratigraphic unit is a thick talus breccia of predominantly carbonate clasts, that rests unconformably above foliated Permian carbonate rocks. The talus breccia evolves in character moving away from the Permian footwall rocks, changing from monolithic carbonate breccia, to heterolithic, volcanic-dominated breccia to coarse, well-bedded to cross-bedded sandstones and grits. These in turn are overlain by the thick succession of massive basalt flows.

Elsewhere the basal contact of the Jurassic strata is an unconformity, overlying Triassic or Permian footwall rocks (Fig. 7d). Where exposed, the upper contact for this strata is a thrust fault contact, with overlying Permian or Triassic rocks in the hangingwall.

Downpour Creek facies

The Downpour Creek facies is exposed north of Downpour Creek on both sides of the pass that separates Downpour Creek from More Creek. To the west, rocks of this facies are cut off by the Forrest Kerr fault. Their eastern limit is the north-striking Downpour Creek fault that juxtaposes them against Lower Jurassic strata (Fig. 8a).

These rocks were previously mapped by Read *et al.* (1989) and Logan *et al.* (2000). Remapping in 2004 has led to a modified structural interpretation and revised stratigraphic context. The Downpour Creek facies is dominated by fine-grained clastic rocks, with less than 10% basalt, diabase, gabbro, and felsic volcanic and intrusive rocks. Clastic rocks are dark grey to black argillite with minor thin beds of orange-weathering ankeritic siltstone and sandstone, and rare granule to pebble conglomerate (Fig. 8b). Laminated siliceous siltstone beds become more common in the higher parts of the sequence, whereas coarser interbeds become more rare.

A variety of volcanic rock suites are exposed in this facies. Lenticular pillow basalt flows, black matrix rhyolite breccia, and cobble conglomerate are present within the thick sedimentary sequence. In addition, the ridgetops to the west and northwest of Downpour Creek are capped by volcanic and intrusive rock. The resistant igneous caprock mapped by Logan *et al.* (2000) includes Lower Jurassic and Middle Jurassic volcanic sequences as well as mafic intrusive bodies. The Lower Jurassic volcanic sequences, like those in the Middle

A.

B.

C.

D.

Figure 7. Mid-Jurassic Sixpack Range facies exposures. A. Polymictic talus breccia. B. Graded bedding in granule conglomerate. C. Crossbedding in pebble conglomerate D. Basal unconformity showing polymictic conglomerate overlying well-foliated Paleozoic Stikine Assemblage tuffs.

Jurassic, have pillow basalts and rhyolites, but also contain varied volcaniclastic rocks including volcanic conglomerates and ash and lapilli tuffs. Complicating the volcanic stratigraphy in this area are stocks of diabase and gabbro that have the same radiating microlites and glomeroporphyritic textures as the extrusive Middle Jurassic basalt mapped at Pillow Basalt Ridge, the Four Corners complex, and the Sixpack Range.

The internal stratigraphy of the Downpour Creek facies is not completely understood. Fossil collections are reported from this unit by Souther (1972), Read *et al.* (1989) and Logan *et al.* (2000). Along the ridgecrest west of the pass between Downpour and More creeks, Late Toarcian conodonts occur at two sites (Read *et al.*, 1989); however, Logan*et al.* (2000) report Bathonian macrofossils from the same area. Further north, Logan *et al.* (2000) collected an Aalenian ammonite. Souther (1972) lists Middle Bajocian macrofossil collections east of the pass. Structures in the Downpour Creek area are complex, involving tight folds and multiple fault strands that significantly modify the single syncline inferred in Logan *et al.* (2000).

On the eastern side of Downpour Creek, fine-grained sedimentary beds of the Downpour Creek facies overlie coarse polymictic conglomerates of the Sixpack Range facies in a gradational, interfingering contact. A similar relationship can be inferred several kilometres to the southwest near the headwaters of Downpour Creek, in spite of extensive fault slivering. There, conglomerates are accompanied by monolithologic, chaotic, volcanic-derived debris-flow breccias and minor basalt flows like those seen farther south in the Sixpack Range. East of Downpour Creek, the conglomerates are relatively thin and overlie plagioclase-phyric volcanic rocks correlated with the lower Hazelton Group (Fig. 8b). Based on these observations, the Sixpack Range facies is interpreted as a basal conglomerate to the finer-grained Downpour Creek facies, and as its more southerly, coarse-grained, more proximal equivalent.

Lower – Middle Jurassic facies summary

The units described above illustrate pronounced facies variations in time and space that characterize the late Early to early Middle Jurassic rift environment between the Eskay Creek mine and More Creek.

Pillow Basalt Ridge facies is a 2000 m thick basaltic sequence with a prominent interval in which rhyolites and rhythmically bedded, siliceous, pyritic siltstones are also important. The PBR basalt, which thins dramatically southwards towards the Eskay Creek mine, is overlain by coarse siliciclastic and felsic breccia deposits of the Iskut River unit, which indicates major felsic volcanic eruption and rapid erosion. This unit records a higher energy depositional environment that developed prior to the onset of Bowser Lake Group sedimentation. By contrast, in the syncline on northwestern Pillow Basalt Ridge, only black argillite interfingers with the uppermost PBR basalts, indicating a more quiescent part of the basin.

The massif north of the Kerr Bend fault contains two distinct facies (Fig. 9). On its eastern side, facing the Iskut River, conglomerates, debris-flow breccias, rhyolites and basalts of the Sixpack Range facies unconformably overlie deformed Paleozoic and Triassic basement. To the west, north of the Kerr Bend fault on the slopes facing west over Forrest Kerr Creek and its northern tributary, thin sediment-free pillow basalt outliers of the Forgold facies unconformably overlie the same basement. These sub-Middle Jurassic unconformities on rocks as old as Paleozoic are unique within the Eskay rift system: everywhere else, the base of the sequence ranges from conformable on slightly older Jurassic strata to an unconformity on Upper Triassic or Lower Jurassic basement.

The relationships between these two facies, north of Kerr Bend fault, to each other and to the Pillow Basalt Ridge facies are not well understood. Clasts in the polymictic conglomerates are correlated with Paleozoic and early Mesozoic rocks in the core of the uplift and with quartz-plagioclase-potassium feldspar porphyry inrusions that are known to occur both in the core of the uplift and to the northwest, along the northern tributary of Forrest Kerr Creek. It seems reasonable to derive these conglomerates from the west. If so, the lack of a basal conglomerate below the pillow basalts on the west side of the Sixpack Range must be explained. A possible scenario is that this area was initially exposed subaerially and eroded, and later became a north-trending rift basin.

Both of these facies are juxtaposed abruptly with the thick, monotonous pillow basalt pile south of the Kerr Bend fault (Fig. 3 and 9). The base of the PBR facies is not exposed. It is not known whether it has a basal conglomerate like the Sixpack Range facies to the northeast, or whether the pillow basalts lie directly on older basement as seen to the northwest.

Facies relationships northwards into the Downpour Creek area are clearer. The coarse, proximal Sixpack Range facies passes northward into basinal sediments and lesser bimodal igneous rocks of the Downpour Creek facies (Fig. 9). The northernmost basalts of the Forgold facies unconformably overlie Lower Jurassic dacites in the headwaters of Downpour Creek, just southwest of the proximal to distal transition in the clastic strata. These basalts are over 200 m thick and have no associated sedimentary strata, like those along strike to the south in the western hangingwall strata above the Kerr Bend fault.

The following scenario integrates the various facies packages (Fig. 3 and 9). The Sixpack Range proximal clastic facies is probably oldest, since it in part underlies the Late Toarcian and younger Downpour Creek basinal

A.

B.

Figure 8. Mid-Jurassic Downpour Creek facies exposures. A. View eastward to the fault contact of black, carbonaceous Downpour Creek facies argillite and siltstone against Lower Jurassic rhyolite on Logan Ridge, east of the Downpour Creek fault. B. Looking northwest towards the pass betweeen Downpour Creek and More Creek. Downpour Creek facies argillites in foreground with thin ankeritic sandstone beds overlie ankeritic lower Hazelton Group volcanics. Topographic linears in background are fault strands related to the main Downpour Creek fault.

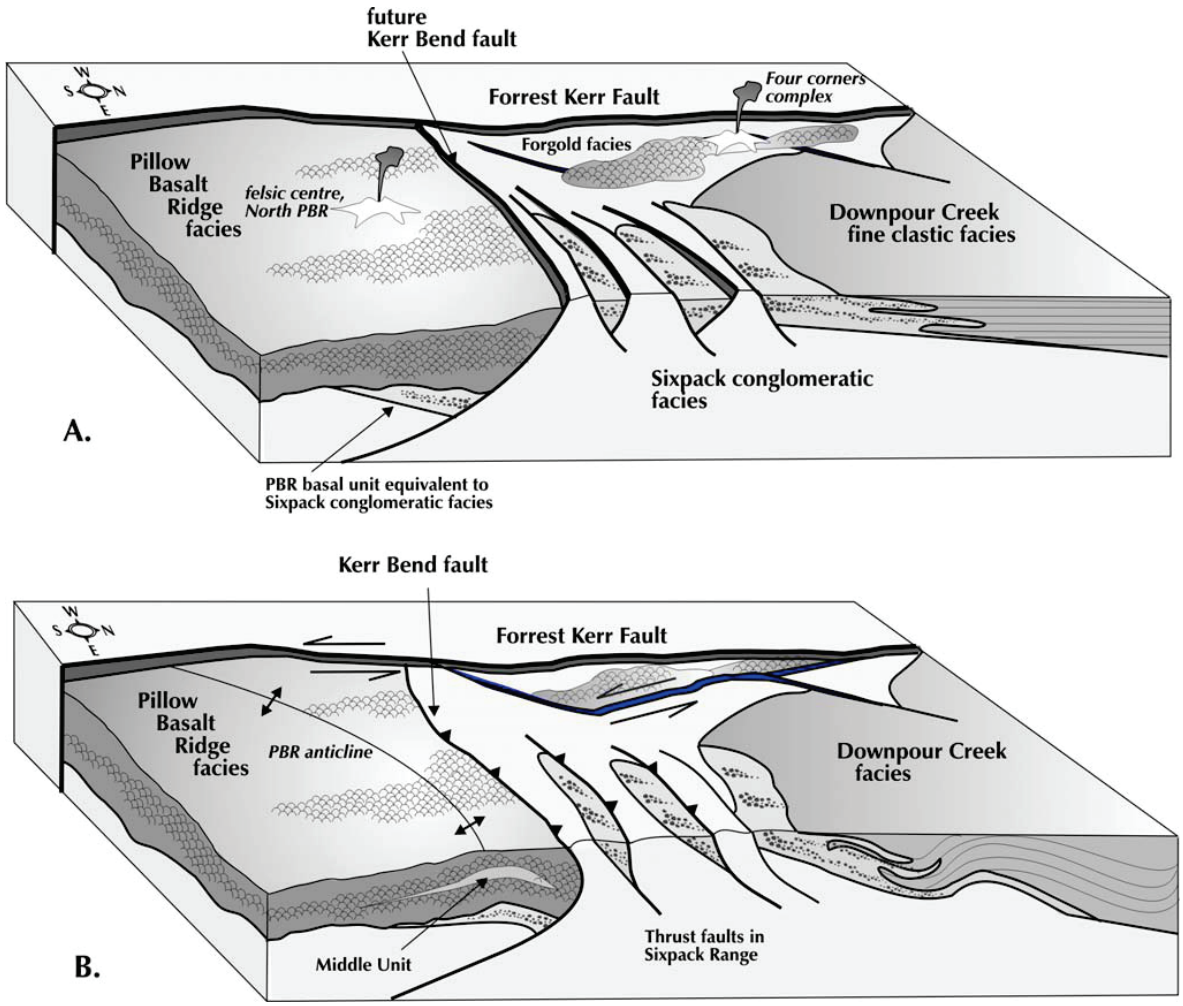

Figure 9. Cartoon block diagrams of map area - view from southeast. Shows the relationships between different mid-Jurassic facies: A. In their inferred syn-rift structural context, and B. during later sinistral shear and basin inversion.

facies. We infer that these two clastic facies were deposited on the eastern and northern flanks of a horst within the Eskay rift system, now preserved as the Paleozoic-Triassic uplift in the core of the Sixpack Range. The horst could have been an elongate, north-tilted block with steepest scarps along its southeastern margin near the present Kerr Bend fault where the coarsest conglomerates and breccias occur. We also infer that the adjacent graben to the immediate south of this scarp filled first with clastic detritus from the north, and later became the site of eruption for the voluminous PBR pillow basalts. The ab sence of a basal conglomerate in the Forgold facies and Four Corners complex suggests that these volcanic rocks were erupted at a still later stage, as faulting and uplift waned and the exposed highlands were drowned.

The Kerr Bend fault separates two distinctive Middle Jurassic facies - a thick pile of basalts to the south versus a clastic-dominated package to the north (Fig. 9). Thrust faults that demarcate abrupt facies and thickness changes may be remobilized original growth faults (McClay *et al.*, 1989). As shown in Figure 9, the locus of the present Kerr Bend fault is interpreted as a remobilized graben-bounding fault which separated the Sixpack Range horst from an adjacent graben to the south. Th e Kerr Bend fault corresponds roughly in position and orientation to the precursor normal fault. Read *et al.* (1989) inferred 2.5 km of post-Middle Jurassic displacement on the Forrest Kerr fault, based on offsets of the northeast- to east-northeast–trending faults and folds such as the PBR anticline. These features, which are only developed near the Forrest Kerr fault, can be related kinematically to sinistral transcurrent motion along it (Fig. 9 and 10).

The change in kinematics to sinistral transpression first steepened the original fault surface, and then overturned it to the south. Continued thrust motion on this fault would have obscured any basal clastic facies

rocks on the southern (PBR) side, by burying them in the footwall.

Since deposition of the Iskut River unit likely post-dates the last movement on the Kerr Bend fault, its Middle to early Late Jurassic fossil age constrains the episode of sinistral motion on the north-trending Forrest Kerr fault and related deformation of the PBR facies to a time immediately after the formation of the Eskay Creek orebodies. Renewed high relief created by offsets on the Forrest Kerr and Kerr Bend faults could account for the high energy sedimentary environment in the unit and gravity transport of olistoliths into the basin. This model is revisited in the discussion of structure in the area.

BOWSER LAKE GROUP

Strata of the Middle to Upper Jurassic Bowser Lake Group overlap the older volcanic sequences along the eastern part of the study area and have been most recently mapped by Evenchick (1991) and Ricketts and Evenchick (1991). To the east, stratigraphy and nomenclature for the Bowser Lake Group in the Spatsizi River map sheet (NTS 104H) have been wholly revised and updated (Evenchick and Thorkelson, 2005).

Regionally, the basal contact of the Bowser Lake Group grades upward from the upper sedimentary strata of the Salmon River Formation (Spatsizi Formation) of the underlying Hazelton Group. The Middle Jurassic boundary between these similar sedimentary packages roughly coincides with the Bajocian-Bathonian transition at 166 Ma.

Anderson (1993) describes the lowest units within the Bowser Lake Group as thin- to thick-bedded, fine- to coarse-grained siliciclastic rocks including turbiditic shale, siltstone, greywacke, fine- to medium-grained sandstone and rare conglomerate. Anderson cautions that these units are indistinguishable in the field from similar rock types at the top of the underlying Salmon River Formation of the Hazelton Group.

Evenchick (1991), mapping in the current study area, correlated black siltstone, fine-grained sandstone and minor to large proportions of chert pebble conglomerate with the Ashman Formation of the Bowser Lake Group. Evenchick and Thorkelson (2005) note that the Hazelton Group - Bowser Lake Group contact is gradational, however, they place the boundary where thin, white-weathering tuffaceous laminae, typical of the upper Spatsizi Formation (Salmon River Formation), are no longer present in black siltstones.

Bowser Lake Group strata are well exposed along Bandit Ridge, an east-trending ridge immediately southwest of the mouth of Downpour Creek. The western contact of this unit is an east-dipping fault against older strata of the Sixpack Range facies. Sedimentary strata of the Bowser Lake Group are highly contorted and disrupted within 500 m of this fault contact. Within this zone, pebble conglomerate units correlated with the Ashman Formation of the Bowser Lake Group display stretched pebbles with length to width ratios of 4:1. For the next 4 km to the east, Bowser Lake Group rock types include a thick, highly folded and faulted succession of siltstone, mudstone, sandstone and rare thin limestone beds.

MOUNT EDZIZA VOLCANIC COMPLEX

The Late Cenozoic Mount Edziza volcanic complex blankets an area of 1,000 km^2, including part of the northwest corner of the project area. The complex is comprehensively described and illustrated in Geological Survey of Canada Memoir 420 (Souther, 1992). Volcanic rocks range in age from 7.5 Ma to 2 Ka. The complex comprises alkaline basalt and hawaiite with lesser intermediate and felsic volcanic flows, and records five major cycles of magmatic activity.

Intrusive Rocks

STIKINE SUITE

Middle to Late Triassic tholeiitic to calcalkaline granitoid plutons of the Stikine Suite intrude Stuhini Group volcanic and sedimentary strata in this region and are interpreted as comagmatic intrusions (Logan *et al.*, 2000). Examples are the small stocks of diorite and gabbro mapped near the south end of the Sixpack Range.

COPPER MOUNTAIN PLUTONIC SUITE

Small ultramafic stocks of the Late Triassic to Early Jurassic Copper Mountain Suite (Logan *et al*., 2000) are distributed throughout this region, but have not been noted in the present map area.

TEXAS CREEK PLUTONIC SUITE

A variety of fine- to medium-grained, commonly porphyritic, leucocratic intrusive rocks found in the map area are correlated with the Early Jurassic Texas Creek Suite (Logan *et al*., 2000). The intrusions appear as simple stocks or as clusters of anastomosing dikes. Intrusions of this suite are important regional loci for porphyry copper-gold, transitional gold, and epithermal gold-silver deposits. In the 2004 map area, a string of small stocks of this age trend northward along both sides of the Forrest Kerr fault (Fig. 5).

THREE SISTERS PLUTONIC SUITE

Fine- to medium-grained equigranular diorite stocks and a small medium-grained gabbro plug cut Lower to Middle Jurassic strata to the northwest of northern Downpour Creek. These plutons are assigned to the Middle Jurassic (179-176 Ma) Three Sisters Suite defined by Anderson (1983).

HYDER PLUTONIC SUITE

The Eocene Hyder Suite forms the eastern margin of the Coast Crystalline Belt to the west of the study area. This continental-scale magmatic event is recorded within the map area by a series of north-trending, fine-grained to aphanitic rhyolite dikes first identified by Souther (1972). One of these north-trending dikes intrudes Triassic strata north and south of the mouth of More Creek (Fig. 5). These intrusions are likely feeders to overlying felsic flows that have been subsequently eroded.

Structure

The large-scale structural framework of the area is dominated by north-striking faults of regional significance (Fig. 5 and 10). The Forrest Kerr fault is the most prominent of these, with a mapped strike length over 50 km, east-side-down throw of more than 2 km and post-mid Jurassic sinistral displacement of more than 2.5 km (Read *et al.*, 1989). It has a number of splays. Some of them bound blocks of mid-Jurassic exposures near the Four Corners complex. Another significant set of fault splays deflects northeastward into the headwaters of Downpour Creek and includes the north-striking Downpour Creek fault, which appears to be cut off by the Triassic Pass fault. Both the Downpour Creek fault and the Triassic Pass fault have down-to-the-west stratigraphic throws, opposite to that on the Forrest Kerr fault. Their northern extensions are inferred to turn northwestward and merge with the main Forrest Kerr fault somewhere along the north branch of More Creek**.** To the south, the Downpour Creek fault may extend along the eastern side of Pillow Basalt Ridge roughly along the outcrop belt of the Iskut River unit (Fig. 5 and 10). Overall, the fault pattern is one of anastomosing, braided strands typical of a regional transcurrent fault system.

The main strand of the Forrest Kerr fault crosses the pass at the head of Carcass Creek on the RDN property between the Downpour Creek and More Creek drainages. It is expressed as a zone of finely comminuted, highly altered fault breccia.

Field relationships show that motion on the Forrest Kerr fault system accompanied as well as post-dated mid-Jurassic bimodal igneous activity. Detailed mapping of strands of the Forrest Kerr fault located east of the main fault near the Four Corners complex showed

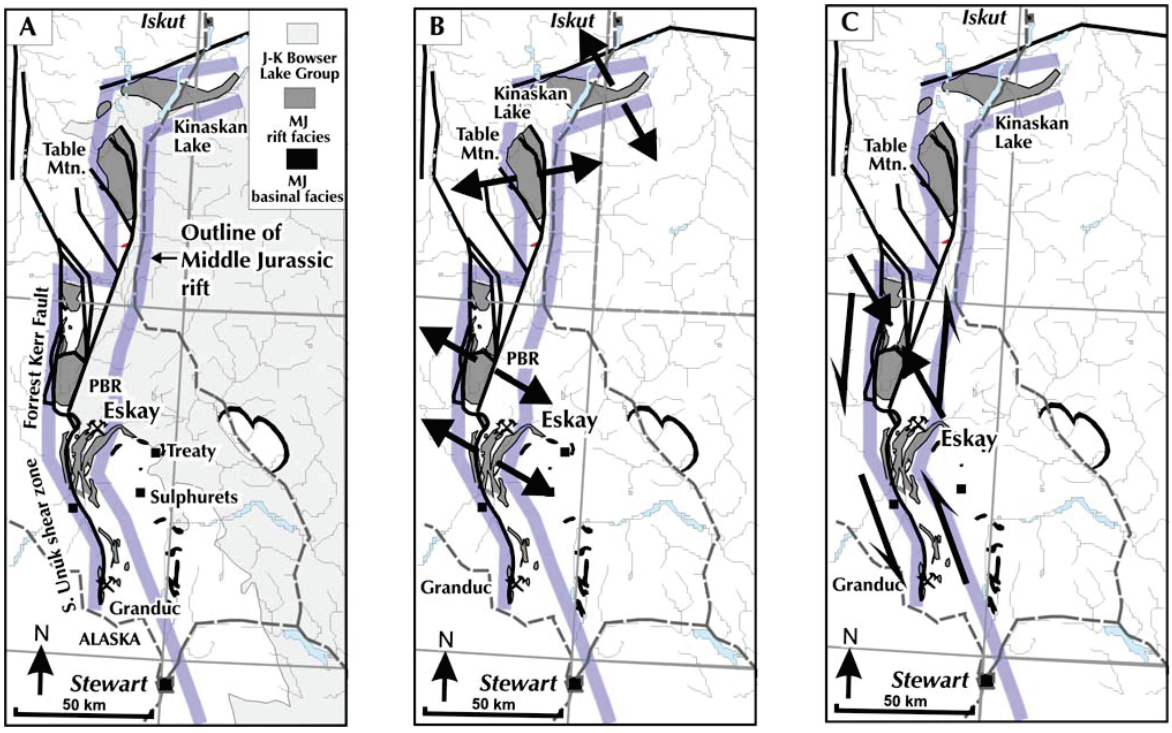

Figure 10. Cartoon regional structural history of west-central Stikinia in mid-Jurassic time. A. Present faults and outcrop areas of mid-Jurassic strata. B. Circa 180 to 174 Ma, the extensional rift regime that gave rise to the bimodal volcanic and related sedimentary sequences. Orientations of tensional features such as dikes and feeder zones suggests straight-on extension in northern part of the belt, and a slight dextral transtensional component in the south, with northeasterly extension. C. Circa 172 to 167 Ma, sinistral strike-slip regime imposed on the pre-existing rift system gives rise to northeasterly compressional features within it.

them to be zones of intense deformation tens of metres wide over a minimum strike length of 2 km. They consist of fault breccia with black argillite matrix probably derived from Triassic strata that crop out nearby. Clasts include disrupted siltstone beds from within the argillite, and exotic fragments such as basalt and plagioclase porphyries. Typically, the clasts are centimetre to decimetre size, but larger basalt blocks are also present. Some of them are strongly altered to carbonate and, less commonly, quartz-carbonate-mariposite assemblages. Mid-Jurassic pillow basalts and the bimodal Four Corners complex lie west of the fault strands and are truncated by minor splays from them. Two outcrops of fault breccia are surrounded by the rocks of the Four Corners complex. One outcrop is in the bottom of a small cirque on the north side of the complex. The cirque walls south of it form a continuous outcrop of basalt and felsite that isolates the northern outcrop of fault breccia from the fault zone farther south. In the other outcrop, fault breccia contains numerous clasts of plagioclase-phyric hypabyssal granodiorite. They are unlike the igneous rocks of the Four Corners complex, but similar to unit Jfp (Jurassic feldspar porphyry) of Read *et al.* (1989). A rhyolite dike cuts off the breccia. Thus construction of the Four Corners igneous complex postdated major motion and brecciation on some splays of the Forrest Kerr fault; however, other splays containing identical breccias outlasted it.

In the main through-going splay that truncates the Four Corners complex to the east, lineations defined by clast elongations generally plunge at less than 25°. Clast asymmetries and shear bands show a consistent sinistral sense of motion both in outcrop and in thin section. Steep lineations, such as slickenlines and clast elongations, are also present but are less common. The pre-Four Corners breccia outcrops contain inconclusive kinematic indicators and poorly developed steep lineations.

A set of east-northeast–striking, south-directed reverse faults and related folds affects the uplifted Paleozoic/Triassic block east of the Forrest Kerr fault (Fig. 5 and 9). The most significant of these, the Kerr Bend fault, first recognized by Read *et al.* (1989), places Paleozoic and younger hangingwall strata on top of the mid-Jurassic basalts of Pillow Basalt Ridge. The layered rocks on Pillow Basalt Ridge are also involved in northeasterly folding. The eastern extents of these faults and folds are truncated by exposures of the Middle to early Late Jurassic Iskut River clastic-felsic unit. Northward deflection of bedding and structures on Pillow Basalt Ridge as they approach the base of the Iskut River unit (Fig. 5) may be related to a north-striking sinistral fault, possibly an extension of the Downpour Creek fault, either along the basal contact or buried beneath the Iskut River unit itself. The coarse, unsorted deposits and olistoliths in this unit are consistent with deposition in a fault-controlled basin. We infer that its western bounding fault lies at or near the present western contact of the unit.

Read *et al.* (1989) calculated a minimum 2.5 km sinistral displacement along the Forrest Kerr fault based on the offset of folds across it. We are in accord with their structural interpretation, although we have modified it in several respects. First, we interpret the Kerr Bend fault and other northeast to east-northeast compressional features as the consequence of the sinistral motion on the north-striking Forrest Kerr fault. Second, detailed work has shifted and realigned the mapped axis of the PBR anticline on Pillow Basalt Ridge such that it does not intersect, and thus does not fold the Kerr Bend fault. Instead, both the PBR anticline and the small syncline to the northwest of it are folds in the footwall strata cut off by the Kerr Bend thrust fault. Read *et al.* (1989) considered the dark grey shale-siltstone unit in the core of the syncline on northwestern Pillow Basalt Ridge to be Bowser Lake Group strata, and structures affecting it – the syncline itself and the Forrest Kerr fault by association – were thought to be post-Bowser, mid-Cretaceous in age. However, the intimate interbedding of the shale and siltstone with pillow basalts (Barresi *et al.*, this volume) indicates that this is an uppermost unit in the mid-Jurassic Hazelton Group sequence. Structures affecting it are only required to be post-mid-Jurassic.

This set of east-northeast– to northeast-striking– folds and reverse faults can be modeled as a compressional transfer zone between the Forrest Kerr fault to the west and the southern extension of the Downpour Creek fault to the east (Fig. 5 and 10). Northeast-striking faults link the two north-striking fault systems into a single sinistral transcurrent zone.

The Triassic Pass fault is located east of the Downpour Creek fault, and truncates it at a low angle (Fig. 5). Its southern, unmapped extension lies in the Iskut River valley. East of the Triassic Pass fault, the Smokey Ridge thrust fault imbricates Triassic and overlying pebbly sandstone on the mountainside immediately north of Downpour Creek (Fig. 5). The fault crops out in several incised gullies. In its footwall, cross-stratified Bowser Lake Group(?) sandstone with scattered chert pebbles and plant debris unconformably overlies Triassic tuffaceous mudstone above a well-developed regolith (Fig. 11). The fault is a zone of strong shearing that places Upper Triassic black phyllite and tuffaceous mudstone on top of undeformed sandstone of the Bowser Lake Group (Fig. 11). A second thrust fault is inferred lower down this slope, in the valley of Downpour Creek, that places the Triassic exposures below the unconformity on top of the Bowser Lake Group section that is exposed on Bandit Ridge, south of Downpour Creek. Folds in the Upper Triassic sequence and in the Bowser Lake Group trend eastward; these are consistent with the orientation of the Smokey Ridge Thrust fault.

The Triassic Pass fault truncates both of these thrust faults, as well as footwall Bowser Lake Group strata. Thus, motion on it must be younger than the Jurassic-Cretaceous Bowser Lake Group.

In the northeastern part of the area, a north-trending, near-vertical fault is exposed both north and south of More Creek. A large quartz-phyric rhyolite dike and a panel of highly sheared tuffaceous sedimentary beds and coal of probable Eocene age occur within the fault zone (Fig. 5 and 10).

MINERAL DEPOSITS

Northwestern BC hosts a variety of mineral deposit types characteristic of magmatic arc environments, including calc-alkaline porphyry copper-gold deposits (Fig. 1 in Schroeter and Pardy, 2004); Eskay Creek-type subaqueous hotspring deposits (Massey, 1999a); Kuroko-type VMS deposits (Massey, 1999b); and low-sulphidation epithermal deposits (Fig. 1 in Schroeter and Pardy, 2004). Near the current study area, intrusive-related Cu-Ni deposits (Lefebure and Fournier, 2000) and Besshi-type VMS deposits (Massey, 1999b) are hosted in rock units that may be present locally. Sedimentary strata of the Bowser Lake Group host coal deposits and have elevated concentrations of molybdenum and nickel (Alldrick *et al.*, 2004c). Recent study of the Bowser Lake Group has shown potential for the generation and accumulation of petroleum (Evenchick *et al.*, 2002; Ferri *et al.*, 2004).

Figure 12 shows the distribution of mineral deposits and prospects in the study area. Occurrences are concentrated in the volcanic strata that pre-date deposition of the Bowser Lake Group. This distribution is reflected in metal concentrations detected in the Regional Geochemical Surveys (*see* Fig. 5 and 7 in Lett and Jackaman, 2004). The metal-rich region lies west of Highway 37 and corresponds to the eastern edge of the Coast Mountains. Bowser Lake Group sedimentary strata, with its coal, petroleum and sediment-hosted metal potential, generally lie east of Highway 37.

Intrusion-related deposit types in or near the study area include porphyry copper-gold deposits, which are particularly common in this region (Schroeter and Pardy, 2004); intrusion-related low-sulphidation epithermal deposits; and magmatic copper-nickel deposits. Volcanic-hosted deposits include both the Eskay Creek deposits and some low-sulphidation epithermal veins (Massey, 1999a). Stratiform or stratabound deposit types include sediment-hosted molybdenum and nickel, Besshi-type sediment-hosted massive sulphide deposits, as well as volcanic-hosted VMS deposits (Massey, 1999b). Limestone units are favourable host rocks for gold-rich skarn deposits (*e.g.*, McLymont Creek).

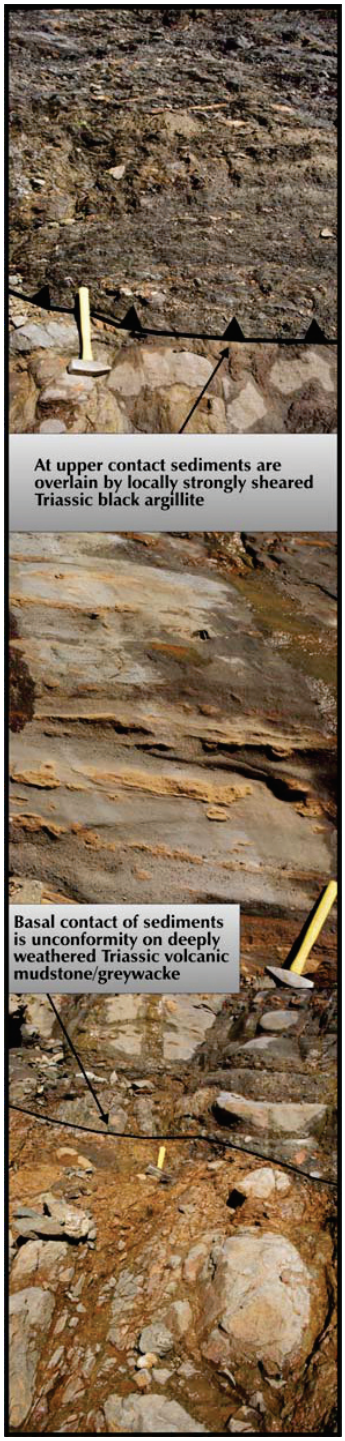

Figure 11. Composite photo of the thin Bowser Lake Group clastic sequence on Triassic basement, in the footwall of the Smokey Ridge thrust fault, which is expressed as highly sheared Triassic argillite overriding the undeformed pebbly sandstones of the Bowser Lake Group. Actual thickness of Bowser sediments in this exposure is about 50 m.

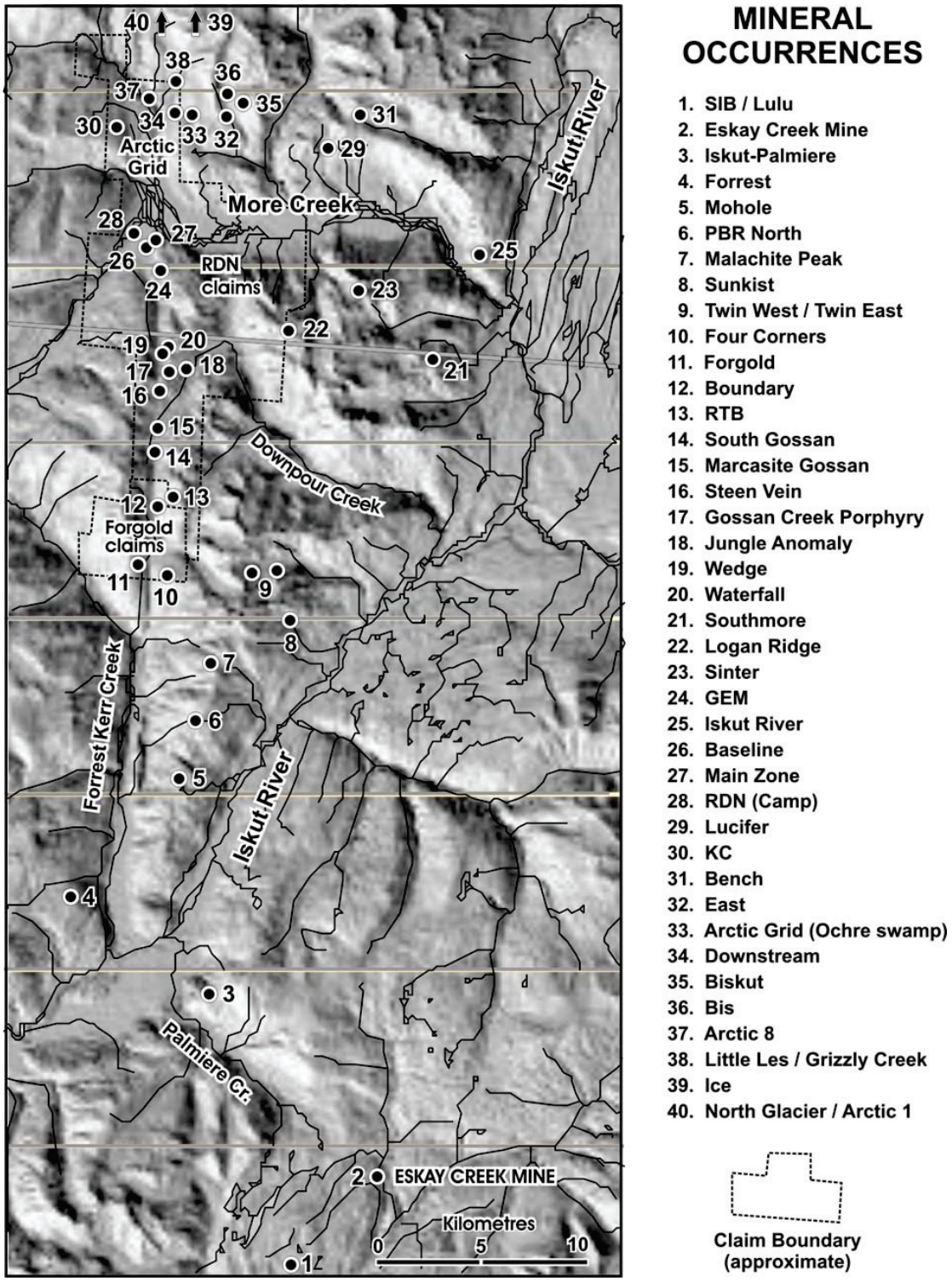

Figure 12. Mineral deposits and prospects in the 2004 map area. Note the concentration of mineral showings along the Forrest Kerr fault.

During the 2004 mapping program, six new mineral showings were located by government geologists working on the Targeted Geoscience Initiative project. As these crews focus on mapping, not prospecting, this is a surprisingly high number of new mineral occurrences, which reflects the high mineral potential of the region. More exploration work is justified based on these discoveries and on the presence of Eskay-equivalent strata in this map area.

The following deposit descriptions are listed from south to north; see Figure 12 for locations.

1. SIB / Lulu (104B 376) (UTM 09 / 0408589E / 6273080N)

This showing crops out near middle of the 9 km long trend of gossans and alteration that extends southwestward from the Eskay Creek mine area. Mudstones interbedded with felsic volcanics host pyrite, stibnite and sphalerite with trace native gold, pyrargyrite and arsenopyrite. A 2002 drillhole intersected 11.7 m grading 19.5 ppm Au and 1703 ppm Ag.

2. Eskay Creek (104B 008) (UTM 09 / 0412514E / 6279588N)

Roth (2002) classifies Eskay Creek as a polymetallic, precious metal rich, volcanogenic massive sulphide and sulphosalt deposit. Ore is contained in a number of stratiform zones and stockwork vein systems that display varied textures and mineralogy. The deposits formed during two periods of early Middle Jurassic hydrothermal activity, both of which were characterized by evolving fluid chemistry and mineralogy. Past production and reserve and resource estimates total 2.34 million tonnes grading 51.3 g/t Au and 2,326 g/t Ag.

3. Iskut-Palmiere (UTM 09 / 0403565E / 6287490N)

Realgar ± orpiment is hosted in both black siliceous siltstones and in a cross-cutting quartz vein. This small outcrop is exposed in a north-draining creek, and lies stratigraphically above a thick dacite unit on the north side of Palmiere (Volcano) Creek. Assays of two grab samples returned arsenic values greater than 1.0%, with negligible associated precious metals. However, creeks draining this low ridge to the north and south returned anomalously high gold grain counts in the heavy mineral concentrates collected during the recent Regional Geochemical Survey (Lett *et al.*, this volume).

4. Forrest (104B 380) (UTM 09 / 0396988E / 62192649N)

This prospect is located on the west side of Forrest Kerr Creek, opposite the south end of Pillow Basalt Ridge. Gold- and silver-b earing quartz-chalcopyrite veins occur in extensive quartz stockworks and individual veins associated with the Forrest Kerr fault. Grab samples assay up to 17.1 g/t Au. Visible gold occurs with bornite and hematite in quartz veins that assay up to 110.4 g/t Au.

5. Mohole (UTM 09 / 0401956E / 6297577N)

A deep drillhole has been completed in central Pillow Basalt Ridge. Hole PBR01-01 was located near the anticlinal fold axis on Pillow Basalt Ridge, to intersect the Eskay Creek horizon ("Contact Mudstone") at depth (see Baressi *et al.*, this volume). This drillhole was completed in two stages. In 2001, Homestake completed the hole to a depth of 1419 m. In 2003 Roca Mines Inc. deepened the hole to 1770 m.

6. PBR North (new showing) (UTM 09 / 0403150E / 6300650N)

On Pillow Basalt Ridge, locally thickened units of weakly pyritic, massive to flow-banded rhyolite are deposited within a succession of pillow lava, massive crystalline basalt flows and interlayered pyritic siliceous siltstones. The thicker rhyolite zones are interpreted as cryptodomes marking eruptive centres; thinner rhyolite units are interpreted as flows. Assays of grab samples collected from the pyritic siltstones have anomalous Zn, Ag and Ba values.

7. Malachite Peak (new showing) (UTM 09 / 0403620E / 6304260N)

North of the Kerr Bend fault, copper-bearing mafic volcanics crop out between 1800 to 2000 m elevation near the crest of Sixpack Range. Host rocks are fine-grained equigranular to weakly augite-feldspar porphyritic basalts. The massive basalt is cut by a network of fine fractures hosting pyrite and chalcopyrite. Malachite is prominent on weathered surfaces and along near-surface fractures.

8. Sunkist (new showing) (UTM 09 / 0406950E / 6305900N)

Ankerite alteration within an east-trending fault forms prominent bright orange gossans near the toe of Fourth Glacier. Best assays from three chip samples are 239 ppm Zn and 279 ppm As .

9. Twin (new showing) Twin East (UTM 09 / 0405840E / 6308160N) Twin West (UTM 09 / 0405120E / 6308015N)

Two prominent orange-weathering gossan zones are exposed on north-facing cliffs near the northeast end of Sixpack Range. A single elongate gossan is divided into two zones where a north-flowing valley glacier cuts through the host strata. The outcrops have not been examined, but this showing may be similar to Sunkist.

10. Four Corners (new showing) (UTM 09 / 0401000E / 6307715N)

A major volcanic centre is preserved northwest of Pillow Basalt Ridge. Numerous rhyolite dikes and flows are emplaced in a sequence of intercalated basalt and sedimentary rocks. Mineralization consists of minor to sparse disseminated pyrite and rare galena.

11. Forgold (104B 378) (UTM 09 / 0399429E / 6309294N)

This property is located west of Downpour Creek and just south of the RDN claimblock. Epithermal gold- and silver-bearing pyrite and chalcopyrite stringer veins assayed up to 30.5 g/t Au and 15.85% Cu (Assessment Report 20,540). Malensek *et al*. (1990) identified three styles of mineralization which are controlled by the Forrest Kerr fault. Chalcopyrite, galena and sphalerite stringers, and quartz-carbonate-sphalerite- galena-chalcopyrite stockwork veins grade up to 2.09 g/t Au. Disseminated chalcopyrite within silicified zones grade up to 112.46 g/t Au and 17.16% Cu. Proximal stocks of monzonite may be genetically associated with the alteration and mineralization.

12. Boundary (RDN) (UTM 09 / 0400040E / 6310950N)

A narrow silicified zone hosts a thin chalcopyrite veinlet. Assays returned anomalous gold values (Savell, 1990). Noranda Exploration Ltd. drilled five holes on this target area in 1991. The best intersection was 11.6 m grading 23.9 g/t Au (Logan *et al.*, 1992 and Awmack, 1997). The best assays obtained from 1998 surface samples were 56.7 ppm Au, 44 ppm Ag, 44 ppm As, 6.34% Cu, 18.7 ppm Hg, 3.900 ppm Pb, and 9,360 ppm Zn (Awmack and Baknes, 1998).

13. RTB (new showing) (RDN) (UTM 09 / 0400710E / 6311425N)

This prospect consists of disseminated and fine fracture-hosted pyrite, chalcopyrite, tetrahedrite and galena in flow-banded rhyolite and adjacent fine sandstone. Rare tetrahedrite and native silver were noted in some samples. Nearby pillow lavas of plagioclase-potassium feldspar porphyry display interbeds and selvages of pyrite- and tetrahedrite-bearing jasper. Best assay results from five chip samples are 0.5% Cu, 2.2% Pb, 8.8% Zn, 245 ppm Ag, 1.4 ppm Au, 2690 ppm Sb, 87 ppm Hg and 499 ppm As.

14. South Gossan (RDN) (UTM 09 / 0399935E / 6313870N)

South Gossan is a large resistant knob of massive dacite flow on the east bank of the headwaters of Downpour Creek. Ubiquitous fine hairline fractures host a weakly developed `stockwork' of pyrite, calcite and quartz. Subsequent w eathering has coated the entire surface of this large outcrop area with striking buff-orange ankeritic weathering. No significant metal values have been obtained (Savell, 1990).

15. Marcasite Gossan (UTM 09 / 0400135E / 6314780N)

This prominent gossan crops out on the east bank of upper Downpour Creek, 900 m north of South Gossan. In this area, strata dip moderately westward with tops up to the west. The showing consists of three stacked dacitic flow units separated by locally fossiliferous siltstone, sandstone and limestone. Dacites are weakly to strongly pyritic, the sedimentary units host only trace to minor pyrite. The middle dacite unit is the most intensely mineralized, and hosts a stockwork of marcasite-pyrite-chalcedony-calcite-pyrobitumen-barite veins. Individual veins range up to 10 cm thick. Mineralization ends abruptly along strike at the north side of the outcrop area against a synmineralization fault. The easternmost, topographically higher but stratigraphically lower, Upper Marcasite Gossan consists of a weaker quartz-chalcedony-pyrite-pyrobitumen stockwork. Savell (1990) reports that gold and base metal values are negligible, but assay results from surface samples include 141 g/t Ag, 2,750 ppm As, 122 ppb Sb, 124 ppm Mo and 5,240 ppb Hg. Even higher values have been obtained from mineralized float boulders near the Upper Marcasite Gossan. Four drillholes completed to date did not intersect mineralization.

16. Steen Vein (RDN) (UTM 09 / 0400290E / 6316195N)

This polymetallic vein crops out in the north wall of the lower gorge of Cole Creek, a small creek that drains southeastward into upper Downpour creek, just south of the Gossan Creek Porphyry. Discovered in 1997, this quartz-galena-sphalerite-tetrahedrite vein follows an east-northeast–trending fault. Chip samples across a true vein width of 2.0 m averaged 279 g/t Ag, 1.86% Pb, 0.77% Zn and 350 ppb Au.

17. Gossan Creek Porphyry (RDN) (UTM 09 / 0400910E / 6317240N)

The Gossan Creek porphyry intrusion (Fig. 5), located near the headwaters of Downpour Creek, roughly correlates with a large bleached gossan (Fig. 13a, b). Three geophysical targets were drill-tested by Noranda in 1991 (Savell and Grill, 1991). DDH 18 intersected argillic-altered feldspar porphyry hosting 5 to 15 % fine- to medium-grained pyrite disseminations and veinlets. From 103.4 to 113.3 m, stringers of sphalerite and chalcopyrite assayed 0.18% Cu, 0.14% Pb, 0.43% Zn 1.17 g/t Ag and 0.07 g/t Au. Other drillholes cut pyritic stockwork with up to 25% fine pyrite.

18. Jungle Anomaly (RDN) (UTM 09 / 0401420E / 6317365N)

This exploration target is a 100 by 450 m soil geochemical anomaly located in thick brush on the west bank of upper Downpour Creek, 2.6 km north of the Marcasite Gossan and just north of the Gossan Creek Porphyry. Samples indicate anomalous Au, As, Ag and Pb values in soils overlying bedrock of clastic sedimentary rocks, rhyolite and basalt. A float cobble of pyritic, silicified argillite collected near the centre of the anomaly assayed 25.44 g/t Au. Pyritic chert float also collected from this area does not occur elsewhere on the extensive property. Subsequent geophysical surveys and drilling have not located a bedrock source.

19. Wedge (RDN) (UTM 09 / 0399975E / 6319070N)

The Wedge prospect crops out low on a west-facing, heavily wooded hillside, just northeast of the headwaters of Carcass Creek at the toe of a glacier, and 5 km south of the current exploration camp. Five drillholes completed in 1990-91 cut mineralized veins in eleven intersections with best assays of 137.8 ppm Au, 62.4 ppm Ag, 2.7% Cu, 0.48% Pb and 3.26% Zn (Awmack and Baknes, 1998).

20. Waterfall (RDN) (UTM 09 / 0400115E / 6319230N)

A quartz-sulphide vein is discontinuously exposed for 50 m (Savell, 1990).

21. Southmore (UTM 09 / 0413310E / 6318760N)

The east wall and south wall of a small north-draining cirque reveal six outcrop areas of strongly gossanous, pyritic, flow-layered white rhyolite. This unit is correlated with the regionally distributed Upper Triassic pyritic rhyolite that also hosts the Bench and Sinter showings. Adjacent units of thin-bedded black siltstone are also pyritic. Associated rock types include buff-weathering sandstone with horizons of wood debris, black limestone, and one rhyolite flow. The strata are cut by a 1.5 m thick sill of flow-banded basalt. Three gossanous outcrops were sampled, the best assays are 28 ppm Mo, 16 ppm Cu, 10 ppm Pb, 25 ppm Zn, 214 ppb Ag, 24 ppm As, 777 ppb Hg and 4 ppm Sb.

22. Logan Ridge (UTM 09 / 0406030E / 6319780N)

A prominent, resistant ridge of intensely gossanous rhyolite spines marks the skyline west of Arrow Creek. Since 1990, this ground has been held as the STOW and PINE claims, and is currently registered as the MOR 8 claims; no exploration results have been reported.

23. Sinter (UTM 09 / 0409560E / 6322175N)

Recent glacier retreat has exposed an extensive area of strong pyritic stockwork, south of More Creek and east of Arrow Creek. During the summer of 1988, the area was explored by Valley Gold Ltd., Noranda Ltd. and Corona Corporation (Bale and Day, 1989). Follow-up work by Noranda Ltd in 1990 (Grill and Savell, 1991) discovered no base or precious metal mineralization, but anomalous mercury (up to 196 ppm Hg), arsenic and antimony were obtained all along the 2 km long trace of the northwest-trending Citadel fault. Barrick Resources sampled the prospect in 2003. An unreported single drillhole was collared at the toe of the west-flowing glacier by Noranda; no results are known. The best assay results from three chip samples collected in 2004 are 122 ppm Cu, 350 ppm Zn, 7 ppm Pb, 24 ppm Ag, 5,750 ppm Ba, 13 ppm Hg and 24 ppm As.

24. GEM (RDN) (UTM 09 / 0399565E / 6322980N)

This prospect crops out 1000 m south of the Main showing on the east side on Carcass Creek, and is hosted in the same massive dacite unit. Discovered by Noranda geologists in 1991 (McArthur *et al.,* 1991), the best assay obtained from grab samples was 5.1 ppm Au. Resampling in 1997 returned a best assay of 2.16 ppm Au and 32 ppm Ag (Awmack, 1997). A soil survey over the area indicates that the dacitic volcanic hostrocks have anomalous Au, Ag, Cu, Pb, Zn, As, Sb and Mn values.

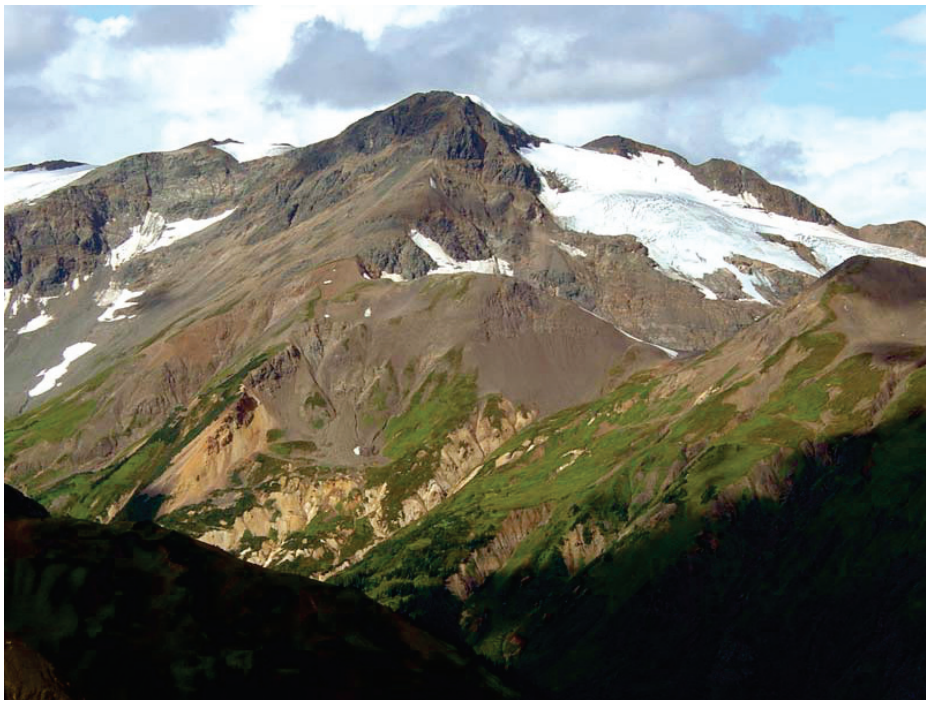

A.

B.

Figure 13. The Gossan Creek Porphyry gossan. A. Looking southwest. The glaciated peak in background lies on the west side of the Forrest Kerr fault. B. The same gossan zone viewed from the south across Downpour Creek

.

25. Iskut River (104G 104) (UTM 09 / 0415471E / 6324464N)

A major (>100 m thick) fossiliferous limestone unit of Upper Triassic age is exposed on cliffs near the mouth of More Creek.

26. Baseline (RDN) (UTM 09 / 0399180E / 6323665N)

This prospect is a quartz vein breccia exposed 240 m southwest of the Main Zone. A chip sample assayed 6.21 g/t Au.

27. Main Zone (RDN) (UTM 09 / 0399355E / 6323810N)

This prospect crops out on the east side of Carcass Creek, 700 m east of the current exploration camp. This showing was discovered by Noranda geologists in 1991 (McArthur *et al.,* 1991) and has remained a focus of exploration efforts on this large property. Host rock is Early Jurassic dacite that is locally porphyritic, spherulitic or silicified. Mineralization consists of disseminated sulphides in areas where the dacite is bleached and silicified. The best assays reported from a series of chip samples (McArthur *et al.,* 1991) are 5 ppm Au, 32.8 g/t Ag, 0.5% Cu, 0.5% Pb, and 10% Zn. A soil survey over the area indicates that the dacitic volcanic rocks have anomalous Au, Ag, Cu, Pb, Zn, As, Sb and Mn values. Subsequent exploration has shown that the prospect is an intensely silicified fault breccia trending 060 degrees (Awmack, 1996); a chip sample across its 8.3 m width returned 3.1 ppm Au, 0.49% Pb and 1.13% Zn. A separate outcrop area 130 m to the west-southwest is called the Club Zone. This 7m long outcrop of silicified breccia returned maximum assays of 2700 ppm Pb, 1205 ppm Zn and 515 ppb Au from three chip samples.

28. RDN (UTM 09 / 0398770E / 6323970N)

The name RDN refers to a large north-trending claim block containing several prospects. The core claims were staked in 1987, predating the discovery of the Eskay Creek 21 Zone. Additional claim blocks to the north and south have been added over the last 17 years. The UTM coordinates above give the location of the current exploration camp. Noranda Exploration Ltd. explored these claims from 1989 to 1991, including a fifteen-hole drill program in 1990 and a further 15 drillholes in 1991. Pathfinder Resources explored the claim block from 1994 to 1996. Rimfire Minerals acquired all the claims in 1997 and conducted soil sampling, geological mapping, trenching and prospecting in 1997 and 1998. Barrick explored the property under option in 2002 to 2003. Northgate Minerals Corporation and Rimfire Minerals completed a nine-hole drill program in 2004, targeting the Wedge Zone, Jungle Anomaly and Marcasite Gossan prospects.

29. Lucifer (104G 145) (UTM 09 / 0407979E / 6329387N)

An extensive carbonate-pyrite-sericite-silica alteration zone has anomalous Au, As, Ba, Cd, Cu, Mo, Pb and Zn values. Country rock is Upper Triassic sedimentary and volcanic rocks intruded by a set of Early Jurassic potassium feldspar megacrystic dikes. Alteration is most intense along steep northeast-trending faults. Two holes drilled on the property in 1991 intersected 1.36 m grading 15 ppm Au and 5.7 m grading 0.7 ppm Au (Dewonck, 1991).

30. KC (RDN) (UTM 09 / 0397140E / 6329780N)

Chalcopyrite veins and veinlets are hosted in Early Jurassic feldspar porphyritic, potassium feldspar megacrystic granodiorite. Several massive chalcopyrite veins up to 12 cm wide are hosted by a dioritic phase of the leucocratic granodiorite (Bobyn, 1991, p.13, 15). The veins are vertical and exposed in a small creek bed over a width of 4 m. Selected grab samples have anomalous Au, Cu and Ag values.

31. Bench (UTM 09 / 0409490E / 6330105N)

A band of massive to semi-massive, fine-grained, bright pyrite crops out at the base of a high cliff of black, pyritic, flow-layered rhyolite near the head of Bench Creek. The upper part of the cliff is faintly banded, black to charcoal rhyolite with a fine dusting of pyrite evenly disseminated throughout the rock. Within the lower 5 m along the base of the cliff, the rhyolite is transected by many fine hairline cracks filled with pyrite. Along most of the length of the cliff, a talus pile of coarse blocks and boulders is piled up against the basal rhyolite layer with the pyritic fractures. At one location near the upstream end of the cliff, the top of the talus pile is lower and exposes 2 feet of massive, fine-grained granular pyrite and semi-massive granular pyrite disseminated in white, fine-grained quartz. The significance of this small showing is its stratabound character and the high probability that this mineralization extends laterally under the blocky talus cover. In 2004, eight samples were collected from this unit along a 2 km strike length. Best assays were 51 ppm Mo, 70 ppm Cu, 44 ppm Pb, 89 ppm Zn, 15 ppb Au, 1099 ppb Ag, 15 ppm As, 2.7 ppm Sb and 394 ppb Hg.

32. East (RDN) (UTM 09 / 0402900E / 6330095N)

Mineralized float samples collected downstream from the Bis prospect assayed 1.9 ppm Au and 771 ppm As.

33. Arctic Grid (RDN) (UTM 09 / 0401400E / 6330165N)

The Arctic Grid is the northernmost claim block of the RDN claim package. The Arctic claims were staked and extensively explored in 1990 by Skeena Resources (Bobyn, 1991). Eight mineral prospects lie on the Arctic claim block: Grizzly Creek (Little Les), North Glacier, Arctic 8, KC, Ice, Bis, Downstream and East. The coordinates above give the location of a large ochre-coloured swamp east of the centre of the claim block.

34. Downstream (RDN) (UTM 09 / 0400485E / 6330215N)

This showing is located 2.5 km downstream of the Grizzly showing, on the southeast bank of Grizzly Creek. Narrow chalcedony veins within pyritic felsite/rhyolite host stringers of massive pyrite up to 5 cm wide. Grab samples from two of these pyrite veins assayed 75 ppm Hg, 580 ppm Sb and 4860 ppm As (Bobyn, 1991; Awmack, 1997).

35. Biskut (104G 146) (UTM 09 / 0403381E / 6331472N)

High on the north slope of More Creek, a 300 by 100 m alteration zone of quartz-sericite-pyrite-clay is developed in Upper Triassic volcanic and sedimentary rocks. Sulphide mineralization locally ranges up to 5% pyrite, with minor galena and arsenopyrite.

36. Bis (RDN) (UTM 09 / 0402915E / 6331215N)

Felsite dike or flow rock hosts 3 to 5% disseminated pyrite and trace arsenopyrite. A grab sample of strongly gossanous felsic rock assayed 5 ppm Au, 570 ppm Cu, 41.9 ppm Ag, 391 ppm As and 124 ppm Mo (Bobyn, 1991, p. 8 and 12).

37. Arctic 8 (RDN) (UTM 09 / 0399065E / 6331145N)

One creek north of Grizzly Creek, and near the unnamed creek's junction with More Creek, several carbonate lenses up to 0.75 m wide are interbedded with greywacke and conglomerate. The carbonate rocks host 1 to 2% galena and trace chalcopyrite and sphalerite (Bobyn, 1991, p. 12 and Map 1). No assays are reported.

38. Little Les / Grizzly Creek (RDN) (104G 079) (UTM 09 / 0400720E / 6331860N)

This is the only prospect on the extensive RDN claim group where pre-1987 exploration is recorded. Initially named Little Les, this prospect has also been named More, Two More and is now referred to as the Grizzly showing on the Arctic Grid, RDN property. To the east of the north branch of More Creek, on the present Arctic Grid, a large gossan is developed where volcanic rocks are intruded by dikes of potassium feldspar megacrystic granodiorite dikes (Folk, 1980). Pyritic alteration hosts trace chalcopyrite, galena, sphalerite, malachite and molybdenite(?). Average grades from 11 chip samples are 0.3% Cu, 1.71 g/t Ag and 0.41 g/t Au. Newmont drilled two short holes on this target in 1970; no results are available (Geology, Exploration and Mining, 1971). Bobyn (1991, p. 12) described porphyry copper-style mineralization exposed over a 300 by 25 m area along the upper part of the northernmost tributary of Grizzly Creek. The host rock is carbonate-chlorite-sericite altered andesitic flows and tuffs. Mineralization is 2 to 5% disseminated chalcopyrite with 1 to 3% disseminated and fracture-fill pyrite. Throughout the area of the showing, stringers of massive chalcopyrite range up to 5 cm wide, with pods and lenses up to 50 cm wide. Trace galena and sphalerite are also present. Mineralization is fracture controlled and best developed proximal to the many feldspar porphyry and felsite dikes, which cut the volcanics.

39. Ice (RDN) (UTM 09 / 0401535E / 6336200N)

Hornblende diorite hosts up to 25% pyrrhotite near the intrusive contact of this large stock (Bobyn, 1991, Map 1). A grab sample assayed 31 ppb Au, 3.7 ppm Ag and 3152 ppm Cu. Similar mineralization occurs in a similar setting 3 km south; in the southwest corner of Upper More 1 claim, on the north bank of the stream immediately northwest of the Grizzly Creek prospect, gossanous cliffs host up to 7% disseminated pyrrhotite and pyrite (Bobyn, 1991, p. 12-13).

40. North Glacier / Arctic 1 (RDN) (UTM 09 / 0400065E / 6337235N)

Mineralized float samples collected from glacial moraines returned assays ranging up to 4.5 ppm Au, 9,034 ppm Cu, 74.6 ppm Ag and 20,147 ppm As.

METALLOGENY

In the map area and in the surrounding region, Upper Triassic mineralization includes large porphyry copper-gold systems (GJ, Galore Creek), Besshi-type VMS deposits (Rock and Roll), pyritic rhyolite/exhalite (Bench, Citadel, Southmore) and vuggy rhyolite dikes and flows with elevated Au, Ag, Hg, Sb and As concentrations (Rainbow). Lower Jurassic mineralization that predates the erosional interval marked by Nassian uplift is represented by large porphyry copper-molybdenum systems (Mary, Red-Chris), stratabound bulk-tonnage epithermal mineralization (Hank), and precious metal-rich skarn deposits (McLymont). Lower to Middle Jurassic mineralization that post-dates the Nassian uplift includes the Griz prospect and many areas of pyritic felsic volcanic units and derived volcaniclastic sedimentary rocks (*e.g.*, Fig. 4 in Simpson and Nelson, 2004), plus the Eskay Creek gold mine and numerous nearby prospects (Lulu, 22 Zone, HSOV).

Exploration Potential

Discovery of a number of small prospects during this season's regional mapping program indicate that the potential of this area has not yet been thoroughly assessed.

Due to the highly dissected terrain, geochemical stream sediment sampling has proven to be a particularly successful and cost-effective tool for assessing the potential of larger areas (Lett and Jackaman, 2004; Lett *et al.*, 2005) and should be equally powerful as a second phase follow-up technique. The middle unit of Pillow Basalt Ridge is favourable for the deposition and preservation of exhalative sulphides and should be selectively prospected. Other areas of quiescent, distal sedimentation will be particularly conducive to the accumulation and preservation of exhalative sulphides (*e.g.*, northern Downpour Creek area).

DISCUSSION AND CONCLUSIONS

This project has provided important new detailed geological surveys of the northern Eskay Rift rocks within the Iskut map area. Tracts of "Eskay equivalent" strata crop out on Pillow Basalt Ridge and north to More Creek. They are correlative in general with sequences mapped in 2003 on Table Mountain, on Willow Ridge and on ridges east and west of Kinaskan Lake (Alldrick *et al.*, 2004a, 2004b)

Fieldwork in 2004 has clarified the nature, stratigraphic and structural context, and mineral potential of the "Eskay equivalent" strata in northern Iskut map area. They can be divided into five separate facies units, Pillow Basalt Ridge, Forgold, Sixpack Range, Downpour Creek and Iskut River. The Sixpack Range is a coarse, proximal, conglomeratic facies (Fig. 7), similar to conglomerates identified in 2003 on Table Mountain and near Kinaskan Lake (Alldrick *et al.*, 2004a, 2004b). They represent rift-margin deposits related to scarps. By contrast, the Forgold basalts rest directly on older basement without intervening clastic units.

Felsic centres are located in the Four Corners complex and the "middle unit" on Pillow Basalt Ridge. Laminated siliceous argillite and rhyolitic tuffaceous siltstones - the "pajama beds" (Anderson, 1993) - are also present at both of these sites.

The Forrest Kerr fault and related faults form the present structural framework for the rift system that localized the Eskay VMS deposit, its host rocks, and correlative strata (Fig. 10). It forms the western boundary of mid-Jurassic exposures as far north as the headwaters of More Creek. Its northern extension is buried under the Mt. Edziza volcanic centre (Fig. 2). North of More Creek, the zone of mid-Jurassic bimodal/sedimentary exposures steps east to the Table Mountain/Kinaskan Lake area. There, it is bounded to the west by local scarps that Alldrick *et al.* (2004b) interpreted as rift margins. Coarse, unsorted conglomerates related to the scarps underlie sedimentary strata containing Toarcian-Bajocian macrofossils.

The trace of the Forrest Kerr fault coincides with a major magnetic lineament (Alldrick, 2000). South of the Iskut River, the Forrest Kerr fault is connected to the Harrymel fault through a complex step-over zone (Read *et al.*, 1989; Alldrick, 2000). This structure continues south to the Granduc mine area, where it is expressed as a 2 km wide zone of transcurrent ductile deformation, the South Unuk shear zone (Lewis, 1992). Uranium-lead dates on syn- and post-kinematic plutons constrain sinistral motion to between 172 and 167 Ma (Fig. 10c; Lewis, 2001).

Geological observations in the present project area are consistent with the interpretation of Read *et al.* (1989) that an episode of sinistral motion on the Forrest Kerr fault post-dated deposition of the Pillow Basalt Ridge strata. The Middle to early Late Jurassic Iskut River unit is interpreted as a fault-related deposit localized along a north-striking sinistral fault that is a splay of the Forrest Kerr fault zone. This offset is contemporaneous with sinistral motion on the South Unuk shear zone. We infer that a regional sinistral shear couple existed along the north-striking bounding faults of the mid-Jurassic rift system, deforming strata and modifying structures created during earlier stress regimes.

Evidence for the stress regime during deposition of the Eskay Creek host rocks and their correlatives consists mainly of observed orientations of rift-related features. These vary along strike of the rift (Fig. 5 and

10). In the Table Mountain area, lines of rhyolite centres and dike swarms are oriented north-northwesterly (Alldrick *et al.*, 2004a, 2004b). This season, a north-northwesterly horizon of pyritic sinters has been discovered on south-central Table Mountain (A. Birkeland, pers comm, 2004). On northern Pillow Basalt Ridge, a line of small rhyolite intrusive centres trends northeasterly (30 degrees). Finally, in the vicinity of the Eskay mine the alignment of felsite centres, feeder dikes and stockwork-style mineralized zones parallel to the fold axis of the northeast-trending Eskay anticline suggests that this fold could be an inverted rift basin (McClay *et al.*,1989).

The combined Forrest Kerr and Harrymel faults provide a possible locus for the western margin of the rift zone. A northerly-trending line of altered Early(?) Jurassic porphyry intrusions lies immediately west of the Forrest Kerr fault along Forrest Kerr Creek (Read *et al.*, 1989; Logan *et al.* , 2000). Similarly, mapping by Equity Engineering and this project team has outlined a northerly trend of Early Jurassic dacite intrusive/extrusive centres east of the fault, near the headwaters of Downpour Creek. The alignment of these centres along the Forrest Kerr fault suggests that it was a zone of crustal weakness in Early Jurassic time, prior to development of the Eskay rift. The east-side-down West Slope fault truncates the Early Jurassic plutons, but is older than the main Forrest Kerr strand (Read *et al.*, 1989). It could have been a mid-Jurassic, graben-bounding normal fault. The Forrest Kerr splay that is cut off by the Four Corners complex is another example of a probable syn-rift fault.

In the Table Mountain area, north-northwesterly tensional features parallel the western rift margin, consistent with orthogonal extension (Alldrick *et al.*, 2004). In contrast, the northeasterly orientation of mid-Jurassic dikes on Pillow Basalt Ridge suggests an oblique component to extension across the north-striking bounding faults (Fig. 10b). Because these features are extensional rather than compressional, movement due to this component would have been opposite to that manifested in the latest mid Jurassic event, *i.e.*, dextral rather than sinistral. Similarly, in the vicinity of the Eskay mine, north-northeasterly extensional features require an oblique stress component. Thus, evidence for dextral, syn-rifting offset is seen in the area from More Creek at least as far south as Tom Mackay Lake. It corresponds to the unique Paleozoic horst and deep graben in this area, evidenced by the unusually thick Pillow Basalt Ridge basalts.

Figure 10 summarizes the inferred structural development of the Eskay rift zone. In mid-Jurassic time, rifting took place in en echelon zones between Kinaskan Lake and the Granduc mine. Over most of the area, orthogonal rifting prevailed. A dextral component across the Forrest Kerr fault led to strong horst and graben development, oblique to the main northerly trend.

In early Bajocian time (172 to 167 Ma), a new stress regime, controlled by a sinistral shear couple across the dominant northerly faults, was superimposed on the rift basins and terminated their development. It caused fault reversal and created local high energy depositional environments in the Iskut River unit.

SUMMARY

Mapping has refined the stratigraphic and structural picture of the More Creek – Palmiere Creek area. Important contributions include the recognition of the near absence of strata representing the lower Hazelton Group, and recognition of regional-scale unconformities that form irregular boundaries between major stratigraphic packages.

Strata deposited within the Eskay rift extend northward through the present map area, displaying a range of different facies which reflect the proximity to volcanic centres and the depositional setting. The Pillow Basalt Ridge facies and the Four Corners complex comprise bimodal volcanic rock types and related sedimentary strata correlative with strata that host the Eskay Creek orebodies to the south.

ACKNOWLEDGMENTS

Magan Havard provided capable field assistance. We thank Dave Mehner, Murray Jones, Dave Caulfield, David Gale, Martin Stewart, Waldo Perez, Arne Birkeland and Richard Mann for valuable discussions in the field. Karl Desjarlais of Interior Helicopters Ltd. provided safe, swift and reliable helicopter support.

REFERENCES

Alldrick, D.J. (1993): Geology and metallogeny of the Stewart mining camp, northwestern British Columbia; *British Columbia Ministry of Energy and Mines*, Bulletin 85, 105 pages.

Alldrick, D.J. (2000): Exploration significance of the Iskut River fault; *British Columbia Ministry of Energy and Mines*, Geological Fieldwork 1999, Paper 2000-1, pages 237-248.

Alldrick, D.J. and Britton J.M. (1992): Unuk River area geology; *British Columbia Ministry of Energy, Mines and Petroleum Resources*, Open File Map 1992-22, scale 1:20 000, 5 sheets.

Alldrick, D.J., Stewart, M.L., Nelson, J.L. and Simpson, K.A. (2004a): Geology of the More Creek-Kinaskan Lake area, northwestern British Columbia; *British Columbia Ministry of Energy and Mines*, Open File Map 2004-2, scale 1:50 000.

Alldrick, D.J., Stewart, M.L., Nelson, J.L. and Simpson, K.A. (2004b): Tracking the Eskay rift through northern

British Columbia - geology and mineral occurrences of the Upper Iskut River area; *British Columbia Ministry of Energy and Mines*, Geological Fieldwork 2003, Paper 2004-1, pages 1-18.

Alldrick, D.J., Jackaman, W. and Lett, R.E.W. (2004c): Compilation and analysis of regional geochemical surveys around the Bowser Basin; *British Columbia Ministry of Energy and Mines*, Geological Fieldwork 2003, Paper 2004-1, pages 163-166.

Alldrick, D.J., Nelson, J.L. and Barresi, T. (2005): Geology of the More Creek - Palmiere Creek area, northwestern British Columbia; *British Columbia Ministry of Energy and Mines*, Open File Map 2005-5, scale 1:50 000.

Anderson, R.G. (1983): The geology of the Hotailuh batholith and surrounding volcanic and sedimentary rocks, north-central British Columbia; unpublished PhD thesis, *Carleton University*.

Anderson, R.G. (1989): A stratigraphic, plutonic and structural framework for the Iskut Map area, northwestern British Columbia: *Geological Survey of Canada*, Current Research, Part E, Paper 89-1 E, pages 145-154.

Anderson, R.G. (1993): A Mesozoic stratigraphic and plutonic framework for northwestern Stikinia, northwestern British Columbia, Canada; *in* Mesozoic Paleogeography of the western United States-II, Dunne, G. and McDougall, K., editors, *Pacific Section SEPM*, Volume 71, pages 477-494.

Anderson, R.G. and Thorkelson, D.J. (1990): Mesozoic stratigraphy and setting for some mineral deposits in Iskut River map area, northwestern British Columbia; *in* Current Research, Part E, *Geological Survey of Canada*, Paper 90-1 E, pages 131-139.

Ash, C.H., Fraser, T.M., Branchflower, J.D. and Thurston, B.Q. (1995): Tatogga Lake project, northwestern British Columbia (104H/11, 12); *in* Geological Fieldwork 1994, Grant, B. and Newell, J.M., editors, *British Columbia Ministry of Energy, Mines and Petroleum Resources*, Paper 1995-1, pages 343-358.

Ash, C.H., Stinson, P.K. and Macdonald, R.W.J. (1996); Geology of the Todagin Plateau and Kinaskan Lake area (104H/12, 104G/9); *in* Geological Fieldwork 1995, Grant, B. and Newell, J.M., editors, *British Columbia Ministry of Energy, Mines and Petroleum Resources*, Paper 1996-1, pages 155-174.

Ash, C.H., Macdonald, R.W.J. and Friedman, P.M. (1997a); Stratigraphy of the Tatogga Lake Area, Northwestern British Columbia (104G/9,16); *in* Geological Fieldwork 1996, Lefebure, D.V., McMillan, W.J. and McArthur, J.G., Editors, British Columbia Ministry of Employment and Investment, Paper 1997-1, pages 283-297

Ash, C.H., Macdonald, R.W.J., Stinson, P.K., Fraser, T.M., Read, P.R., Pustka, J.F., Nelson, K.J., Ardan, K.M., Friedman, R.M. and Lefebure, D.V. (1997b): Geology and mineral occurrences of the Tatogga Lake area, northwestern British Columbia (104G/9E & 16SE, 104H/12NW & 13SW); *British Columbia Ministry of Energy and Mines*, Open File Map 1997-3, scale 1:50 000.

Awmack, H.J. (1996): 1996 geological, geochemical and geophysical report on the RDN 1-10 claims; *British Columbia Ministry of Energy and Mines*, Assessment Report No. 24,719, 32 pages.

Awmack, H.J. (1997): 1997 geological and geochemical report on the RDN 1-10 claims; *British Columbia Ministry of Energy and Mines*, Assessment Report No. 25,336, 29 pages.

Awmack, H.J. and Baknes, M.E. (1998): 1998 geological, geochemical and trenching report on the RDN 1-18 claims; *British Columbia Ministry of Energy and Mines*, Assessment Report No. 25,813, 39 pages.

Bale, W.C. and Day, R.C. (1989): Prospecting assessment report on the Wad, Sinter, and Bill mineral claims; *British Columbia Ministry of Energy and Mines*, Assessment Report No. 19,216, 6 pages.

Barresi, T., Nelson, J.L., Alldrick, D.J. and Dostal, J. (2005): Pillow Basalt Ridge facies - detailed mapping of Eskay Creek equivalent stratigraphy (Iskut River NTS 104B/9, 10, 15, 16); *British Columbia Ministry of Energy and Mines*, Geological Fieldwork 2004, this volume.

Barresi, T. and Dostal, J. (2005): Geochemistry and petrography of Upper Hazelton volcanics - VHMS favorable stratigraphy in the Iskut River and Telegraph Creek Map Areas, northwest British Columbia; *British Columbia Ministry of Energy and Mines*, Geological Fieldwork 2004, this volume.

Bartsch, R.D. (1993): A rhyolite flow dome in the upper Hazelton Group, Eskay Creek area; *in* Geological Fieldwork 1992, *British Columbia Ministry of Energy, Mines and Petroleum Resources*, Paper 1993-1, pages 331-334.

Bobyn, M.G. (1991): Summary report on geological mapping, prospecting, and geochemistry of the Arctic/Upper More Claim Group; *British Columbia Ministry of Energy and Mines*, Assessment Report 21,529, 22 pages.

Breitsprecher, K. and Mortensen, J.K. (2004): BCAge 2004 - a database of isotopic age determinations for rock units in British Columbia; *British Columbia Ministry of Energy and Mines, Geological Survey*, Open File 2004-3.

Dewonck, B. (1991): Assessment report on the Rumsen 1-4 claims for Gzolden Pyramid Resources Inc.; *British Columbia Ministry of Energy and Mines*, Assessment Report No. 21,890, 18 pages.

Ettlinger, A.D. (2001): Eskay Creek 21 Zone; *in* Metallogenesis of the Iskut River Area, Northwestern British Columbia, Lewis, P.D., Toma, A. and Tosdal, R.M., editors, *Mineral Deposit Research Unit*, Special Publication 1.

Evenchick, C.A. (1991): Jurassic stratigraphy of east Telegraph Creek and west Spatsizi map areas, British Columbia; *in* Current Research, Part A, *Geological Survey of Canada*, Paper 91-1A, pages 155-162.

Evenchick, C.A., Poulton, T.P., Tipper, H.W. and Braidek, I. (2001): Fossils and facies of the northern two-thirds of the Bowser Basin, British Columbia; *Geological Survey of Canada*, Open File Report 3956, 103 pages.

Evenchick, C.A., Hayes, M.C., Buddell, K.A. and Osadetz, K.G. (2002): Vitrinite and bitumen reflectance data and preliminary organic maturity model for the northern two thirds of the Bowser and Sustut basins, north-central British Columbia; *Geological Survey of Canada*, Open File Map 4343, scale 1:250 000.

Evenchick, C.A. and McNicoll, V.J. (2002): Stratigraphy, structure, and geochronology of the Anyox Pendant, northwest British Columbia, and implications for mineral exploration; *Canadian Journal of Earth Sciences*, Volume 39, pages 1313-1332.

Evenchick, C.A. and Thorkelson, D.J. (2005): Geology of the Spatsizi River map area, north-central British Columbia; *Geological Survey of Canada*, Bulletin 577.

Ferri, F., Osadetz, K. and Evenchick, C.E. (2004): Petroleum source rock potential of Lower to Middle Jurassic clastics, Intermontane basins, British Columbia; *British Columbia Ministry of Energy and Mines, Resource Development and Geoscience Branch*, Summary of Activities 2004, pages 87-97.

Folk, P.G. (1980): Geological and geochemical geophysical report on the More and Two More mineral claims; *British Columbia Ministry of Energy and Mines*, Assessment Report 9041, 19 pages.

Geology, Exploration and Mining (1971): Little Les; *in* Geology, Exploration and Mining in British Columbia 1971, *British Columbia Ministry of Energy and Mines*, pages 37-38.

Grill, E. and Savell, M. (1991): Geological, geochemical and geophysical report on the Wad, Sinter and Bill mineral claims; *British Columbia Ministry of Energy and Mines*, Assessment Report 21,311, 16 pages.

Gunning, M.H. (1996): Definition and interpretation of Paleozoic volcanic domains, northwestern Stikinia, Iskut River area, British Columbia; unpublished PhD thesis, *University of Western Ontario*, 388 pages.

Kaip, A.W. (1997): Geology, alteration and mineralization on the Hank property, northwestern British Columbia: a near-surface, low-sulfidation epithermal system; unpublished MSc thesis, *University of British Columbia*, 198 pages.

Lefebure, D.V. and Fournier, M.A. (2000): Platinum group element mineral occurrences in British Columbia; *British Columbia Ministry of Energy and Mines*, Geofile Map 2000-2, scale 1:2 000 000.

Lett, R. and Jackaman, W. (2003): Reanalysis of regional stream sediment survey samples from the Iskut River area; *British Columbia Ministry of Energy and Mines*, Geofile 2003-20, 189 pages.

Lett, R. and Jackaman, W. (2004): Iskut River and Telegraph Creek - new exploration opportunities in the BC regional geochemical survey database; *British Columbia Ministry of Energy and Mines*, Geological Fieldwork 2003, Paper 2004-1, pages 199-207.

Lett, R.E., Friske, P.W.B. and Jackaman, W. (2005): The National Geochemical Reconnaissance Program in northwest British Columbia - the Bowser Lake (NTS 104A) Regional Geochemical Survey; *British Columbia Ministry of Energy and Mines*, Geological Fieldwork 2004, Paper 2005-1

Lewis, P. D. (1992): Structural geology of the Prout Plateau region, Iskut River map area, British Columbia; *British Columbia Ministry of Energy, Mines and Petroleum Resources*, Paper 1992-1, pages 521-527.

Lewis, P.D. (2001): Structural evolution of the Iskut River area - preliminary results; *in* Metallogenesis of the Iskut River area, northwestern Bristish Columbia, Lewis, P.D., Toma, A. and Tosdal, R.M., editors, *Mineral Deposit Research Unit*, Special Publication Number 1, pages 63-76.

Lewis, P.D, Macdonald, A.J. and Bartsch, R.D. (2001): Hazelton Group/Bowser Lake Group stratigraphy in the Iskut River area - progress and problems; *in* Metallogenesis of the Iskut River Area, Northwestern British Columbia, Lewis, P.D., Toma, A. and Tosdal, R.M., editors, *Mineral Deposit Research Unit*, Special Publication Number 1, pages 9-30.

Logan. J.M., Koyanagi, V.M. and Drobe, J.R (1990): Geology and mineral occurrences of the Forrest Kerr – Iskut River area (104B/15); *British Columbia Ministry of Energy, Mines and Petroleum Resources*, Open File Map 1990-2, scale 1:50 000.

Logan. J.M., Drobe, J.R. and Elsby, D.C. (1992): Geology, geochemistry and mineral occurrences of the More Creek area, northwestern British Columbia (104G/2); *British Columbia Ministry of Energy, Mines and Petroleum Resources*, Open File 1992-5.

Logan, J.M. and Drobe, J.R. (1993): Geology of the Mess Lake area, northwestern British Columbia (104G/7W); *British Columbia Ministry of Energy, Mines and Petroleum Resources*, Open File 1993-6.

Logan, J.M., Drobe, J.R., Koyanagi, V.M. and Elsby, D.C. (1997): Geology of the Forest Kerr - Mess Creek area, northwestern British Columbia (104B/10,15 & 104G/2 & 7W); *British Columbia Ministry of Employment and Investment*, Geoscience Map 1997-3, scale 1:100 000.

Logan, J.M., Drobe, J.R. and McClelland, W.C. (2000): Geology of the Forest Kerr - Mess Creek area, Northwestern British Columbia (104B/10,15 & 104G/2 & 7W); *British Columbia Ministry of Energy and Mines*, Bulletin 104, 164 pages.

Malensek, G.A., Baker, N. and Cavey, G. (1990): Assessment report on the Forgold project for Santa Marina Gold Ltd.; *British Columbia Ministry of Energy and Mines*, Assessment Report No. 20,722, 30 pages.

MacDonald, J.A., Lewis, P.D., Thompson, J.F.H., Nadaraju, G., Bartsch, R.D., Bridge, D.J., Rhys, D.A., Roth, T., Kaip, A., Godwin, C.I. and Sinclair, A.J. (1996): Metallogeny of an early to middle Jurassic Arc, Iskut River area, northwestern British Columbia; *Economic Geology*, Volume 91, no 6, pages 1098-1114.

Massey, N.W.D. (1999a): Potential for subaqueous hot-spring (Eskay Creek) deposits in British Columbia; *British Columbia Ministry of Energy and Mines*, Open File Map 1999-14, scale 1:2 000 000.

Massey, N.W.D. (1999b): Volcanogenic massive sulphide deposits in British Columbia; *British Columbia Ministry of Energy and Mines*, Open File Map 1999-2, scale 1:2 000 000.

McArthur, G., Campbell, I. And LeBel, J.L. (1991): More Creek project - geological, geochemical and geophysical report on the more 5 and 6 mineral claims; *British Columbia Ministry of Energy and Mines*, Assessment Report Number 22,238, 22 pages.

McClay, K.R., Insley, M.W. and Anderton, R. (1989): Inversion of the Kechika Trough, northeastern British Columbia; *in* Inversion Tectonics, Cooper, M.A. and Williams, G.D., editors, *Geological Society of London*, Special Publication 44, pages 235-257.

Mortensen, J.K., Wojdak, P., MacDonald, R., Gordee, S.M. and Gabites, J.E. (2005): Regional studies of VMS

mineralization and potential within the Early Jurassic Hazelton Group, British Columbia; *British Columbia Ministry of Energy and Mines*, Geological Fieldwork 2004, this volume.

Operation Stikine (1957): Stikine River area, British Columbia (104A, B, G, H, I, J); Map 9-1957.

Read, P.B., Brown, R.L., Psutka, J.F., Moore, J.M., Journeay, M., Lane, L.S. and Orchard, M.J. (1989): Geology, More and Forest Kerr Creeks (parts of 104B/10,15,16 & 104G/1, 2), northwestern British Columbia; *Geological Survey of Canada*, Open File 2094.

Ricketts, B.D. and Evenchick, C.A. (1991): Analysis of the middle to upper Jurassic Bowser Basin, northern British Columbia; *in* Current Research, Part A, *Geological Survey of Canada*, Paper 91-1A, pages 65-73.

Roth, T. (2002): Physical and chemical constraints on mineralization in the Eskay Creek deposit, northwestern British Columbia: evidence from petrography, mineral chemistry, and sulfur isotopes; unpublished PhD thesis, *University of British Columbia*, 401 pages.

Savell, M. (1990): Geological, geochemical and geophysical report on the RDN and GOZ mineral claims; *British Columbia Ministry of Energy and Mines*, Assessment Reprot Number 20,769, 18 pages.

Schmitt, H.R. (1977): Triassic - Jurassic granodiorite monzodiorite pluton southeast of Telegraph Creek, BC; unpublished BSc thesis, *University of British Columbia*, 79 pages.

Schroeter, T.G. and Pardy, J.W. (2004): Lode gold production and resources in British Columbia; *British Columbia Ministry of Energy and Mines*, Open File 2004-1.

Simpson, K.A. and Nelson, J.L. (2004): Preliminary interpretations of mid-Jurassic volcanic and sedimentary facies in the East Telegraph Creek map area; *Geological Survey of Canada*, Current Research 2004-A1, 8 pages.

Souther, J.G., 1972: Telegraph Creek map-area, British Columbia; *Geological Survey of Canada*, Paper 71-44.

A.4: Barresi, T., and Dostal, J. 2005. Geochemistry and Petrography of Upper Hazelton Group volcanics: VHMS-Favourable Stratigraphy in the Iskut River and Telegraph Creek Map Areas, Northwestern British Columbia. In Geological Fieldwork 2004. British Columbia Ministry of Energy, Mines and Petroleum Resources, Paper 2005-1, pp. 39-47.

Geochemistry and Petrography of Upper Hazelton Group Volcanics: VHMS-Favourable Stratigraphy in the Iskut River and Telegraph Creek Map Areas, Northwestern British Columbia

By T. Barresi [1] and J. Dostal[2]

KEYWORDS: Eskay Creek, Eskay Rift, Hazelton Group, geochemistry, petrochemistry, island arc, bimodal volcanism, VMS deposits, Targeted Geoscience Initiative II (TGI-II)

INTRODUCTION

In 2003, the British Columbia Geological Survey and the Geological Survey of Canada initiated a joint project to map lower Middle Jurassic, upper Hazelton Group rocks in the Telegraph Creek and Iskut River map areas of northwestern British Columbia. In this region, the upper Hazelton Group is host to the Eskay Creek volcanic-hosted massive sulphide (VHMS) deposit, as well as numerous showings, prospects and geochemical anomalies, making it one of the most highly prospective regions in British Columbia. The scope of the project includes regional and detailed mapping of the upper Hazelton Group as well as geochemical and geochronological studies. Funding is provided by the British Columbia Ministry of Energy and Mines, and by the Geological Survey of Canada's Targeted Geoscience Initiative II.

This paper is the first of a series that will present and interpret whole rock and mineral chemistry data from the study area. The purpose of studying these data is to better understand the igneous and tectonic processes that were dominant during the formation of the Eskay Creek VHMS deposit, and to determine the significance of similarities and variations in the geochemistry of Eskay Creek time-equivalent volcanic rocks along the length of the Eskay Rift. This study may lead to a better understanding of how whole rock geochemistry can be used as an exploration tool in finding VHMS style mineralization. The data presented in this article are whole rock geochemical analyses of 17 volcanic and related intrusive rocks that were collected during the 2003 field season from the area between More Creek and Kinaskan Lake, in the Telegraph Creek map area (Fig. 1). The focus of this study is on Lower to Middle Jurassic, upper Hazelton Group rocks, which in the study area are assigned to the Willow Ridge Complex (Alldrick *et al.*, 2004a; Alldrick *et al.*, 2004b).

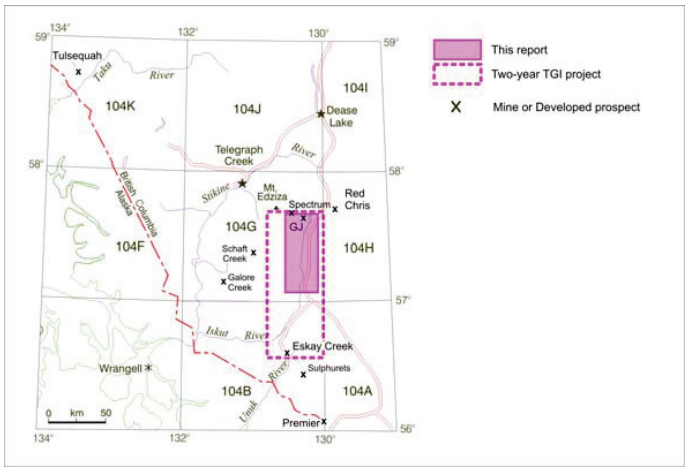

Figure 1. Project location map; modified from Logan *et al.* (2000)

1 – Department of Earth Science, Dalhousie University, Halifax, NS, B3H 3J5 e-mail: TN425520@dal.ca
2 – Department of Geology, Saint Mary's University, Halifax, NS, B3H 3C3

GEOLOGICAL SETTING

The Willow Ridge Complex (WRC) is located within the Stikine Terrane in northwestern British Columbia (Fig. 2). The Stikine Terrane, in the Iskut and Telegraph Creek map areas, is composed of three major pre-accretionary units and two younger, syn- and post-accretionary, units (Alldrick *et al.*, 2004a). The main stratigraphic components are: 1) the metavolcanic and metasedimentary Stikine Assemblage of Devonian to Permian age; 2) island-arc volcanic rocks of the Late Triassic Stuhini Group; 3) Early to Middle Jurassic island-arc volcanic and sedimentary rocks of the Hazelton Group; 4) the Middle Jurassic to Cretaceous Bowser Lake Group, which is a sedimentary overlap assemblage that overlies the eastern margin of the Stikine Terrane units; and 5) the upper Miocene to Holocene Mount Edziza Volcanic Complex.

The Willow Ridge Complex is defined by Alldrick *et al.* (2004a). It is considered to be a part of the Eskay Creek Facies of Anderson and Thorkelson (1990) and is interpreted to have been deposited in a subaqueous volcano-sedimentary environment, typical of rift settings (Alldrick *et al.*, 2004a). Alldrick *et al.* (2004a) describe the WRC as a "thick package of basalt lava flows and feeder dikes, minor interlayered dacite and rhyolite lava flows, breccias, feeder dikes and lava domes, and intercalated volcaniclastic sedimentary rocks". Alldrick *et al.* (2004a) interpret the volcanic rocks within the complex as a bimodal volcanic suite. The full thickness of the complex is uncertain, but on Table Mountain it is at least 4 km thick. The complex is divided into three units: a Lower Basalt Unit, a Middle Sedimentary Unit, and an Upper Basalt Unit, which unconformably overlie older, Stuhini Group or lower Hazelton Group volcanic breccias. All three WRC units have intercalated felsic flows and feeder dikes and sills. The Middle Sedimentary Unit is predominantly composed of clastic rocks but also contains bimodal volcanics, including a north-northwesterly trending line of felsic domes. The reader is referred to Alldrick *et al.* (2004a), Alldrick *et al.* (2004b), and Simpson and Nelson (2004) for detailed maps and descriptions of the geology in the study area.

PETROGRAPHY

The WRC consists of a bimodal, felsic and mafic igneous rock suite. Mafic rocks consist mainly of basalt and minor andesite; felsic rocks are rhyolite.

Mafic rock in the WRC is aphanitic and dark to olive green. Mafic intrusions include dikes and sills, and, on Willow Ridge, stocks assigned to the Three Sisters Plutonic Suite. Extrusive units include massive flows, pillowed flows and pillow breccia, hyaloclastite, and breccias of fluidly shaped clasts typical of fire fountain deposits (Simpson and Nelson, 2004). Basalts and andesites are commonly amygdaloidal and have characteristic white weathering variolites, a devitrification feature. Their primary mineralogy includes densely packed plagioclase laths and clinopyroxene phenocrysts in a devitrified glassy matrix. Amygdules are filled with chlorite and minor quartz and calcite. The primary mineralogy of basalts and andesites is well preserved with the exception of secondary calcite in the matrix and clinopyroxene phenocrysts that are in some cases replaced by chlorite and quartz. Secondary alteration accounts for between 5 and 25% of the modal mineralogy in mafic samples.

Felsic rock in the WRC is aphanitic, white to pale green, commonly spherulitic and rarely has small vesicles/amygdules that are elongated parallel to flow. High-level felsic intrusions include dikes, sills and cryptodomes; extrusive bodies occur as flows, breccias and domes. The rhyolites are generally aphyric, and rarely feldspar porphyritic with potassium feldspar and lesser plagioclase phenocrysts. The groundmass has undergone minor devitrification and is mainly composed of quartz and potassium feldspar. Accessory amounts of sphene are common; sample JN01-08 also contains zircon. The proportion of opaque minerals is low in most samples, but sample JN04-11 contains 14% opaque minerals. The samples have undergone varying degrees of alteration and contain secondary epidote, chlorite, calcite, quartz and white mica. Secondary alteration products account for between 5 and 15% of the modal mineralogy in rhyolite samples.

ANALYTICAL METHODOLOGY AND SAMPLING PROCEDURE

Seventeen samples for whole rock and trace element analysis were collected from surface exposures during regional mapping (Fig. 2; Alldrick *et al.* 2004a; Alldrick *et al.* 2004b). They were selected to represent the least altered instances of the full range of volcanic lithologies that occur commonly in the study area. Four samples (A03-14-7, A03-18-6, JN-07-01 and MS-03-07-02) represent the Triassic Stuhini Group and lower Hazelton Group. The remaining samples are upper Hazelton Group rocks of the Willow Ridge Complex. The data for all samples are presented in Table 1. For the analysis discussed in this paper, four samples are discarded. Sample A03-18-6 is discarded because it is a tuff. Samples A03-14-7 and MS-03-06-05 are discarded due to high degrees of alteration. Sample KS04-23B is discarded because it contains a high proportion of mafic xenocrysts. The remaining samples represent three lithologies: rhyolite, basalt and andesite.

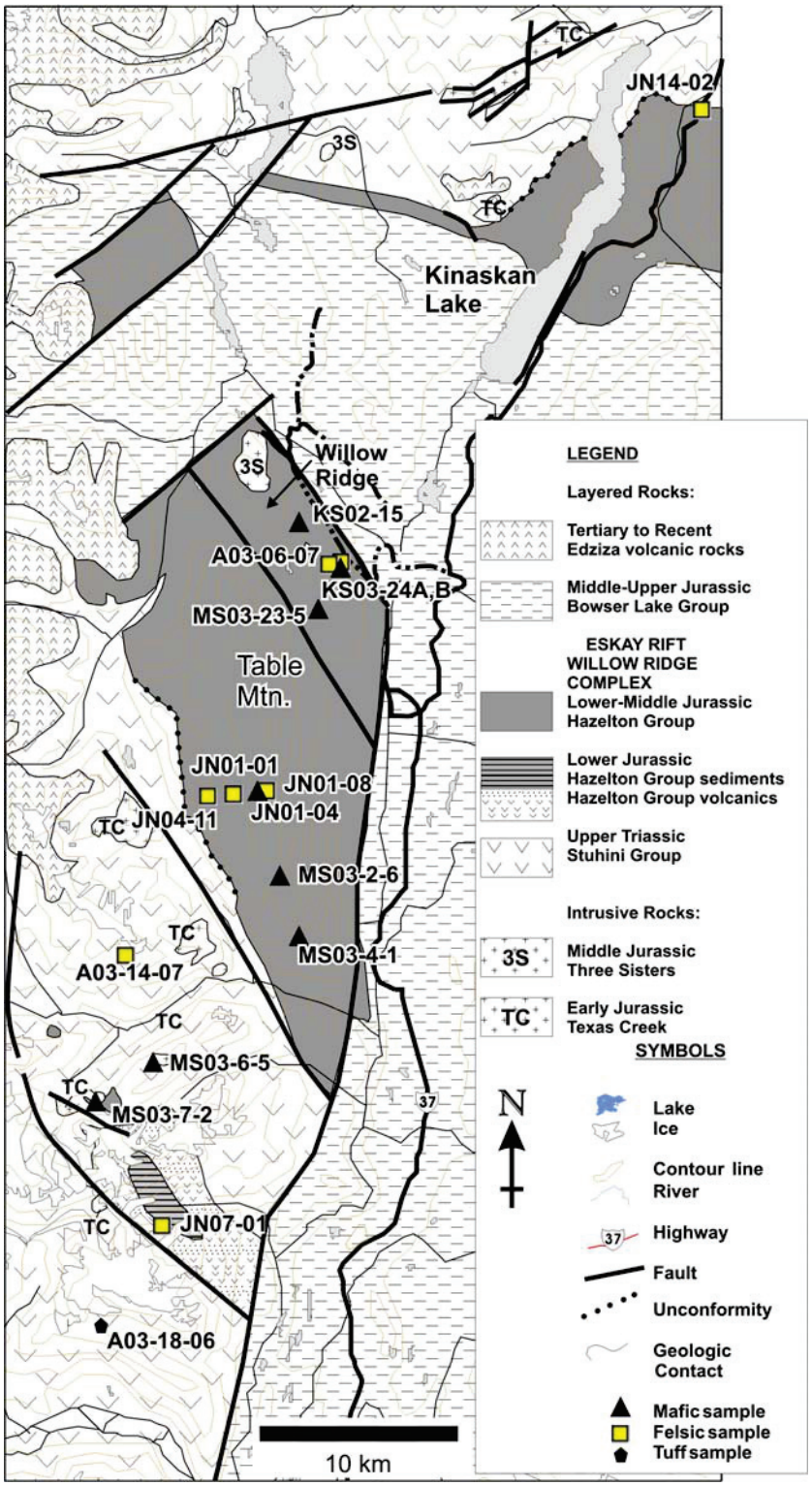

Figure 2. Geology map with sample locations; modified from Alldrick *et al.* (2004a).

TABLE 1. WHOLE ROCK GEOCHEMISTRY OF 17 SAMPLES FROM THE AREA BETWEE N MORE CREEK AND KINASKAN LAKE, IN THE TELEGRAPH CREEK MAP AREA

	WRC Rhyolite					WRC Mafic Rock						Triassic Rock		Discarded Samples			
	A03-06-07	JN01-01	JN01-08	JN04-11	JN14-02	JN01-04	KS02-15	KS03-24A	MS-03-23-05	MS-03-2-6	MS-03-04-01	JN07-01	MS-03-07-02	A03-14-07	A03-18-06	KS03-24B	MS-03-06-05
Northing	421260	416367	417267	415228	437134	417070	418813	421488	420457	419124	418694	412100	410866	409615	409310	421488	412705
Easting	6367558	6357233	6357929	6357218	6390500	6357677	6369407	6367159	6365319	6353741	6351346	6336122	6340927	6349481	6330150	6367159	6342981
SiO_2	82.58	76.48	81.94	69.01	69.87	46.11	47.09	51.77	56.7	61.77	53.91	83.9	52.93	96.58	64.9	71.02	55.34
TiO_2	0.1	0.15	0.23	0.5	0.18	1.51	0.98	1.94	1.73	1.15	1.36	0.12	0.87	0.05	0.94	0.68	0.68
Al_2O_3	8.27	11.84	7.73	12.68	14.06	13.02	16.09	13.64	14.89	13.55	15.06	7.46	18.23	0.87	12.93	13.34	16.38
Fe_2O_3	0.52	1.72	1.37	5.48	3.14	9.75	10.31	13.01	10.85	9.18	10.52	1.62	5.92	0.6	7.51	3.15	6.09
MnO	0.01	0.01	0.01	0.1	0.09	0.18	0.12	0.25	0.1	0.1	0.1	0.01	0.2	0.01	0.01	0.01	0.12
MgO	0.02	0.23	0.49	0.72	0.2	3.35	8.6	4.5	3.17	3.08	5.26	0.15	0.79	0.01	2.56	0.94	1.8
CaO	0.07	0.03	0.31	0.3	0.98	11.47	6.17	2.39	2.25	1.08	3.44	0.21	8.39	0.05	1.19	1	5.15
Na_2O	0.21	4.55	0.23	4.78	3.38	4.4	3.98	0.67	5.67	3.52	4.53	2.18	4.21	0.01	1.89	5.32	3.08
K_2O	6.96	3.07	5.46	1.12	5.19	0.64	0.62	6.03	0.02	2.42	1.13	2.75	1.99	0.18	2.68	2.22	3.83
P_2O_5	0.03	0.01	0.07	0.1	0.05	0.28	0.15	0.74	0.31	0.34	0.31	0.01	0.34	0.01	0.15	0.28	0.3
Ba	0.09	0.15	0.27	0.1	0.15	0.06	0.07	0.17	0.02	0.11	0.11	0.21	0.14	0.03	0.02	0.06	0.2
LOI	0.37	0.98	1.14	4.63	2	8.14	5.32	4.46	3.89	3.31	3.88	0.7	5.48	1.33	4.84	1.35	6.36
Total	99.23	99.22	99.25	99.52	99.29	98.91	99.5	99.57	99.6	99.61	99.61	99.32	99.49	99.73	99.62	99.37	99.33
V (ppm)	11	10	8	16	7	280	169	292	132	52	231	7	136	19	160	65	124
Y	14.55	48.05	31.73	51.76	32.08	35.52	18.47	40.79	39.04	31.04	43.53	42.67	22.63	4.34	19.92	30.98	18.82
Zr	99.19	365.48	216.59	352.68	308.44	147.48	68.5	157.27	189.8	186.33	222.51	253.57	135.22	17.10	163.88	178.48	140.75
Nb	5.00	21.03	11.50	21.88	17.94	13.53	6.17	9.01	14.95	15.08	15.1	20.53	12.34	3.72	10.05	9.19	13.8
La	19.79	26.97	14.15	23.23	32.48	10.96	4.25	15.38	18.35	13.23	15.37	7.68	18.65	6.00	13.81	20.12	16.3
Ce	37.28	53.69	26.26	46.59	60.97	24.58	10.62	31.83	37.28	31.18	33.33	17.29	35.62	13.36	28.78	42.07	30.42
Pr	3.50	6.65	3.53	5.92	7.18	3.48	1.69	4.50	5.06	4.50	4.50	2.44	4.53	1.43	4.34	5.37	3.80
Nd	11.42	27.65	14.46	25.04	27.20	16.36	8.79	20.71	22.54	20.57	20.08	11.22	19.38	5.44	18.90	22.03	16.05
	1.84	6.41	3.17	6.06	5.30	4.39	2.52	5.39	5.47	5.30	5.15	3.57	4.33	0.70	4.54	4.74	3.58
Eu	0.14	1.05	0.58	1.63	0.89	1.40	0.90	1.47	1.33	1.23	1.43	0.67	1.43	0.11	1.24	0.96	0.98
	1.51	6.96	3.87	7.34	5.25	5.66	3.18	6.87	6.63	6.02	6.50	4.93	4.50	0.53	4.63	4.98	3.62
Tb	0.30	1.30	0.73	1.32	0.89	0.98	0.54	1.16	1.10	1.01	1.13	1.04	0.69	0.10	0.72	0.85	0.56
	2.28	8.83	5.20	9.01	5.82	6.49	3.54	7.54	7.04	6.38	7.66	7.26	4.30	0.71	4.43	5.55	3.50
Ho	0.57	1.96	1.19	2.03	1.29	1.41	0.76	1.63	1.50	1.29	1.67	1.63	0.89	0.16	0.87	1.22	0.73
	2.11	6.34	3.81	6.43	4.09	4.28	2.25	4.91	4.43	3.73	5.08	5.08	2.56	0.50	2.48	3.72	2.20
Tm	0.37	1.01	0.59	1	0.64	0.64	0.33	0.72	0.65	0.55	0.77	0.79	0.38	0.07	0.37	0.55	0.33
	2.74	7.15	4.12	6.81	4.48	4.24	2.13	4.81	4.35	3.60	5.14	5.52	2.46	0.60	2.51	3.70	2.27
Lu	0.43	1.08	0.59	0.99	0.64	0.6	0.30	0.70	0.61	0.52	0.75	0.78	0.36	0.09	0.37	0.53	0.32
	3.58	8.74	4.64	7.35	6.55	3.49	1.59	3.65	4.36	4.43	4.79	5.56	3.12	0.32	3.75	3.98	3.28
Ta	0.66	1.06	0.54	0.93	0.90	0.39	0.11	0.45	0.70	0.73	0.56	0.78	0.51	0.06	0.40	0.58	0.51
	13.77	6.07	3.93	6.41	11.43	1.60	0.25	2.26	3.23	3.56	3.30	4.51	3.61	0.42	1.75	5.46	5.75

Processing of samples included the removal of weathered surfaces by selective chip sampling. Samples were pulped in a chrome steel swing mill. The major oxides as well as Ba and V were determined by x-ray fluorescence (XRF) using a fused disc and Siemens spectrometer at Global Discovery Labs in Vancouver, British Columbia. Loss on ignition was determined by fusion at 1100°C. Trace element concentrations, including analyses of Y, Zr, Nb, Hf, Ta, Th and the rare earth elements (REE) were determined by inductively coupled plasma mass spectrometry (ICP-MS) at Memorial University of Newfoundland (rock powders were dissolved with Na_2O_2). The quality of analysis was monitored by simultaneous analysis of standard reference rocks. Major oxides and trace elements have been recalculated to anhydrous for all discussion in this paper. Table 1 contains the results of all original data, which are not recalculated to anhydrous compositions.

WHOLE ROCK GEOCHEMISTRY

WRC Rocks

Analysis of major oxides of metamorphosed and altered rocks, such as those from the WRC, poses difficulties because many major elements have a high degree of mobility. In particular, the hydrothermal alteration of feldspars and glass results in the loss of alkalis (Saeki and Date, 1980), and the formation of chlorite can affect Mg and Fe concentrations (Lentz, 1999). Other major elements, such as Al_2O_3 and TiO_2, are normally considered immobile. For this study an effort was made to collect samples exhibiting the least amount of alteration. However, petrography shows that many samples have been subject to significant alteration. As a result, the emphasis of this study is on trace element geochemistry utilizing mainly the REE and high field strength elements, which are considered to be immobile under low-grade alteration conditions (Whitford *et al.*, 1988; Lentz, 1999).

According to SiO_2 vs Zr/TiO_2 ratios, WRC rocks range, on an anhydrous basis, from basalts and andesites to dacites and rhyolites (Fig. 3). Two samples have very high contents of SiO_2 (83%), indicating that they were affected by secondary SiO_2 enrichment. In addition, petrography shows that secondary quartz is present in some mafic samples, which suggests that the rocks which plot as andesites may be silicified basalt. Because of this apparent SiO_2 mobility, classification of WRC rocks must be done using trace elements. According to Zr/TiO_2 vs Nb/Y ratios, the WRC volcanics are a bimodal rock suite, consisting of mafic rocks that range in composition from basalts to andesite-basalts, and felsic rocks that are all rhyolites (Fig. 4).

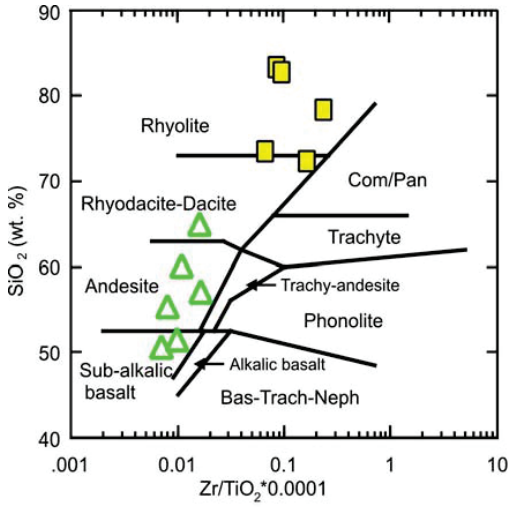

Figure 3. Classification of WRC volcanic rocks; squares = felsic samples, triangles = mafic samples; Com/Pan = comendite and pantellerite; Bas-Trach-Neph = basanite and trachyte and nephelinite; Winchester and Floyd (1977).

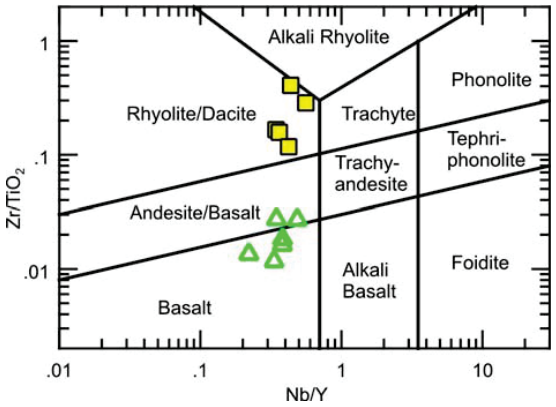

Figure 4. Classification of WRC volcanic rocks according to immobile elements; squares = felsic samples, triangles = mafic samples; Pearce (1996).

Both classification systems agree that the WRC rocks are sub-alkalic. A plot of TiO_2 vs Mg# ($Mg\# = Mg/Mg+Fe_{tot}$) supports the bimodality of the suite, showing that the felsic and mafic rocks form two distinct populations (Fig. 5).

WRC Mafic Rocks

Mafic rocks of the Willow Ridge Complex are basalts and andesites (Fig. 4). According to their negative trend on a TiO_2 vs Mg# diagram (Fig. 5) and overall high TiO_2 values (1.3 – 2%), they have a

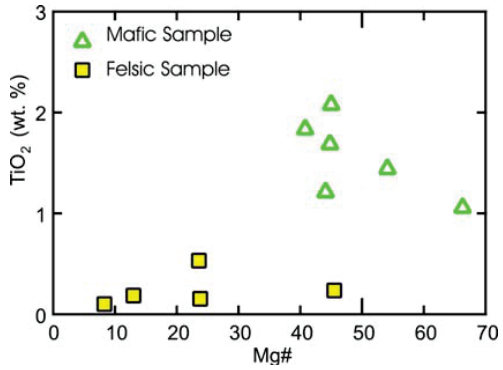

Figure 5. TiO_2 vs MG# (MG# = $Mg/Mg+Fe_{tot}$) plot of WRC mafic and felsic volcanic rocks; shows two unrelated populations; mafic samples have high TiO_2 concentrations and a negative slope.

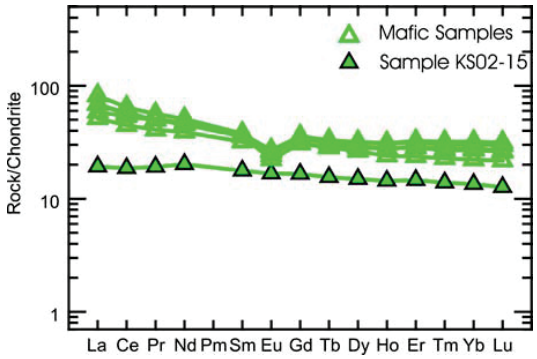

Figure 6. Chondrite normalized REE plot of WRC mafic rocks; Sun and McDonough (1989).

tholeiitic MORB affinity. Rare earth elements (REE) show a slight enrichment in light REE (LREE) (La_n/Sm_n = 1.83), flat heavy REE (HREE) (Gd_n/Yb_n = 1.19) and a small negative Eu anomaly (Fig. 6). Sample KS-02-15 has lower absolute abundance of REE and a nearly flat pattern (La_n/Yb_n = 1.43). Mantle normalized trace element abundance patterns for the mafic rocks show a slight enrichment of strongly incompatible elements, sloping from Th to Sm with a small but distinct negative Nb anomaly (Fig. 7). Sample KS02-15 has lower absolute abundances of incompatible elements than the other mafic samples, and it does not show a negative Nb anomaly. There are no significant systematic differences between the trace element characteristics of basalts and andesites.

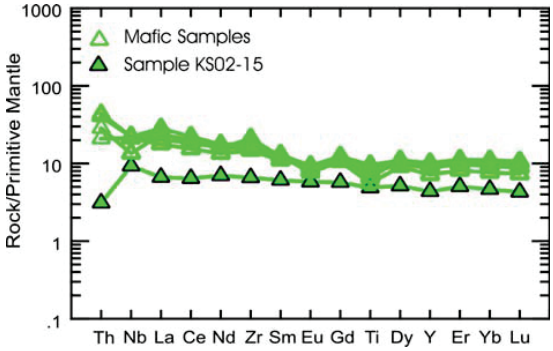

Figure 7. Primitive mantle normalized immobile element plot of WRC mafic rocks; Sun and McDonough (1989).

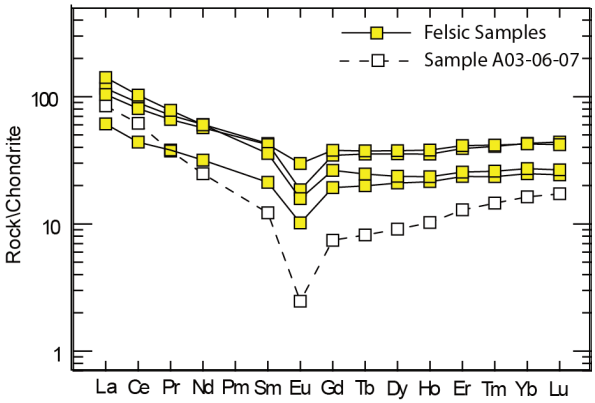

Figure 8. Chondrite normalized REE plot of WRC felsic rocks; Sun and McDonough (1989).

WRC Felsic Rocks

The very high concentrations of SiO_2 (between 72% and 83%) in the rhyolites suggest that at least some samples were affected by secondary silicification. The majority of felsic samples follow the same pattern on REE diagrams and show enrichment in LREE (La_n/Sm_n = 3.01), flat HREE (Gd_n/Yb_n = 0.86) and a slight negative Eu anomaly (Fig. 8). One sample (A03-06-07) has a very different, V-shaped, REE pattern. It has a moderately steep downward slope from La to Sm (La_n/Sm_n = 6.93), a shallow upward slope from Gd to Lu (Gd_n/Yb_n = 0.46) and a strong negative Eu anomaly. Mantle normalized trace element plots also distinguish sample A03-06-07 from the main felsic population (Fig. 9). The four felsic samples that plot together have a

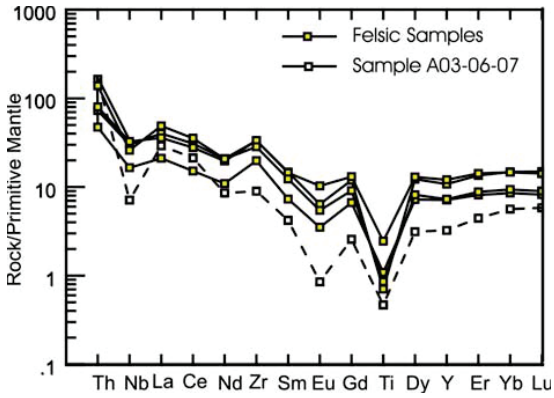

Figure 9. Primitive mantle normalized immobile element plot of WRC felsic rocks; Sun and McDonough (1989).

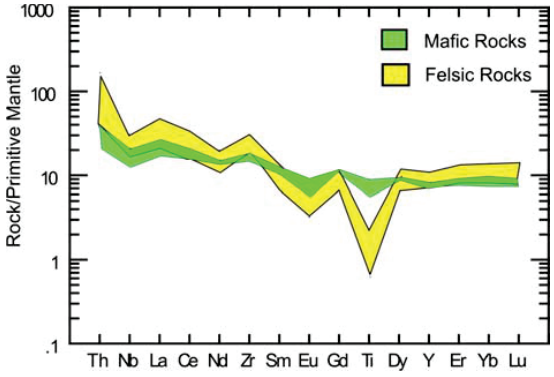

Figure 10. Primitive mantle normalized immobile element plot showing the overlap in element concentrations for WRC felsic and mafic rocks; Sun and McDonough (1989).

shallow downward slope up to Sm with mildly negative Nb, strongly negative Ti and weak positive Zr anomalies. Sample A03-06-07 has a lower absolute abundance of most incompatible elements, a steeper negative slope up to Sm and stronger negative Nb and Eu anomalies.

DISCUSSION

The volcanic rocks of the Willow Ridge Complex form a bimodal, sub-alkalic suite that is consistent with a rifting arc environment. Two sources are proposed for the mafic rocks within the complex. Sample KS02-15, which has a flat REE pattern and a positive Nb anomaly on a mantle normalized profile (Fig. 7), is typical of rift-related basalts generated from asthenospheric mantle. The remaining samples, which are relatively enriched in LREE and incompatible elements such as Th, and have a slight negative Nb anomaly, are derived from sub-arc lithospheric mantle.

Rhyolites in the WRC show a distinct grouping according to Zr/TiO_2 and Nb/Y ratios (Fig. 4). No intermediate or alkali rocks are represented. The absolute abundances of trace elements of rhyolites and basalts overlap (Fig. 10). This precludes the possibility that the rhyolites were derived from fractional crystallization of the basalts. Therefore they must have a different source than the WRC mafic rocks. The most obvious source of the rhyolites is melting of crustal rocks. Sample A03-06-07 has a very different trace element signature than most of the WRC rhyolites; this may be a result of the heterogeneous nature of the crust from which it is derived. A variety of explanations for similar V-shaped REE signatures in felsic rocks are described by Dostal and Chatterjee (1995).

Field relations within the WRC and on a regional scale suggest that the upper Hazelton Group in the Telegraph Creek and Iskut River map areas is rift related. The geochemistry of the WRC is consistent with a rifting arc environment. Bimodal volcanism, as expressed in the WRC, is common of rift environments. The following is the most likely scenario that accounts for the range of volcanic rock compositions found within the WRC. Rift-related decompression melting of the asthenosphere produced mafic magmas represented by sample KS-02-15. However, the majority of the magma, which erupted during the period represented by the WRC, was derived from a sub-arc lithospheric mantle source. Heat derived from the mafic magmas caused partial melting within the crust. This generated felsic magmas, which have similar trace element abundances as the sub-arc mantle derived mafic rocks but different relative enrichment patterns, notably Nb and Ti depletions, which reflect their crustal source. Rift-related faulting allowed these magmas to erupt with minimal mixing, which accounts for the bimodality of the WRC volcanic suite.

Comparison of WRC and Eskay Creek Igneous Rocks

Volcanic rocks from the WRC and the Eskay Creek mine have similar chemical characteristics but there are also some subtle differences between them. Rhyolites at Eskay Creek are significantly enriched in the absolute abundances of REE with respect to basalts. This is similar to the relationship between the rhyolites of the WRC and the one asthenospherically derived mafic sample, but contrasts with the relationships seen between WRC rhyolites and the majority of basalts found in the complex. Significantly, Barrett and Sherlock (1996) indicate that the rhyolite and basalt

magmas at Eskay Creek could be derived from different sources. They suggest that the rhyolites are derived from tholeiitic crustal rocks, and the basalts are derived from primitive mantle. This is also the most likely scenario for the genesis of the rhyolites, and the primitive basalt sample from the WRC. Barrett and Sherlock (1996) also agree that the eruption of primitive basalt at Eskay Creek might be due to rift-related deep faulting. Average element concentrations between Eskay Creek rhyolites and basalts are similar to WRC rhyolites and basalts but there are some differences. Barrett and Sherlock (1996) use approximate values of Zr, Y, Nb and $(La/Yb)_n$ to characterize Eskay rhyolites (Table 2). Willow Ridge Complex and Eskay Creek rhyolites have comparable $(La/Yb)_n$ ratios, but the absolute element concentrations are elevated in the WRC rhyolites. Barrett and Sherlock (1996) characterized Eskay Creek basalts by their range of immobile element concentrations. The ranges of element concentrations in WRC basalts have significant overlap with those of Eskay Creek basalts (Table 3).

Rhyolites from both Eskay Creek and from the WRC have incompatible element characteristics that are consistent with FIII type rhyolites of Lescher *et al.* (1986). These types of rhyolites are host to most of the Archean age VHMS deposits in the Superior Province as well as large tonnage VHMS deposits of other ages worldwide (*e.g.,* Kidd Creek, United Verde).

The bimodal volcanic suite of the WRC shows a marked departure from the volcanism in the lower part of the Hazelton Group. Early Jurassic rocks of the Hazelton Group have dominantly intermediate compositions with a calc-alkaline affinity (Marsden and Thorkelson, 1992). Macdonald *et al.* (1996) interpreted the Early Jurassic volcanic environment to be a partly emergent volcanic arc. The geochemical and field characteristics of the WRC both indicate that a shift occurred from an Early Jurassic arc-related environment to a rifting-arc environment during the Middle Jurassic.

CONCLUSIONS

Volcanic rocks from the Willow Ridge Complex are bimodal. Mafic rocks are rift-related tholeiites and all but the most primitive basalts were derived from the sub-arc lithospheric mantle. Rhyolites are derived from partial melting of a heterogeneous crust. The bimodality of the volcanics from the WRC, and the tholeiitic affinity of the mafic rocks, are consistent with field observations which suggest that the WRC represents a rift environment. Volcanic rocks from the WRC represent a shift from Early Jurassic arc formation to Middle Jurassic arc rifting, which has been observed elsewhere in the region, notably at Eskay Creek. Chemically the WRC volcanic rocks are very similar to those at Eskay Creek but there are some subtle differences in their geochemical signatures. Both WRC and Eskay Creek rhyolites have incompatible element characteristics that are consistent with FIII type rhyolites of Lescher *et al.* (1986). FIII type rhyolites are highly prospective and host most of the Archean VHMS deposits in the Superior province, and many other high tonnage deposits worldwide.

TABLE 2. COMPARISONS OF SELECTED IMMOBILE ELEMENTS IN RHYOLITES FROM ESKAY CREEK AND THE WRC

	Eskay Rhyolite	WRC Rhyolite
Zr	170 ppm	228 ppm
Y	55 ppm	37 ppm
Nb	30 ppm	16 ppm
$(La/Yb)_n$	2-4	2-5

TABLE 3 COMPARISONS OF SELECTED IMMOBILE ELEMENTS IN BASALTS FROM ESKAY CREEK AND THE WRC

	Eskay Basalt	WRC Basalt
TiO_2	1.3–2%	1.1–1.8%
Zr	60–90 ppm	73–235 ppm
Y	25–40 ppm	19–46 ppm
Nb	2–6 ppm	6–17 ppm

ACKNOWLEDGMENTS

We would like to thank Dani Alldrick, JoAnne Nelson, Martin Stewart and Kirstie Simpson for collecting the geochemical rock samples that are described in this article. We also thank JoAnne Nelson and Dani Alldrick for valuable discussions about upper Hazelton Group geology and for their constructive reviews of this article.

REFERENCES

Alldrick, D.J., Stewart, M.L., Nelson, J.L. and Simpson, K.A. (2004a): Tracking the Eskay Rift through northern British Columbia - geology and mineral occurrences of the Upper Iskut River area; *British Columbia Ministry of Energy and Mines*, Geological Fieldwork 2003, Paper 2004-1, pages 1-18.

Alldrick, D.J., Stewart, M.L., Nelson, J.L. and Simpson, K.A. (2004b): Geology of the More Creek - Kinaskan Lake area, northwestern British Columbia; *British Columbia Ministry of Energy and Mines*, Open File Map 2004-2, scale 1:50 000.

Barrett, T.J. and Sherlock, R.L. (1996): Geology, lithogeochemistry and volcanic setting of the Eskay Creek Au-Ag-Cu-Zn deposit, northwestern British Columbia; *Exploration and Mining Geology*, Volume 5, pages 339-368.

Dostal, J. and Chatterjee. A.K. (1995): Origin of topaz-bearing and related peraluminous granites of the Late Devonian Davis Lake pluton, Nova Scotia, Canada: Crystal versus fluid fractionation; *Chemical Geology*, Volume 123, pages 67-88.

Lentz, D.R. (1999): Petrology, geochemistry, and oxygen isotope interpretation of felsic volcanic and related rocks hosting the Brunswick 6 and 12 massive sulfide deposits (Brunswick belt), Bathurst mining camp, New Brunswick, Canada; *Economic Geology*, Volume 94, pages 57-86.

Lescher, C.M., Goodwin, A.M., Campbell, I.H. and Gorton, M.P. (1986): Trace-element geochemistry of ore-associated and barren, felsic metavolcanic rocks in the Superior Province, Canada; *Canadian Journal of Earth Science*, Volume 23, pages 222-237.

Logan, J.M., Drobe, J.R. and McClelland, W.C. (2000): Geology of the Forest Kerr - Mess Creek Area, Northwestern British Columbia (104B/10,15 & 104G/2 & 7W); *British Columbia Ministry of Energy and Mines*, Bulletin 104, 164 pages.

MacDonald, J.A., Lewis, P.D., Thompson, J.F.H., Nadaraju, G., Bartsch, R.D., Bridge, D.J., Rhys, D.A., Roth, T., Kaip, A., Godwin, C.I. and Sinclair, A.J. (1996): Metallogeny of an Early to Middle Jurassic arc, Iskut River area, northwestern British Columbia; *Economic Geology*, Volume 91, no 6, pages 1098-1114.

Marsden, H. and Thorkelson, D.J. (1992): Geology of the Hazelton volcanic belt in British Columbia: Implications for the Early to Middle Jurassic evolution of Stikinia; *Tectonics*, Volume 11, no 6, pages 1222-1287.

Pearce, J.A. (1996): A user's guide to basalt discrimination diagrams; *Geological Association of Canada*, Short Course Notes, Volume 12, pages 79-113.

Saeki, Y. and Date, J. (1980): Computer application to the alteration data of the footwall dacite lava at the Ezuri Kuroko Deposits, Akito Prefecture; *Mining Geology*, Volume 30, pages 241-250.

Simpson, K.A. and Nelson, J.L. (2004): Preliminary interpretations of mid-Jurassic volcanic and sedimentary facies in the East Telegraph Creek map area; *Geological Survey of Canada*, Current Research 2004-A1, 8 pages

Sun, S-S. and McDounough, W.F. (1989): Chemical and isotope systematics of oceanic basalts: Implications for mantle composition and processes; *Geological Society*, Special Publication 42, pages 313-345.

Whitford, D.J., Korsch, M.J., Porritt, P.M. and Craven, S.J. (1988): Rare-earth element mobility around the volcanogenic massive sulfide deposit at Que River, Tasmania, Australia; *Chemical Geology*, Volume 68, pages 105-199.

Winchester, J.A. and Floyd, P.A. (1977): Geochemical discrimination of different magma series and their differentiation products using immobile elements; *Chemical Geology*, Volume 20, pages 325-343.

Appendix B: Supplemental Data

Appendix B.1: Detrital Zircon Data (Chapter 3)

	Age estimates with 1 sigma uncertainty (Ma)							
	$^{207}Pb/^{235}U$	$^{207}Pb/^{235}U$	$^{206}Pb/^{238}U$	$^{206}Pb/^{238}U$	$^{207}Pb/^{206}Pb$	$^{207}Pb/^{206}Pb$	Preferred Age	
Analysis No.	**Ma**	**+/- 1σ Error**	**Ma**	**+/- 1σ Error**	**Ma**	**+/- 1σ Error**	**Ma ***	**+/- 1σ Error**
07JN09-03L1	229.1	6.48	224.2	2.38	244.1	69.01	**224**	**1.67**
07JN09-03L2	225.2	5.87	224	2.26	230.1	63.71	**221.4**	**2.12**
07JN09-03L3	225.4	2.73	222.2	1.08	235.4	29.76	**221.9**	**1.07**
07JN09-03L4	229	6.16	230.6	2.39	248.2	65.58	**230.3**	**2.38**
07JN09-03L5	234.8	10.03	222	3.48	246.1	103.35	**225**	**3.06**
07JN09-03L6	221.9	4.69	220.7	1.8	242.1	51.77	**220.4**	**1.8**
07JN09-03L7	221.6	8.85	221.9	3.18	216.5	97.32	**221.7**	**3.19**
07JN09-03L8	231.9	8.07	231.6	2.8	224.4	85.39	**231.3**	**4.27**
07JN09-03L9	220	7.09	217.2	2.47	229.5	79.08	**216.5**	**2.58**
07JN09-03L10	220	6.38	219.2	2.36	218.1	71.15	**219.6**	**1.87**
07JN09-03L11	252.1	6.98	253.4	2.76	270.2	67.14	**253.1**	**2.75**
07JN09-03L12	228.1	6.78	226.3	2.47	241.5	72.49	**226**	**2.46**
07JN09-03L13	224.1	4.54	221.2	1.76	244.1	49.59	**222.1**	**1.48**
07JN09-03L14	222.5	11.05	219.9	4.04	236.8	119.57	**222.4**	**2.61**
07JN09-03L15	216.3	9.43	211.6	3.03	230.1	106.23	**211.4**	**3.02**
07JN09-03L16	225.6	3.58	225.6	1.41	250.5	38.86	**225.3**	**1.41**
07JN09-03L17	219	4.35	221.1	1.73	236.6	48.65	**220.8**	**1.72**
07JN09-03L18	232	10.82	224.9	4.01	230	112.38	**224.7**	**4.01**
07JN09-03L19	212.5	11.22	219.6	4.39	237.5	126.52	**219.3**	**4.39**
07JN09-03L20	220.4	5.32	221.8	1.94	241.5	59.19	**223.2**	**1.86**
07JN09-03L21	232.6	7	229.8	2.69	257.5	73.11	**229.6**	**2.68**
07JN09-03L22	235.4	2.63	231.2	1.04	223	27.52	**231.1**	**1.04**
07JN09-03L23	223.6	4.83	221.7	1.79	227	53.12	**221.5**	**1.79**
07JN09-03L24	223.1	2.58	221	1.04	221.7	28.48	**220.8**	**1.03**
07JN09-03L25	236.4	6.56	232.9	2.5	226.5	67.86	**232.7**	**2.49**
07JN09-03L26	232	7.65	233.1	2.88	237.8	80.51	**233**	**2.88**
07JN09-03L27	222.7	8.6	223.1	2.86	225	94.64	**223**	**2.86**
07JN09-03L28	225.3	7.53	227.1	2.81	216.4	81.75	**226.9**	**2.81**
07JN09-03L29	228.6	10.44	224.5	3.69	235.7	111.07	**224.3**	**3.69**
07JN09-03L30	228.6	12.68	229.7	4.92	227	132.66	**229.5**	**4.92**
07JN09-03L31	236.6	9.11	215.7	3.27	498.1	90.67	**222.7**	**5.57**
07JN09-03L32	223.2	23.18	222.2	7.51	401.2	237.72	**225.2**	**7.65**
07JN09-03L33	225.3	9.24	220.5	3.23	246.2	99.55	**220.3**	**3.22**
07JN09-03L34	224.7	9.85	227.2	3.29	247.7	106.58	**227.4**	**3.26**
07JN09-03L35	227.9	9.73	227.2	3.12	249.9	104.09	**227.1**	**3.11**
07JN09-03L36	206.1	22.95	209.6	8.3	211.8	257.68	**213.7**	**10.29**
07JN09-03L37	225.5	3.82	222.1	1.45	215.2	41.7	**222**	**1.45**
07JN09-03L38	228.6	9.65	220.2	3.28	240.1	102.62	**219.5**	**3.51**
07JN09-03L39	220.5	9.33	218.2	3.1	234.3	103.18	**218.1**	**3.1**
07JN09-03L40	216.8	11.66	220.4	4.21	226.6	129.7	**220.4**	**4.21**

		Isotopic Ratios with absolute errors						
	Discordancy	$^{207}Pb/^{235}U$	$^{207}Pb/^{235}U$	$^{206}Pb/^{238}U$	$^{206}Pb/^{238}U$	Rho	$^{207}Pb/^{206}Pb$	$^{207}Pb/^{206}Pb$
Analysis No.	%	Ratio	1σ Error	Ratio	1σ Error		Ratio	1σ Error
07JN09-03L1	8.2	0.2531	0.0080	0.0354	0.0004	0.34	0.0511	0.0016
07JN09-03L2	2.7	0.2483	0.0072	0.0354	0.0004	0.35	0.0508	0.0014
07JN09-03L3	5.6	0.2486	0.0034	0.0351	0.0002	0.36	0.0509	0.0007
07JN09-03L4	7.1	0.2530	0.0076	0.0364	0.0004	0.35	0.0512	0.0015
07JN09-03L5	9.8	0.2602	0.0124	0.0350	0.0006	0.33	0.0511	0.0024
07JN09-03L6	8.8	0.2442	0.0057	0.0348	0.0003	0.35	0.0510	0.0012
07JN09-03L7	-2.5	0.2438	0.0108	0.0350	0.0005	0.33	0.0505	0.0022
07JN09-03L8	-3.2	0.2566	0.0100	0.0366	0.0005	0.32	0.0506	0.0019
07JN09-03L9	5.4	0.2419	0.0087	0.0343	0.0004	0.33	0.0508	0.0018
07JN09-03L10	-0.5	0.2419	0.0078	0.0346	0.0004	0.34	0.0505	0.0016
07JN09-03L11	6.2	0.2818	0.0088	0.0401	0.0004	0.35	0.0517	0.0016
07JN09-03L12	6.3	0.2519	0.0084	0.0357	0.0004	0.34	0.0510	0.0016
07JN09-03L13	9.4	0.2470	0.0056	0.0349	0.0003	0.36	0.0511	0.0011
07JN09-03L14	7.1	0.2450	0.0136	0.0347	0.0007	0.34	0.0509	0.0027
07JN09-03L15	8.0	0.2374	0.0115	0.0334	0.0005	0.30	0.0508	0.0024
07JN09-03L16	9.9	0.2488	0.0044	0.0356	0.0002	0.37	0.0512	0.0009
07JN09-03L17	6.6	0.2407	0.0053	0.0349	0.0003	0.36	0.0509	0.0011
07JN09-03L18	2.2	0.2567	0.0134	0.0355	0.0006	0.35	0.0508	0.0026
07JN09-03L19	7.5	0.2328	0.0136	0.0346	0.0007	0.35	0.0509	0.0029
07JN09-03L20	8.2	0.2425	0.0065	0.0350	0.0003	0.33	0.0510	0.0013
07JN09-03L21	10.8	0.2575	0.0087	0.0363	0.0004	0.35	0.0514	0.0017
07JN09-03L22	-3.7	0.2610	0.0033	0.0365	0.0002	0.37	0.0506	0.0006
07JN09-03L23	2.3	0.2464	0.0059	0.0350	0.0003	0.34	0.0507	0.0012
07JN09-03L24	0.3	0.2458	0.0032	0.0349	0.0002	0.38	0.0506	0.0006
07JN09-03L25	-2.8	0.2622	0.0082	0.0368	0.0004	0.35	0.0507	0.0015
07JN09-03L26	2.0	0.2567	0.0095	0.0368	0.0005	0.34	0.0509	0.0018
07JN09-03L27	0.8	0.2452	0.0106	0.0352	0.0005	0.30	0.0507	0.0021
07JN09-03L28	-4.9	0.2484	0.0093	0.0359	0.0005	0.34	0.0505	0.0018
07JN09-03L29	4.8	0.2524	0.0129	0.0354	0.0006	0.33	0.0509	0.0025
07JN09-03L30	-1.2	0.2524	0.0156	0.0363	0.0008	0.35	0.0507	0.0030
07JN09-03L31	56.7	0.2624	0.0113	0.0340	0.0005	0.35	0.0572	0.0024
07JN09-03L32	44.6	0.2459	0.0284	0.0351	0.0012	0.30	0.0547	0.0063
07JN09-03L33	10.4	0.2485	0.0114	0.0348	0.0005	0.33	0.0511	0.0023
07JN09-03L34	8.3	0.2477	0.0121	0.0359	0.0005	0.30	0.0512	0.0025
07JN09-03L35	9.1	0.2516	0.0120	0.0359	0.0005	0.29	0.0512	0.0024
07JN09-03L36	1.0	0.2251	0.0277	0.0330	0.0013	0.33	0.0504	0.0061
07JN09-03L37	-3.2	0.2487	0.0047	0.0351	0.0002	0.35	0.0504	0.0009
07JN09-03L38	8.3	0.2525	0.0119	0.0348	0.0005	0.32	0.0510	0.0023
07JN09-03L39	6.9	0.2425	0.0114	0.0344	0.0005	0.31	0.0509	0.0024
07JN09-03L40	2.7	0.2380	0.0142	0.0348	0.0007	0.33	0.0507	0.0030

	Age estimates with 1 sigma uncertainty (Ma)							
	$^{207}Pb/^{235}U$	$^{207}Pb/^{235}U$	$^{206}Pb/^{238}U$	$^{206}Pb/^{238}U$	$^{207}Pb/^{206}Pb$	$^{207}Pb/^{206}Pb$	Preferred Age	
Analysis No.	Ma	+/- 1σ Error	Ma	+/- 1σ Error	Ma	+/- 1σ Error	Ma *	+/- 1σ Error
05MM0501L1	207.3	2.67	208.2	1.03	202.5	31.83	**208.2**	**1.03**
05MM0501L2	207.9	4.01	206.2	1.48	204.9	47.55	**206.2**	**1.48**
05MM0501L3	207.3	2.47	205.4	0.98	217.3	29.28	**205.4**	**0.98**
05MM0501L4	208.9	2.89	209.7	1.11	204.8	34.17	**209.7**	**1.11**
05MM0501L5	214.1	4.65	217.8	1.82	220.4	53.17	**217.8**	**1.82**
05MM0501L6	208.8	1.34	210.1	0.6	225	15.81	**210.1**	**0.60**
05MM0501L7	211.3	2.74	210.3	1.07	221.1	31.89	**210.3**	**1.07**
05MM0501L8	205.6	2.66	207.1	1.03	194.7	31.98	**207.1**	**1.03**
05MM0501L9	199.7	4.04	203.2	1.54	203.7	49.77	**203.2**	**1.54**
05MM0501L10	207.1	2.44	208	0.95	195.7	29.2	**208.0**	**0.95**
05MM0501L11	207.7	1.79	208	0.75	192.4	21.33	**208.0**	**0.75**
05MM0501L12	207	2.4	207.6	0.96	209.5	28.58	**207.6**	**0.96**
05MM0501L13	206.7	3.81	208.2	1.39	209.4	45.57	**208.2**	**1.39**
05MM0501L14	203.4	5.09	202	1.87	217.3	61.24	**202.0**	**1.87**
05MM0501L15	208.8	2.64	203.7	1.03	197.3	31.27	**203.7**	**1.03**
05MM0501L16	211	3.37	204.5	1.28	273.4	39.02	**204.5**	**1.28**
05MM0501L17	201.9	3.88	206.8	1.57	217.7	47.07	**206.8**	**1.57**
05MM0501L18	204.9	3.11	204.2	1.19	205.6	37.41	**204.2**	**1.19**
05MM0501L19	198.1	4.71	199.8	1.75	198.7	58.45	**199.8**	**1.75**
05MM0501L20	204.9	2.5	202.5	0.98	214.1	30.05	**202.5**	**0.98**
05MM0501L21	197.9	3.11	205	1.16	131.7	39.36	**205.0**	**1.16**
05MM0501L22	203.1	3.47	201.1	1.27	208.6	42.22	**201.1**	**1.27**
05MM0501L23	209.9	3.31	208	1.24	206.7	38.98	**208.0**	**1.24**
05MM0501L24	215.1	5.42	215.5	2.05	217.5	61.76	**215.5**	**2.05**
05MM0501L25	212.1	3.45	210.6	1.27	214.1	40.2	**210.6**	**1.27**
05MM0501L26	210.5	5.8	207.9	2.15	219.1	67.35	**207.9**	**2.15**
05MM0501L27	211.3	3.77	203.4	1.33	288.9	43.56	**203.4**	**1.33**
05MM0501L28	207	2.78	203.7	1.06	220.2	33.05	**203.7**	**1.06**
05MM0501L29	203.2	3.3	200.3	1.21	212.9	40.07	**200.3**	**1.21**
05MM0501L30	205.7	2.06	202.2	0.83	192.3	24.72	**202.2**	**0.83**
05MM0501L31	204.5	3.1	204.9	1.21	221.3	37.32	**204.9**	**1.21**
05MM0501L32	207.2	3.43	209.8	1.31	214.3	40.81	**209.8**	**1.31**
05MM0501L33	214.2	2.85	210.4	1.14	249.6	32.59	**210.4**	**1.14**
05MM0501L34	209.3	3.24	207.1	1.26	213.9	38.07	**207.1**	**1.26**
05MM0501L35	215.6	3.28	212.3	1.24	223.6	37.48	**212.3**	**1.24**
05MM0501L36	215.7	3.4	211.3	1.31	226.5	38.7	**211.3**	**1.31**
05MM0501L37	211.4	3.39	211	1.33	230.7	39.36	**211.0**	**1.33**
05MM0501L38	205.6	2.75	205.2	1.07	223.4	32.88	**205.2**	**1.07**
05MM0501L39	215.8	1.85	217.9	0.78	200.8	21.15	**217.9**	**0.78**
05MM0501L40	209.6	3.18	212.2	1.19	171.5	37.74	**212.2**	**1.19**
05MM0501L41	209.7	2.72	210.7	1.07	219.5	31.95	**210.7**	**1.07**
05MM0501L42	208.9	2.52	210.9	0.99	196.2	29.84	**210.9**	**0.99**
05MM0501L43	214.3	1.88	216	0.79	217.3	21.54	**216.0**	**0.79**
05MM0501L44	221.7	1.71	222.2	0.74	238.9	18.86	**222.2**	**0.74**
05MM0501L45	214	3.37	212.5	1.29	228.4	38.67	**212.5**	**1.29**
05MM0501L46	210	2.77	206.3	1.07	220.8	32.45	**206.3**	**1.07**
05MM0501L47	212.5	2.84	209	1.09	216.5	32.98	**209.0**	**1.09**
05MM0501L48	210.7	3.07	211.4	1.17	221.1	35.91	**211.4**	**1.17**
05MM0501L49	211.1	2.92	210.9	1.11	199.9	34.16	**210.9**	**1.11**
05MM0501L50	215	11.33	228.6	4.7	232	126.02	**228.6**	**4.70**
05MM0501L51	227.2	3.82	210.8	1.37	360.6	40.79	**210.8**	**1.37**
05MM0501L52	212.1	4.56	216.6	1.79	227.1	52.71	**216.6**	**1.79**
05MM0501L53	210.8	2.01	214.2	0.84	201.4	23.33	**214.2**	**0.84**
05MM0501L54	293.4	3.04	289.6	1.25	305.8	25.25	**289.6**	**1.25**
05MM0501L55	214.1	3.85	211.4	1.41	237	44.26	**211.4**	**1.41**
05MM0501L56	207.8	5.25	205.5	1.89	233.6	61.92	**205.5**	**1.89**
05MM0501L57	211.2	3.25	206.4	1.26	205.3	37.87	**206.4**	**1.26**
05MM0501L58	230.2	3.89	214.7	1.45	394.5	40.3	**214.7**	**1.45**
05MM0501L59	225.2	4.31	212.7	1.54	329.4	46.32	**212.7**	**1.54**
05MM0501L60	216.4	2.51	211.1	0.98	228.2	28.46	**211.1**	**0.98**

		Isotopic Ratios with absolute errors						
	Discordancy	$^{207}Pb/^{235}U$	$^{207}Pb/^{235}U$	$^{206}Pb/^{238}U$	$^{206}Pb/^{238}U$	Rho	$^{207}Pb/^{206}Pb$	$^{207}Pb/^{206}Pb$
Analysis No.	%	Ratio	1σ Error	Ratio	1σ Error		Ratio	1σ Error
05MM0501L1	-2.8	0.2265	0.0032	0.0328	0.0002	0.36	0.0502	0.0007
05MM0501L2	-0.6	0.2272	0.0049	0.0325	0.0002	0.35	0.0502	0.0010
05MM0501L3	5.5	0.2265	0.0030	0.0324	0.0002	0.38	0.0505	0.0006
05MM0501L4	-2.4	0.2285	0.0035	0.0331	0.0002	0.36	0.0502	0.0008
05MM0501L5	1.2	0.2347	0.0057	0.0344	0.0003	0.35	0.0506	0.0012
05MM0501L6	6.6	0.2284	0.0016	0.0331	0.0001	0.43	0.0507	0.0004
05MM0501L7	4.9	0.2313	0.0033	0.0332	0.0002	0.36	0.0506	0.0007
05MM0501L8	-6.4	0.2245	0.0032	0.0326	0.0002	0.37	0.0500	0.0007
05MM0501L9	0.2	0.2174	0.0048	0.0320	0.0003	0.35	0.0502	0.0011
05MM0501L10	-6.3	0.2262	0.0030	0.0328	0.0002	0.35	0.0500	0.0006
05MM0501L11	-8.1	0.2270	0.0022	0.0328	0.0001	0.38	0.0499	0.0005
05MM0501L12	0.9	0.2261	0.0029	0.0327	0.0002	0.36	0.0503	0.0006
05MM0501L13	0.6	0.2258	0.0046	0.0328	0.0002	0.33	0.0503	0.0010
05MM0501L14	7.0	0.2218	0.0061	0.0318	0.0003	0.34	0.0505	0.0014
05MM0501L15	-3.2	0.2283	0.0032	0.0321	0.0002	0.36	0.0501	0.0007
05MM0501L16	25.2	0.2310	0.0041	0.0322	0.0002	0.35	0.0517	0.0009
05MM0501L17	5.0	0.2200	0.0047	0.0326	0.0003	0.36	0.0505	0.0010
05MM0501L18	0.7	0.2236	0.0037	0.0322	0.0002	0.35	0.0502	0.0008
05MM0501L19	-0.6	0.2154	0.0056	0.0315	0.0003	0.34	0.0501	0.0013
05MM0501L20	5.4	0.2237	0.0030	0.0319	0.0002	0.37	0.0504	0.0007
05MM0501L21	-55.7	0.2152	0.0037	0.0323	0.0002	0.34	0.0487	0.0008
05MM0501L22	3.6	0.2214	0.0042	0.0317	0.0002	0.33	0.0503	0.0009
05MM0501L23	-0.6	0.2297	0.0040	0.0328	0.0002	0.35	0.0503	0.0009
05MM0501L24	0.9	0.2360	0.0066	0.0340	0.0003	0.35	0.0505	0.0014
05MM0501L25	1.6	0.2323	0.0042	0.0332	0.0002	0.33	0.0504	0.0009
05MM0501L26	5.1	0.2303	0.0070	0.0328	0.0003	0.34	0.0505	0.0015
05MM0501L27	29.6	0.2314	0.0046	0.0321	0.0002	0.33	0.0521	0.0010
05MM0501L28	7.5	0.2261	0.0034	0.0321	0.0002	0.36	0.0506	0.0007
05MM0501L29	5.9	0.2216	0.0040	0.0316	0.0002	0.34	0.0504	0.0009
05MM0501L30	-5.1	0.2246	0.0025	0.0319	0.0001	0.37	0.0499	0.0005
05MM0501L31	7.4	0.2232	0.0037	0.0323	0.0002	0.35	0.0506	0.0008
05MM0501L32	2.1	0.2263	0.0041	0.0331	0.0002	0.35	0.0504	0.0009
05MM0501L33	15.7	0.2349	0.0035	0.0332	0.0002	0.37	0.0512	0.0007
05MM0501L34	3.2	0.2289	0.0039	0.0327	0.0002	0.36	0.0504	0.0008
05MM0501L35	5.1	0.2365	0.0040	0.0335	0.0002	0.35	0.0506	0.0008
05MM0501L36	6.7	0.2367	0.0041	0.0333	0.0002	0.36	0.0507	0.0009
05MM0501L37	8.5	0.2314	0.0041	0.0333	0.0002	0.36	0.0508	0.0009
05MM0501L38	8.1	0.2244	0.0033	0.0324	0.0002	0.36	0.0506	0.0007
05MM0501L39	-8.5	0.2368	0.0023	0.0344	0.0001	0.40	0.0501	0.0005
05MM0501L40	-23.7	0.2292	0.0039	0.0335	0.0002	0.34	0.0495	0.0008
05MM0501L41	4.0	0.2293	0.0033	0.0332	0.0002	0.36	0.0505	0.0007
05MM0501L42	-7.5	0.2285	0.0031	0.0333	0.0002	0.36	0.0500	0.0007
05MM0501L43	0.6	0.2349	0.0023	0.0341	0.0001	0.39	0.0505	0.0005
05MM0501L44	7.0	0.2440	0.0021	0.0351	0.0001	0.40	0.0510	0.0004
05MM0501L45	7.0	0.2346	0.0041	0.0335	0.0002	0.36	0.0507	0.0009
05MM0501L46	6.6	0.2298	0.0034	0.0325	0.0002	0.36	0.0506	0.0007
05MM0501L47	3.5	0.2328	0.0035	0.0330	0.0002	0.35	0.0505	0.0007
05MM0501L48	4.4	0.2307	0.0037	0.0333	0.0002	0.35	0.0506	0.0008
05MM0501L49	-5.5	0.2311	0.0035	0.0333	0.0002	0.35	0.0501	0.0007
05MM0501L50	1.5	0.2358	0.0138	0.0361	0.0008	0.36	0.0508	0.0029
05MM0501L51	41.5	0.2507	0.0047	0.0332	0.0002	0.35	0.0538	0.0010
05MM0501L52	4.6	0.2323	0.0055	0.0342	0.0003	0.36	0.0507	0.0012
05MM0501L53	-6.4	0.2308	0.0024	0.0338	0.0001	0.37	0.0501	0.0005
05MM0501L54	5.3	0.3350	0.0040	0.0460	0.0002	0.36	0.0525	0.0006
05MM0501L55	10.8	0.2347	0.0047	0.0333	0.0002	0.35	0.0509	0.0010
05MM0501L56	12.0	0.2271	0.0063	0.0324	0.0003	0.33	0.0508	0.0014
05MM0501L57	-0.5	0.2312	0.0039	0.0325	0.0002	0.36	0.0502	0.0008
05MM0501L58	45.6	0.2544	0.0048	0.0339	0.0002	0.36	0.0546	0.0010
05MM0501L59	35.4	0.2483	0.0053	0.0336	0.0003	0.35	0.0530	0.0011
05MM0501L60	7.5	0.2375	0.0031	0.0333	0.0002	0.37	0.0507	0.0006

Appendix B.2: Mineral Chemistry (Chapter 5)

Sample ID	Location	Mass % SiO_2	TiO_2	Al_2O_3	Cr_2O_3	FeO	MnO	MgO	CaO	Na_2O	K_2O	Total
FELDSPAR												
1 05tb2-3 1	PBR	65.6	0.0	22.4	0.0	0.1	0.0	0.0	2.7	9.9	0.0	100.6
1 05tb2-3 2	PBR	66.0	0.0	21.9	0.0	0.1	0.0	0.0	2.1	10.4	0.0	100.5
2 05tb2-3 3	PBR	50.1	0.0	31.5	0.0	0.7	0.0	0.3	15.0	3.0	0.0	100.6
2 05tb2-3 4	PBR	50.4	0.0	31.3	0.0	0.7	0.0	0.3	14.9	3.2	0.0	100.8
3 05tb2-3 5	PBR	68.9	0.0	20.7	0.0	0.0	0.0	0.0	0.7	10.2	0.0	100.5
4 05tb2-3 5	PBR	49.6	0.0	31.5	0.0	0.6	0.0	0.3	15.3	3.0	0.0	100.3
5 05tb2-3 7	PBR	68.3	0.0	20.2	0.0	0.0	0.0	0.0	0.5	11.0	0.0	100.1
1 04tb8-2 1	PBR	49.6	0.0	29.4	0.0	0.9	0.0	0.2	13.5	3.7	0.1	97.3
2 04tb8-2 3	PBR	48.4	0.0	29.9	0.0	0.6	0.0	0.2	14.0	3.3	0.1	96.4
3 04tb8-2 5	PBR	50.4	0.0	31.1	0.0	0.7	0.0	0.2	14.5	3.2	0.1	100.3
1 04tb16-6 1	Foremore	67.8	0.0	20.5	0.0	0.1	0.0	0.0	0.8	9.4	0.1	98.7
5 04tb16-6 8	Foremore	65.4	0.0	20.9	0.0	0.1	0.0	0.0	1.7	9.3	0.1	97.4
1 04jn6-5D 5	6 Pack	66.2	0.0	21.0	0.0	0.0	0.0	0.0	1.4	10.7	0.0	99.3
1 04jn6-7D 16	6 Pack	67.6	0.0	20.4	0.0	0.1	0.0	0.0	0.5	11.1	0.2	99.9
2 04jn6-7d 17	6 Pack	63.1	0.1	18.7	0.0	0.3	0.0	0.0	0.0	0.2	15.5	98.0
2 04jn6-7d 18	6 Pack	69.1	0.0	20.4	0.0	0.2	0.0	0.0	0.4	10.8	0.1	101.0
2 04jn6-7d 19	6 Pack	67.7	0.0	20.6	0.0	0.1	0.0	0.0	1.0	10.4	0.0	99.8
5 ms030401 31	Table Mtn	68.4	0.0	20.7	0.0	0.1	0.0	0.0	0.9	10.7	0.0	100.9
3 04tb24-2 45	Table Mtn	69.4	0.0	20.7	0.0	0.3	0.0	0.0	0.9	10.7	0.2	102.2

Sample ID	Si	Ti	Al	Cr	Fe	Mn	Mg	Ca	Na	K	Total
FELDSPAR	Cation Total O=8										
1 05tb2-3 1	2.876	0.000	1.156	0.000	0.003	0.000	0.000	0.125	0.837	0.002	5.00
1 05tb2-3 2	2.888	0.000	1.128	0.000	0.002	0.000	0.000	0.099	0.881	0.002	5.00
2 05tb2-3 3	2.276	0.000	1.687	0.000	0.026	0.000	0.019	0.729	0.263	0.001	5.00
2 05tb2-3 4	2.282	0.000	1.671	0.000	0.026	0.000	0.020	0.724	0.277	0.001	5.00
3 05tb2-3 5	3.025	0.000	1.071	0.000	0.001	0.000	0.000	0.032	0.870	0.001	5.00
4 05tb2-3 5	2.257	0.000	1.690	0.000	0.023	0.000	0.019	0.745	0.265	0.000	5.00
5 05tb2-3 7	2.995	0.000	1.042	0.000	0.002	0.000	0.000	0.023	0.937	0.001	5.00
1 04tb8-2 1	2.316	0.001	1.618	0.000	0.036	0.000	0.014	0.674	0.335	0.006	5.00
2 04tb8-2 3	2.316	0.001	1.662	0.000	0.024	0.000	0.012	0.707	0.301	0.006	5.03
3 04tb8-2 5	2.292	0.002	1.666	0.000	0.027	0.000	0.013	0.707	0.286	0.007	5.00
1 04tb16-6 1	3.048	0.000	1.087	0.000	0.002	0.000	0.000	0.040	0.820	0.003	5.00
5 04tb16-6 8	2.974	0.000	1.118	0.000	0.003	0.000	0.000	0.082	0.819	0.004	5.00
1 04jn6-5D 5	2.927	0.000	1.091	0.000	0.001	0.000	0.000	0.066	0.913	0.001	5.00
1 04jn6-7D 16	2.927	0.000	1.055	0.000	0.002	0.000	0.000	0.023	0.946	0.009	4.96
2 04jn6-7d 17	2.981	0.005	1.042	0.000	0.012	0.000	0.000	0.001	0.023	0.937	5.00
2 04jn6-7d 18	3.011	0.000	1.049	0.000	0.006	0.000	0.000	0.020	0.908	0.006	5.00
2 04jn6-7d 19	2.986	0.000	1.069	0.000	0.002	0.000	0.000	0.048	0.893	0.002	5.00
5 ms030401 31	2.978	0.000	1.065	0.000	0.004	0.000	0.000	0.044	0.906	0.002	5.00
3 04tb24-2 45	2.993	0.001	1.050	0.000	0.011	0.000	0.000	0.043	0.893	0.010	5.00

Sample ID	Location	Mass % SiO_2	TiO_2	Al_2O_3	Cr_2O_3	FeO	MnO	MgO	CaO	Na_2O	K_2O	Total
PYROXENE												
5 05tb2-3 6	PBR	46.4	1.8	6.4	0.3	12.0	0.3	11.4	20.9	0.3	0.0	99.8
4 05tb2-3 8	PBR	46.7	1.5	5.4	0.2	12.1	0.3	11.4	21.5	0.3	0.0	99.3
1 04tb8-2 2	PBR	42.4	2.5	4.8	0.1	17.6	0.4	8.5	20.3	0.4	0.0	97.1
2 04tb8-2 4	PBR	47.1	1.3	3.0	0.1	16.8	0.5	9.8	20.1	0.3	0.0	98.9
2 04tb16-6 3	Foremore	49.9	0.5	3.2	0.3	6.0	0.2	16.8	21.8	0.2	0.0	98.8
4 04tb16-6 5	Foremore	50.8	0.6	1.7	0.0	12.2	0.4	15.3	18.5	0.2	0.0	99.5
4 04tb16-6 6	Foremore	51.8	0.3	1.9	0.2	5.6	0.2	17.9	21.2	0.2	0.0	99.3
4 04tb16-6 7	Foremore	49.9	0.4	3.5	0.8	5.2	0.2	16.6	22.3	0.3	0.0	99.2
6 04tb16-6 9	Foremore	49.8	0.5	2.9	0.1	7.3	0.2	17.1	20.3	0.2	0.0	98.3
6 04tb16-6 10	Foremore	47.8	0.8	3.1	0.0	11.9	0.3	14.4	19.3	0.3	0.0	97.9
3 04jn6-5D 6	6 Pack	52.3	0.3	1.7	0.2	6.5	0.2	17.0	21.0	0.2	0.0	99.5
3 04jn6-5D 7	6 Pack	50.7	0.7	1.7	0.1	11.8	0.4	14.7	18.9	0.3	0.0	99.2
3 04jn6-5D 9	6 Pack	48.9	0.3	1.6	0.2	6.9	0.2	16.9	20.0	0.4	0.0	95.4
3 04jn6-5D 10	6 Pack	50.8	0.4	2.4	0.2	7.0	0.2	16.5	20.8	0.3	0.0	98.7
3 04jn6-5D 11	6 Pack	50.8	0.4	2.1	0.1	7.2	0.2	16.5	21.0	0.2	0.0	98.6
3 04jn6-5D 12	6 Pack	49.5	0.7	1.8	0.0	11.4	0.3	14.4	19.4	0.3	0.0	97.9
5 04jn6-5D 13	6 Pack	51.6	0.4	2.1	0.1	7.3	0.2	16.7	20.8	0.2	0.0	99.4
5 04jn6-5D 14	6 Pack	50.9	0.5	1.2	0.0	14.1	0.5	13.6	18.3	0.3	0.0	99.5
1 ms030401 21	Table Mtn	49.5	0.3	1.4	0.2	8.2	0.3	17.8	18.7	0.2	0.0	96.6
2 ms030401 22	Table Mtn	51.1	0.5	2.3	0.2	7.7	0.2	16.4	21.1	0.2	0.0	99.9
2 ms030401 23	Table Mtn	50.9	0.6	2.5	0.1	8.6	0.2	16.6	19.8	0.2	0.0	99.5
2 ms030401 24	Table Mtn	50.2	0.8	3.1	0.0	9.7	0.2	15.6	19.6	0.2	0.0	99.6
3 ms030401 25	Table Mtn	51.5	0.4	1.7	0.2	7.9	0.2	17.2	19.9	0.2	0.0	99.1
4 ms030401 26	Table Mtn	51.4	0.6	2.4	0.3	8.0	0.2	16.4	20.6	0.2	0.0	100.1
4 ms030401 27	Table Mtn	50.7	0.7	2.8	0.2	8.2	0.2	16.1	20.5	0.2	0.0	99.7
4 ms030401 28	Table Mtn	50.5	0.8	2.9	0.2	8.9	0.2	16.1	19.6	0.2	0.0	99.4
4 ms030401 29	Table Mtn	49.8	1.0	3.3	0.1	10.1	0.3	15.7	19.4	0.3	0.0	99.9
4 ms030401 30	Table Mtn	48.9	1.0	2.7	0.1	14.1	0.3	13.1	18.8	0.3	0.0	99.3
2 04tb24-2 35	Table Mtn	51.8	0.5	2.0	0.1	8.2	0.2	17.2	19.5	0.2	0.0	99.7
2 04tb24-2 36	Table Mtn	51.0	0.7	2.4	0.0	11.8	0.3	15.5	18.2	0.3	0.0	100.1
2 04tb24-2 37	Table Mtn	50.9	0.7	2.0	0.0	12.6	0.4	14.7	18.5	0.3	0.0	100.1
3 04tb24-2 38	Table Mtn	51.4	0.4	2.1	0.1	7.5	0.2	17.1	20.1	0.3	0.0	99.2
3 04tb24-2 39	Table Mtn	50.4	0.7	1.8	0.0	13.7	0.4	15.3	16.8	0.3	0.0	99.4
3 04tb24-2 40	Table Mtn	47.2	1.7	5.9	0.2	8.7	0.2	12.9	22.5	0.4	0.0	99.7
3 04tb24-2 41	Table Mtn	51.1	0.8	2.6	0.1	8.6	0.2	14.8	22.1	0.4	0.0	100.6
3 04tb24-2 42	Table Mtn	48.5	1.5	5.0	0.2	9.0	0.2	13.2	22.5	0.4	0.0	100.4
3 04tb24-2 43	Table Mtn	47.9	1.8	5.1	0.0	10.8	0.2	12.6	21.8	0.5	0.0	100.8
3 04tb24-2 44	Table Mtn	50.8	0.9	2.3	0.0	9.7	0.3	14.3	21.7	0.4	0.0	100.3
3 04tb24-2 46	Table Mtn	49.0	1.5	4.3	0.0	10.6	0.2	12.6	22.4	0.5	0.0	101.2

Sample ID	Si	Ti	Al	Cr	Fe	Mn	Mg	Ca	Na	K	Total
PYROXENE	Cation Total O=6										
5 05tb2-3 6	1.755	0.050	0.286	0.008	0.380	0.008	0.645	0.847	0.021	0.0	4.00
4 05tb2-3 8	1.775	0.044	0.242	0.005	0.383	0.009	0.647	0.873	0.022	0.0	4.00
1 04tb8-2 2	1.691	0.075	0.227	0.002	0.586	0.015	0.507	0.868	0.028	0.0	4.00
2 04tb8-2 4	1.832	0.038	0.137	0.002	0.547	0.015	0.569	0.837	0.024	0.0	4.00
2 04tb16-6 3	1.847	0.013	0.138	0.007	0.185	0.005	0.926	0.863	0.015	0.0	4.00
4 04tb16-6 5	1.904	0.016	0.075	0.000	0.381	0.011	0.853	0.742	0.016	0.0	4.00
4 04tb16-6 6	1.898	0.009	0.084	0.005	0.170	0.005	0.981	0.834	0.013	0.0	4.00
4 04tb16-6 7	1.838	0.011	0.154	0.023	0.160	0.005	0.912	0.879	0.019	0.0	4.00
6 04tb16-6 9	1.852	0.013	0.129	0.002	0.226	0.006	0.947	0.809	0.016	0.0	4.00
6 04tb16-6 10	1.820	0.024	0.140	0.000	0.380	0.011	0.817	0.788	0.021	0.0	4.00
3 04jn6-5D 6	1.924	0.008	0.074	0.007	0.200	0.007	0.934	0.830	0.017	0.0	4.00
3 04jn6-5D 7	1.909	0.019	0.077	0.002	0.373	0.012	0.823	0.762	0.023	0.0	4.00
3 04jn6-5D 9	1.873	0.010	0.071	0.005	0.221	0.007	0.965	0.822	0.027	0.0	4.00
3 04jn6-5D 10	1.889	0.012	0.107	0.007	0.218	0.007	0.912	0.830	0.018	0.0	4.00
3 04jn6-5D 11	1.892	0.012	0.092	0.004	0.224	0.006	0.915	0.836	0.018	0.0	4.00
3 04jn6-5D 12	1.889	0.020	0.079	0.001	0.363	0.011	0.821	0.793	0.023	0.0	4.00
5 04jn6-5D 13	1.905	0.012	0.091	0.004	0.224	0.007	0.919	0.821	0.018	0.0	4.00
5 04jn6-5D 14	1.933	0.014	0.053	0.001	0.448	0.016	0.768	0.745	0.022	0.0	4.00
1 ms030401 21	1.875	0.010	0.065	0.005	0.259	0.009	1.005	0.759	0.015	0.0	4.00
2 ms030401 22	1.881	0.015	0.101	0.006	0.238	0.006	0.902	0.834	0.017	0.0	4.00
2 ms030401 23	1.882	0.016	0.107	0.003	0.266	0.007	0.914	0.786	0.017	0.0	4.00
2 ms030401 24	1.867	0.023	0.138	0.001	0.302	0.008	0.866	0.779	0.017	0.0	4.00
3 ms030401 25	1.907	0.011	0.073	0.005	0.245	0.007	0.949	0.788	0.015	0.0	4.00
4 ms030401 26	1.890	0.015	0.105	0.008	0.245	0.007	0.901	0.811	0.017	0.0	4.00
4 ms030401 27	1.876	0.019	0.120	0.007	0.255	0.006	0.888	0.811	0.018	0.0	4.00
4 ms030401 28	1.876	0.022	0.127	0.005	0.276	0.007	0.890	0.781	0.017	0.0	4.00
4 ms030401 29	1.847	0.027	0.145	0.002	0.313	0.009	0.867	0.772	0.018	0.0	4.00
4 ms030401 30	1.860	0.029	0.119	0.002	0.447	0.010	0.743	0.765	0.024	0.0	4.00
2 04tb24-2 35	1.907	0.013	0.087	0.002	0.252	0.006	0.946	0.771	0.016	0.0	4.00
2 04tb24-2 36	1.896	0.020	0.104	0.001	0.367	0.010	0.857	0.725	0.021	0.0	4.00
2 04tb24-2 37	1.904	0.020	0.088	0.000	0.395	0.012	0.820	0.740	0.022	0.0	4.00
3 04tb24-2 38	1.897	0.011	0.092	0.003	0.231	0.006	0.943	0.797	0.018	0.0	4.00
3 04tb24-2 39	1.898	0.018	0.082	0.000	0.430	0.013	0.861	0.677	0.019	0.0	4.00
3 04tb24-2 40	1.762	0.047	0.260	0.007	0.272	0.006	0.717	0.899	0.031	0.0	4.00
3 04tb24-2 41	1.882	0.022	0.112	0.003	0.264	0.006	0.810	0.874	0.028	0.0	4.00
3 04tb24-2 42	1.798	0.040	0.218	0.005	0.280	0.005	0.731	0.893	0.029	0.0	4.00
3 04tb24-2 43	1.778	0.052	0.222	0.001	0.334	0.008	0.697	0.869	0.039	0.0	4.00
3 04tb24-2 44	1.884	0.025	0.102	0.001	0.300	0.009	0.790	0.864	0.026	0.0	4.00
3 04tb24-2 46	1.811	0.042	0.188	0.001	0.328	0.007	0.696	0.890	0.037	0.0	4.00

Appendix B.3: Geochemical Data (Chapter 5)

Sample	Easting (NAD 83 Zone 9)	Northing (NAD83 Zone9	Location	Group	SiO_2 wt. %	TiO_2 wt. %	Al_2O_3 wt. %	Fe_2O_{3total} wt. %	Fe_2O_3 wt. %	FeO wt. %	MnO wt. %
04TB11-4	402193	6302414	PBR	1	45.1	1.88	15.4	13.1	3.32	8.8	0.18
04TB19-6	401190	6307250	Foremore	1	47.6	0.78	16.0	8.4	1.73	6.0	0.18
04JN12-2D	400200	6316800	Foremore	1	45.3	0.89	17.5	8.7	0.81	7.1	0.13
04JN8-10	431990	6388080	Klastline	1	44.0	0.75	16.8	9.7	4.14	5.0	0.17
04JN8-9B	432060	6387900	Klastline	1	44.4	0.96	16.9	10.2	4.31	5.3	0.17
A04-04-1	401992	6296845	PBR	1	47.7	1.64	14.8	12.1	2.43	8.7	0.20
A04-03-6	401121	6295255	PBR	1	44.3	2.19	14.8	14.8	3.35	10.3	0.19
A04-03-7	401192	6294717	PBR	1	47.2	2.20	14.9	13.4	3.51	8.9	0.19
04TB10-2	403181	6301058	PBR	1	46.1	1.31	15.6	11.3	1.19	9.1	0.20
04TB10-3	403107	6300872	PBR	1	46.9	1.69	15.7	14.5	1.50	11.7	0.16
04TB10-5	403077	6300197	PBR	1	45.7	1.68	15.6	13.2	2.53	9.6	0.20
04TB2-3	401969	6298303	PBR	1	46.3	0.75	17.8	9.5		9.6	0.17
04TB3-3	402978	6299003	PBR	1	47.9	1.27	14.3	13.3	1.30	10.8	0.22
04TB7-3	403159	6301393	PBR	1	47.7	1.61	14.8	12.8	0.80	10.8	0.20
04TB7-4	402856	6301812	PBR	1	46.6	1.74	14.2	13.2	1.53	10.5	0.17
04TB7-6	403220	6302640	PBR	1	46.7	1.84	15.2	12.9	3.34	8.6	0.18
04TB8-2	404198	6302009	PBR	1	45.8	1.96	15.2	13.3	1.96	10.2	0.20
04TB9-2	402440	6300011	PBR	1	50.3	1.44	15.9	10.0		10.8	0.15
04TB2-4	402273	6299055	PBR	1	44.7	1.71	16.1	14.0	1.66	11.1	0.19
04TB24-7A	415314	6352203	Table Mtn.	2	48.5	1.73	13.7	16.5	4.05	11.2	0.23
04TB24-2	416870	6352050	Table Mtn.	2	50.6	1.24	13.8	12.4	3.95	7.6	0.18
04TB24-3	417140	6352270	Table Mtn.	2	50.6	0.95	16.1	9.5	2.72	6.1	0.13
04JN6-6	405382	6303669	6 Pack	2	54.6	0.85	15.1	8.7	2.03	6.0	0.16
04JN6-7D	405693	6303770	6 Pack	2	55.8	0.57	15.6	7.6	1.71	5.3	0.14
04JN6-5D	405382	6303669	6 Pack	2	50.4	1.01	14.3	11.2	2.31	8.0	0.20
04JN1-8A	400954	6311052	Foremore	2	49.0	0.94	14.9	11.5	1.83	8.7	0.29
04TB16-7	400831	6307699	Foremore	2	50.7	1.51	13.3	13.8	2.69	10.0	0.25
04TB19-7A	401249	6307334	Foremore	2	49.5	1.18	14.0	12.0	2.22	8.8	0.24
04TB26-10	401376	6319709	Foremore	2	55.1	0.61	16.2	8.0	0.44	6.8	0.12
04TB16-6	400875	6307870	Foremore	2	49.1	0.99	14.9	10.1	2.32	7.0	0.17
04TB22-14	427281	6385807	Klastline	2	48.9	0.93	15.1	11.6	3.38	7.4	0.14
04TB21-12	426401	6384867	Klastline	2	49.2	0.84	16.0	9.9	2.23	6.9	0.17
04TB2-5	401957	6298485	PBR	2	49.0	1.11	14.0	12.1	0.88	10.1	0.20
04TB4-2	401377	6298321	PBR	2	47.9	1.36	14.1	11.5	1.28	9.2	0.20
04TB5-1	402058	6297875	PBR	2	50.8	1.71	13.0	13.4	1.51	10.7	0.22
Average IRF Rhyolite					80.1	0.14	10.4	1.9			0.03
MS03-23-05	420457	6365319	Table Mtn.	andesite	59.0	1.80	15.5	11.3			0.10

Sample	MgO wt. %	CaO wt. %	Na_2O wt. %	K_2O wt. %	P_2O_5 wt. %	TOTAL wt. %	Cu ppm	Zn ppm	Pb ppm	Co ppm	Ni ppm	V ppm
04TB11-4	6.39	11.14	2.7	0.21	0.21	100.0	44	122	0	45	71	340
04TB19-6	5.64	12.32	3.7	0.84	0.10	100.4	63	89	0	43	118	218
04JN12-2D	7.83	10.39	1.9	0.90	0.09	100.3	36	88	0	42	78	199
04JN8-10	9.39	11.66	1.6	0.27	0.08	100.0	65	83	0	47	212	179
04JN8-9B	7.72	11.74	2.4	0.42	0.11	99.7	75	90	0	45	123	234
A04-04-1	5.78	10.78	2.8	0.68	0.19	100.7	29	120	0	48	63	331
A04-03-6	6.59	10.66	2.4	0.80	0.23	100.2	53	137	0	58	117	372
A04-03-7	5.84	11.16	2.2	0.13	0.24	99.9	50	133	0	59	112	370
04TB10-2	9.03	8.80	2.4	1.85	0.13	100.3	41	102	0	50	128	80
04TB10-3	6.30	8.13	3.8	0.14	0.18	100.3	50	125	0	51	91	319
04TB10-5	6.37	10.93	3.1	0.80	0.18	100.2	39	131	0	55	75	356
04TB2-3	5.66	12.13	2.7	1.07	0.08	100.1	55	91	0	39	55	234
04TB3-3	6.61	9.06	3.4	1.09	0.12	100.1	65	115	0	54	66	333
04TB7-3	6.32	11.08	2.6	0.19	0.19	100.2	39	120	0	51	87	332
04TB7-4	7.25	9.02	3.6	0.32	0.22	99.6	47	111	0	49	72	331
04TB7-6	7.05	9.90	2.3	0.44	0.20	100.0	47	133	0	55	97	347
04TB8-2	6.04	11.64	2.3	0.30	0.28	100.0	38	144	0	48	50	392
04TB9-2	6.29	10.02	2.3	0.49	0.16	100.1	48	114	1	60	131	85
04TB2-4	7.11	10.88	2.0	0.43	0.19	100.2	37	127	0	54	71	343
04TB24-7A	4.37	6.62	4.3	1.55	0.46	100.5	19	130	3	47	-10	499
04TB24-2	6.43	7.99	4.2	0.97	0.19	100.2	23	99	0	44	14	323
04TB24-3	6.48	7.78	3.3	1.37	0.34	100.3	73	98	2	36	68	216
04JN6-6	5.27	6.93	5.5	1.07	0.18	100.6	44	81	2	30	18	194
04JN6-7D	4.32	4.07	4.3	2.75	0.29	100.2	89	74	4	24	17	224
04JN6-5D	7.49	8.46	4.1	0.56	0.13	100.6	49	103	1	44	40	276
04JN1-8A	3.19	7.23	4.5	1.54	0.34	100.5	143	295	64	33	27	252
04TB16-7	6.93	5.69	3.3	1.69	0.23	100.2	34	108	2	43	18	353
04TB19-7A	5.01	9.01	3.8	0.84	0.22	100.3	104	184	29	39	27	299
04TB26-10	2.73	5.12	8.0	0.09	0.27	100.2	0	67	0	21	0	125
04TB16-6	7.60	10.28	3.6	0.42	0.16	100.2	62	93	1	43	59	273
04TB22-14	7.37	8.51	4.3	0.38	0.12	100.4	51	74	0	47	58	276
04TB21-12	7.71	6.56	3.6	2.24	0.18	100.2	55	88	0	41	80	233
04TB2-5	7.03	7.81	3.1	2.75	0.12	100.3	62	97	0	49	50	300
04TB4-2	6.24	11.66	3.1	0.73	0.14	100.0	50	110	0	45	56	328
04TB5-1	4.73	6.96	2.9	3.98	0.25	100.6	37	193	0	33	10	396
Average IRF Rhyolite	0.99	0.16	1.6	3.53	0.05	99.7	112	58	27	23	15	10
MS03-23-05	3.30	2.34	5.9	0.02	0.32	99.6						132

Sample	Sc	Rb	Sr	Ga	Nb	Y	Zr	Ag	Ba	Cr	Cs	Hf
	ppm	ppm	ppm	ppm	ppm	ppm	ppm	ppm	ppm	ppm	ppm	ppm
04TB11-4	42	4	257	20	4.6	41	100	0.0	130	243	1.40	2.9
04TB19-6	33	19	427	13	1.7	21	40	0.0	480	339	0.81	1.1
04JN12-2D	30	16	280	14	1.2	19	37	0.0	463	172	1.00	1.1
04JN8-10	35	6	273	12	1.2	19	43	0.0	345	272	0.96	1.2
04JN8-9B	39	10	867	15	1.6	23	57	0.0	284	214	3.00	1.5
A04-04-1	40	18	85	17	3.7	37	94	0.0	231	84	0.56	2.3
A04-03-6	43	4	238	20	4.0	50	116	0.0	243	275	0.96	3.5
A04-03-7	43	2	157	19	4.3	50	114	0.0	139	276	0.84	3.6
04TB10-2	36	43	288	17	3.0	30	67	0.0	1210	547	2.80	1.9
04TB10-3	41	2	171	18	4.0	39	92	0.0	127	304	2.00	2.5
04TB10-5	43	5	288	19	3.8	38	92	0.0	115	303	0.56	2.6
04TB2-3	35	25	87	15	1.3	20	38	0.0	236	270	0.88	1.1
04TB3-3	44	31	58	17	2.1	32	63	0.0	375	151	1.00	1.8
04TB7-3	40	3	219	19	2.7	39	84	0.0	212	238	1.00	2.2
04TB7-4	41	4	74	18	4.6	40	91	0.0	138	223	0.92	2.4
04TB7-6	43	9	223	19	4.4	42	102	0.0	255	279	0.58	2.7
04TB8-2	42	7	221	21	6.1	44	106	0.0	208	207	0.98	2.8
04TB9-2	35	8	183	18	3.5	34	81	0.0	190	335	1.30	2.1
04TB2-4	43	10	178	20	3.8	40	94	0.0	119	297	1.20	2.4
04TB24-7A	37	31	339	19	6.3	36	93	0.0	1340	16	0.39	2.3
04TB24-2	42	19	460	16	4.3	37	108	0.0	48	57	0.37	2.5
04TB24-3	31	31	507	16	7.6	31	141	0.0	884	158	0.41	2.8
04JN6-6	30	18	184	19	6.9	27	90	0.0	344	34	0.56	2.4
04JN6-7D	28	48	490	15	6.9	15	48	0.0	2250	76	1.30	1.4
04JN6-5D	45	10	292	15	2.3	27	53	0.0	671	166	0.41	1.5
04JN1-8A	20	24	449	17	2.9	24	67	0.0	556	50	2.30	2.1
04TB16-7	38	29	165	19	5.6	42	110	0.0	871	30	1.60	3.2
04TB19-7A	33	15	315	16	2.7	30	69	0.0	354	66	1.10	1.9
04TB26-10	23	1	293	15	5.7	49	163	0.0	276	11	0.09	4.0
04TB16-6	40	7	331	14	3.6	25	53	0.0	82	256	1.10	1.5
04TB22-14	42	5	280	15	2.9	25	56	0.0	234	166	0.04	1.6
04TB21-12	34	35	448	12	3.1	23	54	0.0	699	270	0.38	1.4
04TB2-5	44	43	227	13	2.5	30	61	0.0	1060	149	0.52	1.6
04TB4-2	41	11	125	18	3.1	33	67	0.0	369	193	0.38	2.0
04TB5-1	39	68	35	20	5.7	44	99	0.1	783	19	0.54	2.7
Average IRF Rhyolite	1	95	20	20	24.1	48	240	12.3	433	13	1.56	5.1
MS03-23-05					15.0	39	190		200			4.4

Sample	Mo	Sb	U	La	Ce	Pr	Nd	Sm	Eu	Gd	Tb	Dy
	ppm	ppm	ppm	ppm	ppm	ppm	ppm	ppm	ppm	ppm	ppm	ppm
04TB11-4	0.8	0.3	0.28	6.4	17	2.5	13.0	4.4	1.60	6.2	1.10	7.3
04TB19-6	0.9	0.5	0.21	3.0	8	1.1	5.9	1.9	0.73	2.8	0.48	3.2
04JN12-2D	0.4	0.4	0.06	2.4	7	1.2	6.0	2.1	0.84	3.0	0.49	3.1
04JN8-10	0.3	0.2	0.06	3.0	8	1.3	6.1	2.1	0.81	2.8	0.47	3.0
04JN8-9B	0.3	7.6	0.09	4.2	11	1.7	8.4	2.7	1.00	3.5	0.59	3.6
A04-04-1	0.5	1.9	0.24	5.5	14	2.1	11.0	3.9	1.30	5.4	0.94	5.9
A04-03-6	1.2	0.0	0.22	5.9	16	2.6	14.0	5.1	1.70	7.2	1.20	8.1
A04-03-7	0.9	0.2	0.23	6.0	17	2.7	15.0	5.2	1.70	7.4	1.30	7.9
04TB10-2	0.3	0.0	0.11	4.2	11	1.7	8.8	3.1	1.10	4.5	0.77	4.8
04TB10-3	0.7	0.4	0.15	5.2	14	2.2	12.0	3.9	1.30	5.5	0.98	6.2
04TB10-5	0.6	0.0	0.22	5.6	14	2.2	11.0	4.1	1.40	5.7	1.00	6.3
04TB2-3	0.4	0.3	0.29	2.3	6	0.9	4.8	1.7	0.68	2.6	0.47	3.1
04TB3-3	-0.2	1.6	0.12	3.5	9	1.5	8.0	3.0	1.10	4.3	0.80	5.2
04TB7-3	0.9	0.6	0.22	4.3	12	2.0	10.0	3.8	1.50	5.3	0.91	6.1
04TB7-4	0.4	0.5	0.20	6.5	16	2.6	12.0	4.1	1.40	5.6	0.97	6.3
04TB7-6	0.6	0.6	0.21	6.3	16	2.5	12.0	4.5	1.50	6.2	1.10	6.9
04TB8-2	1.1	0.6	0.28	9.2	22	3.3	16.0	4.7	1.70	6.2	1.10	6.8
04TB9-2	0.6	0.3	0.13	4.6	12	2.0	9.8	3.5	1.30	4.8	0.84	5.4
04TB2-4	0.8	0.7	0.24	5.1	13	2.1	11.0	4.1	1.40	5.7	1.00	6.4
04TB24-7A	1.5	0.0	1.10	14.0	29	3.8	17.0	4.4	1.30	5.3	0.88	5.5
04TB24-2	1.1	0.0	0.54	7.5	18	2.6	12.0	3.6	1.20	5.0	0.85	5.5
04TB24-3	0.3	0.3	0.40	13.0	30	3.9	17.0	4.1	1.20	4.8	0.79	4.9
04JN6-6	1.0	0.4	1.20	11.0	22	2.8	13.0	3.1	1.10	3.9	0.67	4.5
04JN6-7D	0.9	3.1	0.79	7.1	14	1.8	7.9	2.0	0.69	2.4	0.40	2.6
04JN6-5D	0.5	0.0	0.31	4.3	11	1.6	8.0	2.6	0.93	3.6	0.67	4.6
04JN1-8A	0.6	0.6	1.00	9.9	24	3.4	16.0	4.1	1.20	4.4	0.69	4.2
04TB16-7	1.1	0.5	0.68	9.2	21	3.0	15.0	4.2	1.40	5.6	1.00	6.9
04TB19-7A	0.6	0.4	0.52	7.2	17	2.5	12.0	3.6	1.20	4.6	0.77	4.8
04TB26-10	0.0	0.0	0.72	9.0	21	3.2	15.0	4.9	1.30	6.5	1.20	7.8
04TB16-6	0.3	0.3	0.23	5.7	13	1.8	8.7	2.6	0.96	3.5	0.62	4.2
04TB22-14	0.4	0.6	0.37	6.1	14	1.9	8.6	2.5	0.86	3.4	0.61	3.9
04TB21-12	0.4	0.3	0.24	7.4	17	2.3	10.0	2.8	0.87	3.4	0.58	3.6
04TB2-5	0.3	1.5	0.62	3.9	10	1.5	7.7	2.7	0.93	4.0	0.70	4.6
04TB4-2	0.5	2.4	0.20	4.6	11	1.8	9.1	3.2	1.20	4.6	0.81	5.3
04TB5-1	0.5	0.5	0.96	6.7	17	2.6	13.0	4.2	1.40	5.7	1.00	6.9
Average IRF Rhyolite	2.8	31.0	6.66	26.8	55	5.9	22.8	5.0	0.60	6.0	1.09	7.4
MS03-23-05				18.4	37	5.1	22.5	5.5	1.33	6.6	1.10	7.0

Sample	Ho	Er	Tm	Yb	Lu	Ta	Th	St	Be	Bi	Cd	In
	ppm	ppm	ppm	ppm	ppm	ppm	ppm	ppm	ppm	ppm	ppm	ppm
04TB11-4	1.60	4.3	0.68	4.3	0.67	0.80	0.49	0.00	0.7	0.0	0.3	0.09
04TB19-6	0.69	2.1	0.30	2.1	0.33	0.11	0.24	0.04	0.0	0.0	0.0	0.00
04JN12-2D	0.66	1.8	0.80	1.8	0.27	0.09	0.15	0.00	0.0	0.0	0.0	0.06
04JN8-10	0.66	1.9	0.29	1.9	0.31	0.08	0.16	0.06	0.0	0.0	0.0	0.00
04JN8-9B	0.80	2.3	0.35	2.3	0.36	0.10	0.22	0.02	0.0	0.0	0.0	0.13
A04-04-1	1.30	3.8	0.57	3.8	0.60	0.24	0.48	0.12	0.0	0.0	0.0	0.07
A04-03-6	1.80	4.9	0.78	5.0	0.80	0.80	0.44	0.00	0.7	0.0	0.0	0.10
A04-03-7	1.80	5.0	0.75	5.1	0.80	0.27	0.45	0.00	0.7	0.0	0.3	0.10
04TB10-2	1.10	3.0	0.45	3.0	0.46	0.18	0.28	0.10	0.0	0.0	0.0	0.06
04TB10-3	1.30	3.8	0.57	3.7	0.60	0.24	0.42	0.00	1.4	0.0	0.4	0.06
04TB10-5	1.40	4.0	0.61	4.0	0.64	0.25	0.51	0.02	0.6	0.0	0.0	0.08
04TB2-3	0.70	2.0	0.31	2.0	0.33	0.10	0.19	0.04	0.0	0.0	0.0	0.00
04TB3-3	1.10	3.3	0.52	3.5	0.55	0.14	0.24	0.02	0.0	0.0	0.0	0.09
04TB7-3	1.30	3.6	0.55	3.8	0.57	0.17	0.30	0.15	0.6	0.0	0.0	0.08
04TB7-4	1.30	3.7	0.55	3.7	0.60	0.22	0.50	0.14	0.7	0.0	0.0	0.08
04TB7-6	1.50	4.2	0.62	4.3	0.67	0.24	0.47	0.00	0.6	0.0	0.2	0.10
04TB8-2	1.50	4.0	0.60	4.2	0.66	0.32	0.67	0.08	0.7	0.0	0.0	0.11
04TB9-2	1.10	3.2	0.47	3.3	0.50	0.22	0.37	0.34	0.5	0.0	0.0	0.11
04TB2-4	1.40	4.0	0.61	4.0	0.64	0.24	0.50	0.05	0.5	0.0	0.0	0.09
04TB24-7A	1.20	3.3	0.52	3.6	0.56	0.35	2.20	0.50	1.1	0.0	0.0	0.08
04TB24-2	1.20	3.6	0.54	3.7	0.58	0.25	1.30	0.11	0.7	0.0	0.0	0.08
04TB24-3	1.10	3.0	0.46	3.1	0.49	0.40	1.10	0.02	0.9	0.0	0.0	0.06
04JN6-6	0.99	2.7	0.44	2.9	0.44	0.38	2.30	0.09	1.0	0.0	0.0	0.06
04JN6-7D	0.53	1.5	0.23	1.5	0.24	0.40	1.40	0.15	0.7	0.0	0.0	0.00
04JN6-5D	0.99	2.7	0.43	2.8	0.41	0.15	0.59	0.08	0.0	0.0	0.7	0.07
04JN1-8A	0.87	2.3	0.36	2.3	0.34	0.19	1.50	0.13	0.8	0.0	0.9	0.06
04TB16-7	1.50	4.2	0.68	4.4	0.68	0.31	1.50	0.07	1.0	0.0	0.0	0.07
04TB19-7A	1.00	2.9	0.44	2.9	0.47	0.17	0.87	0.12	0.6	0.0	0.4	0.07
04TB26-10	1.80	5.0	0.79	5.6	0.90	0.40	1.90	0.00	0.5	0.0	0.0	0.05
04TB16-6	0.93	2.5	0.40	2.6	0.40	0.20	0.63	0.10	0.0	0.0	0.0	0.05
04TB22-14	0.87	2.5	0.39	2.6	0.43	0.17	0.85	0.00	0.0	0.0	0.0	0.05
04TB21-12	0.78	2.2	0.35	2.3	0.37	0.18	0.56	0.00	0.5	0.0	0.2	0.00
04TB2-5	1.00	3.0	0.46	3.1	0.48	0.16	0.47	0.08	0.0	0.0	0.0	0.08
04TB4-2	1.10	3.2	0.49	3.2	0.51	0.20	0.52	0.02	0.5	0.0	0.0	0.07
04TB5-1	1.50	4.1	0.65	4.3	0.69	0.33	1.40	0.10	0.8	0.0	0.3	0.11
Average IRF Rhyolite	1.64	5.2	0.82	5.3	0.77	1.46	8.23				1.1	0.09
MS03-23-05	1.50	4.4	0.65	4.4	0.61	0.70	3.23					

Sample	Sn	Tl	Te	LOI	H_2O_T	CO_{2T}
	ppm	ppm	ppm	wt. %	wt. %	wt. %
04TB11-4	0.9	0.05	0.0	3.8	3.5	1.0
04TB19-6	0.0	0.19	0.0	4.9	2.2	3.1
04JN12-2D	0.8	0.11	0.0	6.6	3.9	3.4
04JN8-10	0.0	0.04	0.0	6.0	5.8	0.1
04JN8-9B	11.0	0.03	0.0	5.6	4.9	0.1
A04-04-1	0.8	0.14	0.0	3.9	3.1	1.6
A04-03-6	1.2	0.07	0.0	4.0	4.5	0.2
A04-03-7	1.2	0.03	0.0	2.9	3.1	0.2
04TB10-2	0.6	0.42	0.0	4.2	4.1	0.6
04TB10-3	0.7	0.04	0.0	3.0	3.7	0.2
04TB10-5	0.8	0.07	0.0	3.2	3.5	0.4
04TB2-3	0.0	0.22	0.0	3.3	2.2	1.6
04TB3-3	1.0	0.40	0.0	3.1	3.2	0.6
04TB7-3	0.8	0.05	0.0	2.9	3.0	0.6
04TB7-4	0.9	0.05	0.0	4.1	3.8	0.4
04TB7-6	1.5	0.08	0.0	3.7	4.0	0.1
04TB8-2	1.3	0.10	0.0	3.2	3.3	0.6
04TB9-2	0.8	0.13	0.0	2.2	2.4	0.2
04TB2-4	0.7	0.17	0.0	3.3	3.5	0.4
04TB24-7A	1.0	0.19	0.0	2.1	2.8	0.2
04TB24-2	0.8	0.11	0.0	2.3	2.7	0.1
04TB24-3	1.0	0.18	0.0	3.7	3.8	0.4
04JN6-6	0.8	0.08	0.0	2.3	2.5	0.2
04JN6-7D	0.7	0.64	0.0	4.3	3.3	1.6
04JN6-5D	0.5	0.06	0.0	2.9	3.1	0.3
04JN1-8A	0.8	0.20	0.0	6.5	3.4	4.3
04TB16-7	1.0	0.18	0.0	2.8	3.5	0.1
04TB19-7A	0.7	0.13	0.0	4.1	2.8	2.4
04TB26-10	0.6	0.00	0.0	4.1	2.3	2.3
04TB16-6	0.0	0.24	0.0	2.9	3.3	0.1
04TB22-14	0.0	0.04	0.0	3.1	3.6	0.1
04TB21-12	0.5	0.25	0.0	3.8	4.2	0.2
04TB2-5	0.7	0.41	0.0	3.1	3.0	0.9
04TB4-2	0.7	0.17	0.0	3.4	3.1	0.8
04TB5-1	1.0	0.79	0.0	2.6	2.8	0.8
Average IRF Rhyolite MS03-23-05		0.25		1.6		

Sample	Easting (NAD 83 Zone 9)	Northing (NAD83 Zone9	Location	Group	SiO_2 wt. %	TiO_2 wt. %	Al_2O_3 wt. %	Fe_2O_{3total} wt. %	Fe_2O_3 wt. %	FeO wt. %	MnO wt. %
Duplicate analyses run during the above analyses (samples not included in this study)											
Dup 1A					76.70	0.15	10.80	1.20		2.6	0.00
Dup 1B					76.50	0.15	10.70	1.20		2.8	0.00
Dup 2A					63.40	0.92	13.60	6.70	0.59	5.5	0.13
Dup 2B					63.80	0.91	13.70	6.70	0.81	5.3	0.12
Dup 3A					63.60	0.62	17.80	0.30		0.4	0.02
Dup 3B					63.60	0.63	17.90	0.20		0.3	0.02

Sample	MgO wt. %	CaO wt. %	Na_2O wt. %	K_2O wt. %	P_2O_5 wt. %	TOTAL wt. %	Cu ppm	Zn ppm	Pb ppm	Co ppm	Ni ppm	V ppm
Duplicate analyses rur												
Dup 1A	0.18	0.15	0.10	9.31	-0.01	100.2	14	27	24	-5	-10	11
Dup 1B	0.20	0.15	0.10	9.40	-0.01	100.2	11	15	23	-5	-10	8
Dup 2A	2.87	3.62	5.60	1.94	0.22	100.1	-10	153	-1	14	-10	150
Dup 2B	2.84	3.61	5.50	1.86	0.21	100.6	-10	150	2	15	-10	150
Dup 3A	0.16	3.80	10.40	0.06	0.12	99.8	-10	17	-1	-5	-10	36
Dup 3B	0.14	3.74	10.50	0.06	0.14	99.9	-10	16	-1	-5	-10	35

Sample	Sc ppm	Rb ppm	Sr ppm	Ga ppm	Nb ppm	Y ppm	Zr ppm	Ag ppm	Ba ppm	Cr ppm	Cs ppm	Hf ppm
Duplicate analyses rur												
Dup 1A	4.5	145.00	26	9.00	18.00	35.00	195.0	0.3	3040	38	0.64	5.60
Dup 1B	4.3	144.00	23	9.00	18.00	34.00	193.0	0.1	2980	33	0.62	5.60
Dup 2A	20.0	36.00	60	18.00	11.00	50.00	201.0	-0.1	347	50	0.19	5.20
Dup 2B	20.0	36.00	57	17.00	11.00	49.00	196.0	0.1	374	56	0.20	5.30
Dup 3A	6.3	0.45	78	14.00	19.00	28.00	278.0	-0.1	49	18	-0.02	6.50
Dup 3B	6.2	0.44	79	14.00	19.00	28.00	281.0	-0.1	39	19	-0.02	6.60

Sample	Mo ppm	Sb ppm	U ppm	La ppm	Ce ppm	Pr ppm	Nd ppm	Sm ppm	Eu ppm	Gd ppm	Tb ppm	Dy ppm
Duplicate analyses rur												
Dup 1A	4.7	1.3	3.90	13.0	31.0	3.70	14.0	2.70	0.33	3.00	0.60	4.60
Dup 1B	4.7	1.5	3.80	13.0	30.0	3.60	14.0	2.90	0.31	3.00	0.61	4.60
Dup 2A	1.0	0.7	3.00	13.0	30.0	4.10	18.0	5.20	1.10	6.50	1.20	7.70
Dup 2B	1.1	0.5	2.90	13.0	31.0	4.00	18.0	5.30	1.10	6.60	1.20	7.80
Dup 3A	0.6	-0.2	4.60	20.0	48.0	6.40	25.0	5.20	0.93	4.70	0.71	4.10
Dup 3B	0.6	-0.2	4.70	20.0	49.0	6.30	25.0	5.30	0.95	4.60	0.72	4.20

Sample	Ho ppm	Er ppm	Tm ppm	Yb ppm	Lu ppm	Ta ppm	Th ppm	St ppm	Be ppm	Bi ppm	Cd ppm	In ppm
Duplicate analyses rur												
Dup 1A	1.10	3.60	0.63	4.40	0.72	1.10	7.60	0.67	1.7	-0.2	-0.2	-0.05
Dup 1B	1.10	3.50	0.65	4.30	0.70	1.10	7.40	0.69	1.7	-0.2	-0.2	-0.05
Dup 2A	1.70	5.00	0.80	5.50	0.87	0.71	4.70	0.06	1.5	-0.2	-0.2	0.07
Dup 2B	1.70	4.90	0.82	5.40	0.86	0.69	4.80	0.07	1.5	-0.2	-0.2	0.07
Dup 3A	0.87	2.40	0.41	2.90	0.47	1.20	11.00	-0.02	1.1	-0.2	-0.2	-0.05
Dup 3B	0.87	2.40	0.42	2.80	0.46	1.30	11.00	-0.02	1.1	-0.2	-0.2	-0.05

Sample	Sn ppm	Tl ppm	Te ppm	LOI wt. %	H_2O_T wt. %	CO_{2T} wt. %
Duplicate analyses run						
Dup 1A	2.2	1.50	-0.2	0.8	0.4	0.2
Dup 1B	2.0	1.40	-0.2	0.8	0.4	0.3
Dup 2A	2.0	0.36	-0.2	1.2	1.4	0.1
Dup 2B	2.2	0.38	-0.2	1.1	1.5	0.2
Dup 3A	1.1	-0.02	-0.2	2.7	0.2	2.7
Dup 3B	1.1	-0.02	-0.2	2.7	0.2	2.7

Appendix C: Geochronology Methods

CA-TIMS Analyses

CA-TIMS (chemical abrasion thermal ionization mass spectrometry) procedures described here are modified from Mundil et al. (2004), Mattinson (2005), and Scoates and Friedman (2008). After rock samples have undergone standard mineral separation procedures, zircons were handpicked in alcohol. The clearest, crack- and inclusion-free grains were selected, photographed, and then annealed in quartz glass crucibles at 900˚C for 60 hours. Annealed grains were transferred into 3.5 mL PFA screw top beakers, ultrapure HF (up to 50% strength, 500 mL) and HNO_3 (up to 14 N, 50 mL) were added and caps closed finger tight. The beakers were placed in 125 mL PTFE liners (up to four per liner). About 2 mL HF and 0.2 mL HNO_3,of the same strength as acid in beakers containing samples was added to the liners. The liners were slid into stainless steel Parr™ high-pressure dissolution devices, which were sealed and heated to a maximum of 200˚C for 8-16 hours (typically 175˚C for 12 hours). Beakers were removed from liners and zircon was separated from leachate. Zircons were rinsed with >18 MΩ.cm water and subboiled acetone. Then 2 mL of subboiled 6N HCl was added and beakers were set on a hotplate at 80˚-130˚C for 30 minutes, and again rinsed with water and acetone. Masses were estimated from the dimensions (volumes) of grains. Single grains were transferred into clean 300 mL PFA microcapsules (crucibles), and 50 mL 50% HF and 5 mL 14 N HNO_3 were added. Each was spiked with a $^{233\text{-}235}U$-^{205}Pb tracer solution, capped and again placed in a Parr liner (8-15 microcapsules per liner). HF and nitric acids in a 10:1 ratio, respectively, were added to the liner, which was then placed in the Parr high-pressure device, and dissolution was achieved at 240˚C for 40 hours. The resulting solutions were dried on a hotplate at 130˚C, 50 mL 6N HCl was added to microcapsules and fluorides were dissolved in high pressure Parr devices for 12 hours at 210˚C. HCl solutions were transferred into clean 7 mL PFA beakers and dried with 2 mL of 0.5 N H_3PO_4. Samples were loaded onto degassed, zone-refined Re filaments in 2 mL of silicic acid emitter (Gerstenberger and Haase, 1997).

Isotopic ratios were measured using a modified single collector VG-54R thermal ionization mass spectrometer equipped with analogue Daly photomultipliers. Measurements were taken in peak-switching mode on the Daly detector. Analytical blanks are 0.2 pg for U, and up to 5.0 pg for Pb. U fractionation was determined directly on individual runs using the $^{233\text{-}235}$U tracer, and Pb isotopic ratios were corrected for fractionation of 0.23-0.32%/amu, based on replicate analyses of the NBS-982 Pb reference material and the values recommended by Thirlwall (2000). Data reduction employed the Excel-based program of Schmitz and Schoene (2007). Standard concordia diagrams were constructed and regression intercepts, weighted averages calculated with Isoplot (Ludwig, 2003). Unless otherwise noted, all errors are quoted at the 2 sigma,(95%) level of confidence. Isotopic ages were calculated with the decay constants l238=1.55125E-10 and l235=9.8485E-10 (Jaffey et al. 1971). EARTHTIME U-Pb synthetic solutions were analyzed on an on-going basis to monitor the accuracy of results.

LA-ICP-MS detrital zircon analyses

Two 10 Kg + samples of basal Telkwa Formation rock were collected for analyses. Zircons were separated from their host rocks using conventional mineral separation methods, and sectioned in an epoxy grain mount along with grains of an internationally accepted standard (Plešovice, a zircon standard with weighted mean ^{206}Pb/^{238}U date of 337.13 ± 0.37 Ma), and brought to a very high polish. The surface of the mount was then washed for ~10 minutes with dilute nitric acid and rinsed in ultraclean water. Analyses are carried out using a New Wave 213nm Nd-YAG laser coupled to a Thermo Finnigan Element2 high-resolution ICP-MS. Ablation was in a New Wave "Supercell" ablation chamber, which is designed to achieve very high efficiency entrainment of aerosols into the carrier gas. Helium was used as the carrier gas for all experiments, and gas flow rates, together with other parameters such as torch position, were optimized prior to beginning a series of analyses. We typically used a 25 or 30 micrometer spot with 28-32% laser power, and did line scans rather than spot analyses in order to avoid within-run elemental fractions. Each analysis consisted of a 10 second background measurement (laser off)

followed by a ~30 second data acquisition period with the laser firing. A typical analytical session consisted of four analyses of the standard zircon, followed by four analyses of unknown zircons, one standard, one monitor zircon of known age, four unknown analyses, etc., and finally four standard analyses. Data were reduced using the GLITTER software package developed by the GEMOC group at Macquarrie University, which subtracts background measurements, propagate analytical errors, and calculates isotopic ratios and ages. This application generates a time-resolved record of each laser shot. Final ages for contiguous populations of relatively young (Phanerozoic) zircons are typically based on a weighted average of the calculated $^{206}Pb/^{238}U$ ages for 20-25 individual analyses. For detrital zircon samples 60 grains were analysed and displayed on Concordia and probability plots. For the latter $^{206}Pb/^{238}U$ ages are used for grains less than 1 Ga and $^{207}Pb/^{206}Pb$ ages for those greater than 1 Ga; these data were filtered at 10% discordance. Plotting of the analytical results employs ISOPLOT 3.00 software (Ludwig, 2003).

References

Crowley, J.L., Schoene, B. and Bowring, S.A. 2007. U-Pb dating of zircon in the Bishop Tuff at the millennial scale. Geology, **35**: 1123-1126.

Gerstenberger, H., Haase, G. 1997. A highly effective emitter substance for mass spectrometric Pb isotope ratio determinations. Chemical. Geology, **136**: 309–312.

Jaffey, A.H., Flynn, K.F., Glendenin, L.E., Bentley, W.C., Essling, A.M.1971. Precision measurement of half-lives and specific activities of ^{235}U and ^{238}U. Phys. Rev. **C4**: 1889–1906.

Ludwig K.R., 2003. Isoplot 3.00, A Geochronological Toolkit for Microsoft Excel. University of California at Berkely, kludwig@bgc.org.

Mattinson, J.M. 2005. Zircon U-Pb chemical abrasion ("CA-TIMS") method: Combined annealing and multi-step partial dissolution analysis for improved precision and accuracy of zircon ages. Chemical Geology, **220**: 47–66.

Mundil, R. Ludwig, K. R., Metcalfe, I, and Renne, P.R. 2004. Age and Timing of the Permian Mass Extinctions: U/Pb Dating of Closed-System Zircons. Science, **305**: 1760-1763.

Scoates, J.S. and Friedman, R.M. 2008. Precise age of the platiniferous Merensky Reef, Bushveld Complex, South Africa, by the U-Pb zircon chemical abrasion ID-TIMS technique. Economic Geology, **103**: 465-471.

Schmitz, M. D., and Schoene, B. 2007. Derivation of isotope ratios, errors, and error correlations for U-Pb geochronology using ^{205}Pb-^{235}U-(^{233}U)-spiked isotope dilution thermal ionization mass spectrometric data. Geochem. Geophys. Geosyst.,8, Q08006

Sláma, J., Košler, J., Condon, D., Crowley, J., Gerdes A., Hanchar, J., Horstwood, M.,Morris, G., Nasdala, L., Norberg, N. Schaltegger, U., Schoene, B., Tubrett, M., and Whitehouse, M., 2008. Plešovice zircon — A new natural reference material for U–Pb and Hf isotopic microanalysis. Chemical Geology **249**: 1–35.

Stacey, J.S., and Kramers, J.D. 1975. Approximation of terrestrial lead isotopic evolution by a two-stage model. Earth and Planetary Science Letters, **26**: 207–221.

Thirlwall, M.F., 2000. Inter-laboratory and other errors in Pb isotope analyses investigated using a ^{207}Pb–^{204}Pb double spike. Chemical Geology, **163**: 299–322.

Appendix D: Copyright Permissions

November 1, 2014

British Columbia Ministry of Energy and Mines, British Columbia Geological Survey Papers and Open-Files
PO Box 9333
Station Provincial Government
Victoria, B.C.
V8W 9N3

I am preparing my Ph.D. thesis for submission to the Faculty of Graduate Studies at Dalhousie University, Halifax, Nova Scotia, Canada. I am seeking your permission to include manuscript versions of the following papers and open-files as chapters and appendices in the thesis:

Alldrick, D.J., Nelson, J.L. and Barresi, T. 2005. Geology and mineral occurrences of the upper Iskut River area: Tracking the Eskay Rift through northern British Columbia. In Geological Fieldwork 2004, British Columbia Ministry of Energy and Mines, British Columbia Geological Survey Paper 2005-2: 2-39.

Alldrick, D.J., Nelson, J.L., Barresi, T. 2005. Geology of the Volcano Creek - More Creek Area, British Columbia. British Columbia Ministry of Energy, Mines and Petroleum Resources, Open File Map 2005-5, scale 1:50 000.

Alldrick, D.J., Nelson, J.L., Barresi, T., Stewart, M.L. and Simpson, K.A. 2006. Geology of upper Iskut River area, northwestern British Columbia. BC Ministry of Energy and Mines, Open File Map 2006-2, Scale 1:100 000.

Barresi, T., and Dostal, J. 2005. Geochemistry and Petrography of Upper Hazelton Group volcanics: VHMS-Favourable Stratigraphy in the Iskut River and Telegraph Creek Map Areas, Northwestern British Columbia. In Geological Fieldwork 2004. British Columbia Ministry of Energy, Mines and Petroleum Resources, Paper 2005-1, pp. 39-47.

Barresi, T., Nelson, J. 2006. Usk Map Area (NTS 103I/09), Near Terrace, British Columbia: Cross-Sections and Volcanic Facies Interpretation. In Geological Fieldwork 2005, British Columbia Ministry of Energy and Mines, British Columbia Geological Survey Paper 2006-1, p. 21-28.

Barresi, T., Nelson, J.L., Alldrick, D.J., and Dostal, J. 2005. Pillow Basalt Ridge Facies: Detailed mapping of Eskay Creek-Equivalent Stratigraphy in Northwestern British Columbia. In Geological Fieldwork 2004. British Columbia Ministry of Energy, Mines and Petroleum Resources, Paper 2005-1, pp. 31-38.

Nelson, J., Barresi, T., Knight, E. and Boudreau, N. 2006a. Geology and Mineral Potential of the Usk Map Area (NTS 103I/09), Terrace, British Columbia. In Geological Fieldwork 2005, British Columbia Ministry of Energy and Mines, British Columbia Geological Survey Paper 2006-1, p. 149-162.

Nelson, J.L., Barresi, T., Knight, E., Boudreau, N. 2006a. Geology of the Usk Map Area (NTS 103I/9). British Columbia Ministry of Energy and Mines, British Columbia Geological Survey Open File 2006-03.

Canadian graduate these are reproduced by the Library and Archives of Canada (formerly National Library of Canada) through a non-exclusive, world-wide license to reproduce, loan, distribute, or sell theses. I am also seeking your permission for the material described above to be reproduced and distributed by the LAC(NLC). Further details about the LAC(NLC) thesis program are available on the LAC(NLC) website (www.nlc-bnc.ca).

Full publication details and a copy of this permission letter will be included in the thesis.

Yours sincerely,

Tony Barresi

Permission is granted for:

a) The inclusion of the material described above in your thesis
b) For the material described above to be included in the copy of your thesis that is sent to the Library and Archives of Canada (formerly National Library of Canada) for reproduction and distribution.

Name: Lawrence B. Aspler Title: Science Editor. B.C. Geological Survey

Signature: _____ Date: November 17, 2014

November 1, 2014

Canadian Journal of Earth Sciences
Canadian Science Publishing
65 Auriga Drive, Suite 203
Ottawa, ON
K2E 7W6

I am preparing my Ph.D. thesis for submission to the Faculty of Graduate Studies at Dalhousie University, Halifax, Nova Scotia, Canada. I am seeking your permission to include manuscript versions of the following papers and open-files as chapters and appendices in the thesis:

Barresi, T., Nelson, J.L., and Dostal, J. 2015. Geochemical constraints on magmatic and metallogenic processes: Iskut River Formation, volcanogenic massive sulfide-hosting basalts, NW British Columbia, Canada. Canadian Journal of Earth Sciences, 52: 1-20.

Gagnon, J.-F., Barresi, T., Waldron, W.F., Nelson, J.L., Poulton, T.P., and Cordey, F. 2012. Stratigraphy of the upper Hazelton Group and the Jurassic evolution of the Stikine terrane, British Columbia. Canadian Journal of Earth Science 49: 1027-1052.

Canadian graduate these are reproduced by the Library and Archives of Canada (formerly National Library of Canada) through a non-exclusive, world-wide license to reproduce, loan, distribute, or sell theses. I am also seeking your permission for the material described above to be reproduced and distributed by the LAC(NLC). Further details about the LAC(NLC) thesis program are available on the LAC(NLC) website (www.nlc-bnc.ca).

Full publication details and a copy of this permission letter will be included in the thesis.

Yours sincerely,

Tony Barresi

Permission is granted for:

c) The inclusion of the material described above in your thesis
d) For the material described above to be included in the copy of your thesis that is sent to the Library and Archives of Canada (formerly National Library of Canada) for reproduction and distribution.

Name: _____ Title: _____

Signature: _____ Date: _____

NRC RESEARCH PRESS LICENSE TERMS AND CONDITIONS

Feb 02, 2015

This is a License Agreement between Tony Barresi ("You") and NRC Research Press ("NRC Research Press") provided by Copyright Clearance Center ("CCC"). The license consists of your order details, the terms and conditions provided by NRC Research Press, and the payment terms and conditions.

All payments must be made in full to CCC. For payment instructions, please see information listed at the bottom of this form.

License Number	3550820893506
License date	Jan 16, 2015
Order Content Publisher	NRC Research Press
Order Content Publication	Canadian Journal of Earth Sciences
Order Content Title	Geochemical constraints on magmatic and metallogenic processes: Iskut River Formation, volcanogenic massive sulfide-hosting basalts, NW British Columbia, Canada
Order Content Author	Tony Barresi, JoAnne L. Nelson, Jaroslav Dostal
Order Content Date	Jan 1, 2015
Volume number	52
Issue number	1
Type of Use	Thesis/Dissertation
Requestor type	Author (original work)
Format	Print and electronic
Portion	Full article
Order reference number	None
Title of your thesis / dissertation	Tectono-Magmatic and Metallogenic Evolution of the Late Triassic to Middle Jurassic Hazelton Group in Northwest British Columbia
Expected completion date	Mar 2015
Estimated size(pages)	300
Total	**0.00 CAD**
Terms and Conditions	

General Terms & Conditions

Permission is granted upon the requester's compliance with the following terms and conditions:

1. A credit line will be prominently placed in your product(s) and include: for books the author, book title, editor, copyright holder, year of publication; for journals the author, title of article, title of journal, volume number, issue number, and the inclusive pages. The credit line must include the following wording: "© 2008 Canadian Science Publishing or its licensors. Reproduced with permission," except when an author of an original article published in 2009 or later is reproducing his/her own work.

2. The requester warrants that the material shall not be used in any manner that may be derogatory to the title, content, or authors of the material or to Canadian Science Publishing, including but not limited to an association with conduct that is fraudulent or otherwise illegal.

3. Permission is granted for the term (for Books/CDs-Shelf Life; for Internet/Intranet-In perpetuity; for all other forms of print-the life of the title) and purpose specified in your request. Once term has expired, permission to renew must be made in writing.

4. Permission granted is nonexclusive, and is valid throughout the world in English and the languages specified in your original request. A new permission must be requested for revisions of the publication under current consideration.

5. Canadian Science Publishing cannot supply the requester with the original artwork or a "clean copy."

6. If the Canadian Science Publishing material is to be translated, the following lines must be included: The authors, editors, and Canadian Science Publishing are not responsible for errors or omissions in translations.

v1.4

Questions? customercare@copyright.com or +1-855-239-3415 (toll free in the US) or +1-978-646-2777.

Gratis licenses (referencing $0 in the Total field) are free. Please retain this printable license for your reference. No payment is required.

NRC RESEARCH PRESS LICENSE TERMS AND CONDITIONS

Feb 02, 2015

This is a License Agreement between Tony Barresi ("You") and NRC Research Press ("NRC Research Press") provided by Copyright Clearance Center ("CCC"). The license consists of your order details, the terms and conditions provided by NRC Research Press, and the payment terms and conditions.

All payments must be made in full to CCC. For payment instructions, please see information listed at the bottom of this form.

License Number	3550821098249
License date	Jan 16, 2015
Order Content Publisher	NRC Research Press
Order Content Publication	Canadian Journal of Earth Sciences
Order Content Title	Stratigraphy of the upper Hazelton Group and the Jurassic evolution of the Stikine terrane, British Columbia1ESS Contribution 20120051.
Order Content Author	J.-F. Gagnon, T. Barresi, John W.F. Waldron, et al
Order Content Date	Sep 1, 2012
Volume number	49
Issue number	9
Type of Use	Thesis/Dissertation
Requestor type	Author (original work)
Format	Print and electronic
Portion	Extract (< 100 words)
Order reference number	None
Title of your thesis / dissertation	Tectono-Magmatic and Metallogenic Evolution of the Late Triassic to Middle Jurassic Hazelton Group in Northwest British Columbia
Expected completion date	Mar 2015
Estimated size(pages)	300
Total	**0.00 USD**
Terms and Conditions	

General Terms & Conditions

Permission is granted upon the requester's compliance with the following terms and conditions:

1. A credit line will be prominently placed in your product(s) and include: for books the author, book title, editor, copyright holder, year of publication; for journals the author, title of article, title of journal, volume number, issue number, and the inclusive pages. The credit line must include the following wording: "© 2008 Canadian Science Publishing or its licensors. Reproduced with permission," except when an author of an original article published in 2009 or later is reproducing his/her own work.

2. The requester warrants that the material shall not be used in any manner that may be derogatory to the title, content, or authors of the material or to Canadian Science Publishing, including but not limited to an association with conduct that is fraudulent or otherwise illegal.

3. Permission is granted for the term (for Books/CDs-Shelf Life; for Internet/Intranet-In perpetuity; for all other forms of print-the life of the title) and purpose specified in your request. Once term has expired, permission to renew must be made in writing.

4. Permission granted is nonexclusive, and is valid throughout the world in English and the languages specified in your original request. A new permission must be requested for revisions of the publication under current consideration.

5. Canadian Science Publishing cannot supply the requester with the original artwork or a "clean copy."

6. If the Canadian Science Publishing material is to be translated, the following lines must be included: The authors, editors, and Canadian Science Publishing are not responsible for errors or omissions in translations.

v1.4

Questions? customercare@copyright.com or +1-855-239-3415 (toll free in the US) or +1-978-646-2777.

Gratis licenses (referencing $0 in the Total field) are free. Please retain this printable license for your reference. No payment is required.

Appendix E: Maps

Appendix E.1: Nelson, J.L., Barresi, T., Knight, E., and Boudreau, N. 2006b. Geology of the Usk Map Area (NTS 103I/9). British Columbia Ministry of Energy and Mines, British Columbia Geological Survey Open File 2006-03.

In non-digital version of thesis, see inset envelope for map

This appendix has been archived as a supplemental data file (Appendix E1.pdf)

Appendix E.2: Alldrick, D.J., Nelson, J.L. and Barresi, T. 2005b. Geology of the Volcano Creek - More Creek Area, British Columbia. British Columbia Ministry of Energy, Mines and Petroleum Resources, Open File Map 2005-5, scale 1:50 000.

In non-digital version of thesis, see inset envelope for map

This appendix has been archived as a supplemental data file (Appendix E2.pdf)

Appendix E.3: Alldrick, D.J., Nelson, J.L., Barresi, T., Stewart, M.L. and Simpson, K.A. 2006. Geology of upper Iskut River area, northwestern British Columbia. BC Ministry of Energy and Mines, Open File Map 2006-2, Scale 1:100 000.

In non-digital version of thesis, see inset envelope for map

This appendix has been archived as a supplemental data file (Appendix E3.pdf)